The 45th Annual Meeting of the NMR Society of Japan

Abstracts

November 22nd (Wed) – 24th (Fri), 2006

Kyoto University Clock Tower Centennial Hall

ＮＭＲ 2006

主催：東京 NMR 懇談会

日時：平成 18 年 12 月 16 日(土)
会場：東京大学 薬学部総合研究棟 2 階講堂　　東京メトロ丸ノ内線、本郷三丁目駅 徒歩 5 分

テーマ 構造生物学はわれわれに何を与えるか？

09：30　開　　場　　モーニング・サービス（パンと飲み物）
10：00　開会挨拶　　嶋田 一夫（東大・院薬系・BIRC,AIST）

セッション1　座長：阿久津 秀雄
10：10　油田細菌が産出する生界面活性剤アルスロファクチンの NMR 解析
池上 貴久（阪大・蛋白研）
10：50　テロメア DNA 及びテロメア結合タンパク質の構造・機能とテロメア長制御
片平 正人（横浜市大・国際総合科学）
11：30　NMR 測定条件における蛋白質の凝集防止と安定化
若松 馨 （群馬大・工）

昼　　食(12:10-13:10)

セッション2　座長：甲斐荘 正恒
13：10　高精度・高特異的な化学反応を触媒する遺伝暗号翻訳系酵素の反応機構の時間分解能構造解析
濡木 理 （東京工大・生命理工）
13：50　電子顕微鏡によるタンパク質の単粒子構造解析法：結晶を用いない方法による対称性の少ない構造の解析
佐藤 主税（産総研 脳神経情報部門＆生物情報解析センター）
14:30　実験結果と計算の融合による蛋白質－低分子ドッキングと薬物スクリーニング
福西 快文（産総研 生物情報解析研究センター）

コーヒー ＆ ティー・ブレーク(15:10－15:30)

セッション3　座長：寺尾 武彦
15:30　シルクの固体 NMR 構造解析
朝倉 哲郎（東京農工大・工）
16:10　天然変成タンパク質と動的構造
西村 善文（横浜市大・総合理学研究科）
16:50　好中球活性酸素発生系の構造生物学 －細胞質因子のドメインの構造と制御機構－
稲垣 冬彦（北大・薬）

懇親会 （於：薬学図書館ホール、18:00～ 無料です）
シンポジウム・懇親会への参加ご希望の方は、準備の都合上できるだけ事前に下記 E-mail、Fax でお知らせください。グループでまとめて頂けると好都合です。参加費無料

連絡先：〒113-0033 東京都文京区本郷 7-3-1 東京大学大学院薬学系研究科 嶋田 一夫
FAX 03-5814-4810　E.mail　nmr2006@iw-nmr.f.u-tokyo.ac.jp

Supporting Organizers

Conference Sponsor

The Nuclear Magnetic Resonance Society of Japan

Conference Co-sponsors

Japanese Society for Magnetic Resonance in Medicine
The Japanese Biochemical Society
The Pharmaceutical Society of Japan
The Society of Polymer Science, Japan
Protein Science Society of Japan
The Biophysical Society of Japan
Japan Society for Bioscience, Biotechnology, and Agrochemistry
The Physical Society of Japan
The Japan Society for Analytical Chemistry

Conference Organization

Executive committee

Chair	Masahiro Shirakawa
Vice-Chairs	Yutaka Ito
	Hidehito Tochio

Programming committee

Solution NMR	Shin-ichi Tate
	Masato Katahira
	Yutaka Ito
	Hidekazu Hiroaki
	Chojiro Kojima
Solid state NMR	Toshimichi Fujiwara
	Koji Saito
NMR imaging and in vivo	Yoshiteru Seo
	Jun Kikuchi
Technical and theoretical developments of NMR	Peter Güntert
	Toshio Yamazaki

Access to Kyoto University Clock Tower Centennial Hall

京都大学百周年時計台記念館（京都市左京区吉田本町）

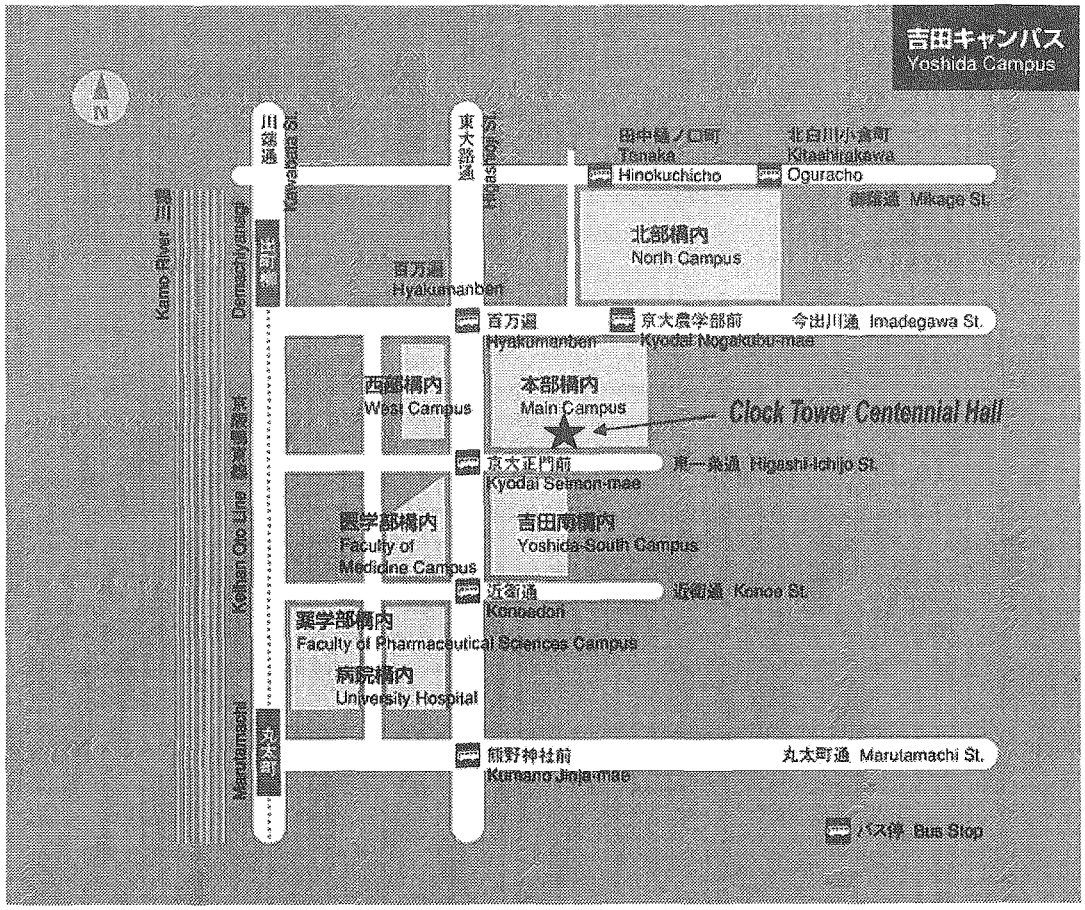

Transportation to Kyoto University from Kyoto JR Station

[To take a taxi]

The taxi ride will take about 20 minutes and cost about 1,800 yen.

[To take the bus: Kyoto City bus]

The bus ride will take about 30–35 minutes and cost 230 yen.

206: bound for Kitaoji Bus Terminarl via Higashiyama St.
Get off "Hyakumanben".

17: bound for Ginkaku-ji via Kawaramachi St.
Get off "Hyakumanben".

第 45 回 NMR 討論会
The 45th Annual Meeting of the NMR Society of Japan

会期: 11 月 22 日(水)－24 日(金)
22 – 24 November 2006

会場: 京都大学百周年時計台記念館 (京都市左京区吉田本町)
The Clock Tower Centennial Hall, Kyoto University

第一日 11 月 22 日(水)
Day 1: Wednesday, 22 November

第一会場 (百周年記念ホール), Centennial Hall
(9:50-12:30)

A-4: Solution NMR: Application to genomic science
A-5: Solution NMR: Organic and natural products, lipids, polysaccharides & Chemical biology
A-6. Solution NMR: Inorganic and analytical chemistry
Organizer: Chojiro Kojima (Nara Institute of Science and Technology)
(English session)

第二会場 (国際交流ホール), International Conference Hall
(9:50-10:30)

C-1: NMR imaging: Methodology and applications
Organizer: Yoshiteru Seo (Dokkyo Medical University)
C-2. In vivo NMR, Metabolomics and molecular imaging

Organizer: Jun Kikuchi (RIKEN)
(Japanese session)

(10:30-12:30)
B-3. Solid NMR: Application to polymer science
B-4. Solid NMR: Application to materials science
B-5. Solid NMR: Liquid crystals and membranes
Organizer: Koji Saito (Nippon Steel Corporation)
(Japanese session)

(12:30-13:00)
核磁気共鳴学会総会 Meeting of the NMR Society of Japan

(13:00-14:00)
昼食＆ポスターセッション Lunch & poster presentations

(14:00-15:00)
ポスターセッション, コアタイム （説明義務ポスター番号：奇数番号） Poster presentations (continued)

第一会場 （百周年記念ホール）, **Centennial Hall**
(15:00-18:25)
B-3. Solid NMR: Application to polymer science

B-4. Solid NMR: Application to materials science
B-5. Solid NMR: Liquid crystals and membranes
Organizer: Koji Saito (Nippon Steel Corporation)
(English session)

(18:30-19:30)

A-3. Solution NMR: Application to proteins, nucleic acids and their complexes.
Organizers: Masato Katahira (Yokohama City University), Hidekazu Hiroaki (Yokohama City University) and Yutaka Ito (Tokyo Metropolitan University)
(English session)

第二会場　（国際交流ホール），**International Conference Hall**

(15:00-16:30)

ポスター賞申込者　口頭発表　Poster award presentations

(16:40-17:20)

A-4: Solution NMR: Application to genomic science

A-5: Solution NMR: Organic and natural products, lipids, polysaccharides & Chemical biology

A-6. Solution NMR: Inorganic and analytical chemistry

Organizer: Chojiro Kojima (Nara Institute of Science and Technology)

(Japanese session)

1LJ9　Control of the polarization of surrounding water by a protein detected in terms of δ_{H2O}

○Kazuko Mizuno[1], Takuya Yamamura[1], Takunori Harada[2] Reiko Kuroda[3] ([1]Department of Applied Chemistry and Biotechnology, Faculty of Engineering, University of Fukui, [2]ERATO-SORST,JST, [3]Graduate School of Arts and Sciences, Univ. of Tokyo) 6

1LJ10　Metabolomic approach of plant cellular chemical biology by flow probe system

○Miho Izumikawa[1], Takashi Hirayama[2,3], Kazuo Shinozaki[1,3], and Jun Kikuchi[1,4] ([1]Plant Science Center, RIKEN Yokohama Institute, [2]International Graduate School of Arts and Sciences, Yokohama City University, [3]Plant Molecular Biology Laboratory, RIKEN, [4]Graduate School of Bioagriculture Sciences, Nagoya University) 6

(17:30-19:30)

D-1. Calculation, simulation and data analysis

D-2. NMR theory

D-3. Instrumentation

D-4. Quantum computer

Organizers: Peter Güntert (RIKEN) and Toshio Yamazaki (RIKEN)

(English session)

1LE16　Analysis of NMR Data Obtained by Fast Spectroscopy

○Martin Billeter, Daniel Malmodin, Wolfgang Bermel (Gothenburg University, Gothenburg/Sweden) 4

1LE17　Fast and Smart Protein Structure Determination by NMR

○Markus Zweckstetter (Department for NMR-based Structural Biology, Max Planck Institute for Biophysical Chemistry, Germany) 4

1LE18　Automated Protein Structure Determination from NMR Spectra

○Peter Güntert and Blanca López-Méndez (Tatsuo Miyazawa Memorial Program, RIKEN Genomic Sciences Center, Japan) 4

第二日　**11 月 23 日(木)**

Day 2:　Thursday, 23 November

第一会場　（百周年記念ホール），**Centennial Hall**

(9:30-13:00)

Plenary session

2LE1　SAILing to the Future: Toward the next-generation world de facto standard in protein NMR spectroscopy

○Masatsune Kainosho (CREST/JST & Tokyo Metropolitan University/Nagoya University) 7

2LE2　○Mitsuhiko Ikura (Division of Signaling Biology, Ontario Cancer Institute and Department of Medical Biophysics, University of Toronto, Canada)) 7

(13:00-14:00)
昼食 Lunch

第一会場 （百周年記念ホール）, **Centennial Hall**
(14:00-16:40)
C-1. NMR imaging: Methodology and applications
Organizer: Yoshiteru Seo (Dokkyo Medical University)
(English session)

(16:40-18:30)
A-3. Solution NMR: Application to proteins, nucleic acids and their complexes.
Organizers: Masato Katahira (Yokohama City University), Hidekazu Hiroaki (Yokohama City University) and Yutaka Ito (Tokyo Metropolitan University)
(English session)

(18:40-20:30)
懇親会 Banquet

第三日 **11月24日(金)**
Day 3: Friday, 24 November

第一会場 (百周年記念ホール), **Centennial Hall**
(9:30-13:00)
B-1. Solid NMR: Methodology
B-2. Solid NMR: Application to biological science
Organizer: Toshimichi Fujiwara (Osaka University)
(English session)

第二会場 (国際交流ホール), **International Conference Hall**
(9:30-11:10)

A-3. Solution NMR: Application to proteins, nucleic acids and their complexes.

Organizers: Masato Katahira (Yokohama City University), Hidekazu Hiroaki (Yokohama City University) and Yutaka Ito (Tokyo Metropolitan University)

(Japanese session)

(11:20-13:00)

C-2. In vivo NMR, metabolomics and molecular imaging

Organizer: Jun Kikuchi (RIKEN)

(English session)

B-2. Application to biological science

B-3. Application to polymer science

). Technical and theoretical developments of NMR

D-1. Calculation, simulation and data analysis

D-2. NMR theory

D-3. Instrumentation

Wednesday, November 22

English Session

1 LE1

Stucture and Function Elucidation of Two Unknown Proteins from Helicobacter pyroli

Bong-Jin Lee
College of Pharmacy, Seoul National University, San 56-1, Sillim-Dong, Kwanak-Gu, Seoul 151-742, Korea

The H. pyroli proteins of which molecular weight are around 20 kDa were selected for the investigation of their 3-dimensional structures by NMR. 76 target genes of H. pyroli were selected and cloned into E. coli expression vector. pET/BL21(DE3) was chosen as an expression system of target proteins. Many proteins were successfully expressed in *E.coli* and could be obtained in soluble fraction after cell lysis. Because NMR spectra of Hp0894 and Hp0495, of which function is unknown, showed good resolution, we determined solution structures of these proteins and elucidated their function. We found that Hp0894 is Archaeal RelE like toxin and Hp0495 has structural homology with Pyrociccus horikoshi NikR. Structures and Function of these proteins will be discussed.

1 LE2

Structural proteomics of animals and a plant

Takanori Kigawa[1,2], Yutaka Muto[1], Fumiaki Hayashi[1], Kazuhiko Yamasaki[1,3], Hiroshi Hirota[1], Peter Güntert[1], Toshio Yamazaki[1], Mayumi Yoshida[1], Mikako Shirouzu[1], Akiko Tanaka[1], Yoshihide Hayashizaki[1], Kazuo Shinozaki[4], Osamu Ohara[5,6], Sumio Sugano[7], and Shigeyuki Yokoyama[1,8]

[1]RIKEN Genomic Sciences Center, [2]Interdisciplinary Graduate School of Science and Engineering, Tokyo Institute of Technology, [3]Age Dimension Research Center, National Institute of Advanced Industrial Science and Technology, [4]RIKEN Plant Science Center, [5]Kazusa DNA Research Institute, [6]RIKEN Research Center for Allergy and Immunology, [7]Institute of Medical Science, The University of Tokyo, and [8]Graduate School of Science, The University of Tokyo

RIKEN Structural Genomics/Proteomics Initiative (RSGI) (http://www.rsgi.riken.jp) was organized by RIKEN Genomics Sciences Center (GSC) and RIKEN SPring-8 Center in 2001. RSGI has been integrated into the National Project on Protein Structural and Functional Analyses ("Protein 3000"), organized by the Ministry of Education, Culture, Sports, Science, and Technology, as one center of the program for comprehensive studies. The RSGI aims to study both structures and molecular functions of protein families. In this framework, RIKEN GSC is mainly targeting mouse, human, and *Arabidopsis thaliana* proteins, from the viewpoint of domain families involved in phenomena of biological and medical importance.

Domain(s) belonging to selected families are further screened in terms of the suitability for the structure determination. The *E. coli* cell-free protein synthesis system is used for protein expression method because it is more suitable for efficient expression of a large number of constructs than in vivo protein expression systems. In the initial stage of screening, the domain fragments are synthesized by small-scale cell-free reactions. A number of different expression constructs are tested for the productivity and the solubility of the product, and good constructs are selected. Experiments in this initial stage is now fully automated with the integrated system "The Cell-Free eXpress", which is able to synthesize 768 samples in 9 hours. In the next stage, milligram quantity of ^{15}N-labeled samples are prepared in parallel using a dialysis cell-free system, and then, partially purified with an affinity chromatography.

Keywords: NMR spectroscopy, Structural genomics, Structural proteomics, Cell-free protein synthesis, Protein domain.

This procedure is also fully automated and 96 samples in sub-milligram to milligram quantity can be prepared within a half day. Throughout the screening stages, the protein samples were prepared directly from PCR-amplified linear DNA fragments without any cloning procedures. In the third stage, ^{1}H-^{15}N HSQC spectra are measured to investigate whether selected domains are properly folded, and thus, suitable for structure determination. The winners in the third screening stage are subjected to larger-scale cell-free production of the uniformly $^{13}C/^{15}N$-labeled samples for the NMR spectroscopy, and then step to structure determination. A part of the samples that are judged to be more suitable for the X-ray crystallography are prepared in the selenomethionine-substituted form for structure determination by MAD phasing.

The large-scale NMR facility housing 40 high-field NMR spectrometers have been constructed at RIKEN Yokohama Campus. We have developed several key software such as a program package, KUJIRA, which is used for systematic and interactive NMR data analysis, and the program CYANA for automated structure calculation. Thanks to these programs, structure determination process by NMR have been dramatically accelerated.

In these 4 years, we have determined about 900 structures by NMR spectroscopy according to this workflow, indicating that a high-throughput pipeline for NMR structure determination have been established.

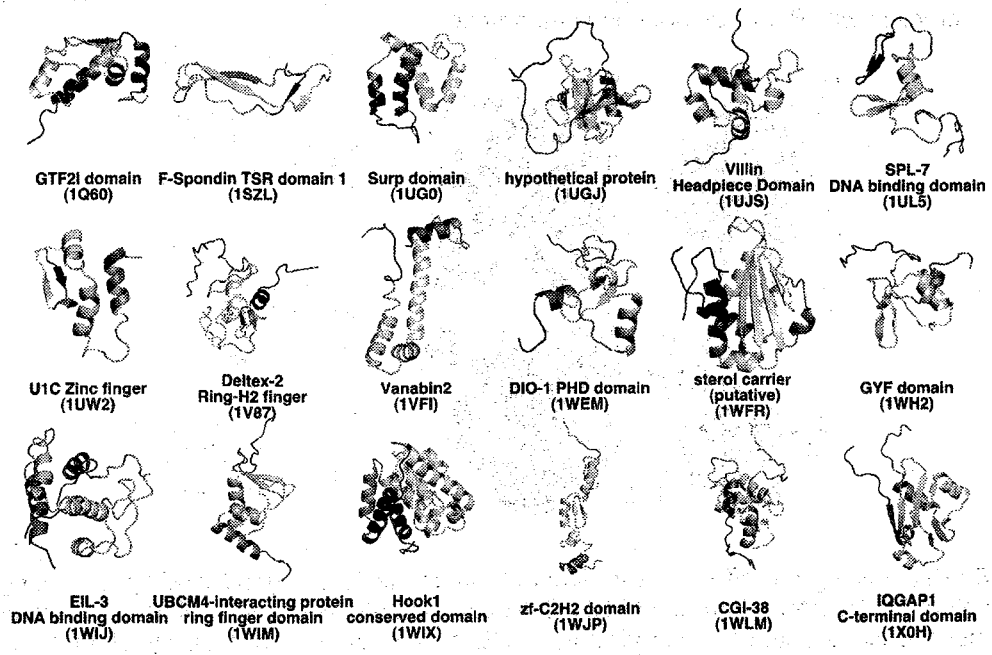

Figure. A part of 'novel' structures we determined and deposited to PDB.

1 LE3

Chelerythrine and sanguinarine docks at distinct sites on Bcl_{XL} that are not the classic "BH3 binding cleft"

Yong-Hong Zhang[1], Anirban Bhunia[1], Kah Fei Wan[2], Mei Chin Lee[2], Shing-Leng Chan[2], Victor C.-K. Yu[2] and Yu-Keung Mok[1]

[1]Department of Biological Sciences, National University of Singapore, Singapore 117543, and [2]Institute of Molecular and Cell Biology, 61 Biopolis Drive (Proteos), Singapore 138673

Proteins of the Bcl-2 family are central regulators of apoptosis. Ratio of the levels of pro-survival and pro-apoptotic members of the family is thought to be an important factor for determining the sensitivity of the mammalian cells to apoptotic stimuli. High levels of expression of pro-survival members such as Bcl_{XL} in human cancers were frequently found to be a good prognostic indicator predicting poor response to chemotherapy. The pro-survival members of the Bcl-2 family mediate their effects through heterodimerization with the BH3 region of the pro-apoptotic members. Structural analyses of the binding complex of the BH3 peptide and Bcl_{XL} showed that a hydrophobic groove termed "BH3 binding cleft" is the docking site for the BH3 region. Chemical mimetics of the BH3 region such as BH3I-1 that target the "BH3 binding cleft" indeed exhibit pro-apoptotic activities. Chelerythrine (CHE) and sanguinarine (SAN) are natural benzophenanthridine alkaloids that are structurally homologous to each other. CHE was previously identified as an inhibitor of Bcl_{XL} function from a high throughput screen of natural products, but its mode of interaction with Bcl_{XL} has not been determined.

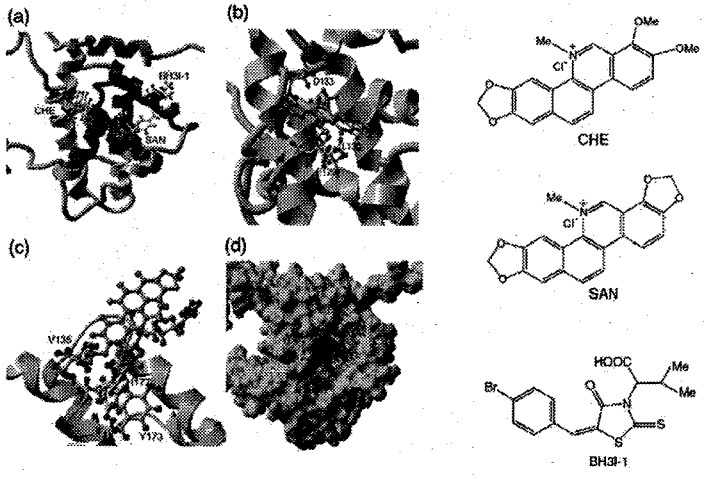

By determining the effect of site-directed mutagenesis on ligand binding and using saturation transfer difference (STD) NMR experiments, we have verified locations of these docked ligands. Surprisingly, CHE and SAN bind separately at the "BH groove" and BH1 region of Bcl_{XL} respectively, different from the "BH3 binding cleft" where other known inhibitors of Bcl_{XL} target.

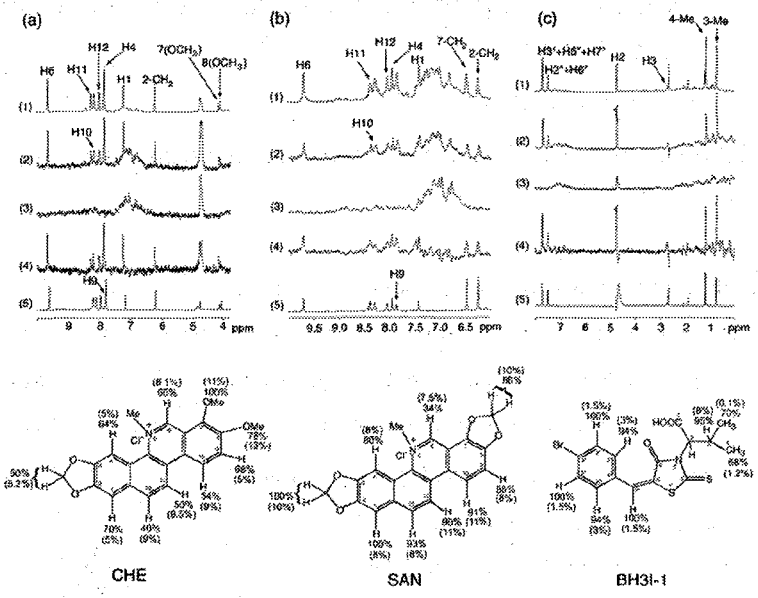

Interestingly, certain residues on the flexible loop between helices α1 and α2 of Bcl_{XL} are also perturbed upon CHE, but not SAN or BH3I-1 binding. Although CHE and SAN are similarly effective as BH3I-1 in displacing bound BH3 peptide, they are much more effective in inducing apoptosis, raising the possibility that CHE and SAN might be able to antagonize other pro-survival mechanisms in addition to the one that involves BH3 region binding.

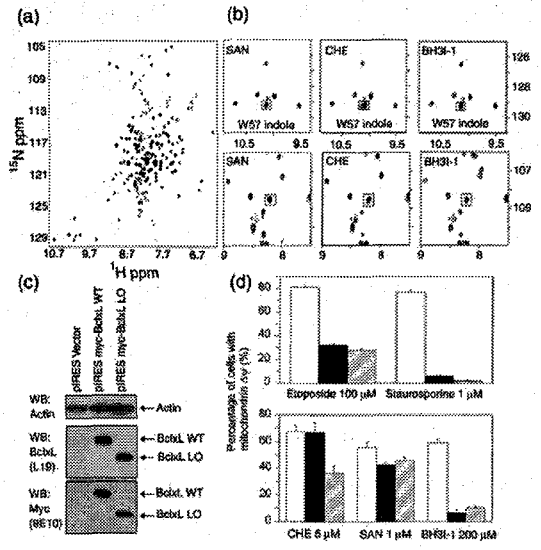

Keywords: Chelerythrine, Sanguinarine, Bcl_{XL}, apoptosis, BH groove

1 LE4

Nucleotide flipping in CXG trinucleotide repeats induced by small ligands

Chojiro KOJIMA

Graduate School of Biological Science, Nara Institute of Science and Technology, Ikoma, Nara 630-0192, Japan.

Trinucleotide repeat expansions in genomic DNA are the molecular basis of a growing number of hereditary diseases. The characteristic feature of these diseases is a phenomenon termed as anticipation. A longer repeat length would lead to the increasing disease severity and decreasing age at onset in succeeding generations. The mechanism of $(CAG)_n$, $(CTG)_n$, and $(CGG)_n$ repeats expansion is considered to correlate to the increased stability of the metastable hairpin form consisting of CXG/CXG triads involving X-X mismatches. Ligands binding to $(CXG)_n$ repeats would be important molecular probes for determining the repeat length and the repeat expansion mechanism. Recently we have reported the base flip-out structure of the first identified ligands, naphthyridine– azaquinolone (NA), complexed with the CAG/CAG triad using $^{13}C^{15}N$-labelled DNA and heteronuclear multi- dimensional NMR techniques (Nakatani K. *et al.* and Kojima C., *Nat. Chem. Biol.*, 2005). Here we show new NMR structures of two ligands, naphthyridine dimer (ND) and naphthyridine carbamate dimer (NC), complexed with the CGG/CGG triad.

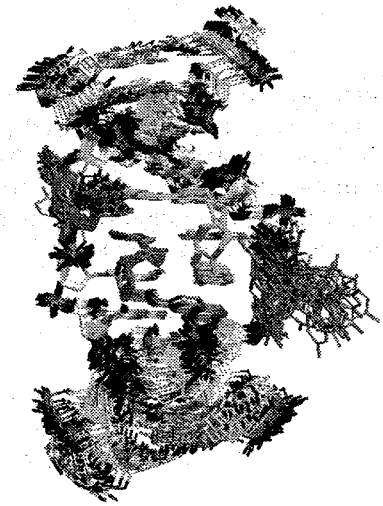

Figure 1. NMR structures of NA-CAG/CAG complex. 30 complex structures are superimposed focusing on A6, G7, A17, G18, NA1, and NA2 residues.

Signals from free DNA and the drug-DNA complex were observed separately on a slow-exchange timescale for all drug-DNA complexes. The stoichiometry was easily and unambiguously determined to be 2:1 (drug:DNA). The ^1H-^1H NOESY, TOCSY, DQF-COSY

Keywords: DNA, mismatch binding ligand, naphthyridine, azaquinolone, triplet repeat

and natural abundance ^{1}H-^{13}C HSQC spectra of the 1:2 complex were recorded. Proton resonances were completely assigned including H5' and H5". The distance restraints were obtained from the complete relaxation matrix method, MARDIGRAS. Residual dipole coupling constraints were obtained from DQF-COSY and ^{1}H-^{13}C HSQC spectra using Pf1 phage. The determined solution structure of the complex revealed the invasive ligands binding to the G-G mismatch and flanking G-C base pairs, causing the widowed cytosines to flip out from base-stack. Hydrogen-bond pairs between drugs and DNA, naphthyridine-guanine, were well stacked in the right-handed DNA helix, showing structural mimicry of Watson–Crick base pairing. These features were also found in NA-DNA complex structure. Thus, these drugs belong to a new family that the small molecular ligand induced the base flipping of the nucleotide base in the Watson-Crick base pair. We will present the results of AMBER molecular dynamics simulations of these complexes, and discuss about a new type base-stacking which is stabilizing the flipped nucleotides.

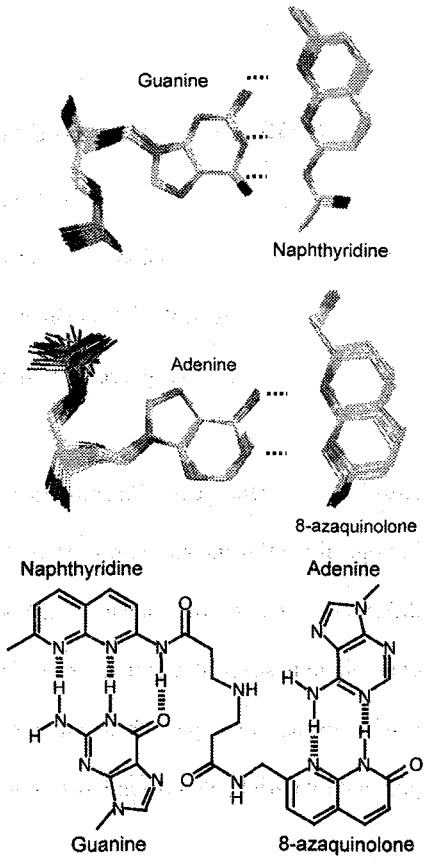

Figure 2. Superimposed NMR structures of NA-CAG/CAG complex for the hydrogen bonding between guanine and naphthyridine (top) and adenine and 8-azaquinolone (middle). Naphthyridine chromophore is complementary in hydrogen bonding surface to guanine, whereas 8-azaquinolone is complementary to adenine (bottom).

NMR methods for study of unusual DNA structures

Anh Tuân Phan

Division of Physics and Applied Physics

School of Physical and Mathematical Sciences

Nanyang Technological University, Singapore

Besides the canonical Watson-Crick double helix, DNA can adopt other biologically relevant structures. Here I present methods used in our studies of different aspects of unusual DNA structures, including stoichiometry, unambiguous spectral assignment, internal motion and structure characterization. I will discuss examples from studies of i-motif and G-quadruplex structures adopted by C-rich and G-rich DNA sequences.

Keywords: unusual DNA structures; G-quadruplex; i-motif; low-enrichment site-specific labeling; unambiguous spectral assignment

1 LE6

磁場勾配パルスを用いた ^{1}H-^{89}Y 直接および ロングレンジ相関法と有機金属化学への応用

独立行政法人理化学研究所
○越野広雪，西浦正芳，侯 召民

^{1}H-^{89}Y Direct and Long-range Heteronuclear Correlations Using Pulsed Field Gradients in Organometallic Chemistry

RIKEN
Hiroyuki Koshino, Masayoshi Nishiura, and Zhaomin Hou

Multinuclear NMR spectra are very useful for studying the structures of multinuclear metal complexes. We developed ^{1}H-^{89}Y PFG-HMQC and HMBC methods and applied to a tetranuclear yttrium polyhydride cluster complex $[(C_5Me_4SiMe_3)_4Y_4H_7(THF)_2]\cdot[B(C_6F_5)_4]$ (1) and some cluster complexes including half-sandwich rare earth metal complexes.

新しい有機金属触媒の開発，触媒反応の解析において溶液 NMR による構造解析は重要である。大部分の新規有機金属錯体の構造は X 線結晶構造解析によって明らかにされているが，反応を行う溶液中の構造解析は必須であり，NMR はその主要な分析手法である。有機金属触媒の活性中心にあり，その核となる金属原子にはスピン 1/2 で高分解能 NMR に適した多核は少なく無いが，従来は低周波の多核 NMR の場合 10mm φ の直接観測用のプローブが一般的であり，主に多量の試料を用いた 1 次元 NMR の測定，解析が行われていた。しかしスピン 1/2 の低周波多核の観測に ^{1}H 観測の HMQC 法や HMBC 法などのインバース法を適用できれば，様々な相関の観測，帰属が可能になり，溶液 NMR による有機金属触媒の構造解析に有効であると期待された[1)]。

新規な有機金属触媒として開発している有機金属錯体の中にはイットリウムなどの希土類元素を含む化合物が多い。イットリウム(^{89}Y)はスピン -1/2，天然存在比は 100%であり，今回実験に用いた 14.1T で ^{1}H の 600MHz に対し，^{89}Y は 29.4MHz の周波数で，^{1}H-^{89}Y のインバース法による感度向上が期待された。プローブは市販品が無く，の磁場勾配パルスと低周波多核は ^{15}N(60.8MHz)から ^{103}Rh(18.9MHz)までの直接観測と

キーワード：^{89}Y-NMR，PFG-HMBC，有機金属，希土類金属触媒，多核 NMR

こしのひろゆき，にしうらまさよし，ほうしょうみん

^{1}H のインバースによる観測が可能な 5mm φ の FG5LTH プローブを日本電子（株）に製作依頼したものを使用した。装置は JEOL-ECA600 を使用した。本プローブを適用できるスピン 1/2 の核種と天然存在比を共鳴周波数の高い順に並べて以下に示した。^{15}N(0.37%), ^{169}Tm(100%), ^{89}Y(100%), ^{109}Ag(48.2%), ^{183}W(14.4%), ^{107}Ag(51.8%), ^{57}Fe(2.19%), ^{103}Rh(100%)。

測定と解析の例としてポリヒドリド錯体[2,3]のひとつである，$[(C_5Me_4SiMe_3)_4Y_4H_7(THF)_2]\cdot[B(C_6F_5)_4]$ (1)に対して ^{1}H-^{89}Y PFG-HMQC[4]および ^{1}H-^{89}Y PFG-HMBC[5]を測定した。HMBC 法は通常のパルスシークエンスから low path J フィルターを取り除いたものを使用した。化合物(1)の構造は X 線結晶構造解析により図 1 のように決定されているが，C_6D_5Cl 中の NMR の解析により溶液中でも同様な構造であることを明らかにした。すなわち全ての H-Y の直接結合の相関が観測でき，２種の ^{89}Y の化学シフトと，積分強度 4H 分の μ_2-H(dd, ^{1}J=42, 34Hz)，2H 分の μ_3-H(dt, ^{1}J=8, 21Hz)，４つの Y 全てと結合している 1H 分の μ_4-H(br. s)の帰属も明らかにした。置換基のあるシクロペンテニル基 $C_5Me_4SiMe_3$ の結合位置もメチル基からイットリウムへのロングレンジ相関を観測することにより可能であった。この他，興味深い触媒活性を有するハーフサンドイッチ型希土類金属錯体[6]など幾つかの応用例を示し，直接観測より高感度で相関情報の得られる ^{1}H-^{89}Y PFG-HMQC および ^{1}H-^{89}Y PFG-HMBC などのインバース測定の有用性について報告する。

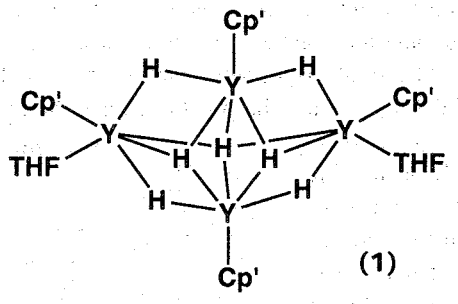

(1)

Fig. 1 Structure of tetranuclear yttrium polyhydride cluster complex compound **1**. Cp' = $C_5Me_4SiMe_3$, THF = tetrahydrofuran,$[B(C_6F_5)_4]$ anion is omitted.

参考文献

1)鵜澤洵，越野広雪，有機合成化学協会誌, **1996**, *54*, 354.

2) T. Shima and Z. Hou, *J. Am. Chem. Soc.*, **2006**, *128*, 8124.

3) Y. Luo et al, *Organometallics*, **2005**, *24*, 4362.

4) R. E. Hurd, and B. K. John, *J. Magn. Reson.*, **1991**, *91*, 648.

5) W. Willker et al, *Magn. Reson. Chem.*, **1993**, *31*, 287.

6) W.-X. Zhang et al, *J. Am. Chem. Soc.*, **2005**, *127*, 16788.

From Simple to Advanced Solid-State NMR: the Analysis of Structure and Dynamics of Materials in Organic Devices

Hironori Kaji[1,2]
[1]Institute for Chemical Research, Kyoto University, Uji, Kyoto 611-0011, JAPAN and [2]Structural Ordering and Physical Properties, PRESTO, JST

Recent developments of organic devices, such as organic light-emitting diodes (OLEDs) and organic field effect transistors (OFETs), are attracting for applications of organic light-emitting and carrier transport materials to these devices. Over the last several years, we have attempted to pursue the precise analyses of such materials using not only simple but also advanced solid-state NMR. Here, we show our recent results on light-emitting materials used for organic devices.

One example is the clarification of the relationship between the structure and light-emitting properties of tris(8-hydroxyquinoline) aluminum(III) (Alq_3).[1,2] Alq_3 is one of the most widely used materials in OLEDs and the relation between the structure and the luminescent wavelength is of recent interest; yellowish-green emissions are observed for Alq_3 in the α-crystalline and amorphous states, whereas blue emissions are found for Alq_3 in the γ- and δ-crystalline states. Some groups consider that the different emissions are originated from the different intermolecular ligand packings. Others consider the difference from the different isomeric states: As shown in Fig. 1, Alq_3 has two different isomers, meridional and facial isomers. The three ligands are different for the meridonal, while they are equivalent in the facial. Detailed X-ray diffraction experiments have been carried out,[3-6] however, even the crystal structures have not been well characterized.

Figure 1 shows the experimental dipolar decoupled ^{27}Al magic angle spinning (MAS) NMR spectra of Alq_3.[1] For α- and amorphous Alq_3, broad spectral patterns are observed. These spectra are not reproduced by single asymmetry parameters, η, indicating the structural disorders. In contrast, γ- and δ-Alq_3 provide sharp patterns, and the best-fit simulations are obtained for $\eta = 0$ and 0.24, respectively. The DFT calculation for a single facial Alq_3 molecule predicts the axially symmetric pattern with $\eta = 0$, indicating that the γ-Alq_3 is composed of the facial isomer. No effects of intermolecular packings are found. The DFT calculation for facial Alq_3 in the δ-crystalline form[5] gives $\eta = 0.26$.[7] This value agrees well with our experimental result, $\eta = 0.24$, indicating the non-zero η value for δ-Alq_3 is originated from the crystalline intermolecular packing. These results are supported by CP/MAS ^{13}C NMR experiments.[2]

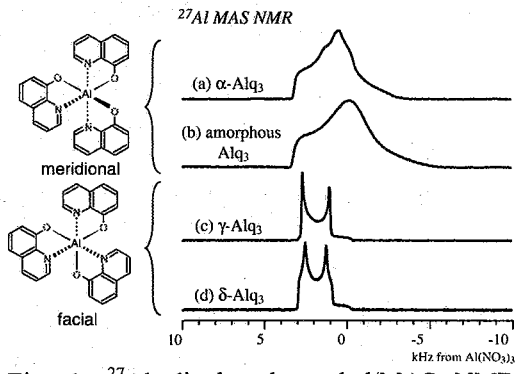

Fig. 1. ^{27}Al dipolar decoupled/MAS NMR spectra of α-, amorphous, γ-, and δ-Alq_3. Alq_3s in the meridional and facial isomeric states are shown at the left.

The meridional and facial isomers can

Keywords: organic light-emitting diodes / solid-state NMR / amorphous / carrier transport materials / light-emitting materials

be more clearly distinguished by recently-developed two-dimensional double-quantum solid-state NMR, 2D DOQSY.[8] Figure 2(a)-(c) shows the experimental 2D DOQSY spectra of ^{15}N-doubly labeled Alq_3. We can distinguish the two isomeric states from the difference of strongest peak positions (black parts in the spectra). From the simulated patterns of meridional (Fig. 3(d), (e)) and facial Alq_3 (Fig. 3(f)), it is clearly found that α- and amorphous Alq_3 are composed of the meridional isomer, whereas δ-Alq_3 are composed of the facial isomer. The blue-shifted fluorescences for γ- and δ-Alq_3 are thus found to be originated from the different isomeric states.

Second example is the relationship between the dynamics and emission wavelengths of tetraphenylpyrene (TPPy). TPPy is an excellent material for organic light-emitting FETs,[9] which shows unusual photoluminescence characters[10]: The well-purified TPPy (TPPy(A)) emits blue fluorescence. In contrast, the emission color changes into green for thermally annealed TPPy (TPPy(B)). Although the single crystal X-ray diffraction and CP/MAS ^{13}C NMR experiments cannot distinguish these samples, clear differences are observed for ^{1}H and ^{13}C spin-lattice relaxation experiments. TPPy (B) sample exhibits shorter relaxation times, indicating that TPPy (B) is more mobile than TPPy (A) on the time scale of ~ 10^9 Hz. The luminescence of TPPy(B) changes into blue by lowering temperatures, and the difference of the dynamics is considered to be the origin of the different fluorescence wavelength in these two TPPy samples.

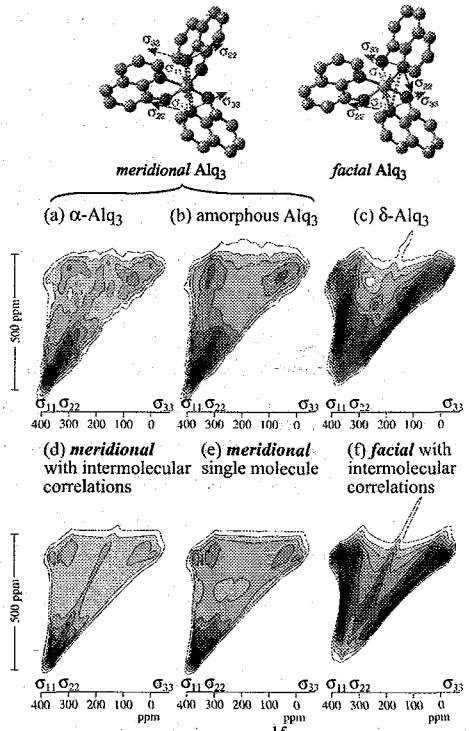

Fig. 2. Experimental ^{15}N 2D DOQSY spectra of (a) α-, (b) amorphous, and (c) δ-Alq_3. The best-fit spectra are shown at the corresponding lower column (d) – (f).

The studies on charge transport materials will be also shown in the presentation. The related topics will be presented in the poster session.

Acknowledgement. H. K. thanks Prof. C. Adachi and T. Oyamada for the studies on TPPy.

References

(1) Kaji, H. et al., *Jpn. J. Appl. Phys.* **2005,** 44, 3706.
(2) Kaji, H. et al., *J. Am. Chem. Soc.* **2006,** 128, 4292.
(3) Brinkmann, M. et al., *J. Am. Chem. Soc.* **2000,** 122, 5147.
(4) Braun, M. et al., *J. Chem. Phys.* **2001,** 114, 9625.
(5) Colle, M. et al., *Chem. Commun.* **2002**, 2908.
(6) Rajeswaran, M.; Blanton, T. N. *J. Chem. Crystallogr.* **2005,** 35, 71.
(7) Utz, M. et al., *Appl. Phys. Lett.* **2003,** 83, 4023.
(8) Schmidt-Rohr, K. *Macromolecules* **1996,** 29, 3975.
(9) Oyamada, T. et al., *J. Appl. Phys.* **2005,** 98, 074506.
(10) Oyamada, T. et al., *Chem. Phys. Lett.* **2006,** 421, 295.

TWIST GLASS TRANSITION IN π-CONJUGATED POLYMERS *

Koji Yazawa[1], Yoshio Inoue[1], Takakazu Yamamoto[2], and Naoki Asakawa[1] †

1) Department of Biomolecular Engineering and 2)Chemical Resources Laboratory, Tokyo Institute of Technology. 4259 Nagatsuta-cho, Midori-ku, Yokohama, Kanagawa 226-8501, Japan, email:nasakawa@bio.titech.ac.jp

Abstract: The molecular structure and dynamics of regioregulated poly(3-butylthiophene) (P3BT), poly(3-hexylthiophene)(P3HT), and poly(3-dodecylthiophene) (P3DDT) were investigated using Fourier transform infrared absorption (FTIR), solid state ^{13}C nuclear magnetic resonance (NMR), and differential scanning calorimetry (DSC) measurements. In the DSC measurements, the endothermic peak was obtained around 340 K in P3BT, and assigned to enthalpy relaxation that originated from the glass transition of the thiophene ring twist in crystalline phase from results of FTIR, ^{13}C cross-polarization and magic-angle spinning (CP-MAS) NMR, ^{13}C spin-lattice relaxation time measurements, and centerband-only detection of exchange (CODEX) measurements. We defined this transition as *twist-glass transition*, which is analogous to the plastic crystal - glassy crystal transition.

A. Introduction

POLY(3-ALKYLTHIOPHENE)s (P3ATs) show great promise as electronic and optoelectronic devices such as light-emitting diodes and field-effect transistors. Particularly, the regioregular versions of P3ATs have received much attention because they show high crystallinity and high conductivity because of improvement of main chain packing.

The dynamic structure of P3AT is important to find out physical properties such as thermochromism, in which the twist motion of the thiophene ring is thermally excited[1]. *Conformon* is an elemental excitation related to such molecular structural defects that it behaves as an interrupter of π-conjugation. Therefore, the dynamics as well as dimension and density of conformons are related closely to the conjugation length of the π electron[2,3,6,7]. No studies are available for the molecular dynamics of P3ATs in spite of its importance.

In this study, we shall give attention to the dynamics of quasi-ordered phases, particularly twist motion of thiophene main chain in the crystalline state of P3ATs. At first, we observed an endothermic peak for poly(3-butylthiophene)(P3BT) in DSC measurements, and peak shifts of C_β-H out-of-plane deformation region in FTIR measurement around 340 K. Next, we also investigated the dynamics of P3BT around the transition by ^{13}C CP-MAS NMR ,^{13}C spin-lattice relaxation time measurements (T_{1C}), and centerband-only detection of exchange(CODEX) measurements, and show evidence of the glass transition with respect to the twist motion. We define this transition as *twist glass transition*, which is an example analogous to PC-GC transition.

B. Experimentals

Regioregular HT (head-to-tail)-type poly(3-butylthiophene) (P3BT), poly(3-hexylthiophene)(P3HT), and poly(3-dodecylthiophene) (P3DDT) were purchased

*Keywords: glass transition, π-conjugated polymers, relaxation time, CODEX, molecular dynamics

†やざわこうじ、いのうえよしお、やまもとたかかず、あさかわなおき

from Rieke Metals Inc. and were used without further purification.

We carried out variable temperature ^{13}C cross-polarization and magic-angle s pinning (CPMAS), T_{1C}, and centerband-only detection of exchange (CODEX)[4] measurements using a NMR spectrometer (GSX-270; JEOL) operating at 270 MHz for ^{1}H and 67.9 MHz for ^{13}C. For CPMAS measurements, experimental conditions were set up with 90° pulse length of 5.2 μs, contact time of 2 ms, recycle delay of 10 s, and the MAS rate of 3.2 kHz. The ^{13}C chemical shifts were referenced externally to the methyl carbon resonance of hexamethylbenzene at 17.36 ppm. We used Torchia method for T_{1C} measurements. For CODEX measurements, experimental conditions were set up with 90° pulse length of 5.0 μs, contact time of 2 ms, recycle delay of 10 s, and the MAS rate was monitored by fiber optics and set at 5000±2Hz. Pure-exchange CODEX spectra are obtained by measuring a reference spectrum with durations of t_m and t_z interachanged and subtracting the CODEX spectrum from it. Original powder samples were used. We also carried out variable temperature proton transverse relaxation time (T_{2H}) measurements.[8,10]

C. Results and Discussion

We performed ^{13}C spin-lattice relaxation time measurements for P3ATs using Torchia method at various temperatures to investigate the molecular dynamics. An Arrhenius plot of the spin-lattice relaxation rate ($R_1 = T_1^{-1}$) for each carbon is shown in Fig. 1.

For the side chains (Fig. 1(a)), each R_1 value was obtained using a simple exponential fitting curve. Figure 1(a) shows the subtle change of slopes around 333 K, but the decrease of R_1 was observed throughout the measured temperature range with heating (from 303 K to 373 K). This tendency is visible in the extremely narrowed regime according to the classical Bloembergen-Pound-Purcell (BPP) theory, indicating that the side chains behave similarly to liquid, which is also observed in ^{13}C CP-MAS NMR spectra. The subtle change of slopes was inferred to result from the conformation change of the main chain because it would be difficult to believe that further changes in average conformation should occur in a liquid state. On the other hand, the relaxation of main chain carbons showed no single exponential decay in the measured temperature range. For that reason, we tried to fit the decay curves using a Kohlraush-Williams-Watts (KWW) function.

In general, the KWW function is used to express magnetization near and below the glass transition temperature (T_g) because the distribution of the relaxation rate gave rise to non-exponential recoveries. Temperature dependence of R_1 for each aromatic carbons is shown in Figs. 1(b). Figure 1(b) shows that the main chain must be in the slow-motion regime because of the increase of R_1 with heating. More noteworthy is the fact that discontinuous changes are apparent around 333 K.

In many cases, a similar tendency is apparent in ^{2}H NMR measurements, at the glass transition for many glassy formers including polymers such as polybutadiene and polystyrene. In the case of NMR spin-lattice relaxation measurements, we can distinguish three temperature regions for the arguments of glass transition. (i) $T < T_g$: The R_1 of glass formers is dominated by slow β-process (Johari-Goldstein process), which follows the Arrhenius-type thermal activation process below T_g. (ii) $T_g < T < 1.2T_g$: Both α process and the Johari-Goldstein process affect R_1. Where the α process is described as stretched exponential functions. (iii) $T > 1.2T_g$: R_1 is dominated only by α process.

Below 333 K, we observed the Arrhenius-type thermally activated process for all carbons. That tendency is similar to the Johari-Goldstein process. Over 333 K, although the measured temperature

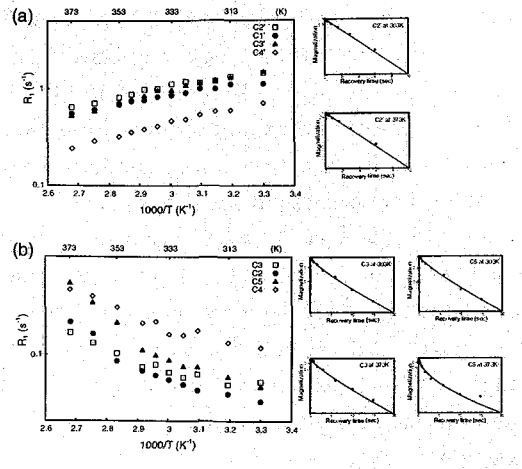

FIG. 1: Plots of ^{13}C spin-lattice relaxation rate R_1 as a function of 1000/T for P3BT; the alkyl side chain (a) and the main chain (b). Typical decay curves are also shown for the butyl C2' carbon, and for the thiophene C3 and C5 carbons at 303 K and 373 K (insets).

range is insufficient to consider the condition of (ii) or (iii) because of the limitation of available temperature range of our instrument, discontinuous changes can be a fingerprint for the effect of α processes.

To detect more direct evidence of the twist-glass transition, we tried to perform CODEX measurements at 303K and 353K where are lower and higher than the transition temperature, respectively. Fig. 2(a) and (b) show CODEX spectra (S), reference spectra (S_0), and pure-exchange spectra ($\Delta S = S - S_0$) at 303K and 353K, respectively, with mixing time of t_m = 120 ms, t_z = 0.8 ms and CSA recoupling time of Nt_r = 1ms. At 303K, no significant change is observed between S and S_0, consequently ΔS shows a weak signal; that is, sufficient motion of thiophene with detectable motional amplitude during Nt_r (=1ms) does not occur below the twist glass transition temperature. At 353K, on the other hand, the pure-exchange spectrum shows the signal of thiophene. It indicates that thiophene main chain undergoes reorientation during the mixing time (t_m = 120 ms) and consequently the motion attenuates recoupling of CSA. This is a direct evidence of thiophene twisting above the twist-glass transition. Fig. 2(c) shows the normalized exchange intensity as a function of t_m. The mixing-time dependence of CODEX can be expressed as

$$\Delta S/S_0(t_m) = \frac{M-1}{M} - \frac{M-1}{M}\exp(-\frac{t_m}{\tau_c})^{\beta}, \qquad (1)$$

where τ_c is the correlation time, β is the stretching parameter, and M is the number of equivalent orientational sites accessible in the motional process. Using this equation the correlation time of thiophene twist is found to be τ_c = 31.4 ms (τ_c^{-1} = 31.8 Hz) at 353K. However, it is difficulat to determine this value as a characteristic rate of thiophene twist because the twist motion show a large dispersion because of the structural modulation waves as observed in the similar polymer P4MTz.

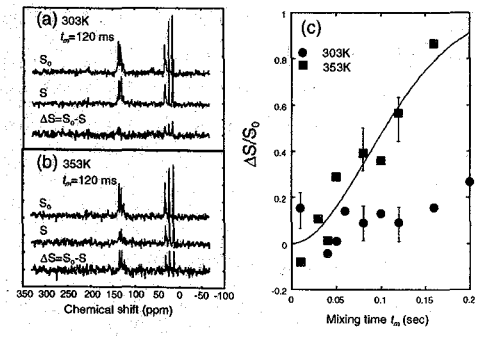

FIG. 2: A pure-exchange spectrum (ΔS) from a CODEX measurement (S) and a reference spectrum without exchange (S_0) at 303K (a) and 353K (b). ΔS was generated by subtraction of S from S_0. $\Delta S/S_0$ of thiophene twisting at 303 K and 353 K were plotted as a function of t_m (c).

I. CONCLUSION

Solid-state structure and dynamics of the regioregulated HT-P3ATs, especially P3BT, were in-

vestigated using FTIR and ^{13}C NMR spectroscopies. The DSC measurements show that P3BT has an endothermic transition that occurred in the crystalline phase around 340 K. The FTIR measurements show that the shifts of absorption maximum for the out-of-plane mode of the thiophene C_β-H band were observed, which is consistent with DSC results. In the ^{13}C CPMAS NMR measurements, the methyl moiety shows the transition from two or more states to a unique state. Furthermore, T_{1C} and CODEX measurements indicate that there exists a glass transition of thiophene ring twist in the crystalline phase. Its enthalpy relaxation shows an endothermic peak in DSC traces. To P3BT, we attempted to apply the idea that it is a glassy crystal-plastic crystal transition. We assigned each peak in FTIR to a specific phase. A phase diagram of P3BT is shown in Fig. 3. At temperatures higher than the melting point (T > 540 K), the polymer is surely an isotropic liquid assigned to 836 cm^{-1} in the FTIR spectrum. At 340 K < T < 540 K, mostly plastic crystal (820 cm^{-1}) exists, where the polymer undergoes the twist motion of thiophene. Below 340 K, two states exist in which the glassy crystal (825 cm^{-1}) has thiophene rings that are frozen with various angles and crystals without twisting (810 cm^{-1}).

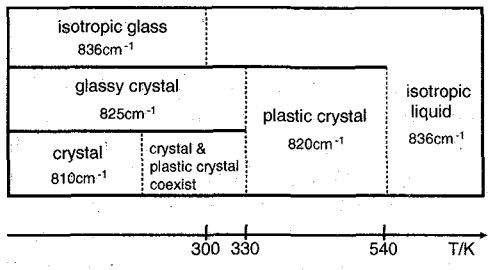

FIG. 3: A proposed phase diagram of P3BT. The IR absorption bands for the C_β-H bond out-of-plane deformation are also shown.

[1] O. Ingänas, W.R. Salaneck, J.-E. Oästerholm, and J. Laakso: *Synth. Met.* **22** 395 (1988).

[2] J. Corish, D. E. Feeley, D. A. Morton-Blake, F. Beniere, and M. Marchetti: *J. Phys. Chem. B* **101**, 10075 (1997).

[3] K. Iwasaki, H. Fujimoto, and S. Matsuzaki: *Synth. Met.* **63**, 101 (1994).

[4] E. R. deAzevedo, W. -G. Hu, T. J. Bonagamba, and K. Schmidt-Rohr: *J. Am. Chem. Soc.* **121**, 8411 (1999).

[5] K.Yazawa, Y.Inoue, T.Yamamoto, and N.Asakawa, *Phys.Rev.B*, in press.

[6] S.Mori, Y.inoue, T.Yamamoto, and N.Asakawa, *Phys.Rev.B*, 71, 054205(2005).

[7] N.Asakawa, M.Ohira, K.Yazawa, T.Yamamoto, and Y.Inoue, arXiv:cond-mat/0507515.

[8] N.Asakawa, K.Matsubara, and Y.Inoue, *Chem.Phys.Lett.*, 406,215(2005).

[9] Naoki Asakawa, *Koubunshikakou*, 53, 552(2004).

[10] N.Asakawa, T.Kajikawa, K.Sato, M.Sakurai, Y.Inoue, and T.Yamamoto, *J.Mole.Struct.*, 602-603, 455(2002).

Low-Field NMR Approaches for the Characterization of Polymer Materials

Kay Saalwächter

Institut für Physik, Martin-Luther-Universität Halle-Wittenberg
Friedemann-Bach-Platz 6, D-06108 Halle, Germany
Email: kay.saalwaechter@physik.uni-halle.de

In this contribution, I demonstrate the application of proton multiple-quantum (MQ) NMR to the characterization of elastomer microstructure [1-3], gel-point determination and the quantitative analysis of systems that gel in dilute solution and in the bulk [4]. Other low-field NMR developments include robust and reliable approaches to determine the crystallinity and monitor the crystallization kinetics and the mobile-phase mobility in semicrystalline polymers [5], as well as spin-diffusion studies of the domain sizes in block copolymers.
MQ NMR at low field is indeed a robust, reliable, and quantitative method to study elastomer microstructure, structural heterogeneities, and chain dynamics [1]. Recent work includes quantitative relationships between the NMR observables and the cross-link density of diene rubbers [2] and the analysis of chain dynamics in the same type of systems [3]. Some of our findings are in marked contrast to earlier observations, and suggest that a number of models commonly used to analyze chain motion in elastomers (and ultimately to explain their mechanical behavior) are in need of revision.

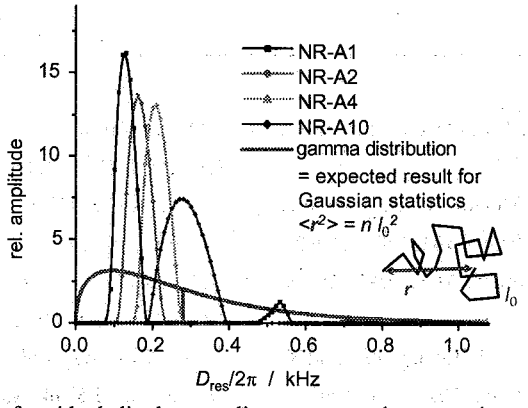

Fig. 1: Distributions of residual dipolar couplings, measured on a series of natural rubber with increasing sulphur content (1,2,4 and 10 phr) by MQ NMR at low field. A comparison of the distribution for NR-A10 with the result expected from Gaussian network theory indicates major discrepancies [2].

As an example, Fig. 1 shows distributions of residual dipolar couplings for a series of natural rubber with increasing cross-link density. The non-zero coupling arises from network chain fluctuations that are rendered anisotropic by the cross-links. Its average is directly proportional to

Keywords: multiple-quantum NMR, elastomers, heterogeneities, gel point, polymer crystallization

the cross-link density and therefore reflects macroscopic properties like the elasticity or the equilibrium degree of swelling. The distributions are, however, much narrower than predicted by the common Gaussian network theory. This indicates that the dynamics of individual chain segments is homogeneous. Cooperative packing effects that go beyond simple single-chain models are therefore important and thus need to be incorporated in any molecular theory of rubber elasticity.

As a second example, Fig. 2 demonstrates the use of a mixed magic sandwich echo (MSE) in combination with a CPMG train for a quantitative assessment of polymer crystallinity. Crystallites are rigid and exhibit a solid-like FID, the full detection of which must include overcoming the relatively long 10 μs dead time of a typical low-field instrument. The refocusing afforded by the MSE is near quantitative, as can be seen in an isothermal crystallization experiment. The ensuing longer mobile-phase decay must be corrected for B_0 field inhomogeneities, as is best achieved by a CPMG train. The signal decay is then dominated by the dynamics of the chains in the interlamellar regions and reflects morphological details.

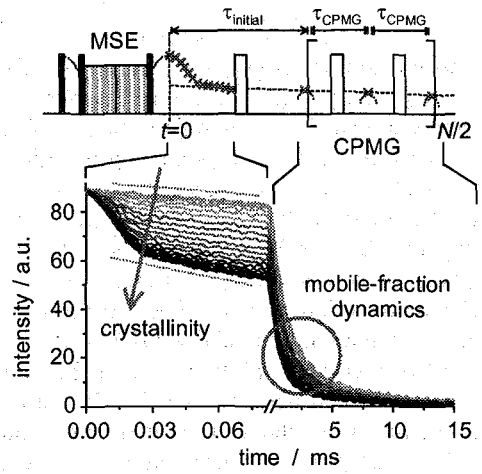

Fig. 2: A combined pulsed magic-sandwich echo (MSE) Carr-Purcell-Meiboom-Gill (CPMG) pulse sequence for the real-time detection of polymer crystallinity and mobile-phase mobility on low-field instruments. The signal traces are for syndiotactic poly(propylene) measured every 5 minutes under conditions of isothermal crystallization of at 378 K [5].

References:

[1] KS et al., J. Chem. Phys. **119** (2003) 3468-3482; KS, *J. Am. Chem. Soc.* **125** (2003) 14684.
[2] KS, B. Herrero, M. A. López-Manchado, *Macromolecules* **38** (2005) 9650-9660.
[3] KS, A. Heuer, *Macromolecules* **39** (2006) 3291-3303.
[4] KS, R. G. Liu, W. Oppermann, M. Gottlieb, submitted.
[5] A. Maus, C. Hertlein, KS, *Macromol. Chem. Phys.* **207** (2006) 1150-1158.

Y-89 MAS-NMR Determination of Local Oxygen Defect Structure around Yttrium Ions for Oxide Ion Conductors

H. Maekawa[1,2,3,*], K. Kawata[1], T. Yamamura[1,2], J. Kawamura[2,3,4], Y.P. Xiong[5], N. Sakai[5], H. Yokokawa[5]

1. Graduate School of Engineering, Tohoku University, Aramaki Aoba 6-6-02, Sendai, 980-8579, Japan

2. Center for Interdisciplinary Research, Tohoku University, Aramaki Aoba 6-6-02, Sendai, 980-8578, Japan

3. CREST, Japan Science and Technology Corporation, Kawaguchi 332-0012, Japan

4. Institute of Multidisciplinary Research for Advanced Materials, Tohoku University, 2-1-1 Katahira, Aoba-ku, Sendai, 980-8577, Japan

5. Fuel Cell Group, AIST Tsukuba Central 5, National Institute of Advanced Industrial Science and Technology, 1-1 Higashi, Tsukuba, Ibaraki 305-8565, Japan

INTRODUCTION

Ceria-zirconia-yttria solid solution (CeO_2-ZrO_2-$YO_{1.5}$) was focused in development of solid oxide fuel cells (SOFCs), firstly as the reaction compound found at the interface of yttria-doped ceria (YDC) and yttria-stabilized zirconia (YSZ). YSZ is a promising electrolyte in SOFC, and YDC may be used as anodes [1], as coating materials on electrolyte, or as an intermediate layer between the electrode and the electrolyte.

Many attempts have been already made to fabricate composite materials, which may have both chemical stability of YSZ and high catalytic activity of YDC. However, when such a composite is prepared by a wet process followed by a sintering process at high temperatures, the inter-diffusion of cerium and zirconium components is often observed at the interface, which results in the formation of (CeO_2-ZrO_2-$YO_{1.5}$) solid solutions. These solid solutions exhibit lower ionic conductivities in the middle of the solubility range, therefore it may cause some degradation of the cell performance [2]. On the other hand, ceria–zirconia solid solutions have been focused from the viewpoint of interesting catalytic activity and mixed conductivity. The CeO_2–ZrO_2–$YO_{1.5}$ solid solution is also focused as a promising material for oxygen permeable membranes, which can be applied to electro-catalytic reactors or oxygen gas separators [2,3].

The local coordination structure around specific ions doped into crystalline ionic conductors provides fundamental information on the ion migration mechanism. Especially, the local oxygen defect structure and its preferential location in specific ions have great importance on understanding ionic migration mechanism in solid state ionics materials. High-field and high resolution solid-state nuclear magnetic resonance (NMR) is a powerful tool for elucidating local structure of ions in solids. Although ^{89}Y is NMR active, few investigations have been carried out due to its low sensitivity [4,5]. Recently, our group reported ^{89}Y NMR measurements of YSZ by means of a high-field and a high-resolution solid-state magic angle sample spinning (MAS)-NMR and clarified the compositional dependence of the yttrium coordination number and the local defect structure. The objective of the present paper is to investigate local structure around yttrium in $[(CeO_2)_x(ZrO_2)_{1-x}]_{0.8}(YO_{1.5})_{0.2}$ (x=0–1) by adopting a ^{89}Y MAS-NMR spectroscopy.

Keywords: ceria, zirconia, yttria, Y-89 NMR, oxygen defect, local structure

EXPERIMENTAL

The sample composition was selected at $[(CeO_2)_x(ZrO_2)_{1-x}]_{0.8}(YO_{1.5})_{0.2}$ (x=0–1.0, 0.1 step). Powders of the reagent grade starting materials, CeO_2, ZrO_2, Y_2O_3, and Gd_2O_3 (Wako Co. Ltd.), were ball milled in ethanol and pressed into pellets. Pellets were sintered at 1923 K for 10 h. X-ray diffraction was measured by PW-1800 (Philips, The Netherlands) using a Cu(K_α) target. The peaks in the range of 2θ=50–100° were collected for lattice constant determination, in which silicon powder was used as an internal reference.

An ECA-600 (JEOL) spectrometer operating at a 14 T magnetic field was utilized. The resonance frequency of ^{89}Y was 29.41 MHz. A single tuned 6 mmϕ MQ-MAS probe (JEOL) was used. The spinning rate of the 6 mmϕ rotor was set to 10 kHz. Repetition time was 5 s and 10,000–50,000 scans were accumulated. 1 M YCl_3 was used as the chemical shift standard. Peak separation and integration were performed by the Winfit program [6]. Each sample was doped with 0.2 mol% Gd_2O_3 to shorten the NMR reputation time.

RESULTS AND DISCUSSIONS

CZY samples were confirmed as a single phased cubic fluorite form by XRD measurements. The lattice parameter followed Vegard's law. The spin-lattice relaxation time (T_1) of spin I = 1/2 nuclei in solids is generally quite lengthy, typically as long as several hours. To complete NMR measurements within a reasonable accumulation time, a small amount of paramagnetic impurity was introduced. The amount of paramagnetic impurity (Gd_2O_3) was set to 0.2 mol%, which shortens the T_1 values by 5–15 s and has minimum influence on the quantitative analysis of peak intensities. The ^{89}Y MAS-NMR spectra of CZY samples are shown in Fig.1. The compositional dependence of spectra was observed. Spectra consisted of two major peaks, indicated as peaks I and II, respectively.

All spectra were well simulated by a Gaussian–Lorentzian model. The main peak I at 85–90 ppm and a very small sub peak II at 190–195 ppm were observed for $(ZrO_2)_{0.8}(YO_{1.5})_{0.2}$ sample, which is consistent with our previous report [4]. By the substitution of zirconium to cerium, the intensity of peak II grew progressively, whereas the intensity of peak I decreased.

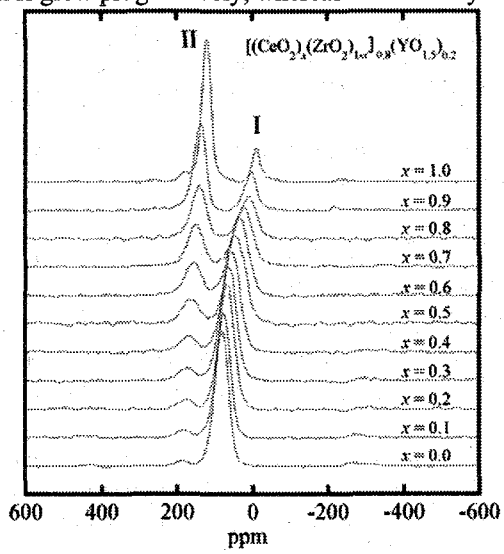

Fig.1. ^{89}Y MAS-NMR spectra of $[(CeO_2)_x(ZrO_2)_{1-x}]_{0.8}(YO_{1.5})_{0.2}$ (x=0–1.0, 0.1 step).

Yttrium ions surrounded by different numbers of oxygen atoms could be identified as separated peaks in the spectrum [4,5]. In the ideal cubic fluorite structure, cations (Ce^{4+}, Zr^{4+},

Y^{3+}) are surrounded by 8 nearest neighbor oxygen atoms. The coordination number will decrease when an oxygen defect was formed within the coordination polyhedron. Taking into account the previously determined values of ^{89}Y NMR chemical shifts [4,5], peaks I and II can be assigned to 8 and 7 coordination yttrium, respectively. The relative amount of yttrium ions for different coordination numbers can be directly determined from the peak intensities.

The result of the peak separations, including the integral intensity, full width at half maximum (FWHM) and the chemical shift are summarized in Fig. 3. The chemical shift reflects the degree of the magnetic field shielding of the nuclei. A systematic negative shift reflects a change in the chemical bonding nature between Y and O atoms with substituting zirconium to cerium. The increase of the FWHM at medium composition, as shown in Fig.3, may be related to a wider distribution of local chemical species, and may be related to the possible existence of the miscibility gap in this material which was explained in terms of the positive (repulsive) interaction parameters between ZrO_2 and CeO_2 [2]. By the substitution of zirconium to cerium, a decrease of 8-ccordinated yttrium and an increase of 7-coordinated yttrium were observed.

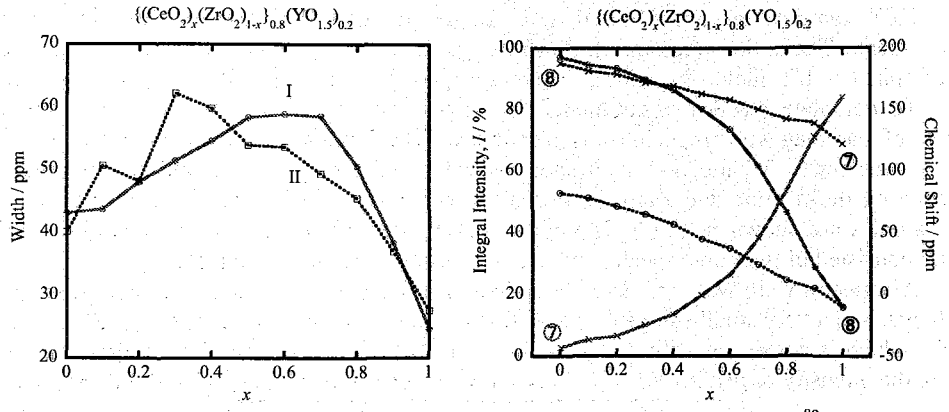

Fig.2. (Left) Full width at half maximum (FWHM) of peaks I and II observed for ^{89}Y NMR spectra of $[(CeO_2)_x(ZrO_2)_{1-x}]_{0.8}(YO_{1.5})_{0.2}$ (x=0–1.0, 0.1 step). (Right) Integral intensity (bold line) and chemical shift (dotted line) of ^{89}Y NMR peaks. Circled number indicates the coordination number.

With increasing yttria content, oxygen vacancies are formed to keep the charge neutrality, which can be written as follows,

$$Y_2O_3 \rightarrow 2Y'_{Ce+Zr} + 3O_O^{\times} + V_O^{\bullet\bullet}. \qquad (1)$$

The composition of CeO_2-ZrO_2-Y_2O_3 system can be written by using the yttrium ion content, y, and the oxygen vacancy concentration δ,

$$((Ce+Zr)_{1-y}Y_y)O_{2-\delta} = (1-y)[(Ce+Zr)O_{2-\delta_{(Ce+Zr)}}] \cdot y[YO_{2-\delta_Y}], \qquad (2)$$

where $\delta_{(Ce+Zr)}$ and δ_Y are the oxygen vacancy concentration around Ce+Zr and Y, respectively. Oxygen vacancy concentration is given by the charge neutrality condition,

$$\delta = [V_O^{\bullet\bullet}] = [Y'_{Ce+Zr}]/2 = y/2. \qquad (3)$$

The average coordination numbers for the cations expected from the random distribution of cerium, zirconium and yttrium ions, C_{ideal} can be expressed by the experimentally determined avarage coordination number of yttrium ion, C_Y, and average coordination number of cerium and zirconium ion, C_{Ce+Zr}, as follows,

$$C_{ideal} = 8 \cdot (1-\delta/2) = 8-2y = y \cdot C_Y + (1-y) \cdot C_{Ce+Zr}, \qquad (4)$$

$$C_Y = 8 \times I_8 + 7 \times I_7, \qquad (5)$$

where I_n is the integral intensity of the NMR peak for n coordinated yttrium ion.

The oxygen vacancy concentration can be defined as,

$$\delta_Y = 2 - C_Y / 4 \quad (6)$$

$$\delta_{(Ce+Zr)} = 2 - C_{Ce+Zr} / 4 . \quad (7)$$

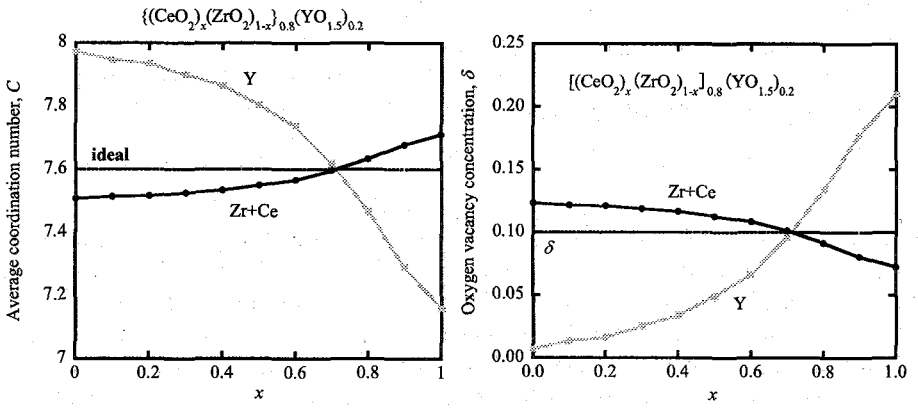

Fig. 3. (Left) Average coordination number of cations for $[(CeO_2)_x(ZrO_2)_{1-x}]_{0.8}(YO_{1.5})_{0.2}$ (x=0–1.0, 0.1 step).determined from ^{89}Y MAS-NMR peak separation. (Right) Oxygen vacancy concentration around cations calculated from eqs. (4) ~ (7).

As clearly shown in Fig. 3, oxygen vacancies are preferentially located to zirconium ions for $(ZrO_2)_{0.8}(YO_{1.5})_{0.2}$ end member composition. By the substitution of zirconium to cerium, oxygen vacancy start to form around yttrium ions. This can be understood by the difference of site preference of zirconium and cerium cations, where zirconium prefer 7-coordinated site whereas cerium prefer 8-coordinated site, respectively, in the cubic fluorite lattice. The present results give a quantitative measure of the degree of preference of the oxygen vacancy on each cations, for the first time.

ACKNOWLEDGEMENTS

The present work was supported in part by the Grant-in Aid for Scientific Research on Priority Area Nanoionics (439) by the Ministry of Education, Culture, Sports and Technology.

REFERENCES

1. M. Mogensen, T. Lindegaard, U.R. Hansen, G. Mogensen, J. Electrochem. Soc., 141, 1994, 2122-2128
2. N. Sakai, K. Kawaji, Y.P. Xiong, H. Kishimoto, T. Horita and H. Yokokawa, J. Electroceramics, 13, 2004, 677-682
3. N. Sakai, T. Hashimoto, T. Katsube, K. Yamaji, H. Negishi, T. Horita, H. Yokokawa, Y.P. Xiong, M. Nakagawa and Y. Takahashi, Solid State Ionics, Vol. 143 , 2001, 151-160.
4. K. Kawata, H. Maekawa, T. Nemoto and T. Yamamura, Solid State Ionics, Article in press, 2006
5. P. Florian, M. Gervais, A. Douy, D. Massiot and J.-P. Coutures, J. Phys. Chem. B 105, 2001, 379-391.
6. D. Massiot, F. Fayon, M. Capron, I. King, S. Le Calve, B. Alonso, J.-O. Durand, B. Bujoli, Z. Gan, G. Hoatson, Magn. Reson. Chem. 40 (2002) 70-76.

1 LE11

多核種高磁場固体NMRを利用した無機系材料の構造解析

新日本製鐵（株）先端技術研究所[1]　○齋藤公児、下田啓士、金橋康二、藤部康弘
日本電子（株）[2]　根本貴弘

Industrial Application of Multi Nuclear Solid State NMR (^{17}O,^{25}Mg,^{27}Al,^{43}Ca) at High Field (16.4T) and Super High Field (21.8T)

Nippon Steel Corporation, Advanced Research Technology Labo.[1], JEOL[2]

○Koji Saito1,Keiji Shimoda1, Yasuhiro Tobu1, Koji Kanehashi1, Takahiro Nemoto2

<Abstracts>

A new approach to structural analysis of inorganic polymer, we called slag which is by products of steel making, has been proposed using multi-nuclear solid state NMR at high magnetic field that is capable of obtaining the structural information of each element composing the slag such as Si, Al, Mg, O, Ca and effective to both crystalline and non-crystalline solid materials. It is concluded that the combination of multi-nuclear MQMAS and hetero nuclear correlation spectroscopy methods with isotope label technique at high magnetic field is a very effective for characterization of inorganic materials and especially well suited to the analysis of slag that are low crystallinity in contrast to X-ray diffraction (XRD).The NMR approach to protein science is very similar and useful and helpful to analyze the chemical structure of inorganic materials toward to three dimensional structure using solid state NMR.

A new approach to structural analysis of inorganic polymer, we called slag which is by products of steel making, has been proposed using multi-nuclear solid state NMR at high magnetic field that is capable of obtaining the structural information of each element composing the slag such as Si, Al, Mg, O, Ca and effective to both crystalline and non-crystalline solid materials. Toward to making three dimensional structure analysis of slags, we make three strategy like below

1) Nuclear : introduced isotope labeling (^{25}Mg,^{17}O, ^{43}Ca)
2) Magnet : using suitable high field magnet for each nuclei
3) Resonance : applied hetero-nuclear correlation spectroscopy methods

1) Nuclear : introduced isotope labeling (^{25}Mg,^{17}O, ^{43}Ca)[1-4)]

In this study, we applied mainly ^{27}Al and ^{25}Mg and ^{17}O and ^{43}Ca solid state NMR two types of steel -making slags. In ^{27}Al NMR measurements, drastic improvement of spectral resolution at high magnetic field (16.4T) 5QMAS experiment clarified the existence of at least 11 chemical sites of Al in slag. And, we successfully obtained ^{25}Mg 3QMAS spectra in slags, when special probe has been developed to overcome low sensitivity. Additionally, solid state ^{17}O NMR is very useful and powerful tools for the structural analysis of oxygen in various inorganic materials. However, quite low sensitivity on NMR is main difficulty point. And then, we tried to synthesize each ^{17}O-labeled stating materials such as $Ca(*OH)_2$, Al_2*O_3 and $Si*O_2$ in order to overcome low sensitivity(Fig.1).

高磁場固体NMR、多核NMR、アモルファス材料、MQMAS

○さいとうこうじ、しもだけいじ、かねはしこうじ、とうぶやすひろ、ねもとたかひろ

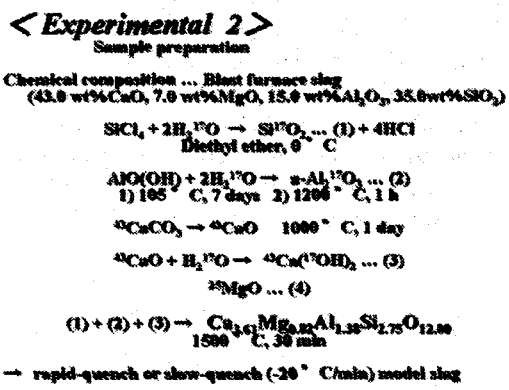

Fig.1 Sample preparation using isotope labeling

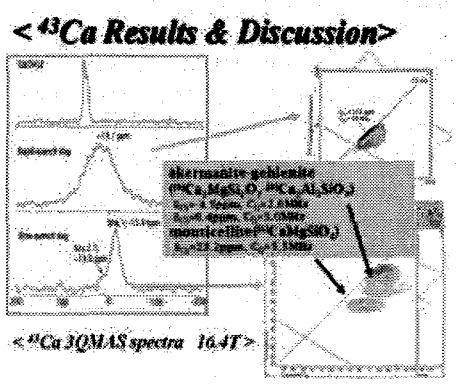

Fig.2 ^{43}Ca-MQMAS of slags

Using these materials, the formation of slag network was investigated at 1273 to 1673K by ^{17}O MQMAS. The process of network formation of oxygen in slag could be observed by means of ^{17}O full labeled materials at each temperature. Moreover, ^{17}O selective labeled materials became possible to assign each peak in spectra of full-labeled materials. ^{27}Al-^{17}O CP/MAS methods were applied in order to make connectivity clearly. We first applied ^{43}Ca 3 and 5QMAS NMR spectroscopy for ^{43}Ca-enriched model slags(Fig.2). Local environments of Ca^{2+} ions in slow- and rapid-quench model slags were found to be different each other. The slow-quench slag has well-defined CaO_8 polyhedra in a crystalline form, although the rapid-quench slag is considered to have CaO_6 octahedral species as a main component. From above mentioned results, multi-nuclear solid state NMR is proved to be a very effective method in characterization of the slag. The structural information on divalent cations such as Mg^{2+}, Ca^{2+}, and Fe^{2+} should have important aspects in magmatic liquids and its quenched glasses because of their abundance in the Earth's interior. The local structure around Mg^{2+} in silicate melts and glasses has been investigated by several researchers, nevertheless little is confirmed on its coordination state. Nuclear magnetic resonance (NMR) spectroscopy is an advantageous method to analyze a specific element in multi-components system. In the present study, we applied ^{25}Mg MQMAS NMR to investigate the Mg local environments in $CaMgSi_2O_6$ glass in comparison with its crystalline counterpart, diopside.

2) Magnet : using suitable high field magnet for each nuclei [5-7)]

Recent new development of a super conducting magnet can make a new application field for solid state NMR. Especially, NIMS in Tsukuba succeeded in the development of 930 MHz (21.8T) solid state NMR system. In this paper, we would like to show two topics which have new finds in industrial application when this developed high field solid state NMR system is applied. Optimization of the drying process conditions for a steel-making converter in a steel works is very important since the process is off-line and time-consuming. However, it is very difficult to optimize drying process conditions (temperature, surface active agents, etc.), because the refractory mortar of steel converter is made of very complicated and mixture materials. To help understanding, we have analyzed the refractory mortar using solid state NMR at 16.4T because the refractory mortar is an amorphous material; it means X-ray method can't give useful information. And then, we got new chemical structural information of the refractory mortar using ^{27}Al MQMAS at 16.4T. And also, we have first demonstrated the structural analysis of these

complex materials using very high field 930MHz (21.8T) solid state NMR. This paper shows the effect of magnetic field strength in these materials on ^{27}Al MAS and MQMAS spectra (Fig.3). In particular, we find several new chemical sites using 21.8T with compared to the result of ^{27}Al MQMAS at 16.4T (Fig.4). At the same time, some relaxation information (T_1) of the refractory mortar will be discussed because of high resolution MAS spectra at 21.8T. It is clear that solid state NMR at high field give useful information to analyze complicated materials. Using this data, we can adjust and design the drying process and time in steel works. The another topics is application of 17O for amorphous-ALPO. New results for amorphous-ALPO using 930 solid state NMR system will be discussed.

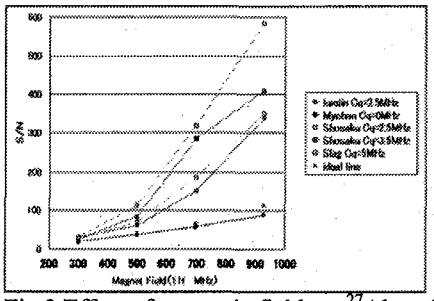

Fig.3 Effect of magnetic fields to ^{27}Al nuclei

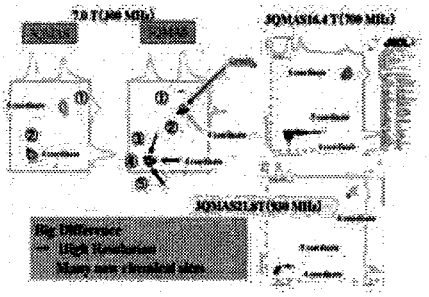
Fig.4 Effect of magnet fields to refractory mortar

3) Resonance : applied hetero-nuclear correlation spectroscopy methods [8-10)]

Extensive researches on aluminophosphate ($AlPO_4$) have been performed because of its industrial needs. While crystalline $AlPO_4$-based molecular sieves such as zeolites were investigated by many kinds of measurements, there are few structural analyses of amorphous $AlPO_4$ (*a*-$AlPO_4$). Solid-state NMR is capable of characterizing the structure of amorphous materials that is difficult by using diffraction methods. Previously, ^{27}Al MQMAS study indicated useful information of aluminum sites and distributions of *a*-$AlPO_4$[1]. Double resonance method gives clear information of heteronuclear correlation for materials. For example, ^{31}P{^{27}Al}HETCOR spectrum of crystalline AlPO4-14 easy to detect correlations between P-Al [11)].

However, single nuclear analysis indicates only local structure, and one of hetero-nuclear correlation gives limited information on amorphous material. In the case of the structural analysis of amorphous material should be need the information on multi-nuclear and all of hetero-nuclear correlations.

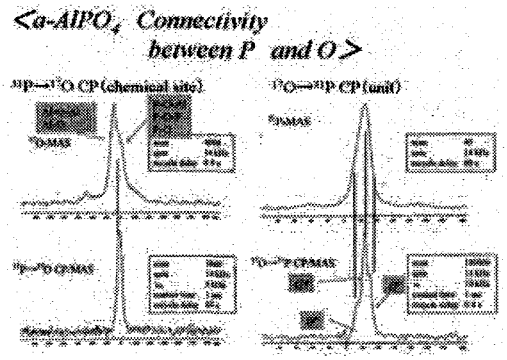

Fig.5 The results of Mutual CP for a-ALPO

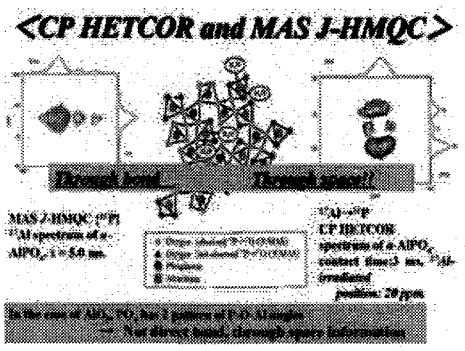

Fig.6 The results of CP HETCOR and MAS-HMQC for a-ALPO

In this research, we aim to structure analysis on a-$AlPO_4$. We prepared ^{17}O-enriched a-$AlPO_4$ and carried out multi-nuclear and each hetero-nuclear correlations analysis by solid state NMR. As a result, all local structure and each correlation elucidate the 3D networks on a-$AlPO_4$ as indicated below.

1. ^{31}P MAS, ^{17}O MQMAS and ^{27}Al MQMAS; All spectra indicated multi-sites and distributions.
2. Mutual ($^{31}P \leftrightarrow {}^{17}O$) CP MAS NMR (Fig.5) ; $^{17}O\{^{31}P\}$CP MAS spectrum clearly showed that three different phosphorus environments correspond to Q_2, Q_3 and Q_4
3. $\{^{31}P\}^{27}Al$ MAS-J-HMQC, and $^{31}P\{^{27}Al\}$ 3QMAS/HETCOR (Fig.6): MAS-J-HMQC spectrum indicated a-$AlPO_4$ has all types of the $^{[4],[5],[6]}$Al-O-P bonds. And 3QMAS/HETCOR indicated four P local environments exist.
4. $^{17}O\{^{27}Al\}$MQMAS/HETCOR; Detail discussion will be in my lecture.

Various measurements of solid state NMR could realize multi-nuclear and all of hetero-nuclear correlation analysis on amorphous material.

It is concluded that the combination of multi-nuclear MQMAS and hetero nuclear correlation spectroscopy methods with isotope label technique at high magnetic field is a very effective for characterization of inorganic materials and especially well suited to the analysis of slag that are low crystallinity in contrast to X-ray diffraction (XRD).The NMR approach to protein science is very similar and useful and helpful to analyze the chemical structure of inorganic materials toward to three dimensional structure using solid state NMR.

Acknowledgments

This work is partially supported by Special Coordination Funds for Promoting Science and Technology. I would like to thank Mr.M.Hatakeyama Mr.M.Nishiura (NSC) about their cooperation and also, Dr.T.Iijima (Kyoto University), Mr.K.Hasegawa (JEOL) , and Dr.T.Shimizu(NIMS) about their collaboration.

References

1)M. Hatakeyama, T. Nemoto, K. Kanehashi and K. Saito, Chem. Lett. 34, 684 (2005)
2)K. Shimoda, Y. Tobu, K. Kanehashi, T. Nemoto, and K. Saito, Chemistry Letters 34, 1588 (2005)
3)K. Shimoda, Y. Tobu, K. Kanehashi, T. Nemoto and K. Saito, Solid State NMR. 30, 114(2006)
4)K.Kanehashi and K.Saito; J.Magn.Reson.submitted
5)K.Kanehashi and K. Saito:, Fuel Processing Technology 85 (2004) 873
6)K.Kanehashi and K. Saito:, Energy & Fuel, 18, (2004) 1732
7)K.Saito, K.Kanehashi and M.Hatakeyama, Chem.Lett.,(2006) in pess
8)K,Kanehashi and K.Saito, ; , Chem. Lett., No.7,668-669, (2002)
9)K.Kanehashi and K.Saito,; J.Noncry.Solid ,in press (2006)
10)T. Iijima, K. Kanehashi, K. Saito, M. Hatakeyama and T. Nemoto, Chem. Lett. 34, 1380 (2005)
11) H. Kraus Journal Physical Chemistry 100 (1996) 16336

1 LE12

Advanced Dipolar NMR Techniques for Structural Studies of Disordered Materials

Hellmut Eckert

Institut für Physikalische Chemie, WWU Münster

Because of their straightforward relationship with internuclear distance information, homo- and heteronuclear magnetic dipole-dipole couplings have particular significance in solid state NMR applications for structural studies. Modern solid state nuclear magnetic resonance methodology affords a number of new powerful techniques to quantify such dipolar couplings under high-resolution (magic angle spinning) conditions and is hence potentially very suited to yield distance information in solids for simple two- or three-spin systems. In contrast, disordered materials such as defective crystals, glasses or nanocomposites present important new challenges, as the interactions have typically multi-spin character, the order of the spin system is usually not known and most likely subject to distribution, and many of the nuclei involved are influenced by nuclear electric quadrupolar couplings at the same time.

One of the most promising dipolar recoupling techniques available is the rotational echo double resonance (REDOR) method, which takes advantage of the high resolution afforded by magic angle spinning to provide site-resolved dipole coupling information. We have recently developed this method for the dipolar analysis of multi-spin systems, including those with quadrupolar nuclei, to extract reliable second moment values specifying average magnetic dipole-dipole couplings. Based on such second moment values various types of internuclear distance correlations have been characterized (see figure 1), constituting medium-range order in a series of ion-conducting glasses.

Keywords: dipolar coupling, REDOR, glasses, solid electrolytes

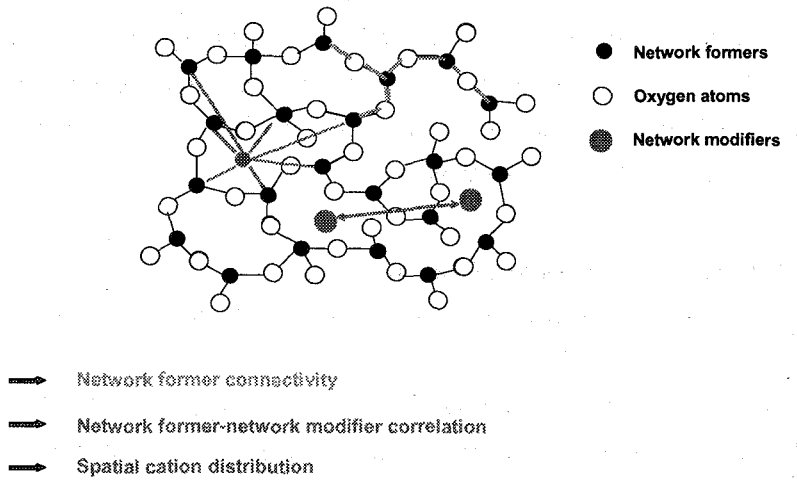

Figure 1: sketch of the various types of medium-range order in glasses, involving distance correlations among network former species (a), between network former species and network modifier species (b) and between network modifier species (c), respectively

With regard to (a), quantitative information about interatomic connectivities and spatial correlations on the 300 to 500 pm distance scale have been obtained between ^{11}B, ^{27}Al, and ^{31}P nuclei in the glass framework of numerous alkali borophosphate and alumophosphate glasses. Using this approach, it was possible to quantify the extent of B-O-P and Al-O-P linking in these systems [1,2]. These glasses do not present statistical connectivities but rather their structures are dominated by a strong preference for heteroatomic B-O-P and Al-O-P linkages. More recent extensions of our approach towards other systems has helped to clarify the structural roles of non-traditional network former species such as TeO_2, MoO_3, and WO_3 and their influence upon macroscopic physical properties.

With regard to (b), spatial correlations have been probed between the framework nuclei ^{11}B, ^{31}P, and ^{29}Si on the one hand, and the nuclei ^{6}Li, ^{7}Li, and ^{23}Na associated with the network modifier species on the other. Using this approach, composition dependent data have provided quantitative information on the extent of cation clustering in alkali borate, phosphate and silicate glasses, [3-5]. Similar insight is

independently available from NMR results probing the spatial correlations between the nuclei associated with the network modifier ions (approach c). For example, ^{6}Li-^{7}Li double resonance NMR studies reveal a large difference in cation clustering tendency between lithium silicate and lithium borate glasses [6]. The extension of such experiments to mixed-alkali glasses has also led to important new insights regarding the mutual immobilization of cations in glasses containing more than one network modifier species [7] ("mixed alkali effect").

[1] L. Zhang, H. Eckert, *J. Phys. Chem.* B **2006**, 110, 8946.

[2] S. Elbers, W. Strojek, L.Koudelka, H. Eckert, *Solid State Nucl. Magn. Reson.* **2005**, *27*, 65.

[3] J. D. Epping, W. Strojek, H. Eckert, *Phys. Chem. Chem. Phys.* **2005**, *7*, 2384

[4] U. Voigt, H. Lammert, H. Eckert, H. Heuer, *Phys. Rev. B* **2005**, *72*, 064207

[5] W. Strojek, H. Eckert, *Phys. Chem. Chem. Phys.* **2006**, *8*, 2276.

[6] S. Puls, H. Eckert, to be published

1 LE13

NMR studies of membrane associating proteins involved in metal homeostasis

Yutaka Ito[1,2], Kaori Kurashima-Ito[2], Kayano Moromisato[1], Masaki Mishima[1], Teppei Ikeya[3,4], Sundaresan Rajesh[5], Kaoru Nishimura[5], Jonathan Heddle[5], and Jeremy Tame[5]

[1]Tokyo Metropolitan University, 1-1 Minami Osawa, Hachioji, Tokyo 192-0397, Japan; [2]RIKEN, 1-7-29 Suehiro, Tsurumi, Yokohama 230-0045, Japan; [3]RIKEN Genomic Sciences Center, 1-7-22 Suehiro, Tsurumi, Yokohama 230-0045, Japan; [4]SAIL-Technologies, 1-1-40 Suehiro, Tsurumi, Yokohama 230-0045, Japan; [5]Yokohama City University, 1-7-29 Suehiro, Tsurumi, Yokohama 230-0045, Japan

Recent developments on protein stable isotope labelling and TROSY-based NMR measurements were applied to a 31kDa (285 a.a.) nucleotide-binding domain of human mitochondrial ABCB6 (ABCB6-C) and a 56kDa (502 a.a.) *Escherichia coli* NikA.

Human ATP-binding cassette, sub-family B, member 6 (ABCB6) is a mitochondrial ABC transporter, and presumably contributes to iron homeostasis. Aimed at understanding the structural basis for the conformational changes accompanying the substrate-transportation cycle, we have studied the C-terminal nucleotide-binding domain of ABCB6 (ABCB6-C) in both the nucleotide-free and ADP-bound states by heteronuclear multidimensional NMR and homology modelling. A nonlinear sampling scheme was utilised for indirectly acquired ^{13}C and ^{15}N dimensions of all 3D triple-resonance NMR experiments, in order to overcome the instability and the low solubility of ABCB6-C. The backbone resonances for approximately 25 % of non-proline residues, which are mostly distributed around the functionally important loops and in the Helical domain, were not observed for nucleotide-free form of ABCB6-C. From the pH, temperature and magnetic field strength dependencies of the resonance intensities, we concluded that this incompleteness in the assignments is mainly due to the exchange between multiple conformations at an intermediate rate on the NMR timescale. These localised conformational dynamics remained in ADP-bound ABCB6-C except for the loops responsible for adenine base and α/β-phosphate binding. These results revealed that the localised dynamic cooperativity, which was recently proposed for a prokaryotic ABC MJ1267, also exists in a higher eukaryotic ABC, and is presumably shared by all members of the ABC family. Since the Helical domain is the putative interface to the transmembrane

キーワード　ABCB6, NikA, OppA, TROSY, 重水素化, 非線形サンプリング

いとう ゆたか, くらしま かおり, もろみさと かやの, みしま まさき, いけや てっぺい, すんだれさん らじぇしゅ, にしむら かおる, Jonathan Heddle, Jeremy Tame

domain, this cooperativity may explain the coupled functions between domains in the substrate-transportation cycle.

Nickel is an essential cofactor for a number of bacterial enzymes, while high concentrations of nickel are toxic to cells, owing to its high affinity for DNA and ability to disrupt enzyme activity. Bacteria have evolved several efficient transport systems to maintain Ni homeostasis for the normal functioning of enzymes involved in ureolysis, methane biogenesis and hydrogen metabolism. The *E. coli* ATP-dependent ABC-type transporter encoded by the *nik* operon, the NikABCDE permease, is implicated in the specific transport of Ni from the periplasm to the cytoplasm. The mature periprasmic NikA (502 a.a., 56kDa) is the primary nickel-binding component and mediator of the chemotactic response away from nickel. NikA exhibits significant sequence similarity to the oligopeptide binding protein OppA, a periplasmic binding protein (PBP). We had initiated the NMR backbone resonance assignments of apo-NikA, which will provide a framework for the analyses of structure and dynamics of NikA in solution. Assignments for more than 86% of non-proline residues were obtained by the analysis of TROSY-based triple-resonance experiments. The incompleteness in the assignments was caused by line broadening of cross peaks in ^{1}H-^{15}N TROSY-HSQC spectra, thus providing scarcely observable cross peaks in triple-resonance spectra for these $^{1}H^{N}$-^{15}N correlations. Indeed, 20-30 isolated but largely broadened cross peaks were observed in ^{1}H-^{15}N TROSY-HSQC spectra. Incomplete exchange of amide ^{2}H to ^{1}H was ruled out, since the ^{1}H-^{15}N TROSY-HSQC spectra of 6 M guanidine hydrochloride-unfolded and refolded NikA failed to reveal new correlation cross peaks. Mapping the residues with missing assignments onto the crystal structure of NikA revealed that they were mainly localised around the nickel-binding site, which is surrounded by two lobes in NikA. Thus changes in the relative orientation of two lobes in the nickel free state in solution, caused by intrinsic conformational flexibility around the hinge region, is probably responsible for the exchange broadening of the $^{1}H^{N}$-^{15}N correlation cross peaks.

A similar triple-resonance approach was employed for *Salmonella* periplasmic oligopeptide-binding protein OppA (517 a.a.) D419N mutant. Backbone $^{1}H^{N}$, $^{13}C^{\alpha}$, $^{13}C'$, ^{15}N and side chain $^{13}C^{\beta}$ resonances were assigned for more than 89% non-proline residues in OppA(D419N) (OppA has 31 proline residues). In common with the case of NikA, the unassigned residues were mainly localised around the ligand-binding site of the crystal structure of OppA, suggesting the shared ligand-recognition mechanism of periplasmic binding proteins

1 LE14

An NMR spectroscopic approach to the ubiquitin-proteasome system

○Eri Sakata[1], Akira Sumiyoshi[1], Hiroaki Sasakawa[2], Yoshiki Yamaguchi[1], Koichi Kato[1,2]

[1]Graduate School of Pharmaceutical Sciences, Nagoya City University

[2] Institute for Molecular Science

Ubiquitin (Ub) and ubiquitin-like protein (Ubl) are covalently attached to the target substrate through isopeptide linkage between their carboxyl termini and amino groups of lysine residues of acceptor molecules. These post-translational modifications operate as if they provided additional domain(s) to control the functions and fates of the target proteins in cells. Especially, the polyubiquitin chain acts as a principal signal for proteasomal protein degradation. Although the ubiquitination pathways are known to require the sequential activities of Ub-activating enzyme (E1), Ub-conjugating enzyme (E2) and Ub-ligase (E3), the structural basis for the mechanisms to control these cascade reactions remain to be understood. We performed NMR analyses of the molecular recognition mechanisms of these enzymes that regulate the ubiquitination reactions.

In the process of ubiquitination, E2 is a key enzyme that recognizes E1, carries covalently activated Ub and transfers Ub in concert with E3. Nedd8, one of various ubiquitin-like modifiers ligated in a manner similar to the ubiquitination pathway, is covalently attached to the cullin subunit of SCF complex and thereby up-regulates the ubiquitin ligase activity by enhancing the recruitment of E2 to this complex. However, the underlying mechanisms of the activation of the SCF complex remain unclear. Here we examined a possible interaction of Nedd8 with Ubc4, which is an ubiquitin-E2 enzyme that catalyzes the formation of polyubiquitin chains upon neddylation of cullin1. The NMR data demonstrate that Nedd8 binds ubiquitin-E2 (Ubc4), but not Nedd8-E2 (Ubc12). The

Keywords; Ubiquitin-proteasome system, Solution structure, Protein-protein interactions
Spin label

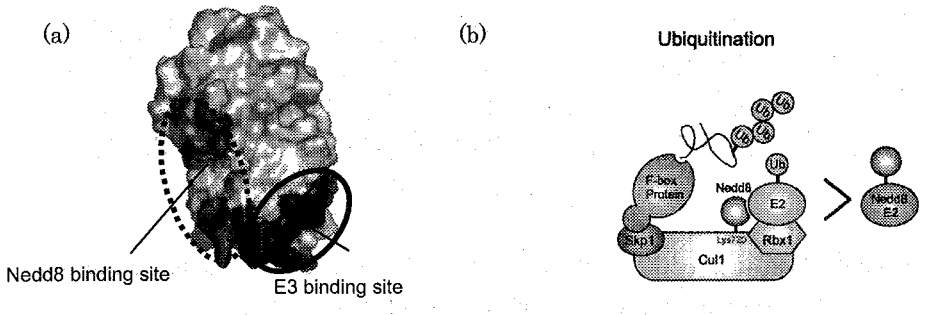

Figure 1 (a) Representation of the binding interface of Ubc4. Nedd8 directly binds a surface area adjoining the Rbx1-binding site of Ubc4 through its hydrophobic surface (b) Schematic mechanism for the role of the Neddylation. The recruitment of ubiquitin-E2 conjugates to SCF complex is enhanced upon neddylation by cooperative binding of Nedd8 and Rbx1 to the E2 enzyme.

Nedd8-binding site is distinct from but adjoins the putative E3-binding site on Ubc4 through its hydrophobic surface. These data imply that once Nedd8 is attached onto the cullin subunit, it forms the active platform for selective recruitment of ubiquitin-charged E2 in cooperation with Rbx1, excluding Ubc12-Nedd8 complex. On inspection of NMR data, we will also discuss structural basis of elongation of ubiquitin chain by E2.

There exist enzymes that are able to remove ubiquitin from target proteins. These deubiquitinating enzymes contribute to reversible ubiquitin-conjugation systems that regulate protein functions. Ataxin-3, a product of a causative gene of Machado-Joseph disease, is composed of the N-terminal Josephin domain, two or theree Ub-interacting motif and a polyglutamine tract. It has recently been shown that the Josephin domain acts as a deubiquitinating enzyme. We performed NMR analyses of the interaction between the 20-kDa Josephin domain and Lys48-linked di-Ub (K48-Ub_2) isotopically labeled in a unit-selective manner by an enzymatic reaction *in vitro*. We demonstrated that the hydrophobic surfaces of both Ub units, which surround the isopeptide linkage, were involved in the interaction with the Josephin domain. To determine the orientation of polyubiquitin chain with respect to the Josephin domain, we prepared K48-Ub_2 with site-specific spin labeling. On the basis of the paramagnetic relaxation enhancement data, we identified the amino acids residues of the Josephin domain in close spatial proximity of the unpaired electron in the complex. We propose a hypothetical model of the interaction between the Josephin domain and K48-linked polyubiquitin chain.

1 LE15

サブミリ秒 H/D 交換法と NMR によって観測されたアポミオグロビンの折り畳み中間体の構造ゆらぎ

(京大院・工[1]、TSRI[2]、Spring-8[3]、北大・理[1,4]、阪大・蛋白研[5])
○鵜澤尊規[1]、西村千秋[2]、秋山修志[3]、石森浩一郎[1,4]、高橋聡[5]、H. Jane Dyson[2]、Peter E. Wright[2]

Conformational fluctuation of the kinetic intermediate in apomyoglobin folding detected by submillisecond H/D exchange coupled with NMR

[1]*Faculty of Engineering, Kyoto University*
[2]*Department of Molecular Biology, The Scripps Research Institute*
[3]*RIKEN Harima Institute SPring-8 Center*
[4]*Faculty of Science, Hokkaido University*
[5] *Institute for Protein Research, Osaka University*
○Takanori Uzawa[1], Chiaki Nishimura[2], Shuji Akiyama[3], Koichiro Ishimori[4], Satoshi Takahashi[5], H. Jane Dyson[2], Peter E. Wright[2]

Proteins search a lot of conformations on the energy surface biased toward the folded conformations to fold into their native structures. The conformational search in the kinetic intermediate ensemble which is practically expressed as conformational fluctuation, however, remains poorly understood. Thus motivated, we used submillisecond H/D exchange combined with NMR to understand the fluctuation in the early folding intermediate of apomyoglobin. As a result of analyzing the proton occupancies at 0.4ms and 6ms of the refolding time, we successfully found the strong protections for A and G helices, the moderate protections for B and H helices and the weak protections for a part of B, C and E helices at 0.4ms. Moreover, the protections at 6ms were close to those at 0.4ms. On the other hand, the fractions of the exchangable amide-hydrogen (NH_{open}) in the B, C and E helices possessed significant values at 0.4ms, but decreased at 6ms. The change of NH_{open} without the change of the protection was interpreted to be caused by the fluctuation of B, C and E regions in the kinetic intermediate ensemble. After the complete packing of the regions which are still fluctuating at 6ms, apomyoglobin folds into the native state.

【序論】蛋白質は天然状態に折り畳む際、エネルギー地形上で構造をゆるがせることで多くの構造を探索していると考えられるが、折り畳み中間体アンサンブルにおいてどのように天然構造に折り畳む構造を探しているのかは、未だ良く理解されて

キーワード：protein folding, H/D exchange, rapid mixing
うざわたかのり、にしむらちあき、あきやましゅうじ、いしもりこういちろう、たかはしさとし、ジェーンダイソン、ピーターライト

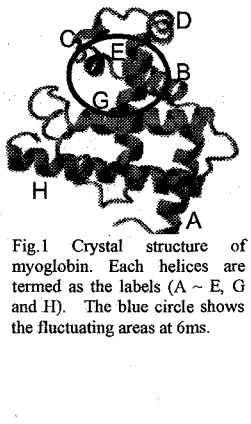

Fig.1 Crystal structure of myoglobin. Each helices are termed as the labels (A ~ E, G and H). The blue circle shows the fluctuating areas at 6ms.

いない。本研究では、折り畳み過程に関する研究が大きく進んでいるアポミオグロビン(apoMb)の折り畳み中間体を、高速溶液混合と水素重水素(H/D)交換法とNMR測定法を組み合わせて観察することで、apoMbの中間体においてどの領域がゆらいでいるのか、およびこれらの領域の折り畳みに果たす役割について知ることを目的とした。

【実験】中間体アンサンブルにおける構造探索過程を残基レベルで評価するため、H/D交換法を用いた（Scheme1）。この方法を用いる事で、アミドプロトンのプロトン占有率のpH依存性から、各残基のk_{op}、k_{cl}およびゆらいでいる状態（Open状態）にあるアミドプロトンの割合を示すNH_{open}状態の割合を見積もることができる。

$$NH_{close} \underset{k_{cl}}{\overset{k_{op}}{\rightleftharpoons}} NH_{open} \xrightarrow{k_{ex}(pH)} ND_{exchanged}$$

Scheme 1. Exchange process in the H/D exchange method. The exchange reaction of an amide-hydrogen has been interpreted based on the protected state that is non-exchangeable (NH_{closed}), the open state that is exchangeable (NH_{open}) and the exchanged state $ND_{exchanged}$. k_{op} and k_{cl} are the local opening and local closing rates. k_{ex} is the exchange rate of the unprotected amide and varies with pH ($k_{ex}=k_{ex}(pH7)\times10^{(pH-7)}$).

pH2 で変性した apoMb を高速溶液混合技術で急激に pH6 へジャンプさせ折り畳み反応を開始した。0.4ms もしくは 6ms の折り畳み時間の後、H/D 交換 pH パルス（pD7~10.7）を 3.6ms 間あて、pD を 6 に下げた。得られたサンプルの HSQC スペクトルを測定し、各シグナル強度の H/D 交換時の pD に対する変化を調べた。

【結果と考察】得られた結果をHvidtの式(Krishna et al. (2004) *Methods* **34**, 51–64.)でフィットすることで、アミドプロトンの安定性の指標となるk_{cl}/k_{op}とNH_{open}を見積もった（Fig.2）。

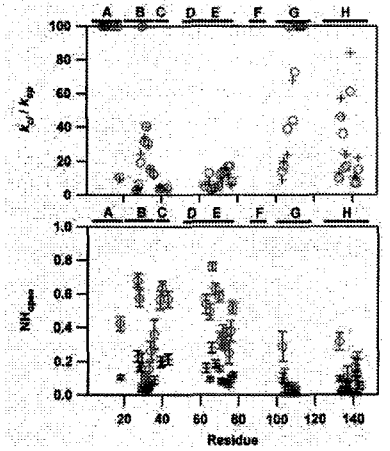

Fig. 2 Estimated k_{cl}/k_{op} (upper panel) and NH_{open} (lower panel) for 0.4ms (red circles) and 6ms (blue crosses) of refolding time.

A、Gヘリックス領域における残基はHvidtの式でフィットできないほど、非常に高いk_{cl}/k_{op}を持っていた。他のヘリックス領域と比較した結果、A,G > H,B > C,Eの順に安定なヘリックスを形成していることが明らかとなった。これは、これまでA,B,G,Hヘリックスが等しくアポミオグロビンの折り畳みの核となっていると考えられていたことに対して、A,Gヘリックスがより重要であることを示唆している。さらに、0.4msと 6msのk_{cl}/k_{op}には顕著な違いがないことは、ヘリックスの更なる安定化は起きていないことを示している。

一方、NH_{open}の割合は時間に依存することが明らかとなった。特にB,C,Eヘリックス領域におけるNH_{open}は、0.4msから 6msにかけて大きく減少していることが明らかとなった。これらの結果は、折り畳み反応開始後 0.4msでは、A,B,G,Hヘリックスが形成された中間体アンサンブルのうち 30~60%のB,C,E領域はゆらいでいるものの、6msになるとゆらいでいる領域の割合が減少し、弱いヘリックス(k_{cl}/k_{op}=~10)を形成した中間体の割合が増加したと解釈できた。さらに、6msにおいても未だ揺らいでいる領域（Fig.2におけるNH_{open}>15%の領域をFig.1 の青色円で示した）の存在は、apoMbは天然状態に折り畳むためには、これらの領域のゆらぎが最終的なパッキングによって抑えられることが必要である事を示唆している。

Analysis of NMR Data Obtained by Fast Spectroscopy

Martin Billeter, Daniel Malmodin, Wolfgang Bermel

Abstract

NMR spectroscopy is a unique method for the structural, dynamic and functional characterization of proteins in solution, playing an essential role in several large-scale structure genomics initiatives. Nevertheless, the laborious and often difficult interpretation of the NMR spectra continues to limit the potential of NMR protein structure analysis. "Fast spectroscopy" NMR data acquisition, followed by adequate computational tools, can provide signal frequencies and intensities that, due to their high dimensionality, cannot be recorded with conventional approaches.

Coupling of evolution periods in NMR experiments is a very promising approach that has recently attracted much attention for its substantial savings in measurement time. Another novel concept, which already proved useful in many types of NMR applications, is multi-way decomposition. These (and related) techniques allow significant speed-ups when performing resonance assignments, extracting structural data or screening for ligands (drug discovery). The combination of these approaches (implemented in the program PRODECOMP) provides the following advantages: Highly similar information to what would be found in a corresponding full-dimensional spectrum is extracted from a set of projected spectra. All experimental spectra are used simultaneously, avoiding sensitivity loss associated with individual examination of the spectra. Aliasing caused by the linear combinations of individual shifts in the projected spectra is automatically resolved, allowing for better resolution due to smaller spectral widths. Reconstructions of various high-dimensional spectra, including the corresponding full-dimensional spectrum, become straightforward and free of artifacts. Novel applications include the analysis of NMR data sets yielding unambiguous spin systems with ≥ 10 nuclei.

1 LE17

Fast and Smart Protein Structure Determination by NMR

Markus Zweckstetter
Department for NMR-based Structural Biology, Max Planck Institute for Biophysical Chemistry, Am Fassberg 11, 37077 Göttingen, Germany

NMR spectroscopy provides high-resolution structural information of biomolecules in near-physiological conditions. Although significant improvements were achieved in NMR spectroscopy in the last 20 years, the increase in genome sequencing data has created a need for rapid and efficient methods of NMR-based structure determination. NMR data acquisition can be accelerated significantly, when sensitive spectrometers are combined with new methods for sampling chemical shifts in multidimensional NMR experiments. Therefore, data analysis and in particular the requirement to assign side chain chemical shifts to specific atoms is the major bottleneck of rapid NMR-based structure determination. Here, we present a method, termed FastNMR (FAst STructure determination by NMR), which enables automatic, high-resolution NMR structure determination of domain-sized proteins.(1) Starting from unassigned, experimental NMR data, high-resolution structures of three proteins were determined without manual intervention in less than 24 hours. This included the automatic *de novo* structure determination of the 65-residue cone snail neurotoxin conkunitzin-S2.

Residual dipolar couplings (RDCs) can be measured in a weakly aligned macromolecule, for which the large one-bond internuclear dipolar interactions no longer average to zero. RDCs are exquisitely sensitive to bond vector orientation and offer many new opportunities in NMR studies of proteins in solution. For charged liquid crystalline media the magnitude and orientation of the solute's alignment tensor can be predicted with reasonable accuracy from the three-dimensional charge distribution and shape of a macromolecule using the program PALES.(2,3) The ability to predict dipolar couplings for a given protein structure provides possibilities for the differentiation between monomeric and homodimeric states, conformational analysis of dynamic systems such as oligosaccharides, refinement of nucleic acid structures, determination of the relative orientation of protein domains, validation of structures of protein complexes and classification of protein fold families on the basis of unassigned NMR data. PALES has recently been used for the determination of the relative arrangement of monomers within coiled-coil proteins in solution.(4) In addition, PALES was used to obtain insight into the conformational behaviour and molecular alignment of intrinsically unstructured proteins, such as α-synculein, which is the major component of aggregates in the brains of Parkinson's disease patients.(5)

(1) J. Korukottu, M. Bayrhuber, P. Montaville, Y-S. Jung, V. Vijayan, S. Becker, M. Zweckstetter (2006), *Angew. Chem. Int. Ed.*, in press.
(2) M. Zweckstetter, A. Bax (2000), *J. Am. Chem. Soc.* **122**, 3791-3792.
(3) M. Zweckstetter, G. Hummer, A. Bax (2004), *Biophys. J.* **86**, 3444-3460.
(4) M. Zweckstetter, J.R. Schnell, J.J. Chou (2005), *J. Am. Chem. Soc.* **127**,11918-11919.
(5) L. Skora, M.-K. Cho, H.-Y. Kim, S. Becker, C.O. Fernandez, M. Blackledge, M. Zweckstetter (2006), *Angew. Chem. Int .Ed.*, Epub Sep. 28.

Keywords: NMR spectroscopy, automatic, protein structure, FastNMR, PALES, unfolded

Automated Protein Structure Determination from NMR Spectra

Peter Güntert and Blanca López-Méndez
Tatsuo Miyazawa Memorial Program, RIKEN Genomic Sciences Center,
1-7-22 Suehiro-cho, Tsurumi, Yokohama 230-0045, Japan

Fully automated structure determination of proteins in solution (FLYA) yields, without human intervention, three-dimensional protein structures starting from a set of multidimensional NMR spectra. Integrating existing and new software, automated peak picking over all spectra is followed by peak list filtering, the generation of an ensemble of initial chemical shift assignments, the determination of consensus chemical shift assignments for all ^{1}H, ^{13}C and ^{15}N nuclei, the assignment of NOESY cross peaks, the generation of distance restraints, and the calculation of the three-dimensional structure by torsion angle dynamics. The resulting, preliminary structure serves as additional input to the second stage of the procedure, in which a new ensemble of chemical shift assignments and a refined structure are calculated. The three-dimensional structures of three 12–16 kDa proteins computed with the FLYA algorithm coincided closely with the conventionally determined structures. Deviations were below 0.95 Å for the backbone atom positions, excluding the flexible chain termini. 96–97% of all backbone and side-chain chemical shifts in the structured regions were assigned to the correct residues. The purely computational FLYA method is suitable to substitute all manual spectra analysis, and thus overcomes a main efficiency limitation of the NMR method for protein structure determination.

Keywords: protein structure calculation; automated assignment; CYANA; FLYA

Here we present a fully automated computational approach that is capable to solve 3D protein structures using as experimental input data only the amino acid sequence and a set of multi-dimensional NMR spectra. In analogy to automated crystallographic systems for high-throughput macromolecular structure determination, we have achieved complete automation of NMR protein structure determination by combining and extending software packages that carry out individual steps in NMR structure determination into an integrated system.

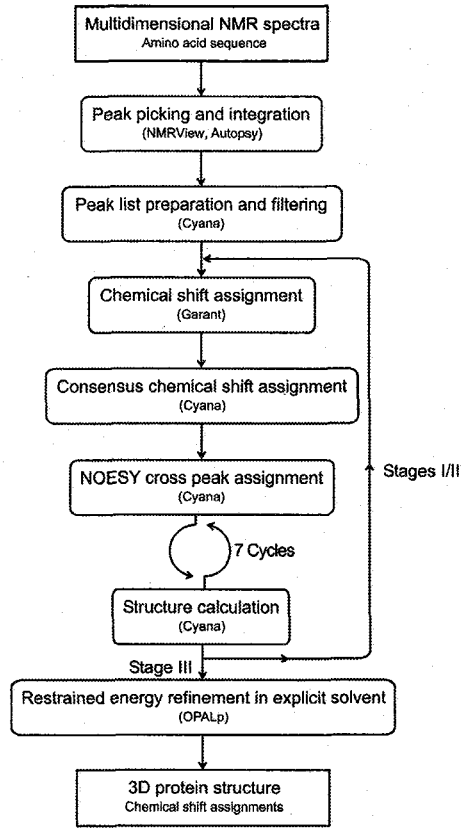

Flowchart of the fully automated structure determination algorithm, FLYA.

The results of the FLYA structure determinations of three proteins show that fully automated NMR structure determination of proteins up to 140 amino acid residues is possible now. The method is purely computational and can cope with the amount of overlap and artifacts present in typical, experimental NMR spectra. It is straightforward to further improve the results by interactive improvements of the peak lists, corrections of erroneous chemical shift assignments, and/or additional conformational restraints for torsion angles, hydrogen bonds, residual dipolar couplings, etc. Various extensions of the basic FLYA algorithm can be envisaged.

López-Méndez, B. & Güntert, P. Automated protein structure determination from NMR spectra. *J. Am. Chem. Soc.* 128, 13112-13122 (2006).

Wednesday, November 22

Japanese Session

1 LJ1

Magic-Echo DANTE による固体 MRI 用スライス選択法

筑波大学大学院 数理物質科学研究科 1、横浜創英短大 情報工学科 2
○ 増本秀史 1、橋本雄幸 2、松井 茂 1

Tailored Slice-Selection in Solid-State MRI by DANTE under Magic-Echo Line Narrowing

H. Masumoto,* T. Hashimoto, † and S. Matsui,*
**Graduate School of Pure and Applied Sciences, University of Tsukuba, Tsukuba, Ibaraki 305-8573*
† Department of Information Technology, Yokohama Soei Junior College, Yokohama, Kanagawa 226-0015

The slice selection method is well-established in liquid-state MRI. The sinc-shaped soft RF pulse applied under the presence of a field gradient achieves the almost ideal slice selection. This selection scheme, however, does not work in solid-state MRI where the T_2 of the object is much shorter than the soft RF pulse. Although a few slice selection methods have been proposed for solid-state MRI (1-3), each method suffers from its own problem like poor selectivity, technical difficulty, etc. Here, we describe a simple slice selection method for solid-state MRI by combining DANTE (4) with Magic-Echo (ME) line narrowing (5). Our method is technically less demanding and permits tailoring the profile of the slice for the first time in solid-state MRI.

The original DANTE sequence consists of regularly spaced N short RF pulses. The flip angle of each pulse is defined by α_i (i = 1, 2, 3,...,N) and is identical. During the pulse spacing τ_D, free precession occurs, leading to the frequency dependent RF excitation. Since the frequency dependence can be converted to the spatial dependence by application of a field gradient G, slice selection can be attained by the DANTE sequence. For combining the DANTE sequence with the ME line narrowing sequence without degrading the line narrowing efficiency, it is necessary to apply the DANTE RF pulses at the ME peaks where the spin time evolution is free from the dipolar interaction. The ME DANTE pulse sequence is schematically depicted by the upper sequence in Fig. 1. The ME DANTE excitation is followed by the suitable ME sequence with reversed gradient pulses for rephasing the signal. The rephased signal is then sampled for monitoring the slice profile.

It is important to note that by introducing an appropriate modulation into the original DANTE sequence as shown by the lower sequence in Fig. 1, one can control the shape of the slice profile arbitrarily. The sinc modulation leads to a rectangular shape that is an ideal slice profile.

To demonstrate the utility of the ME DANTE slice-selection method, we

キイワード： slice selection, MRI, DANTE, magic echo, line narrowing

ますもとひでふみ、はしもとたけゆき、まついしげる

have made numerical simulations of the DANTE experiments based on the Bloch equations and further performed the ME DANTE experiments on a test sample of adamantane. Also, we have carried out the DANTE experiments on a water sample for comparison. The results will be reported in the presentation.

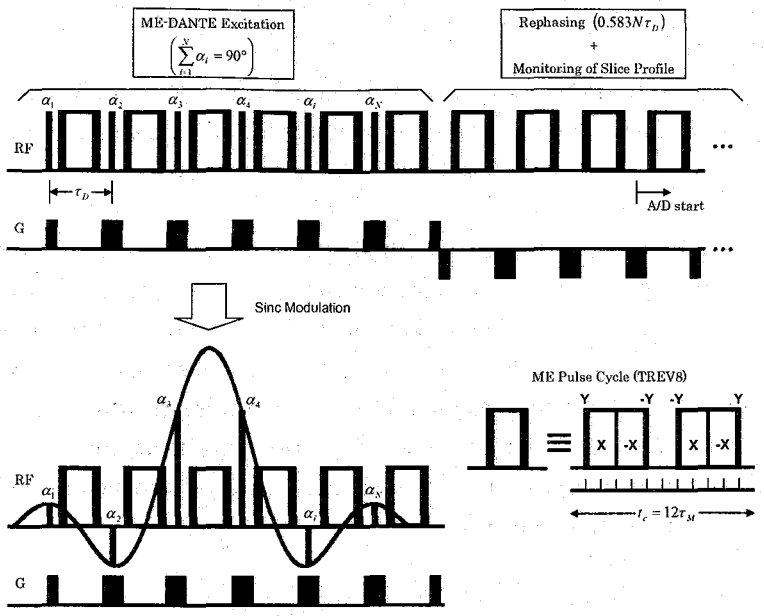

Fig. 1. The original (upper) and sinc-modulated (lower) DANTE sequences combined with the ME line narrowing sequence. The ME sequence of TREV8 (5) has been employed with the cycle time t_c = 360 μ s which is equal to the DANTE pulse spacing τ_D. The width of 90° pulse (filled) was 2.5 μ s.

Acknowledgement: We thank the late Professor Tamon Inouye for encouragement and continuing support.

References:

(1) R. A. Wind, J. H. N. Creyghton, D. J. Ligthelm, and J. Smidt, *J. Phys. C: Solid State Phys.*, **11**, L223 (1978).
(2) D. G. Cory, J. B. Miller, and A. N. Garroway, *J. Magn. Reson.* **90**, 544 (1990).
(3) S. Matsui, *J.Magn Reson.* **97**, 335-341 (1992).
(4) G. Bodenhausen, R. Freeman, and G. A. Morris, *J. Magn. Reson.* **23**, 171 (1976).
(5) S. Matsui, *Chem. Phys. Lett.* **179**, 187-190 (1991); S. Matsui, *J.Magn Reson.* **95**, 149-153 (1991); S. Matsui, *J.Magn Reson.* **98**, 618-621 (1992); S. Matsui, Y. Ogasawara, and T. Inouye, *J. Magn. Reson.* **A 105**, 215-218 (1993); S. Matsui, M. Nonaka, T. Nakai, and T. Inouye, *Solid State NMR* **10**,39-44 (1997); M. Nonaka, S. Matsui, and T. Inouye, *J. Magn. Reson.* **145**, 315-318 (2000); S. Matsui and S. Saito, *J.Magn Reson.*, **149**, 103-109 (2001); S. Matsui, S. Saito, T. Hashimoto, and T. Inouye, *J.Magn Reson.* **160**, 13-19 (2003).

1 LJ2

マウス脳内超偏極^{129}Xeのダイナミクス精密測定

(大阪大学大学院医学系研究科保健学専攻)
○秋山かずえ , 金子暁里 , 木村敦臣 , 藤原英明

Precise Analysis on the Dynamics of Hyperpolarized ^{129}Xe in Mouse Brain

(Division of Health Sciences,Graduate School of Medicine,Osaka University)
○Kazue Akiyama , Atsuomi Kimura

Hyperpolarized ^{129}Xe gas is being watched with interest as an useful NMR probe , because we can perform the precise measurement of rCBF and gCBF with the gas. However , the behavior and the character of HP ^{129}Xe is not yet turned out clearly. For example , comparing with proton , hyperpolarized gases show complex relaxation processes. RF pulses cause not only general longitudinal relaxation but depolarization. In present study , the relaxation constant that was proposed before and that can express the depolarization rate of hyperpolarized gas was improved precisely in mouse brain .

背景

近年、NMR信号を増幅し高感度化を図る方法として 超偏極^{129}Xeガスを使用したNMR法が注目されつつある。Xeは脂溶性の希ガスであり血中に溶けて脳組織に拡散するため、脳血流量の精密測定を実現する新たなprobeとして期待されている[1]。しかし、脳内における^{129}Xeの動態、性質を表すパラメータはまだ正確には決定されていない。超偏極ガスはRFパルス照射後、通常の縦緩和に加えRFパルスによる脱偏極の影響を受ける事が分かっている。今回、マウスの脳中に溶解した^{129}Xeにおいてこれまでに発表してきた脱偏極速度をより精密に測定する方法を発表する。

方法

麻酔をかけたマウスにレーザーで超偏極させた^{129}Xeガスを自家製のマスクを通して持続的に吸入させた。^{129}Xeガスが脳組織に十分に溶解するのを待ち、ガスを吸入させた状態のままフリップ角θのRFパルスを繰り返し時間TRで連続的に照射した。このようにして得られた^{129}Xe信号の溶解相ピークのみを取り出して積分値を計測し、次に示す式.[1]にfitting することにより得られた減衰曲線から脱偏極定数αを算出した。θには約20° を使用しTRは0.27、0.37、0.47secで行った。

キーワード：Dynamics、Hyperpolarized ^{129}Xe、Mouse、Brain

著者ふりがな：あきやま かずえ、かねこ あかり、きむら あつおみ、ふじわら ひであき

$$\frac{C_{Brain}(t)}{C_{Brain}(0)} = A + (1-A)e^{-\beta t} \qquad [1]$$

但し、$A = \frac{\alpha}{\beta}$ ， $\alpha = \frac{F_{Brain}}{\lambda_{Brain}} + \frac{1}{T_{1Brain}}$ ， $\beta = \frac{F_{Brain}}{\lambda_{Brain}} + \frac{f(1-\cos\theta)}{TR} + \frac{1}{T_{1Brain}}$ である。

$C_{Brain}(t)$,$C_{Brain}(0)$：時間t、0での信号強度

F_{Brain}：perfusion rate (ml blood/ml tissue/sec)

λ_{Brain}：血液-脳組織間の分配係数

f：TR間に脳組織に流入する^{129}Xe量

T_{1Brain}：脳組織中における^{129}Xeの縦緩和時間

結果・考察

得られた^{129}Xe-MR信号の溶解相ピークの例をFig.1に示す。この溶解相ピークのTR毎の積分値をグラフ化したものがFig.2である。◆は実測値であり、これを理論式[1]に近づくように最小二乗法でfittingする事により実線のような減衰曲線が得られた。θ=約 20°、TR=0.27、0.37、0.47secで測定したそれぞれの減衰曲線から得たA、βの値からαを導き出した。Aの平均値は0.349、βは0.547であり、その結果0.177というαの値を得た。前述のαの式にF_{Brain}、λ_{Brain}の文献値(前者 1.4 (ml blood/ml tissue/min) [2]、後者 0.79 [3])をそれぞれ代入しT_{1Brain}の値を算出するとT_{1Brain}=10.1secであった。これはラットの脳で報告されている約12sec [4]という結果と比較すると妥当な結果であると言える。

これまでの^{129}XeのT_{1Brain}測定はXeガスの供給を止める事により得られたwashout曲線からT_{1Brain}を算出する方法で行われていたため、測定時のマウスの呼吸状態の影響を大きく受けてしまう。しかし、この方法では肺機能の影響を考慮する必要がなく、より正確なT_{1Brain}測定が可能であると結論付けられる。

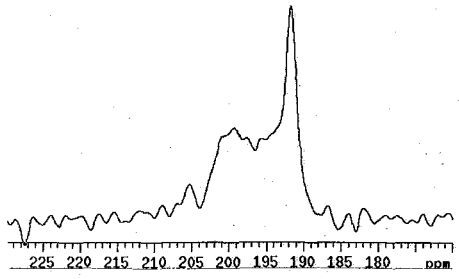

Fig.1 An example of ^{129}Xe spectrum acquired in the mouse brain in vivo.

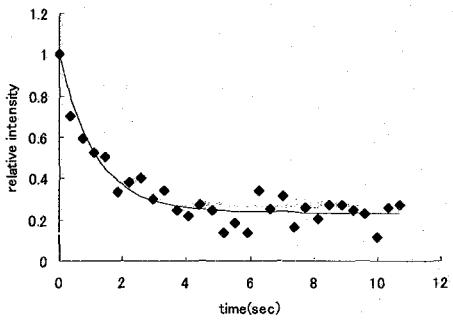

Fig.2 Kinetics of the ^{129}Xe gas signal in a mouse brain.

参考文献

1）Magn Reson Med 2003 ;49 :1041-1018 , 2）J Appl Physiol 1980 ;49 :178-183 , 3）Magn Reson Med 1996 ;36 :340-344 , 4）Magn Reson Med 2004 ;51 :843-847,

Solid-state NMR Characterization of Order-Disorder Phenomena in Polymer Crystals

National Institute for Advanced Industrial Science and Technology,
Research Institute of Nanotechnology,[1]
Research Institute for Innovation in Sustainable Chemistry[2]
Toshikazu Miyoshi,[1] Wei Hu,[1] Hideaki Hagiwara,[2] Li, Yongjin,[1] and Akira Kaito[1]

The polymer crystalline structures have been successfully investigated using traditional X-ray diffraction methods. X-ray diffraction method generally requires long range structural orders. Therefore, it is not easy applied to characterize polymer crystals with disordered packing structures in a short range. [1)] On the other hand, solid-state ^{13}C NMR is potentially sensitive to local chain packing structures. Here, we investigate the chain packing structure for well known crystalline polymers, polyolefines (*isotactic*-polypropylene (*i*PP) and *isotactic*-poly(3-methyl-1-butene)(*i*P3M1B)), using high power ^{1}H decoupling and 2D ^{13}C-^{13}C INADEQUATE at natural abundance. Consequently, we will show newly structural information on order-disorder phenomena for chain packing structures, and advantage of solid-state NMR for characterization of disordered crystals over X-ray.

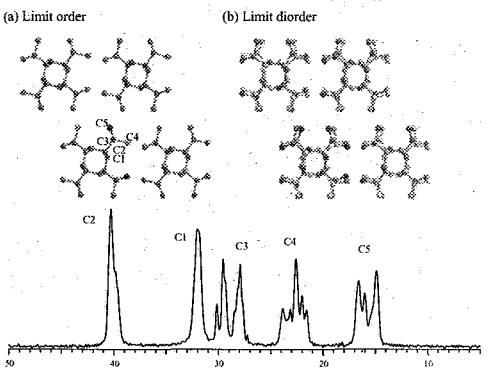

Figure 1. Two crystalline packing models, "limit order" and "limit disorder" for *i*P3M1B proposed by X-ray diffraction analysis, and ^{13}C CPMAS NMR spectrum for *i*P3M1B crystalline region, with a $T_{1\rho H}$ filter at 240 K.

Disordered Packing Structure by ^{13}C-^{13}C INADEQUATE There are several X-ray diffraction investigations on crystalline packing structures for iP3M1B crystalline region. In the latest, Corradini *et al.* revised packing structures and proposed two packing models, "limit order" and "limit disorder" models as shown in Figure 1.[2)] The former shows completely an ordered structure, on the other hand, the latter includes statistically disordered up- and down-ward chains in each site. Both the calculated X-ray diffraction patterns on the basis of the former and latter satisfy the experimental diffraction patterns, because conformations and crystal lattice parameters are same in both structures. This indicates that X-ray technique is difficult to differentiate the former from the latter. Here, we apply solid-state NMR techniques for characterizing packing structure for *i*P3M1B. Figure 1 shows ^{13}C CPMAS NMR spectrum for *i*P3M1B crystalline region, with a $T_{1\rho H}$ relaxation time filter which suppresses the amorphous signals, demonstrating that side-chain CH, (C3), nonequivalent two CH_3 (C4 and C5) carbon apparently give 3, 5, and 4 resonances, respectively. These resonance numbers deny the ordered packing structures, since the ordered structure allows carbon signals adopting only two kinds of different environments, meaning two kinds of the closest contact distances with neighboring chains. However, the obtained spectrum is not enough to conclude the

Key words / high resolution solid state NMR / INADEQUATE / polymer crystal / order-disorder

disorder model. Therefore, we apply ^{13}C-^{13}C 2D INADEQUATE technique for further improving spectral resolution using chemical shift dispersions due to packing and double quantum coherence. In order to improve spectral sensitivity, temperature was decreased up to 240 K and decoupling power and positions are carefully checked. Consequently, we obtained ^{13}C-^{13}C 2D INADEQUATE spectrum for *i*P3M1B crystalline region, with a total machine time of 190 hours. It is demonstrated all carbon connectivity is shown in 2D MAP, and especially, side-chain resolution is improved, as shown in Figure 2. It is consequently found that the side-chain carbons have 8 signals, especially, C5 carbon signals give the clearest pattern. Considering packing models, it is concluded that *i*P3M1B chains crystallize with up- and down-disorders in each site. Furthermore, line fitting using Gaussian functions to 1D line shape indicates signal population for each resonance distributes between 8% and 21 %, which is not consistent with the averaged value, 12.5 % expected from the "limit disorder" model. It is concluded that *i*P3M1B chain in the crystalline region includes up- and down-ward chains in each site, and disorder is not statistically.

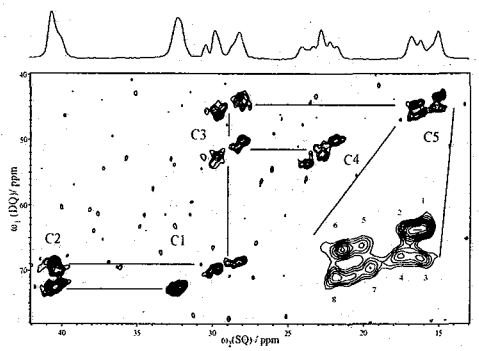

Figure 2. ^{13}C-^{13}C 2D INADEQUATE spectrum for iP3M1B at 240 K in natural abundance. This sequence includes ^{1}H $T_{1\rho H}$ filter which suppress amorphous signals. The total experimental time is 168 hours.

Disorder-Order Phenomena by solid-state NMR It is well known that α form (most stable form) of *i*PP also has up- and down-disorders depending on crystallization or annealing temperatures. For this polymer, X-ray diffraction has been applied for analyzing how disordered and ordered structures changes depending on annealing times[3] and crystallization time.[4] On the other hand, there are also several works on high resolution solid state ^{13}C NMR for *i*PP.[5-7] Nevertheless, interpretation on the line shape is not consistent with the results obtained by X-ray diffraction. In this work, we re-investigate line-shape analysis on disorder-order phenomena using ^{13}C CPMAS NMR. Firstly, we will show how disorder and order structures contribute to NMR spectrum. Here, we apply high power proton TPPM dipolar decoupling with a field strength of 110 kHz during signal detection periods, for discriminating order structure from the disorder. Secondly, newly structural information for ordered structure is demonstrated by NMR. Finally, it is demonstrated that disorder-order phenomena could be quantatively characterized by solid-state NMR, and compare with the result by X-ray diffraction. Through this work, it is shown why solid-state NMR is particularly suitable for characterizations on disordered structures.

References

1) Rosa, C. D., *et al.*, *Macromol. Symp.*, **2001**, *175*, 215-224. 2) Corradini, P., *et al.*, *Eur. Polym. J.*, **1970**, *6*, 281. 3) Auriemma, F., *et al.*, *Macromolecules*, **2000**, *33*, 8764. 4) Radhakrishnan, J., *et al.*, Polymer, **1998**, *39*, 2995. 5) Bunn, A., *et al.*, *Polymer*, **1982**, *23*, 694. 6) Caldas, V., *et al.*, *Magn. Reson. Chem.*, **1994**, *32*, S72. 7) Saito, S., *et al.*, *Macromolecules*, **1990**, *23*, 3256.

1 LJ4

NMR法から決定したpoly(ε-L-lysine)の結晶化度

（防大応化）○浅野敦志、村田義文、田中千香子

NMR Determination of Crystallinity of poly(ε-L-lysine)

Atsushi Asano, Yoshifumi Murata, Takuzo Kurotsu
Department of Applied Chemistry, National Defense Academy, Japan
e-mail: asanoa@nda.ac.jp, TEL: 046-841-3810, ex.3596

Crystallinity of poly(e-L-lysine) (ε-PL) was estimated by analyzing the differences in the ^{1}H spin-spin relaxation times (^{1}H-T_2), the ^{13}C spin-lattice relaxation times (^{13}C-T_1), and the ^{13}C NMR signal shapes between the crystalline and the non-crystalline phases. The observed ^{1}H relaxation curve showed the sum of Gaussian and exponential decays. Similarly, the observed ^{13}C relaxation curves were double exponential. The ^{13}C NMR spectrum of ε-PL was divided into the narrow and the broad lines by utilizing the intrinsic differences in the ^{1}H spin-lattice relaxation time in the rotating-frame between them, which are attributed to the crystalline and the non-crystalline phases, respectively. Even though the crystallinity is obtained from the identical NMR measurements, the estimated values are different with each other. The crystallinity estimated from the ^{1}H-T_2 differences was 75.8 ± 0.1 % at 60 °C and 60.7 ± 0.4 % at 80 °C. From the ^{13}C-T_1 differences, the value was estimated to be 62 ± 11%. Furthermore, the value estimated from the NMR signal separation was 54 ± 5%. In this study we have explained these discrepancies by the difference in susceptibility among the experiments for the inter-phase, which exists in-between the crystalline and the amorphous phases.

【はじめに】結晶化度は結晶性ポリマーの物性を左右する重要なパラメータの一つである。しかし、測定方法によりその値が異なることも良く知られている。例えば、レーヨンはX線法からは約40%と算出されるが、密度法では約30%、ヨウ素吸着法では約50%と値が異なる[1]。NMR法は、結晶化度やハードセグメントなどの定量に有効であり、結晶／非晶、ハード／ソフトなどの比率の算出によく用いられている。NMR法では、このような相構造の違いを、構成しているドメインの運動性の違いとして、あるいは構造の秩序性の違いとして評価することで比率を算出することが可能である。運動性の違いは、緩和時間の違いとして捉えることが可能である。また、秩序性の違いは、スペクトルに現れるピークの線幅の違いや化学シフト値の違いとして捉えられる。しかし、運動性と構造の秩序性が必ずしも１：１で対応しているわけではないため、同じNMR法から得ているにもかかわらず、得られる結晶化度の値が異なる場合が存在する。特に高分子の場合、結晶と非晶の間に存在する中間相の運動性と秩序性が一致せず、求められた結晶化度の値が異なることがある。この違いを結晶化度が高く高融点のポリε-L-リジンを用いて、^{1}H-T_2と^{13}C-T_1、さらにスペクトルのピーク分離から得られた値を比較し、検証した。

Keywords：結晶化度, poly(ε-L-lysine), 固体^{13}C NMR, ^{13}C-T_1, ^{1}H-T_2, スペクトルの分離

著者ふりがな：あさのあつし、むらたよしふみ、たなかちかこ

【結果と考察】図１は、^{1}H核の共鳴周波数が25MHzのパルスNMR装置（JEOL MU25）を用いて、ソリッドエコー法から得られたpoly(ε-L-lysine)(ε-PL)の実測のFIDである。測定温度は80℃である。観測されたFIDは、１種類のガウス関数と２種類の指数関数で表され、3成分に分類される。ガウス関数成分は結晶相由来であり、その割合は約61%である。また中間相は約21%、非晶相が約18%と算出される。しかし測定温度を60℃に変更すると観測されるFIDは1種類のガウス関数と1種類の指数関数の和となり、その成分はそれぞれ76%、24%となる。室温においても同様である。 60℃と80℃で結晶相の割合と非晶相の割合が一致しないという結果は、ε-PLの融点が約170℃であり、ガラス転移点も約50℃近傍であることを考慮すれば、運動性の割合と相の割合が一致していないことを示している。一方、室温で測定した^{13}C-T_1の緩和曲線は2種類の指数関数の和として観測される。緩和時間の遅い成分は主に結晶成分由来であり、その比率は約62%となる。この観測結果は以前^{13}C-T_1から得られた63%という値[2]と良く一致している。これら一連の緩和時間の観測結果は、ε-PL が結晶相、非晶相、中間相からなるが、緩和時間の違いから明確に中間相を区別することが困難であることを示している。^{1}H-T_2の測定結果をみると、80℃での中間相の割合が非晶成分を上回っている。60℃では中間相の成分が観測されず、その結晶成分が80℃で観測された中間成分の割合だけ増えている。このことは、室温からガラス転移点までは、中間相の運動性が結晶成分に匹敵していることを示す。運動性は温度に依存しているため、 緩和時間から結晶化度を算出する際には注意が必要である。特に融点の高いサンプルの場合、室温近傍の温度では運動が遅いため、中間相が結晶相の運動と同程度の周波数成分を持ち、算出される値が異なってしまう。そこで、構造の秩序性が反映される^{13}Cスペクトルの個々のピークを分離して結晶化度を算出した。図２にはスペクトルの分離を示したが、ここで求められた値は約54%となった。^{13}C-T_1から求めた値と比べると10%程度の差がある。これはスペクトルに反映されたシャープな信号が結晶相のみを反映し、ブロードな信号が中間相と非晶相の秩序が乱れた成分を反映するからである。

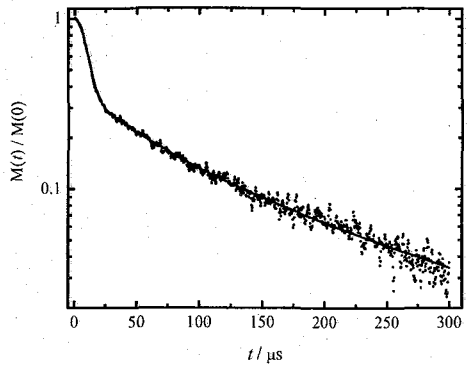

Figure 1. Observed and normalized free induction decay by the solid-echo pulse sequence with the period of 12 μs between two π/2 pulses at 80 °C. The horizontal shows the echo time. The decay is least square fitted by a Gaussian – exponential – exponential curve with the individual relaxation time.

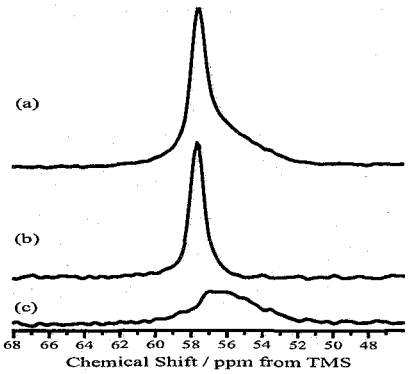

Figure 2. Expanded ^{13}C CPMAS NMR spectrum at the $C_\alpha H$ region: (a) whole spectrum, (b) the separated signal into the crystalline phase, and c) into the non-crystalline phase.

[1] 土田英俊、 “高分子の科学” 、培風館、p.43-44, 1975.
[2] S. Maeda et al., *J. Mol. Struc.*, **655**, 149 (2003).

1 LJ5

^{129}Xe NMR 法によるガラス状高分子の微細高次構造評価

名工大院・工　○浅野朋子, 吉水広明, 辻田義治

Structural Evaluation of Glassy Polymer by means of ^{129}Xe NMR

Graduate School of Engineering, Nagoya Institute of Technology
○Asano Tomoko, Hiroaki Yoshimizu, Yoshiharu Tujita

In this study, the ^{129}Xe NMR spectra of ^{129}Xe in the glassy polymers under various pressures of Xe are observed in order to find out what is reflected in ^{129}Xe NMR signals. The relationships among the ^{129}Xe NMR chemical shifts, the Xe sorption properties, and ^{129}Xe NMR linewidth were investigated. ^{129}Xe NMR chemical shifts and ^{129}Xe NMR linewidth are follow the Dual-mode sorption model, and they can be separated Henry and Langmuir sites. Linewidth of Henry site is narrower than that of Lngmuir site. ^{129}Xe NMR linewidth of glassy polymers decrease with increasing pressure, and that is with the Xe fraction of Henry site to sorption amounts is increasing. The estimation of the both sites of NMR signals can provide detailed structure of glassy polymers.

[目的] 近年, プローブとして Xe を用いる ^{129}Xe NMR 法は高分子の構造及び物性を評価する効果的方法として注目されている. これまでに, Xe を試料内に存在させ, 観測される NMR シグナルからミクロボイドサイズ及び数の評価を行ってきたが, NMR ピーク線幅は運動性及びミクロボイド分布の双方を反映すると解釈され, 定性, 定量的にガラス状高分子の構造と結びつけるのは困難と考えてきた. 本研究は ^{129}Xe NMR 法によって得られる様々なデータから解析可能なガラス状高分子の構造を明らかにする目的で行った.

[実験] Xe は名古屋興産(株)社製のものを用いた. サンプルには PPO, PS, PVC を用いた. 試料膜は全て溶液キャスト法により調製した. Xe 収着測定は CAHN 社製精密電子天秤(CAHN-2000)を用い, 重量法により行った. ^{129}Xe NMR 測定は Varian 社製 Unity 400 plus NMR 分光計を用いて行った. 各サンプルを外径 10mm の耐圧ガラス製(シィアイテクノ(株)社製)の NMR 管に約 0.5g 充填した後, 十分乾燥してから所定の圧力に相当する Xe を導入した. Xe 導入後少なくとも 24 時間放置した後に, 観測周波数 110.5MHz にてシングルパルス法で測定した.

キーワード : ^{129}Xe NMR, ミクロボイド, Xe 収着測定, ガラス状高分子

○あさのともこ, よしみずひろあき, つじたよしはる

[結果と考察] Xe 収着測定を行ったところ，各サンプルともガラス状高分子に特有な二元収着型の収着等温曲線を示した．最小二乗法を適応して二元収着パラメータを算出し，更に Henry，及び Langmuir サイトの相対収着量を算出した．

次に各サンプルに種々の圧力で Xe を収着させて ^{129}Xe NMR 測定を行った．NMR 化学シフト値は Xe 収着量の増加に伴い低磁場シフトした．化学シフト値を Xe 収着量に対してプロットしたところ，非線形的なシフトを示した．これに加え，得られた ^{129}Xe NMR スペクトルが対称性の良い単一のピークを示したことから，Xe 原子は Henry サイトと Langmuir サイト間を，NMR 観測タイムスケールにおいて速い速度で交換していると言える．そのため Fast Exchange モデルの適応により，Henry 及び Langmuir サイトの化学シフトを見積もることが可能である．

Figure 1 に ^{129}Xe NMR スペクトル線幅(半値幅)を Xe 圧力に対してプロットした．Henry，Langmuir 両サイトの相対収着量及び予測線幅から見積もった線幅(Table 1)も同時に示す．ガラス状高分子はゴム状高分子と異なり Xe 圧力増加に伴い線幅が顕著に先鋭化する．Henry，Langmuir 両サイトの線幅を比較すると，Henry サイトの線幅の方が狭く，Henry サイトに収着した Xe 分率の増加により線幅の先鋭化が説明可能と言える．これまでの研究によってゴム状高分子の線幅は，Xe 原子の運動性だけではなく，高分子鎖セグメントのミクロブラウン運動を反映しているとの知見が得られた．ガラス状高分子における Henry サイトの線幅も Xe の運動性，即ち拡散性を反映していると考えられる．これより Xe のガラス状高分子中の拡散性は高分子の局所分子運動にも影響を受けていると言える．また Langmuir サイトの線幅は，ミクロボイドサイズ及び分布を反映していると考えられる．PVC はガスバリア性高分子であり，非常に低い拡散性を示す．これは Henry 及び Langmuir サイトの線幅がブロードであることからも示唆される．また非常に低い拡散性は Henry サイトの運動性の低さよりも，個々のミクロボイドサイズの小ささがより大きく影響していると考えられる．

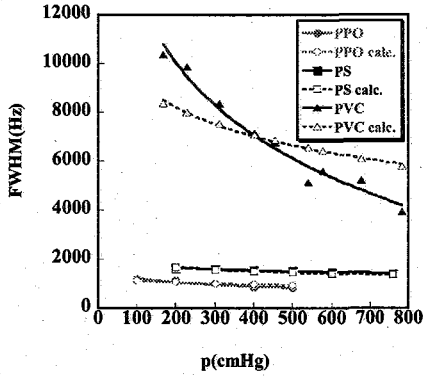

Figure 1 ^{129}Xe NMR peak width of ^{129}Xe in samples plotted against pressure of Xe.

	d_H [Å]	C_H' [cm^{3}STP/cm^3$_{polym}$]	Langmuir site Linewidth [Hz]	Henry site Linewidth [Hz]
PPO	6.55	30.9	1300	500
PS	5.12	28.4	3300	900
PVC	4.52	26.3	10400	1000

Table 1 Calculated linewidth of Henry and Langmuir sites, C_H', and microvoid size

以上より，^{129}Xe NMR 化学シフト及び線幅はともに二元収着モデルに従うと示唆され，各サイトの値よりガラス状高分子の微細高次構造の評価が可能と言える．

1 LJ6

固体ＮＭＲを用いたステアリン酸アルミニウムの構造研究

東京工業大学・院・理工　○黒木重樹

Structural Investigation of Aluminum Stearates using Solid State NMR

Department of Chemistry and Materials Science, Tokyo Institute of Technology
Shigeki Kuroki

Aluminium Stearate is one of the metal soap which used as a lubricant in the production of polyamides and thermosetting plastics. It is used as a thickening agent in the production of varnishes and lacquers. It is also used as a water repellent agent and hydrophobic agent. There exist three kinds of aliminium strearate such as mono($Al(C_{17}H_{35}COO)(OH)_2$), di($Al(C_{17}H_{35}COO)_2(OH)$) and tri($Al(C_{17}H_{35}COO)_3$). Until now the crystal structure of these compounds has never exactly determined. In this study, the crystal structure of these three aliminium strearates is discussed by ^{27}Al MAS, MQMAS and ^{13}C CP/MAS NMR spectroscopies. The similarity of the ^{27}Al MAS spectra of these three compounds shows that the molecules pack in the same manner in crystalline phase.

[緒言] 一般に長鎖脂肪酸やナフテル酸、ロジン酸などの有機酸の金属塩を総称して“せっけん”と言うが、金属せっけんとはこのような金属塩のうちアルカリ金属以外の金属塩を言う。アルカリ金属せっけんは普通、アルカリせっけんまたは単にせっけんと呼ばれているが、それと金属せっけんの大きな違いは、アルカリせっけんが水に溶解しやすいのに対し、金属せっけんは一般に水に不溶である点である。金属せっけんはアルカリせっけん同様、極性—無極性からなる分子構造を有することにより、今日においてはプラスチック、顔料、セメント、金属加工、潤滑油、医薬、化粧品などの様々な分野で、潤滑剤、分散剤、撥水剤、離型剤、乾燥剤、触媒安定剤、殺菌剤などとして不可欠の存在となっている。

金属せっけんの結晶構造は、粉末Ｘ線回折法により解明が行われてきた。その結果、長鎖脂肪酸の金属せっけんはその脂肪酸と類似の回折像を示し、層状構造をとっていることが明らかになっている。しかし、アルカリせっけん同様、変態があることが知られており、その詳細な結晶構造に関しては単結晶を用いたＸ線回折の研究がほとんどなされていないため、解明されていない。

本研究で取り扱うアルミニウムせっけんには理論的に $AlOOCR(OH)_2$（モノソープ）、$Al(OOCR)_2OH$（ジソープ）、$Al(OOCR)_3$（トリソープ）（Ｒはアルキル基）の３つの構造物が可能であり、工業製品はこれらの混合物である。

そこで本研究では、代表的なアルミニウムせっけん、ステアリン酸（$C_{17}H_{35}COO-$）アルミニウムを研究対象とし、固体 ^{27}Al および ^{13}CNMR スペクトルからモノ、ジ、およびトリの３つのステアリン酸アルミニウムの結晶構造に関する議論を行った。

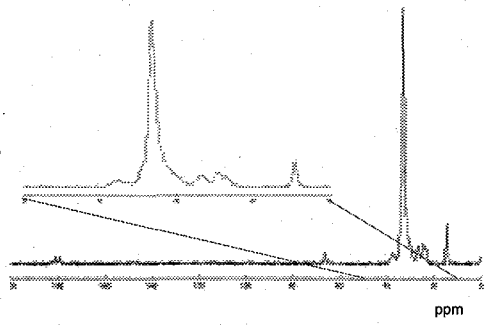

Fig.1 150.9 MHz ^{13}C CP/MAS spectrum of Aluminium distearate at room temperature.

Aluminum Stearates / Crystal Structure / ^{27}Al MQ-MAS / ^{13}C CP-MAS

くろき　しげき

[実験]今回用いた試料は、モノおよびジステアリン酸アルミニウムは和光純薬から、トリジステアリン酸アルミニウムは関東化学から購入した。NMR スペクトルは CP/MAS プローブの付属した BrukerBiospin 社 DSX300 および Av600 を用い測定を行った。

[結果と考察]まず、Fig.1 に室温におけるアルミニウムジステアレートの ^{13}CCP/MAS スペクトルを示す。他のモノ、トリのスペクトルもほぼ同じスペクトルを示した。カルボニル炭素の領域に 181.2 と 179.4ppm の 2 本の信号が観測されている。このうち、181.2ppm はステアリン酸のカルボキシル基の化学シフトとほぼ一致するので、遊離ステアリン酸に帰属した。179.4ppm の信号はアルミニウムと結合したカルボニル基に帰属できる。一方、長鎖アルキル基のメインの CH_2 基は 33.3ppm に現れ、長鎖アルキル基が三斜晶または単斜晶のパッキングをしていることがわかる。先ほど述べたようにモノ、トリも同様のパッキングをしている。50℃以上での測定では、長鎖アルキル基のメイン CH_2 基は 32.7ppm に現れ、長鎖アルキル基が斜方晶のパッキングに変化したとがわかる。

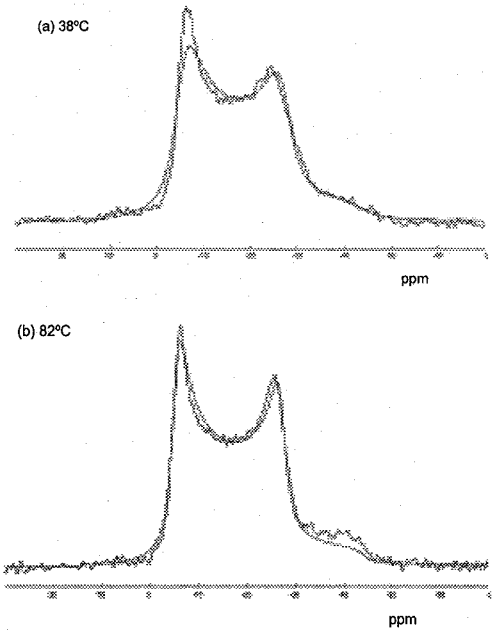

Fig.2 156.4 MHz ^{27}Al MAS spectrum of Aluminium distearate at 38 (a) and 82 (b) °C.

Fig.2 に 38℃および 82℃におけるアルミニウムジステアレートの ^{27}Al MAS スペクトルを示す。他のモノ、トリにおいてもほぼ同様なスペクトルが得られ、分子のパッキングの仕方が同様であることを示している。

スペクトルシミュレーションの結果、38℃において、化学シフトδ=1.0 ppm、核四極子結合定数 C_Q=8.57MHz、電場勾配非対称パラメータη=0.09、82℃ではδ=0.9 ppm、C_Q=8.58MHz、η=0.05 であった。温度変化によってほとんどスペクトルの変化は見られないが、電場勾配の軸対称性がよくなり、理論と実測スペクトルの一致がよくなっている。これは、分子のある任意の軸に関する対称性が上がっていることを意味する。

Fig.3 に 38℃におけるアルミニウムジおよびトリステアレートの ^{27}Al MQMAS スペクトルを示す。1DMAS スペクトルでは同様のスペクトルを示したが、MQMAS スペクトルからトリステアレートのほうには 1 つ以上の Al サイトの存在が明らかになった。

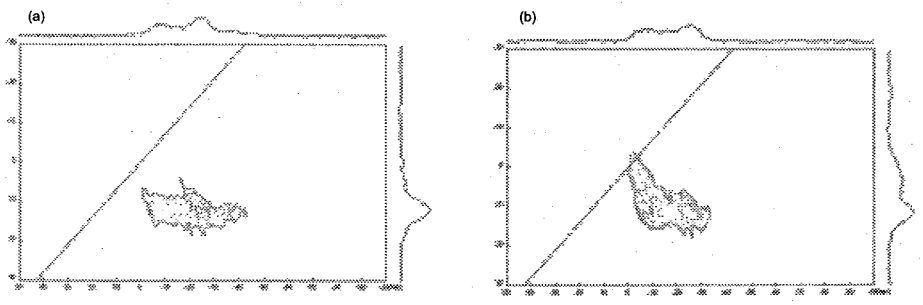

Fig.3 ^{27}Al MQMAS spectra of Aluminium distearate (a) and Aluminium tristearate (b)at 38°C.

1 LJ7

強磁場(21.8T)固体二次元交換NMRによるメソポーラスなBCNの構造解析

(物質・材料研究機構[1], 京大・理[2])
○村上美和[1], 清水禎[1], 丹所正孝[1], Vinu Ajayan[1], 有賀克彦[1], 森利之[1], 竹腰清乃理[2]

Structural Analysis of Mesoporous BCN Using Two-dimensional Exchange NMR in Solids at High Magnetic Field of 21.8 T

[1]National Institute for Materials Science
[2]Graduate School of Science, Kyoto University
M.Murakami[1], T.Shimizu[1], M.Tansho[1], A.Vinu[1], K.Ariga[1], T.Mori[1], K.Takegoshi[2]

Microstructures of mesoporous BCN and mesoporous BN have been examined by using two-dimensional ^{11}B-^{11}B exchange NMR at 21.8 T, which suggests a "pillar and wall" structure for mesoporous BCN, while a wall-only structure for mesoporous BN.

【序】近年、900MHz級NMRマグネットが実用化され、ライフサイエンス分野のみならず、固体材料の解析にも適用されつつある。本研究では、触媒活性や分子ふるい等の用途が期待される、新規に合成したメソポーラスな炭窒化ホウ素(MBCN)および窒化ホウ素(MBN)について21.8 Tの強磁場固体NMRを用いて構造解析を検討した。

【実験】MBNおよびMBCNは既報[1]に従い合成した。^{11}B MAS NMR測定には、JEOL社製ECA930分光器(21.8 T)およびECA500分光器(11.7 T)を用いた。^{11}B-^{11}B二次元交換スペクトルの測定にはNOESYと同様の3パルス法を使用し、各パルス幅は2.0μsで測定した。

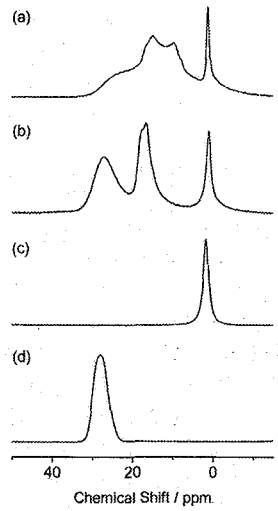

Figure 1. ^{11}B MAS NMR spectra in powdered MBCN (a) and (b), cBN (c), and hBN (d); (a) observed at 11.7 T, while (b)–(d) at 21.8 T.

【結果と考察】11.7 Tの静磁場下で、MBCNの^{11}B MAS NMRを測定した場合には、四極子相互作用の影響により、シグナルの分離が不十分であったが、21.8 Tの静磁場下で測定した場合には、図1に示すように、良好に分離した3つのシグナルを観測できた。

---

mesoporous material, BCN,Two-dimensional Exchange NMR, High Magnetic Field

むらかみみわ、しみずただし、たんしょまさたか、ヴィヌアジャヤン、ありがかつとし、もりとしゆき、たけごしきよのり

これらのうち、0.94 ppmと27.2 ppmのピークは立方晶窒化ホウ素(cBN)および六方晶窒化ホウ素(hBN)との比較より各々窒素４配位ホウ素、窒素３配位ホウ素に相当すると考えた。16.6 ppmのピークについては、元素分析の結果から炭素を含むBN構造ではないかと考えている[2]。ここでは、このホウ素を含炭素BNと書く。

図２に２D交換スペクトルを示す。交換時間 0.01 秒では対角ピークしか観測されなかったが(図 2(a))、0.5 秒では、0.94 ppmと 16.6 ppmのピークの間にクロスピークが観測された（図 2(b)）。さらに交換時間を１秒まで伸ばしても、新たなクロスピークは観測されなかった。そこで、MAS 速度をこれまでの 16 kHz から 10 kHz に落として測定したところ、交換時間１秒で、27.2 ppm のピークと他のピークの間に新たなクロスピークが観測された(図 2(c))。クロスピークの強度がMAS速度に依存していることから、磁化移動は ^{11}B-^{11}B 双極子相互作用に起因するものと考えられる。従って、図 2(b)は、0.94 ppm の窒素４配位ホウ素と含炭素 BN は３配位ホウ素に比べて近い位置にあることを示している。３、４配位ホウ素の構造を考えると、メソポーラス BCN は４配位ホウ素と含炭素 BN からなる立体的な構造のドメインが３配位ホウ素による平面的な構造をもったドメインとつながった構造になっていると思われる。我々はこの構造を"pillar and wall" 構造と名づけ、メソポーラシティとの関係を検討している。より高温で合成された MBN では"pillar"に対応するピークが小さく、その構造は、ほぼ"wall"だけの構造と考えられる。これらの結果は現在投稿中である[3]。

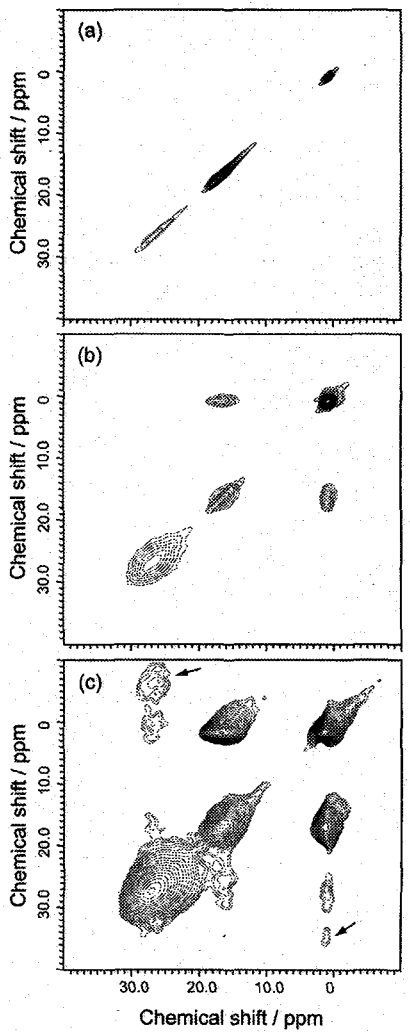

Figure 2. ^{11}B-^{11}B 2D exchange spectra of MBCN at mixing time of 10 ms (a), 500 ms (b), and 1 s (c). The MAS frequencies were 16 kHz for (a) and (b), and 10 kHz for (c). The two peaks marked with arrows are spinning side bands.

[1] A. Vinu et al., *Chem. Mater., 17*, 5887-5890 (2005).
[2] M. Murakami et al., *Chem. Lett., 35*, 986-987 (2006).
[3] M. Murakami et al., to be submitted.

1 LJ8

アンフォテリシンBが脂質膜中で形成する複合体の構造解析：フッ素原子の導入と REDOR 法の利用

（阪大院理）○葛西祐介・松森信明・土川博史・梅川雄一・大石徹・村田道雄

Membrane Permeabilizing Assembly of Amphotericin B - REDOR Experiments for Fluorine-labeled Antibiotics and Sterols

Yusuke Kasai, Nobuaki Matsumori, Hiroshi Tsuchikawa, Yuichi Umegawa, Tohru Oishi, Michio Murata

Department of Chemistry, Graduate School of Science, Osaka University, 1-16 Machikaneyama, Toyonaka, Osaka 560-0043, Japan

Amphotericin B (**1**, AmB), a polyene macrolide antibiotic, is still the drug of choice for treatment of systemic fungal infections. Its antifungal action is presumed to be formation of a barrel-stave type ion-permeable channel across lipid bilayers. However, no experimental evidence has been obtained for the information of this molecular assemblage due to a lack of appropriate methodology. We applied solid state NMR methodology, rotational echo double resonance (REDOR), to investigate the structure of the membrane permeabilizing assembly. ^{19}F-labeled AmB and sterols were synthetically prepared, and uniformly ^{13}C-labeled AmB was produced biosynthetically. Solid state NMR experiments of the labeled antibiotics and sterols in DMPC membrane showed significant REDOR dephasing, indicating the close vicinity of AmB/AmB and AmB/sterol in membrane.

アンフォテリシンB (**1**, AmB) は放線菌 *Streptomyces nodosus* より単離された抗生物質であり、強力な抗真菌活性と耐性菌のできにくい性質から、発見以来 50 年近く経た現在も医薬用抗真菌剤として重要である[1]。一方で腎毒性などの副作用が問題となっており、その軽減に向けた研究開発が活発になされている。AmB は疎水性のポリエン領域と親水性のポリオール領域を有する両親媒性化合物であり、細胞膜中でステロールと共に会合して樽板タイプのイオン透過性チャネルを形成して活性を発現すると言われている (Figure 1b)[2]。しかし長年の膨大な研究にもかかわらず、会合体の構造やステロールの役割などは推測の域を出ていない。

近年、固体 NMR は膜タンパクや膜結合ペプチドの構造解析に広く用いられているが、AmB 複合体の解析にも適用可能であると考えた。特に REDOR (rotational echo double resonance) 法[3]は異種原子核間の距離を与えるため、会合体形成の基盤となる二分子間相互作用の解析に適している。標識原子として、約 10 Å までの距離測定が可能な ^{13}C-^{19}F を選択し、Figure 1 に示したフッ素標識体を合成化学的手法により[4-6]、

amphotericin B, REDOR, isotope label, ion channel, self-assembly
かさいゆうすけ・まつもりのぶあき・つちかわひろし・うめがわゆういち・おおいしとおる・むらたみちお

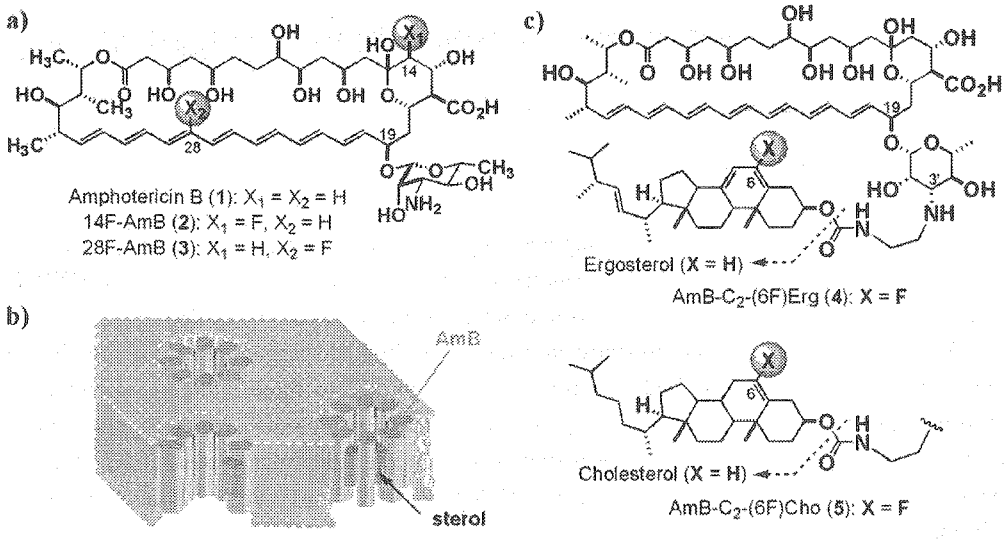

Figure 1. a) Structures of amphotericin B (AmB) and its fluorine-labeled entities. b) Barrel-stave model for AmB in phospholipid membrane. c) Structures of AmB-fluorosterol covalent conjugates.

全 ^{13}C 標識化 ([U-^{13}C]) AmB (標識率 50%) を生合成的手法により調製した。AmB/ステロール相互作用解析では、[U-^{13}C]AmB とフッ化ステロールを共有結合で連結することで、分子間相互作用の安定化を図った[6]。DMPC 膜中での連結体 **4** および **5** の $^{13}C\{^{19}F\}$RDX 測定[7]により、AmB のポリエン部に有意な REDOR 減衰を観測することに成功した。$\Delta S/S_0$ 値を通常の REDOR 理論式[8]に適用し、得られた距離情報を制限として分子力場計算を行った結果、AmB-ステロール間の疎水性相互作用を再現する配座が得られた (Figure 2)。このように、連結による相互作用の安定化および ^{13}C-^{19}F REDOR 測定による距離情報は、AmB 複合体の構造解析に有用であるのみならず、他の非ペプチド性物質に対しても適用可能な方法論であると考える。

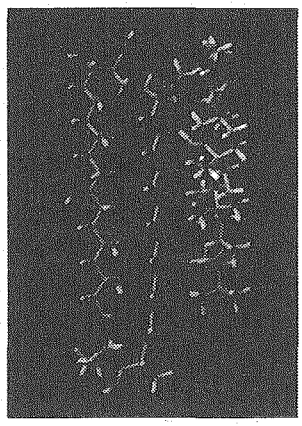

Figure 2. One of low-energy conformations for AmB-C_2-(6F)Erg **4** suitable for channel formation in a membrane.

発表時には AmB/AmB 相互作用解析として、フッ素化 AmB **3** と全炭素標識化 AmB の脂質膜中での固体 NMR 測定の結果も併せて報告する予定である。

ref. 1) Hartsel, S.; Bolard, J. *Trends Pharmacol. Sci.* **1996**, *17*, 445-449. 2) De Kruijff, K.; Demel, A. R. *Biochim. Biophys. Acta* **1974**, *339*, 57. 3) Gullion, T.; Schaefer, J. *J. Magn. Reson.* **1989**, *81*,196-200. 4) Matsumori, N. et al. *Bioorg. Med. Chem. Lett.* **2005**, *15*, 3565-3567. 5) Tsuchikawa, H. et al. *Tetrahedron Lett.* **2006**, *47*, 6187-6191. 6) Matsumori, N. et al. *Chem. Biol.* **2004**, *11*, 673. 7) Mehta, A. K.; Schaefer, J. *J. Magn. Reson.* **2003**, *163*, 188-191. 8) Mueller, K. T. *J. Magn. Reson. A* **1995**, *113*, 81.

1 LJ9

タンパク質が周辺の水の分極を制御することを実証するための水プロトンのケミカルシフトの測定

(福井大院工, ERATO-SORST[1], 東大院総合[2]), ○水野和子, 山村卓矢, 原田拓典[1], 黒田玲子[2]

Control of the polarization of surrounding water by a protein detected in terms of δ_{H2O}

(Dep. Appl. Chem. Biotech., Univ. of Fukui) K. Mizuno, T. Yamamura, (ERATO-SORST, JST) T. Harada, (Graduate School of Arts and Sciences, Univ. of Tokyo) R. Kuroda

We present a new paradigm to study an origin of folding and unfolding of proteins. In the paradigm, a protein is described to have a specific ability to modify the polarization of surrounding water by folding or unfolding as a controller of surrounding water. In this work to prove the paradigm, we carried out measurements of circular dichroism and chemical shift of water protons for β-amyloid (1-40) in Tris-HCl buffer solutions varying concentration of trifluoroethanol.

Introduction. We studied so far effects of alkyl alcohols and halogenoalcohols, e.g 2-chloroethanol, on conformation of proteins, and we found that these have much stronger denaturing abilities than corresponding alkyl alcohols. To interpret the origin of the folding, we have been studying the effects of organic solvents on the polarization of the water in aqueous binary mixtures, by measuring IR and NMR spectra of the solutions. We found that chemical shifts of water protons, δ_{H2O}, measured with the differences in the bulk volumetric magnetic susceptibilities corrected precisely could give a good measure of the polarization of the water in the solutions.[1] Thus, we studied the concentration dependences of δ_{H2O} in aqueous binary mixtures of various compounds. We observed that anomalous polarization of water occur in dilute concentrations of N-methylacetamide or dimethylsulfoxide, whereas the polarization of water molecules becomes much smaller than that of pure water in concentrated solutions of dimethylsulfoxide or 1,4-dioxane, as shown in Fig.1

We did not consider the effects of protein itself on the polarization of water in the solutions but those of only denaturing reagents, before we observed the great changes in the polarization of water. The curves in Fig. 1 suggest that proteins may have potential to modify the polarization of water molecules around it depending on the composition and sequence of the amino acids in it, because of various properties of their residues. From the investigation above, it is necessary for us to construct a new paradigm which involves the relationship between protein and water to explore the origin of folding and unfolding of proteins.

Outline of our paradigm. The outline of a new paradigm we present is described as follows; 1) The images of the water and the proteins for the paradigm ; water is a liquid the hydrogen(H)-bonding strength of which can be varied over much wider range than other

a new paradigm for protein and water, origin of folding, chemical shift of water protons

みずの かずこ, やまむら たくや, はらだ たくのり, くろだ れいこ

liquids, and proteins have their own specific potential to modify the (H)-bonding strength of surrounding water. 2) Perturbations in temperature, pressure, or species and composition of additives, etc., are propagated to a protein as the changes in the H-bonding strength of the bulk water in the solutions. 3) The protein receives the changes in the bulk water and responses by changing its conformation to counteract the changes in the H-bonding strength of the water around the protein according to Le Chatelier's Principle. 4) Folding and unfolding result in the changes in the H-bonding strength of the water, respectively, and the control of the H-bonding strength of the surrounding water is one of the most important functions of proteins.

Experiments and Methods.

CD spectra of β-amyloid (1-40) at 0.1mg/ml in Tris-HCl buffer solutions of pH 7.42 were recorded at room temperature varying concentration (v/v) of trifluoroethanol(TFE). Percentage of the helix and β-structure motifs estimated by the CONTIN/LL program[2] (base set 4) are plotted vs. the vol% of TFE in Fig.2. ^{1}H-chemical shifts of [Tris-HCl buffer solution + TFE] and [Tris-HCl buffer solution + TFE + β-amyloid (1-40)] were measured with external double reference method[1] at 23.0℃.

Results and Discussion

The chemical shift of water protons, δ_{H2O}, for [Tris-HCl buffer solution + TFE] are plotted as the differences from the value of δ_{H2O} for the buffer solution vs. vol% of TFE. Over the range of 5~25vol%, H-bonding property becomes stronger than that of the buffer solution, but it is weaker at 50vol%. The effect of protein on the H-bonding property of water is plotted as the changes in δ_{H2O} from the value for [Tris-HCl buffer solution + TFE] vs. vol% of TFE. Fig. 2 shows that the protein plays roles so that the effect of TFE on δ_{H2O} may be counteracted following context of the paradigm .

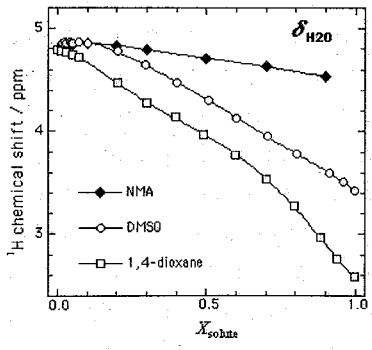

Fig.1 δ_{H2O} for the water in aqueous binary mixtures of N-methylacetamide, dimethyl sulfoxide, and 1,4-dioxane at 25.0℃

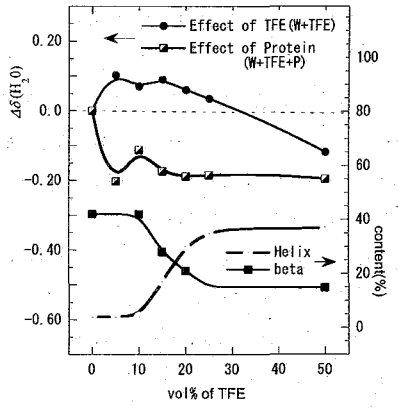

Fig.2 Effects of TFE and the protein on the δ_{H2O} sulfoxide, and 1,4-dioxane at 25.0℃

1. Mizuno, K; Tamiya, Y.; Mekata, M. *Pure Appl. Chem.* **2004,** *76,* 105.
2. Sreerama, N.; Woody, R. W. *Anal. Biochemistry,* **2000,** *287,* 252.

1 LJ10

Metabolomic approach of plant cellular chemical biology by flow probe system

Miho Izumikawa[1], Takashi Hirayama[2,3], Kazuo Shinozaki[1,3], and Jun Kikuchi[1,4]
[1]RIKEN Plant Science Center, Yokohama, Japan、[2]Int. Grad. Sch. of Arts and Sci., Yokohama City Univ., Yokohama, Japan、[3]Plant Mol. Biol. Lab., RIKEN, Tsukuba, Japan、[4]Grad. Sch. Bioagri. Sci., Nagoya Univ., Nagoya, Japan

Metabolomics uses a combination of data-rich analytical chemical methods such as nuclear magnetic resonance spectroscopy and mass spectrometry together with chemometrics for profiling metabolism and interpreting metabolic fingerprints in complex biological systems. The methods have been applied in many areas of relevance to pharmaceutical research and development. Comprehensive analysis of the metabolome can contribute to mechanism of action studies for small molecules discovered in phenotypic screens. This rapidly developing field of metabolic profiling includes the use of NMR in gene function analysis and the identification of metabolic pathways (1,2). Recently a general protocol for using comparative NMR metabolomics data to infer in vivo efficacy, specificity and toxicity of chemical leads within a drug discovery program has been described (3). Plant metabolites are characterized by an enormous chemical diversity, every plant having its own complex set of metabolites. This variety poses analytical challenges, both for profiling multiple metabolites in parallel and for the quantitative analysis of selected metabolites. Spectacular advances in plant metabolomics offer new possibilities, together with the aid of systems biology, to explore the extraordinary complexity of the plant biochemical capacity (4). One element of classical systems analysis treats a system as a black or gray box, the inner structure and behavior of which can be analyzed and modeled by varying an internal or external condition, probing it from outside and studying the effect of the variation on the external observables. The result is an understanding of the inner make-up and workings of the system. The equivalent of this in biology is to observe what a cell or system excretes under controlled conditions-the 'metabolic footprint' or exometabolome - as this is readily and accurately measurable (5,6).

key word : cellular chemical biology, plant metabolism, metabolic profiling, chemical response, flow probe

The focus of this presentation concerns the use of NMR spectroscopy for metabolic analyses and, in particular, its use in pharmacology/toxicology for examining the metabolic profile of plant cells. Plant cells are very sensitive to various external chemical stimuli, selected from plant primary metabolites, the impact stress conditions on the plant metabolome appeared in phenotype. In addition, NMR experiments exhibit invisible metabolic phenotype. We monitored the metabolic profile of two types of plant cell system by ^{1}H and multi-dimensional NMR techniques.

Arabidopsis T87 cell line and cyanobacteria *Synechocystis* sp. PCC6803 were selected as model plant cell system, the chemical responses on their metabolism against ~400 compounds including plant primary metabolites were visually observed and analyzed by 1D-^{1}H NMR. Since the NMR-based approach has the advantage of comparison of different samples, spectral subtractions between various chemical stimuli were collected to estimate the metabolic influences among those chemicals. We developed Z-matrix analysis to classify enormous 1D spectra and to pull out remarkable signals, Z-matrix means the difference between an intensity and its average divided by a standard deviation. In *Arabidopsis* T87 cells, 20 chemicals showed high Z-matrix (over 8) from among 218 chemicals, on the other hand, in *Synechocystis* sp. PCC6803, it was 9 among 244 chemicals. These chemicals were not quite corresponded (Figure 1).

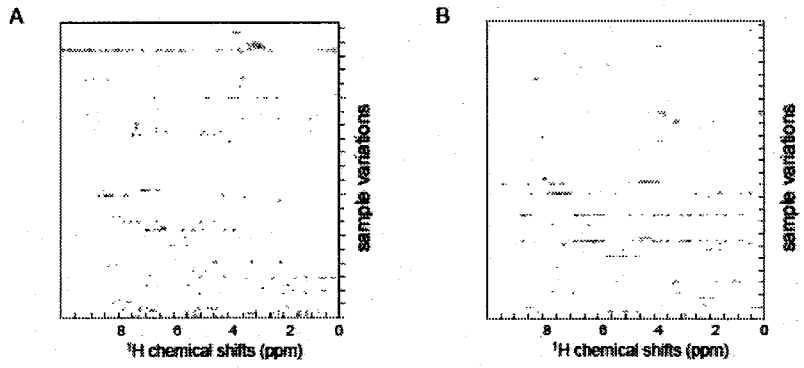

Figure 1 : Z-matrix analysis of ^{1}H-NMJR spectra responded with over 200 chemical stimulus. A; *Arabidopsis* T87. B; *Synechocystis* sp. PCC6803. The bin width was set to 0.05ppm, and the data were estimated and graphs were drawn by using Microsoft Excel. Z-matrix with over 6 and under –6 were highlighted.

Interestingly, in *Arabidopsis* T87, 13 among 20 chemicas caused visible phenotype changes, but in *Synechocystis* sp. PCC6803, 7 among 9 chemicals were silent. This result reflects that plant cell is more sensitive to external stimuli than bacteria.

As shown in Figure2, invisible metabolic changes are appeared to 1D-^{1}H NMR spectra, but to know the details about chemical responses on metabolism, multi-dimensional NMR analyses are required. Most of the main metabolites in plant cells are labeled from uniformly ^{13}C-labeled glucose, they show us qualitative and quantitative chemical responses in metabolism on ^{1}H-^{13}C HSQC spectra.

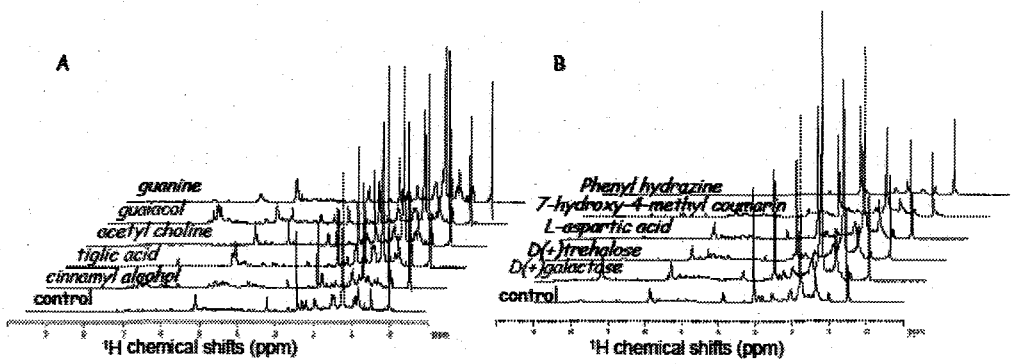

Figure 2 : 1D-^{1}H NMR spectra. A; *Arabidopsis* T87. B; *Synechocystis* sp. PCC6803. Italics are sources of chemical stimulus.

The chemical stimulated cells were cultured with ^{13}C-labeled glucose, after 4-5 days incubation, the cells were collected and extracted with HFA-HEPES buffer. The extracts were measured by HSQC experiment, the remarkable signal intensities were summarized in Figure 3. In the case of galactose, some amino acids, sugars, organic acids, in spite of that they are main primary metabolites, showed higher intensities than a control.

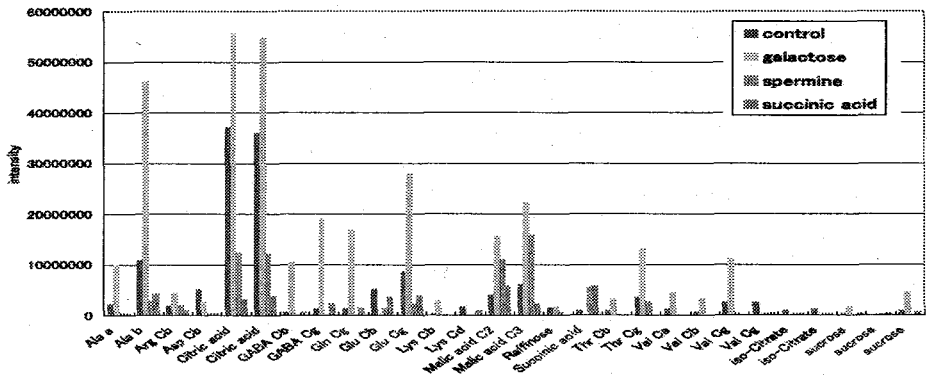

Figure 3 : The signal intensities of characteristic metabolites on HSQC analysis. HSQC experiments were carried out on Bruker DRX-500, DRU-700, and the signals were assigned by using the program SpinAssign (Chikayama *et al.*). These chemicals caused visible phenotype changes on *Arabidopsis* T87.

In addition, since cyanobacteria excretes the metabolites out of the cell, the external components were analyzed by using a flow probe. We will present a chemical screening system and the results, also a new methodology to pursue the time course metabolism following chemical stimuli by using a flow probe system.

References

1 Lindon, J. C.; Holmes, E.; Nicholson, J. K. *Curr. Opin. Mol. Therap.* **2004**, *6*, 265-272.

2 Harrigan, G. G.; Brackett, D. J.; Boros, L. G. *Mini-Rev. Med. Chem.* **2005**, *5*, 13-20.

3 Forgue, P.; Halouska, S.; Werth, M.; Xu, K. M.; Harris, S.; Powers, R. *J. Proteome Res.* **2006**, *5*, 1916-1923.

4 Oksman-Caldentey, K. M.; Saito, K. *Curr. Opin. Biotech.* **2005**, *16*, 174-179.

5 Kell, D. B.; Brown, M.; Davey, H. M.; Dunn, W. B.; Spasic, I.; Oliver, S. G. *Nat. Rev. Microbiol.* **2005**, *3*, 557-565.

6 Villas-Boas, S. G.; Noel, S.; Lane, G. A.; Attwood, G.; Cookson, A. *Anal. Biochem.* **2006**, *349*, 297-305.

Thursday, November 23

English Session

SAILing to the Future

Toward the next-generation world de facto standard in protein NMR spectroscopy

Masatsune Kainosho

CREST/JST & Tokyo Metropolitan University/Nagoya University

NMR spectroscopy can determine the three-dimensional structure of proteins in solution. Nevertheless, its potential has been limited by the difficulty of interpreting NMR spectra in the presence of broadened and overlapped resonance lines and low signal-to-noise ratios. We have developed stereo-array isotope labelling (SAIL) method that can overcome many of these problems by applying a complete stereo- and regiospecific pattern of stable isotopes, which is optimal with regard to the quality and information content of the resulting NMR spectra. SAIL utilizes exclusively chemically and enzymatically synthesized amino acids for cell-free protein expression. We demonstrate for a calicium binding protein calmodulin (17.2 kDa), E. coli peptidyl proryl cis-trans isomerase EPPIb (18.2 kDa), Streptomyces subtilisin inhibitor SSI (23 kDa as homo dimmer), Arabidopsis thaliana hypothetical protein At3g16450 (32kDa), and maltodextrin-binding protein MBP (41kDa) that the SAIL method offers sharpened lines, spectral simplification without loss of information, and the ability to rapidly collect the structural restraints required to solve a high-quality solution structure for proteins. Since the SAIL approach allows us to determine the protein structure twice as large as commonly solved by NMR and thus makes a large class of proteins newly accessible to detailed solution structure determination. We are also trying to extend the method to even larger, and more difficult systems, such as protein complexes or

proteins integrated in biological membranes. Some perspectives of the SAIL approach will also be given.

"Optimal isotope lebelling for NMR protein structure determinations", M. Kainosho *et al.*, *Nature*, **440**, 52-57(2006)

2 LE2

Mitsuhiko Ikura[a,b]

[a]*Division of Signaling Biology, Ontario Cancer Institute*
[b]*Department of Medical Biophysics, University of Toronto, Canada*

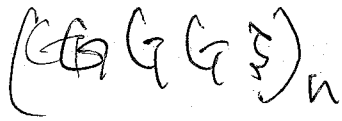

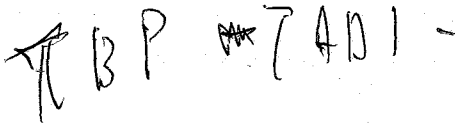

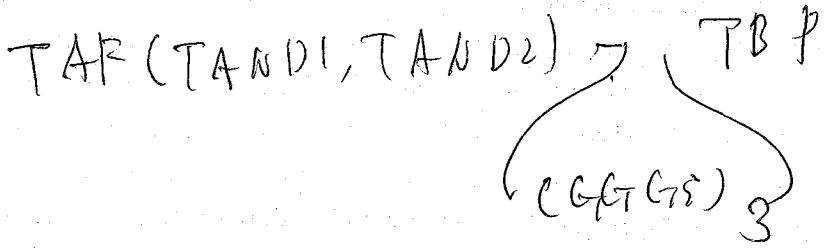

Structure and Function of the N-terminal Domains of the SUMO Ligase PIAS Family

Heisaburo Shindo

Tokyo University of Pharmacy and Life Science, National Institute of Agrobiological Sciences, and RIKEN Genomic Science Center

A small ubiquitin-like modifier, so-called SUMO, is a protein that is structurally similar to ubiquitin. Like ubiquitin, SUMO is covalently attached to certain lysine residues of specific target proteins, and such SUMO modification is called SUMOylation which occurs in common in the eukaryote kimgdom. In contrast to ubiquitination, however, sumolylation does not promote the degradation of proteins, but instead alters a number of different functions of proteins, depending upon the protein substrate in question. These functions include properties such as stabilization of target proteins, activation or suppression of various transcription factors, subcellular localization in nucleus, and maintenance of chromatin structure and so on.

Pathway of sumoylation is very similar to that of ubiquitination. That is, SUMO is initially linked to activation enzyme E1 in ATP-dependent manner, and then transferred to conjugation enzyme E2. Sumoylation of target proteins requires SUMO ligase E3 in the most cases, although SUMO ligases are not essential for cell growth. It may recognize both conjugate enzyme E2 and certain target proteins and serves as a catalyst for sumoylation whose mechanism is not well-understood. Thus, structural study of SUMO ligase E3 as well as its specific interaction with target proteins is important to understand SUMO modification processes in cells.

Three different types of SUMO ligases E3 have been reported. The first E3 group comprises a large protein family of PIAS which shares a common RING finger-like structure. A second type of SUMO E3 protein found in mammalians is RanBP2, which is part of the nuclear pore complex without sequence homology to the PIAS family. The third type of SUMO ligase Pc2 belongs to the polycomprotein family and stimulates sumoylation of the C-terminus binding protein, resulting in the recessive mode of chromatin. The PIAS family (also called Siz family in yeast and plants) is most extensively studied, which shares both RING and SAP domains, while Siz proteins in plants comprise another unique domain, PHD finger (plant homeodomain). The RING finger is described as recognition site for conjugate enzyme E2, whereas the N-terminal domains including SAP and PHD are not well characterized yet.

Keywords: SUMO ligase, PIAS and Siz, SAP domain, NMR structure, DNA binding

Here, I present the structures and intermolecular interactions of the N-terminal domains of SUMO ligases E3 from mammalian, yeast and rice. The followings will be discussed:

(1) Solution structures of the N-terminal domains of the PIAS/Siz family

We have previously determined the solution structure of the N-terminal domain of hsPIAS1, showing a unique 4-helix bundle, up-down-extended loop-down-up topology with a crossover of the loops connecting two helixes. As for the N-terminal domain Siz1(1-111), the structure is composed of five α-helixes and unstructured region (1-21) of Siz1. Topology of the first four α-helices are very much similar to that of hsPIAS1(1-65). As for the N-terminal domain of OsSiz1(1-104), the structure is very much similar to that of hsPIAS(1-65), although α-helices and loops are quite different in length.

(2) **DNA binding site identified by ^{15}N and ^{1}H chemical shift perturbations**

The N-terminal domains of both hsPIAS and ScSiz1 exhibit a binding ability to DNA. Although the individual residues strongly perturbed in chemical shift index are different between two, they are almost all located within the SAP motif in the N-terminal domain. It will be interesting to test auto-sumoylation of the N-terminal domains of PIAS proteins and to see if the sumoylation affects on DNA binding, if any.

(3) Interaction of the N-terminal domain with SUMO target proteins such as p53, lef-1 HMG box and c-jun as assessed by GST-pull down assay

Transcription factors such as tumor suppressor protein p53 and lymphoid enhance factor Lef-1 are known to be the substrates for SUMO modification. GST pull-down assay and Western blotting showed that the N-terminal domain hsPIAS1(1-65) can interact with both p53 and lef-1 HMG box.

(4) Characterization of the PHD finger (107-177) of OsSiz1

Very recent x-ray crystallographic and NMR studies on tumor suppressor ING2 and nucleosome remodeling factor NURF demonstrated that the PHD finger plays a role in the recognition of H3K4me3 histone code, and thus in chromatin regulation and signaling. It is very interesting to test whether or not the PHD finger of OsSiz has a binding capability to trimethylated lysines.

(5) Prosperity of NMR study on structural biology

Finally, I will address a few comments on the above matter, although it is the heavy theme for me to say something about.

Exploring Biological Supramolecular Systems by NMR

Hideo AKUTSU

Institute for Protein Research, Osaka University

To understand biological activities organized in order, investigations on biological supramolecular systems such as membrane proteins in membranes and a variety of energy conversion systems are important. However, the methodologies for structural analysis of supramolecular systems are still poor. Although X-ray crystallography is a powerful method, crystallization of membrane system, for example, is very difficult. While electron microscopy can handle membrane system directly, it also needs two-dimensional crystals for high-resolution analysis. High-resolution NMR is a powerful method to investigate biological molecules not only from structural point of view but also functional one. However, NMR has drawbacks on sensitivity and resolution. When I started my career in this field, NMR was used mainly for structure determination of simple organic molecules. The sensitivity and resolution of NMR were significantly improved in last three decades thanks to high field superconducting magnets and sophisticated pulse techniques. NMR is now becoming an important method for the investigations on biological supramolecular systems.

The size limit is a serious problem for solution NMR. The size limit is caused by the signal broadening due to rapid transverse relaxation in a slowly tumbling molecule and by the signal overlapping due to the huge number of resonating nuclear spins in a protein. The former has been improved by means of deuteration of the protein and innovative pulse techniques. Development of TROSY spectroscopy has contributed to a revolutionary improvement of the resolution of ^{1}H-^{15}N and ^{1}H-^{13}C (aromatic) correlation spectra. The combination of deuteration and TROSY raised the molecular mass limit to more than 50 kDa.

F_OF_1-ATP synthase is a multisubunit enzyme that catalyzes ATP synthesis in oxidative phosphorylation and photophosphorylation. H^+-ATP synthase is also know as a sophisticated molecular motor. This enzyme consists of two components, F_O and F_1. The simplest F_1 (F_1-ATPase) comprises five kinds of subunits with a stoichiometry of $\alpha_3\beta_3\gamma\delta\varepsilon$. The molecular mass is about 360 kDa. In the crystal structure of F_1 from bovine heart mitochondria (MF_1), the three catalytic sites are not equivalent. The β subunit in F_1 takes on the closed form in the presence of a bound nucleotide, while it takes on the open form in its absence. We have applied segmental isotope-labeling by intein splicing reaction to the β subunit of F_OF_1-ATP synthase, and have succeeded in obtaining the detailed information on the conformational change of the β subunit monomer (1-3). A new insight into the mechanism of the F_1 rotation and proton translocation across F_o has emerged through

application of NMR methodology to the subunits and subcomplexes. It was shown that a driving force of the F_1 rotation is the conformational change of the β subunit from thermophilic *Bacillus* PS3, which carries the catalytic site, from open to closed forms on ligand binding.

The structure of ATP synthase subunit *c* from PS3, TF_oc, in an organic solvent (chloroform : methanol = 3:1) was also determined by NMR (4). The determined structure of TF_oc takes on a stable hairpin structure. The hairpin structures were also reported for the subunit *c* of *E.coli*, EF_oc. However, the structures for TF_oc and EF_oc are significantly different in the direction of side chain of the conserved acidic amino acid residue (Glu56 in TF_oc and Asp61 in EF_oc) essential for the H^+-translocation. The conformational change depending on pH was not detected for TF_oc in contrast to EF_oc. It was concluded that the energy barriers among the multiple orientations of two helices in the hairpin are not high enough to discuss the conformation of subunit *c* in F_o as have done for EF_oc. On the basis of these results, a new model for the H^+-translocation mechanism was proposed (4).

Solid-state NMR is a promising method for investigations of membrane proteins and supramolecular systems because there is no size limit. We have been developing multidimensional solid-state NMR under MASS for the structural analysis of uniformly and specifically isotope-labeled samples (5-10). Newly developed methods were applied to H^+-ATPsynthase γ subunit and Mastoparan X bound to the lipid membrane. Mastopran X is a wasp venom and known to activate a G-protein. Uniformly and specifically labeled Mastoparans X were bound to DPPC-DPPG bilayer membranes under a hydrated condition. Its structure and its location in the membrane wad determined in detail (6, 7). The secondary structure analysis of H^+-ATPsynthase γ subunit, a transmembrane protein, in solid state was also successfully carried out (5).

It can be concluded that the combination of solution and solid-state NMR is a powerful approach to investigate biological supramolecular systems.

References:

1) H. Yagi, T. Tsujimoto, T. Yamazaki, M. Yoshida, and H. Akutsu, *J. Am. Chem. Soc.*, **126**, 16632-16638 (2004). **2)** K. Tozawa, H. Yagi, K. Hisamatsu, K. Ozawa, M. Yoshida, and H. Akutsu, *J. Biochem.*, **130**, 527 - 533 (2001). **3)** H. Yagi, K. Tozawa, N. Sekino, T. Iwabuchi, M. Yoshida, and H. Akutsu, *Biophys. J.*, **77**, 2175-2183 (1999). **4)** T. Nakano, T. Ikegami, T. Suzuki, M. Yoshida, H. Akutsu, *J. Mol. Biol.*, **358**,. 132-144 (2006). **5)** M. Kobayashi, Y. Matsuki, T. Fujiwara and H. Akutsu, *J. Biomol. NMR*, in press. **6)** E. Harada, Y. Todokoro, H. Akutsu and T. Fujiwara, *J. Am. Chem. Soc.*, **128**, 10654-10655 (2006). **7)** Y. Todokoro, I. Yumen, K. Fukushima, S.-W. Kang, J.-S. Park, T. Kohno, K. Wakamatsu, H. Akutsu and T. Fujiwara, *Biophys. J.*, **91**, 1368-1379 (2006). **8)** T. Fujiwara, Y. Todokoro, H. Yanagisita, M. Tawarayama, T. Kohno, K. Wakamatsu and H. Akutsu, *J. Biomol. NMR*, 28, 311-325 (2004). **9)** T. Fujiwara, T. Shimomura, Y. Ohigashi, and H. Akutsu, *J. Chem. Phys.*, **109**, 2380-2393 (1998). **10)** T. Fujiwara, K. Sugase, M. Kainosho, A. Ono, A(M) Ono, and H. Akutsu, *J. Am. Chem. Soc.*, **117**, 11351-11352 (1995).

Mapping protein energy landscapes by NMR relaxation dispersion

David D. Boehr, Daniel J. Felitsky, Kenji Sugase, H. Jane Dyson, Peter E. Wright
Department of Molecular Biology, The Scripps Research Institute, La Jolla, California, USA 92037.

NMR is a widely used method for determining the three-dimensional structures of proteins and other biomolecules in solution. However, protein structures are not static, and molecular motions are central to their biological functions. It is essential to move beyond our largely static view of protein structure towards an understanding of the dynamics and thermodynamics of conformational change and their relationship to protein function. NMR relaxation experiments provide a powerful approach to direct experimental characterization of protein dynamics on a broad range of time scales, ranging from ps to ms, and allow direct mapping of the protein energy landscape. Recently developed relaxation dispersion experiments permit quantitative analysis of the dynamics and thermodynamics of slow conformational fluctuations in proteins and of the kinetics of protein-ligand interactions and coupled folding and binding events. Applications of NMR to study the role of protein motions in the catalytic function of the enzyme dihydrofolate reductase (DHFR) will be described. Our experiments reveal active site conformational fluctuations on a time scale that is directly relevant to the structural transitions involved in progression through the catalytic cycle. Flexibility in the active site loops appears to be harnessed by the enzyme to control the flux of substrate, product, and cofactor, and to correctly position the reactants in the active site prior to the hydride transfer step. Progress through the catalytic cycle involves a dynamic energy landscape, where each intermediate populates excited states in which the protein conformation corresponds to that of the preceding or following intermediate in the cycle. NMR also provides detailed insights into the coupled folding and binding processes that mediate the physiological functions of intrinsically disordered proteins. In particular, relaxation dispersion measurements provide an especially powerful approach for mapping the folding pathway, providing novel insights into the mechanism of coupled folding and binding, and allowing structural characterization of transient encounter complexes.

Contrast enhanced microimaging at 700 MHz

Gary J Cowin*, Guy Weerasinghe#, Samantha South#, Andrew Tuck^, Graham J. Galloway* and Ian M. Brereton*§

Centre for Magnetic Resonance* Queensland NMR Network§, Centre for Integrated Preclinical Drug Development# and Queensland Centre for Schizophrenia Research^, University of Queensland, Brisbane, Australia.

Magnetic resonance research has been constantly striving for higher image resolution. One result of this goal is constantly increasing magnet strengths for both human and animal imaging systems. We are investigating the improvements in microimaging that can be achieved by increasing the magnetic field strength from 4.6T, in a horizontal animal MRI system, to 16.4 T in a vertical animal system. As the first step, we chose fixed rat brains to look at the microimaging potential at the two field strengths without physiological interference. The increase in field strength was accompanied by a doubling of the T1 times, thus requiring longer TR. We are investigation the use of paramagnetic metals to counter this restriction on TR and hence signal-to-noise per unit time and to increase contrast in fixed adult and neonatal tissue.

Adult rats were perfusion fixed with 4% paraformaldehyde, for control animals, or with the addition of 5% OptiMARK (Mallinckrodt) gadolinium contrast agent. The brain, kidneys, heart and liver ware removed and set in a 5 ml flat bottomed tube containing 0.5% agarose gel. Newborn mouse brains were drop fixed in 4% formalin solution. The brains were then removed and 0.1% PBS containing 4 mM MnCl or 5% OptiMARK (Mallinckrodt) gadolinium contrast agent for 48 hrs then set in a 5 ml flat bottomed tube containing 0.5% agarose gel.

Images of the fixed tissue were obtained on two Bruker (Ettlingen, Germany) systems:

Magnet	Gradient strength	Rise time	Rf coil	spectrometer
4.6T	1.8 G/mm	280 μs	35 mm SAW	AVANCE
16.4T	14.7 G/mm	110 μs	25mm Birdcage	AVANCE II

Both systems were running ParaVision 4.0. FLASH 3D protocol was used for image acquisition with isotropic image resolution from 200 μm to 30 μm. Maximum imaging time was limited to approximately 12 hours.

The effect of magnet field strength upon relaxation times for the fixed adult brain tissue at 4.6T and 16.4T was characterised by an approximate doubling of the T1 and a halving of the T2 and T2*. Addition of the Gd contrast agent OptiMARK to the perfusion medium resulted in a approximate 10 times decrease in the T1 time. This has a dramatic effect upon the signal-to-noise that can be acquired per unit time. Only small decrease in the T2 and T2* resulted from the addition of Gd.

Keywords: Microimaging, paramagnetic contast agents, fixed brain, rat, mouse

Signal-to-noise became limiting at 4.6T at $(100\mu m)^3$ without Gd and at $(75\ \mu m)^3$ with Gd and at 16.4T at $(50\ \mu m)^3$ without Gd and at $(30\ \mu m)^3$ with Gd. However, image contrast within the brain was greater with Gd at both field strengths. We are currently achieving 3D images of Gd perfused whole rat brains with an isotropic resolution of 30 μm, illustrated in figure 1. Further optimisation of the hardware and sequences on new 16.4T microimaging system, should enable finer image resolution to be achieved.

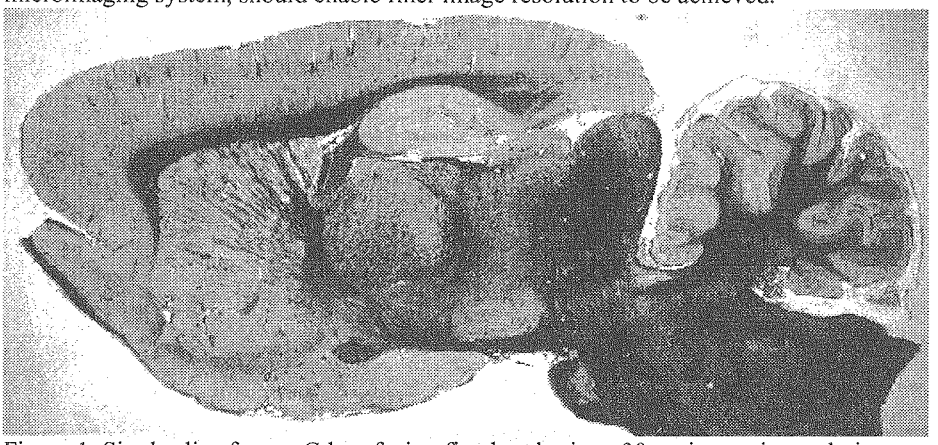

Figure 1. Single slice from a Gd perfusion fixed rat brain at 30μm isotropic resolution. TR=50 ms, TE=13 ms, FOV=28X14X14 mm, matrix=920X460X460, ns=8, acq.14 hrs.

Neonatal mouse brains are a challenge for standard MRI investigation due to the combination of small size and poor regional contrast, resulting from limited myelination in neonatal. Paramagnetic metal ions have potential to enhance signal-to-noise and improve regional contrast. In contrast to adult animal where perfusion fixation is possible, newborn mice are routinely drop fixed. The GD complex OptiMARK did not appear to be taken up by the drop fixed brains, resulting in a black rim around the brains (Fig. 2). In comparison, MnCl was taken up by the brain and enhanced regional contrast in the fixed newborn mouse brain.

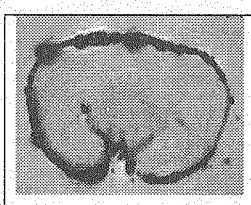

Figure 2
Poor uptake of OptiMARK

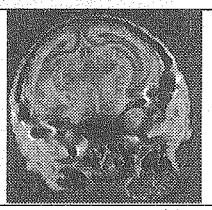

Figure 3
Contrast enhancement of newborn mouse brain with MnCl

These preliminary results illustrate great potential for the use of paramagnetic ions for improving signal-to-noise per unit time and contrast in newborn brains. This is ideally matched with ultra high field MRI systems to achieve extremely fine image resolution.

MR Cardiac Imaging: From mice to men

F Fidler[1,2], PhD ,KH Hiller[1,2], PhD and PM Jakob[1,2], PhD

[1]University of Würzburg, Dept. of experimental Physics 5, Germany

[2]Research Center for Magnetic Resonance Bavaria e.V. (MRB), Würzburg, Germany

In the last few years, magnetic resonance imaging (MRI) becomes the attractive non invasive imaging modality for experimental animal research. Animal models offer the great opportunity to investigate both pathophysiological questions and drug development. The understanding of mammalian genome allows the increased generation of animal models for studying cardiovascular development, changes and function. MRI is used to characterize the phenotype of such models by the functional effects of gene expression or gene knock-out directly or by the resulting morphological consequences. The non invasiveness of the MRI examinations lead to advanced monitoring of progression of chronic heart disease and regression during therapy since it offers the opportunity of measurements in the same animal at different time points.

MRI allows high accurate three-dimensional characterization of cardiac structure and function within the same examination. Detailed morphological is provided by this technique at a high resolution (<100µm) allows the quantification of volumetric and functional changes in hearts especially when underlying ventricular remodelling after myocardial infarction or in dilated cardiomyopathy[R1], but also in vascular disorders such as chronic occlusive arterial disease and restenosis.

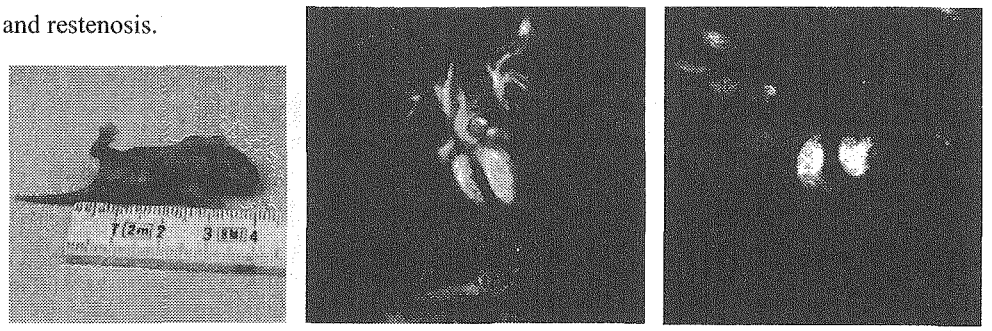

Figure 1: Cine-MRI on newborn mice [F. Wiesmann et al. Am J Physiol 278(2):2000]

The variety of parameters that can be addressed as well in animal models and humans is hugh. The well established Cine-technique allows the investigation and accurate determination of

Keywords: cardiac imaging, cardiac function, perfusion, MR spectroscopy, contrast agent

morphologic and functional consequences in the cardiovascular system, such as compartment volumes, wall thickness and mass or planimetry of valve areas. Figure 1 shows example images from a Cine-MRI dataset on newborn mice. Combined with a phase contrast velocity mapping, wall motion can be detected precisely[R2].

Perfusion can be addressed by spin labelling technique without the application of contrast agent, contrast agent application can be used to measure additionally the regional blood volume (rbv)[R3]. This technique, first applied to rat heart, have been transferred to both the smaller mice and to human application[R4].

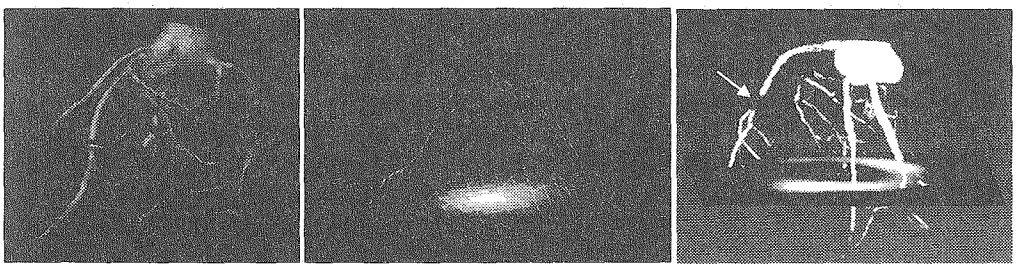

Figure 2: Left: 3D-Angiography of rat heart. Middle: Coronary flow profile. [S. Köhler et al. MRM50:2003] Right: Fusion image angiography with ^{31}P CSI of infarct [M. Nahrendorf et al. Am J Physiol Heart 285:2003].

Visualization of coronaries with 3D-Angiography can be achieved on isolated rat and mice heart, as shown in figure 2. Phase contrast flow measurements cover a wide range, from flow profiles in coronaries to flow quantification in the aorta of the mice.

Different aspects of the infarct are imaged with proton MRI based on diffusion or high resolution T_2^* imaging[R5]. These techniques are suitable to visualize muscle fibre orientation. Spectroscopic imaging based on ^{23}Na[R6] or ^{31}P MRI can show detailed information of the infarct (figure 2).

A relatively new field are highly specific contrast agents which bind to specific receptors. With the use of these new contrast agents one is able to image specific processes like apoptosis[R7].

References:
[R1]: Shapiro EP et al. Circ 79:1989
[R2]: Streif JUG et al. MRM 49:2003
[R3]: Waller C et al. Circ 103:2001
[R4]: Fidler F et al. J Cardiovasc Magn Reson 6(2):2004
[R5]: Köhler S et al. MRM 49(2):2003
[R6]: Neuberger T et al. MAGMA 17(3-6):2004
[R7]: Hiller KH et al. Mol Imag 5(2):2006

Water transport in neural cells in vivo and cell culture

Yoshiteru Seo[1], Yoshie Imaizumi[1], Mika Yokoi[1], Kazuto Watanabe[1], Takashi Ogino[2]

[1]Dept. of Regulatory Physiology Dokkyo Medical University School of Medicine, [2]Dept. of Biochemistry and Cellular Biology, National Institute of Neuroscience, National Center of Neurology and Psychiatry

The brain consists of 3 water compartments: intravascular water, interstitial water and intracellular water. In order to analyze water metabolism in brain, we have to determine kinetic parameters of water transport between these compartments. In this report, we have estimated water permeability of neural/glial cells in brain of Claudin-5 knocked out mice in vivo, and also detected water permeability of cultured neural cells from cerebral cortex. All NMR experiments were done by an AMX-300wb (7 T) with micro2.5 gradient.

[Water permeability in vivo]

A relaxation reagents (gadolinium-diethylene triamine-N,N,N',N",N"-penta acetic acid (Gd-DTPA^{2-}) was applied to estimate water permeability of the neural/glial cells in mice. In the intact mice, the longitudinal relaxation rates ($1/T_1$) showed minimal changes (< 0.1 s^{-1}) even the $1/T_1$ of blood water was accelerated more than 40 s^{-1} by Gd-DTPA^{2-}. It is suggested that the normal blood-brain barrier (BBB) have very low water permeability. The anatomic basis for BBB resides in tight junctions (TJs) of brain endothelial cells in addition to their limited transcytosis. The claudin-5 was identified as a major TJ cell adhesion molecule in brain endothelial cells. In the claudin-5 knocked out mice, Gd-DTPA^{2-} can pass through the modified BBB. From the dose-dependency of Gd-DTPA (Fig. 1), a water efflux rate from the neural/glial cells (k_n = 3.82 ± 0.58 s^{-1}) was detected which is corresponding to a diffusional water permeability of ca. 0.8 • 10^{-3} cm s^{-1}.

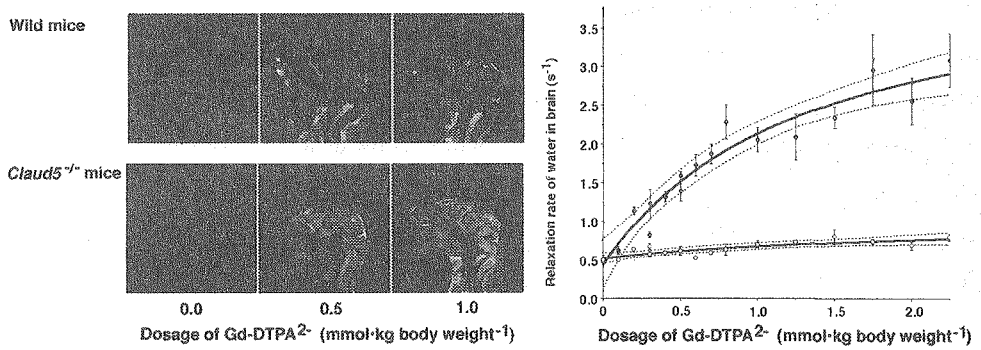

Fig. 1 Median section of T_1-weighted images of wild-type and claud5$^{-/-}$ brain and the relationship between the $1/T_1$ of water in brain and the dosage of injected Gd-DTPA^{2-}. Filled and open circles represent $1/T_1$ of the wild and claud5$^{-/-}$ brain, respectively. The bold and dotted lines are the results of fitting and 95% confidence limits, respectively, based on a simple two-compartment exchange model.

Key words: ^{1}H-NMR, ^{1}H-MRI, T_1 relaxation, relaxation reagent, diffusive water permeability

[Water permeability of primary cultured neural cells]

The diffusive water permeability of primary cultured neural cells from mouse brain cortex was measured by using Gd-DTPA^{2-}. Cortex of newborn mice were minced, separated by trypsin and DNAase, then neural cells were incubated in DH10 medium for 2 to 3 days. Then, resuspended by collagenase and DNAase in DH10 medium with 10 mM Gd-DTPA^{2-}. The shape of neural cells are rotational ellipsoid, and its longer and shorter diameters were 12.1 ± 1.4 and 9.5 ± 1.2 μm (mean ± SEM, n=100), respectively. The final cytocrit was 5 – 7.5 %. A typical T_1 relaxation is shown in Fig. 2. The rate constant for water efflux from the neural cells was estimated to be ca. 5 s^{-1} at 29°C which would be consistent with diffusive water permeability (P_d) of ca. 1 x 10^{-3} cm s^{-1}. This value is almost the same value we have estimated in vivo, and also is the same range of those obtained in perfused rabbit submandibular gland (3 x 10^{-3} cm s^{-1}), *Necturus* gallbladder (1.6 x 10^{-3} cm s^{-1}) and human red blood cells (2.4 to 4.7 x 10^{-3} cm s^{-1}).

Activation energy of water transport through the cell membrane (E_a) was estimated from temperature dependence (5–30°C) of the rate constant for water efflux. From the slope of Arrenius plot, E_a value is estimated to be ca. 8 kcal/mol. This activation energy is much smaller than that obtained in the lipid bilayer vesicles (12-14 kcal/mol), and is in the same range of red blood cells with AQP1 (E_a = 5 kcal/mol). Thus, this indicates that water transport of neural cells might be done by a channel-mediated pathway, and suggests contribution of AQP water channel.

[Conclusion]

We have obtained almost the same values of water permeability of neural/glial cells in brain in vivo and in primary cultured neural cells from mice cortex. We are now under preparation to identify the water transporting channel in neural cells, and also plan to measure the primary culture of glial cells.

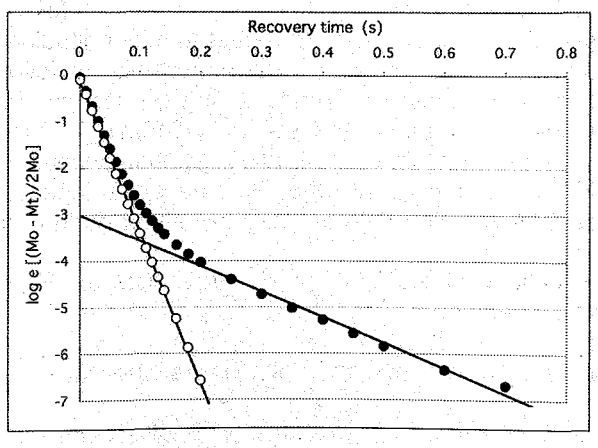

Fig. 2 T_1 relaxation of water in neural cell suspension with 10 mM Gd-DTPA^{2-} at 29°C. The rate constant of the slow component was 5.5 ± 0.2 s^{-1} with a fraction of magnetization of 5.3 ± 0.5 %. The fast component obtained by subtraction of the fitted slow component from the original data (○), and the rate constant was 32.5 ± 0.2 s^{-1}.

Double Quantum Filtered NMR Microimaging and Spectroscopy of Nerves and Connective Tissues

Gil Navon, Hadassah Shinar Uzi Eliav and Galit Saar
School of Chemistry, Tel Aviv University, Tel Aviv 69978, Israel

Background:

The ^2H spectrum of deuterated water molecules interacting with ordered structures such as oriented collagen fibers consists of a pair of quadrupolar split satellites. The frequency difference between the satellites transitions, ν_Q, is a weighted average of the splittings of the water molecules bound to the different binding sites on the collagen fibers, ν_i, and their fractions P_i relative to the total content of water molecules exchanging with these sites according to the following equation:

$\nu_Q=\Sigma\nu_i P_i (3\cos^2\theta_i-1)/2$ [1]

θ_i is the angle between the direction of the director of the quadrupolar interaction and the magnetic field.

In biological tissues, where there is a large amount of water molecules which does not interact with the anisotropic sites, or when the splitting is small relative to the linewidth, the split lines will be masked by the large signal of isotropic water. This problem is overcome by the use of double quantum filtered (DQF) NMR techniques where the large isotropic signal of the bulk water molecules is filtered out, allowing a clear observation of the split satellites. The basic DQF pulse sequence is given by:

$90°\text{-}\tau/2\text{-}180°\text{-}\tau/2\text{-}90°\text{-}t_{DQ}\text{-}90°$ (Acq) [2]

With proper phase cycling allowing only the magnetization obtained from the DQ coherences to be observed. t_{DQ} is the double quantum evolution time and τ is the creation time of the second rank tensors. By choosing the appropriate value of τ one can depict specific tissue characterize by specific value of ν_Q. In the spectrum obtained by the pulse sequence in Eq. 2 the satellites signals appear in antiphase. In order to obtain in-phase spectrum we use the pulse sequence given in Eq. 3 (1):

$90°\text{-}\tau\text{-}90°\text{-}t_{DQ}\text{-}90°\text{-}\tau\text{-}90°\text{-}t_{ZQ}\text{-}90°$(Acq) [3]

where t_{ZQ} is the evolution time for the zero-quantum (longitudinal magnetization) coherence. This pulse sequence gives us the opportunity to follow magnetization transfer due to exchange processes occurring during t_{ZQ}. Hence, this in-phase DQF (IP-DQF) pulse sequence is also denoted as DQF-MT. One-dimensional ^2H spectroscopic images can be obtained by introducing phase encoding gradients during the t_{DQ} time periods in sequences [2] and [3]. The advantage of introducing the gradients during the DQ evolution time is that their effect during this time period is doubled.

In the talk two applications of the DQF pulse sequences to ^2H spectroscopy and microimaging will be presented.

1. ^2H DQF-MT NMR Measurements of Inter-Compartmental Water Exchange in Nerves.

The rate of water transport to and from the axon is of a central importance in the physiology of signal conductance in nerves. As the neuronal activity is characterized by ionic fluxes which lead to osmotic gradients, fast water redistribution is essential to insure proper function. Here we report the application of the DQF-MT pulse sequence for the measurement of the water exchange among the compartments in bovine optic nerve.

The nerves of the peripheral and central nervous systems comprise axons ensheated by many layers of the myelin and embedded in a matrix of oriented collagen fibers of the endoneurium and the epineurium. ^2H DQF spectra of nerves equilibrated in deuterated saline consists of quadrupolar split satellites representing the water in the different nerve compartments. The main advantages of this technique are the enhanced resolution due to the filtering of the isotropic signal and the ability to excite selectively the water in the different compartments. This is demonstrated in Fig 1, where different compartments having different average quadrupolar interaction ν_Q are depicted for different τ values. Thus in ^2H DQF-MT NMR spectra of isolated bovine optic nerve equilibrated in deuterated saline as a function of τ with very sort t_{ZQ} four compartments are observed. In line with our previous findings (2) we assign signal C to the intraaxonal water and signal B to the epineurium. Signals A and D are probably due to the myelin and the endoneurium water. We have previously utilized the separation of the DQF spectra to measure the relaxation times and the water diffusion constants in each compartment (3). However the use of the DQF-MT method allows for the determination of water exchange between the inter and the intraaxonal compartments as well.

The ^2H DQF spectra of porcine optic nerve equilibrated in deuterated saline is shown in Fig. 2 as a function of the exchange time. We have found that the buildup time constant for signal C as well as the decay of signals A and D are triexponential with time constants of 1.4 (20%), 30 (80%) and 100 (100%) ms. The short (minor) component is tentatively assigned to spin diffusion, the intermediate to inter-compartment water exchange and the long to T_1 decay.

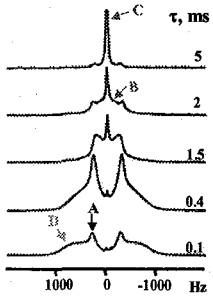

Fig. 1

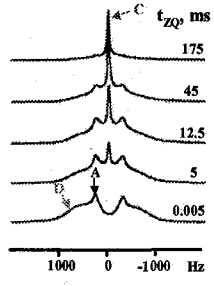

Fig. 2

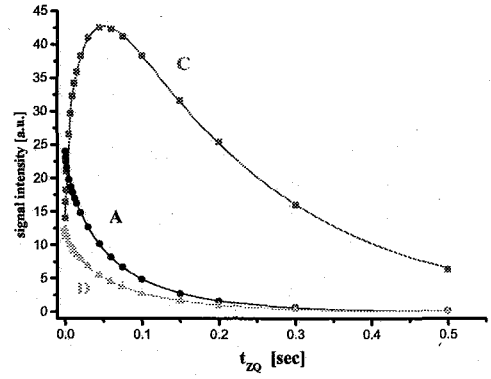

Fig. 3

2. **Multinuclear NMR and Microscopic MRI Studies of the Articular Cartilage Nanostructure.**

Osteoarthritis is a common disease afflicting a large proportion of the population throughout the world and is considered a major health problem. It involves the erosion of the articular cartilage. Articular cartilage has exceptional viscoelastic biomechanical properties that allow its function as a load bearing, minimizing the effects of stresses applied to the joints. The strive to understand the physiochemical origin of these

properties on the basis of the interrelationship between the major constituents of the cartilage, namely collagen and proteoglycans has attracted many investigations. Unlike many techniques that require sectioning, slicing and decalcification of the tissue, NMR spectroscopy and microscopic MRI have the advantage that the physiochemical properties of the tissue can be studied non- invasively on intact samples.

All ^2H measurements were performed on cylindrical cartilage plugs, with a diameter of about 8 mm, after equilibration in deuterated saline for 1-2 hours. The plugs were then wiped and placed in a 10 mm OD NMR tube with supporting Teflon inserts. The tube was filled with fluorinated oil (Fluorinert, FC-77, 3M), which has low water solubility and the same magnetic susceptibility as water.

Information about the spatial distribution of the quadrupolar splittings is obtained from the one-dimensional DQF spectroscopic imaging pulse sequences, obtained by introducing phase encoding gradients during the t_{DQ} time periods in sequences [2] and [3]. An example is given in Fig. 4 where the x axis represents the spectral dimension and the y axis represents the spatial dimension. Some spectra extracted from the image at different spatial locations are also given in the figure. Two pairs of quadrupolar split satellites with a splitting of about 900 and 500 Hz are observed in the calcified and radial zones. Further from the bone the intensity of the signal with the large splitting decreases and the smaller splitting becomes dominant. The splitting was not resolved in the intermediate zone and a small splitting is again detected in the surface zone. This phenomenon was found in all the cartilage bone plugs measured, yet the frequency differences between the satellites as well as their relative intensities vary from sample to sample.

We have found that the splitting depends on the orientation of the plug relative to the magnetic field. When the surface of the plug is parallel to the field the quadrupolar splittings in the calcified and radial zones was approximately half of that observed at the perpendicular orientation as expected for a well ordered system with the director of the interaction aligned perpendicular to the surface of the plug. Thus the ^2H 1-D DQF spectroscopic image agrees with the known collagen architecture in articular cartilage where the fibers are well ordered throughout the calcified and the radial zones, aligned perpendicular to the bone surface, then bend in the intermediate zone and align parallel to the surface of the cartilage in the superficial zone. During this bending they pass through the magic angle where the quadrupolar splitting vanishes.

One of the functions of articular cartilage is to withstand recurrent pressure applied in everyday life. In previous studies osmotic pressure has been used to mimic the effects of mechanical pressure. In the present study the response of the collagen network of intact and proteoglycans (PG) - depleted cartilage to mechanical and osmotic pressures are compared (4,5). An example of the effect of 0.5 MPa (about 5 atm.) mechanical load and osmotic stress on the ^2H IP-DQF spectroscopic images of cartilage-bone plugs is shown in Fig. 5. Major differences were found in the zones near the bone between the effects of the two types of application of pressure for both intact and depleted plugs. While the order is lost in these zones as a result of mechanical load, it is preserved under osmotic pressure. For both intact and PG-depleted plugs under osmotic stress most of the collagen fibers become disordered. Our results indicate that different modes of strain are produced by unidirectional mechanical load and the isotropic osmotic stress. Thus osmotic stress can not serve as a model for the effect of load on cartilage in-vivo.

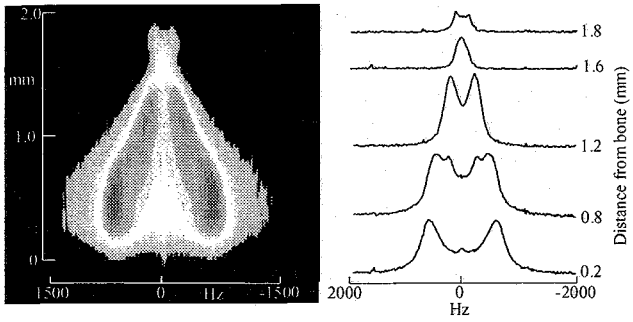

Fig. 4

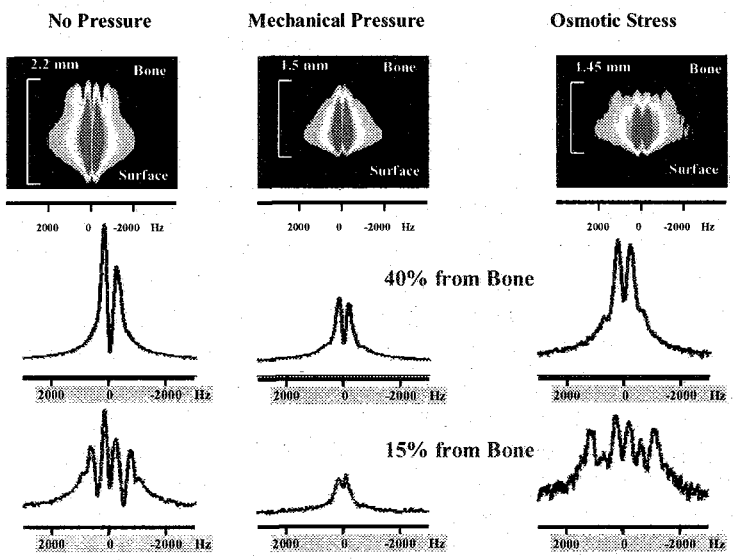

Fig. 5

References:

1. U. Eliav et al. J. Magn. Reson. 137;295 (1993).
2. H. Shinar et al. J. Magn. Reson 129; 98 (1997).
3. Y. Seo et al., Magn. Reson. Med. 42; 461 (1999).
4. H. Shinar et al. Magn Reson Med 48;322 (2002).
5. G. Saar, H. Shinar, G. Navon , Eur. Biophys. J. (In Press).

2 LE10

4.7T MRIで定量化したヒト脳の形態

（国立環境研）○三森文行、高屋展宏、渡邉英宏

Shape of the human brain quantified by 4.7T MRI

(National Institute for Environmental Studies) F.Mitsumori, N.Takaya, H.Watanabe

Structural data for the human brain was quantified based on the 3-dimensional anatomical image obtained at 4.7T on 77 healthy subjects. High magnetic field is beneficial for the high sensitivity leading to the high spatial resolution and for the high tissue contrast leading to the precise tissue discrimination. From the quantified structural data the age dependent change in grey, white matters and CSF were analyzed. The size of corpus callosum revealed the difference between male and female brain.

【はじめに】近年、ヒト脳のMRI画像解析の精密化、定量化により、脳の発達・形成に関する研究に新しい展開が見られる。たとえば、４～２１歳にわたる健常被験者の追跡研究により、大脳皮質の発達が後頭葉から前頭葉に向かって進むことなどが明らかになってきた[1]。我々は2003年以来、4.7T 高磁場人体用MRI分光計を用いて健常被験者の脳の形態情報の集積と解析法の検討を進め、これまでの3年間で77名の被験者の測定を終了した。本報告では、主として３次元T_1強調画像に基づく形態の定量解析から脳の大きさ、形態の年齢依存性、性差などがどこまでとらえられるか、高磁場MRIを用いた脳の形態解析の可能性と限界について論じたい。

【方　法】MRI測定にはOxford Magnet Technology社の4.7T磁石（ボア径925mm）を接続したVarian Inova分光計を用いた。信号検出器は口径30cmの頭部用^{1}H TEM型検出器を用いた。国立環境研究所医学研究倫理審査委員会の認めた健常被験者 77 名についてMRI測定を実施し、全頭の３次元MDEFT画像、高速スピンエコー画像、T_1, T_2分布画像等の測定を行った。このうちMDEFT画像測定法の最適化やT_2測定については昨年までの学会で報告してきた[2,3]。MDEFT画像データセットは３次元Fourier変換処理の後、dielectric effectによる画像信号強度の不均一をBrain Voyagerソフトウェアの６次多項式補正により平滑化した後、主としてStatistical Parametric Mappingソフトウェア（SPM99）の組織分画モジュールを用いて皮質（GM）、白質（WM）、脳脊髄液（CSF）の確率画像を得た。各組織の体積は画像ピクセルごとにそれぞれの組織の確率とピクセル体積を掛け合わせることにより得た。全頭での解析に加え、側脳室、脳梁等、脳内の特異的部位の抽出や解析も進めている[4]。

【結果と考察】高磁場の高感度を利して３次元の各方向 1mmの分解能を有する高精細画像をルーチンで測定することが可能である。また、灰白質、白質組織のT_1緩和時間の差の拡大により、従来の予測に反して、組織間コントラストを向上しより精度の高い組織識別が実現できた。一方、dielectric effectによる脳中心部での信号強度の増強は高次の多項式関数を用いることに均質化することが可能であった。Fig.1 に脳の１断面における組織分画の例を示す。均質化処理を行わないと誤って分画されてしまう大脳基底核部位や周辺の脳回部位の灰白質も正確に識別されている。Fig.2 に全頭で解析したGM、WM、CSFの体積を男女それぞれに年齢別にプロットした結果を

Keywords: high field MRI, human brain, tissue segmentation, shape, grey matter

みつもり　ふみゆき、たかや　のぶひろ、わたなべ　ひでひろ

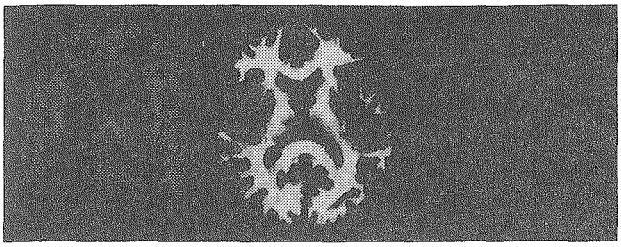

Fig.1. Grey Matter (red, left), White Matter (green, middle), and CSF (blue, right) segmented from the 3D MDEFT image of a human brain.

示す。これより、男性灰白質体積は $V_{GM} = -3.2x + 828$ (ml), (xは年齢) の関係（相関関係の有無のピアソン検定：$p < 0.05\%$）に従って年齢とともに減少するのに対し、女性灰白質体積は $V_{GM} = 0.31x + 616$ と、年齢依存性がほとんど見られなかった。女性脳データを詳細に検討すると、20 歳代の若年齢層の傾向が 30 歳代以降の傾向と逆転しているように見受けられる。そこで、女性脳を 20 歳代 (n=14)と 30 歳代以降(n=22)の 2 群に分けてその年齢依存性の回帰直線を求めると、図 2 cに示すように両群で年齢に対して相反する傾向が得られた。ピアソンの相関の検定の結果、若年女性の逆転した傾きは 14.5 で、危険率 5%以下で有意であった。なお、20 歳代前半群、後半群の灰白質体積の平均値では、nが小さいこともあり、有意差は認められなかった。これまで、若年女性脳でこのような特異的年齢依存性が報告されたことはなく、今後さらに測定例を増やして検討する必要がある。側脳室体積の年齢依存性は全頭で得られた男女差を支持する結果を示した。

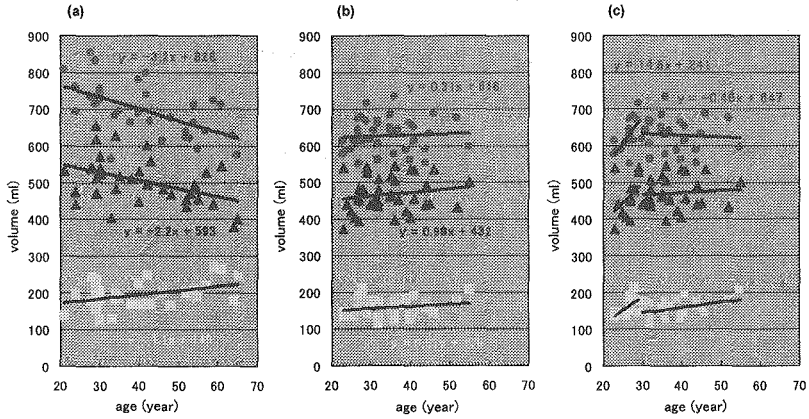

Fig.2. Age dependent change in the volume of grey, white matters, and CSF (a) in male, and (b,c) in female. The regression analyses were performed on entire age group in (a) and (b), while in (c) it was separately performed at 20's and the rest.

【結　語】4.7T 高磁場 MRI より得られたヒト脳の形態解析は加齢に伴う脳の変化や性差を十分に解析できる精度が得られることが明らかになった。

【参考文献】

[1] N.Gogtay, J.N.Giedd, L.Lusk et al. PNAS 101, 8174 (2004).
[2] 高屋展宏、渡邉英宏、三森文行、第 43 回 NMR 討論会、1P106、2004. 11 （東京）.
[3] F.Mitsumori, H.Watanabe, N.Takaya, M.Garwood, The 1st Asia-Pacific NMR Symposium, BLS12 (2005).
[4] 高屋展宏、渡邉英宏、三森文行、第 45 回 NMR 討論会、2006. 11 （京都）.

2 LE11

Paramagnetic Relaxation Enhancement for Investigations of Large-Scale Dynamics in Macromolecular Binding Process

Junji Iwahara°, Chun Tang, Charles D. Schwieters, G. Marius Clore

Laboratory of Chemical Physics, National Institute of Diabetes and Digestive and Kidney Disease, National Institutes of Health, Bethesda, MD 20892-0520, USA

Macromolecular binding event is not simply a two-state exchange between free and bound forms. In fact, previous kinetic investigations have suggested that the process of a specific complex formation goes through intermediate states called as target search or encounter complexes and the presence of such states greatly accelerate the overall process. How do individual components bind to each other at intermediate states in terms of structure? How dynamic are they? Although these are very important questions for understanding macromolecular recognitions, structural biology has not given adequate answers yet. It is because the very low populations at equilibrium and dynamic nature of such states make the investigations extremely difficult. We have developed the very powerful NMR method to analyze the transient intermediates in macromolecular binding at equilibrium. The method that makes use of the intermolecular paramagnetic relaxation enhancement (PRE) provides information about the structures and dynamics of the intermediates whose populations are as low as ~1%, if the exchange between intermediate and ground states is in fast exchange regime. In the presentation, the principle of the method and the applications to investigations of the target search process in the homeodomain-DNA interactions and the encounter complexes in protein-protein association will be demonstrated.

References

1) Iwahara, J., Schwieters, C.D., Clore, G.M. (2004) *J Am Chem Soc* 126, 12800-12808.
2) Iwahara, J., Clore, G.M. (2006) *Nature* 440, 1227-1230.
3) Tang, C., Iwahara, J., Clore, G.M. (2006) *Nature*, in press.
4) Iwahara, J., Zweckstetter, M., Clore, G.M. (2006) *Proc Natl Acad Sci USA* 103,15062-15067.

Keywords
paramagnetic relaxation enhancement; protein-DNA complex; protein-protein complex; intermediates; dynamics.

RNA Dynamics and Structural Adaptation

Qi Zhang, Charles Fisher, Alexandar Hansen, Melissa Getz, Xiaoyan Sun, and Hashim M. Al-Hashimi*

University of Michigan, 930 N. University, Ann Arbor, MI, 48109

Ribonucleic acids (RNA) often function by adaptively changing conformation in response to specific cellular signals ranging from recognition of proteins and small metabolite molecules to changes in temperature and pH. These transitions often involve large-scale changes in secondary structure and/or significant alterations in the RNA global architecture. Although RNA structures are believed to code for internal mobility that enable such transitions to take place specifically, these dynamical properties remain poorly understood. Methods based on NMR spin relaxation and residual dipolar couplings (RDCs) offer a unique opportunity to site-specifically visualize RNA motions occurring at ps-ms timescales. However, quantitative application of these techniques generally requires that internal motions are not correlated to overall reorientation. While this "decoupling approximation" appears to be valid for many globular proteins, it can generally break down in extended RNA systems which tend to be composed of loosely linked helical domains that can reorient relative to one another in such a way to effect large changes in the properties of overall reorientation.

Here, we describe implementation of an elongation strategy that allowed us to decouple internal motions in RNA from overall reorientation. Application of 15N and 13C spin relaxation and RDC methods revealed hierarchical motional modes spanning picosecond librations, nanosecond collective motions of A-form helical domains, and micro-to-millisecond structural transitions. Our results uncover a universe of internal motions occurring at nanosecond timescales that evade detection by conventional NMR spin relaxation methods because they occur at timescales approaching overall rotational diffusion. We present direct evidence that this uncovered network of motional modes is coded for by subtle elements in the RNA sequence and that it gives rise to dynamical changes in the RNA conformation that allows adaptive recognition of chemically diverse targets.

In the domain-elongation strategy, the size of a terminal RNA domain is elongated using a stretch of Watson-Crick base-pairs. This results in an elongated RNA (E-RNA) which has a hydrodynamic shape and thus overall diffusion/alignment properties that are less sensitive to internal motions, including collective dynamics of helical domains. Furthermore, by slowing down overall tumbling, the elongation broadens the sensitivity of NMR relaxation, which is limited to internal motions occurring at timescales faster than overall tumbling. To avoid an increase in NMR spectral

Key words: RNA dynamics, adaptive recognition, TROSY, spin relaxation, and residual dipolar couplings

overlap, two constructs are prepared in which alternating unlabelled A/U and G/C base pairs are used for elongation using otherwise uniformly 13C/15N-labeled G/C and A/U nucleotides respectively. In this manner, NMR data can be acquired over the entire RNA target while keeping elongation residues "NMR invisible".

Using this strategy, we were able to resolve a manifold of highly coupled motional modes in the transactivation response element (TAR) RNA from HIV-1 that otherwise evade detection due to motional couplings. TAR is one of the best examples of an RNA that can adopt different conformations and thereby bind to chemically diverse targets. Based on 13C and 15N spin relaxation data, we observe variable base and sugar picosecond fluctuations within helical domains that move collectively at diffusion-limited nanosecond timescales across a short, functionally important, and highly mobile bulge linker. These motional modes lead to spontaneous changes in the conformation that correlate quantitatively with those that follow adaptive recognition of diverse targets. Thus, sub-nanosecond internal motions in free TAR allow its structure to vary adaptively so to bind chemically diverse targets.

By combining the domain-elongation strategy with RDC measurements, we obtained structural evidence that the free transactivation response element (TAR) RNA from HIV-1 dynamically samples all of its seven previously reported ligand-bound structures. These bound structures differ significantly (all-atom rmsd = 4.7 Å) and feature TAR bound to peptides, divalent ions, and five chemically distinct small molecules. By exploiting the elongated domain as a reference frame, we were able to compute expected RDCs for each TAR structure. While poor agreement is observed between the experimentally measured RDCs and values computed for any given structure, very good agreement is observed with the dynamical averages of the computed RDCs. We further demonstrate that TAR mutants can be prepared with altered dynamical properties that code dynamic access to only a sub-set of the TAR conformational sub-states that feature coaxially aligned helices. The binding properties of these TAR mutants to the above five ligands will be characterized and correlated to the conformational sub-states they are appear to access spontaneously.

The domain-elongation strategy provides a new approach for resolving motional modes in RNA spanning picosecond to millisecond timescales. Our results suggest that the adaptive changes in RNA conformation that take place upon ligand binding actually occur dynamically in the free RNA.

Structural Biology of Functional RNA and DNA

Akimasa Matsugami[1], Daisuke Koizumi[1], Takako Ohyama[1], Masashi Inada[1], Hiroaki Tsuchibayashi[1], Takashi Nagata[1], Yan Xu[2], Yuuki Noguchi[2], Hiroshi Sugiyama[2], Kunio Kikuchi[3], Takuya Umehara[3], Fumiko Nishikawa[3], Satoshi Nishikawa[3] and Masato Katahira[1,4,5]
[1]Yokohama City Univ., [2]Kyoto Univ., [3]AIST, [4]RIKEN, [5]JST, PRESTO

①Structure of human telomeric DNA under physiological ionic conditions

Human telomeric DNA is 5-8 kb long and composed of the repetition of d(TTAGGG) sequence, with a 3' single-stranded overhang of about 200 nucleotides. DNA which is rich in guanosine residues tends to form quadruplex with guanine-quartet planes as core structure. Telomere DNA is rich in guanosine residues and thus its quadruplex structure is supposed to play certain roles in the regulation of telomere length. Particularly, the finding that the activity of the telomerase is inhibited by the formation of the quadruplex has drawn the great attention in terms of the development of novel anticancer drugs.

The solution structure of telomeric DNA in the presence of Na^+ was reported to be antiparallel basket-type quadruplex by NMR.[1] Later, the crystal structure of telomere DNA in the presence of K^+ was determined, and the quite different structure of parallel propeller-type quadruplex was found.[2] This structure is similar to the solution structure found for GGA triplet repeat DNA in the presence of K^+.[3,4] Currently, the solution structure of human telomeric DNA in the presence of K^+ is a hot unanswered question, as this structure is believed to be biologically most relevant when high intracellular K^+ concentration is concerned.

The difficulty of the structure determination in the presence of K^+ comes from the fact that the corresponding NMR spectrum is poor due to the existence of conformational heterogeneity. We have overcome the difficulty by introducing proper substitution of guanines with 8-bromoguanines.[5,6] It is known that an 8-bromodeoxyguanosine takes on the *syn* conformation. It was demonstrated that the substitution of a guanosine in the *syn* conformation with an 8-bromoguanosine increased the thermal stability of the quadruplex structure, allowing the determination of the *syn/anti* conformations. This method has been applied to explore the major structure of human telomeric DNA in K^+ solution. We have tried to stabilize, or "freeze", the major structure of human telomeric DNA with the proper incorporation of 8-bromoguanines. We synthesized many derivatives of human telomeric DNA with various kinds of 8-bromoguanine substitutions. The positions to incorporate 8-bromoguanines were optimized on the basis of the following guides; when the proper guanosine which takes on *syn* in the major native structure is substituted with an

Key words: telomere, aptamer, RNA, structure

8-bromoguanosine, (i) CD spectrum should not change a lot, if any, and (ii) the thermal stability should increase. Thus, we reached the optimum pattern of the substitution which most stabilizes the major native quadruplex structure. Then, we have determined the structure stabilized by proper incorporation of 8-bromoguanines. Thus, we have succeeded to determine the major structure of human telomere DNA in the presence of K^+.

The determined structure is neither the antiparallel basket-type quadruplex nor the parallel propeller-type quadruplex. It is notable that four guanine-tracts take on the mixed-parallel/antiparallel, or (3+1) architecture, in which three guanine-tracts are aligned parallel and the other guanine-tract being antiparallel.

The mixed-parallel/antiparallel structure has also been proposed by Ambrus *et al.*[7] Very recently, the mixed-parallel/antiparallel structure has been determined by Luu *et al.*[8] They have overcome the difficulty by mutating the residues flanking the four guanine tracts. The mutations stabilized a structure probably through the introduction of the extra interaction. Actually, the formation of an extra base pair involving the mutated residue is found.[8] Although the strategy to overcome the difficulty is different between our group and the other groups, the consistent results have been obtained from both the sides.

②Structural analyses of other functional DNA and RNA

Structural analyses on other functional DNA and RNA, such as the RNA aptamer for a gene regulatory element of virus and 4' S DNA which exhibits resistance to nuclease, will also be presented. Structural analyses on RNA/DNA-binding proteins such as Musashi and hnRNP A1 may also be presented.

References

1. Wang, Y. *et al.* (1993) *Structure* **1**, 263-282.
2. Parkinson, G. N. *et al.* (2002) *Nature* **417**, 876-880.
3. Matsugami, A. *et al.* (2001) *J. Mol. Biol.* **313**, 255-269
4. Matsugami, A. *et al.*. (2003) *J. Biol. Chem.* **278**, 28147-28153.
5. Sugiyama, H. *et al.* (2006) *Bioorg Med Chem.* **14**, 5584-5591.
6. Matsugami, A. *et al.* (2006) *Nucleic Acids Symp. Ser.* **No. 50**.
7. Ambrus, A. *et al.* (2006) *Nucleic Acids Res.* **34**, 2723-2735.
8. Luu, K. N. *et al.* (2006) *J. Am. Chem. Soc.* **128**, 9963-9970.

Thursday, November 23

Japanese Session

2 LJ1

NMRインターフェースマイクロチップ“MICCS”の開発と“MICCS-NMR”の応用

（日本電子1、神戸薬大2、横国大分析セ3）○高橋　豊[1]、櫻井智司[1]、上田昌史[2]、中越雅道[3]、内海博明[1]、宮田興子[2]、内藤猛章[2]

Development of a NMR Interface Microchip "MICCS" and Its Applications using "MICCS-NMR"

(JEOL[1], Univ. of Kobe[2], Yokohama Nat. Uni.[3]) Y. Takahashi[1], S. Sakurai[1], M. Ueda[2], M. Nakakoshi[3], H. Utsumi[1], K. Miyata[2], T. Naito[2]

Abstract: Development of a new micro fluidic device for NMR “MICCS” and its application using “MICCS-NMR were described. MICCS can be used with standard NMR probes for 5mm O. D. sample tubes. It was connected to syringes with capillary tubes. The reagent solutions were introduced into the MICCS by syringe pumps, and were mixed in a Y-shaped channel. Herein we report the direct observation of a boron complex by ^{1}H and ^{11}B MICCS-NMR. The complex has been proposed as a key intermediate in the radical addition of the oxime ether mediated triethylborane(Et_3B) that produce amine derivatives. The results from MICCS-NMR indicate good consistency with those from 2D and 3D DOSY methods.

【はじめに】マイクロチップは、微小空間を利用し様々な化学プロセスを高効率に実行できる可能性を持つ。特に、合成化学への応用は、反応の高効率化・省試薬，省スペース化・安全性などの観点から、その実用化が期待されている。合成化学における反応の過程を考える上で、反応中間体の解析は非常に重要である。NMR は中間体の解析において有力なツールであると考えられるが、実際にはその解析は難しいことが多い。なぜなら反応中間体は、多くの場合不安定であったり、その寿命が短かったりするためである。そこで我々は、ミクロンオーダーの流路を持つガラス製のセル“MICCS”を開発し（MICCS：MIcro Channeled Cell for Synthesis monitoring）[1]、NMR プローブ内における化学反応を、直接観測することを試みた。トリエチルボラン（Et_3B）とオキシムエーテル類を反応させると、Et_3B をラジカル開始剤としてアミン類を高収率で得ることができるが[2]、本反応機構は、ホウ素－オキシムエーテル錯体を経て生成物に至ると推測されていた。我々は、DOSY 法によって、その不安定中間体の解析を行い、反応機構を証明した[3]。今回は、^{1}H および ^{11}B の MICCS-NMR を用いてその解析を行ったので報告する。

キーワード：反応モニター、NMR セル、MICCS, MICCS-NMR、不安定中間体

たかはしゆたか、さくらいさとし、うえだまさし、なかこしまさみち、
うつみひろあき、みやたきょうこ、ないとうたけあき

【実験】MICCS の写真を Fig. 1 に示す。MICCS は、試薬導入用配管を接続するための樹脂（PEEK）製の部品と、混合・反応・検出用のミクロ流路を備えたガラス製部品とから構成される。PEEK 部品は高砂電気工業株式会社に、ガラス製部品はマイクロ化学技研株式会社に作製を依頼した。

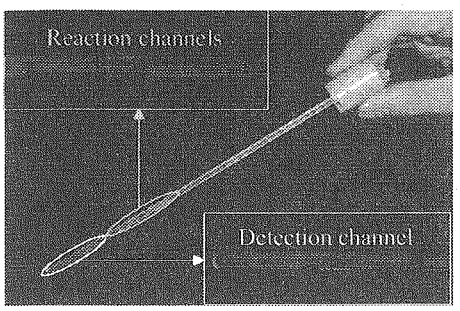

Fig. 1. Photograph of MICCS.

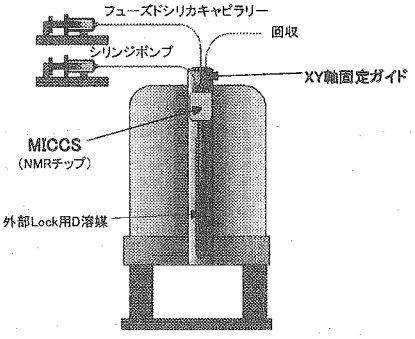

Fig. 2. Schematic diagram of MICCS-NMR.

NMR 装置には、日本電子製 JNM-ECA シリーズを用いた。MICCS のガラス部分を 5 mmϕ の試料管に挿入し、ホルダー&ローターに固定してマグネットに導入、測定を行った。MICCS-NMR 装置の概略を Fig. 2 に示す。

^{1}H MICCS-NMR では、MICCS の 3 つの導入口を使用し、オキシムエーテル、トリエチルボラン、メタノール（各 1M ジクロロメタン溶液）をそれぞれ導入した。各試料の流量比を徐々に変化させることで、反応させる試料の割合を調節し、そのときの ^{1}H-NMR をそれぞれ測定した。

【結果と考察】^{1}H MICCS-NMR で得られた結果を Fig.3 に示す。オキシムエーテルに徐々にトリエチルボランが加えたことにより、スペクトルはオキシムエーテルのものから中間体のものへと変化した。更に、メタノールを添加し始めると、スペクトルは生成物へと変化し、最後にはトリエチルボランとメタノールのみとなった。また、得られたスペクトルは、DOSY 法によって得られたスペクトルと良く一致していた。

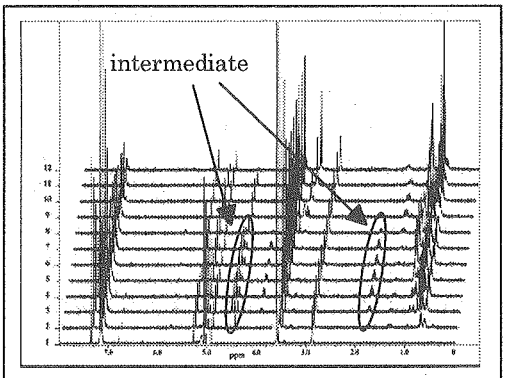

Fig. 3. 2D-dispray of ^{1}H-NMR spectra.

【文献】

1) Y. Takahashi et al., *Micro TAS*, 2, 464 (2004).
2) H. Miyabe, C. Ushiro, M. Ueda, K.Yamakawa, T. Naito, *J. Org. Chem.*, 65, 176 (2000).
3) M. Nakakoshi, M. Ueda, S. Sakurai, O. Miyata, M. Sugiura, T. Naito, *Magn. Reson. Chem.*, 44, 807 (2006).

2 LJ2

Pairwise cross-correlated relaxation experiments for the determination of backbone dihedral angles of peptides that bind weakly to target molecules

○Hideo Takahashi[1], Yumiko Mizukoshi[2], and Ichio Shimada[1,3]

[1]Biological Information Research Center (BIRC), National Institute of Advanced Industrial Science and Technology (AIST), [2]Japan Biological Information Research Center (JBIRC), Japan Biological Informatics Consortium (JBIC), [3]Graduate School of Pharmaceutical Sciences, The University of Tokyo

Cross-correlated spin relaxation (CCR) between two different relaxation mechanisms can provide valuable information about macromolecular structure and dynamics. Reif et al. have developed a method utilizing CCR between interresidual dipolar fields of ^{15}N-^{1}H (residue i+1) and $^{13}C^{\alpha}$-$^{1}H^{\alpha}$ (residue i) internuclear vectors, denoted as $\Gamma_{H\alpha C\alpha,HN}(\Psi)$ (Figure 1a), to measure the backbone dihedral angle Ψ of proteins. However, since a single relaxation rate can give rise to a multiplicity of dihedral angles, there is a limitation in the use of CCR in angle determination. Therefore, Yang et al. developed an alternative experiment to measure Ψ, based on CCR between intraresidual $^{13}C^{\alpha}$-$^{1}H^{\alpha}$ dipolar and $^{13}C'$ (carbonyl) chemical shift anisotropy (CSA) relaxation mechanisms, $\Gamma_{H\alpha C\alpha,C'}(\Psi)$ (Figure 1b). It has been shown that the number of possible Ψ angles can be considerably reduced by combining measurements from these two experiments. This can lead to unambiguous determination of dihedral angles in favorable cases. In the case of the backbone dihedral angle Φ, a similar strategy is followed, which utilizes intraresidual ^{15}N-^{1}H dipolar/$^{13}C^{\alpha}$-$^{1}H^{\alpha}$ dipolar CCR, $\Gamma_{HN,H\alpha C\alpha}(\Phi)$ (Figure 1c) and interresidual $^{13}C'(i\text{-}1)$ CSA/$^{13}C^{\alpha}(i)$-$^{1}H^{\alpha}(i)$ dipolar CCR, $\Gamma_{C',H\alpha C\alpha}(\Phi)$ (Figure 1d). Since the pulse sequences for these experiments utilize or partially utilize HNCA type coherence transfer, the evolution of $^{1}J_{NC\alpha}$ and $^{2}J_{NC\alpha}$ spin couplings are active during the ^{15}N evolution period. These

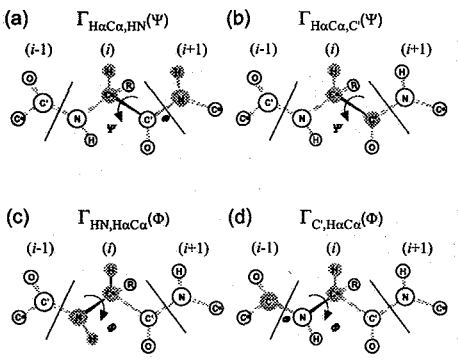

Figure 1 Schematic representation of the four cross-correlated spin relaxation rates associated with the determination of backbone dihedral angles Φ and Ψ. (a) $\Gamma_{H\alpha C\alpha,HN}(\Psi)$; (b) $\Gamma_{H\alpha C\alpha,C'}(\Psi)$; (c) $\Gamma_{HN,H\alpha C\alpha}(\Phi)$; (d) $\Gamma_{C',H\alpha C\alpha}(\Phi)$.

Keywords: cross-correlated relaxation, dipole-dipole interaction, chemical shift anisotropy, dihedral angle, peptide

couplings hamper a simple derivation of these CCR rates. Therefore, in order to obtain $\Gamma_{HN,H\alpha C\alpha}(\Phi)$ and $\Gamma_{C',H\alpha C\alpha}(\Phi)$, time-consuming three-dimensional experiments were performed to discriminate intraresidual and interresidual correlations. Interresidual CCR rates obtained previously were subtracted from the measured CCR rates.

Here, we present novel and simple two-dimensional versions of the quantitative CCR experiments for measuring $\Gamma_{HN,H\alpha C\alpha}(\Phi)$ and $\Gamma_{C',H\alpha C\alpha}(\Phi)$. In order to refocus interresidual $^2J_{NC\alpha}$ evolution, the experiments utilize intra-HNCA type coherence transfer to generate multiple quantum (MQ) coherences, $4N_xC'_z(i\text{-}1)C^{\alpha}_x(i)$ or $4N_zC'_x(i\text{-}1)C^{\alpha}_x(i)$, for obtaining $\Gamma_{HN,H\alpha C\alpha}(\Phi)$ or $\Gamma_{C',H\alpha C\alpha}(\Phi)$, respectively. The contribution from other coherences is also discussed and an appropriate setting of the evolution delays is presented. These CCR experiments were applied to ^{15}N- and ^{13}C-labeled human ubiquitin. The relevant CCR rates showed a high degree of correlation with the Φ angles observed in the X-ray structure.

Significant benefit is expected when these CCR experiments are applied to peptides which weakly bind to target molecules (TrCCR experiments), since it is difficult to obtain dihedral angle restraints of such bound peptides from J coupling or secondary chemical shift values. By utilizing these CCR experiments ($\Gamma_{HN,H\alpha C\alpha}(\Phi)$ and $\Gamma_{C',H\alpha C\alpha}(\Phi)$) in combination with those previously established ($\Gamma_{H\alpha C\alpha,HN}(\Psi)$ and $\Gamma_{H\alpha C\alpha,C'}(\Psi)$), we could determine high resolution structures of peptides that bind weakly to large target molecules.

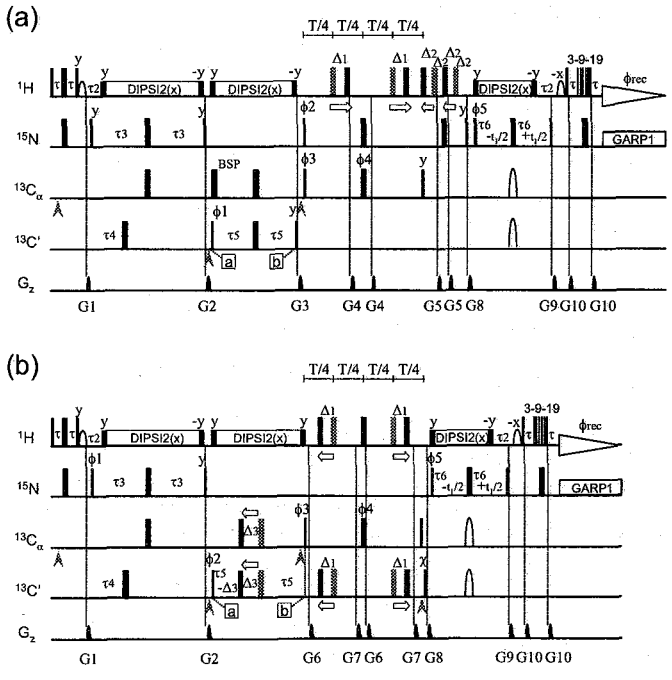

Figure 2 Pulse scheme for quantification of cross-correlated relaxation rates (a) $\Gamma_{HN,H\alpha C\alpha}(\Phi)$ and (b) $\Gamma_{C',H\alpha C\alpha}(\Phi)$. Narrow and wide pulses indicate 90° and 180° pulses, respectively. Two open shapes in the middle of 2τ6 indicate a 180° pulse, applied as a single 500 μs adiabatic Chirp pulse which simultaneously inverts $^{13}C^{\alpha}$ and $^{13}C'$ spins. The delays used are $\tau = 2.25$ ms, $\tau_2 = 5.5$ ms, $\tau_3 = 26$ ms, $\tau_4 = 16.5$ ms, $\tau_5 = 4.5$ ms, $\tau_6 = 20$ ms, $\Delta_1 = 0.89$ ms, $\Delta_2 = 0.49$ ms, $\Delta_3 = 1.78$ ms, and T = 28 ms [can be optimized if a C^{α} selective 180° pulse (ϕ4) is applied to refocus the $^1J_{C\alpha C\beta}$ coupling. Gray rectangles in the "reference" measurement are placed so that scalar couplings are refocused. In the "cross" measurement, these pulses are shifted (hatched rectangles) to allow (a) evolution under $^1J_{C\alpha H\alpha}$ and $^1J_{NH}$, and (b) refocusing of the carbonyl chemical shift and evolution under $^1J_{C\alpha H\alpha}$. The phase cycling is (a) ϕ1 = 4(x), 4(-x); ϕ2 = 2(y), 2(-y); ϕ3 = y, -y; ϕ4 = 8(x), 8(y); ϕ5 = y + States-TPPI; ϕ_{rec} = x, 2(-x), x, -x, 2(x), 2(-x), 2(x), -x, x, 2(-x), x; (b) ϕ1 = 8(y), 8(-y); ϕ2 = x, -x; ϕ3 = 2(x), 2(-x); ϕ4 = 4(x), 4(y); ϕ5 = y + States-TPPI; ϕ_{rec} = x, 2(-x), x, -x, 2(x), 2(-x), 2(x), -x, x, 2(-x), x; χ = y ("reference") or x ("cross").

2 LJ3

効率的なタンパク質リン酸化修飾手法の開発: リン酸化 Crk-II の構造解析への応用

([1]北海道大学大学院薬学研究院、[2]日本学術振興会、[3]タンパク 3000)

○小橋川　敬博[1,2]、内藤　雅人[1]、稲垣　冬彦[1,3]

Effective method for protein phosphorylation and its application for structural analysis of phosphorylated Crk-II

○Yoshihiro Kobashigawa[1,2], Masato Naito[1], Fuyuhiko Inagaki[1,3]

([1]Graduate School of Pharmaceutical Sciences, Hokkaido Univ., [2]JSPS, [3]Protein3000)

Protein phosphorylation is a major post-translational modification that regulates cellular signal transduction. Although substrate proteins are phosphorylated by their specific kinases, cognate pairs of substrates and kinases are still elusive. In addition, phosphorylation is mediated through indirect as well as direct interaction between kinases and substrates, which makes difficult to effectively prepare phosphorylated proteins *in vitro*. Here we show a novel protein phosphorylation method that utilizes artificially introduced cognate binding modules into substrates and enzymes. This enhances the local concentration of substrates around enzymes so that the enzymatic reaction proceeds efficiently. We prepared a substrate protein that contains a SH3 domain, and a kinase containing a SH3 binding motif. This method was successfully applied for preparation of phosphorylated $^{13}C/^{15}N$-labeled CrkII, and followed by NMR structural analysis.

タンパク質のリン酸化は生体内シグナル伝達に関わる主要な翻訳後修飾の一つである。生体内では特定の基質を特定のキナーゼがリン酸化するが，そのペアについては未だ同定されていない場合が多い。また，リン酸化反応は基質とキナーゼの間の直接的，もしくは複数のアダプター分子を介した間接的な相互作用を介して行われる。そのため，リン酸化タンパク質の大量調製は一般には困難であり，基礎研

Fig.1. Schematic representation of the protein phosphorylation system using the artificially introduced cognate binding modules.

キーワード：SH3,　module,　motif,　interaction,　kinase

○こばしがわ　よしひろ、ないとう　まさと、いながき　ふゆひこ

究，応用研究の妨げとなっている。本研究では，互いに相互作用するドメインをキナーゼと基質に人為的に融合させたタンパク質をデザインすることにより，基質と酵素の局所濃度を高めリン酸化反応を効率的に行う手法を開発した (Fig. 1)。また、それをリン酸化Crk-IIの$^{13}C/^{15}N$ラベル体の大量調製に応用した。

Crk はキナーゼからのシグナルを small G にリンクするアダプター分子であり、主に接着斑において機能する。細胞骨格の再構成、細胞運動性、細胞増殖等に関わり、ヒトの肉腫、肺癌、乳癌、脳腫瘍等で発現の亢進が見られる。Crk-II は SH2-SH3-SH3 のドメイン構造 (Fig. 2) よりなり、2 つの SH3 ドメインの間のリンカー領域に存在する Y221 が Abl によりリン酸化されることにより不活性化されることが知られている。本研究ではリン酸化状態の Crk-II の構造を NMR により決定した。

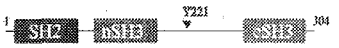

Fig.2. Domain structure of Crk-II.

ドメイン間相互作用を利用した効率的なリン酸化

最初に Abl による Crk-II のリン酸化を行った。キナーゼドメインのみからなるコンストラクトおよびキナーゼドメインの C 末端側に Crk-II の N 端側 SH3 ドメイン (nSH3) の結合配列である PXXP モチーフを付加したコンストラクトによるリン酸化を試みた。リン酸化は CBB 染色および Crk-II の Y221 に対するリン酸化特異的な抗体を用いた免疫染色により確認した。その結果、PXXP モチーフを付加することにより数十分の 1 のキナーゼで同程度のリン酸化効率が得られた。基質タンパク質を Vav(170-375)に変えた場合においても、相互作用モジュールを Grb2 の C 端側 SH3 ドメインと RXXK モチーフに変えた場合においても同様の結果が得られた。ちなみに、Vav(170-375)の生体内におけるキナーゼは Src Family Kinase であり、Abl は本来のキナーゼではない。さらに同手法の応用として，大腸菌によるリン酸化タンパク質の発現を目的としてキナーゼと相互作用ドメイン，任意の基質タンパク質の遺伝子を挿入可能なマルチクローニングサイトを含む発現ベクターを作製し，実際に Vav(170-375)を発現させたところ，ほぼすべてリン酸化体として得られた。

リン酸化Crk-IIの立体構造

本手法を用いて$^{13}C/^{15}N$ラベル体リン酸化Crk-IIの大量調製を行い, NMRによる構造決定を行った (Fig. 3) 。その結果、Y221 を自己のSH2 ドメインが認識しており、標的分子の結合が阻害されていることが示された。また、SH2 とnSH3 の間にあるリンカー領域がnSH3 の標的分子認識部位の一部をマスクされていることが示唆され、実際に滴定実験およびpull-down assayにより確認された。これにより、Crk-IIのリン酸化による不活性化機構の一端が構造的に示された。

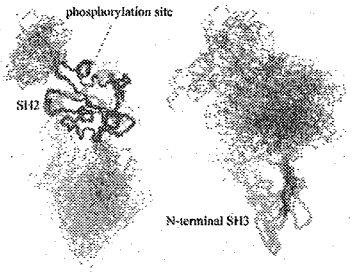

Fig.3. Solution structure of phosphorylated Crk-II superimposed on SH2 (left) and on nSH3 (right).

NMR測定条件下でのタンパク質凝集の抑制

[1]群大工、[2]三菱化学生命研、[3]福岡女子大環境理
○ 向瓏[1]、稲岡斉彦[1]、石井毅[1]、細田和男[1]、小堀可奈子[1]、川合美菜子[1]、向井秀仁[2]、佐藤一紀[3]、河野俊之[2]、若松馨[1]

Prevention of protein aggregation under conditions specific to NMR measurements

([1]Faculty of engineering, Gunma University, [2]Mitsubishi Kagaku Institute of Life Sciences, [3]Department of Environmental Science, Fukuoka Women's University)
Long Xiang[1], Toshihiko Inaoka[1], Takeshi Ishii[1], Kazuo Hosoda[1], Kanako Kobori[1], Minako Kawaai[1], Hidehito Mukai[2], Kazuki Sato[3], Toshiyuki Kohno[2], Kaori Wakamatsu[1]

In solution NMR measurements of proteins, sample conditions are set up such that protein molecules are in the monodispersive state. It is because the aggregation of protein molecules leads to severe broadening of NMR resonances hence to poor signal resolution and low signal-to-noise ratio. Here we show that some proteins and peptides aggregate under conditions specific to NMR measurements: chemical shift reference compound, D_2O, and NMR sample tube. We also show the methods to circumvent such aggregation. With several simple precautions, the lifetime of protein samples for NMR can be greatly extended.

【緒言】

溶液NMRにおいて、タンパク質の凝集はみかけの分子量を増大させシグナルの感度と分離を悪化させる。そこで、バッファー組成などを検討する事によってタンパク質分子が単分散状態である条件を設定する。しかし、動的光散乱測定等では単分散であると判断されるサンプルもNMRを測定するとブロードなシグナルを与える事がある。NMR測定に固有な条件を検討したところ、NMRサンプル管のガラス表面、化学シフト基準物質であるDSS、重水中の不純物がタンパク質やペプチドを凝集させる事がわかった。

【結果】

(1) ガラス表面によるタンパク質の凝集:

m4I3C(14)とGi1 α の混合物をNMRサンプル管に入れた時の凝集をFig. 1に示す。サンプル管をシリコナイズしていないと混合物は強く白濁するが(左)、シリコナイズ処理を1回(中央)すると濁度が下り、3回処理すると全く濁らなくなった(右)。

ガラスのミクロビーズの表面をシリコナイズ処理するとタンパク質の吸着量が増えるという結果があるが、NMRサンプル管と同様な管に対する吸着量はシリコナイズ処理によって低下する事はあっても、増える事は無かった(タンパク質の種類で異なる)。

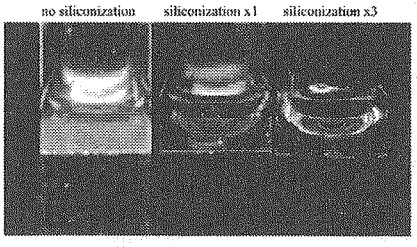

Fig. 1: Glass furface-induced aggregation of protein/peptide mixture. The times of siliconization treatment of NMR sample tube was 0 (left), 1 (middle), and 3 (right).

タンパク質　ペプチド　凝集　ケイ素化合物

こうりゅう　いなおか よしひこ　いしい たけし　ほそだ かずお　こばり かなこ　かわあい みなこ　むかい ひでひと　さとう かずき　こうの としゆき　わかまつ かおり

(2) 化学シフト基準物質によるペプチドの凝集:

m4I3C(14)の水溶液に化学シフトの基準物質であるDSSを添加するとペプチドのシグナルがブロードになった(上)。また、DSSのメチルシグナルもブロードであった。

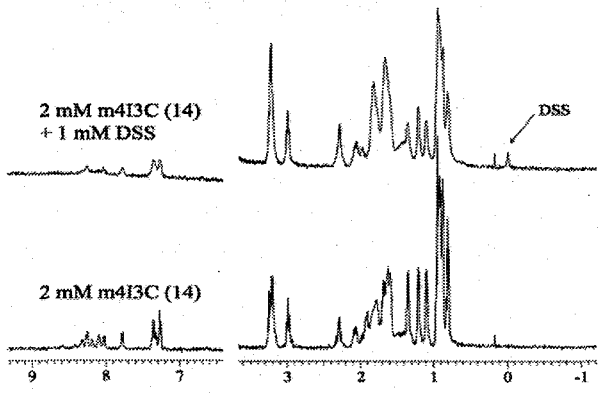

Fig. 2: DSS-induced aggregation of peptide. 1D proton spectrum of m4I3C(14) in the absence (bottom) and presence (top) of DSS.

(3) 重水中の不純物による凝集:

市販の重水には約0.15 ppmに不純物のプロトンシグナルが観測される事がある(Fig. 2, bottom)。重水中のこの不純物は両イオン交換樹脂で除去できるが、精製した重水を用いると、PC/PS/CHAPSOのバイセルに入れたマガイニン2のシグナルが1.7倍高くなった(Fig. 3)。

市販の重水を原子吸光で分析したところ、0.1 ppm程度のケイ素を含む事がわかった。また、タンパク質やペプチドの水溶液にケイ酸を添加すると微量でも凝集を引き起した。

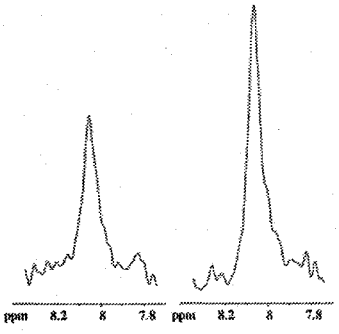

Fig. 3: Purification of D_2O sharpens HSQC signal of magainin 2 in bicelle.
Left: D_2O without purification,
Right: D_2O purified with ion-exchange resin.

【考察】

タンパク質の立体構造をNMRで決定するためにはタンパク質が長期間安定に単分散の状態で存在する必要がある。しかし、生理的意義の高いサンプルほど不安定でかつ凝集しやすい。例えば、大腸菌のタンパク質に比べてヒトのタンパク質は凝集しやすく、また単独のタンパク質に比べて複合体(タンパク質/タンパク質、タンパク質/ペプチド、タンパク質/核酸)は凝集しやすい。そこで、タンパク質を凝集させる要因を極力排除する必要がある。今回、NMR測定に固有の条件でタンパク質やペプチドが凝集しうる事を示したが、これらの凝集原因は簡単な処理で除去できる。質の良いスペクトルを得る事が従来困難であったサンプルの構造が、これらの注意を払う事によって決定できるようになると期待される。

2 LJ5

Application of the wheat germ cell-free protein synthesis system to NMR studies on protein structure

Masato Shimizu, Koichi Akiyama, Eugene Hayato Morita
Integrated Center for Sciences, Ehime University

Introduction

To understand living organisms, it is indispensable to analyze the relationships between structure and functions of proteins which govern the homeostasis of the cell. To fulfill this need, techniques for cell-free protein synthesis systems are rapidly being improved. Comparing the traditional gene manipulating techniques (overexpression of recombinant proteins), with a cell-free translation system, one can synthesize larger proteins at high speed, and as accurately as ones by *in vivo* translation, and can express proteins that would interfere with the host cell physiology. One of the most convenient and reliable types of eukaryotic cell–free translation systems is based on wheat germ embryos containing all the components for translation in a concentrated dried state and ready for protein synthesis after germination. With the use of heteronuclear multidimensional NMR techniques (1-5), we demonstrated that wheat germ cell-free protein synthesis system provides enough amounts of proteins (mg sale of proteins per ml reaction mixture), and synthesized proteins holds the native structure and biological activities. This means that such a cell-free system is applicable to the analysis of the relationships between protein structures and functions. In particular, a wheat germ cell-free protein synthesis system was shown to be a convenient way to synthesize amino-acid selectively labeled proteins (2-5).

In this study, we have further developed the noble way to synthesize the proteins with low solubility using detergents. From TOF-MASS analysis, we also found that the in some case, N-terminals of the synthesized proteins have the heterogeneity. N-terminal methionine residues of proteins synthesized with this system can be lost and the addition of CH_3CO might occur at the same time.

Materials and Methods

Protein Synthesis—For NMR studies, four-hundred micrograms aliquots of the synthesized mRNAs were dissolved in 600 μl of a dialysis buffer, and then mixed with a wheat germ extract (ZOEGENE Corporation) for protein synthesis . This mixture was dialyzed against the dialysis buffer containing 20 amino acids (labeled with ^{15}N; 0.3 mM each) for 2 days. Labeled amino acids of cell-free grade were purchased from Taiyo Nippon Sanso Corporation. After the synthesis, synthesized proteins were purified with appropriate chromatographic techniques and concentrated to a protein concentration of 50 μM.

Detergent Selection-To find the most appropriate detergents for protein synthesis, we synthesized the proteins in 1/10 scale of NMR sample preparation with or without detergents. In this study, we tested the four detergents (Brij35, Brij58, TritonX-100, and NP-40) with 0.1% concentration.

Measurement of NMR Spectra—D_2O, as an NMR lock, was added to the concentrated protein

Key Words: Cell-free, Wheat germ, Amino-acid selective labeling, N-terminal modification

solution to the level of 10%. Two-dimensional ^{1}H-^{15}N HSQC spectra of the protein were obtained with a DMX-500 (Bruker) equipped with a cryogenic probe system, and 512 scans were averaged. The data were processed using NMRPipe on a Linux workstation. ^{1}H and ^{15}N chemical shifts were referenced according to the method of Wishart *et al.* (1995).

Results and Discussion

In case for the synthesis with kinase domain of human Jak1 protein tyrosine kinase, we have tested the effect of four detergents. Without detergents, kinase domain is synthesized as the insoluble materials. In the presence of 0.1% detergents, more than 50% of the synthesized proteins are solubilized. However, Brij35 and Triton X-100 provided lower yield of the protein synthesis. Especially, in the presence of Brij35, almost no proteins are synthesized. Within these 4 detergents, NP-40 provided the highest yield. In case of other proteins, NP-40 and Brij35 also provided the highest and the least yield, respectively. This means that Brij35 must strongly inhibit the translation pathway of wheat germ cell-free protein synthesis system. We now compare the biological activities of the solubilized kinases to find the most effective detergents providing the active kinase domain for structural and functional analyses. Another important problem is the molecular mechanism of which detergents solubilize the insoluble proteins with lower concentration than critical micelle concentration (CMC), and we also try to clarify this.

In case of calmodulin (CaM), we have observed two different molecular weights for synthesized protein. Comparing the calculated molecular weight in consideration of the amino acid sequence of CaM, observed molecular weights correspond to the molecular weights of (CaM-Met), and (CaM-Met+CH_3CO). This means that the synthesized CaM with wheat germ cell-free system lacks the N-terminal Met, and addition of CH_3CO occurs in some ratio. This will give the structural variation in N-terminal region, and this tendency was also identified in ^{1}H-^{15}N HSQC spectrum of CaM synthesized with this system.

Acknowledgement

This work was supported by the Research Promotion Bureau, Ministry of Education, Culture, Sports, Science and Technology (MEXT), Japan, under contract No. 17-211, and grants for the National Project on Protein Structural and Functional Analyses. NMR and TOF-MASS measurements were performed at Venture Business Laboratory in Ehime University.

References

[1] Morita, E.H., Sawasaki, T., Tanaka, R., Endo, Y., and Kohno, T., *Protein Sci.* **12**, 1216–1221 (2003).

[2] Morita, E.H., Shimizu M., Ogasawara T., Endo, Y., Tanaka R., and Kohno T., *J. Biomol. NMR* **30**, 37–45 (2004).

[3] Morita E.H. Tanpakushitsu Kakusan Koso, **50**, 1361-1366 (2005).

[4] Morita E.H., Bunko Kenkyu, **55**, 274-283 (2006)

[5] Shimizu, M., Ikegami, T., Akiyama, K., and Morita E.H., J. Biochem 140, 453-456 (2006).

2 LJ6

Development of a workflow tool in solution protein NMR: Olivia

Masashi Yokochi, Yoshihiro Kobashigawa, Shinji Sekiguchi
and Fuyuhiko Inagaki
Department of Structural Biology, Graduate School of Pharmaceutical Sciences,
Hokkaido University, N-12, W-6, Kita-ku, Saporo, 00-0812, Japan

Introduction

Over the last five years we have designed, implemented and distributed a NMR resonance assignment analysis system called Olivia for help of determination of solution protein structure. Olivia is designed to share the whole of NMR assignment processes without losing confidence level as same as first analyzer could have. Remembering workflow of the NMR analysis, there must be solutions for quality management of the analysis that anyone can summon multiple spectra accounting assignment decision and that anyone can correct it and synchronize the results within all relevant spectra. From this point of view, NMR spectroscopic analysis has been considered as closed work even in a same laboratory. That is why holding the result solely quite so differs from sharing assignment processes in the sense of sharing confidence information together. It's possible if real-time assignment assessment services, assignment navigation tools and its visualization technique are cooperatively developed in a system. We present Olivia as a workflow tool for solution protein NMR analysis by introducing various techniques that cover from NMR data acquisition (FID) to assessment of structure determination (PDB).

Highlights

As for assessment services, we have developed peak list, spectra, and structure based evaluation techniques respectively. Fig.1 shows both concept and implementation of unique spectra based evaluation technique. Graph of lower part of 3D NOESY spectra represents direct spectral correlation coefficients: Pearson's product moment correlation coefficient, Spearman's rank correlation coefficients and Kendall's tau. In this case, transpose NOE resonances raise all correlation coefficients. Fid.2 shows structure based evaluation technique, horizontal lines over resonance represents near distance NOEs derived from structure information.

Keywords: NOE assignment

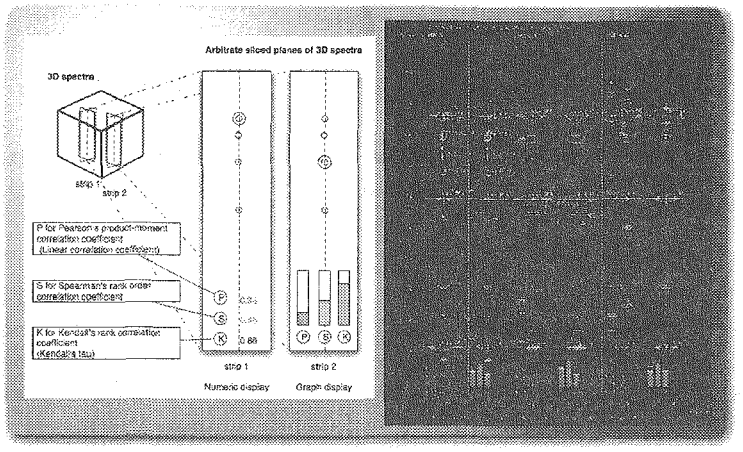

Fig. 1

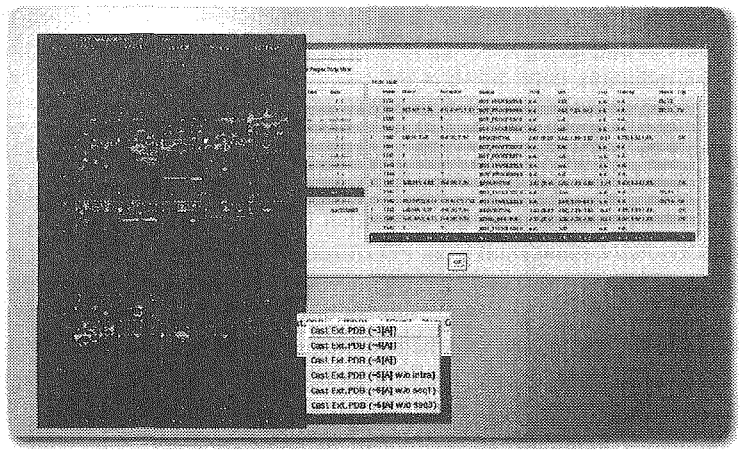

Fig.2

User support

Developer team has been formed to adopt Olivia to the latest NMR technology and to improve user interface, functionality and performance continuously. We already opened official web site, http://fermi.pharm.hokudai.ac.jp/olivia/, which distributes source files, development news and documents including user's manual. And we provides user's community site concurrently. User's feedback information has been utilized to improve the system.

System requirements

Olivia would run on any UNIX variants such as: FreeBSD, Irix, Linux, Mac OS X and Solaris, The system is designed to work with NMRPipe well, but Azara, UCSF(Sparky), NMRView and XEASY are supported. For the NOE ambiguous assignment program with MD and SA, you can choose from CYANA 2 and ARIA 2.

A laptop NMR spectrometer[1]

Kazuyuki Takeda [2]
Graduate School of Engineering Science, Osaka University, Japan

ABSTRACT: The digital circuits for an NMR spectrometer have been built into a single chip of Field-Programmable Gate-Array (FPGA), with which a laptop-sized, home-built spectrometer has been constructed.

1. Introduction

Application of NMR spectroscopy has been diversified into a wide variety of scientific and engineering fields. In order to meet various demands from various fields, commercial NMR spectrometers are very carefully designed and well built. In some cases, however, one may have reasons for wanting a home-built spectrometer. For example, some exotic experiments may require modification to hardware inside the spectrometer; it is formidable to do it in the commercial spectrometer.

In this work, it is shown that a handy and operational NMR spectrometer can be built by combining the latest semiconductors devices and RF components. The spectrometer presented here has three channels, each of which is capable of outputting RF of up to 400 MHz, and modulating the amplitude, phase, and frequency of the RF irradiation.

The key strategy for developing this spectrometer is to fully exploit a *Field-Programmable Gate-Array* (FPGA). An FPGA is an LSI composed of a large number of *programmable* logic gates, in which digital circuits, called IP-cores ("IP" stands for "Intellectual Property"), can be built with hardware description codes. An FPGA is attractive in the sense that (i) circuit components are, once developed, re-usable, (ii) the individual circuits built in an FPGA run *concurrently*, (iii) circuits in the chip are re-configurable as many times as necessary, and (iv) development requires only a personal computer and a download cable. In principle, an FPGA can realize any digital circuits within limitations set by the available number of logic elements and the operation speed. In this work we aimed at letting *a single FPGA chip* do all the digital jobs required for an NMR spectrometer. These include (a) triple pulse programmers, (b) Direct Digital Synthesizer (DDS), (c) a digital receiver composed of a digital quadrature demodulator and a digital low-pass filter, and (d) PC interfaces for command/data transfer. The FPGA chip used in this work is EP2C70F672C8, which is one of "Cyclone II" devices by Altera Inc. Its 27x27 mm package has 68,416 logic elements, 1,152,000 RAM bits, 150 multipliers, 4 PLLs, and 622 I/O pins.

2 Architecture of the spectrometer

Fig. 1 describes the block diagram of one of the three RF channels. In this architecture, two RF sources, denoted by DDS(I) and DDS(II), are used; the former is phase-tunable and frequency-fixed at 20 MHz, while the latter is frequency-tunable and phase-fixed. In order to generate a signal with an intended frequency f, the frequency of DDS(II) is set to f+20 MHz. Each of DDS(I) and DDS(II) is equipped with *two* RF sources, which have an identical frequency but are out of phase by 90°. The quadrature signals from DDS(I) and DDS(II) are sent to an image reject mixer, which generates the frequency f without the image frequency f+40 MHz. The signal is then amplitude-modulated with a multiplier, and finally pulse-modulated with an RF switch to generate the excitation pulses. The control words for the RF-phase, frequency, amplitude, transmitter gate, power-amplifier unblanking, etc., are provided by a pulse programmer described below.

[1] *Key Words:* Field-Programmable Gate Array (FPGA), IP-core, Pulse programmer, Direct Digital Synthesizer (DDS), Digital receiver

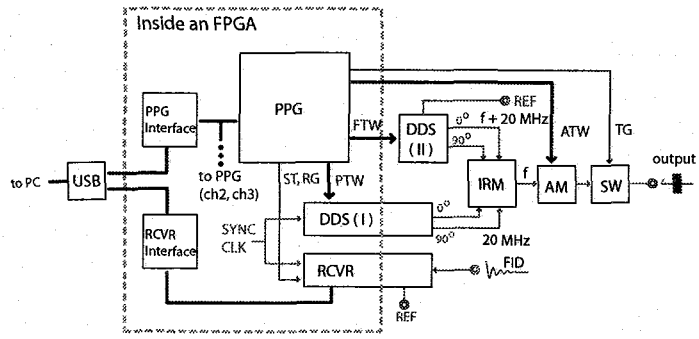

Fig. 1. A block diagram for one of three RF channels developed in this work. The glossary is as follows. PPG: Pulse Pro-Grammer, DDS: Direct Digital Synthesizer, IRM: Image-Reject Mixer, AM: Amplitude Modulator, SW: SWitch, RCVR: ReCeiVeR, FTW: Frequency-Tuning Word, PTW: Phase-Tuning Word, ATW: Amplitude-Tuning Word, TG: Transmitter Gate, RG: Receiver Gate, and ST: Sampling Trigger.

2.1 Pulse programmers

The design of the pulse programer is based on a prototype developed by Prof. Takegoshi at Kyoto University. The original one used ~100 ICs on several circuit boards and enormous wire connections among them. Here, the VHDL[2] codes were written that reproduces this pulse programmer. It operates at a clock frequency of 100 MHz, and has a 40-bit timer counter. Thus, the time resolution is 10 ns and it can count up to 10 ns$\times 2^{40} > 10000$ sec. One 32-bit loop counter and two 16-bit loop counters are also incorporated, which can be nested so that an iteration of up to $2^{32} \times 2^{16} \times 2^{16} = 2^{64}$ times is possible. The pulse programmer has 64 line outputs, which is used to control amplitude, phase, frequency, transmitter gate, and power-amplifier unblanking for an individual RF channel.

In this work we went further to incorporate the separate, three identical pulse programmers inside the FPGA for up to triple-resonance experiments. It was as easy as calling a subroutine in computer programming, once the code for a single pulse programmer has successfully been written. Rather than a single pulse programmer with much more line outputs, we have chosen to put the separate, independent pulse programmers for controlling the individual RF channels because in some cases, e.g, in TPPM decoupling, they are needed to run asynchronously. In this sense, the concurrent property makes an FPGA quite advantageous over a microprocessor, which is also capable of digital jobs but operates sequentially.

2.2 DDS

Direct digital synthesis (DDS) is a technique to generate a frequency- and phase-tunable signal by using digital data processing, which is nowadays becoming an alternative to traditional analog synthesis. For the 20 MHz signal generator, DDS(I), all the DDS circuits except for the non-digital components, such as an DA converter and a low-pass filter, have been embedded in the FPGA, as schematically described in Fig. 2(a). Fig. 2(b) shows the signal monitored at the output of the DA converter (AD9740, Analog Devices) driven with the control word generated by the digital part of DDS built inside the FPGA. The DDS(I) operates at a clock frequency of 160 MHz to generate the 20 MHz signal, so that $160/20 = 8$ discrete steps per period are visible in the signal. The rapid voltage change between the steps indicates the existence of higher-frequency Fourier components, which can be removed by passing the signal through the low-pass filter, as shown in Fig. 2(c).

[2]VHDL is one of typical hardware description languages. Another typical one is Verilog.

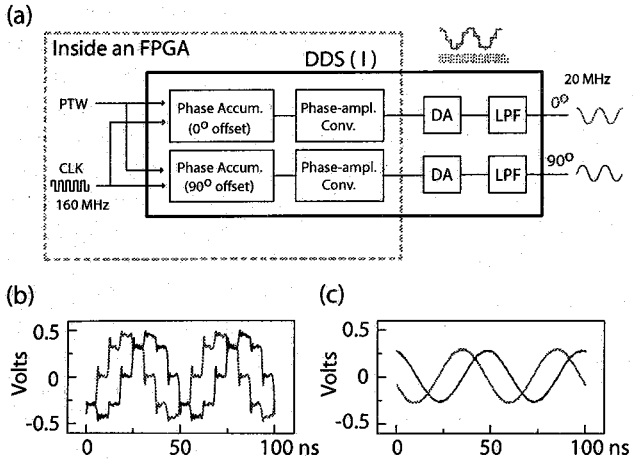

Fig. 2. (a) A Diagram for the phase-tunable DDS synthesizer with a fixed frequency at 20 MHz. The digital components, a phase accumulator and phase-to-amplitude converter, were built inside the FPGA by writing the VHDL codes. A 160 MHz clock is used to generate the 20 MHz signal. The control word for the DA converter is thus updated every 6.25 ns, as shown in (b), and the fundamental harmonic is extracted through a low-pass filter, as demonstrated in (c). For image-reject mixing, two 20 MHz signals are generated whose phase is shifted exactly by 90°.

On the other hand, for the other frequency source, DDS (II), the required frequency (up to ~400 MHz) is too high to be implemented in the same manner. Accordingly, a DDS-dedicated LSI, AD9858 (Analog Devices), was used, which can be driven with a clock frequency of 1 GHz. Since the maximum output frequency of a DDS system is typically ~ 0.4 times the clock frequency, it can generate a signal of up to 0.4 × 1 GHz ~400 MHz. The programming of an AD9858 chip is carried out by the pulse programmer.

2.3 Signal acquisition

Fig. 3(a) is a diagram describing the receiver. The NMR signal with a frequency $f + \Delta$ is down-converted with respect to the reference frequency f+20 MHz of DDS(II) into the intermediate frequency (IF) at Δ+ 20 MHz, and the IF signal is digitized by a 14-bit AD converter (AD9245, Analog Devices) operating at 80 Msps. The digitized IF signal is then sent to the digital receiver built inside the FPGA, and *digitally processed* in the following manner. Firstly, the Δ+ 20 MHz IF is digitally demodulated into in-phase (I) and quadrature (Q) components having a frequency (Δ+ 20 MHz) - 20 MHz = Δ. In order to demonstrate digital quadrature demodulation, a signal with successive frequency jumps (20.2, 21, and 20.5 MHz) generated by DDS(II) was connected to the input (indicated by a star in Fig. 3(a)) of the AD converter. As shown in Fig. 3(b), the digital quadrature demodulator has successfully converted the input signal into the I and Q components with frequencies Δ of 0.2, 1, and 0.5 MHz.

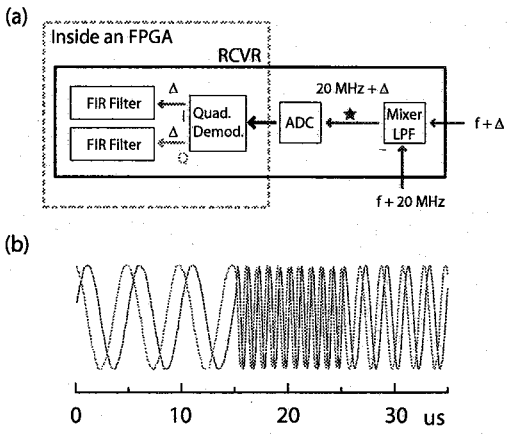

Fig. 3. (a) A diagram for the receiver composed of non-digital parts (a mixer and an AD converter), and the digital parts (a quadrature demodulator and digital FIR filters) built inside the FPGA. For the mixer used was AD831 (Analog Devices), which is equipped with a low-pass filter whose cutoff frequency is determined by external capacitors. (b) Demonstration of quadrature demodulation performed digitally inside the FPGA. See the text for detail.

The AD-conversion rate of 80 MHz, which is exactly 4 times the demodulation reference frequency of 20 MHz, was convenient for writing the VHDL codes for demodulation, because the multiplication factors $\sin(2\pi t \cdot 20\text{MHz})$ and $\cos(2\pi t \cdot 20\text{MHz})$ used in the demodulation process can only take 0,1, and -1 at the 80 MHz clock edge, and the operation becomes much simpler.

Secondly, each of the I and Q components of the signal is passed through a Finite Impulse Response (FIR) low-pass filter, also written in VHDL. Fig. 4 demonstrates, as an example, the effect of a 31-stage, Hamming-window FIR filter with a cutoff frequency of 1.5 MHz. In this experiment, a frequency-jumped signal, switched from 20.2 to 22.5 MHz in 6 steps, was generated by DDS(II) and was digitized, and then quadrature-demodulated in the same way as in the measurement shown in Fig. 3. In the demodulated signal shown in Fig. 4(a), the observed frequency was varied from 0.2 (=20.2-20) to 2.5 (=22.5-20) MHz. When this signal is further passed through the FIR filter, the amplitude of the signal above the cutoff frequencies was significantly reduced, as seen in Fig. 4(b). The FIR digital filters with various cutoff frequencies were incorporated, from which the user can select the appropriate one according to the sampling interval, or spectral width, of an individual experiment.

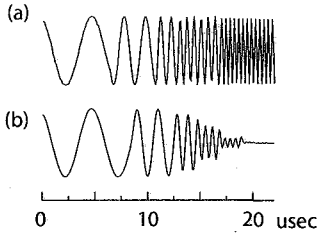

Fig. 4. A signal (a) without, and (b) with the digital FIR low-pass filter with a cutoff frequency of 1.5 MHz.

The processed data is finally sent to a PC through a USB cable. The same USB cable also serves for transferring a pulse program from the PC to the spectrometer. In order to manage transfer of both pulse programs and NMR signals via a single USB line, a USB breadboard purchased from HuMANDATA Ltd. was used, which is equipped with a two-channel USB IC FT2232C (FTDI).

In summary, a laptop-sized, three-channel NMR spectrometer has been built. By packing the required digital circuits into a single FPGA chip, the system has become pretty compact. Thus, one can, for example, take the spectrometer out of the laboratory. It is also possible to modify the system so as to meet the specific needs of the user. The author hopes and believes that this work could lower the barriar of building a hand-made spectrometer in a laboratory, and promote exotic and exciting NMR experiments.

The snapshot of the spectrometer is presented in Ref. [2].

References

[1] K. Takeda, *Single-chip pulse programmer on field-programmable gate-array*, 47th ENC (2006).

[2] K. Takeda, *Packing digital circuits for an NMR spectrometer into a single chip*, poster session.

2 LJ8

微量試料用 microMAS プローブの開発と生体高分子への応用

(農工大・工[1])
°山内 一夫[1]、高橋 塁[1]、朝倉 哲郎[1]

Development of MicroMAS Probehead and Its Application to Biopolymers

(Department of Biotechnology, Tokyo University of Agriculture and Technology[1])
°Kazuo Yamauchi[1], Rui Takahashi[1], and Tetsuo Asakura[1]

The probehead (microMAS) is developed for high-resolution solid state NMR observation of mass limited samples. Microrotors with 1mm o.d. or 0.5mm o.d. are developed, it has the capability of observation wit sub-micro gram to 500μg of the sample. The probehead gives extremely high sensitivity of the spectra and largely improves the limit of detection for solid state NMR. As the results, the NMR spectra of μg order samples could be successfully observed using conventional 400 MHz NMR within a few hours. Here, we introduce some applications for the structure determination of the biopolymers with microMAS probehead, including REDOR experiments using triple-microMAS probehead.

緒言

NMR の最大の弱点は他の分析機器と比較して、その感度の低さにある。実際、従来の固体 NMR 測定では、ミリグラム単位、マイクロリットル単位のサンプル量が必要であった。従って、例えば微量しか得られない生体物質については、固体 NMR の測定が事実上、不可能となる場合もあった。このような微量サンプルの系を固体 NMR の測定対象にするためには、微量サンプルにターゲットを絞った、感度の高い NMR 測定技術の開発が必要となる。

現在、NMR の高感度化技術は外部磁場の高磁場化など、いくつか行われているが、装置やサンプルの観点から汎用的に微量物質を感度よく測定する方法としてマイクロコイル NMR プローブを用いることは非常に有利である。我々は微量でも高感度・高分解能で観測可能な固体 NMR 用の microMAS プローブを開発し(Fig.1)、検出限界の飛躍的な向上を実現してきている [1)-3)]。これにより今まで観測が事実上不可能であったミリグラム以下の試料であっても観測が可能となった。

マイクロコイルコイル NMR を用いた応用例は多岐にわたるが、本発表においては特にニーズの高い生体試料測定の可能性を検討した。

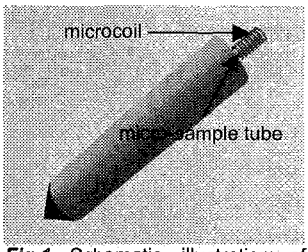

Fig.1 Schematic illustration of microMAS rotor. Samples are set in the micro-sample tube and rotate with conventional rotor.

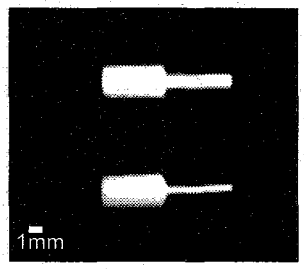

Fig.2 A photo of micro -MAS rotor. Rotor diameter is 1 mm (up) and 500 μm (down), it rotates up to 12 kHz.

プローブ製作

マイクロコイルプローブは ^{13}C 観測、^{1}H デカップリングの CP/MAS を行うことができるシングルコイルダブルチューンの LC 回路で構成されるもの、1mm のローターを用いるために、ソレノイド型の RF コイルは回転中ローターと接触し破損しないようにコイル内径 1.2mm のものを用いた。

microcoil, MicroMAS, mass-limited sample, silk fibroin, solid state NMR
やまうちかずお、たかはしるい、あさくらてつお

サンプル管は Fig.2 に示すようなサンプル量に応じて、ジルコニア製の外径 1mm 内径 500μm および外径 500μm 内径 300μm のものを使用した。マイクローターは、通常ローターと同軸接続する形となっているために回転は通常ローターと同じように行う事ができる。本サンプル管では 10kHz で安定した回転を確認した。また、3日以上の長時間測定でも安定して回転することが確認できた。

さらに、^{13}C,^{15}N 観測、^{1}H デカップリングの REDOR などの測定を目的とした同様の 3 チャンネルプローブの製作を行った。(Fig.3)

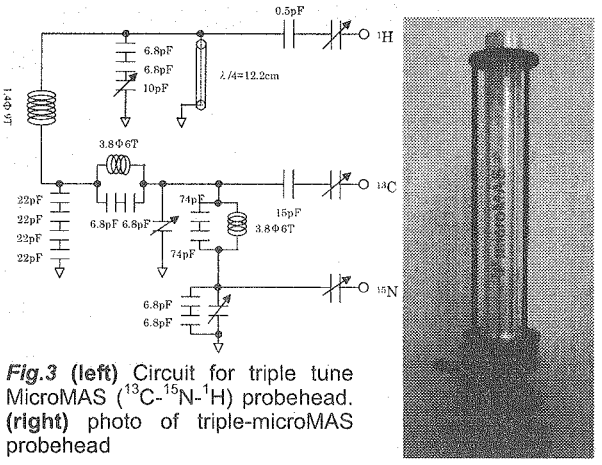

Fig.3 **(left)** Circuit for triple tune MicroMAS (^{13}C-^{15}N-^{1}H) probehead. **(right)** photo of triple-microMAS probehead

測定・プローブ評価

原子間の距離情報は生体高分子の構造情報を得るために非常に重要である。REDOR などの双極子相互作用を利用した距離測定手法は、正確・精密な距離情報が得られるが、プローブをはじめとする装置の信頼性も重要となってくる。このような点から今回製作した triple-microMAS プローブを用いて距離が既知のサンプルであるグリシンの距離測定を行いプローブの性能を評価した。

Fig.4 に REDOR の ΔS/Soff カーブと理論曲線を示す。今回測定したカルボニル炭素とアミド窒素の距離は単結晶より 2.48Å と出ているが、今回測定した結果は±0.1Å 以内の誤差で一致している。特に NcTr が長くなっても理論曲線と一致している点が特筆すべき点である。microcoil が非常に強いデカップリングフィールド(200KHz)を用いることが出来るため、プロトンとの双極子相互作用が十分に打ち消されているためであると考えられる。

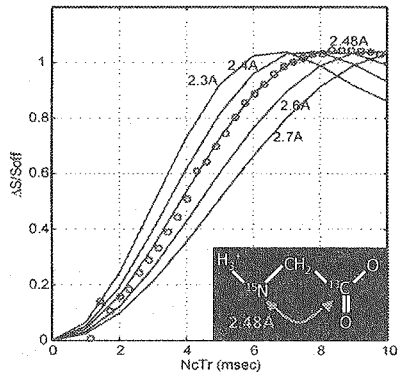

Fig.4 REDOR ΔS/Soff plot of [1-^{13}C, ^{15}N]Gly. Simulated line show the theoretical values for 2.3, 2.4, 2.48, 2.6, and 2.7Å. The experimental result fit to 2.48 Å and it agrees with crystallographic result.

発表では microMAS プローブを用いた実サンプルへの応用を含めて発表する予定である。

謝辞

この開発は独立行政法人科学技術振興機構の先端計測分析技術・機器開発事業による成果である。

参考文献

1) K. Yamauchi, J.W.G. Janssen A.P.M. Kentgens, *J. Magn. Reson.* **167**, 87. (2004).
2) K. Yamauchi, T. Imada, T. Asakura, *J. Phys.Chem. B,* **109**, 17689.(2005).
3) K. Yamauchi, T. Asakura, *Chem. Lett.***35**, 426.(2006).

気体原子の光ポンピングによるアルカリ塩の核スピン偏極

兵庫県立大[A], Princeton University

○石川潔[A], B. Patton, Y. -Y. Jau, and W. Happer

Nuclear spin polarization of alkali-metal salt by optically pumping atomic vapor

University of Hyogo[A], Princeton University

K. Ishikawa[A], B. Patton, Y. -Y. Jau, and W. Happer

We report the nuclear spin polarization of solid alkali-salt by optically-pumping atomic vapor. Here, CsH salt was used as a model solid. The enhancement of NMR signals was measured at N_2 pressure over a range of 10 to 700 Torr. Spin polarization was successfully transferred to solid nuclei at the lower pressures. We will discuss the mechanism of spin transfer from atomic vapor to solid.

光ポンピングにより、電子スピンのみならず、あらゆる物質において核スピンを偏極することは、古くからの挑戦である。その中で、アルカリ金属原子気体の光ポンピングと、それを利用した希ガス原子の核スピン偏極は、応用面から見ても成功を収めてきた。凝縮系の核スピン偏極に関しては、これまで、有機分子結晶の交換交差と固態効果を利用したレーザースピン偏極、イオン結晶の常磁性不純物を光ポンピングした動的核スピン偏極、光を使用せず極低温・強磁場でラジカル分子などを利用した動的核スピン偏極などが実現されている。しかし、個々の系に特化した手法や装置に頼らざるを得ず、汎用性にかける。ここでは、アルカリ金属原子の光ポンピングを利用した固体中の核スピンを偏極する新たな

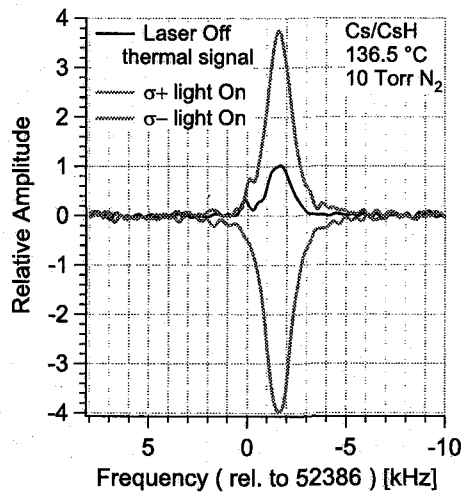

Figure 1: Signal enhancement of ^{133}Cs nuclei in CsH salt by optically pumping Cs vapor. Polarity of enhanced signals was reversed with circular polarization changed. Spin polarization was transferred from polarized vapor to nuclear spin in salt. At buffer-gas pressure of 10 Torr, the enhanced signals were nearly four times larger than thermal signal.

optical pumping, spin polarization, alkali-metal salt, surface interaction

いしかわ きよし、 ぱっとん ぶらいあん、じゃう やんゆう、はーぱー うぃりあむ

手法を提案し、水素化セシウムの核スピン偏極の実験結果について報告する。

実験では、Cs 原子の水素化物を使って Cs イオンの NMR 信号を観測した。磁場は 9.4 T、共鳴周波数は 52.39 MHz、レーザー波長は Cs D_1 線 (894 nm)、温度は 130 ~ 170 °C である。図 1 は、緩衝ガス圧力 10 Torr で光ポンピングしたときの信号増大のようすを示す。熱平衡状態の共鳴信号に比べ、σ_+ 偏光でポンピングすると信号の大きさが 3.7 倍になる。レーザー光を σ_- 偏光にすると、信号の極性が変わり約 4 倍である。実験手法として従来のレーザー動的核偏極と異なる点は、試料温度が比較的高温であること、マイクロ波などを照射しないことである。FID 信号観測のため RF 単パルスを使用するだけであるのは、希ガス原子のスピン交換光ポンピングと似ている。単純で汎用な手法ほど、今後、重要になると思われる。

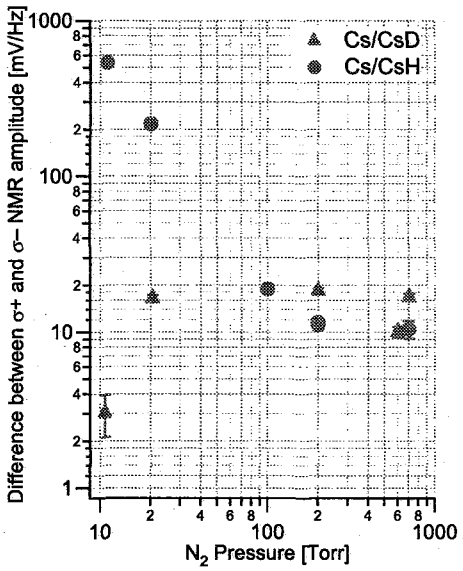

Figure 2: Pressure dependence of signal enhancement. The larger signals were observed at the lower pressures.

本研究が立ち上がった元来の目的は、生体のイオンチャンネルへの応用である。そのためには、さらに偏極率を上げるとともに、多くのイオンでスピン偏極する必要がある。そもそも、気体のアルカリ金属原子から固体の核スピンに偏極がなぜ移行するのか。現時点で候補となる機構は、以下のものであろう。

1. 化学交換で単に原子が置き換わっているだけ。
2. 気相からアルカリ金属原子が吸着して、核スピン間の磁気相互作用で移る。
3. 電子スピン偏極した原子が固体表面に衝突して、スピン交換相互作用で移る。
4. 偏極電子スピンが伝導帯に注入され、固体の核スピンが偏極する。
5. 固体の色中心の電子スピンを経由し、核スピンが偏極する。

図 2 は、信号増大の緩衝ガス圧力依存性である。緩衝ガス圧が低いほど固体の核スピン偏極率が向上する傾向にある。気体原子の核スピンは、高磁場では電子との結合が弱いので、光学遷移では偏極しない。緩衝ガスとの衝突により初めて核スピン偏極する。実験結果は、気体原子の核スピン偏極は重要でないことを支持し、上記 1. 2. を排除する。

Friday, November 24

English Session

3 LE1

Multidimensional Solid-State NMR of Nanocrystals, Fibrils and Membrane Proteins: High Resolution Spectra Leading to Structure

W. Trent Franks,[1] Benjamin J. Wylie,[1] Kathryn D. Kloepper,[1] Heather L. Frericks,[1] Ying Li,[2] Donghua H. Zhou,[1] Deborah A. Berthold,[1,3] Sanjeewa Rupasinghe,[4] Aleksandra Z. Kijac,[2] Lai Lai Yap,[3] Robert G. Gennis,[1,2,3] Stephen G. Sligar,[1,2,3] Mary A. Schuler,[2,4,5] Jerome Baudry[1] and Chad M. Rienstra[1,2,3,*]

Univ. of Illinois at Urbana-Champaign, Departments of Chemistry,[1] Biophysics & Computational Biology,[2] Biochemistry,[3] Plant Biology[4] and Cell & Structural Biology[5] 600 South Mathews Avenue, Urbana, Illinois, USA 61801

http://www.scs.uiuc.edu/~rienstra

Recent advances in magic-angle spinning solid-state NMR spectroscopy enable highly resolved spectra to be measured in a variety of proteins of broad interest to biochemists. Multidimensional methods applied to uniformly isotopically enriched proteins obviate the traditional requirement of site-specific isotopic labeling. Here we show several examples of advanced techniques applied to several biochemical systems.

(1) In the nanocrystalline model protein GB1, especially high spectral resolution and sensitivity enable a completeness of signal assignments not previously observed in any solid protein. Line widths of ~0.1 ppm are observed in many cases, and methods to measure distances and orientation-dependent spectroscopic parameters result in a very high-resolution (~0.5 Å backbone RMSD) structure.

(2) Studies of the fibrillar protein α-synuclein yield insights into several aspects of its role in neuronal physiology and dysfunction implicated in Parkinson's disease. We have examined the wild type and several mutant forms of α-synuclein in micelle-associated complexes by solution NMR and vesicle-associated and fibrillar states accessible only to solid-state NMR. Our experimental data demonstrate an important structural role for domains that include the early-onset mutation sites in the protein.

(3) Our new instrumental capabilities now permit the routine acquisition of multidimensional chemical shift correlation spectra in membrane proteins ranging in molecular weight from 15 to ~150 kDa. Examples include membrane scaffolding proteins derived from apolipoprotein A-I, *E.coli* proteins involved in disulfide-bond transfer, cytochrome P450 monooxygenases and the 1,291-residue cytochrome bo_3 ubiquinol oxidase, the largest protein so far studied using 3D magic-angle spinning techniques. Although technical challenges remain in order to complete the assignments and perform high-resolution structural analysis, substantial progress is demonstrated in the acquisition and partial analysis of data sets in these challenging membrane protein systems. 2D and 3D spectra demonstrate resolution of many hundreds of signals, and we show the promise of 4D magic-angle spinning methods for substantially enhancing the resolution and size range accessible to this type of solid-state NMR, in combination with molecular modeling techniques for simplification of spectral interpretation.

References

"Constant-time through-bond ^{13}C correlation spectroscopy for assigning protein resonances with solid-state NMR spectroscopy", Chen, L.; Olsen, R. A.; Elliot, D. W.; Boettcher, J. M.; Zhou, D. H.; **Rienstra, C. M.**; Mueller, L. J.; *J. Am. Chem. Soc. (Communication)* **2006,** *128*, 9992-9993.

"Determinations of ^{15}N chemical shift anisotropy magnitudes in a uniformly-^{15}N,^{13}C-labeled microcrystalline protein by 3D magic-angle spinning NMR spectroscopy", Wylie, B. J.; Franks, W. T.; **Rienstra, C. M.**, *J. Phys. Chem. B* **2006**, *110*, 10926-10936.

"Backbone conformational constraints in a microcrystalline U-^{15}N labeled protein by 3D dipolar-shift solid-state NMR spectroscopy", Franks, W. T.; Wylie, B. J.; Stellfox, S. A.; **Rienstra C. M.**, *J. Am. Chem. Soc. (Communication)* **2006**, *128*, 3154-3155.

"Site-specific ^{13}C chemical shift anisotropy measurements in a uniformly-^{15}N,^{13}C-labeled microcrystalline protein by 3D magic-angle spinning NMR spectroscopy", Wylie, B. J.; Franks, W. T.; Graesser, D. T.; **Rienstra, C. M.**, *J. Am. Chem. Soc. (Communication)* **2005**, *127*, 11946-11947.

"Magic-angle spinning solid-state NMR spectroscopy of the ß1 immunoglobulin binding domain of protein G (GB1): ^{15}N and ^{13}C chemical shift assignments and conformational analysis", Franks, W. T.; Zhou, D. H.; Wylie, B. J.; Money, B. G.; Graesser, D. T.; Frericks, H. J.; Sahota, G.; **Rienstra, C. M.**, *J. Am. Chem. Soc.* **2005,** *127*, 12291-12305.

"Magic-angle spinning solid-state NMR of a 144 kDa membrane protein complex: E. coli cytochrome bo_3 oxidase", Frericks, H. L.; Zhou, D. H.; Yap, L.; Gennis, R. B.; **Rienstra, C. M.**, *J. Biomol. NMR.*, in press **2006**. (Published online, Sep. 9, 2006).

"Structural analysis of nanoscale self-assembled discoidal lipid bilayers by solid-state NMR spectroscopy", Li, Y.; Kijac, A. Z.; Sligar, S. G.; **Rienstra, C. M.**, *Biophys. J.*, in press **2006**. (Published online, Aug. 11, 2006).

Keywords

Chemical shielding anisotropy, magic-angle spinning, molecular modeling, proteins, recoupling

Structure and Dynamic Pictures of Membrane Proteins and Membrane Associated Peptides as Revealed by Solid State NMR

Akira Naito
Graduate School of Engineering, Yokohama National University 79-5 Tokiwadai, Hodogaya-ku, Yokohama 240-8501, Japan

Introduction

It is important to elucidate structure and dynamic pictures of membrane bound biomolecules to gain insight into the structure function relationship. Solid state NMR provides detailed information on the pictures for particularly membrane associated biomolecules. Magnetically oriented vesicle systems (MOVS) can provide unique information on structure and orientation with respect to the membrane surface if one analyzes the chemical shift anisotropies of the sequentially labeled carbonyl carbons of the backbones of peptides. Magic angle spinning (MAS) experiment is a powerful means to elucidate structure and dynamics of membrane proteins. Particularly REDOR-filtered experiments allow to selectively observe a labeled nucleus of a particular amino acid among them whose inter-nuclear distance is very close. When fast magic angle spinning (f-MAS) experiment is applied, one can expect a better resolution in the membrane associated biomolecules. On the other hand, sample heating, cross-polarization efficiency, pressure effects have to be considered in the f-MAS experiment. Pressure effect by f-MAS has not yet been well characterized, although this would be one of the important parameters to make change of the dynamics and structures of membrane proteins. We also discuss photo-illumination experiments in the membrane proteins during f-MAS. This experiment is particularly useful for retinal proteins where retinals are activated by photo-illumination. We will demonstrate following three systems to gain insight into the structure function relationship by means of solid state NMR.

Structure and orientation of bombolitin II

Structure and orientation of bombolitin II (BLT2) bound to DPPC membrane were determined by solid-state ^{31}P and ^{13}C NMR spectroscopy to understand the hemolytic activity of the peptide. ^{31}P NMR spectra showed that BLT2-DPPC membranes with a peptide-to-lipid molar ratio of 1:10 were disrupted into small particles below the Tc and grew large elongated vesicles whose long axis is oriented parallel to the static magnetic field through a membrane fusion process above Tc. ^{13}C NMR spectra of site-specifically ^{13}C-labelled at the backbone

Keywords: Solid state NMR, Membrane protein, Membrane associated peptide, Magnetically oriented vesicle system, REDOR

carbonyl carbons of BLT2 were analyzed to determine the structure, dynamics, and orientation of BLT2 bound to the magnetically oriented vesicle systems (MOVS). It was revealed that the membrane-bound BLT2 adopts an α–helical structure and laterally diffuses in the membrane, rotating around the membrane normal with the tilt angle of the helical axis at 33^0. REDOR experiments further showed that BLT2 adopts a rigid straight α–helical structure. These results suggest that the mechanism of membrane fusion induced by BLT2 is attributed to insertion of BLT2 into the lipid bilayer, perturbing the lipid bilayer structure to promote lipid-mixing between adjacent vesicles for membrane fusion

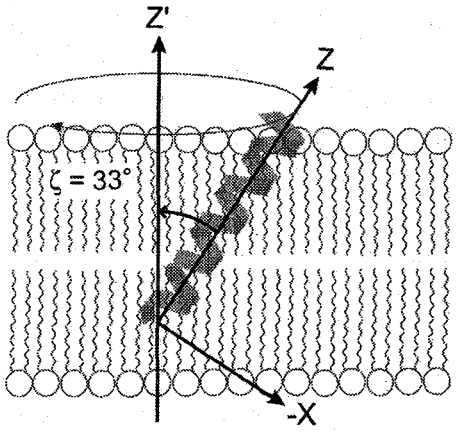

Figure 1: Schematic representation of dynamic structure and orientation of BLT2 bound to DPPC bilayer from analyses of the ^{13}C chemical shift anisotropies. Z' axis is the rotation axis of BLT2, which is paralle to the membrane normal

Structure and dynamics of bacteriorhodopsin

Bacteriorhodopsin (bR) is an integral membrane protein in purple membrane of *Halobacterium Salinarum* and contains retinal covalently linked to Lys216 through a protonated Schiff base. bR consists of seven transmembrane α–helices and shows a function as a light-driven proton pump. bR also shows a variety of local motions for the respective areas such as in the transmembrane, the interfacial area and the C-terminus. These dynamic features may correlate with the function of membrane proteins. We therefore examine the local structures and dynamics of specific positions near retinal by observing ^{13}C NMR spectra of [3-^{13}C]Ala-bR, [1-^{13}C]Val-bR and [2-^{13}C]Val-bR under a magic angle spinning (MAS) condition. It turned out that Ala residues in the vicinity of retinal showed higher mobility compared to those of other Ala residues in α–helices as judged from the ^{13}C isotropic chemical shifts. Further, pronounced change in the mobility due to the induced pressure under a f-MAS condition was observed at the signal position of 16.6 ppm. We have further detected pressure induced isomerization of retinal in bR by ^{15}N CP-MAS NMR spectra of [ζ-^{15}N]Lys-labeled bR. In the ^{15}N NMR spectra, both all-*trans* and 13-*cis* retinal configurations have been observed at 148.0 and 155.0 ppm, respectively, with the intensity ratio of 1 at the MAS frequency of 4 kHz in the dark. The signal intensity of 13-cis retinal at

155.0 ppm was increased when the MAS frequency was decreased from 12 kHz to 4 kHz. It is, therefore, clearly demonstrated that increased pressure induced by f-MAS frequency generated isomerization of retinal from all-*trans* to 13-*cis* state in the bR. This pressure induced isomerization may cause the change in motion of Ala residue located near the retinal (Ala81) to be more flexible. ^{13}C spin-lattice (T_1) and spin-spin relaxation times (T_2) were measured in [1-^{13}C]Val-bR. It turned out that Val residues in the interfacial area have fast motion with the frequency of 10^8 Hz, as revealed from T_1 values. On the other hand, Val residues in α-helices have less components of motions with the frequency of 10^4 Hz. These results indicate that bR has a variety of motions in various parts of the membrane proteins depending also on retinal configurations. Backbone conformations near tyrosine in bR corresponding to all-*trans* and 13-*cis* retinal configurations in the dark were investigated for Tyr-X peptide bonds by using double amino acid labeling with [1-^{13}C],[^{15}N]X-bR by means of REDOR-filtered experiments. Two ^{13}C NMR peaks were observed for REDOR-filtered spectrum of Tyr185 in the dark as shown in Figure 2. These two signals are attributed to the bR with all-*trans* and 13-*cis* retinals. All-*trans* peak intensity was increased in the light adapted state as revealed by photo-illumination experiment, while the 13-*cis* state increased for pressure-adapted state. These results clearly indicate that protein structure depends on the retinal configurations.

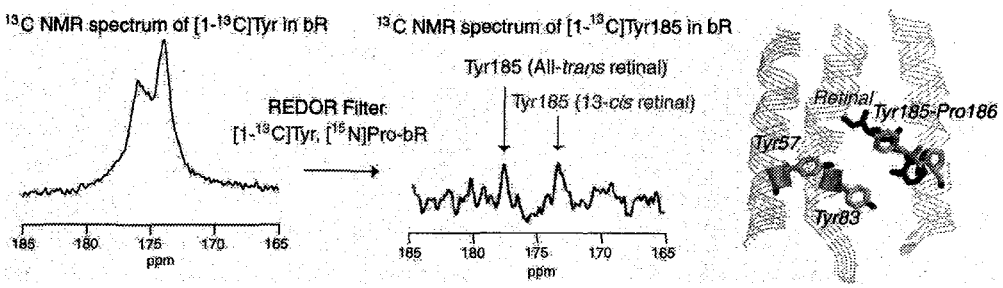

Figure 2: ^{13}C CP-MAS and REDOR filtered ^{13}C NMR spectra of [1-^{13}C]Tyr, [^{15}N]Pro-bR and structure of bR in the vicinity of retinal.

Signal transduction mechanism of phoborhodopsin complex

Pharaonis phoborhodopsin (*p*pR or sensory rhodopsin II) is a negative phototaxis receptor through complex formation with its cognate transducer (*p*HtrII) from *Natronomonas pharaonis*, leading to the photo-induced signal transduction. We examined ^{13}C CP- and DD-MAS NMR spectra of [3-^{13}C]Ala-labeled *p*pR, *p*pR(1-220) and D75N mutant (an activated state) complexed with *p*HtrII, in order to reveal accompanied dynamics changes and

particularly a possible role of a C-terminal α–helical region protruding from the cytoplasmic surface in the signal transduction processes. The C-terminal α–helix in the cytoplasmic side consists of two regions, more static stem (Ala221) and flexible tip (Ala228, 234, 236 and 238) regions, corresponding to the NMR peaks of [3-^{13}C]Ala ppR at 15.9 and 16.7-16.9 ppm, respectively. The latter tip portion of the C-terminal a-helix turned out to be participated also in the complex formation, in addition to the transmembrane α–helices, to result in motions with lowered frequency as judged from the suppressed peaks. In contrast, such spectral changes were not anymore present when *p*pR changes to D75N in the *p*HtrII complex. In fact, dynamics changes were induced to accelerate fluctuations in the C-terminal α–helix of *p*pR during the process of photo-activation of *p*pR-*p*HtrII complex (to D75N-*p*HtrII) as observed by solid state ^{13}C NMR. In contrast, it turned out that fluctuation frequency of the cytoplasmic α–helices of the transducer ([1-^{13}C]Ala-*p*HtrII) complexed with D75N as an activated form was lowered by one order of magnitude. It appears that this caused by a switching of pairs in the helix- helix interactions in the cytoplasmic C-terminal α–helices of *p*HtrII from *p*pR to *p*HtrII itself, concomitant with the loosened interactions in the transmembrane and C-terminal α–helices of *p*pR caused by the disrupted salt-bridges (Figure 3). This finding gains insight into a signal relay pathway in the initial step of phototaxis receptor and its cognate transducer protein.

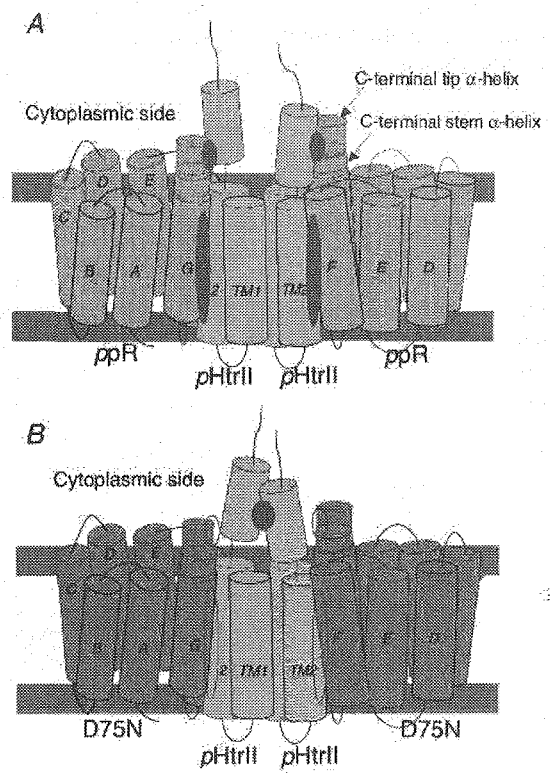

Figure 3: Schematic representation of the manner of interaction of the C-terminal α–helical tip region in ppR (A) and D75N (B) with the transmembrane and cytoplasmic α–helicies of pHtrII(1-159). The helix-helix interactions between the cytoplasmic α–helices are also presented. Elliptical gray area and open area show the enhanced and weakened interaction parts, respectively.

Solid-state NMR on (membrane) protein complexes

Ovidiu C. Andronesi, Gitta Angerstein, Manuel Etzkorn, Henrike Heise, Adam Lange, Robert Schneider, Karsten Seidel, Marc Baldus

Max Planck Institute for Biophysical Chemistry, Solid-state NMR, Department for NMR-based Structural Biology, 37077 Göttingen, Germany

Keywords: MAS, Membrane proteins, potassium channel, rhodopsin, solid-state NMR

Solid-state Nuclear Magnetic Resonance (ssNMR) offers increasing possibilities to study protein complexes at atomic level[1]. Such investigations not only include the determination of 3D molecular structure, but also provide access to probe molecular motion. In our contribution, ssNMR pulse schemes that permit to investigate such aspects using a singly, uniformly labelled sample will be discussed and applications in the following research areas will be shown:

A) ssNMR on a chimaeric Kv1.3 Channel

Potassium (K^+) channels are part of a gene super-family of cation channels that play important roles in regulating cellular excitability. K^+ channels contain a conduction pore and a selectivity filter that catalyze, similar to the active site of an enzyme, the transport of K^+ ions across the plasma membrane. X-ray crystallography has revolutionized our understanding of ion channel structure and function (see, e.g. [2]). SsNMR, on the other hand, provides assess to the study of molecular structure and dynamics of ion channels in a lipid bilayer environment where protein functionality is often most easily established and maintained. For example, we have used two-dimensional ssNMR to study how the structural aspects of high affinity toxin-binding to a chimaeric Kv1.3 channel (KcsA-Kv1.3[3]). Using uniformly labelled toxin or channel, changes in ssNMR resonance frequency and structure were monitored on the level of individual residues (Figure). Our studies revealed that, upon toxin binding, structural rearrangements of both constituents occur[4] and provide the spectroscopic reference to study ligand binding in an important class of membrane proteins. As we will show, they also enable the residue-specific monitoring of channel activation by 2D ssNMR.

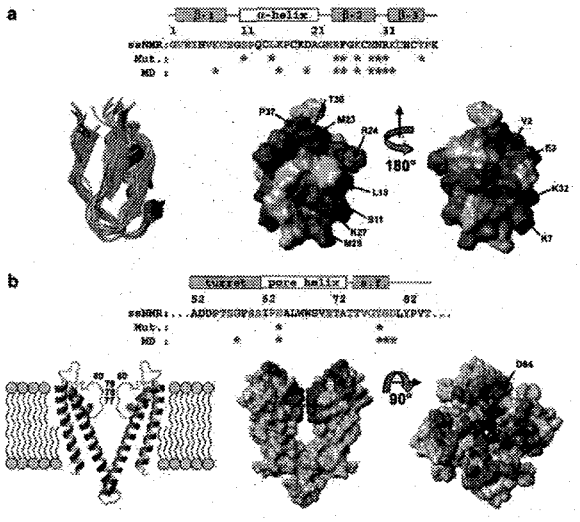

Pendolesi
10~22 μs.

B) Seven-helix membrane receptor in native membranes

While ssNMR hence has made considerable progress in probing ligand binding to membrane proteins, the determination of entire 3D structures of larger, membrane embedded proteins has thus far been complicated by the length of the amino-acid sequence, the high repetitiveness of hydrophobic residues and the limited spectral resolution due to the dominant influence of a single type of regular (α-helical or β-sheet) secondary structure. In principle, spectral crowding can be reduced by advanced labelling approaches, but may be precluded by protein expression levels and/or costs of labelled starting materials. We show that uniform (^{13}C,^{15}N) isotope labelling which is straightforward in many cell-based expression systems, the addition of a well selected set of amino acids in natural abundance (i.e., reverse labelling[5, 6]) and the application of ssNMR methods that separate spectroscopic signals of mobile, static and water-exposed protein segments can be used to monitor structure and topology of an entire seven-helix receptor in native membranes using a single, isotope-labelled sample.

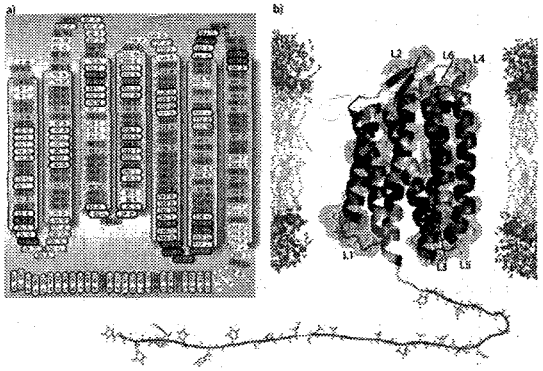

Our approach is demonstrated on sensory rhodopsin II from *Natronomonas pharaonis* (NpSRII), a seven-helix (A-G) membrane protein containing retinal as cofactor which is bound to a lysine residue via a protonated Schiff base.[7] SsNMR experiments were conducted on NpSRII samples containing four dominant residue types V, L, F, and Y in natural abundance (i.e., U[^{13}C,^{15}N\(V,L,F,Y)] NpSRII, Figure). Our spectra were recorded on proteoliposomes at 800 MHz (^{1}H resonance frequency) and permit to investigate 3D structure, topology and intrinsic dynamics of a seven-helix membrane receptor in native membranes by two-dimensional ssNMR[8].

C) Protein folding and aggregation.

Similar ssNMR methods can also provide the spectroscopic basis for studying protein folding and aggregation at the level of individual residues and in real time. For example, we report on recent progress to determine the 3D fold of fibrils consisting of α-synuclein by multidimensional solid-state NMR [6].

References

[1] M. Baldus, *Curr. Opin. Struct. Biol.* **2006**, in press.

[2] R. MacKinnon, *FEBS Lett.* **2003**, *555*, 62-65.

[3] C. Legros, V. Pollmann, H. G. Knaus, A. M. Farrell, H. Darbon, P. E. Bougis, M. F. Martin-Eauclaire, O. Pongs, *J. Biol. Chem.* **2000**, *275*, 16918-16924.

[4] A. Lange, K. Giller, S. Hornig, M.-F. Martin-Eauclaire, O. Pongs, S. Becker, M. Baldus, *Nature* **2006**, *440*, 959-962.

[5] G. W. Vuister, S. J. Kim, C. Wu, A. Bax, *J.Am.Chem.Soc.* **1994**, *116*, 9206-9210.

[6] H. Heise, W. Hoyer, S. Becker, O. C. Andronesi, D. Riedel, M. Baldus, *Proc. Natl. Acad. Sci. U. S. A.* **2005**, *102*, 15871-15876.

[7] J. P. Klare, V. I. Gordeliy, J. Labahn, G. Büldt, H.-J. Steinhoff, M. Engelhard, *FEBS Lett.* **2004**, *564*, 219-224.

[8] M. Etzkorn, S. Martell, O. C. Andronesi, K. Seidel, M. Engelhard, M. Baldus, *Angew. Chem., Int. Ed. Engl.* **2006**, in press.

Structural analysis of biomolecular complexes by solid-state NMR distance analysis

Toshimichi Fujiwara and Hideo Akutsu
Institute for Protein Research, Osaka University

Solid-state NMR enables the structural determination of biological molecular complexes in unoriented solids. Proteins/peptide in lipid bilayers, fibrous proteins such as amyloid fibers, and huge molecular assemblies are typical targets of the solid-state NMR structural analysis. Though the atomic-resolution structures are essential in understanding the biological functions, X-ray diffraction and solution NMR do not provide sufficient structural information on noncrystalline large complexes. We will present the usefulness of magic-angle spinning solid-state NMR based on dipolar couplings for the structural analysis of ^{13}C uniformly labeled biomolecular complexes as follows.

Atomic structure of bacteriochlorophyll (BChl) *c* assembly in chlorosomes was determined by solid-state NMR. Chlorosomes are light harvesting (LH) antenna complexes of green photosynthetic bacteria. Pigments arrangements are optimized generally by protein complexes in plants and purple photosynthetic bacteria. In chlorosomes, however, no proteins are involved in the LH systems. This allows the self-organization of pigments at a higher density, and makes chlorosome a dedicated device for light harvesting under very dark conditions such as in a deep sea. The atomic structure model of the chlorosome based on NMR revealed its roles in efficient light capture and excitation transfer to reaction centers. In this study we have developed a procedure for the structure determination by using polarization transfer matrix analysis of ^{13}C–^{13}C spin diffusion experiments. About 100 internuclear distances obtained were assigned to intermolecular spin pairs in the BChl *c* assembly simultaneously with the

Keywords: solid-state NMR, magic-angle spinning, bilayer membrane, chlorosome, mastoparan-X

structure optimization under ^{13}C–^{13}C distance constraints.

A peptide structure[1] and its interactions with phospholipids in bilayer membranes were determined by ^{13}C-NMR observation of $^{2}H/^{31}P$-selective ^{1}H-depolarization under magic-angle spinning. A solid-state NMR method was developed to observe the signals due to ^{13}C spins of a peptide in the close vicinity of ^{31}P and ^{2}H spins in deuterated phospholipids bilayers. This method, ^{13}C-NMR observation of $^{31}P/^{2}H$-selective ^{1}H-depolarization,[2] was applied to a fully ^{13}C,^{15}N labeled 14-residue peptide, mastoparan-X, forming an α-helix. The ^{13}C-NMR spectral analysis for ^{1}H–^{2}H and ^{1}H–^{31}P dipolar interactions provided the angles for the helix orientation with respect to the membrane at the precision 5° and the depth where the helix is located in the membrane at the precision of 1 Å.

References

1. Y. Todokoro., et al., *Biophys. J.*, **91**, 1368 (2006).
2. E. Harada, et al., *J. Am. Chem. Soc.*, **128**, 10654 (2006).

Transmembrane Helix Interactions in Membrane Protein Folding, Function, Misfolding and Disease

Steven O. Smith, Takeshi Sato, Mahiuddin Ahmed and Saburo Aimoto
Department of Biochemistry and Cell Biology, Center for Structural Biology, Stony Brook University, U.S.A.; Institute for Protein Research, Osaka University, Osaka, Japan

Helix interactions in membrane protein channels, transporters and receptors are critical for both protein structure and function. I will describe our work using solid-state NMR spectroscopy to establish how transmembrane helices associate in membrane environments and how helix motions are coupled to membrane protein function. One of the conclusions which emerges from our analysis is that there are statistically significant differences between helix interactions in membrane proteins and soluble α-bundle proteins. We observe a higher diversity of membrane protein interactions and find that there is a high propensity of small and polar residues in tightly packed helix interfaces in membrane proteins. These results indicate that membrane proteins have at least two general 'motifs' for mediating helix interactions. Both membrane and soluble proteins exhibit "knobs-into-holes" packing exemplified by "leucine zippers". Membrane proteins, on the other hand, have a second general motif, exemplified by the dimer interface of glycophorin A, in which small and polar residues form smooth surfaces that allow very close approach of the backbones of interacting helices. The close approach of transmembrane helices permit interhelical hydrogen bonding by Ser and Thr residues.

The structure of the transmembrane dimer of glycophorin A (right) exemplies the close approach of transmembrane helices in membrane proteins (*1*). Glycophorin A has a well characterized GxxxG motif. The two glycines in this motif (Gly79 and Gly83, shown as van der Waals spheres) pack closely in the helix interface and allow interhelical hydrogen bonding of Thr87 (not shown).

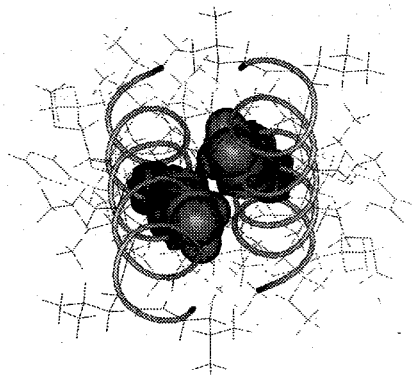

I will also describe recent work on the role of glycine in the misfolding of membrane proteins and the formation of amyloid fibrils associated with Alzheimer's and a wide range of other neurodegenerative diseases. It is known that these fibrils have a cross β-sheet structure where main chain hydrogen bonding occurs between β-strands in the direction of the fibril axis. However, the structural basis for how the membrane-spanning helix is converted into β-sheet or how protofibrils associate into fibrils is not known. We have proposed that glycine plays a role in the structural transitions leading to amyloid-like fibrils. Specifically, we show that the GxxxG motif, which mediates helix interactions in membrane proteins, provide key packing surfaces when they occur in β-sheets. We show that glycines in the glycophorin A transmembrane helix promote extended β-strand formation when the helix partitions into aqueous environments and stabilize the packing of β-sheets in the formation of amyloid-like fibrils.

Keywords: solid-state NMR, helix interactions, Alzheimer's disease, amyloid, GxxxG

Based on these results, we have recently found that in the Aβ amyloid fibrils associated with Alzheimer's disease, Met35 packs against Gly33 in the C-terminus of Aβ40 and against Gly37 in the C-terminus of Aβ42 (2). We have taken advantage of this structure to design a new class of inhibitors that prevents fibril formation. We show that peptide inhibitors based on a GxFxGxF framework disrupt sheet-to-sheet packing and inhibit the formation of mature Aβ fibrils as assayed by thioflavin T fluorescence and electron microscopy. The GxFxGxF motif is complementary to the IxGxMxG motif found in the C-terminal sequence of the Aβ40 and Aβ42 peptides. *Importantly*, the designed peptide inhibitors significantly reduce the toxicity induced by Aβ42 on cultured rat cortical neurons.

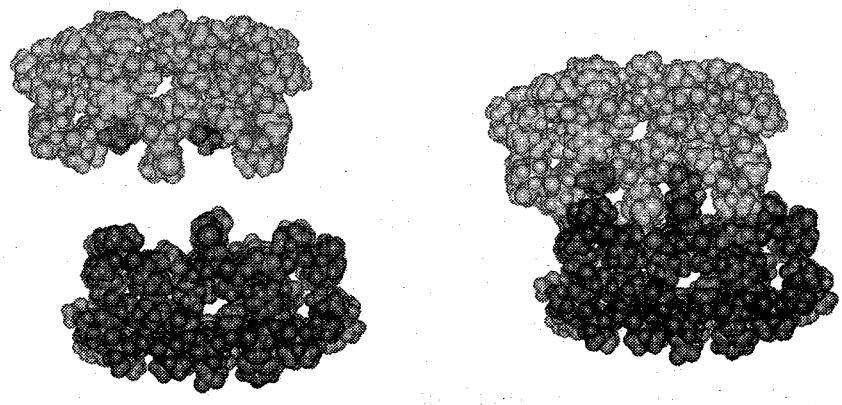

In the Aβ40 and Aβ42 fibrils, the individual β-strands pack in a parallel and in-register orientation that allows the glycines to form long channels in the protofibril surface. The figure above shows how "ridges-into-grooves" packing allows two protofibrils to associate to form a mature fibril.

(1) Smith, S. O., Song, D., Shekar, S., Groesbeek, M., Ziliox, M., and Aimoto, S. (2001) Structure of the transmembrane dimer interface of glycophorin A in membrane bilayers. *Biochemistry 40*, 6553-6558.

(2) Sato, T., Kienlen-Campard, P., Ahmed, M., Liu, W., Li, H., Elliott, J. I., Aimoto, S., Constantinescu, S. N., Octave, J. N., and Smith, S. O. (2006) Inhibitors of amyloid toxicity based on β-sheet packing of Aβ40 and Aβ42. *Biochemistry 45*, 5503-5516.

GXMXG

GXXXGXXXG Gly

for (OH)

binding

G G

Structure Analysis of the Crystalline Region of Silkworm Silks by Solid-state NMR

Michi Okonogi and Tetsuo Asakura
Department of Biotechnology,
Tokyo University of Agriculture and Technology, Koganei, Tokyo 184-8588 JAPAN

Silks are a wide class of fibrous proteins with properties which intrigue scientists ranging from structural engineers to polymer chemists and biomedical researchers. The elucidation of the structure and structural changes of silk fibroin before and after spinning is important for the understanding of the origin of such impressive mechanical properties, and to gain further insights for the de novo design of artificial proteins.[1)]

In this talk we will discuss the structure of silk fibroins from the well-known domesticated silkworm, *Bombyx mori*, and the wild silkworm, *Samia cynthia ricini* studied with solid-state NMR. Emphasis will be laid on the crystalline region, because this region is thought to contribute greatly to the strength and stiffness of these silks. Furthermore, the primary sequence differs considerably between *B. mori* and *S. c. ricini* especially in the crystalline region, namely, the former mainly consists of Ala-Gly repetitions and the latter is composed of poly-Ala with lengths $(Ala)_{12\text{-}13}$. The use of stable isotope labeled sequential model peptides is very useful in determination of detailed local structure.

B. mori silk fibroin before and after spinning

The structures of the crystalline region of *B. mori* silk fibroin before and after spinning (silk I and silk II respectively) were determined using an appropriate model peptide, $(AG)_{15}$, with several solid-state NMR methods; ^{13}C 2D spin-diffusion solid-state NMR and rotational echo double resonance (REDOR) NMR techniques along with the quantitative use of the conformation-dependent ^{13}C CP/MAS chemical shifts. Conclusively, the silk I structure has been determined to be a repeated β-turn type II structure[2)], and the silk II structure has been determined to be a lamellar structure[3),4)].

S. c. ricini silk fibroin before and after spinning

The structures of *S. c. ricini* silk fibroin before and after spinning were determined using a model peptide, $GGAGGGYGGDGG(A)_{12}GGAGDGYGAG$, which is a typical repeated sequence of the silk fibroin, with the solid-state NMR methods mentioned above. The precise structure was elucidated for the pre-spinning structure, where the poly-Ala sequence takes a typical α-helix pattern with a tightly wound helical structure at both terminal regions of the poly-Ala sequence[5)]. For the post-spinning structure however, precise structure elucidation is still in progress. From several ^{13}C and ^{15}N solid-state NMR experiments, it has been shown that the poly-Ala regions form β-sheet structures. However, inhomogeneous β-sheet structures are clearly observed from the broad and asymmetric Ala Cβ ^{13}C resonances in the ^{13}C CP/MAS NMR spectrum. By extending our studies to the structural analysis of alanine

Keywords: Silk Fibroin, Crystalline region, *Bombyx mori*, *Samia cynthia ricini*, Anti-parallel and parallel β-sheet structures

oligomers, as will be mentioned below, we investigated the origin of this inhomogeneity.

Highlight topic:

Anti-parallel and parallel β-sheet structures co-existing in *S. c. ricini* silk fiber

One possibility of the origin of the inhomogeneous β-sheet structure in *S. c. ricini* silk fiber may be due to the presence of both anti-parallel and parallel β-sheet structures, which is difficult to distinguish by only analyzing silk fiber and its model peptide mentioned above.

The alanine tripeptide (Ala_3) is known to form both anti-parallel (AP) and parallel (P) β-sheet structures, depending on the solvent composition during crystallization. Therefore, we selected this peptide as the initial step to investigate both types of β-sheet structure by solid-state NMR. By combining selective stable-isotope labeling of Ala_3 with ^{13}C CP/MAS NMR and 2D RFDR (Radio Frequency Driven Recoupling), we accurately assigned all ^{13}C resonances, including the distinction between the two nonequivalent molecules for each β-sheet structure[6]. Differences in dynamics were also studied by ^{13}C T_1 measurements of AP- and P-Ala_3. Compared to the AP-structure the P-structure shows a 0.9 ppm shift to low field for the central Ala Cβ and 2-3 times longer T_1 for all Ala Cβ, Cα, and carbonyl carbons. Similar results were also observed for Ala_4, which we recently succeeded in preparing both AP- and P-structures. Using these differences in both chemical shift and T_1 values, we assigned the parallel and anti-parallel β-sheet ^{13}C resonances in the asymmetric and broad methyl spectra of [3-^{13}C]-Ala silk fiber of *S. c. ricini*.

Further investigations using ^{15}N and ^{17}O NMR together with theoretical chemical shift calculations, and an extension of ^{13}C NMR studies on Ala_4, Ala_5, Ala_6, and Ala_7, will also be discussed in our presentation. NMR parameters obtained from these studies will be useful for not only distinguishing anti-parallel and parallel β-sheet structures co-existing in *S. c. ricini* silk fiber, but also other types of silks as well, such as spider dragline silk.

Acknowledgement TA acknowledges supports from the Asahi Glass Foundation, Insect Technology Project, Japan, Agriculture Biotechnology Project, Japan and Grant-in Aid for Scientific Research by the Ministry of Education, Culture, Sports, Science and Technology of Japan (18105007).

References

1) Asakura, T.; Kaplan, D. L., Silk production and processing. In *Encyclopedia of Agricultural Science*, Ed.by C.J.Arutzen, Academic Press: NY, **1994**; 4, p 1-11.
2) Asakura, T.; Ohgo, K.; Komatsu, K.; Kanenari, M.; Okuyama, K., *Macromolecules* **2005,** 38, 7397-7403
3) Asakura, T.; Yao, J.; Yamane, T.; Umemura, K.; Ulrich, A. S., *J. Am. Chem. Soc.,* **2002,** 124, 8794-8795.
4) Asakura, T.; Nakazawa, Y.; Ohnishi, E.; Moro, F., *Protein Sci.,* **2005,** 14, 2654-7.
5) Nakazawa, Y.; Asakura, T., *J. Am. Chem. Soc.,* **2003,** 125, 7230-7.
6) Asakura, T.; Okonogi, M.; Nakazawa, Y.; Yamauchi, K., *J. Am. Chem. Soc.,* **2006,** 128, 6231-8.

3 LE7

Metabolite mixture analysis attracts NMR researcher's attention

Jun Kikuchi[1,2,3,4]

[1]*RIKEN Plant Science Center,* [2]*Grad. Sch. Bioagri. Sci., Nagoya Univ. ,* [3]*CREST, JST,* [4]*Int. Grad. Sch. Arts Sci., Yokohama City Univ.*

Since plants can produce a variety of useful metabolites using light energy and simple compounds, plant metabomics gain much attention not only for basic science but also for applied science. Firstly, I will summarize how we have extended uniform stable isotope labeling technologies in higher plants (1-4), such as *Arabidopsis*, *Rice*, *Wheat* and *Populus*. The ^{13}C labeling allows more accurate molecular identifications by use of our original Java software **SpinAssign**, searching our original standard database. In addition to this, the ^{13}C labeling can be used in metabolic flux analysis of plant cells at atomic level. Furthermore, we have observed nicely resolved ^{1}H-^{13}C cross peaks of non-extracted, insoluble small and macromolecules by magic-angle-spinning NMR experiments. These approaches can be applied for plant biomass characterization such as wood material processing, bioenergy production etc. Secondary, the plant biomass can be also used as nutritional resources in animal and symbiotic bacterial systems. I will introduce how the ^{13}C labeled plants can be decomposed by animal organs and symbiotic gut microflora. We also investigated symbiotic relationship of two gut microflora system by their ^{13}C labeling and *in vivo* NMR. Finally, I will review how technological advancements will contribute in NMR-based metabomics. The most disadvantage of NMR is its week sensitivity, which can be overcome by use of cryogenically cooled probe and careful choice of solvent system [4]. In spite of this, ^{13}C-dynamic nuclear polarization enables significant signal enhancement of purified small molecules, which can be also applied in multi-component system by careful use of radical doping [5].

References

1) Kikuchi, J., Shinozaki, K. & Hirayama, T. "Stable isotope labeling of *Arabidopsis thaliana* for an NMR-based metabolomics approach" *Plant Cell Physiol.* **45**, 1099-1104 (2004).

2) Kikuchi, J. & Hirayama, T. "Hetero-nuclear NMR-based metabolomics" *Biotech. Agri. Forest.* **57**, 94-101 (2006).

3) Kikuchi, J. & Hirayama, T. "Practical aspects of uniform stable isotope labeling of higher plants for a hetero-nuclear NMR-based metabolomics" *Methods Mol Biol*, (in press).

4) Kikuchi, J. and Akamine, K. (2006) "*in vivo* NMR" *J. Spect. Soc.* (in press).

5) Horiuchi, T., Takahashi, M., Kikuchi, J., Yokoyama, S. & Maeda, H. (2005) "Effect of dielectric properties of solvents on the quality factor for a beyond 900 MHz cryogenic probe model" *J. Magn. Reson.* **174**, 33-41.

6) Blazina, D, Kikuchi, J. and Reynolds, S. "Application of DNP-NMR to plant science". *32th Int. Conf. Magn. Reson. Biol. System* 210.

DNP NMR in multi-component systems

Steven Reynolds[1], Jun Kikuchi[2] and Damir Blazina[1]

[1] Oxford Instruments Molecular Biotools Ltd., Tubney Woods, Abingdon, Oxon, UK
[2] RIKEN Plant Science Center, Suehiro-cho, Tsurumi-ku, Yokohama, Japan

One of the main limitations of NMR spectroscopy, in particular when applied to heteronuclei, is its relatively low sensitivity. This is caused by the low natural abundance of the respective NMR active isotopes (e.g. 1% for ^{13}C) and by the low polarisation of the sample. The extent of polarisation is linked to the relative populations of spin states, which is typically in the region of 5-20 ppm and reflects the very small amount of sample that actually contributes to the NMR signal.

One way of increasing the sensitivity of NMR is to create an enhanced, non-Boltzmann spin state population, which yields enhanced NMR signals. The approaches used to achieve this are generally referred to as "hyperpolarisation techniques", and perhaps the most generally applicable is dynamic nuclear polarisation (DNP). DNP has been shown to yield signals for ^{13}C and ^{15}N nuclei in solution-state NMR that are enhanced by over 10,000 times in comparison with conventional NMR spectra.[1] The technique involves cooling a sample to <4 K in a strong magnetic field (B_0 = 3.35 T) in the presence of a trityl radical.[2] Under such conditions, the unpaired electrons on the trityl radical become strongly polarised, and this polarisation can be transferred to nearby atomic nuclei using microwave irradiation ($\nu \approx$ 94 GHz). Once the polarisation has built up to a sufficient level (typical over 0.5-4hours), the sample is dissolved by the injection of an aliquot (typically 3–5 mL) of hot solvent and rapidly (<1 s) transferred to a conventional NMR spectrometer for measurement. During sample polarisation the NMR spectrometer is available to other users.

The DNP enhancements that can be obtained are governed by the appropriate choice of radical. We investigate this by reference to compounds relevant to plant science, including sugars, lipids and peptides. Natural abundance ^{13}C DNP NMR spectra are shown, which exhibit significantly enhanced signal intensities compared to conventional NMR spectroscopy. By careful sample preparation, a mixture of hydrophilic, lipophilic and amphiphilic samples can be polarised. Interactions between components in this mixture can be detected by changes in the associated ^{13}C NMR spectra. Furthermore, the application of DNP to plant science is discussed.

References:
1. Ardenkjaer-Larsen, J. H.; Fridlung, B.; Gram, A; Hannson, G.; Hansson, L.; Lerche, M.H.; Servin, R.; Thaning, M.; Golman, K. *Proc. Nat. Acad. Sci.* **2003**, *100*, 10158.
2. Wolber, J.; Ellner, F.; Fridlund, B.; Gram, A.; Johannesson, H.; Hansson, G.; Hansson, L.H.; Lerche, M.H.; Mansson, S.; Servin, R.; Thaning, M.; Golman, K.; Ardenkjaer-Larsen, J. H. *Nucl. Inst. Meth. Phys. Res. A* **2004**, *526*, 173.

Variation of ^{1}H-NMR in Saliva of Healthy Young Females

○ Seizo Takahashi[1], Takashi Ogino[2] and Yukiharu Yamaguchi[3]

1. Department of Chemical and Biological Sciences, Japan Women's University
2. National Institute of Neuroscience, NCNP
3. Division of Clinical Technology, Pfizer Global R & D, Pfizer Japan Inc.

Saliva could be a valuable reporter of physiology because of an intermediate character as a biofluid between blood and urine. Human saliva has mostly been analyzed by chromatography, although NMR spectroscopy has advantages over it in many respects. The aim of this study was to get an insight into the intra- and inter-subject variability of physiological response to the internal hormones of females as a model of drug response. We have reported previously that the concentrations of salivary metabolites are extensively varied depending on many factors. It was hard to detect as a result the periodic change due to the hormonal control of females. Thus, the present study was focused on the time course of individual subjects to look for the intra-subject variance compared with the inter-subject variance.

Materials and Methods

Saliva was collected in Sallivet™ (ca. 2mL) immediately after waking in every morning for 30 days, and stored in a deep freezer (-80 degree C) for 2 years. The specimens from 4 subjects who showed clean periodic basal body temperature oscillation were sampled for NMR measurements. Spectra were acquired on a Bruker AMX-400WB spectrometer under the following conditions:

SQ: NS=64, TD=16K, SW=10ppm, TE=296K, P18=5s

DQ: NS=256, D2=5ms, rests are same as SQ

Results and Discussions

We found that strong resonance scatter in the log-normal distributions among samples while most peaks fall in the gamma distributions. When the logarithmic intensities of points in the frequency domain spectra were sorted to the descending order, spectral intensities of salivary metabolites was found to fit into 2 linear functions. The result indicates that the scale rule is applicable to the distribution of salivary metabolites.

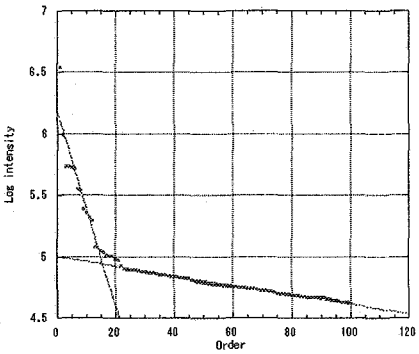

Fig. 1 Log-intensity of a salivary spectrum sorted to the descending order

Keywords: metabolite, intensity distribution, intra/inter subject variation, double quantum

The first group exhibits distinct peaks but highly scattered from sample to sample than the other group. The gradient of the fitted line to the second group is stable and could become a measure of the overall concentration of the sample as well as the ordinate value. The ordinate information has most frequently been used for the measure of concentration; however it is vulnerable to the change in baseline roll and level. The gradient value would be better as an indicator of the salivary concentration.

Salivary NMR is characteristic to the double quantum spectra (DQ) where molecules of no internal spin-spin coupling are observable. Fig. 2 exhibits the daily change of the spectral intensity of acetate methyl from a subject. It was shown that the behavior of SQ and DQ was similar but the ratios of DQ abainst SQ+DQ were differently behaved. There was a correlation between the SQ and DQ intensities, but not for the ratio against SQ and little against DQ intensities. The ratio could be regarded as a measure of mole fraction bound to the macro-molecules in a dynamic equilibrium of metabolites in saliva. The result above shows that spectral intensity of DQ depends on the molar concentration of samples as shown by SQ intensity, but that the mole fraction is independent to the concentration of molecules present in saliva. Fig. 2 shows that the variation of molar concentration is larger than that of mole fraction except for certain days. It needs to be studied for the origin of sudden change in ratios at certain days.

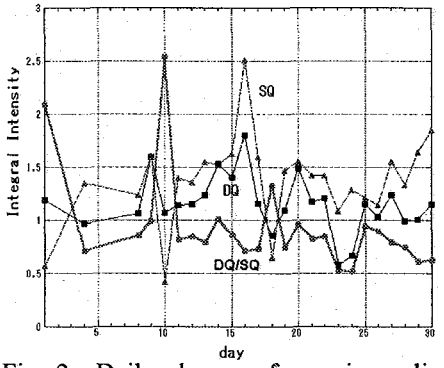

Fig. 2 Daily change of morning saliva measured by the integral intensity of logarithmic SQ, DQ, and DQ/(SQ+DQ) ratios.

Acetate was shown previously to distribute in a lognormal shape. Thus the variation of acetate concentration between intra- and inter-subjects was compared in the logarithmic SQ intensity of methyl resonance. The standard deviation of intra-subjects was 0.15 which was significantly smaller than 0.26 of 30 subjects. The result suggests that each subject may be different in the physiological expression of metabolites. However, single information such as acetate concentration alone suffers from the highly scattered level to defy the difference between two subjects. To overcome this difficulty, metabonimics was indispensable which uses a number of metabolite concentrations at a time. It should be noted, however, that most metabolite concentrations exhibit the gamma distribution, but the the proper analytical method is not known for the data set with gamma distributions.

Chasing the daily change, it became clear that the group one resonance, namely the high intensity signals, are mostly determined by other factors than the hormonal control. In order to look for the hormonal effect in the salivary spectra, the present study revealed that the second group should be intensively explored.

3 LE10

Non-targeted NMR Metabolomics: Evaluation disease status in toxin-induced diabetic nephropathy rat using ^{1}H spectra of urine

* Tadashi Nemoto[1], Itiro Ando[1,2], Kazunori Arifuku[3], Taeko Kataoka[1], Kenji Kanazawa[1], Yasuhiro Natori[4] and Masako Fujiwara[3]

[1]Biological Information Research Center, National Institute of Advanced Industrial Science and Technology (AIST) [2]Environmental Research Center Ltd., [3]JEOL DATUM LTD, [4]Department of Clinical Pharmacology, International Medical Center of Japan

One of the metabolomics technologies, so-called NMR-based metabolic profiling is an easy and powerful tool to detect abnormality, to assess, and to evaluate metabolomics status. By this method, simple water-suppressed 1d spectra of urine samples were accumulated then subjected to statistical analysis to get useful 2 or 3 dimensional views.

We have been trying to push back the front raw of this methodology using normal (healthy) and hypertensive male rats to detect physiological difference(s) without any big stress. In this paper, we tried to evaluate toxin-induced diabetic nephropathy in Wister rats.

Streptozotocin (STZ) treated rats (11 week-old, 15 males) and controls (same, 5 males) were reared and urine samples were collected once a week as 24hr pooled condition from 1 to 4 weeks just after STZ treatment. All samples were immediately frozen in –30°C freezer until NMR measurements. After a minimum treatment of samples such as centrifuge, addition of PBS and D_2O, water-suppressed 1D proton spectra were accumulated on a JEOL ECA-500 spectrometer. All fids were directly processed by 'ALICE2 for Metabolome' software package (Version 1.0) to get a Principal Component Analysis (PCA) score plot (Figure).

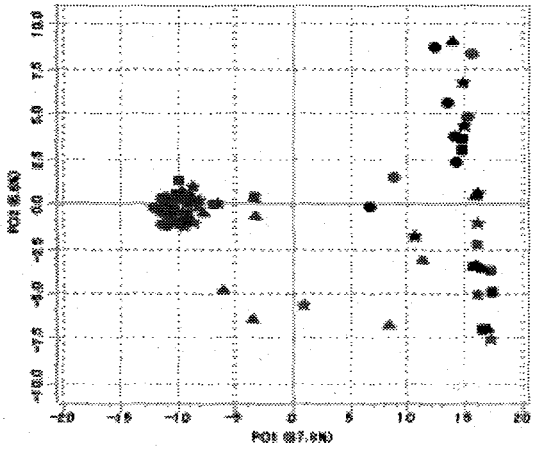

The valued of PC1 (x-axis) and that of PC2 (y) were 88% and only 6.6%, respectively. In this score plot, on the left center, there was an apparent dataset-cluster. When back to spectra, it was found that major effect on this score plot was the presence of glucose signals with significant strength. There were considerable numbers of STZ-treated data points spread among controls'. These were the outliers and detailed analyses of these have been completed. By trajectory analysis, 4 of

Keywords: metabolomics, multivariate analysis, diabetes, urine, nephropathy

the STZ-treated animals were insufficiently responded. Three of them were recovered from toxin treatment. After several weeks, these 3 individuals have been killed and thus, NMR-metabolic profiling can evaluate the efficiency of toxin treatment in early stage, which will greatly reduce the animal rearing cost.

Using the spectral data of successfully established diabetes model rats, further PCA have been carried out. Glucose signal region were removed from the datasets and re-calculated again (Figure). In the figure, the data points 'normal' diabetes rats were aligned to make a new cluster. In the cluster, there was one rat that was gradually moved out to right upper direction was found. Combined with biochemical information, it was found that rat was completely diabetes but it was only one exceptional: this individual did not produce albuminuria (albumin-containing urine) within entire rearing period.

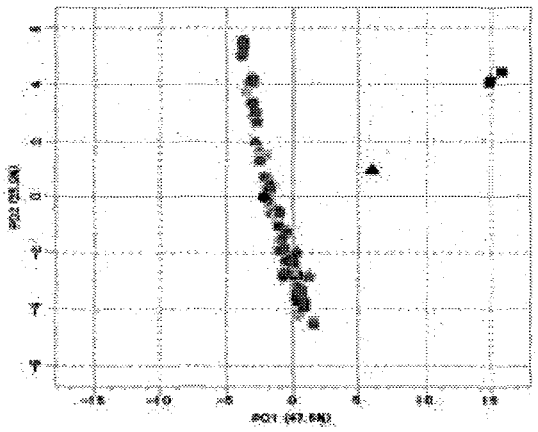

Thus, NMR-metabolic profiling method, one of non-targeted metabolomics analysis figures out important keys in the animal experiments and represent them very simple way.

References

Pattern Recognition Analysis for Classification of Hypertensive Model Rats and Diurral Variation Using 1H-NMR Spectroscopy of Urine., M. Fujiwara, K. Arifuku, I. Ando, and T. Nemoto, *Anal. Sci.*,2005, **21**, 1259-1262.

3 LE11

MAGICAL
難溶性高分子量タンパク質のための新規帰属方法

(三菱化学生命科学研究所)
○河野俊之

MAGICAL: A Novel Signal Assignment Method for Large and Less Soluble Proteins

Mitsubishi Kagaku Institute of Life Sciences (MITILS)
Toshiyuki Kohno

NMR signal assignments method based on 3D or 4D NMR measurements ever reported have some drawbacks: First, the concentrations of target proteins should be high. Second, it is difficult to assign all the NMR signals in case of larger proteins. Third, the target proteins should be stable for weeks. To overcome these drawbacks, we have developed a novel assignment method (MAGICAL) based on the completely selective labeling method. With this method, we can now easily assign all the NMR signals of large proteins at lower (0.1-0.2 mM) concentration, only with 2D NMR measurements, even in the case of larger proteins. This method may also be applied to proteins that are not stable to be analyzed by long 3D NMR measurements. Furthermore, we can assign the signals very rapidly because the assignment strategy is very simple and straightforward.

従来のタンパク質の主鎖のNMRシグナルの完全帰属方法は、3次元や4次元NMRスペクトル測定を基本としていた。しかし、多次元NMRによる帰属方法を難溶性高分子量タンパク質に適用しようとすると、いくつかの問題点が有った。(1)多次元NMR測定のためには高濃度の試料を必要とするので、溶解度の低いタンパク質は解析できない。(2)高分子量タンパク質の場合は多次元NMRを用いてもシグナルの重なりが激しく解析が困難になる。(3)多次元NMRを複数測定する必要が有るので、目的タンパク質が室温において数週間安定に保たれていなければならない。、我々は、この問題点を解決するために、無細胞タンパク質合成系を基にした以下の方法を開発してきた。(1)小麦胚芽無細胞タンパク質合成系を用いて、標識した目的タンパク質を無精製または簡易精製するだけで、長時間のNMR測定に耐えられるようにする技術。(2)無細胞タンパク質合成に数種類のアミノ酸代謝阻害剤を加えることで、20種類のどのアミノ酸でも完全選択的に標識可能な技術。(3)完全選択的なアミノ酸標識技術を応用し、系統的なコンビナトリアルアミノ酸標識方法(MAGICAL法:Method for AssiGnments with Intelligent Combinatorial Amino acid Labeling)を用いることにより、目的タンパク質のNMRシグナルの完全帰属が可能な新規方法。

これらの方法を用いることにより、高分子量タンパク質であっても、100-200 μM の溶解度があって数日間安定なタンパク質であれば、2次元NMR測定を行うだけで、簡便に主鎖のシグナルの完全帰属が可能になった。

小麦胚芽無細胞蛋白質合成 選択的標識 2次元NMR 帰属 高分子量タンパク質

こうのとしゆき

MAGICAL法

MAGICAL法による ^{1}H-^{15}N HSQC の各シグナルの帰属の仕方は以下の通りである。

(1)一種類のアミノ酸残基のみを選択的に $^{13}C/^{15}N$ 二重標識し、その他の 19 種類のアミノ酸を ^{15}N のみで標識した目的タンパク質を 20 種類調製する。

(2)一種類のアミノ酸残基のみを $^{13}C/^{15}N$ 二重標識し、その他の 19 種類のアミノ酸を ^{15}N のみで標識した目的タンパク質の2次元 HN(CO)及び2次元 HN(CA)スペクトルを比較し、HN(CA)スペクトルに存在し、かつ HN(CO)スペクトルに存在しないシグナルを得ることで、^{1}H-^{15}N HSQC スペクトルにおける各シグナルが、どのアミノ酸の種類に属するかを決定する。

(3)一種類のアミノ酸残基のみを $^{13}C/^{15}N$ 二重標識し、その他の 19 種類のアミノ酸を ^{15}N のみで標識化した目的タンパク質の HN(CO)スペクトルから、それぞれのシグナルがどの種類のアミノ酸残基の後ろにある残基かを決定する。

(4)(2)(3)の結果とアミノ酸配列表から、アミノ酸の並びを利用してシグナルの帰属を行う。

(5)連続するアミノ酸の並び方が同一のものが2ヶ所以上あるものについては、2次元 H(N)CA と2次元 H(NCO)CA スペクトルを用いて、さらに手前の帰属済みの残基から帰属を決定する。手前の残基が同様の状況により帰属が不確定である場合は、さらに手前の残基から順次帰属を行う。必要に応じて H(N)CO と H(NCA)CO の組み合わせも使う。

高分子量タンパク質の場合には、重水素化したアミノ酸を用い、$^{13}C/^{15}N$ 標識のアミノ酸を $^{13}C/^{15}N/D$ の三重標識に、^{15}N 標識のアミノ酸を $^{15}N/D$ の二重標識に変更し、測定もTROSYベースのものに変更するが、基本的な考え方は上記と同じである。

我々は、このMAGICAL法をさまざまなタンパク質に適用してきた。そして、200 μM 程度の溶解度しかなく、3日程度しか安定でないタンパク質でも主鎖の全シグナルの帰属が可能であること、250 残基程度のタンパク質であれば、1週間の測定と1週間の解析時間で帰属が可能であることを確認してきた。また、300 残基を超え、500 μM 以下の溶解度しかなく、25 ℃以下でのみ安定でありしかも構造多形を持っているような、従来法では解析が著しく困難であるタンパク質でもほぼ全てのシグナルの帰属が可能であることを見いだした。本講演では、MAGICAL法の現状とさまざまな適用例について議論する予定である。

NMR approach of the investigation of cellar surface proteins

Ichio Shimada[a,b]

[a]*Department of Physicalchemistry, Graduate School of Pharmaceutical Sciences, University of Tokyo, Tokyo, Japan*

[b]*Biological Information Research Center, BIRC, National Institute of Advanced Industrial Science and Technology, AIST, Aomi Koto-ku, Tokyo, Japan*

Collagen plays a critical role not only in providing the mechanical strength for extracellular matrices, but also in mediating a variety of cellular processes, including cell attachment, cell development, and diseases through interaction with other matrix proteins and cell-surface receptors. Discoidin domain receptor 2 (DDR2), which belongs to the receptor tyrosine kinase family, is a receptor for fibrillar collagen. DDR2 is expressed in heart, skeletal muscle, lung, brain, kidney, and connective tissue and is overexpressed in some tumor cells. DDR2 regulates cell proliferation, adhesion, and motility. In addition, DDR2 controls extracellular matrix remodeling by influencing the expression and activity of matrix metalloproteinases. The direct interaction of collagen with the discoidin (DS) domain in the extracellular region of DDR2 activates its intracellular tyrosine kinase, leading to the downstream intracellular signaling.

Here, we report the collagen recognition mode of the DS domain. The DS domain was expressed in *Pichia pastris* and purified to homogeneity. Surface plasmon resonance study indicated the dissociation constant of 15 μM for the DS domain binding to collagen type II, which is typical collagen binding affinity for the collagen-binding protein. The solution structure of the DS domain has been determined, exhibiting a distorted jellyroll fold, consisting of eight β-strands. The structure of DS was almost similar to those of coagulation factors V and VIII C1, C2 domains and neuropilin-1 b1 domain. Then, the binding site on the DS domain to fibrillar collagen has been determined by transferred cross-saturation (TCS) experiment. The residues with high reduction ratio of the HSQC peak intensities are mainly distributed on the top surface of the DS domain, showing that collagen binds to the DS domain at the top surface: loop 1, loop4, loop6. The identified collagen-binding site of the DS domain is composed of the hydrophobic residues, Trp52, Cys73, Ile112, Phe114, and Met174, and a set of positively and negatively charged residues, Arg105 and Glu113. These features may reflect the specificity of the DS domain for collagen. The collagen-binding site of the DS domain shows no structural similarity to other known collagen-binding proteins. The diversity of collagen-binding mode will be discussed, based on the three dimensional structure and collagen-binding site.

Pressure perturbation NMR spectroscopy for protein dynamics

Kazuyuki Akasaka[1, 2]

[1]Department of Biotechnological Science, Kinki University, Kinokawa-shi 649-6493;
[2]RIKEN SPring-8 Center, 1-1-1- Kouto, Mikazuki-cho, Hyogo 679-5148, Japan

Proteins are molecules designed to work under physiological conditions. For example, protein function is obviously related to the thermal energy available under the physiological condition. After thousands or more basic protein structures have been determined, one of the next major targets of NMR spectroscopy would be to explore the delicate dynamic design of proteins for adjusting their functions under respective physiological conditions such as temperature, pressure and pH.

The dynamics of protein is unique in two ways; Firstly, the biologically relevant fluctuation of a protein may span an extremely wide frequency range (ps~ks). Secondly, the fluctuation may also span a wide conformational space from the bottom of the folding funnel to nearly the top of it under physiological conditions. Up until now, however, our knowledge on protein structure is highly biased toward the bottom of the energy landscape and our knowledge on protein dynamics is also centered on fast dynamics typically in the time range of ps~ns.

Pressure perturbation is useful in effectively expanding NMR target to lower frequency motions and higher energy portions of the energy landscape (*1, 2*). Pressure perturbation to proteins can be both mechanical (A) and thermodynamic (B) in nature. While the mechanical part of the perturbation discloses usually high frequency motions (ps~ns) of conformers in the bottom of the energy landscape, the thermodynamic part of the perturbation discloses slower, cooperative motions and transitions to conformers higher in the energy landscape. The high sensitivity of thermodynamic response to pressure within a few kbar range is generally assured for most globular proteins in solution from two general thermodynamic properties of naturally occurring proteins, "Marginal Stability" (*1*) and "Volume Theorem" (*3*).

Pressure perturbation combined with NMR is unique in that it can disclose "shape" changes of a protein molecule associated with fluctuation. In favorable cases, the shape change can be expressed even in atomic coordinates, as were done recently for hen lysozyme at 2 kbar (~mechanical response) (*4*) and and ubiquitin at 3 kbar (thermodynamic response) (*5*), respectively.

Key Words: pressure perturbation, mechanical response, thermodynamic response, energy landscape, volume theorem

References

1. K. Akasaka, Highly fluctuating protein structures revealed by variable pressure NMR. *Biochemistry (Current Topics)* 42, 1875-1885(2003).
2. K. Akasaka, Probing Conformational Fluctuation of Proteins by Pressure Perturbation. *Chemical Reviews* 106, 1814-1835 (2006).
3. C. B. Anfinsen *Science 181*, 223-230 (1973).
4. M. Refaee, T. Tezuka, K. Akasaka and M. P. Williamson, Pressure-dependent changes in the solution structure of hen egg-white lysozyme. *J. Mol. Biol.* 327, 857-865 (2003).
5. R. Kitahara, S.Yokoyama and K. Akasaka, NMR snapshots of a fluctuating protein structure. Ubiquitin at 30 bar – 3kbar. *J. Mol. Biol.* 347, 277-285 (2005).

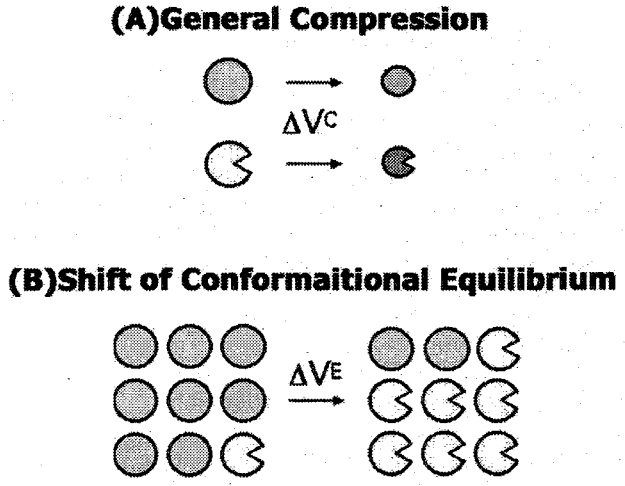

Fig. 1. Image of mechanical (A) and thermodynamic (B) response of proteins to pressure.

Biomolecular structure and dynamics from solution state residual dipolar couplings measured in multiple alignment media

Ke Ruan, Kathryn Briggman, Devon Sheppard, and Joel R. Tolman
Department of Chemistry, Johns Hopkins University, 3400 N. Charles St., Baltimore, MD, USA 21218

Dipolar coupling interactions occur between pairs of magnetic nuclei and thus, like the scalar coupling, produce a fine structure or splitting of individual resonances in the NMR spectrum. When a molecule tumbles in solution such that all orientations relative to the magnetic field are assumed with equal probability, dipolar interactions contribute only to relaxation properties and not to the frequencies of lines in the NMR spectrum. As the assumption of orientational isotropy normally holds to a high level of approximation for molecules in solution, contributions to line splittings from dipolar couplings is not generally observed. The introduction of a very weak degree of molecular alignment causes the introduction of residuals of these dipolar couplings into the spectrum while largely preserving the high resolution characteristic of solution state NMR. As is well known, these residual dipolar couplings (RDCs) are related to both the distance between the coupled nuclei as well as their orientation relative to global molecular axes (Figure 1). Indeed, RDCs have become one of the standard tools employed in biomolecular structure determination. They have played a particularly important role in studies of multi-domain systems or extended systems in which long-range order has been traditionally difficult to establish using shorter range restraints such as the NOE. In addition to their structural content, RDCs also represent potentially valuable probes of biomolecular dynamics or flexibility. This aspect of RDCs arises from the fact that they are a time average over all orientations of the bond relative to a molecular frame, occurring on a timescale faster than milliseconds. The challenge is to separate contributions to the observed RDC which arise due to orientational and motional properties. In general, this requires that complementary sets of RDCs be acquired under different anisotropic solvent conditions.

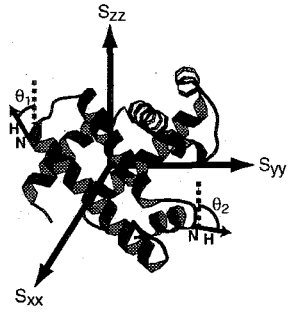

Figure 1 Measured RDCs depend on the orientation of the internuclear vector relative to a molecular-fixed coordinate system.

The nature of molecular alignment is mediated by interactions between the biomolecular solute and the anisotropic solvent, usually referred to as the alignment medium. The use of different alignment medium often leads to a different net alignment of the biomolecule, which allows complementary information

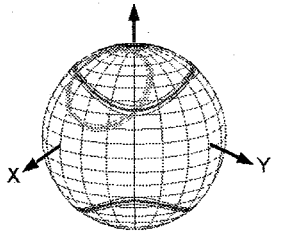

Figure 2 The use of two different alignment media restrains the possible bond orientations to the intersection between two flattened cones. Use of more than two media produces an overdetermined situation and can allow dynamics to be characterized.

Keywords: dynamics, alignment, residual dipolar couplings, acrylamide gels, ubiquitin

to be acquired (Figure 2). This is a fundamental aspect for the study of biomolecular dynamics using RDC methods. We will discuss techniques by which the acquisition of RDCs using > 5 different alignment media can allow the determination of amplitudes (ie generalized order parameters) and asymmetries of motion for individual amide N-H bonds. The characterization of dynamics using multi-alignment RDCs can proceed based on a set of structural coordinates[1] or even in a completely *de novo* fashion,[2] in which RDC-based order parameters and mean bond orientations are determined simultaneously. As these RDC approaches also provide generalized order parameters, they nicely complement established ^{15}N spin relaxation methods. Notably, the two methods are sensitive to different timescales: picosecond to nanosecond timescales in the case of ^{15}N spin relaxation and picosecond to millisecond timescales in the case of RDCs.

One of the major difficulties associated with multi-alignment RDC approaches to the study of dynamics is purely experimental. Although five independent alignments are required to separate orientational and dynamic contributions to RDCs, it remains quite challenging to obtain data which correspond more than three independent alignment tensors. In general this is because the array of available alignment media, although chemically distinct, induce molecular alignment by means of fundamental steric and electrostatic interactions. As such, the resulting molecular alignment tensors often exhibit a substantial degree of linear dependence. These difficulties are exacerbated by the near lack of experimental control which one has over the alignment tensor which results from use of a given alignment medium.

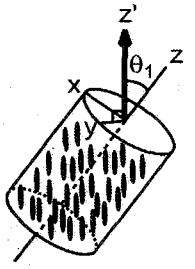

Figure 3 Modulation of alignment by variation of the angle θ_1 between the bacteriophage Pf1 ordering director and the axis of strain applied to a polyacrylamide gel.

We have been exploring means by which greater experimental control over the alignment can be achieved. Our approach to this problem is to utilize a single composite alignment medium comprised of aligned bacteriophage Pf1 particles embedded in a strained polyacrylamide gel matrix (Figure 3). Using this composite medium, molecular alignment can be modulated by varying the angle between the directors of ordering for the Pf1 and strained gel matrix, by varying the ionic strength or concentration of the Pf1 particles.[3] This observation reveals the important role of symmetry in restricting our ability to modulate molecular alignment. Our goal is to achieve control over macroscopic factors governing the net alignment, thus allowing the acquisition of multi-alignment RDC data with greater predictability while maintaining a homogeneous chemical environment. We will discuss our progress towards the prediction of the resultant alignment tensors using this medium in the context of an application to human ubiquitin.

References:

(1) a. Meiler, J.; Prompers, J. J.; Peti, W.; Griesinger, C.; Bruschweiler, R. *J. Am. Chem. Soc.* **2001**, *123*, 6098-6107. b. Peti, W.; Meiler, J.; Bruschweiler, R.; Griesinger, C. *J. Am. Chem. Soc.* **2002**, *124*, 5822-5833.
(2) a. Tolman, J. R. *J. Am. Chem. Soc.* **2002**, *124*, 12020-12030. b. Briggman, K. B.; Tolman, J. R. *J . Am. Chem. Soc* **2003**, *125*, 10164-10165.
(3) Ruan, K.; Tolman, J. R. *J . Am. Chem. Soc.* **2005**, *127*, 15032-15033.

Lanthanide Labelling for Structure Determination of Protein-Ligand Complexes

Guido Pintacuda, Michael John, Xun-Cheng Su, Ah-Young Park, Nicholas E. Dixon, Christophe Schmitz, Thomas Huber*, Peter Wu, Kiyoshi Ozawa, Gottfried Otting

Research School of Chemistry, Australian National University, Canberra, Australia
*Department of Mathematics, University of Queensland, Brisbane, Australia

A novel NMR strategy was developed which uses the paramagnetic effects from lanthanide labelled proteins to achieve rapid 3D structure determinations of protein-protein and protein-ligand complexes. The pseudocontact shifts induced by a site-specifically bound lanthanide ion yield the coordinate system of the magnetic susceptibility tensor in the molecular frames of the two molecules. Simple superposition of the tensors detected in the two protein molecules brings them together in a 3D model of the protein-protein complex. The method is demonstrated with the 30 kDa complex between two subunits of *Escherichia coli* polymerase III, comprising the N-terminal domain of the exonuclease subunit ε and the subunit θ, using straightforward ^{15}N-HSQC spectra.

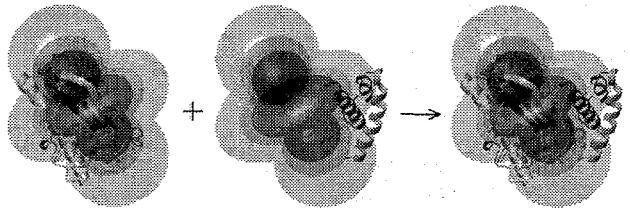

Figure 1: iso-surfaces of pseudocontact shifts originating from a bound Dy^{3+} ion in the active site of epsilon, plotted onto ε (grey ribbon) and θ (yellow ribbon), yield the structure of the complex by rigid-body docking

In addition, methods for rapid assignments of the paramagnetic NMR spectra are presented, as well as chemical methods for site-specific lanthanide labelling of proteins. A second application involves the determination of the binding site, orientation, and conformation of a small ligand molecule bound to the lanthanide labelled protein from one-dimensional ^{1}H and ^{13}C NMR experiments.

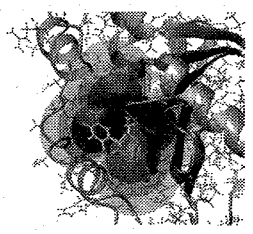

Figure 2: Structure of the epsilon-thymidine complex determined by pseudocontact shifts.

Keywords: ^{15}N-HSQC, pseudocontact shift, lanthanides, cell-free protein expression, epsilon-theta complex

Finally, applications of cell-free protein expression will be shown.

References

G. Pintacuda, M. A. Keniry, T. Huber, A. Y. Park, N. E. Dixon, G. Otting (2004) Fast structure-based assignment of ^{15}N-HSQC spectra of selectively ^{15}N-labeled paramagnetic proteins. *J. Am. Chem. Soc.* 126, 2963-2970.

M. John, A. Y. Park, G. Pintacuda, N. E. Dixon, G. Otting (2005) Weak alignment of paramagnetic proteins warrants correction for residual CSA effects in measurements of pseudocontact shifts. *J. Am. Chem. Soc.* 127, 17190-17191.

G. Pintacuda, A. Y. Park, M. A. Keniry, N. E. Dixon, G. Otting (2006) Lanthanide labeling offers fast NMR approach to 3D structure determinations of protein-protein complexes. *J. Am. Chem. Soc.* 128, 3696-3702.

K. Ozawa, P. S. C. Wu, N. E. Dixon, G. Otting (2006) ^{15}N-labelled proteins by cell free protein synthesis: strategies for high-throughput NMR studies of proteins and protein-ligand complexes. *FEBS J.* 273, 4154-4159.

M. John, G. Pintacuda, A. Y. Park, N. E. Dixon, G. Otting, (2006) Structure determination of protein-ligand complexes by transferred paramagnetic shifts. *J. Am. Chem. Soc.*, in press

X. C. Su, T. Huber, N. E. Dixon, G. Otting (2006) Site-specific labelling of proteins with a rigid lanthanide binding tag. *ChemBioChem,* in press

Structure of the split PH domain and distinct lipid-binding properties of the PH-PDZ supramodule of alpha-syntrophin

Wenyu Wen[1, 2], Jing Yan[1, 2], Weiguang Xu[1], Jia-fu Long[1], and Mingjie Zhang[1]

[1] Department of Biochemistry, Molecular Neuroscience Center, Hong Kong University of Science and Technology, Clear Water Bay, Kowloon, Hong Kong, People's Republic of China

[2] These two authors contributed equally to this work

Pleckstrin homology (PH) domains play diverse roles in cytoskeletal dynamics and signal transduction. Split PH domains represent a unique subclass of PH domains that have been implicated in interactions with complementary partial PH domains 'hidden' in many proteins. Whether partial PH domains exist as independent structural units alone and whether two halves of a split PH domain can fold together to form an intact PH domain are not known. Here, we solved the structure of the PH_N-PDZ-PH_C tandem of alpha-syntrophin. The split PH domain of alpha-syntrophin adopts a canonical PH domain fold. The isolated partial PH domains of alpha-syntrophin, although completely unfolded, remain soluble in solution. Mixing of the two isolated domains induces de novo folding and yields a stable PH domain. Our results demonstrate that two complementary partial PH domains are capable of binding to each other to form an intact PH domain.

The split PH domain of the PH_N-PDZ-PH_C tandem from α-syntrophin adopts the same fold as the two halves linked together

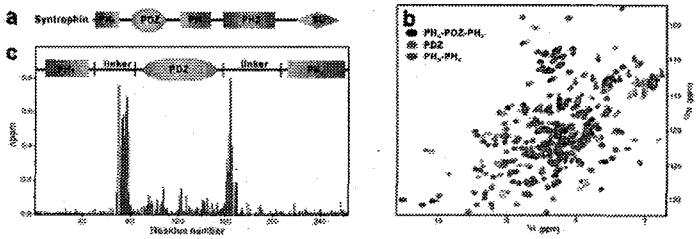

Figure 1: Comparison of the split PH and PDZ domains in the PH_N-PDZ-PH_C tandem and in their respective isolated state. **(a)** Schematic diagram showing the domain organization of syntrophins. **(b)** Superposition plots of ^1H, ^{15}N HSQC spectra of the PH_N-PDZ-PH_C tandem (black), the isolated PDZ domain (green), and the joint PH_N-PH_C domain (red). **(c)** Plot of chemical shift changes as a function of residue number of the split PH and PDZ domains in the PH_N-PDZ-PH_C tandem and in their respective isolated forms. The combined ^1H and ^{15}N chemical shift changes are defined as: $\Delta_{ave} = [(\Delta\delta_{HN})^2 + (\Delta\delta_N \times \alpha_N)^2]^{1/2}$. $\Delta\delta_{HN}$ and $\Delta\delta_N$ represent chemical shift differences of amide proton and nitrogen chemical shifts between the PH_N-PDZ-PH_C tandem and the isolated PH and PDZ domains, respectively. The scaling factor (α_N) used to normalize the ^1H and ^{15}N chemical shifts is 0.17. The domain organization of the PH_N-PDZ-PH_C tandem is indicated at the top of the plot.

Keywords: split PH domain, lipid binding, syntrophin

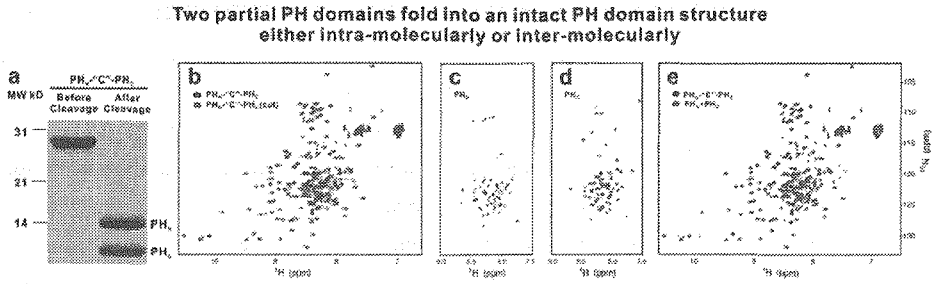

Figure 2: Folding and interaction of the two isolated, partial PH domain fragments. (a) SDS-PAGE showing the purification of the joined PH_N-"C"-PH_C domain and cleavage of the domain into PH_N and PH_C fragments (b) Overlay plot of the ^1H, ^{15}N HSQC spectra of the joined PH_N-"C"-PH_C (black) and its protease cleaved form (red). (c&d) ^1H, ^{15}N HSQC spectra of the isolated PH_N (c) and PH_C (d) fragments. (e) Overlay plot of the ^1H, ^{15}N HSQC spectra of the joined PH_N-"C"-PH_C (black) and the 1:1 mixture of the two halves of the split PH domain (red).

We further showed that the PH_N-PDZ-PH_C tandem forms a functionally distinct supramodule, in which the split PH domain and the PDZ domain function synergistically in binding to inositol phospholipids.

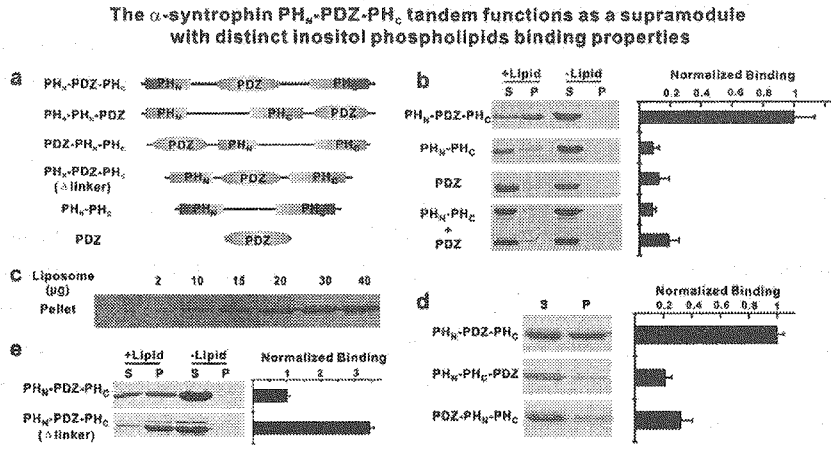

Figure 3: The PH_N-PDZ-PH_C supramodule binds to brain liposomes with enhanced avidity. (a) Schematic diagrams showing the various forms of proteins purified for liposome binding assays. (b) Brain liposome binding assays of the PH_N-PDZ-PH_C tandem and its fragments. "S" and "P" denote proteins recovered in the supernatants and pellets, respectively, in the centrifugation-based liposome binding assays. (c) Dose-dependent binding between the PH_N-PDZ-PH_C tandem and the brain liposome. In this assay, the amount of the PH_N-PDZ-PH_C tandem is fixed at 10 μM, and the concentration of liposome varies. The liposome-bound PH_N-PDZ-PH_C tandem is recovered in the pellet in the binding assay. (d) Lipid binding of the two mutants of the PH_N-PDZ-PH_C tandem. In these two mutants, the PDZ domain was placed either at the front or after the split PH domain. In these mutants, the PH domain and the PDZ domain were connected by a flexible "Gly-Ser-Gly-Gly-Ser-Gly-Gly-Ser-Gly-Ser" linker. (e) Lipid binding of a PH_N-PDZ-PH_C tandem mutant with the two connecting linkers shortened to 6 residues.

In addition to alpha-syntrophin, we also determined the three-dimensional structure of the split PH domain of Phospholipase C-gamma1. Similar to the structure of split PH domain of alpha-syntrophin, the split PH domain of the enzyme folds into a canonical PH domain fold with high thermostability. The SH2SH2SH3 insertion between the two halves of the split PH domain has negligible impact on the conformation of the PH domain. (supported by grants from the Research Grants Council of Hong Kong)

3 LE17

膜関連 AAA-ATPase の N-terminal domain の構造生物学

(横浜市大院・国際総合科学)
○ 廣明秀一

Structural biology of N-terminal domains dissected from membrane related AAA-ATPases.

Hidekazu Hiroaki
International Graduate School of Arts and Sciences, Yokohama City University

Some of AAA-ATPases are working with membrane associating events, such as membrane fusion, invaginated membrane formation and protein transport across membrane. These AAA-ATPases usually possess unique N-terminal segment of approximately 100 to 500 amino acids in length. We searched several isolatable domains from these sequences, and if found, determined their structures and molecular functions. Examples include MIT domain from hVps4b, N-domain from mouse kp60 and N-domain of mouse PEX1 (PEX1-ND). First two domains adopt into up-and-down three helix bundle fold, whereas PEX1ND adopts a double-psi-barrel fold with b-barrel fold similar to other type II AAA-ATPases, such as VCP and NSF. Interestingly, two of them ($Vps4^{MIT}$ and PEX1-ND) showed substantial phosphoinositides-binding activities. The residues responsible for maintaining their folding and function are further discussed.

<Background>

AAA ("ATPase associated with various cellular activities")-ATPases are found in all three domains of life and play an important role as molecular chaperones, including the dissociation of protein complexes and protein translocation. AAA-ATPase has two classes, type I and type II, which contain one and two copies of the AAA cassette, respectively. There are some AAA-ATPases located in organelle membranes whose function is closely related to maintenance, formation and translocation of the organellar membranes. As example, Vps4 is involved in the of formation of invaginated membrane structures at multivesicular bodies (MVBs) in concert with the ESCRT-III complex. Whereas native Vps4 is found in the cytosol, an ATPase-defective mutant of Vps4b has been observed to accumulate at the endosomal membranes. PEX1 belongs to the class of type II AAA-ATPases, whose function is indispensable for normal peroxisomal biogenesis including the critical step of peroxisomal protein import and peroxisomal membrane fusion, with associating another type II AAA-ATPase, PEX6 . PEX1-PEX6 complex is involved in the dissociation of ubiquitinated PEX5 from the peroxisomal membrane. There are other membrane-associated type II AAA-ATPases. NSF, and its yeast ortholog Sec18, are responsible for heterotypic membrane fusion mainly in exocytic pathways. α-, β- and γ–SNAPs are known to be the most important targets of NSF. VCP and yeast CDC48, are involved in ER-associated protein degradation (ERAD) as well as in remodeling of the Golgi and nuclear membrane. Although the specific target of VCP

キーワード：AAA ATPase、オルガネラ膜、ホスホイノシタイド結合ドメイン、微小管

著者ふりがな：ひろあきひでかず

unfoldase activity remains unclear, there are several adaptor molecules, p47, Ufd1 / Npl4, VCIP135, Derlin-1 and VIMP, which may determine VCP functions.

To explore any membrane-associating and other functional domains from the N-terminal regions of AAA-ATPases, we developed a combined approach of structural biology with bioinformatics. Firstly, an extensive sequence analysis was done for these type I and type II ATPases. Secondly, a laboratory-scale high-throughput method for constructing expression vectors of the domains of interest was developed[1]. Thirdly, the structures were determined by using both NMR and X-ray crystallography. Finally, an evolutionary trace analysis was used to determine the residues critical for protein-lipid interaction.

<Results and discussion>

We have determined the solution structure of the MIT (microtubule interacting and trafficking) domain isolated from the NH_2-terminus of human Vps4b[2]. The molecular function of this domain remains unclear. MIT domain is a small protein module that is conserved in proteins of diverged function, such as Vps4, sorting nexin 15 (SNX15), and spastin. The MIT domain adopts an 'up-and-down' three-helix bundle. There is a shallow crevice between helices A and C that may serve as a protein-binding site. The loop between helices A and B has been shown to bind a Ca^{2+} ion. Furthermore, the MIT domains derived from Vps4 as well as SNX15a have been shown to be capable of binding phosphoinositides in a Ca^{2+}-dependent fashion. We proposed that the MIT domain is a novel membrane-binding domain involved in endosomal trafficking.

We also identified a putative domain from the N-terminal region of katanin p60 (kp60-ND)[3]. katanin is another microtubule severing enzyme. The structure determination of kp60NTD is under-way. Currently, a global fold of up-and-down three helical bundle is obtained, which is similar to $hVps4b^{MIT}$, although there is no obvious sequence similarity. Further structural comparison with kp60-ND and $hVps4b^{MIT}$ will be discussed.

We then determined the crystal structure of the N-terminal domain of mouse PEX1 (PEX1-ND)[4]. The structure showed a striking structural similarity between its N-terminal domain (ND) and those of other membrane related AAA-ATPases, such as valosin-containing protein (VCP/p97). VCP-ND serves as an interface to its adaptor proteins p47 and Ufd1, whereas PEX1-ND's physiological interaction partner remains unknown. Here we found that NDs isolated from VCP, as well as PEX1 bind phosphoinositides. PEX1-ND appears to preferentially bind phosphatidylinositol-3- and -4- monophosphate, whereas VCP-ND displays broad and non-specific lipid binding[5]. Although NSF, CDC48 and Ufd1 have structures similar to VCP, they displayed a lipid specificity similar to that of PEX1-ND in the assays. By mutational analysis, we demonstrate that a conserved arginine surrounded by hydrophobic residues is essential for lipid binding, despite very low sequence similarity between PEX1 and VCP.

<References>

1) Goda N., Tenno T., Takasu H., Hiroaki H. and Shirakawa M. *Protein Science* **13**, 652-658 (2004).

2) Takasu, H., *et al. Biochem Biophys Res Commun.*, **334** 460-465 (2005).

3) Iwaya N., *et al. J Biomol NMR, in press* (2006).

4) Shiozawa K., *et al. J. Biol. Chem*, **279** 50060-50068 (2004).

5) Shiozawa K., *et al. FEBS J.*, **273** *in press* (2006).

The combinatory use of relaxation dispersion and variable-pressure NMR for protein dynamics analysis: D1 domain of annexin I

Ryo Kitahara[1], Matthieu Gallopin[2], Christian Roumestand[3], Shigeyuki Yokoyama[1,4,5], Erick Guittet[2], Kazuyuki Akasaka[6], and Carine van Heijenoort[2]

[1]RIKEN SPring-8 Center, Japan, [2]CNRS-ICSN, Gif-syr-Yvette, FRANCE, [3]CNRS, INSERM, France, [4]RIKEN GSC, Japan, [5]The University of Tokyo, Japan, [6]Kinki University, Japan

Summary: Several NMR approaches have been proposed to study dynamic motions of proteins in solution. Here, we show that the combined use of the relaxation dispersion NMR and variable pressure NMR enables one to better estimate a series of kinetic and thermodynamic parameters of inter-converting conformers of proteins.

Recently, NMR relaxation dispersion methods and variable pressure NMR proved to be very valuable to probe the dynamic nature of proteins and to relate this dynamics to the function. Relaxation dispersion experiments allow the monitoring of conformational fluctuations mostly in μs-ms timescale, while variable pressure NMR is useful for exploring protein dynamics in a wider conformational space and timescale [1-4]. Furthermore, the latter method allows one to examine directly the structures of high-energy alternative conformers resulting from such fluctuations [1]. Here, our concern is whether the two proposed approaches are looking at same dynamic motions of proteins, especially the μs-ms motion. We examined the dynamics of D1 domain of annexin I (A1D1, 81 residues) using the two approaches.

^{15}N relaxation dispersion NMR experiments have been carried out at a series of magnetic fields, 500, 600, 700, 800 MHz and temperatures, 288, 298, 308K, and variable pressure experiments (~ 3 kbar) at 500 MHz and 800 MHz at 293K. ^{15}N relaxation experiments showed significant chemical exchange for residues in localized segments of the sequence (**Fig. 1**). Interestingly, all HSQC cross-peaks of these residues were remarkably broadened or split into two in the nitrogen axis under high pressure. Some examples are shown in **Fig.2**. This reflects probably a decrease in exchange rates under increasing pressures. Hence it enables direct measurements of chemical shift difference ($\Delta\omega$) and relative populations of the two exchanging states, resulting in a reliable calculation of forward and reverse interconversion rates (k_{on}, k_{off}) from the relaxation dispersion data (R_{ex}). Otherwise, pressure dependence of the relative populations, namely the equilibrium constant, provides the Gibbs free energy difference (ΔG) and partial molar volume difference (ΔV) between the two states. In addition, broadening and splitting were observed on cross-peaks of many other residues in the proton axis under high pressure. This implies that the series of ^{15}N relaxation dispersion approaches at multiple magnetic fields can observe backbone motions in a limited timescale. We propose that the joint use of the relaxation dispersion and variable-pressure NMR approaches enables one to better estimate a series of kinetic and thermodynamic parameters of protein's inter-converting conformers.

Key words: high pressure NMR, relaxation dispersion NMR, protein dynamics, thermodynamics

きたはら りょう、 マシュー ガロピン、クリスチャン ルーメスタンド、よこやま しげゆき、エリック ギテ、あかさか かずゆき、カリーナ ヘイノールト

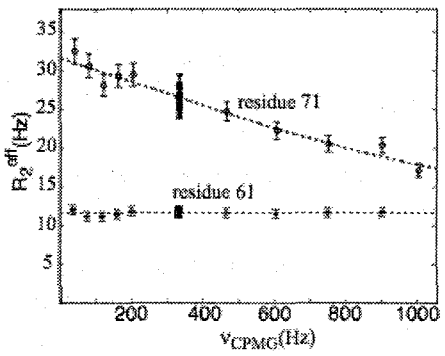

Fig. 1. NMR relaxation dispersion data for residues 61 and 71, revealing the presence of a large exchange contribution for residue 71. The data were performed on a Bruker Avance500 spectrometer, on a sample containing 1mM A1D1, pH4, 298K and 1 bar.

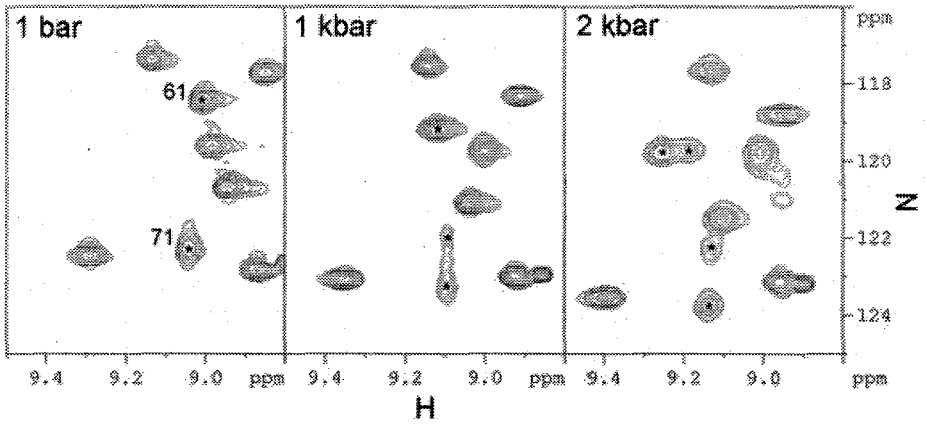

Fig. 2. Splitting and broadening of HSQC cross-peaks of D1 domain of annexin I at ^{1}H-500MHz, pH4.4 and 293 K under representative pressures. The cross-peak of residue 71 splits in N-axis, while that of residue 61 splits in H-axis with pressure.

References

[1] Ryo Kitahara, Shigeyuki Yokoyama and Kazuyuki Akasaka. NMR snapshots of a fluctuating protein structure. Ubiqutin at 30 bar-3 kbar. ***J. Mol. Biol.*** **347**, 277-285 (2005).

[2] Ryo Kitahara, Akira Okuno, Minoru Kato, Yoshihiro Taniguchi, Shigeyuki Yokoyama and Kazuyuki Akasaka. Cold denaturation of ubiquitin at high pressure. ***Mag. Res. Chem.*** **44,** s108-s113 (2006).

[3] Ryo Kitahara, Yoshiki Yamaguchi, Eri Sakata, Takeshi Kasuya, Keiji Tanaka, Koichi Kato, Shigeyuki Yokoyama, Kazuyuki Akasaka. Evolutionally conserved intermediates between ubiquitin and NEDD8. ***J. Mol. Biol. In press.***

[4] Ryo Kitahara, Shigeyuki Yokoyama, and Kazuyuki Akasaka. A New Paradigm of Protein Structures by Variable Pressure NMR. *分光研究* **55**, 10-20 (2006).

高圧 NMR によるシトクロム *c* の酸化還元電位調節に関わる内部運動の解析

(筑波大院数物[1]、広大院生物圏[2]、理研播磨[3]、近畿大[4]) 高山 J 真一[1]、高橋陽太[1]、三上真一[1]、太 虎林[1]、河野 慎[1]、三田 肇[1]、○山本泰彦[1]、三本木至宏[2]、北原 亮[3]、横山茂之[3]、赤坂一之[3,4]

High Pressure NMR Characterization of Internal Motion Responsible for the Regulation of redox potential of Cytochrome *c*

Shin-ichi J. Takayama[1], Yo-ta Takahashi[1], Shin-ichi Mikami[1], Hulin Tai[1], Shin Kawano[1], Hajime Mita[1], ○ Yasuhiko Yamamoto[1], Yoshihiro Sambongi[2], Ryo Kitahara[3], Shigeyuki Yokoyama[3], and Kazuyuki Akasaka[3,4]

[1]Dept. of Chem., Univ. of Tsukuba, [2]Graduate School of Biosphere Sci., Hiroshima Univ., [3]Structural and Molecular Biology Laboratory, RIKEN Harima Institute at Spring-8, and [4]School of Biology-Oriented Science and Technology, Kinki Univ.

H. thermophilus cytochrome c_{552} exhibits a unique dynamic property (Zhong *et al.*, *PNAS* (2004)), which is manifested in the biphasic behavior of the temperature dependence of its redox potential (Takahashi *et al.*, *Biochemistry* (2006)). Variable-temperature and -pressure NMR studies of the protein revealed a conformational transition between two different protein structures, which slightly differ in the conformation of the loop bearing the axial Met residue. The thermodynamic properties of the reduction of this protein possessing two different loop conformations suggested that the heme environment in the protein structure which emerges at lower temperature is more polar, as a result of the altered orientation of the loop with respect to the heme due to its conformational change, than that in the protein structure at higher temperature. The present study clarified the importance of the protein dynamics for both enthalpic and entropic regulation of the redox potential of the protein.

序 論

私共は、好熱性水素細菌 (*Hydrogenobacter thermophilus*) シトクロム c_{552} (HT) と緑膿菌 (*Pseudomonas aeruginosa*) シトクロム c_{551} (PA) を研究対象として、シトクロム *c* における酸化還元電位 (E_m) 調節の分子機構の解明を目指している[1-7]。HT と PA のアミノ酸配列の相同性は 56%であり、お互いの立体構造は類似しているが、両者の E_m には約 60 mV の差がある。E_m の熱力学的解析から、両者の E_m の差は主に還元反応に伴うエンタルピー変化の寄与の差に起因することが明らかになっている[1, 2]。本研究では、赤坂ら[8]により開発された高圧 NMR により、HT と PA の内部運動を解析し、ヘム近傍のループ領域のコンフォメーション変化のダイナミクスが E_m の調節に重要であることを明らかにした。

結果と考察

酸化型 HT の NMR スペクトルで、常磁性シフトして観測されるヘム側鎖プロトンに由来するシグナルは、低温で異常なブロードニングを示した (Figure 1)。また、これらのシグナルは、室温でも高圧にするとブロードニングした。さらに、圧力 2000 bar での-20 ℃までの温度変化では、シグナルは温度低下に伴って連続的に低磁場シフトすると共に、-20 ℃で先鋭化した。これらのシグナルのスピン-格子緩和時間は温度を変えてもほぼ一定である

Keyword : 高圧 NMR、シトクロム *c*、酸化還元電位、内部運動、ヘム電子構造

たかやま J. しんいち、たかはしようた、みかみしんいち、たいこりん、かわのしん、みたはじめ、やまもとやすひこ、さんぼんぎよしひろ、きたはらりょう、よこやましげゆき、あかさかかずゆき

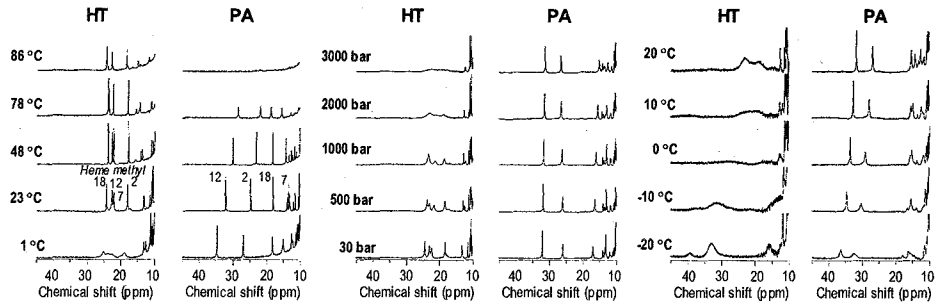

Figure 1. Downfield-shifted portions of ^{1}H NMR spectra of the oxidized HT and PA at various temperatures (Left), various pressures at 25 ℃ (center), and various temperatures at 2000 bar (right).

ことから、このブロードニングはHTの内部運動に起因すると推測された。一方、PAのシグナルでは、温度や圧力の変化に伴うこのようなブロードニングは観測されなかった。

高圧でのシグナルの線幅の増大は、内部運動が圧力の上昇に伴って遅くなることを示しており、運動に伴う活性化体積が正で大きいことを反映している。つまり、HTでは、比較的大きな構造変化を伴う内部運動が起きていることを示している。常温と-20 ℃でのヘムメチルプロトンシグナルのシフト値は、相互変換する2状態それぞれに由来すると考えられることから、変換速度は~10^4 s^{-1}であると見積もられた。HSQCシグナルの温度および圧力依存性（Figure 2）から、ヘム近傍のループ領域（Figure 3）に内部運動の存在が示唆されたことから、この領域のコンフォメーションが2状態の平衡として存在していることが推測された。溶媒への露出表面積が大きいループのコンフォメーションは、疎水性相互作用により影響を受けると考えられるが、温度低下に伴う溶媒の誘電率の増大により疎水性相互作用は強くなるため、結果的にループのコンフォメーションは低温で変化すると推測される。PAにも同様なループは存在するが、そのコンフォメーションが低温でHT同様に変化しない理由としては、X線結晶構造[9]で示されているアミノ酸4残基の間でのユニークな水素結合ネットワークにより固定されているからであると考えられる。HTの場合、温度に対するE_mのプロットは直線にはならないが[1]、ループのコンフォメーション変化が原因であると考えられる。

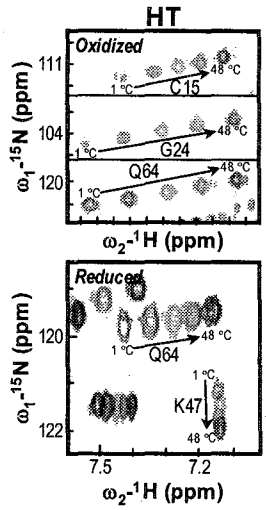

Figure 2. Superpositioning of ^{15}N/^{1}H HSQC N_εH cross-peaks for C15, K47, S53, Q64 of ^{15}N uniformly labeled HT in 90 % H_2O/10 % D_2O, pH 6.00, and various temperatures from 1 to 48 ℃.

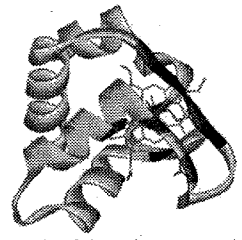

Figure 3. Schematic representation of HT (PDB: 1YNR). The residues in the reduced protein of which the ^{15}N/^{1}H HSQC cross-peaks exhibited broadening at lower temperatures and Pro residues are indicated in dark grey and black, respectively.

References
[1] Y. Takahashi *et al.*, *Biochemistry*, 45, 11005-11011 (2006).
[2] S. J. Takayama *et al.*, *Biochemistry*, 44, 5488-5494 (2005).
[3] K. Oikawa *et al.*, *J. Biol. Chem.*, 280, 5527-5532 (2005).
[4] S. Uchiyama *et al.*, *J. Am. Chem. Soc.*, 126, 14684-14685 (2004).
[5] N. Tachiiri *et al.*, *J. Biol. Inorg. Chem.*, 9, 733-742 (2004).
[6] N. Terui *et al.*, *J. Am. Chem. Soc.*, 125, 13650-13651 (2003).
[7] Y. Yamamoto *et al.*, *J. Am. Chem. Soc.*, 124, 11574-11575 (2002).
[8] K. Akasaka, *Chem. Rev.*, 106, 1814-1835 (2006).
[9] Y. Matsuura *et al.*, *J. Mol. Chem*, 156, 389-409 (1982).

PAN640

Friday, November 24

Japanese Session

3 LJ1

翻訳開始因子 eIF4A に結合するアプタマーの２つのヘアピン部分の立体構造

(1 千葉工大・工・生命環境科学科, 2 東大・医科研, 3JST・CREST)
○ 坂本泰一 1,2,3, 小黒明弘 2, 河合剛太 1, 大津　敬 2, 中村義一 2,3

Solution Structures of Two Hairpin Loops of an RNA Aptamer against Mammalian Initiation Factor 4A

([1]Department of Life and Environmental Sciences, Faculty of Engineering, Chiba Institute of Technology, [2]Department of Basic Medical Sciences, Institute of Medical Science, University of Tokyo, [3]CREST, JST)
Taiichi Sakamoto[1,2,3], Akihiro Oguro[2], Gota Kawai[1], Takashi Ohtsu[2], Yoshikazu Nakamura[2,3]

An RNA aptamer against mammalian initiation factor 4A (eIF4A) has been selected from combinatorial libraries by *in vitro* selection (SELEX). Site-directed mutation and truncation experiments revealed that a 58-nucleotide long structure (APT58, 58 nucleotides long) of this aptamer is required for efficient recognition of eIF4A. To understand the structural basis of APT58's global recognition of eIF4A, we determined the solution structure of two essential nucleotide loops (AUCGCA and ACAUAGA) within the aptamer using NMR. The AUCGCA loop and the ACAUAGA loop are stabilized by a U-turn motif and an AUA tri-nucleotide loop motif, respectively. The both loops contain non-canonical A:A base pairs. Considering the known structural and functional properties of APT58, we propose that the Watson-Crick edges of C7 and C9 in the AUCGCA loop are directly involved in the interaction with eIF4A.

１．はじめに

標的物質に結合する DNA/RNA を試験管内で選択する方法（SELEX 法）は，ある病因タンパク質を標的とした場合に、診断薬や治療薬として期待することができる．翻訳開始因子 eIF4A は，mRNA の 5′-UTR の構造をほぐす RNA helicase であり，mRNA 上のリボソーム結合部位を提示するのに必要なタンパク質であるが，黒色腫において過剰発現することが報告されており，癌との関係が注目されている．我々はすでに，eIF4A（46 kDa）に結合して，翻訳を阻害するアプタマー（APT58）の取得に成功している [1]．そこで，アプタマーの立体構造を明らかにすることによって，より高い活性を持つアプタマーを設計することを計画している．

Keywords: RNA aptamer, Hairpin loop, Initiation factor 4A, AA base pair

さかもとたいいち，おぐろあきひろ，かわいごうた，おおつたかし，
なかむらよしかず

SELEX 法により得られたアプタマーは，2つのヘアピン部分と1つの内部ループ部分を持つ 58 残基の RNA である（図1）．APT58 を2つのドメインに分けて eIF4A との結合を調べたところ，各ドメインだけでは eIF4A と結合しないことがわかっている．よって，APT58 はその構造全体で eIF4A と結合することにより，高い親和性（解離定数 50 pM）および高い特異性を示していると考えられる．また，eIF4A は N 末端ドメインと C 末端ドメインの2つのドメインからなり，各ドメインと APT58 との結合を調べたところ，APT58 は eIF4A のそれぞれのドメインだけでは結合しないことがわかっている．よって，APT58 は eIF4A の一部分ではなく全体の構造を認識していることが示唆されている．

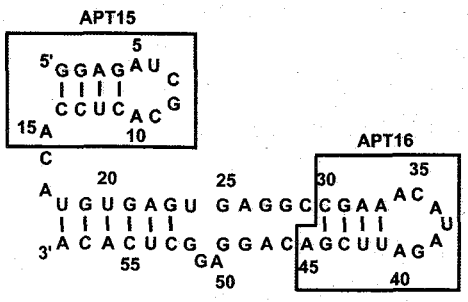

Fig. 1. Secondary structure of the APT58. The APT15 and the APT16 is indicated by boxes.

APT58 と eIF4A の相互作用メカニズムを明らかにするためには，それらの複合体の原子座標レベルでの解析が必要である．しかし，NMR による構造解析では，58 残基の RNA を解析することですら容易ではない．そこでまず，APT58 をドメインごとに分割し，それぞれの立体構造を決定した後にアプタマーの全体構造をモデリングすることを試みた．今回は，断片化により得られた2つのヘアピン部分（APT15 および APT16）について立体構造を明らかにしたので報告する[2)]．

2．方法

APT15 および APT16 の調製には，T7 RNA polymerase による *in vitro* 転写系あるいは RNA 自動合成機を用いた．それぞれの RNA 試料をポリアクリルアミド電気泳動法によって精製した後，APT15 については 10 mM リン酸ナトリウム緩衝液（pH 6.5）に溶解し，APT16 および APT20 については 20 mM リン酸ナトリウム緩衝液（pH 6.5），50 mM 塩化ナトリウムの溶液に溶かした．

DRX-600 および DRX-500（Bruker）を用いて，10℃で測定を行った．NMR シグナルの帰属については，定法に従い，おもに NOESY スペクトルを用いた．さらに，HNN-COSY により，塩基対形成を調べた．HCCH-COSY および HCCH-TOCSY により，リボースのシグナルの帰属を行い，HCCH-TOCSY を用いてアデノシンの H2 プロトンのシグナルを帰属した．NOESY スペクトルから距離の情報を得て，2D TOCSY，2D DQF-COSY，2D HP-COSY および HCP スペクトルからねじれ角の情報を得ることができた．

NMR スペクトルより得られた情報を用いて，プログラム discover により simulated annealing (SA)を行った．ランダムな 100 個の構造を初期構造として計算し，これらの構造の中で総エネルギーの低い 20 個の構造を選んだ．計算には，amber

の力場を用い，拘束条件の force constant としては，距離情報を 50 kcal mol^{-1} $Å^{-2}$，ねじれ角情報を 120 kcal mol^{-1} rad^{-2} とした．

3．結果および考察

図 2 のようにイミノプロトンシグナルを帰属し，さらに塩基やリボースのプロトンについてもシグナルを帰属した．APT15 については 155 個の距離情報および 45 個のねじれ角情報が得られ，APT16 については 228 個の距離情報および 46 個のねじれ角情報が得られた．これらの拘束条件を用いて SA を行い，図 3 の立体構造を得ることができた．APT15 および APT16 の両方の構造について，総エネルギーの低い 20 個の構造のそれらの平均構造に対する重原子の R.M.S.D.はともに 0.87 Å であり，よく収束していることがわかった．ループ部分の局所的な収束度を調べるため，重原子の R.M.S.D.を計算すると，APT15 のもつ AUCGCA ループは 0.52 Å であり，APT16 のもつ ACAUAGA ループは 0.88 Å であった．ループ部分に着目しても，立体構造計算の結果が収束していることがわかった．

APT15 のもつ AUCGCA ループは図 4A に示す A:A 塩基対を含むことがわかった．さらに，U6 と C7 の間のリン酸ジエステル結合のバックボーンがターンをする U-ターンモチーフであ

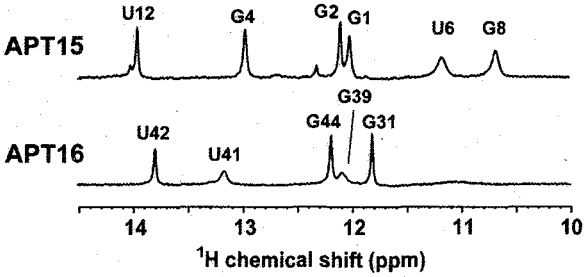

Figure 2. NMR spectra of exchangeable protons for APT15 and APT16. Imino proton assignments are denoted with residue numbers.

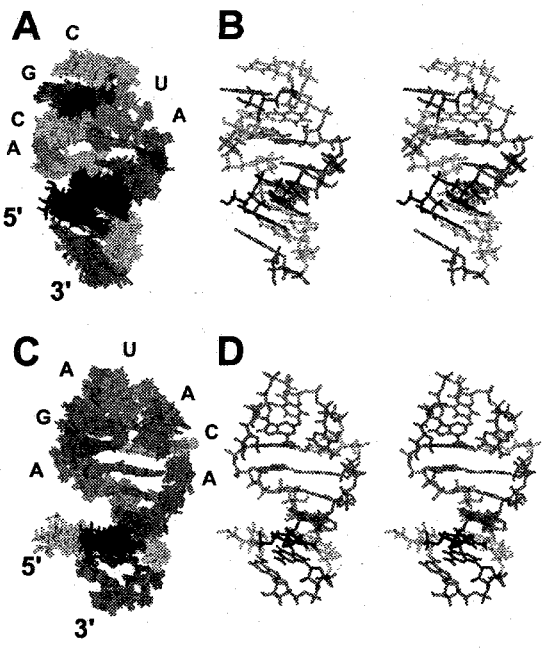

Figure 3. Tertiary structures of the APT15 and the APT16. A: A superposition of final 20 structures of the APT15. B: Stereo view of the minimized average structure of the APT15. C: A superposition of final 20 structures of the APT16. D: Stereo view of the minimized average structure of the APT16.

ることがわかった．U-ターンモチーフでは，U6 の N3 と G8-C9 の間のリン酸基と水素結合を形成し，U6 の 2′OH と G8 の N7 の間で水素結合を形成することによって構造を安定化している．

APT16 のもつ ACAUAGA ループは 7 残基からなるループと予想されていたが，実際は図 4B に示す A:A 塩基対をステム部分に含み，C:G 塩基対で閉じた AUA のトリループであることがわかった（図 2 において，ブロードではあるが，G39 に由来するイミノプロトンシグナルが観測されている）．AUA トリループでは，A38 がループの内側に入り，A36 が溶液中に露出している．A36 の N6 アミノ基が A34-C35 の間のリン酸基と水素結合を形成することによって，その立体構造を安定化している．

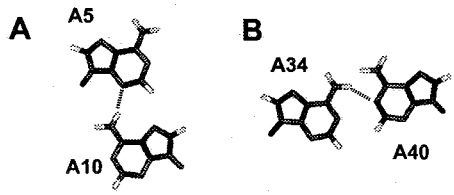

Figure 4. Schematic representation of non-canonical A:A base pairs in the APT15 (A) and the APT16 (B).

ACAUAGA ループを安定な UUCG ループに置換すると，eIF4A との親和性が低くなるが，結合できる．よって，APT16 の部分は相互作用には直接は関わっていないがその柔軟性が必要なのだろうと考えている．一方，AUCGCA ループの C7 あるいは C9 を他の塩基に置換すると，eIF4A に全く結合できなくなることがわかっている．AUCGCA ループの U-ターンモチーフでは C7 および C9 の官能基が外側を向いており，それらの官能基と eIF4A が相互作用していると考えられる．また，U-ターンを壊すような変異を導入すると，結合活性が下がることから， eIF4A はその特徴的な立体構造も認識していると考えられる．

4．今後の展望

eIF4A のヘリカーゼ活性の発現には，inchworm メカニズムが考えられており，そのメカニズムでは N 末端ドメインと C 末端ドメインの動きにより開いた構造と閉じた構造になることが重要である．我々は，APT58 がその両方のドメインに結合することによって，eIF4A の動きを止め，その機能を阻害しているのではないかと考えている． この阻害メカニズムを明らかにするには，APT58 の全体構造の解析が必要である．そこで現在，まだ構造のわかっていない部分である内部ループの構造解析を行っている．今後は，内部ループ部分の構造を決定し，さらに残余双極子相互作用の情報を用いて各ドメイン間の相対的な角度情報を解析することによって，APT58 の全体構造モデルを構築する．さらに，eIF4A との相互作用解析を行う予定である．

参考文献

1) Oguro A., Ohtsu T., Svitkin Y.V., Sonenberg N., and Nakamura Y. (2003) *RNA* **9**, 394-407.
2) Sakamoto T., Oguro A., Kawai G., Ohtsu T., and Nakamura Y. (2005) *Nucleic Acids Res.* **33**, 745-54.

3 LJ2

GTF2Iドメインリピートの溶液中での構造

1 理化学研究所ゲノム科学総合研究センター
2 東京大学理学系研究科、3 横浜市立大学

○片山由貴子[1]、林文晶[1]、栃尾尚哉[1]、小柴生造[1]、井上真[1]、原田拓志[1]、矢吹孝[1]、青木雅昭[1]、木川隆則[1]、好田真由美[1]、白水美香子[1]、寺田貴帆[1]、林崎良英[1]、横山茂之[1,2]、廣田洋[1,3]

Solution structures of GTF2I domain repeats of TFII-I

1. RIKEN Genomic Sciences Center, 2. Graduate School of Science, University of Tokyo, 3. Graduate School, Yokohama City University

○Yukiko Doi-Katayama[1], Fumiaki Hayashi[1], Naoya Tochio[1], Seizo Koshiba[1], Makoto Inoue[1], Takushi Harada[1], Takashi Yabuki[1], Masaaki Aoki[1], Takanori Kigawa[1], Mayumi Yoshida[1], Mikako Shirouzu[1], Takaho Terada[1], Yoshihide Hayashizaki[1], Shigeyuki Yokoyama[1,2], Hiroshi Hirota[1,3]

General transcription factor TFII-I is reported as an unusual transcriptional regulator that associates with both basal and signal-induced transcription factors. TFII-I is consisted of six GTF2I repeat domains called I-repeats R1-R6. It is known that the GTF2I repeat domains are located within the critical region of the Wiliams-Beuren syndrome deletion. Nevertheless, the structure and function of GTF2I domains have not been known clearly except that the domain contains helix-loop-helix motif from the result of gene and biological analyses. Here we have determined the 3D solution structure of five GTF2I domains and have found that they have a common fold but have varieties in the surface potential distribution.

GTF2Iドメインは基本転写因子TFII-Iファミリーのタンパク質上に存在する繰り返しドメインであり、その配列は種に関わらず高く保存されている。TFII-Iは基本転写およびシグナル誘導転写の両方に機能する基本転写因子として、またTFII-Iをコードする遺伝子*GTF2I*がWilliams-Beuren症候群の患者の遺伝子欠損部位に位置する遺伝子として知られていることから、その機能研究については多数の報告がある。これに対し、GTF2Iドメインの構造および機能についての詳細はこれまで明らかにされておらず、構造に関してはGTF2IドメインのみならずTFII-Iにおいても報告されていなかった。そこで、我々はGTF2Iドメインの機能の解明を目的として、マウスおよびヒトのTFII-I上に繰り返されるGTF2Iドメイン数種について、それらの溶液中での構造を解析し、それぞれの特徴について明らかにしたので以下に報告する。

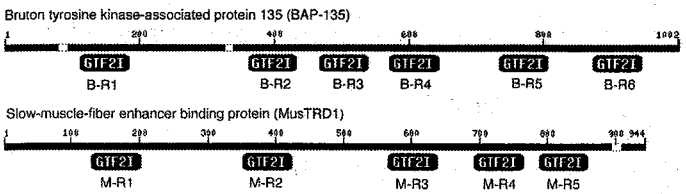

Figure 1.
Sequences of target proteins

本研究で用いたタンパク質は、Bruton tyrosine kinase-associated protein 135 (BAP-135)およびSlow-muscle-fiber enhancer binding protein (MusTRD1)である。BAP-135には6個、MusTRD1には5個のGTF2Iドメインが繰り返し存在する。このうち、これまでにBAP-135上のR1 (B-R1)、R2 (B-R2)、R5 (B-R5)およびMusTRD1上のR1 (M-R1)、R5 (M-R5)の構造解析を行った。

各GTF2Iドメインは、各遺伝子フラグメントを用いた大腸菌無細胞発現系にて $^{13}C/^{15}N$標識体を調製し、それぞれ約1 mMの溶液 (H_2O/D_2O (9/1) 20 mM リン酸化ナトリウム緩衝液 (pH 7.0), 100 mM NaCl, 1 mM *d*-DTT) に調製した。NMR測定は、25° Cで各種スペクトル(HNCO, HNCA, HNCACB, CBCA(CO)NH, and (HCA)CO(CA)NH, HBHA(CO)NH, HBHANH, CC(CO)NH, HCCH-TOCSY, CCH-TOCSY, ^{15}N HSQC, ^{13}C HSQC) を測定し、化学シフトの帰属を行った。NOE情報は、3D ^{15}N- and ^{13}C-edited NOESY スペクトルより得た。構造計算にはCYANA 1.0および2.0を用いた。

いずれのGTF2Iドメインも Helix-loop-helixと逆平行ベータシートに加え、それらの間のふたつのターンを含むループとヘリックスからなるaababという共通トポロジーをもち、B-R5のみC末側にもうひとつヘリックスを持つことが明らかになった。これらの主鎖はよく一致しているのに対し、各ドメインの分子表面の電荷分布にはそれぞれ特徴が認められた。この特徴が各ドメインの機能に大きく関与していることが示唆された。

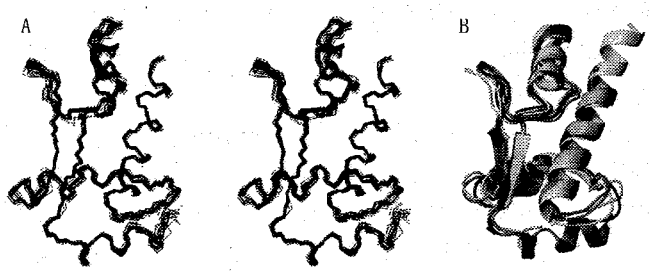

Figure 2.
Structure of GTF2I domain
(A) Stereopair view of the best fit of 20 structures of GTF2I domain B-R5.
(B) Ribbon diagrams of GTF2I domains fitting of the secondary structures of the B-R1, B-R2, B-R5, M-R1, and M-R5.

GTF2I domain; transcription factor; NMR; protein structure

かたやまゆきこ、はやしふみあき、とちおなおや、こしばせいぞう、いのうえまこと、はらだたくし、やぶきたかし、あおきまさあき、きがわたかのり、よしだまゆみ、しろうずみかこ、てらだたかほ、はやしざきよしひで、よこやましげゆき、ひろたひろし

3 LJ3

転移交差飽和法による Plastocyanin-Photosystem I 間電子輸送メカニズムの解析

○小川　雄大[1]、上田　卓見[1,2]、寺沢　宏明[1]、嶋田　一夫[1,3]
[1]東京大学大学院薬学系研究科　[2]JBIRC、JBIC、[3]BIRC、AIST

Structural basis of the electron transport between Photosystem I and Plastocyanin using the transferred cross-saturation method

○Yuuta Ogawa[1], Takumi Ueda[1,2], Hiroaki Terasawa[1], Ichio Shimada[1,3]
[1] Graduate School of Pharmaceutical Sciences, the University of Tokyo
[2] JBIRC, JBIC　[3] BIRC, AIST

The electron transport between Plastocyanin (Pc) and thylakoid membrane protein, Cytochrome b_6f (Cyt b_6f) and Photosystem I (PSI), is essential for photosynthetic light reactions of plants. For the elucidation of the electron transport mechanism, we used the transferred cross-saturation (TCS) methods to identify the residues of Pc interacting with PSI and Cyt b_6f. Based on the results of the TCS experiments of reduced Pc with PSI micelles, Cyt b_6f micelles, and thylakoid membrane vesicles containing both PSI and Cyt b_6f, we conclude that residues in loops 3 and 7 are important for both PSI-binding and Cyt b_6f-binding, whereas residues in loops 1 and 5 are predominantly responsible for the PSI-binding.

[Introduction]　膜タンパク質は、シグナル伝達、イオンや生体物質の輸送および透過、エネルギーの合成および代謝などの重要な働きを担っている。一方、膜タンパク質の多くは、他の生体分子と膜タンパク質複合体を形成したり、立体構造やサブユニット構成、機能の維持に脂質二重膜の条件を必要としたりするため、立体構造解析が困難な、巨大かつ不均一な状態にある。

チラコイド膜中に存在する Photosystem I (PSI)および Cytochrome b_6f(Cyt b_6f)は、複数のサブユニットおよび補酵素からなる、それぞれ分子量約 50 万、20 万の膜タンパク質複合体である。分子量約 1 万の可溶性銅タンパク質である Plastocyanin(Pc)は、Cyt b_6f から電子を受け取り、光励起した PSI に電子を受け渡す。この電子輸送

keyword : membrane protein, transferred cross-saturation, NMR,
transient protein-protein interaction, paramagnetic proteins

著者ふりがな：○おがわ　ゆうた、うえだ　たくみ、てらさわ　ひろあき、
しまだ　いちお

反応は、光を利用して ATP および NADPH を産生する、光合成明反応の一部である。

PSI、Cyt b_6f、Pc の単体での立体構造はすでに解かれているが、複合体状態の立体構造はまだ解かれていない。一方、Pc の変異体を用いた実験から、Pc の hydrophobic patch(Loop 1, 3, 5, 7)と acidic patch(Loop4 の D42-E45)に存在する残基(Fig.1B)が、Cyt b_6f、PSI との相互作用に関与していることが提唱されている。しかし、これまでに変異体解析が行われた残基は、種間で保存されたものに限られている。したがって、Pc-PSI および Pc-Cyt b_6f 間の相互作用メカニズムの詳細は未だ不明である。そこで本研究では、Pc の PSI 相互作用部位および Cyt b_6f 相互作用部位を構造生物学的手法により明らかにすることを目指した。

[Materials & Methods] 安定同位体標識を施したホウレンソウ由来 Pc を、大腸菌 BL21 (DE3) Tuner™ に発現させ、先行論文の方法にしたがって精製した。PSI、Cyt b_6f をそれぞれ総タンパク質量の 20%、5%程度含むチラコイド膜ベシクルを、ホウレンソウの葉のチラコイド膜を超音波処理することにより調製し、さらに dextran/polyethyleneglycol の水性二相分離により、内向きと外向きのベシクルを分離した。n-dodecyl-β-D-maltothiopyranoside により可溶化した PSI ミセルおよび n-undecyl-β-D-maltopyranoside により可溶化した Cyt b_6f ミセルを、先行論文の方

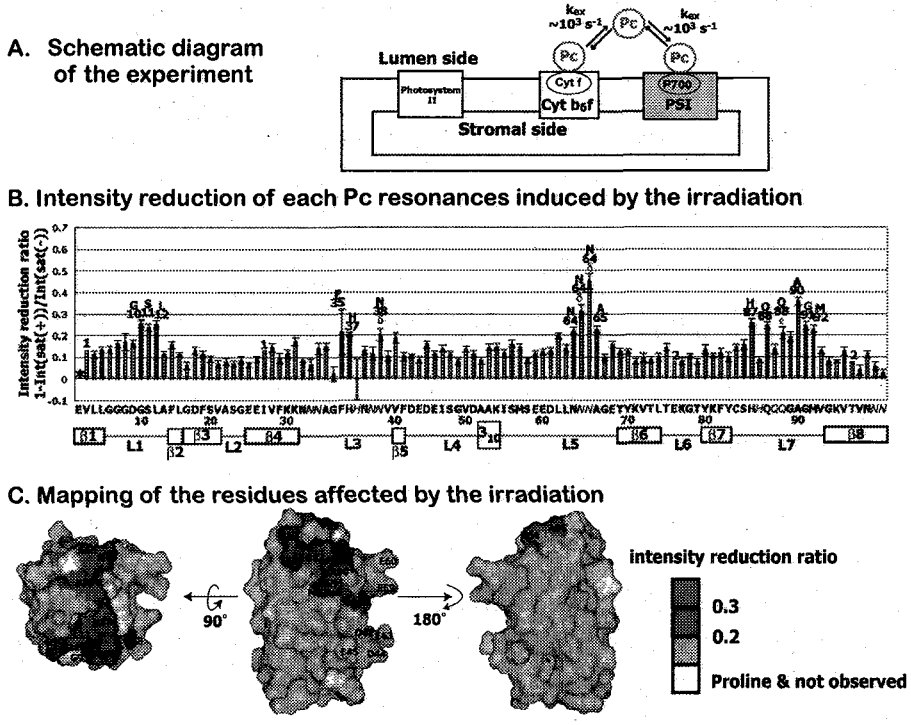

Fig.1 Identification of the residues of Pc interacting with PSI and /or Cyt b_6f by the TCS experiments with thylakoid vesicles

法にしたがって、ホウレンソウの葉より調製した。Flash photolysis および stopped-flow 解析により、得られた PSI および Cyt b_6f が電子輸送活性を保持していることを確認した。

[Results & Discussion] Pc-PSI および Pc-Cyt b_6f 間相互作用の解離速度は、10^3 s^{-1} 程度であると報告されている。そこで本研究では、転移交差飽和法(Transferred Cross-Saturation, TCS)により、Pc の PSI および Cyt b_6f への相互作用部位を決定することにした。はじめに、Cyt b_6f および PSI のサブユニットが欠落していない状態で解析を行うために、PSI、Cyt b_6f を両方含むチラコイド膜ベシクルを用いて TCS 実験を行った(Fig.1)。Cyt b_6f および PSI の Pc 相互作用部位が外側を向いたベシクルと還元型 Pc を混合して TCS 実験を行った結果(Fig.1B)、Pc の hydrophobic patch 中の Loop1(G10、S11、L12)、Loop3(F35、H37、N38)、Loop5(L62、N64)、Loop7(Q88、A90、G91、M92)由来のシグナルに、ラジオ波照射にともなう強度減少が観測された。一方、acidic patch に存在する残基(D42、E43、D44、E45)のシグナル強度減少は観測されなかった。また、Cyt b_6f および PSI の Pc 相互作用部位が内側を向いたベシクルを用いた TCS 実験では、有意なシグナル強度減少は観測されなかった。

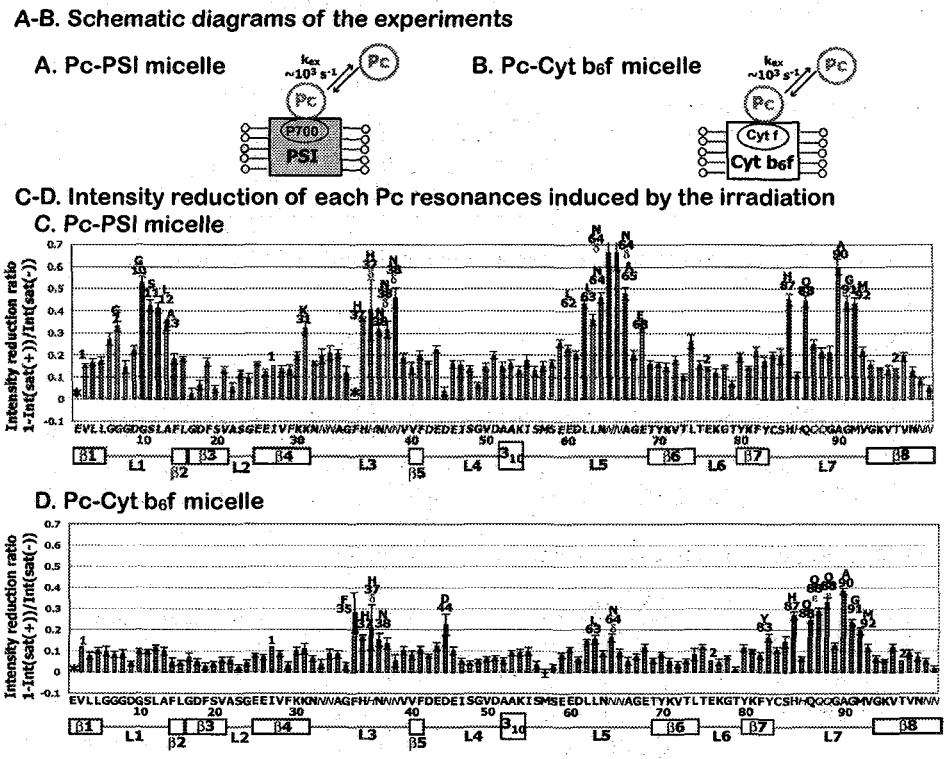

Fig.2 Discrimination of the PSI-binding and Cyt b_6f-binding sites by the TCS experiments with PSI and Cyt b_6f micelles

次に、Pc の PSI との相互作用部位と Cyt b_6f との相互作用部位を区別するために、界面活性剤で可溶化した PSI ミセルおよび Cyt b_6f ミセルを用いて TCS 実験を行った(Fig.2)。PSI ミセルと還元型 Pc を用いた TCS 実験の結果(Fig.2C)、Pc の Loop1、Loop3、Loop5、Loop7 に由来するシグナルに強度減少が観測された。一方、Cyt b_6f ミセルと還元型 Pc を用いた TCS 実験の結果(Fig.2D)、Pc の Loop3、Loop7 に由来するシグナルに強度減少が観測された。

以上の TCS 実験の結果より、Pc の Loop3 と Loop7 中の残基は Cyt b_6f と PSI 両方との相互作用に重要であり、Loop1 と Loop5 中の残基は PSI との相互作用に主に関与すると結論した。これらの TCS 実験により決定された PSI 相互作用部位および Cyt b_6f 相互作用部位中の残基に変異を導入し、Pc-PSI および Pc-Cyt b_6f 間の電子輸送活性を調べた結果、野生型よりも有意に活性が低下していた。この結果は、TCS 実験の結果を支持している。

Pc の acidic patch 中の残基の変異体は、野生型よりも PSI および Cyt b_6f との電子輸送活性が低いことが示されている。一方、本研究の TCS 実験では、acidic patch 中の残基に由来するシグナルには有意な強度減少が観測されなかった。この結果は、acidic patch 中の残基と PSI および Cyt b_6f との相互作用が、最終的な複合体の安定化にはあまり寄与しないが、Pc が PSI および Cyt b_6f に近接し、初期の複合体が形成される段階に重要であることを示している可能性がある。

酸化型 Pc は、ここまでの TCS 実験で用いてきた還元型 Pc と非常に類似した立体構造を持つが、PSI に対する親和性が還元型 Pc よりも 10 倍程度弱いことが知られている。この親和性の差は、反応後酸化型になった Pc の PSI からの解離を促進し、反応回転率を向上させると考えられる。現在、酸化型 Pc と PSI との相互作用の TCS 解析により、親和性の差が生じるメカニズムを解明することを試みている。

3 LJ4

NMR structure of rice phytochrome B PAS1 domain and its dimerization mechanism

○Toshitatsu Kobayashi[1], Masaki Mishima[1], Ryo Tabata[1], Kayo Akagi[2], Nobuya Sakai[2], Etsuko Kato[2], Paul Reay[2], Rintaro Suzuki[2], Makoto Takano[3], Toshimasa Yamazaki[2], and Chojiro Kojima[1]

[1]Graduate School of Biological Sciences, Nara Institute of Science and Technology, 8916-5 Takayama, Ikoma, Nara 630-0101, Japan, [2]Biochemistry Department, and [3]Photobiology and Photosynthesis Research Unit, National Institute of Agrobiological Sciences, 2-1-2 Kannondai, Tsukuba, Ibaraki 305-8602, Japan

Phytochrome is a dimeric chromoprotein that detects the quantity, quality and duration of red or far-red light, and can modulate plant growth and development throughout the entire life cycle of plants. Phytochrome possesses two PAS domains that contain determinants necessary for nuclear translocation and signal transduction. Here the solution structure of PAS1 domain of *Oryza sativa* (rice) phytochrome A (PHYA) and phytochrome B (PHYB) is determined by solution NMR. These PAS1 domain structures maintained typical PAS fold except for the Bβ strand missing in PHYB. The core region of loss-of-function missense mutations (Quail-box) was located on the β-sheet. The surface structure of the PAS1 domain, especially on the β-sheet side, was perturbed by these mutations, such as A759V and G776R for rice PHYB revealed by the HSQC spectra. The PAS1 domain with the N-flanking hinge region formed a stable dimer for PHYB, and the deletion mutants clearly showed that this N-flanking region is necessary. On the other hand, the corresponding region of PHYA did not form dimer. A series of point mutation experiments in the N-flanking region suggested that the positively charged residues were necessary to form the dimer. Especially the residue

KEYWORD
Plant Phytochrome PAS domain Dimerization Structural determination

R663 is dominant since the R663D mutant disrupted the dimer. The N-flanking region of PHYB is a kind of glue to stabilize the dimer, and this dimerization process regulated by positive charge might be related to the function.

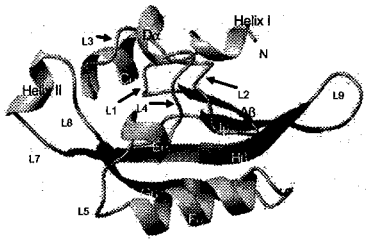

Figure 1. The solution structures of rice PHYB$^{666-782}$.
Schematic ribbon diagrams of the energy-minimized average structures of PHYB$^{666-782}$ are shown.

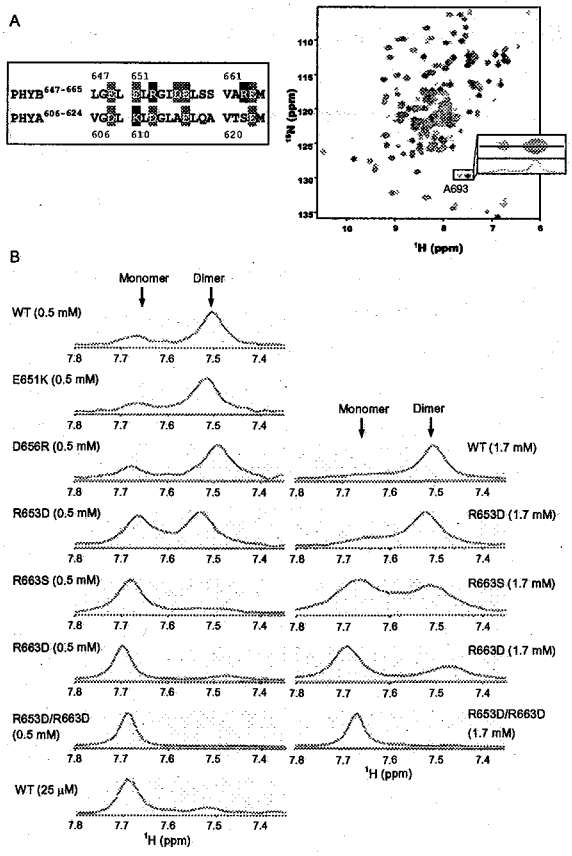

Figure 2. Dimerization property of site-directed mutants of PHYB$^{647-782}$.

(A) Sequence alignment between PHYB$^{647-665}$ and PHYA$^{606-624}$. Negatively and positively charged residues within the hinge-region are drawn in white characters on red and blue backgrounds, respectively. Arrows indicated residues with different charge between PHYA and PHYB. (B) The ^{1}H-^{15}N HSQC spectra of rice PHYB$^{647-782}$ at protein concentration of 0.5 mM. Expanded region of A693 signal on the ^{1}H-^{15}N HSQC and one-dimensional slice at 129.6 ppm (^{15}N) are displayed. (C) One-dimensional slices at 129.6 ppm (^{15}N) of WT and missense mutants of PHYB$^{647-782}$ are displayed. Left (~ 7.7 ppm) and right (~ 7.5 ppm) indicated monomer and dimer of PHYB$^{647-782}$, respectively.

3 LJ5

SUMO-3 (Small Ubiquitin-like Modifier-3) と SBM (SUMO binding motif) 複合体の構造解析

(京大院工[1]、熊本大発生研[2]、阪大蛋白研[3])
○関山直孝[1]、斉藤寿仁[2]、池上貴久[3]、杤尾豪人[1]、白川昌宏[1]

SUMO-3 (Small Ubiquitin-like Modifier) RECOGNITION BY A SUMO BINDING MOTIF

[1]*Department of Molecular Engineering, Kyoto University*
[2]*Department of Regeneration Medicine, Institute of Molecular Embryology and Genetics, Kumamoto University*
[3]*Institute for Protein Research, Osaka University*
○Naotaka Sekiyama[1], Toshihito Saitoh[2], Takahisa Ikegami[3], Hidehito Tochio[1], Masahiro Shirakawa[1]

Posttranslational modification by small ubiquitin-like modifier (SUMO) has been implicated in the regulation of a variety of cellular events. Although four SUMO isoforms have been reported for mammals (SUMO-1 to -4), the differences between *in vivo* functions of SUMO-isoforms are still not yet well understood.

The functional properties of SUMO isoforms may reflect their ability to mediate distinct protein-protein interactions. Previous studies have shown that SUMO can non-covalently bind to other proteins or substrates through SUMO binding motif (SBM). We studied the interaction between SUMO-3 and the peptide containing the SBM of MBD1-containing chromatin-associated factor (MCAF) by isotope-aided NMR spectroscopy. After resonance assignments of SUMO-3 or the peptide in their complex form by triple-resonance spectroscopy, chemical perturbation experiments were performed using ^{15}N-labeled SUMO-3 or the peptide. The result suggests that the binding surface of SUMO-3 for the peptide is similar with that of SUMO-1 for SBMs observed in previously reported structures.

【序論】SUMO (Small Ubiquitin-like Modifier) はユビキチン様タンパク質のひとつである。ユビキチンと類似の機構を用いて他のタンパク質を修飾することで、転写調節、DNA 修復、細胞周期、局在性変換の細胞機能を制御している。ヒトには SUMO のアイソフォームとして、SUMO-1, 2, 3 が存在する。SUMO-2 と SUMO-3 のアミノ酸配列の相同性は 95%であるのに対し、SUMO-1 と SUMO-2/3 の相同性はそれぞれ 46%、48%

キーワード： SUMO、SBM、NMR 構造解析
せきやまなおたか、さいとうとしひと、いけがみたかひさ、
とちおひでひと、しらかわまさひろ

と低い。このことから、SUMO-1 と SUMO-2/3 の機能的な差異に興味が持たれる。

SUMO の機能分担は、それぞれのアイソフォームが異なるタンパク質間相互作用を媒介することで行われていると考えられている。相互作用の媒介には SUMO と結合するコンセンサス配列 (SBM; SUMO binding motif) の存在が示唆されており特定が進められている。最近、SUMO-2/3 に結合する SBM が遺伝子制御に関与する MCAF に存在することが、共同研究者である熊本大学の斉藤教授のグループにより示された。そこで、SUMO-3 と MCAF 由来の SBM の複合体の立体構造を決定し、SUMO-3 の分子認識を明らかにすることを目指した。

【実験】$^{13}C/^{15}N$ ラベル SUMO-3 は、GST 融合タンパク質として大腸菌により発現し、アフィニティーおよびゲルろ過クロマトグラフィーにより精製した。$^{13}C/^{15}N$ ラベル MCAF 由来の SBM (MCAF-SBM) は、GST 融合タンパク質として大腸菌により発現し、アフィニティーおよび逆相クロマトグラフィーにより精製した。NMR 測定は、Bruker 社製の 500, 700, 800MHz の各 NMR 装置を用い、解析に必要な多核多次元測定を行った。Beffer 条件は、20mM Phosphate (pH 6.8), 298K である。

【結果と考察】SUMO-3 と MCAF-SBM の結合部位を同定するため、$^{13}C/^{15}N$ ラベル SUMO-3 と MCAF-SBM、および $^{13}C/^{15}N$ ラベル MCAF-SBM と SUMO-3 の滴定実験を行った。複合体中の SUMO-3 および MCAF-SBM の主鎖の化学シフトの帰属を行い、^{15}N HSQC 化学シフト摂動法により、SUMO-3 と MCAF-SBM の結合表面を推定した。

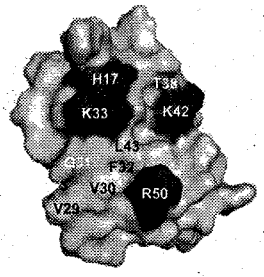

Fig.1 Binding surface of SUMO3 identified by chemical shift perturbation (PDB code: 1U4A, Ding, H. *et al., Biochemisty,* 2005).
Hydrophobic, basic, and hydrophilic residues in the peptide binding surface are colored in yellow, blue, and sky-blue, respectively.

これまでに報告されている SUMO-1 と SBM の結合様式としては、SUMO-1 のβ-strand とα-helix の間に存在する疎水性パッチに SBM がはまり込む機構である。今回の実験からも、SUMO-3 と MCAF-SBM の結合には SUMO-3 表面の疎水性パッチの関与が示されたが、その周りを覆う静電的な残基に SUMO-1 との相違が見られた (Fig.1) 。次に MCAF-SBM の滴定実験から、疎水性パッチに結合している MCAF-SBM の残基は、現在までに報告されている SBM と類似の配列に対応する 4 残基であった。しかし、この周辺に存在するアスパラギン酸、グルタミン酸の化学シフトも大きく変化していることから、疎水性パッチを覆う静電相互作用の違いが SUMO のアイソフォーム間の認識を区別していることが示唆される。

SUMO-3 と MCAF-SBM の結合様式を詳細に解析するには、さらなる構造学的な知見が必要である。今後は、MCAF-SBM の側鎖の化学シフトの帰属を行い、NOESY 測定による距離情報をもとに立体構造計算を行い、SUMO-3 と MCAF-SBM の結合に重要なアミノ酸残基を原子レベルで解明する。

3 LJ6

Asymmetric ^{13}C-^{13}C polarization transfer under dipolar-driven rotational resonance in magic-angle spinning NMR

○ Ryutaro Ohashi and K. Takegoshi
Graduate School of Science, Kyoto University

A two-dimensional (2D) homonuclear exchange NMR spectrum in solids often shows an asymmetric cross-peak pattern, which disturbs quantitative analysis of peak intensities. In case when magnetization is prepared using cross polarization (CP), the asymmetry can naively be ascribed to non-equilibrium initial magnetization. For example, suppose we observe a 2D exchange spectrum of two spins A and B, with the initial magnetization being prepared by CP with an unequal intensity ratio, say, 120 : 80. After a mixing time long enough to achieve internal equilibrium among A and B, the intensity ratio would become 100 : 100 if the spin-lattice relaxation can be ignored. Then the resulting 2D spectrum may be schematically represented in Fig. 1, showing an asymmetric 2D spectrum. Therefore, we modify a theory of 2D exchange NMR for three $\pi/2$ pulses[1] to take into account of different CP enhancement factors. The dotted lines in Fig. 2 are the best-fit curves from the developed theory. In Fig. 2, the dotted lines apparently deviate from the experimental data in 2D ^{13}C-^{13}C exchange spectra of [2,3-^{13}C] *l*-alanine (2,3-Ala) under DARR recoupling[2] (squares), confirming further that the different CP enhancement can not fully explain the observed asymmetry.

We furthermore develop a theory to describe polarization transfer in a two-spin system under DARR recoupling. By taking account of effects of the partial spectral overlap among ^{13}C signals, which is a unique feature of DARR recoupling, and ^{1}H-^{1}H flip-flop exchange, we can successfully explain the observed mixing-time dependence of the peak intensities of 2D ^{13}C-^{13}C DARR exchange spectra of 2,3-Ala. Here, we separate each l-magnetization (l = A or B) into two groups; $M_{l1}(\tau_m)$ is the magnetization involved in the transfer and $M_{l2}(\tau_m)$ is that not involved in the transfer (Fig. 3). We assume M_{l1} and M_{l2} can exchange magnetizations with a rate k_l (the intra-spin exchange rate), and the ratio of the initial magnetizations is given by $M_{l1}(\tau_m = 0) : M_{l2}(\tau_m = 0) = \lambda_l : 1-\lambda_l$. The solid lines in Fig. 2 are the best-fit ones. It was shown that the four-sites model can explain the observed mixing-time dependence of the diagonal and cross peaks.

[1] J. Jeener, et al., J. Chem. Phys. **71** 4546 (1979).
[2] K. Takegoshi, et al., J. Chem. Phys. **118**, 2325 (2003).

Key Words: 2D NMR, exchange NMR, polarization transfer, rotational resonance

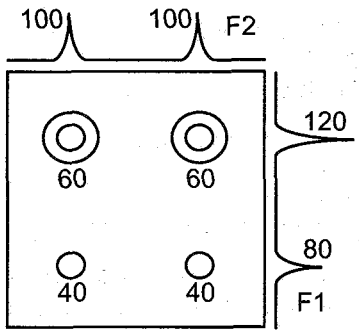

Fig. 1: Schematic illustration of a 2D contour spectrum of two exchanging magnetizations starting from non-equilibrium initial magnetization with a ratio of 120 : 80. The projection spectrum in the first domain (F1) thus shows two peaks with the intensity ratio of 120 : 80, while that in F2 assumes thermal equilibrium (100 : 100). Each figure associated with the peaks denotes its relative intensity.

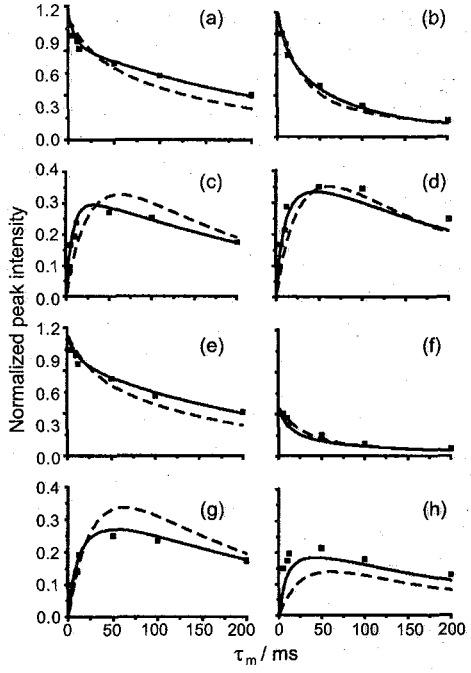

Fig. 2. Mixing-time (τ_m) dependencies of peak intensities of a_{AA} [(a) and (e)], a_{BB} [(b) and (f)], a_{AB} [(c) and (g)], and a_{BA} [(d) and (h)].
Dotted and solid lines are the best-fit curves including the CP effect, and both of the CP effect and the four-sites model, respectively.
Squares represent experimental data.
(a)-(d) were taken at a CP contact time of 700 μs and (e)-(h) at 50 μs.
Each peak intensity is given by taking the largest peak intensity at corresponding contact time, a_{BB} (τ_m = 5 ms) at CT = 700 μs or a_{AA} (τ_m = 5 ms) at CT = 50 μs, as 1.0.
A and B represent methine and methyl carbon in [2,3-^{13}C] *l*-alanine, respectively.

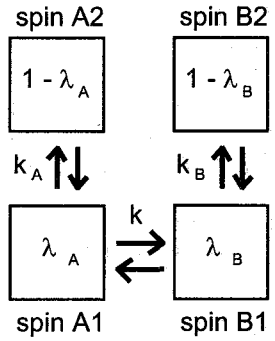

Fig. 3. Schematic model to express the magnetization exchange process of a two-spin (A and B) system under DARR recoupling.
The magnetization of each spin is divided into two groups as represented by boxes; one that can exchange polarization as indicated with arrows.

マイクロコイルを用いた 強いRF照射下におけるMQMASの研究

○犬飼宗弘[1]、武田和行[1]
大阪大学大学院基礎工学研究科

Studies on MQMAS NMR of half-integer Quadrupolar nuclei under strong rf pulses

○Munehiro Inukai[1], Kazuyuki Takeda[1]
[1]Graduate School of Engineering Science, Osaka University, Japan

Abstract: Multi-quantum excitation and conversion efficiencies were stulied in a spin-$\frac{3}{2}$ system under very strong rf irradiation, which was realized by combining a microcoil and MAS experiments.

Most references mentioning the practical tips of MQMAS[1] experiments recommend to use the maximum available rf power for the MQ excitation and conversion pulses so as to attain the best sensitivity of MQMAS spectra[2]. However, this may not be the case for unconventional cases where the rf-filed amplitude (ν_1) is as large as the magnitude of a quadrupolar interaction. Although the optimal ν_1 for a given quadrupolar coupling constant is predictable by numerically simulating the time evolution of the density matrix according to the Liouville-von Neumann equation, no experimental verification has been made in the regime of ν_1 exceeding 300 kHz.

In this work, we have examined MQ excitation and conversion efficiencies for various ν_1 amplitudes up to ca. 1 MHz. Such strong rf irradiation has been realized with a microcoil[3]. We present a coin-shaped microcoil probe developed to accomodate a microcoil with MAS experiments, and show that, for large ν_1, the MQ excitation and conversion efficiencies exhibit oscillation that can be accounted for theoretically. Experiments are demonstrated with ^{23}Na(S=3/2) nuclei in a polycrystalline sample of sodium sulfite.

Our strategy for combining microcoil and MAS experiments is schematically described in Fig. 1. A capillary sample tube was stuck through a cap of a pencil-type 4 mm rotor. With the conventional compressed-air blowing, the capillary could be spun together with the rotor, and one end of the capillary sticking out of the rotor was inserted into the microcoil. A balanced resonant circuit composed of a microcoil and capacitors was fabricated on a coin-sized, disk-shaped circuit board, the microcoil being placed at the center of the board. This coin-shaped probe is capable of attaching itself to a spinning module with minimum amount of modification to an existing MAS probe[4]. Stable spinning of capillary inside the microcoil up to 6 kHz was realized. Moreover, the microcoil with a diameter of 0.8 mm has brought ν_1 of up to ca. 1 MHz into practice with a 300 W power amplifier. From nutation spectra of aqueous solution of NaCl, the ν_1 inhomogeneity was estimated to be ca. 10%.

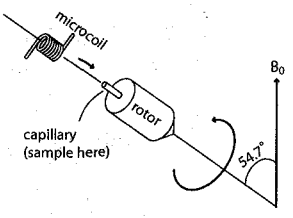

Fig. 1. Schematic description of the way employed in this work to enable microcoil MAS

Experiments were carried out using 0.1 mg polycrystalline sample of sodium sulfite packed in a glass capillary (o.d.: 0.5 mm, i.d.: 0.3 mm). We used a basic two pulses pulse sequence for the separate examinations of the triple-quantum excitation and the triple-to-single quantum conversion efficiencies. The former was studied through measurement

[0] Keyword: microcoil, MQMAS
いぬかいむねひろ、たけだかずゆき

of the absolute value of the echo amplitude for various widths and intensities of the first pulse, while those of the second pulse were fixed. The conversion efficiency was studied in a similar manner. All measurements were perfomed at room temperature in a magnetic field of 11.7 T, which corresponds to the ^{23}Na resonance frequency of 132.2 MHz. The sample spinning frequency was 3.5 kHz.

Fig. 2-3 show the echo amplitudes for various excitation and conversion pulse intensities and widths, which reflect the triple-quantum excitation and triple-to-single quantum conversion efficiencies. For relatively weak rf amplitudes ($\nu_1 < 200$ kHz), the echo intensities show monotonic behavior. On the other hand, oscillation is clearly visible for larger rf amplitudes. This oscillatory behavior can be explaned by considering the MQ transition moments from the system Hamiltonian. We show that the larger the rf amplitude, the more prominent the oscillation is. This work provides a simple guideline for selecting the optimum rf pulse width, particularly when very strong rf irradiation is available.

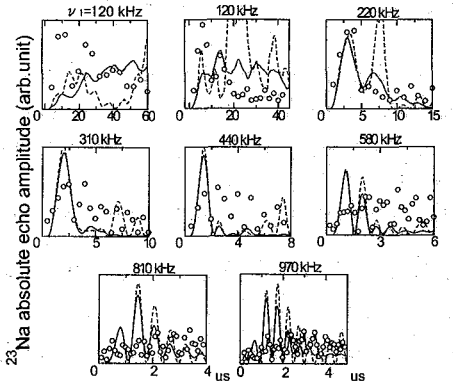

Fig. 2. Excitation efficiency of triple-quantum coherence for a spin-3/2 in a powder sample for various ν_1. $e^2qQ/h = 1.2$ MHz, $\eta = 0$ and $\nu_r = 0$ were assumed. Solid and broken lines represent the simulated dependence with 10% and without ν_1 inhomogeneity.

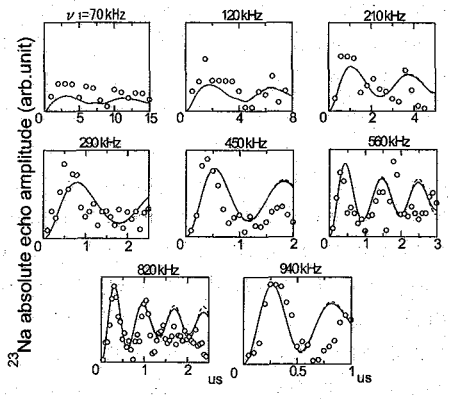

Fig. 3. Conversion efficiency of triple to single-quantum coherence for a spin-3/2 in a powder sample for various ν_1. $e^2qQ/h = 1.2$ MHz, $\eta = 0$ and $\nu_r = 0$ were assumed. Solid and broken lines represent the simulated dependence with 10% and without ν_1 inhomogeneity.

[1] L. Frydman, J.S. Harwood, J. Am. Chem. Soc. 117 (1995) 5367.
[2] J-P. Amoureux, M. Pruski, D. P. Lang, C. Fernandez, J. Magn. Reson. 131 (1998) 170.
[3] D. L. Olson, T. L. Peck A. G. Webb, R. L. Magin, J. V. Sweedler Science. 270 (1995) 1967.
[4] K. Takeda, Coin-sided probe for solid-state NMR, 46th ENC (2005).

^{13}C-^{13}C Homonuclear Cross Polarization through Dipolar Coupling or J Coupling: a Potential Solid-State NMR Method

Qing Luo[1], Yuichi Shimoikeda[2], Hironori Kaji[1], Fumitaka Horii[1],
1.Institute for Chemical Research, Kyoto university, Uji, Kyoto 6111-0011, Japan
2. JEOL, Akishima, Japan

[Introduction] Observations of the homonuclear cross polarization are reported. It can be achieved through dipolar coupling or J-coupling determined by experimental conditions. Through homonuclear cross polarization, we can detect the homonuclear interactions by one dimensional NMR measurements. Comparing with two-dimensional NMR methods used for the detection of homonuclear interactions, this technique is much more rapid. For solid state organic and polymer materials, homonuclear correlations, i.e. ^{13}C-^{13}C interaction, contain important structural information. Homonuclear cross polarization also provides a potential way of rapid assignments of resonance lines.

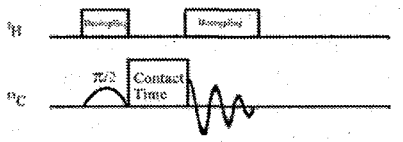

Figure 1. The pulse sequence of the simplest homonuclear cross polarization.

[Experimental] The scheme of homonuclear cross polarization is similar to the normal CP. First the magnetization of a spin is established and then transferred to another spin. The difference is that the magnetization is transferred from $S_1 \rightarrow S_2$ but not $I \rightarrow S$. So, selective excitation is needed to build the initial magnetization. Further more, 2 radio frequency (RF) spin locking in the normal CP is replaced by 1 RF spin locking to achieve the cross polarization. The simplest pulse sequence is shown in Figure 1. In the ^{13}C channel, an initial selective 90° soft pulse excites the magnetization of a specific carbon and it is subsequently spin-locked by the radio-frequency field. To increase the selectivity of the selective excitation and experimental sensitivity, some techniques including $^{1}H/^{13}C$ CP, DANTE and shaped pulses can be combined to achieve selective excitation (Figure 2). When not specially described, the on-resonance frequency of the spin locking is on the center of the spin pairs of interest.

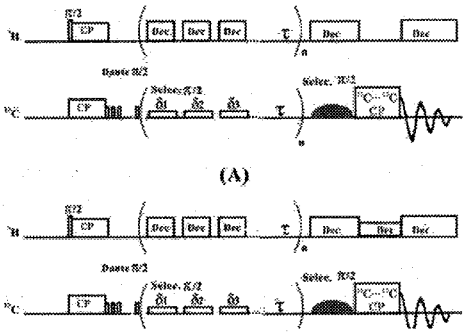

Figure 2. The pulse sequence of the modified homonuclear cross polarization. $^{1}H/^{13}C$ CP is used to build the magnetization of ^{13}C and the magnetization of one spin is selectively rotated to Z axis by a DANTE pulse. Waiting until the magnetization in XY plane of the other spins is relaxed, the magnetization of the selected spin is rotated to XY plane. During the waiting time, some soft pulses can be applied as pre-saturation to other spins. During the spin locking time, whether the proton decoupling should be applied depends on the experimental proposes. When proton decoupling is used, the amplifier (B_1) of the proton channel should be carefully set to avoid the ^{1}H-^{13}C cross polarization.

The spectra were recorded on a Chemagnetics CMX-400 NMR spectrometer equipped with a 7.5 mm or 4 mm double-resonance probe. The samples used are 99% ^{13}C-enriched β-alanine and natural abundant adamantane.

Keywords: Homonuclear Cross Polarization, Dipolar Coupling, J coupling,

[Results and Discussions]

Homonuclear cross polarization through dipolar interaction

β-alanine has 3 chemically inequivalent carbons. However, only 2 peaks can be observed in the ^{13}C NMR spectrum because the resonances of the 2 CH_2 groups are overlapped (35.5ppm). The spectra of homonuclear cross polarization experiments of β-alanine under MAS speed of 3 kHz with various contact times are shown in Figure 3. No proton decoupling was applied during the spin locking. When the contact time is in the range of 1 ms to 16 ms, the intensity of the peak of carbonyl carbon is increased with the increase of contact time, indicating a typical CP phenomenon.

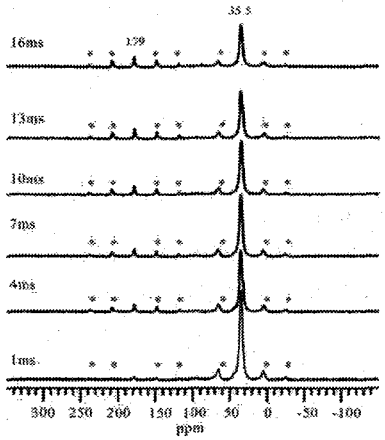

Figure 3. The spectrum of selective homonuclear Hartmann-Hahn method in ^{13}C-enriched beta-alanine with the homonuclear comtact time from 1 ms to 16 ms. The MAS speed is 5kHz.

Homonuclear cross polarization through J coupling

Adamatane (ADM) is a soft solid material. The ^{13}C MAS (5kHz) spectrum of ADM shows a liquid-like high resolution, rendering that the anisotropic interaction is completely suppressed by molecular motions. In the homonuclear cross polarization spectra of ADM, a doublet signal with a split of about 30 Hz can be observed. The doublet is due to the J-coupling between directly bonded CH and CH_2 carbon. The presence of the J-split indicates that the residue homonuclear dipolar interaction is in a negligible level comparing with the J-coupling. It is therefore concluded that the homonuclear cross polarization occur through the J-coupling rather than the residue dipolar coupling. When the MAS speed is higher than 10 kHz, the efficiency of the homonuclear cross polarization of ADM is not decreased. This also supports our deduction because J-coupling is an isotropic interaction and will be not suppressed by MAS.

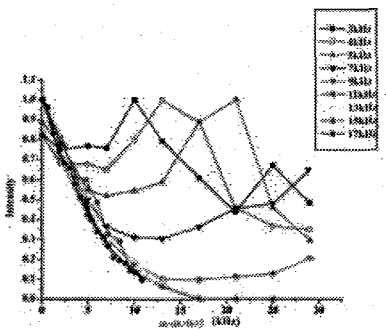

Figure 4. The offset dependence of the homonuclear cross polarization

The homonuclear cross polarization of ADM is found to be very sensitive to the frequency offset of the spin locking pulse. It is due to that J coupling is much weaker than dipolar coupling.

By applying the proton decoupling during the spin locking time, effective homonuclear cross polarization can also been achieved on β-alanine at MAS speed higher than 11 kHz. In that case, the homonuclear cross polarization is induced through J coupling as well as residue dipolar interaction.

3 LJ9

Solid-state MAS NMR of membrane integrating protein, H^+-ATP synthase subunit *c*

M. Kobayashi, I. Yumen, T. Fujiwara, and H. Akutsu
Institute for Protein Research, Osaka University
CREST JST, Suita, Osaka 565-0871

Introduction

Solid-state NMR (SSNMR) for structural determination of biomolecules has been rapidly developed in the last decade. Our target protein for structural analysis is H^+-ATP synthase subunit *c* from *E. coli* (79 residues). One of the recent strategies for structural determination of peptides and proteins by SSNMR is the analysis of uniformly [^{13}C, ^{15}N] labeled samples under magic-angle spinning (MAS). Proteins in microcrystalline states provided high resolution spectra, leading to successful signal assignment for small proteins. The crystallization of membrane proteins is usually performed in the presence of a surfactant. However, the structure and function of a membrane protein in detergent micelles may be different from those in membranes. It is important to apply the SSNMR method to a membrane protein in non-crystalline membranes.

In SSNMR spectral analysis of transmembrane proteins, small dispersion of the NMR signals could be a problem. Generally, the amino acid composition of an integral membrane protein includes more hydrophobic residues with low variety. Small transmembrane proteins prefer α-helical conformations, which lead to signal overlapping because of similar secondary shift. To overcome this problem, the inter-residue correlations are mandatory. In the case of a uniformly labeled sample, we can obtain an all inter-residual aliphatic carbon correlations. Spectral simulation can be applied to assign the signals and to determine the secondary structure of a uniformly labeled sample.

The structural analysis of subunit *c* in membranes by SSNMR is our final objective. First, we have investigated the pure subunit *c* in the solid state because this sample gave intense signals due to small sample volume. Following this, we prepared membrane embedded samples by detergent dialysis method. We can evaluate the membrane protein folding in reconstitution procedure by observed chemical shift. Preliminary secondary structure analysis of subunit *c* in lipid bilayer was performed on the basis of intra-residue ^{13}C correlation spectrum.

Experimental

We performed 2D ^{13}C homonuclear correlation experiments with RFDR and SPC^Z5, and a heteronuclear correlation experiment, an $N-C^{\alpha}C^{\beta}$ one, to obtain the intra-residue correlation.

Key words :
solid-state NMR, MAS, membrane protein, signal assignment, secondary structure

In order to obtain the inter-residue correlation, 2D and 3D N_{i+1}–$(C'C^{\alpha}C^{\beta})_i$ and 2D $(C^{\alpha}C^{\beta})_{i+1}$–$(C'C^{\alpha}C^{\beta})_i$ experiments were performed. Most spectra were recorded at 11.74 T. RFDR and 3D N_{i+1}–C'_i–C^{α}_i correlation spectra were recorded at 14.09 and 16.44 T, respectively. Dipolar interactions for ^{13}C and ^{15}N transferred the magnetization during the mixing period. The initial magnetization was prepared by cross-polarization from the proton magnetization.

We utilized structure-based chemical shift prediction programs, SHIFTS, SHIFTX, and PROSHIFT to analyze structure-dependent shifts. Spectral simulation based on the prediction of chemical shifts and the calculation of cross peak intensities was performed. Optimized simulation spectra were obtained so as to minimize RMSD between experimental and simulation spectra. In order to predict backbone dihedral angles ϕ and ψ from the chemical shifts of $^{13}C^{\alpha}$, $^{13}C^{\beta}$, $^{13}C'$, and $^{15}N^{H}$, we utilized the TALOS program.

Results

The protein took on a unique structure even in the solid state from the ^{13}C linewidths of about 1.7 ppm. On the basis of several inter- and intra-residue ^{13}C–^{13}C and ^{13}C–^{15}N chemical shift correlations, 78% of C^{α}, 72% of C^{β}, 62% of C' and 61% of N^{H} signals were assigned, which provided the secondary structure information for 84% of the 79 residues. Here, inter-residue aliphatic carbon correlation involving Gly, Ala and inter-residue heteronuclear correlation involving Gly, Pro, and a higher resolution in the 3D spectrum were useful for the sequence specific assignment. Predicted backbone dihedral angles and the deduced secondary structure of subunit *c* based on the optimized simulation spectrum were shown. It revealed that the subunit *c* in the solid state could be specified by α-helices with a loop structure in the middle (at sequence 41–45) as in the case of the solution structure in spite of additional extended conformations at 76–79 at the C-terminus. In view of the distorted signal shapes and suppressed signal intensities for M17G18L19, this part may take heterogeneous conformations.

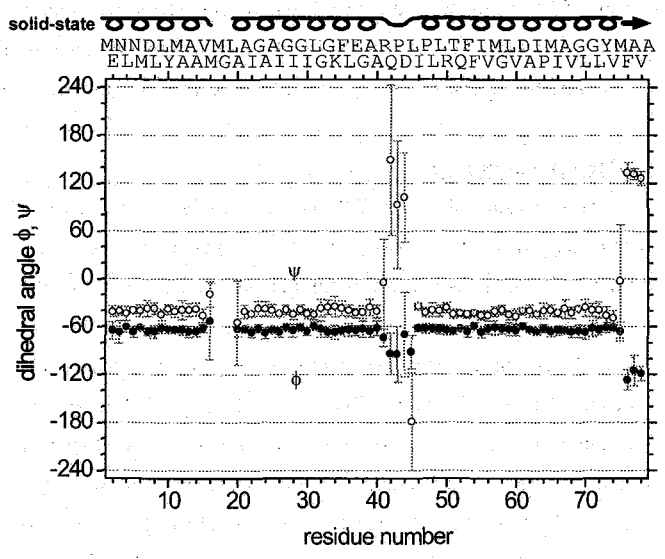

Predicted backbone dihedral angles and the deduced secondary structure of subunit *c* based on the optimized simulation spectrum. The dihedral angles, ϕ and ψ, were predicted by TALOS.

3 LJ10

Pressure effects on retinal isomerization and protein dynamics in bacteriorhodopsin by fast magic angle spinning solid-state NMR

○ Izuru Kawamura[1] Yoshiaki Degawa[1] Satoru Tuzi[2] Katsuyuki Nishimura[3] Hazime Saitô[4] and Akira Naito[1]

[1]*Graduate School of Engineering, Yokohama National University,*
[2]*Department of Life science, University of Hyogo,*
[3]*Institute for Molecular Science,* [4]*Center for Quantum Life Science, Hiroshima University*

Magic Angle Spinning (MAS) is a standard technique to obtain high-resolution spectra by solid-state NMR and the rotation frequency of 50 kHz is now available. There are a lot of points to be considered such as the efficiency of dipolar decoupling (DD) and cross polarization (CP), sample temperature and pressure for sample etc. in fast MAS experiments. Especially, pressure effects on hydrated fluid sample as membrane proteins have not been well considered although it is an important parameter. Bacteriorhodopsin (bR) is a membrane protein with retinal in purple membrane. We have detected pressure effects for [ζ-^{15}N]Lys-labeled bR by a fast MAS NMR. In the ^{15}N CP-MAS NMR spectra, both all-*trans* and 13-*cis*, 15-*syn* retinal configurations have been observed at 148.0 and 155.0 ppm, respectively at the MAS frequency of 4 kHz in the dark. The signal intensity of 13-*cis* retinal at 155.0 ppm was increased when the MAS frequency was increased to 12 kHz and subsequently decreased to 4 kHz. It is, therefore, demonstrated that increased pressure induced by fast MAS frequencies generated isomerization from all-*trans* to 13-*cis* retinal in bR.

1. Bacteriorhodopsin

Bacteriorhodopsin (bR), from *Halobacterium salinarum*, is a 26 kDa membrane protein that consists of 7 transmembrane helices with a retinal covalently linked to Lys216 through protonated Schiff base. BR absorbs light to cause retinal photoisomerization from all-*trans* to 13-*cis*, 15-*anti* state followed by unidirectional cycle of proton transfer reactions. The retinal configuration in the dark-adapted bR coexists as all-*trans* and 13-*cis*, 15-*syn* states with the isomeric ratio close to 1 (Figure 1). When light is illuminated, the population of all-*trans* state is increased. This all-*trans* populated state is a light adapted state. The population of 13-*cis*, 15-*syn* state can be increased when the pressure is applied in the dark. Here, we call this 13-*cis* populated state a pressure adapted one, which has not been well characterized yet.

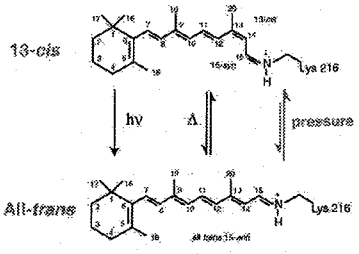

Figure 1. Isomerization pathways between 13-*cis*, 15-*syn* and all-*trans* retinal configurations in bR. The NMR signals of the protonated Schiff base (-C=N-) are a sensitive probe in the changes of retinal

Key words; Solid state NMR, Fast MAS, Pressure Effects, Bacteriorhodopsin, Retinal Isomerization

2. Materials & Methods [ζ-^{15}N]Lys-, [3-^{13}C]Ala-, [1-^{13}C]Val-bR in purple membrane were used for this study. The sample was excess humidity pellets and placed in 4.0 mm o.d. ZrO_2 rotor for fast MAS experiments. *In situ* continuous light-illumination was made through optical fiber from outside of magnet to the top part of rotor in which the top part was tightly sealed with a cap made of optical fiber glued to the rotor, to activate bR by light and to prevent dehydration of sample during rotor spinning. Photo-illumination in the ZrO_2 rotor was achieved without contact between optical fiber and optical fiber cap while MAS measurements. The spinning frequencies were varied in the range of 4-12 kHz and 90° pulse was 5.1 μs. Probe setting temperature was set at 293K during MAS experiments of various rotor frequencies. Variable amplitude CP with two pulse phase modulation (TPPM) decoupling was employed for CP-MAS experiment. ^{15}N chemical shift was externally referred to 11.59 ppm for the amino nitrogen of glycine form NH_4NO_3. Sample temperature on MAS frequencies was calibrated using $PbNO_3$ prior to the series of experiments. Pressure on the samples was naturally applied by the centrifugal force induced by MAS frequency. Since the centrifugal force is proportional to the diameter of rotor and the square of rotor frequency, pressure of inner wall of the ZrO_2 rotor can be estimated 80 atm for the frequency of 12 kHz.

3. Results & discussion Figure 2 (A)-(D) show the ^{15}N CP-MAS NMR spectra of [ζ-^{15}N]Lys-bR in the spectral range between 100 and 200 ppm. Both ^{15}N NMR signals due to all-*trans* and 13-*cis* retinal configurations in the dark were observed at 148.0 and 155.0 ppm under the MAS frequency of 4 kHz (Fig. 2(A)). When the MAS frequency was increased up to 12 kHz, the ^{15}N NMR signals of Schiff base of retinal showed broadening (Fig. 2 (B)). The signal intensity of the 13-*cis* retinal at 155.0 ppm increased as the MAS frequency was decreased from 12 to 4 kHz (Fig. 2(C)). Retinal configurations caused hysteresis by the fast MAS experiments. When temperature was increased to 313K corresponding to the temperature at 12 kHz and subsequently decreased to 293K by keeping the rotor speed of 4 kHz, the signal of 13-*cis* was not increased. These results clearly indicate that isomerization from all-*trans* to 13-*cis* occur in the presence of pressure about 80 atm. A white light was irradiated continuously to bR and significant increase of the signal of all-*trans* was observed (Fig. 2(D)). In conclusion, the proportions of retinal isomers are the same as the dark-adapted state bR, which is shifted from all-*trans* to 13-*cis* rich state by the application of pressure and from 13-*cis* to all-*trans* rich state by the photo-illumination. Pressure induced dynamical and conformational change of bR will be discussed in terms of retinal isomerization.

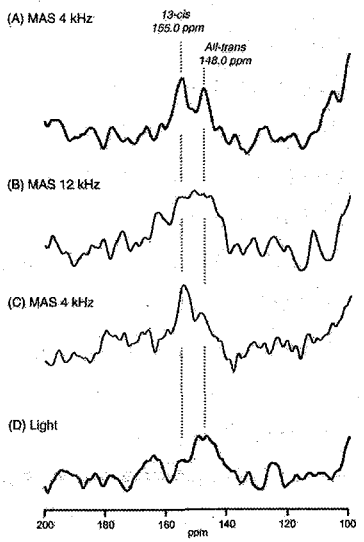

Figure 2. ^{15}N CP-MAS NMR spectra of [ζ-^{15}N]Lys-labeled bR at MAS frequency of 4 and 12 kHz((A) and (B)), respectively. Spinning frequency was decreased from 12 kHz to 4 kHz (C). *In situ* light-irradiation measurement(D).

3 LJ11

Inhibition of phospholipase C-δ1 activity by U73122 studied by solid state NMR spectroscopy

○Satoru Tuzi, Masaaki Nakano, Maiko Hasegawa, Masashi Okada, and Hitoshi Yagisawa
Graduate School of Life Science, University of Hyogo

1-[6[[17β-3-Methoxyestra-1,3,5(10)-trien-17-yl-]amino]hexyl]-1H-pyrrole-2,5-dione (U73122) is widely used as a selective phospholipase C (PLC) inhibitor to study the signal transduction mechanism in the cell. Addition of U73122 in a buffer surrounding the cell to make the final concentration to 10 μM is known to inhibit the intracellular PLC activity. A molecular mechanism of the inhibition of the PLC activity by U73122 is, however, still remains unclear. In this study, we investigated effects of U73122 on the structure and dynamics of PLC-δ1 by using mass spectroscopy and solid state NMR spectroscopy. PLC-δ1 is included in the signal transduction pathway, and hydrolyzes phosphatidylinositol 4,5-bisphosphate (PIP_2) in the plasma membrane as a response to an increase in the intracellular Ca^{2+} concentration to produce the second messengers, diacylglycerol and inositol 1,4,5-trisphosphate.

Experimental procedure: Rat PLC-δ1 was expressed in *E. coli* grown in complex or M9 media containing 20 amino acids. ^{13}C labeled alanine was introduced into the PLC-δ1 as a probe for ^{13}C NMR spectroscopy by replacement of alanine in the M9 medium by [3-^{13}C]alanine. For the mass spectroscopy, PLC-δ1 was treated with U73122 or U73343 in 20 mM MES buffer (pH6.5) for 30 min at 20°C. Mass spectra were obtained for an intact, U73122 treated- and U73343 treated-PLC-δ1 with Voyager MALDI TOF-mass spectroscopy. Hydrolyses of phosphatidylinositol (PI) in vesicles (molar ratio of PC:PI:PIP_2 = 75:20:5) by PLC-δ1 in the presence and the absence of U73122 were traced by changes in intensities of ^{31}P NMR signals of the initial product of the PI hydrolysis, inositol 1,2-cyclicphosphate (IcP) and the final product formed from IcP by PLC-δ1, inositolphosphate (IP). The hydrolysis was started by addition of $CaCl_2$ to achieve the final concentration of 1 μM into the suspension (20 mM MES (pH6.5)) containing PLC-δ1 and the PC/PI/PIP_2 vesicle. Cross polarization-magic angle spinning (CP-MAS) and single pulse excitation dipolar decoupled-MAS (DD-MAS) ^{13}C NMR spectra of the membrane bound PLC-δ1 were measured for PLC-δ1 forming complex with PIP_2 in the vesicles (PC:PIP_2 = 95:5) suspended in 20 mM MES buffer (pH6.5) without Ca^{2+}. ^{31}P and ^{13}C NMR spectra were obtained with Chemagnetics Infinity-400 spectrometer

Key words: solid state NMR, phospholipase C-δ1, U73122, signal transduction, inhibitor

(^{13}C: 100.6 MHz) at 20°C.

Results and Discussion: An increase in mass of PLC-δ1 treated with U73122 revealed that about five U73122 molecules were attached to PLC-δ1 through covalent bonds. These chemical modifications of the PLC-δ1 are ascribed to reactions between a maleimido group of U73122 and the sidechains of Cys residues exposed to the surface of PLC-δ1. No change in mass was induced by U73343, an analog of U73122, in which the maleimido group is replaced by a succinimido group. The time course of ^{31}P NMR spectra indicated that 10 μM U73122 does not entirely abolish the hydrolysis activity of PLC-δ1. A rate of formation of IcP from PI was, however, markedly reduced, whereas a formation rate of IP and a final amount of IP were not affected by U73122. This suggests that U73122 reduces efficiency of hydrolysis of the membrane embedded PI by PLC-δ1. Similarity of DD-MAS ^{13}C NMR spectra of [3-^{13}C]Ala labeled intact- and U73122 treated-PLC-δ1 revealed that no drastic change in the conformation of PLC-δ1 is induced by U73122. CP-MAS ^{13}C NMR spectra were, however, remarkably affected by the treatment with U73122. As shown in Fig. 1, an increase in the cross polarization efficiency between ^{1}H and ^{13}C in either the lipid or the protein was induced in the presence of U73122. This suggests that the interactions between the hydrophobic steroid moieties of U73122 covalently linked to the surface of PLC-δ1 and the hydrophobic inner layer of the membrane anchor PLC-δ1 at the membrane surface. The membrane insertion of U73122 may restrict orientation and motional freedom of PLC-δ1 at the membrane surface and reduce efficiency of collision between the active site and the substrate embedded in the membrane.

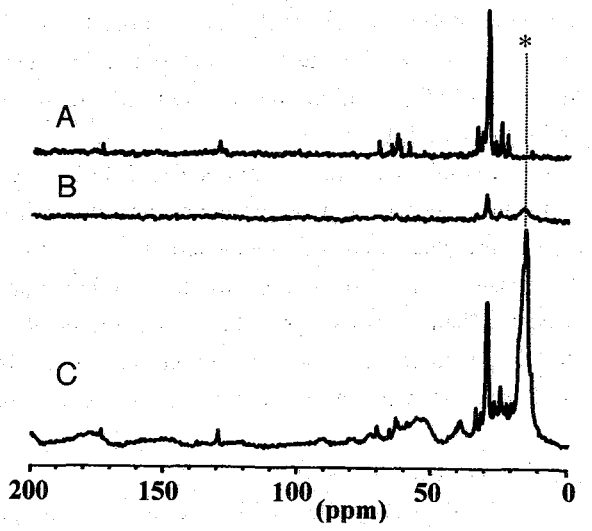

Fig. 1 CPMAS ^{13}C NMR spectra of PC/PIP_2 vesicle (PC:PIP_2 = 95:5) (A), intact PLC-δ1 - PC/PIP_2 vesicle complex (B), and PLC-δ1 treated with U73122 - PC/PIP_2 vesicle complex (C) suspended in 20 mM MES buffer (pH6.5) in the absense of Ca^{2+}. An astarisk indicates the signals of [3-^{13}C]Ala residues.

3 LJ12

固体 ^{1}H MAS NMR による ウシラクトフェリシンと酸性リン脂質二重膜との 特異的相互作用解析およびその抗菌作用の解明

○梅山万左子[1]，吉良敦史[2]，内藤晶[1]
（[1]横浜国大・院工，[2]アルバック）

Interaction of Bovine Lactoferricin with Acidic Phospholipid Bilayers and Elucidation of its Antimicrobial Activity as Revealed by Solid-state ^{1}H MAS NMR Spectroscopy

○Masako Umeyama[1], Atsushi Kira[2], Akira Naito[1]
[1]Graduate School of Engineering, Yokohama National University,
[2]Research and Development Division, ULVAC. Inc.

【Introduction】

Bovine lactoferricin (LfcinB) is an antimicrobial peptide released by pepsin cleavage of lactoferrin. It consists of 25 amino acid residues with the sequence of Phe-Lys-Cys-Arg-Arg^{5}-Trp-Gln-Trp-Arg-Met^{10}-Lys-Lys-Leu-Gly-Ala^{15}-Pro-Ser-Ile-Thr-Cys^{20}-Val-Arg-Arg-Ala-Phe^{25} forming a disulfide bond between Cys^{3} and Cys^{20}. In this work, we investigated the specific interaction of LfcinB with acidic phospholipid bilayers with the weight percentage of 65% dimyristoylphosphatidylglycerol (DMPG), 10% cardiolipin (CL) and 25% dimyristoylphosphatidylcholine (DMPC) as a mimic of cell membrane of *Staphylococcus aureus* by means of quartz crystal microbalance (QCM), solid-state ^{31}P, ^{13}C and ^{1}H NMR spectroscopy. Moreover, it was elucidated by means of potassium ion selective electrode (ISE) that a molecular mechanism of the antimicrobial activity of LfcinB could be attributed to the pore formation induced by LfcinB.

A combined study of solid-state ^{31}P DD-static and ^{1}H MAS NMR separately provides dynamic properties of polar group and acyl chains in lipid bilayers, respectively. Gel-to-liquid crystalline phase transition temperatures (Tc) in the mixed bilayer systems were determined by measuring the temperature variation of relative intensities of acyl chains in ^{1}H MAS NMR spectra. Changes of chemical shift was observed at CH(β) peak of phospholipids in ^{1}H MAS NMR spectra to be caused by ring current effect from Trp. These results suggest that Trp residues exist at the interfacial region of acidic phospholipid bilayers.

【Materials and methods】

LfcinB was synthesized by means of a solid phase method. After removing protecting groups and cleavage from the resin, the synthesized peptides were purified using a high performance liquid chromatography (HPLC). The disulfide bridge between Cys^{3} and Cys^{20}

Keywords: Antimicrobial peptide, Acidic phospholipid bilayers, Solid-state ^{1}H MAS NMR spectroscopy, Gel-to-liquid crystalline phase transition, Ring current shift

was formed by air oxidation at pH 8.5 and then the crude LfcinB was purified by HPLC. A mixture of 65% DMPG, 10% CL and 25% DMPC was dissolved in the solvent with chloroform and methanol. The solvent was subsequently evaporated in vacuo, followed by hydration with Tris buffer (20 mM Tris, 100 mM NaCl and pH 7.5). A freeze-thaw cycle was repeated, followed by incubating the samples for overnight at 40 °C.

【Results and discussion】

QCM measurements were performed to show that affinity of LfcinB for acidic phospholipid bilayers was higher than that for neutral phospholipid bilayers. It was also revealed that the association constant of LfcinB was larger than that of lactoferrin.

^{31}P DD-static NMR spectra indicated that LfcinB interacted with acidic phospholipid bilayers and bilayer defects were observed in the bilayer systems because isotropic peaks were clearly appeared. Gel-to-liquid crystalline phase transition temperatures (Tc) in the mixed bilayer systems were determined by measuring the temperature variation of relative intensities of acyl chains in ^{1}H MAS NMR spectra (Fig. 1). Tc values of DMPC, acidic phospholipid and LfcinB-acidic phospholipid bilayer systems were determined to be 23.0℃, 21.5℃ and 24.0℃, respectively (Fig. 2). ^{13}C DD-MAS NMR spectra indicated that LfcinB interacted with the part of glycerol group Cα in phosphatidylglycerol of phospholipids. Moreover, changes of chemical shift caused by ring current effect from Trp were observed at CH(β) peak in ^{1}H MAS NMR spectra. These results suggest that Trp residues exist at the interfacial region of lipid bilayers.

To characterize the bilayer defects, potassium ion permeation across the membrane was observed by ISE measurements. The experimental results suggest that LfcinB caused pores in the acidic phospholipid bilayers. Because these pores lead the permeability across the membrane, the molecular mechanism of the antimicrobial activity could be attributed to the pore formation in the bacterial membrane induced by LfcinB.

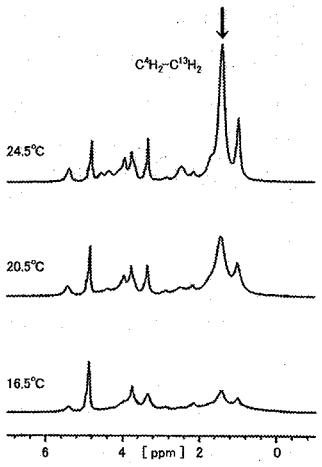

Fig. 1 Temperature variation of solid-state ^{1}H MAS NMR spectra of acidic phospholipid bilayers. The signals with arrow indicate the methylene protons of acyl chains.

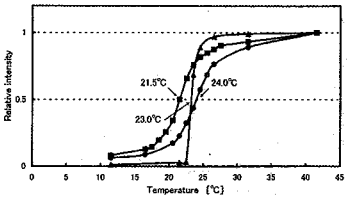

Fig. 2 Plot of relative intensities of ^{1}H MAS NMR signals of methylene protons of acyl chains in LfcinB-acidic phospholipid bilayer systems. Tc values of LfcinB-acidic phospholipid bilayer systems were determined by taking the mid points of the curves of the intensity variations.

【References】 M. Umeyama, A. Kira, K. Nishimura, A. Naito, *Biochim. Biophys. Acta* (2006) in press.

Induction of Morphological Changes in Model Lipid Membranes and the Mechanism of Membrane Disruption by a Large Scorpion-derived Pore-forming Peptide

Kaoru Nomura*, Gilles Ferrat*#, Terumi Nakajima*, Herve Darbon#, Takashi Iwashita* and Gerardo Corzo*‡

*Suntory Institute for Bioorganic Research, Mishima-Gun, Shimamoto-Cho, Wakayamadai 1-1-1, Osaka 618-8503, Japan. #AFMB, CNRS UMR 6098 and Universités d'Aix-Marseille I and II, 31 Chemin Joseph Aiguier, 13402 Marseille Cedex 20, France ‡Institute of Biotechnology-UNAM, Av. Universidad 2001, Cuernavaca, Morelos, 62210, Mexico.

The orientation and pore-forming mechanisms of pandinin 1 and 2 (pin1 and pin2) [1], which are antimicrobial peptides isolated from venom of the African scorpion *Pandinus imperator*, were studied using ^{31}P, ^{13}C, ^{1}H solid-state and multidimensional solution-state nuclear magnetic resonance (NMR) spectroscopy [2, 3]. A high-resolution NMR solution structure of pin2 has known to be composed of a single α-helix, whereas pin1 has the two distinct α-helical regions moving around the central hinge region

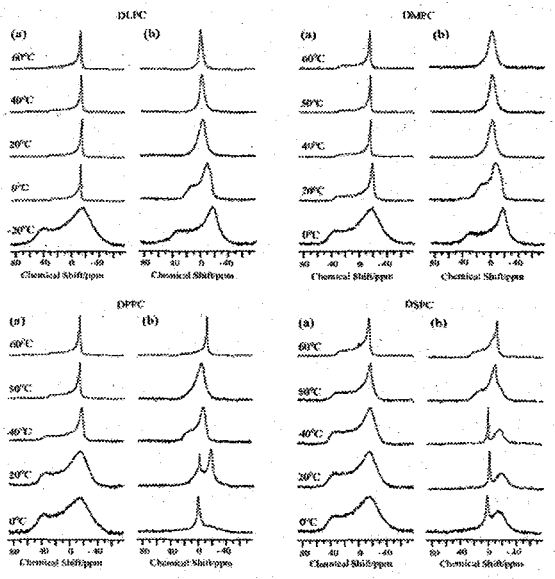

Figure 1. ^{31}P NMR spectra of dispersions of four kinds of saturated phosphatidyl-cholines, DLPC, DMPC, DPPC, and DSPC, in the (a) absence and (b) presence of pin1 (P/L=1:20) at various temperatures.

Key words : antimicrobial peptides, membrane disruption, solid-state NMR

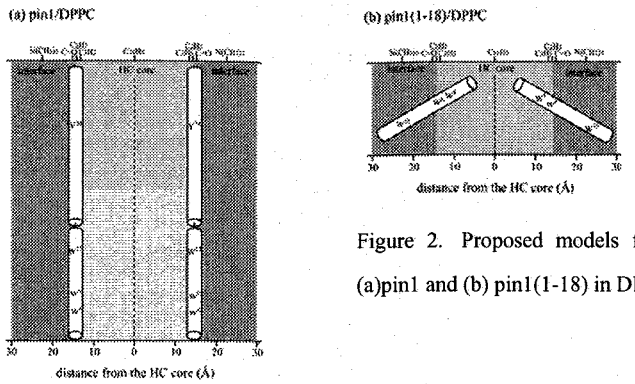

Figure 2. Proposed models for orientation and location of (a)pin1 and (b) pin1(1-18) in DPPC lipid bilayer above T_m.

which contains Pro[19]. ^{31}P NMR spectra of lipid membrane in the presence of pin1 at various temperatures indicated that pin1 induces various lipid phase behaviors depending on the acyl chain length and charge of phospholipids. Notably, it was found that pin1 induced formation of the cubic phase in shorter lipid membranes above T_m. In contrast, in the presence of pin2, it was found that membrane lysis occurres at temperatures below the liquid crystal-gel phase transition of the lipid bilayers. ^{1}H MAS chemical shift measurements suggest that pin1 is located at the membrane-water interface approximately parallel to the bilayer surface. Solid-state NMR results correlated well with the observed biological activity of pin1 in red blood cells and bacteria. On the other hand, differential scanning calorimetry measurements showed that pin2 induced negative curvature strain in lipid bilayers. The ^{13}C chemical shift values of synthetic pin2 labeled at Gly^3, Gly^8, Leu^{12}, Phe^{17}, or Ser^{18} under static or slow magic angle spinning conditions, indicate that pin2 penetrates the membrane with its average helical axis perpendicular to the membrane surface. Furthermore, amide H-D exchange experiments of ^{15}N-Ala^4, Gly^8, and Ala^9 triply labeled pin2 suggest that this peptide forms oligomers and confirms that the N-terminal region creates membrane pores.

References

1. G. Corzo, P. Escoubas, E. Villegas, K. J. Barnham, W. HE, R. S. Norton, and T. Nakajima. (2001). *Biochem. J. 359*, 35-45.

2. K. Nomura, G. Corzo, T. Nakajima, and T. Iwashita. (2004) *Biophys. J. 87*, 2497-2507.

3. K. Nomura, G. Ferrat, T. Nakajima, H. Darbon, T. Iwashita and G. Corzo. (2005) *Biophys. J. 89*, 4067-4080.

Poster Session

Odd numbers: Wednesday, 14:00-15:00

Even numbers: Friday, 14:00-15:00

P001

New two dimensional triple resonance NMR experiments without necessity of isotopic labeling

Michal MALON, Hiroyuki KOSHINO

RIKEN (The Institute of Physical and Chemical Research), 2-1 Hirosawa, Wako,

Saitama 351-0198, Japan

Two dimensional triple resonance NMR experiments have been explored in this study with the aim to overcome limitations of classical HMBC (heteronuclear multiple bond correlation) experiment. Applications can be found in the field of NMR spectroscopy of organic, organometallic and inorganic compounds, synthetic as well natural compounds.

Experiments correlating three magnetically active nuclei may be based on INEPT (Insensitive Nuclei Enhanced by Polarization Transfer) transfer and following HMQC (heteronuclear multiple quantum correlation) experiment [1], or two consecutive INEPT transfers [2]. HXY-experiments exploiting indirect proton detection allow us to study one or even two magnetically diluted half-spin nuclei such as ^{13}C (1.07 %), ^{15}N (0.37 %), ^{29}Si (4.68 %), ^{119}Sn (8.59 %), ^{183}W(14.31 %), ^{195}Pt (33.83 %) and others, at natural abundance. Spectra can be measured as original 3D-experiments or one evolution period may be removed which results in 2D experiments using triple resonance. This approach is favourable in case that only one or a few nuclei of X-type are present in the studied compound. Then, significant experimental time will be saved.

The INEPT/HMQC experiment. Up to now, the pulse sequences based on the INEPT/HMQC scheme have been used in the case of HCP [1], HCF [3,4] and HPW [5] experiments. All the experiments use advantage of two nuclei in a 100 %-natural abundance (^1H, ^{31}P or ^1H, ^{19}F) providing excellent sensitivity. Used coupling constant values, dimensionality and other details are listed in **Table 1**.

The double INEPT experiment. Pulse sequences based on the double INEPT scheme has been used in the case of HCP [6], HPC [5] and HPN [5] experiments, but more interestingly, they have been shown to be effective in the case of HCSi [7,8,10], HCSn [9] and HCPt [11] experiments (Table 1). These experiments correlate protons to two magnetically diluted nuclei without necessity of isotopic labeling and provide excellent results. However, it's worthwhile to emphasize that those studies usually exploited $^1J_{CH}$ and relatively large $^nJ_{XY}$.

Keywords: triple resonance; two dimensional; natural abundance; long-range correlation; proton detection

Table 1. Published applications of 2D or 3D triple resonance experiments.

Type of experiment	Experiment (dimensionality)	Compound	J_{XH} (value, Hz)	J_{XY} (value, Hz)	Reference
INEPT/HMQC	HCP (3D)	diphosphine	^1J (160)	^2J (20)	[1]
INEPT/HMQC	HCF (3D)	polymer	^1J (152)	^2J (40)	[3,4]
INEPT/HMQC	HPW (2D)	W(0)-complex	^2J (44)	^1J (300) ^3J (10)	[5]
Double INEPT	HCP (3D)	oligonucleotide	^1J (167)	^nJ (19)	[2]
Double INEPT	HCP (3D)	polymer	^1J (140)	^1J (60)	[6]
Double INEPT	HCSi (3D)	polymer	^1J (140)	^2J (5)	[7]
Double INEPT	HCSi (3D)	polymer	^1J (140)	^1J (60) ^2J (7)	[8]
Double INEPT	HCSn (3D)	polymer	^1J (140)	^1J (310) $^{2,3}J$ (50) ^3J (20)	[9]
Double INEPT	HCSi (3D)	polymer	^1J (140)	^1J (96) ^nJ (13) ^nJ (5)	[10]
Double INEPT	HCPt (2D)	Pt(II)-complexes	^1J (140)	^4J (35, 30)	[11]
Double INEPT	HPC (2D)	cyclic carbene	^4J (8.1)	^nJ (40)	[5]
Double INEPT	HPN (2D)	azide	^nJ (7)	^nJ (25)	[5]
Double INEPT	HPN (2D)	diazaphosphole	^2J (50)	^nJ (15)	[5]

We have adapted the pulse sequences described in the literature and examined both groups of experiments. We have tested and evaluated the pulse programs using HPC, HCP, HSiC and HCSi experiments and focused on using long-range coupling constants, both ^nJ(H,X) and ^nJ(X,Y), which were not studied intensively before. Consequently, some slight modifications including application of additional pulse field gradients (PFG), spinlocking and more complicated phase cycles had to be done to improve efficiency, artifact and strong t_1-noise suppression. Finally, we have developed pulse programs based on the INEPT/HMQC and double INEPT schemes which allow us to correlate protons indirectly to the third nucleus (Y) up to 5 or 6 bonds in case that long-range coupling constants $^nJ_{HX}$ and $^nJ_{XY}$ are used.

The 2D-HXY-INEPT/HMQC pulse sequence diagram is shown in Figure 1. Experimental details are included under the diagram.

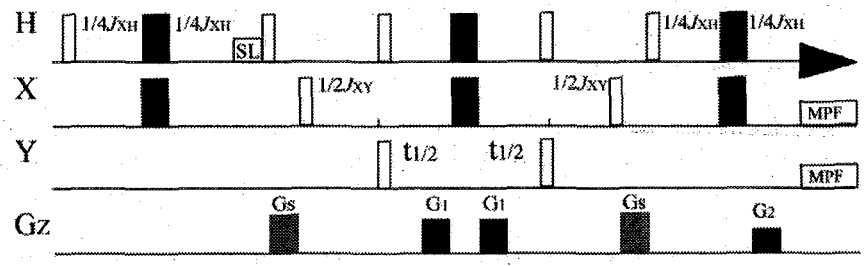

Figure 1. The 2D-HXY-INEPT/HMQC pulse sequence diagram. Open and solid rectangles represent 90 and 180 degree pulses, respectively. Composite pulses (90x/240y/90x) are favourable instead of 180 degree pulses applied to X nucleus. G1 and G2 are pulse field gradients used for H-Y gradient selection and the ratio of gradient strengths has to be as follows: $G2 = 2G1\gamma(Y)/\gamma(H)$. Gs and SL represent homospoil gradients and spinlocking, respectively, used to improve the suppression of unwanted magnetization. Heteronuclear decoupling may be applied to X, Y or both X and Y during acquisition. Spectra are processed in the magnitude mode in $F1$.

The 2D-HXY-double INEPT pulse sequence diagram is depicted in Figure 2. Details are described under the pulse sequence.

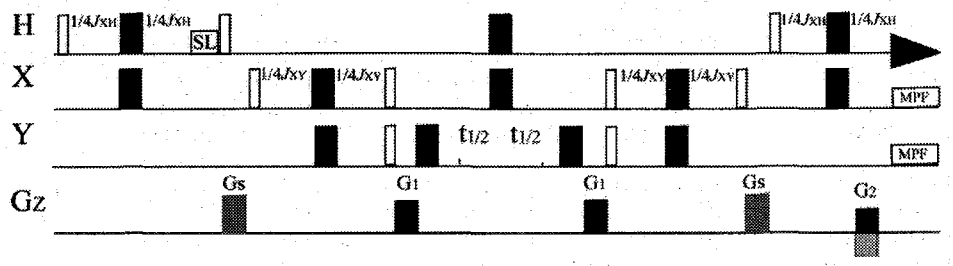

Figure 2. The 2D-HXY-double INEPT pulse sequence diagram. Open and solid rectangles represent 90 and 180 degree pulses, respectively. Composite pulses (90x/240y/90x) are favourable instead of 180 degree pulses applied to X and Y nuclei. G1 and G2 are pulse field gradients used for H-Y gradient selection and the ratio of gradient strengths has to be as follows: $G2 = 2G1\gamma(Y)/\gamma(H)$. To achieve P/N-type selection, G2 is inverted for every other FID. Gs and SL represent homospoil gradients and spinlocking, respectively, used to improve the suppression of unwanted magnetization. Heteronuclear decoupling may be applied to X, Y or both X and Y during acquisition. Spectra are processed in the phase sensitive mode (Echo-Antiecho or PN-type) in *F*1.

As an example, usefulness of the 2D-HSiC-double INEPT experiment will be demonstrated on silicon containing compound 4-(*tert*-butyldimethylsiloxy)phenol. The structure of compound is very simple, but the assignment of aromatic carbon signals based on classical 2D experiments is very difficult. Aromatic ring is characterized by four ^{13}C signals at 115.98, 120.80, 149.34 and 149.71 ppm. Former two signals belong to two methine carbons, while latter two are quaternary carbons. The ^{1}H-^{13}C-PFG-HMBC experiment did not provide any correlation from *tert*-butyldimethylsilyl portion to aromatic carbons. Moreover, aromatic proton signals are severely overlapped which complicates analysis. We decided to use triple resonance experiment and measured the phase sensitive 2D-HSiC-double INEPT experiment described above (Figure 2). The resultant spectrum, structure of the compound and used acquisition parameters are shown in Figure 3. The spectrum revealed correlation signals from both groups of methyl protons to methine carbon at 120.80 ppm which is three bonds far from silicon atom, and to quaternary carbon at 149.34 ppm which is two bonds far from silicon. When the measurement was repeated using $^{n}J_{CSi}$ value optimized to 1.7 Hz, the quaternary carbon signal was significantly suppressed, but weak correlation to another methine carbon was apparent (115.98 ppm). Thus, methyl protons of *tert*-butyl group were indirectly correlated to carbon via seven bonds.

All the spectra are recorded on a JEOL ECA 600 MHz NMR spectrometer equipped with an 5mm inverse triple-resonance $^{1}H/^{13}C/X$ probehead, where X can be tuned over the range of resonance frequencies from ^{31}P (242.9 MHz) to ^{15}N (60.8 MHz), and z-axis pulse field gradients.

Although the pulse sequences of 2D triple resonance experiments are related to 3D experiments, the measurement itself and data processing are based on routine knowledge of 2D experiments. Thus these experiments are available to common NMR users and can be useful in the study of suitable organic, organometallic and inorganic compounds.

More detailed information about experiments and other interesting applications will be presented during the Annual Meeting.

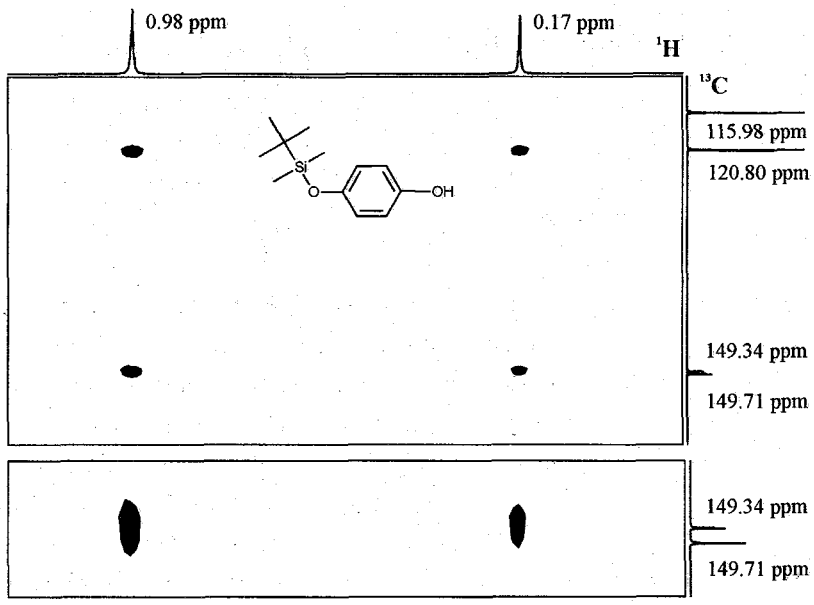

Figure 3. Expansions of the ^{1}H detected 2D-^{1}H-^{29}Si-^{13}C-double INEPT correlation spectrum of 4-(*tert*-butyldimethylsiloxy)phenol. Parameters were adjusted as follows: $^{n}J_{HSi}$ = 6.7 Hz, $^{n}J_{CSi}$ = 2.5 Hz, G1:G1:G2 = 60:60:30.18%, Gs = 75%, durations of PFGs were 1 ms, relaxation delay 2.5 s, 16 scans, 64 increments.

References

[1] S. Berger, P. Bast, *Magn. Res. Chem.* **31** (1993) 1021-1023.

[2] J. P. Marino, H. Schwalbe, C. Anklin, W. Bermel, D. M. Crothers, C. Griesinger, *J. Am. Chem. Soc.* **116** (1994) 6472-6473.

[3] L. Li, P. L. Rinaldi, *Macromolecules* **29** (1996) 4808-4810.

[4] L. Li, P. L. Rinaldi, *Macromolecules* **30** (1997) 520-525.

[5] D. Gudat, *Magn. Reson. Chem.* **41** (2003) 253-259.

[6] T. Saito, R. E. Medsker, H. J. Harwood, P. L. Rinaldi, *J. Magn. Reson. A* **120** (1996) 125-128.

[7] M. Chai, T. Saito, Z. Pi, C. Tessier, P. L. Rinaldi, *Macromolecules* **30** (1997) 1240-1242.

[8] M. Chai, Z. Pi, C. Tessier, P. L. Rinaldi, *J. Am. Chem. Soc.* **121** (1999) 273-279.

[9] W. Liu, T. Saito, L. Li, P. L. Rinaldi, R. Hirst, A. F. Halasa, J. Visintainer, *Macromolecules* **33** (2000) 2364-2369.

[10] W. Liu, P. L. Rinaldi, L. Galya, J. E. Hansen, L. Wilczek, *Organometallics* **21** (2002) 3250-3257.

[11] D. Argyropoulos, E. Hoffmann, S. Mtongana, K. R. Koch, *Magn. Reson. Chem.* **41** (2003) 102-106.

P002

異性体混合試料に対するDOSY法によるシグナル分離

（日本電子（株）・応用研究グループ[1]、
日産化学工業（株）・分析研究部[2]、千葉大学・分析センター[3]、
横浜国立大学・分析機器評価センター[4]）
○櫻井智司[1]、敷井和彰[2]、内海博明[1]、関宏子[3]、中越雅道[4]

Separation of signals by DOSY for mixtures of isomers

(Application & Research Group, JEOL Ltd.[1],
Analysis Research Dept., Nissan Chemical Industries Ltd.[2],
Chemical Analysis Center, Chiba University[3],
Instrumental Analysis Center, Yokohama National University[4])
Satoshi Sakurai[1], Kazuaki Shikii[2], Hiroaki Utsumi[1],
Hiroko Seki[3], Masamichi Nakakoshi[4]

The DOSY is a technique to separate the NMR spectrum for the mixture by using the difference of the self-diffusion coefficients. Therefore, it was thought that the separation for mixture which species have closed molecular weights is not enabled because those diffusion coefficients are very closed also. But, in previous this meeting, we proved DOSY method is useful for separating the spectrum of mixture which species have closed molecular weights. We think that this difference of diffusion coefficients are caused from the differences of volume and the interaction for solvents. Then, we examined the key factor of the difference of the diffusion coefficients by using the mixture of the isomer. In the results, we confirmed the possibility of a spectrum separation by the DOSY method.

【緒言】DOSY法は、分子の自己拡散係数の差を利用して、混合試料中のNMRスペクトルを分離する手法である。このため、分子量が近い試料間の分離は、拡散係数が近いため行えないという認識が一般的であった。昨年の本会で、我々はエストロンとβ-エストラジオールの混合試料（分子量差：2）、およびミリスチン酸イソプロピルとジヒドロベンゾピレン、アピゲニンの混合試料（差ほぼなし）に対する、DOSYによるスペクトル分離の結果を示し、分子量がほぼ等しくてもDOSY法でスペクトル分離できることを証明した。この拡散係数の違いには、分子体積や溶媒との相互作用などの違いが考えられる。そこで今回は、異性体の混合試料を用い、拡散係数の違いの主要因が何であるかを検討し、DOSY法によるスペクトル分離の可能性を確認した。

キーワード：DOSY、diffusion coefficient、isomer

さくらいさとし、しきいかずあき、うつみひろあき、せきひろこ、なかこしまさみち

【実験】DOSY 測定は JNM-ECX400 で行った。試料には、ネロールとゲラニオールの各 19.4 mM の CD_3OD 溶液と $CDCl_3$ 溶液を用いた。試料管には外径 3 mm の試料管を用い、測定の主なパラメータは以下の条件で行った。拡散時間 Δ=200 ms、磁場勾配パルス幅 δ=2.6 ms、磁場勾配強度 G=0.1～33 G/cm（16 ステップ）。

また、分子体積計算には CAChe WorkSystem V5.02 ソフトウェアを用いた。ネロールとゲラニオールそれぞれについて、MOPAC の AM1 パラメータにより構造最適化を行ない、得られた値を実験に用いた。

【結果】CD_3OD 溶媒に対する DOSY スペクトルを Fig.2 に示す。CD_3OD 溶液、$CDCl_3$ 溶液ともに、ネロールとゲラニオールのシグナルが拡散係数の差によって分離され、それぞれの溶媒における両成分の拡散係数の比率は等しかった。また、ネロールとゲラニオールのそれぞれの体積は、ネロールが 193.9 Å^3、ゲラニオールが 203.3 Å^3 であった。

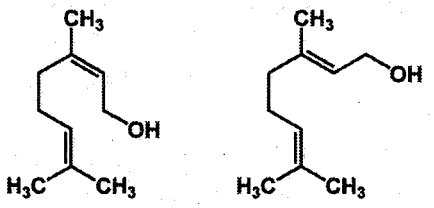

Fig.1 Structures of nerol and geraniol

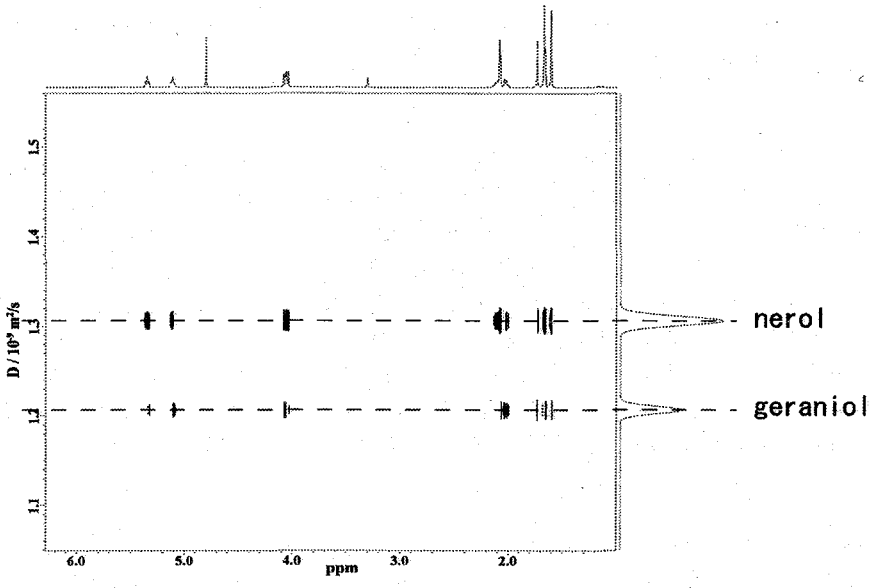

Fig. 2 ^{1}H-DOSY spectrum of mixture in CD_3OD

【考察】異性体であるネロールとゲラニオールの混合試料も、拡散係数の差によって DOSY によりスペクトル分離をすることができた。また、その拡散係数の比率が親水性溶媒と疎水性溶媒とで等しかったことと、体積計算の結果より、その拡散係数の差の主要因は分子体積によるものと考えられる。

P003

Projection Reconstruction NMR 法による タンパク質測定の高速化

(1北大・院薬・構造生物、2Varian, Ltd)
○関口真二1、Eriks Kupce2、横地政志1、稲垣冬彦1

Rapid Acquisition of Protein using Projection Reconstruction NMR

([1]Department of Structural Biology, Graduate School of Pharmaceutical Sciences, Hokkaido University, [2]Varian, Ltd)
Shinji Sekiguchi[1], Eriks Kupce[2], Masashi Yokochi[1], Fuyuhiko Inagaki[1]

Projection-reconstruction method is one of reduced dimensionality experiments, in which time evolutions in indirect dimensions are incremented not independently but simultaneously. This method reconstructs multidimensional spectra from several set of projection spectra and reduces NMR machine time. Here, we applied this method to determine the three dimensional structure of proteins. The data were collected using $^{15}N/^{13}C$ labeled Grb2 C-terminal SH3 domain complexed with peptide. We modified the several pulse sequences in Varian BIOPACK for projection-reconstruction measurements, and analyzed the data by NMRPipe and some originally developed tools.

【はじめに】

NMR 法はタンパク質の立体構造解析の手法として主要なものであるが、立体構造の決定に至るまでに複数の多核多次元測定を行う必要がある。一般的な三次元測定においてその測定時間は十数時間から数日かかり、四次元測定に至っては一週間かけても十分な分解能が得られない。PR-NMR 法は多次元スペクトルのすべてを測定するのではなく、それを二次元にまで落とした投影スペクトルを角度を変えて複数枚測定することにより測定時間を短縮し、その投影スペクトルから元の多次元スペクトルを再構築する、という方法である。

本研究では当研究室で用いられている Varian 社の NMR 分光器とそのコンソールアプリケーション VNMR と、NMR データ解析ソフト NMRPipe を用いて PR-NMR 法による測定と解析を行うための方法を確立し、実際にタンパク質のシグナルを解析、帰属した。

【方法】

今回の測定サンプルには ^{13}C, ^{15}N でラベルした Grb2 の SH3 ドメイン(159-217)の Gab1 由来ペプチド複合体を用いた。この試料について Varian UNITY INOVA 600 を用いて 25℃で測定した。測定したスペクトルは Varian BIOPACK から主鎖由来シグナルの帰属のために HNCO、HN(CO)CA、HNCACB、CBCA(CO)NH、HBHA(CO)NH、脂肪族側鎖由来シグナ

キーワード projection-reconstruction、構造解析、高速化

○せきぐちしんじ、えりっくすくぷちぇ、よこちまさし、いながきふゆひこ

ルの脂肪族側鎖由来シグナルの帰属のために C(CO)NH、H(CCO)NH、CCH-TOCSY、HCCH-TOCSY を用いた。その際、projection angle(pra)を array として測定したデータを適切に並び替えることにより擬似的な三次元スペクトルとした。それにより一つのパルスシーケンスによる測定を 1 つの FID ファイルとして扱うことができ、NMRPipe へのスムーズな橋渡しが可能となった。NMRPipe を用いて FT し、複数の Projection スペクトルを得ることができた。この Projection スペクトルから逆ラドン変換により多次元スペクトルを再構築した。しかしこの方法を用いた場合では再構築したスペクトルの観測幅が ^{15}N と ^{13}C で同じになってしまうため、HNCO などの観測幅があまり違わない場合は問題はないが、HNCACB など観測幅が異なる場合無駄な領域ができ十分な分解能が得られなかった。そのため図 1 に示したように pra の増加に伴い観測幅を調整するようにパルスを変更したもので測定を行った。

【結果、考察】

投影枚数を 18 枚で行ったところ、通常のスペクトルとほとんど遜色のない結果が得られた。他の条件を通常の測定と同様にしたところ、測定時間を通常の 1/3 以下にまで減らすことができた。分解能、S/N 比ともに帰属を行うのに十分なものであり、実際に NMRPipe による自動ピークピック、AutoAssign による自動帰属を行ったところ、プロリンを除く 55 残基中通常の測定法では 36 残基、一方 PR-NMR 法による測定では 33 残基正しく帰属できた。また手動によるピークピックおよび帰属では双方とも 51 残基帰属できた。また脂肪族側鎖帰属では CCH-TOCSY や HCCH-TOCSY の投影スペクトルを参考に C(CO)NH、H(CCO)NH ベースで帰属を行い通常の測定法と同程度帰属することができた。現在どの程度まで投影枚数を減らせるかを検討し測定時間のさらなる減少をはかることを試みている。またスペクトルを芳香族側鎖帰属に必要なものも測定し、完全な帰属が可能かどうか検討中である。

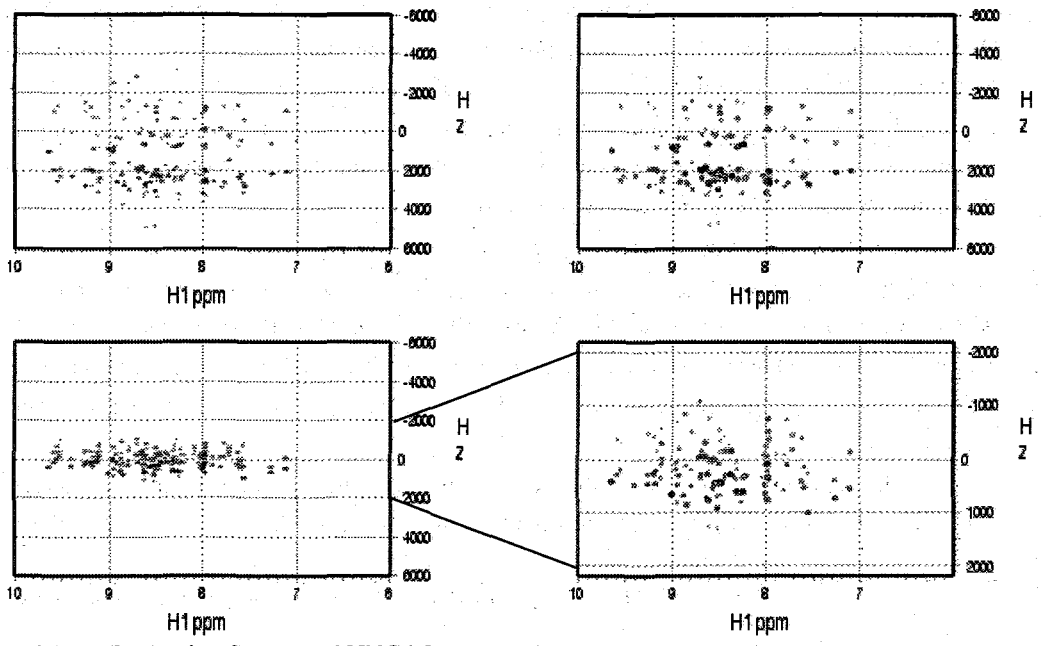

Fig 1. Projection Spectra of HNCACB
(Top:pra=0° 、Bottom:pra=80° 、Left:SW normal、Right:SW slided)

P004

Rapid acquisition of high resolution triple-resonance spectra using nonlinear sampling and maximum entropy reconstruction

Yoshiki Shigemitsu[1], Takahiro Anzai[1], Markus Wälchli[2], Masaki Mishima[1] and Yutaka Ito[1,3,4]

[1]Graduate School of Sciences, Tokyo Metropolitan University, 1-1 Minami-Ohsawa, Hachioji, Tokyo 192-0397, Japan; [2]Bruker Biospin, 3-21-5 Ninomiya, Tsukuba, Ibaraki 305-0051, Japan; [3]Research Group for Bio-supramolecular Structure-Function, RIKEN, 1-7-29 Suehiro-cho, Tsurumi-ku, Yokohama 230-0045, Japan; [4]CREST, JST

Triple resonance NMR experiments, which are commonly utilised for the backbone resonance assignments of proteins, usually require high sample concentration (~ 1 mM). For the analysis of relatively larger proteins, 4 to 6 3D triple-resonance NMR spectra are usually measured in order to reduce the ambiguity caused by signal overlapping, and each requires 1~3 days measurement time. Low solubility and/or low stability of proteins during the NMR measurements sometimes prevent us from applying heteronuclear multidimensional NMR experiments. Technologies enabling rapid measurements of multidimensional NMR data are therefore very useful for these "difficult" samples. Also these techniques meet the requirement from structural genomics projects.

Nonlinear sampling scheme in combination with maximum entropy processing (MaxEnt) is one of the most promising approaches for the rapid detection of multidimensional NMR data. With this technique high resolution can be achieved in much shorter experiment times. Advantages of MaxEnt include the fact that it makes no assumptions regarding the number or type of resonances and can handle arbitrary line shapes. MaxEnt has also been shown to robustly handle data with low S/N ratios.

In this presentation we report our recent applications of the nonlinear sampling/MaxEnt processing scheme to our "difficult" samples, human mitochondrial ABCB6-C, *Thermus thermophilus* RecX, yeast YUH1, and a 59kDa salmonella OppA. We also present the backbone resonance assignment of proteins in living *E. coli* cells, in which the nonlinear sampling scheme played crucial role in rapid acquisition of triple-resonance spectra.

The application of the nonlinear sampling scheme enabled us to measure 3Dtriple-resonance NMR spectra of equivalent quality with approximately 1/3~1/8 duration,

キーワード：異種核多次元 NMR、nonlinear sampling、MEM、projection reconstruction

著者ふりがな：しげみつ　よしき、あんざい　たかひろ、まるくす　ヴぇるひり、
みしま　まさき、いとう　ゆたか

when compared with employing a conventional sampling scheme. This showed that this approach is very effective for the experiments of protein samples with lower stability. The efficiency of nonlinear sample scheme was also demonstrated for the case of 4D experiments (Figure1). The time gained from this scheme can be used to increase the number of scan, suggesting that this approach is also effective for protein samples with lower solubility. Furthermore, nonlinear sampling was shown to be robustly applicable for the processing of 3D NOESY-type spectra, which contain relatively large number of cross peaks with a variety in intensity.

We also discuss the efficiency and accuracy of the nonlinear sampling scheme by comparing the spectra with those obtained by using the recently developed projection reconstruction method, which has been shown to be sufficiently competitive approach for the rapid measurements of heteronuclear multidimensional NMR spectra.

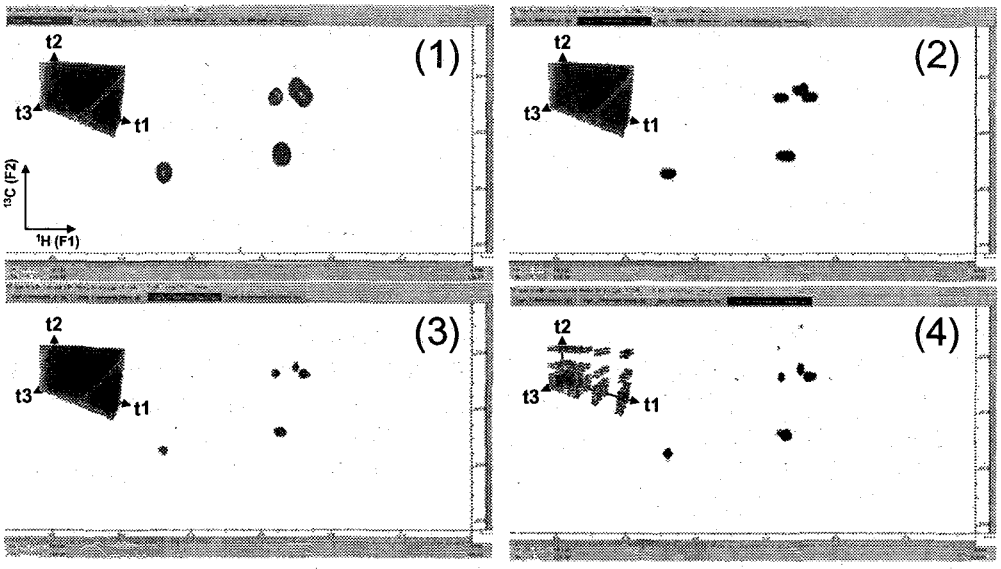

Figure1

2D (^{13}C'-^{1}H^{N}) slices extracted from 4D HCC(CO)NH spectra of a ^{13}C/^{15}N-labelled 11kDa protein. The raw data has 32* (^{1}H, t_1) x 16* (^{13}C, t_2) x 12* (^{15}N, t3) x 512* (^{1}H^{N}, t4) complex points.

(1) Zerofilling(ZF) + Fourier transformation (FT) for all four dimensions.

(2) ZF + FT for F4 (acquisition) and F1 (indirect ^{1}H), and 2D MaxEnt processing for (^{13}C) and F3 (^{15}N).

(3) ZF + FT for F4, and 3D MaxEnt processing for F1, F2 and F3.

(4) Simulate the nonlinearly sampled data [16* (t1), 10* (t2) and 8* (t3)]. ZF + FT for F4, and 3D MaxEnt processing for F1, F2 and F3.

P005

MAGICAL法の高分子量タンパク質への応用

（三菱化学生命科学研究所）
○田中利好、小松千江子、小林邦子、田中剛史、河野俊之

Application of MAGICAL for Large Proteins

Mitsubishi Kagaku Institute of Life Sciences (MITILS)
Rikou Tanaka, Chieko Komatsu, Kuniko Kobayashi, Takeshi Tanaka, and Toshiyuki Kohno

We have developed a novel NMR signal assignment method applicable to larger, less soluble, and unstable proteins. With this method, we can obtain enough information to assign all the NMR signals with diluted sample, even in the case of larger proteins such as 40 kDa. This method does not need complicated analyses, resulting in the unambiguous assignments. Here, we demonstrate the application of this method to larger proteins.

我々は、従来のタンパク質のＮＭＲシグナル帰属法では必須だった、低分子量、高濃度、安定性といった厳しい制限事項を大幅に緩和することが可能な、新しいＮＭＲシグナルの帰属方法（ＭＡＧＩＣＡＬ法）を開発した。この方法を用いると、分子量４万程度のタンパク質においても、従来法よりはるかに低濃度の試料で必要な情報が全て得られ、複雑な解析も不要で、容易にＮＭＲシグナルの完全な帰属が可能となる。本研究では、このＭＡＧＩＣＡＬ法を高分子量タンパク質に適用した。

ＭＡＧＩＣＡＬ法

ＭＡＧＩＣＡＬ法による ^{1}H-^{15}N HSQC の各シグナルの帰属の仕方は以下の通りである。

(1)一種類のアミノ酸残基のみを選択的に ^{13}C/^{15}N 二重標識し、その他の 19 種類のアミノ酸を ^{15}N のみで標識した目的タンパク質を 20 種類調製する。

(2)一種類のアミノ酸残基のみを ^{13}C/^{15}N 二重標識し、その他の 19 種類のアミノ酸を ^{15}N のみで標識した目的タンパク質の２次元 HN(CO)及び２次元 HN(CA)スペクトルを比較し、HN(CA)スペクトルに存在し、かつ HN(CO)スペクトルに存在しないシグナルを得ることで、^{1}H-^{15}N HSQC スペクトルにおける各シグナルが、どのアミノ酸の種類に属するかを決定する。

(3)一種類のアミノ酸残基のみを ^{13}C/^{15}N 二重標識し、その他の 19 種類のアミノ酸を ^{15}N のみで標識化した目的タンパク質の HN(CO)スペクトルから、それぞれのシグナルがどの種類のアミノ酸残基の後ろにある残基かを決定する。

(4)(2)(3)の結果とアミノ酸配列表から、アミノ酸の並びを利用してシグナルの帰属を行う。

(5)連続するアミノ酸の並び方が同一のものが２ヶ所以上あるものについては、２次元 H(N)CA と２次元 H(NCO)CA スペクトルを用いて、さらに手前の帰属済みの残基から帰属を決定する。手前の残基が同様の状況により帰属が不確定である場合は、さらに手前の残基から順次帰属を行う。

小麦胚芽無細胞蛋白質合成　選択的標識 ２次元ＮＭＲ　帰属　高分子量タンパク質

たなかりこう、こまつちえこ、こばやしくにこ、たなかたけし、こうのとしゆき

以下に、大腸菌チオレドキシンタンパク質における帰属例を示す。大腸菌チオレドキシンは、以下の配列（Fig.1）のようにフェニルアラニン残基を４つ持ち、Fig.2(a)に示すように、フェニルアラニン残基だけを ^{15}N 標識したものの HSQC スペクトルでは４つのシグナルが観測される。また、Fig.2(b)に示すように、セリン残基を ^{13}C/^{15}N 二重標識し、他のアミノ酸を ^{15}N 標識したものの HN(CO)スペクトルにおいては、３つあるセリン残基の後ろの残基の HN シグナルが観測される。(a)と(b)のスペクトルで一致するシグナルは、セリン残基の後ろにあるフェニルアラニン残基であるから、アミノ酸配列から判断して、図中に矢印で示したシグナルは、F12 であると決定される。同様にしてアミノ酸の並びかたが一通りである残基については、同様の方法ですべて一意的な帰属ができる。I72 と I75 のように手前の残基が両方ともグリシンであるような場合には、H(N)CA と H(NCO)CA のスペクトルを用い、Cαの化学シフトを介することにより、残基番号を特定できる。

```
SDKIIHLTDD SFDTDVLKAD GAILVDFWAE WCGPCKMIAP ILDEIADEYQ 50
GKLTVAKLNI DQNPGTAPKY GIRGIPTLLL FKNGEVAATK VGALSKGQLK 100
EFLDANLA 108
```

Fig.1 Amino acid sequence of *E. coli* thioredoxin.

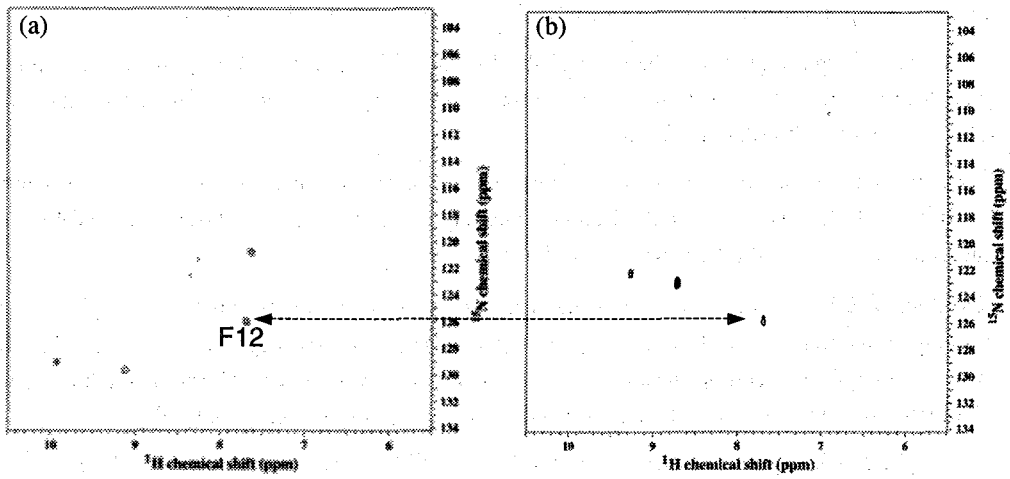

Fig. 2 HSQC spectrum of ^{15}N Phe labeled thioredoxin (a) and HN(CO) spectrum of ^{13}C/^{15}N Ser labeled and ^{15}N the other amino acids labeled thioredoxin.

この方法を高分子量タンパク質に適用するためには、重水素化したアミノ酸を用い、^{13}C/^{15}N 標識のアミノ酸を ^{13}C/^{15}N/D の三重標識に、^{15}N 標識のアミノ酸を ^{15}N/D の二重標識に変えて他は同様にしてタンパク質を合成し、測定を行えば良い。また、HN(CO)、HN(CA)、H(N)CA、H(NCO)CA の測定を全て TROSY タイプの測定に変更することも分子量増大によるシグナルの線幅の増大や感度低下を抑えるのに有効である。このような工夫により、分子量４万以上のタンパク質においても、低濃度のサンプルを用い、簡便にシグナルの帰属を行うことが可能になった。本学会では、ＭＡＧＩＣＡＬ法を高分子量蛋白質に適用した例を発表する。

STUDY OF THE HYDROPHOBIC CAVITY OF β-CRYPTOGEIN THROUGH LASER-POLARIZED XENON NMR SPECTROSCOPY

Ha Phuong Thu[1)], *Patrick Berthault, Gaspard Huber*[2)]

[1)] Institute of Chemistry, Vietnamese Academy of Sciences and Technology

[2)] DSM/DRECAM/Service de Chimie Moleculaire, URA CEA/CNRS 331, CEA/Saclay, FRANCE

Introduction: Elicitins are small proteins that induce a hypersensitive response in plants, even including necrosis, cell death, and subsequently lead to an unspecific systemic-acquired resistance against other pathogens. Their ability to bind sterols has also been recognized and elicitins represent a class of sterol carrier proteins. Moreover the binding of sterol seems to be a prerequisite in elicitin recognition by their receptor. The crystal structure of β-cryptogein, a 10 kDa elicitin, has been determined by X-ray diffraction, as well as that of other basic elicitin. The solution structure of β-cryptogein has also been determined by NMR. It has five α-helices, three disulfide bridges and contains a large inner hydrophobic cavity.

In 2001, it was noticed that β-cryptogein contains structural motifs similar to those of nonspecific lipid transfer proteins (ns-LTP). However ns-LTP can't bind sterols.

The morphology and behaviour of the hydrophobic cavity of β-cryptogein thus appear very different from those of ns-LTPs and deserve further investigation in view of the biological relevance of sterol binding in elicitins.

It seemed interesting to study them through our recently introduced tools using xenon-based NMR [1,2,3]. By using thermal dissolved and laser-polarized gas in liquid-state NMR, the interaction of xenon with β-cryptogein has been studied.

Experimental: For all the experiments under xenon pressure, solutions containing lyophilized β-cryptogein without any buffer in D_2O (450 µl) were previously degassed in the NMR tube through several freezepump-thaw cycles. The pH value was about 7.4 (no pH adjustment). Medium-wall NMR tubes (Wilmad 524-PP) closed by J. Young valves were used.

The NMR experiments were run on a Bruker DRX600 spectrometer (14 Tesla) at 293 K. Laser-polarized xenon was produced in the batch mode by using the apparatus and protocol previously described [4].

Laser-polarized xenon was transferred by condensation through a vacuum line into the NMR tube containing the protein solution. This operation occurred in the fringe of the NMR superconductive magnet in order to avoid important loss of polarization during xenon sublimation and freezing [5].

The SPINOE (spin polarization-induced nuclear Overhauser spectroscopy) experiments[6,7] were performed on a solution containing lyophilized β-cryptogein in D2O (1.6

mM). 96% Xe from Chemgas was used. The concentration of dissolved gas was 5.2 mM, considering a xenon solubility of 44 $\mu MkPa^{-1}$ at 293 K.

Results and Discussions: The typical NMR spectra, acquired with different mixing times (300, 500 and 700 ms) were shown in figure 1. Two successive spin polarization-induced nuclear Overhauser spectroscopy experiments performed with the same amount of dissolved laser-polarized gas exhibited significant response of the protons in through-space interaction with xenon. After assigning the protons, 30 Xe-H interactions are detected. These protons are situated in the inner core of the protein.

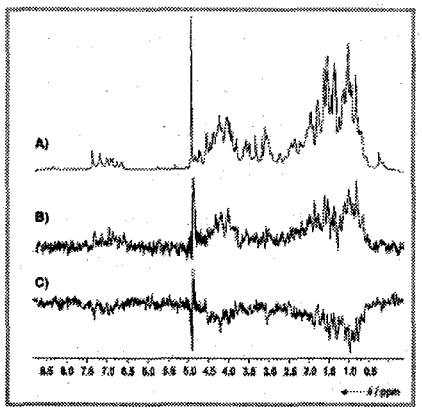

Figure 1: ..... A) ^{1}H-NMR spectrum of β-cryptogein in D_2O. SPINOE subspectra with B) positive or C) negative xenon polarization.

Conclusion: These results support the idea that xenon is a good probe for hydrophobic protein regions.

References

1. C. Landon, P. Berthault, F. Vovelle, H. Desvaux, Protein Sci. 2001, 10, 762-770
2. P. Berthault, C. Landon, F. Vovelle, H. Desvaux, C. R. Acad. Sci. Ser. IV Biophys, 2001, 2, 327-332
3. L. Dubois, P. Da. Silva, C. Landon, J.G. Huber, M. Ponchet, F. Vovelle, P. Berthault, H. Desvaux, J. Am. Chem. Soc. 2004, 126, 15738-15746
4. H. Desvaux, T. Gautier, G. le Goff, M. Petro, P. Berthault, Eur. Phys. J. D 2000,12, 289-296.
5. M. Gatzke, G. D. Cates, B. Driehuys, D. Fox, W. Happer, B. Saam, Phys. Rev. Lett. 1993, 70,690-693
6. G. Navon, Y.-Q. Song, T. Room, S. Appelt, R. E. Taylor, A. Pines, Science 1996, 271, 1848-1851

P007

Signal enhancement by improved extraction procedures and its application to metabolic flux analysis

○Yasuyo Sekiyama[1], Takashi Hirayama[2,3,4], Kazuo Shinozaki[1,] and Jun Kikuchi[1, 2, 3,5]

[1] RIKEN Plant Science Center, [2] Int. Grad. Sch. of Arts and Sci., Yokohama City Univ., [3]CREST, JST, [4]RIKEN Envioron. Mol. Biol., [5]Grad. Sch. of Bioagri. Sci., Nagoya Univ.

Introduction

Metabolomics is an approach for comprehensive analysis of time-related biochemical responses and reactions in the cell. NMR techniques can provide information of the global pool of all measurable metabolites, including both soluble low molecular weight compounds and insoluble macromolecules. We have been developing new methodologies for metabolomics by combination of stable isotope labeling and multi-dimensional hetero-nuclear NMR analysis [1-3]. In the last meeting, we reported that hexafluoroacetonedeuterate (HFA)/HEPES-d_{18} buffer is useful not only for comprehensive extraction of a variety of metabolites but also to obtain constant chemical shifts in NMR spectra for unambiguous assignment of each signal [4]. However, the HFA extraction sometimes causes significant broadening of NMR signals and decreases detectable signals in multi-dimensional NMR spectra especially in the case of bacteria and animals. In this conference, we describe the improved extraction methodologies that can be applicable for a wide range of organisms and their application to metabolic flux analysis (Fig.1).

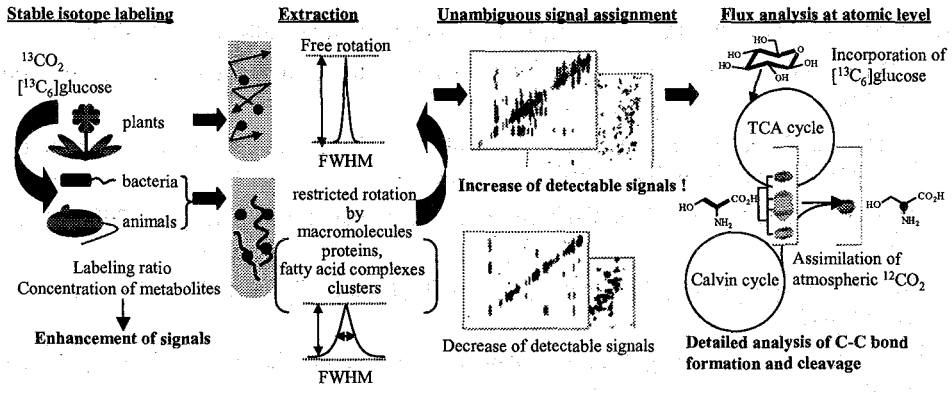

Figure 1. Concept of this study for improvement of NMR-based metabolomics approach.

Keywords: metabolomics, stable isotope labeling, extraction procedure, metabolite identification, metabolic flux analysis

Extraction methodologies

The problem of spectral overlap in 2D spectroscopy encountered in NMR-based metabolomics can be alleviated by increasing the spectral dimensionality to 3D. Several powerful schemes for establishing *J* connectivity, which is useful for unambiguous assignment of metabolites, rely on transferring magnetization in several steps. We expected that a large amount of macromolecules extracted by HFA causes the increase in the line width and the decrease in the efficiency of magnetization transfer by spin-spin relaxation. In order to establish extraction methodologies which can be applicable for a wide range of organisms, we reinvestigated extraction methodologies using photosynthetic bacteria, *Rhodobacter sphaeroides* IL106, which shows pronounced broadening of NMR signals and gives less than 10 cross peaks in the 3D HCCH-COSY spectrum. Although we tried to remove macromolecules in HFA/HEPES extract by ultracentrifugation, ultrafiltration, and gel filtration, the quality of NMR spectra were not improved. Therefore, we evaluated a series of NMR solvents by distribution of FWHM (full width at half-maximum) of the signals observed in ^{1}H-^{13}C HSQC spectra. Non-polar organic solvents, such as CD_3OD, acetone-d_6, iPrOD-d_8 and CD_3CN exhibited significantly nallowing of line width. Examples of the resulting histograms are shown in Fig. 2. Furthermore, we evaluated the solvency of these solvents by the number and total intensity of the ^{1}H-^{13}C HSQC signals measured by both 700 MHz NMR with cryogenic probe and 500 MHz NMR with conventional probe (Fig. 3). While little differences in the distribution of the line width were observed among the 4 solvents described above, CD_3OD dissolved about two times of metabolites those extracted by the other 3 solvents. Therefore we decided to optimize extraction system using CD_3OD. Compared to these non-polar organic solvents, polar aqueous solvents seemed to suffer the sensitivity loss of the 700 MHz NMR with cryogenic probe. The observation can be deduced to be the dielectric loss of ionic

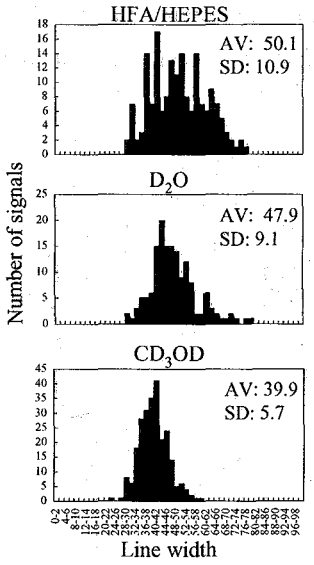

Figure 2. Distribution of FWHM of ^{1}H-^{13}C HSQC signals of ^{13}C-labeled *R. sphaeroides* in various solvents (700 MHz with cryogenic probe, 298K). FWHM value in these histograms are given by $[(f_2$ FWHM$)^2+$ (0.35 x f_1 FWHM$)^2]^{1/2}$. Average (AV) and standard deviation (SD) are indicated in each histogram.

aqueous solutions, especially at higher magnetic field, as predicted by Horiuchi et al. [5]

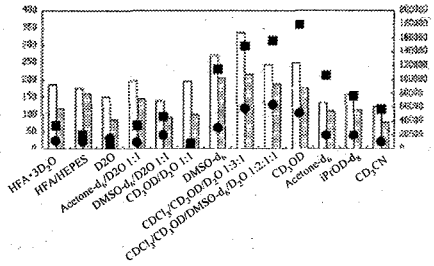

Figure 3. Comparison of ^{1}H-^{13}C HSQC spectra of ^{13}C-labeled *R. sphaeroides* in various solvents.
□ - - Number of signals observed at 700 MHz with cryogenic probe
■ - - Number of signals observed at 500 MHz with conventional probe
■ - - Total intensity observed at 700 MHz with cryogenic probe
● - - Total intensity observed at 500 MHz with conventional probe

To keep pH and chemical shifts constant, we optimized concentration of HEPES buffer as described in the case of HFA system [4]. Based on the solubility of metabolites and line width of the NMR signals, we determined the concentration of HEPES as 10 mM (CD_3OD/200 mM HEPES = 95:5). Only 3% of the ^{1}H-^{13}C HSQC signals showed slight chemical shift changes ($\Delta\delta_c$ 0.2-3.0 ppm, $\Delta\delta H$ 0.001-0.2 ppm) when 2 mM citrate was added to the CD_3OD/HEPES extracts of *R. sphaeroides*. In order to confirm that the CD_3OD/HEPES is widely versatile, we compared the quality of ^{1}H-^{13}C HSQC spectra of HFA/HEPES and CD_3OD/HEPES extracts of a variety of organisms. Line width was significantly decreased and detectable signals were increased by CD_3OD/HEPES extraction (Fig. 4). We also examined other organisms, poplar (plant), *Escherichia. coli* (bacteria), and *Bombyx mori* (animal). Similarly, effects of line narrowing by CD_3OD/HEPES extraction were remarkable in bacterial and animal samples that seem to contain a large amount of macromolecules.

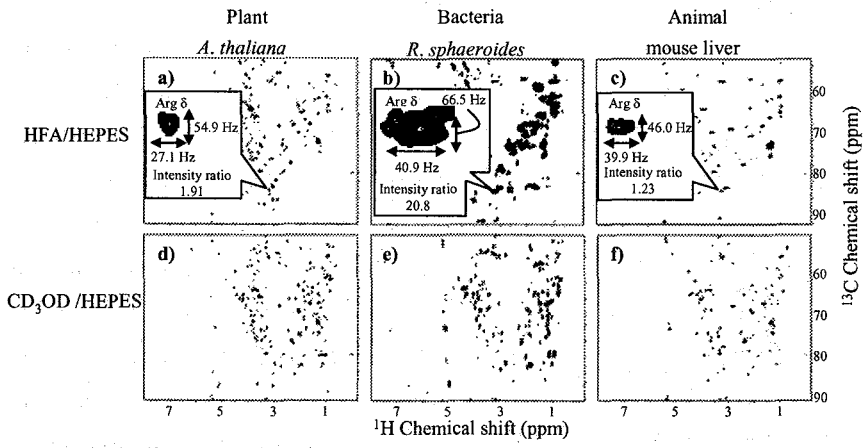

Figure 4. ^{1}H-^{13}C HSQC spectra of a series of ^{13}C-labeled organisms (500 MHz). a) HFA/HEPES extract of *A. thaliana*, b) HFA/HEPES extract of *R. sphaeroides*, c) HFA/HEPES extract of mouse liver, d) CD_3OD/HEPES extract of *A. thaliana*, e) CD_3OD/HEPES extract of *R. sphaeroides*, f) CD_3OD /HEPES extract of mouse liver. Enlargements of the Arg δ signal were depicted in a), b) and c) with FWHM values and intensity ratio.

Detailed assignments of the metabolites observed in CD_3OD/HEPES extracts are now in progress. Furthermore, we are going to obtain information about the insoluble biopolymers, which is required for understanding the all functions of metabolites and metabolic fluxes in whole cells, by high-resolution magic angle spinning (HR-MAS) analysis.

Application to metabolic flux analysis at atomic level

In addition to the aforementioned advances, we are also establishing a methodology for the uniform stable isotope labeling of plants and metabolic flux analysis. Improved extraction methodology and quality of the NMR spectra will make it possible to assign all soluble metabolites and monitor the metabolic fluxes in detail. We monitored the incorporation ratio of [$^{13}C_6$]glucose into *A. thaliana* and contribution of atmospheric $^{12}CO_2$ assimilation by LC-MS and ^{1}H -^{13}C HSQC spectra (Fig. 5a). To obtain information about the biochemical reactions, C-C bond formation and cleavage of main metabolites were analyzed based on the ^{13}C-^{13}C coupling pattern (Fig. 5b). A detailed time-course of the labeling and the differences in the ^{13}C-incorporation profiles of the major metabolites will be discussed at the conference.

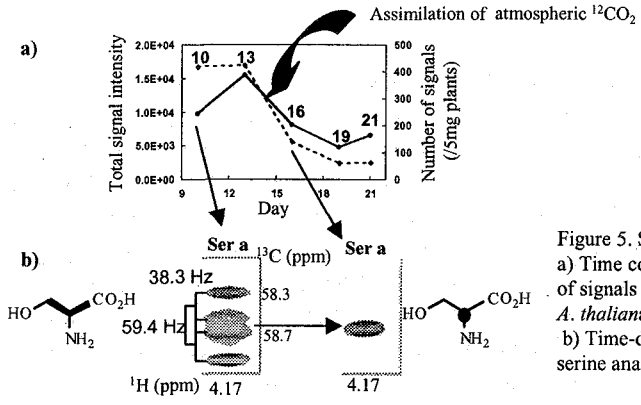

Figure 5. Strategies for metabolic flux analysis. a) Time course of the total intensity and number of signals observed in ^{1}H-^{13}C HSQC spectra of *A. thaliana* grown on [$^{13}C_6$]glucose medium.; b) Time-dependent C-C bond cleavage of serine analyzed by ^{13}C-^{13}C coupling constant.

- References -

[1] Kikuchi, J.; Shinozaki, K. and Hirayama, T. (2004) *Plant Cell Physiol.* 45, 1099-1104.

[2] Kikuchi, J. and Hirayama, T. (2005) *Biotech. Agri. Forestry* 57, 94-101.

[3] Kikuchi, J. and Hirayama, T. (2006) *Methods Mol. Biol.* (in press).

[4] Sekiyama, Y. et al. (2005) The 44th Annual NMR Meeting and Asia-Pacific NMR Symposium.

[5] Horiuchi, T. et al., (2005) *J. Magn. Reson.*, 174, 34-42.

P008

Mg^{2+}-induced conformational changes of C-terminal domain of calmodulin

Wakana Ohashi, Toshio Yamazaki, Hiroshi Hirota
RIKEN Genomic Sciences Center

[Summary]
EF-hands, major Ca^2 binding motifs, play important rules such as modulator of Ca^2 signals and Ca^2 buffers through the Ca^{2+} binding/release. While EF-hands bind to Ca^2 with high affinity and selectivity, some EF-hands also bind to Mg^{2+} with lower affinity. Here, we performed the structural analysis of the Mg^{2+}-loaded form of C-terminal domain of calmodulin containing two EF-hands (EF-hand III and EF-hand IV). For the structural analysis of the Mg^{2+}-loaded form of C-terminal domain of calmodulin, we constructed a mutant where two aspartates were substituted for the two glutamates at –Z position of EF-hand. Mg^{2+} titration experiment showed that Mg^{2+} binds to EF-hand IV first. The solution structure of Mg^{2+}-loaded form had typical EF-hand structure, helix-loop-helix structure. From the comparison of EF-hand structures, it was found that EF-hand III of Mg^{2+}-loaded form is similar to apo form and EF-hand IV is similar to Ca^{2+}-loaded form.

[Introduction]
EF-hands sense the transient increase of cytosolic Ca^{2+} concentration from less than 0.1 μM in resting cells to 1-10 μM in an activated cells and bind to the Ca^{2+} even in the presence of an excess amount of Mg^{2+}. The intracellular concentration of Mg^{2+} is on the order of mM, which is about $10^{4}\sim^{5}$ fold higher than that of Ca^{2+}. Mg^{2+} has similar physical and chemical properties to Ca^{2+} and can bind to EF-hands. Calmodulin, highly ubiquitous EF-hand protein in eukaryotic cells, is responsible for converting the intracellular Ca^{2+} signal into a wide range of physiological processes through the Ca^{2+} binding/release to the EF-hand motif. Previous studies have shown that Mg^{2+} binds to EF-hand of calmodulin and some of the calmodulin targets display decreased affinities for calmodulin in the presence of an excess amount of Mg^{2+}. While the tertiary structure of calmodulin for apo and Ca^{2+}-loaded form has been determined, the structure of Mg^{2+}-loaded form is still unsolved. Here, we performed NMR studies on the Mg^{2+}-loaded form of EF-hand of C-terminal domain of calmodulin. For the structural analysis, the optimization of experimental condition including the mutagensis was performed. The information of Mg^{2+} binding property was obtained by titration experiments. Using the C-terminal domain of calmodulin mutant, the solution structure of Mg^{2+}-loaded form was solved.

[Methods]
A mutant where two aspartates were substituted for the two glutamates at –Z position of EF-hands of C-terminal domain of calmodulin was constructed. The ^{15}N- and ^{13}C, ^{15}N –labeled proteins were produced by the E.coli expression systems and purified by anion

Keywords: EF-hand, calmodulin, Mg^{2+}

exchange chromatography and hydrophobic interaction chromatography. For the titration experiments, the samples was prepared as 1 mM of uniformly ^{15}N -labeled protein in 10 mM MES (pH6.5), 100 mM KCl and 95:5 of H_2O: D_2O. The Mg^{2+} titration experiments were performed by recording a series of ^{15}N HSQC spectra with uniformly ^{15}N-labeled protein in the presence of increasing amounts of Mg^{2+} ranging from 1 to 100 molar equivalent ratios. The samples used for the structural determination were prepared as 1 mM of uniformly1 ^{15}N- or ^{13}C, ^{15}N-labeled protein in 10 mM MES (pH6.5), 100 mM KCl, and 100 mM $MgCl_2$, and 95:5 of H_2O: D_2O. NMR spectra were measured at 323K on Bruker AVANCE600. Resonance assignments were made by analyses of a series of multidimensional heteronuclear NMR spectra. The structure calculation was performed using CYANA (1.0.7).

[Results and Discussion]

Mg^{2+} binds to EF-hand IV first and then binds to EF-hand III.

The protein was titrated with various concentrations of Mg^{2+} (i.e., 1, 2, 3, 4, 5, 6, 7, 8, 9, 10, 20, 30, 40, 50, 60, 70, 80, 90 and 100 mol equiv/protein). The glycine residues at G96 and G132 are located at the fourth position of the 12-residue loop in EF-hands III and IV, respectively. When the 3 equivalent of Mg^{2+} was added to the protein, the resonances of G132 displayed substantial line broadening, whereas the resonances of G96 remained almost unchanged. When the 10 equivalent of Mg^{2+} was added to the protein, the resonances of G96 displayed substantial line broadening, suggesting that Mg^{2+} interacts to EF-hand IV loop first and then interacts to EF-hand III loop.

Solution Structure of Mg-loaded form of C-terminal domain of calmodulin mutant

The structure was calculated by use of upper limit distance constraints inferred from NOEs and backbone dihedral angle constraints based on the TALOS program. The structure of the entire polypeptide main-chain has been defined except for the loops of EF-hands III and IV and at the amino and carboxyl terminal. Some resonances from residues in the EF-hands III and IV loop region exhibited very weak NMR intensities. The secondary structure of Mg^{2+}-loaded C-terminal domain of calmodulin mutant is very similar to that seen in the reported structure of calmodulin. However, the overall tertiary fold of Mg^{2+}-loaded C-terminal domain of calmodulin mutant is different from the overall folds of apo and Ca^{2+}-loaded C-terminal domain of calmodulin wild type. Structure comparison was made in the EF-hands III and IV between the Mg^{2+} -loaded form and apo form and between the Mg^{2+} -loaded form and Ca^{2+}-loaded form, respectively, using the RMSDs of the main-chain atoms. It was found that the structure of EF-hand III of the Mg^{2+} -loaded form resembles to that of apo form and the structure of EF-hand IV is similar to that of Ca^{2+}-loaded form.

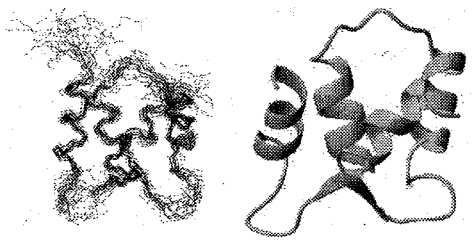

Fig. Solution structure of Mg^{2+}-loaded form of C-terminal domain of calmodulin mutant (Left). Superimposition of 20 structures (Right) Ribbon diagram

P009

human tripartite motifタンパク質ファミリーのRINGドメインの溶液構造

（理研・GSC[1]，東工大院総理[2]，東大院理[3]）
○宮本和英[1]，木川隆則[1,2]，栃尾尚哉[1]，佐藤真奈美[1]，苫米地由里[1]，小柴生造[1]，井上真[1]，横山茂之[1,3]

Solution Structure of the RING domain of the human tripartite motif protein family

([1]RIKEN Genomic Sciences Center, [2]Interdisciplinary Graduate School of Science and Engineering, Tokyo Institute of Technology, [3]Graduate School of Science, University of Tokyo)
○ Kazuhide Miyamoto[1], Takanori Kigawa[1,2], Naoya Tochio[1], Manami Sato[1], Yuri Tomabechi[1], Seizo Koshiba[1], Makoto Inoue[1], Shigeyuki Yokoyama[1,3]

The tripartite motif (TRIM) is comprised of an N-terminal RING domain, one or two B-box domain, and a coiled-coil domain. Many TRIM function as E3 ubiquitin ligases *via* its RING domain. However, the TRIM RING structure remains unknown. In this study, we determined the solution structure of the RING domain of the human TRIM32 by NMR spectroscopy. The RING domain binds two zinc atoms in a stable cross-brace fashion. The structural core consists of one α-helix and three β-strands. The structure was found to have a highly-conserved hydrophobic groove, which was identified as the putative binding site of E2s. This site is significant similar to those of the previously known RING structures, suggesting that the RING domain binds to the E2s in a similar manner. This is the first report of the RING structure of the TRIM family, and therefore provides a molecular basis for further understanding the function of the TRIM family in biological processes.

[序論]

TRIMタンパク質ファミリーは，RINGドメインおよびB-boxドメインからなるTRIM motifをN末端に有していることが特徴であり，GBBB syndrome，familial mediterranean fever，mulibrey nanism，Limb girdle muscular dystrophyといった疾病に関ることが知られている[1]．TRIMタンパク質に含まれるTRIM motifのRINGドメインには，E3ユビキチンリガーゼとして機能するものがあると知られているが，未だその構造は分かっていない．そこで，本研究では，TRIM motifのRINGの構造とその機能との関連性を明らかにする為に，Limb girdle muscular dystrophyに関与する653残基からなるTRIM32

RING domain, TRIM, cell-free synthesis, zinc binding protein, NMR

みやもとかずひで，きがわたかのり，とちおなおや，さとうまなみ，とまべちゆり，こしばせいぞう，いのうえまこと，よこやましげゆき

の RING ドメイン(TRIM32 RING)の溶液構造を NMR 法で決定した．今回決定した RING 構造は，TRIM RING の最初の構造であり，既知の RING 構造との比較検討も行った．

[方法]

無細胞タンパク質合成系により、$^{13}C/^{15}N$標識されたTRIM32 RINGを調製した。Bruker社のAVANCE600 およびAVANCE700 を用いる多核多次元NMR測定後、得られたスペクトルをNMRPipe、NMRViewおよびKujiraで解析することにより、主鎖および側鎖の帰属を行った。^{15}N-edited NOESYと^{13}C-edited NOESYのNOE自動帰属と立体構造計算にはCYANA-CANDID(ver.2.0.17)を用いた。

[結果と考察]

CYANA-CANDID を用いる立体構造計算の結果，得られた構造を Fig.1 に示した．１本のα-helix と３本のβ-strand から構成され，二つの ZN(II)と結合した classical な RING FOLD であることが分かった． 既知の RING 構造との electrostatic surface の比較・検討を行ったところ，類似した hydrophobic cleft があることを見出し，これを putative E2-binding site と同定した．今回始めて TRIM RING の構造解析が行われたことによって，TRIM RING は，他の E3 RING と同じ manner で E2 と結合することが分かった．

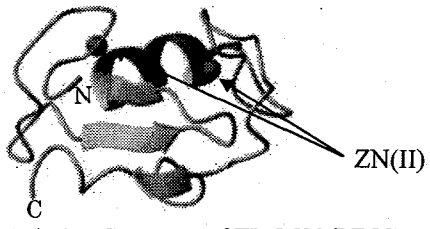

Fig. 1　Solution Structure of TRIM32 RING

References

[1] E. Kudryashova, D. Kudryashov, I. Kramerova and M. J. Spencer, JMB, **354**, 413-424(2005).

P010

Exhaustive Structural Analysis by NMR Reveals a Diverse World of the Pleckstrin Homology Domain

([1]RIKEN GSC, [2]JEOL, [3]The University of Tokyo, [4]Kazusa, [5]RIKEN RCAI and [6]Tokyo Institute of Technology)

○ Hua Li[1], Tamiji Nakanishi[1], Manami Sato[1], Tetsuya Suetake[1], Misao Yoneyama[1], Tadashi Tomizawa[1], Naoya Tochio[1], Kohei Saito[1], Fumiaki Hayashi[1], Nobuaki Nemoto[2], Kenya Izumi[1], Takushi Harada[1], Makoto Inoue[1], Seizo Koshiba[1], Takaho Terada[1], Akiko Tanaka[1], Sumio Sugano[3], Yoshihide Hayashizaki[1], Osamu Ohara[4,5], Takanori Kigawa[1,6], and Shigeyuki Yokoyama[1,3]

The PH domain (pleckstrin homology domain) is the 11th most abundant domain in the human genome (*1*), and it occurs in a wide range of proteins involved in cellular signaling, cytoskeletal organization, membrane trafficking and other processes (*2, 3*). The PH domain was originally identified in 1993 as a stretch of 100~120 amino acids that appears twice in the platelet protein pleckstrin. Structural characterization of several PH domains quickly followed their identification. Each of the PH domain structure determined possesses an almost identical core β-sandwich structure, despite their pair-wise sequence identities are quite low, ranging from about 10% to 30%. GSC, RIKEN performed an exhaustive structural analysis and characterization of the PH domain because of its wide distribution in the human genome, low pair-wise sequence identity and functional diversity. Up to now, more than 60 structures of the PH domains have been deposited in PDB, about half of which was contributed by GSC, RIKEN. All of the PH domain NMR samples were ^{13}C, ^{15}N-labeled, and synthesized by the cell-free protein expression system (*4, 5*). First, the amino acid sequence of the PH domain selected by GSC is distributed almost evenly over the primary sequence space of the PH domain. The detailed structural characterization suggested that most of the PH domains may have functions other than phosphoinositide binding, the best described function of the PH domain (Fig. 1). Finally, each of the PH domain structure is hopefully to serve as a template for the homology modeling, which is limited because of the low sequence identity.

Key words: PH (pleckstrin homology) domain, phosphoinositide binding, NMR, cell-free protein expression system

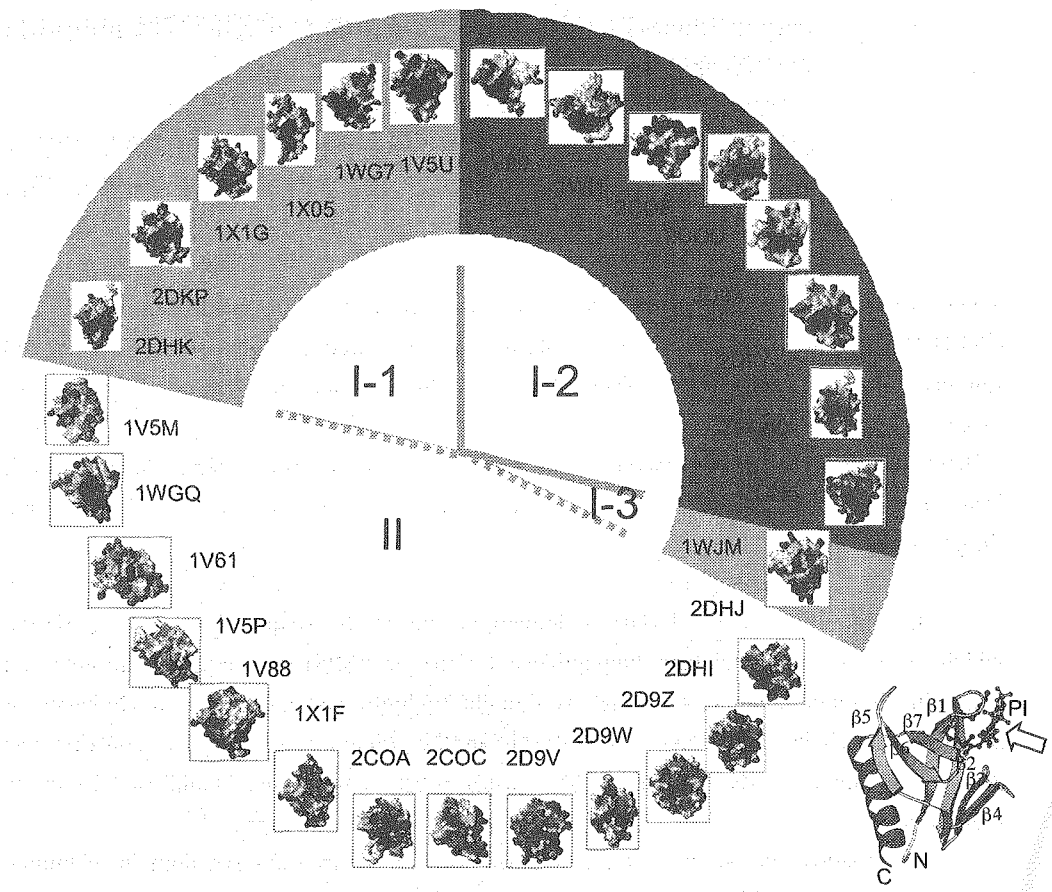

Fig. 1 Classification of the PH domain according to its phosphoinositide (PI) binding affinity. The electrostatic potential surface of each PH domain studied in GSC is shown along with its PDB accession code. The consensus sequence ($KX_n[K/R]XR$, X is any residue type) is reported for the PH domain that binds PI using its β1-β2 and β3-β4 loops. The PH domains are classified into two groups according to the consensus sequence: Group I, the PH domain that is capable of binding PI, and Group II, the PH domain that does not bind PI or binds PI very weakly. Moreover, according to how much they satisfy the consensus sequence and the binding site, the PH domains in Group I are divided into three subgroups, Group I-1, the PH domain that binds PI strongly, Group I-2, the PH domain that binds PI with intermediate affinity, Group I-3, the PH domain binds PI using β1-β2 and β5-β6 loops. A representative structure of the PH domain in complex with PI (PDB code: 1fao) is shown in the lower right panel. The arrow gives the direction along which the electrostatic potential surface drawing of each PH domain is made.

References:
1. International Human Genome Sequencing Consortium (2001) *Nature* **409**, 860-921.
2. Lemmon, M. A. and Ferguson K. M. (2000) *Biochem. J.* **350**, 1-18.
3. Lemmon, M. A. (2004) *Biochem. Soc. Trans.* **32**, 707-711.
4. Kigawa, T., Yabuki, T., Yoshida, Y., Tsutsui, M., Ito, Y., Shibata, T. and Yokoyama, S. (1999) *FEBS Lett.*, **442**, 15-19.
5. Kigawa, T., Yabuki, T., Matsuda, N., Matsuda, T., Nakajima, R., Tanaka, A. and Yokoyama S. (2004) *J. Struct. Funct. Genomics*, **5**, 63-68.

P011

Isopeptidase-T1 の UBA ドメインの C 末端領域は ubiquitin との結合に寄与する

（理研・GSC[1]，東工大院総理[2]，東大院理[3]）
○趙　晨華[1]，木川　隆則[1,2]，栃尾　尚哉[1]，加藤　真菜美[1]，佐藤真奈美[1]，小柴　生造[1]，原田　拓志[1]，渡辺　暁[1]，田仲　昭子[1]，横山茂之[1,3]

The C-terminal region of isoT-1 UBA domain contributes to its ubiquitin-binding

([1]RIKEN Genomic Sciences Center, [2]Interdisciplinary Graduate School of Science and Engineering, Tokyo Institute of Technology, [3]Graduate School of Science, University of Tokyo)
○Chenhua Zhao[1], Takanori Kigawa[1,2], Naoya Tochio[1], Tadashi Tomizawa[1], Manami Kato[1], Manami Sato[1], Seizo Koshiba[1], Takushi Harada[1], Satoru Watanabe[1], Akiko Tanaka[1], and Shigeyuki Yokoyama[1,3]

The ubiquitin-associated (UBA) domain is one of the frequently occurring motifs, which recognizes ubiquitin tags. Isopeptidase T (isoT or USP5) is an abundant protein and exists in all mammalian cells, which is thought to hydrolyze the isopeptide linkages of polyubiquitin chains and play a critical role in the ubiquitin recycling. It contains one ZnF-UBP domain in its N-terminus and two UBA domains (isoT-1 and isoT-2) in its C-terminus.

In this study, we determined the solution structure of isoT-1 UBA domain of human isopeptidase T by NMR spectroscopy. We found that isoT-1 UBA domain consisted of a typical UBA fold, a three-helix bundle structure, and an additional unique structured C-terminal region which was usually unstructured in other UBA domains. The isothermal titration calorimetry (ITC) and NMR perturbation experiments revealed that isoT-1 UBA domain had remarkable high affinity for ubiquitin and its largely hydrophobic surface contributed to the binding. A shorter construct which lacks the C-terminal region was found to form a folded structure, although its ubiquitin-binding affinity was much lower. These results indicate that the unique structured C-terminal region is indispensable for the ubiquitin-binding of isoT-1 UBA domain.

[序論]

UBA ドメインは約 45 残基から構成され、脱 ubiquitin 化酵素などに共通に見られるド

isopeptidaseT, ubiquitin, USP5, UBA domain, NMR, ITC

ちょうしんか，きがわたかのり，とちおなおや，かとうまなみ，さとうまなみ，こしばせいぞう，はらだたくし，わたなべさとる，たなかあきこ，よこやましげゆき

メインとして最初に同定された。UBP（ubiquitin specific protease ）ファミリーに属するIsopeptidase TはisoT-1及びisoT-2 の二つのUBA domainを含んでおり、polyubiquitin鎖のリサイクルに強く関与していることから、この2つのUBAドメインはubiquitinの認識に深く関与していることが示唆されている。しかしながら、これらUBAドメインの立体構造は未だわかっていない。そこで、Isopeptidase T の UBA ドメインのmonoubiquitin及びpolyubiquitin鎖の認識機構及び機能制御を構造生物学的な観点から解明する為に、本研究では、Isopeptidase T の isoT-1 UBA domain の溶液構造をNMR法で決定した。さらに、ITC (Isothermal titration calorimetry) によるubiquitinとのKdの測定や、NMR perturbationの実験により異なるコンストラクトとの比較も行った。

[方法]

無細胞タンパク質合成系により、$^{13}C/^{15}N$ 標識されたisoT-1 UBA ドメインを調製した。Bruker社のAVANCE600およびAVANCE800を用いる多核多次元NMR測定後、得られたスペクトルをNMRPipe、NMRViewおよびKujiraで解析することにより、主鎖および側鎖の帰属を行った。^{15}N-edited NOESY と ^{13}C-edited NOESY のNOE自動帰属と立体構造計算にはCYANA-CANDID(ver.2.0.17)を用いた。

[結果と考察]

CYANA-CANDID を用いる立体構造計算の結果，得られた構造を Fig.1 に示した。今回立体構造を決定した isoT-1 UBA domain の構造と、PDB 登録されている既知のUBAの構造とを比較・検討した。この結果、既知のUBAのFOLDと同様に、3本のヘリックスから構成されているが、3本目のヘリックスからC末端までに長く延びたループが構造形成に深く関与しているという新規の知見を得た。このC末端のループが果たす役割を ubiquitin 結合という観点から解明するために、ITC 測定及び NMR perturbation実験を行った。ubiquitinとのKdは46.4μmで、配列上にMGFというモチーフのところに信号が大きく動いていることがわかった。また、C末端領域を切った短いコンストラクトも作り、^{15}N-HSQC スペクトルから何らかの構造を取っていることがわかり、ubiquitinとのKdが著しく低くなることもわかった。Isopeptidaseの isoT-1 UBA domainのC末端領域の役割がubiquitinとの結合に大きく寄与していることが初めてわかった。

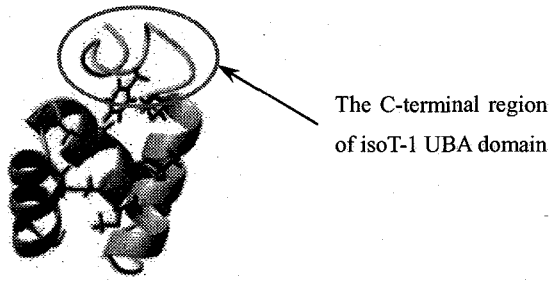

Fig. 1 Solution Structure of isoT-1 UBA domain in isopeptidase T

P012

圧力可変NMRによる蛋白質cavity周辺における立体構造の揺らぎ
−T4 リゾチーム cavity 変異体−

([1]近畿大学・生物理工学 [2]理化学研究所SPring-8 [3]オレゴン大学化学科 [4]理化学研究所GSC [5]東京大学・理学 [6]グローニンゲン大学生物物理化学)

○ [1]前野覚大 [2]北原亮 [3]Frederick W. Dahlquist [4,5]横山茂之 [6]Frans A. A. Mulder [1,2]赤坂一之

Variable pressure NMR reveals conformational fluctuation around cavities in a protein: A cavity mutant of T4 Lysozyme

[1]Akihiko Maeno, [2]Ryo Kitahara, [3]Frederick W. Dahlquist, [2,4,5]Shigeyuki Yokoyama, [6]Frans A. A. Mulder and [1,2]Kazuyuki Akasaka

[1]Dep. of Biotec. Sci., Grad. Sch.of Biology-Oriented Sci. and Tec., Kinki Univ., [2]RIKEN SPring-8 Center, [3]Inst. of Mol. Biol. and Dep. of Chem., Univ. of Oregon, USA, [4]RIKEN Genomic Sciences Center, [5]Grad. Sch.l of Sci., Univ. of Tokyo, [6]Dep. of Biophy. Chem., Univ. of Groningen, Netherlands

We have carried out $^{15}N/^{1}H$ TROSY-HSQC experiments on wild type (WT) and the cavity-creating mutant (L99A) of T4 lysozyme at pressures between 3 and 300 MPa. In L99A, a large cavity (atomic defect) containing a water molecule is created in the hydrophobic core part of T4 lysozyme. With increasing pressure, some cross-peak intensities of L99A were reduced preferentially for residues surrounding the cavity, while all the cross-peaks remain intact for WT. This indicates that the folded L99A conformer fluctuates to a lower-volume conformer with preferential disorder around the cavity, which increases population at higher pressure. The fact that the preferential reduction of cross peaks in L99A is not accompanied by the appearance of typical "denatured" signals suggests that the disordered segments are likely to be multi-conformational or undergo relatively slow motions in millisecond ~microsecond time range. In any case, the result verifies that L99A has an alternative conformer with a slightly higher free energy with local fluctuations around the cavity.

The presence of a higher energy conformer with fluctuations around the cavity was previously detected by relaxation dispersion NMR spectroscopy [Mulder et al. Nat. Struct. Biol., 2001, 8, 932-935, Nikolai R. Skrynnikov et al., J. Am. Chem. Soc., 2002, 124, 12352-12360]. Our present result supports the above conclusion from independent measurements using pressure. Interestingly, a recent high-pressure crystallography study revealed that the number of water molecules within the cavity of L99A increases considerably

Key word:High pressure NMR, relaxation dispersion NMR,conformational fluctuation, cavity

著者; まえの あきひろ、きたはら りょう、ふれでりっく だるくぃいすと、よこやま しげゆき、ふらんす むるだあ、あかさか かずゆき

with increasing pressure [Collins et al., PNAS, 2005, 102, 16668-16671]. Combined with the latter observation in crystal, it is likely that the higher energy, low-volume conformer is associated with the higher degree of penetration of water molecules into the cavity.

蛋白質の構造揺らぎは、その機能発現メカニズムの観点から重要と考えられている。本発表では比較的遅い、すなわちマイクロ秒からミリ秒で生じる構造揺らぎと分子内キャビティーの関係について議論する。T4 リゾチームの野生型(WT)とキャビティー変異体(L99A)に対して 3 から 300MPaまでの圧力範囲で二次元$^{15}N/^{1}H$ TROSY-HSQC 測定を行った。加圧に伴い、WTとは対照的に分子内キャビティーを持つL99A変異体では、キャビティー周辺の残基における信号強度が選択的に減少した。加圧に伴う信号強度の減少は、それらの部位でより体積の小さな高エネルギー状態に構造転移したことを示す。変性状態を示す新たな信号の出現は見られなかった事から、この高エネルギー構造は、キャビティー周辺でマイクロ秒からミリ秒オーダーで揺らいだ構造をしていると考えられる。同様に、緩和拡散NMR測定法によりキャビティー周辺領域で化学交換が観測されている。[Mulder et al. Nat. Struct. Biol., 2001, 8, 932-935, Nikolai R. Skrynnikov et al., J. Am. Chem. Soc., 2002, 124, 12352-12360] (**Fig. 1**)。両測定法による結果がほぼ一致した事から、緩和拡散NMR測定法と高圧NMR測定法はともに、マイクロ秒—ミリ秒で揺らぐ高エネルギー構造を検出しているといえる。興味深い事に、加圧によりキャビティー内の水分子の数が増加することが高圧X線結晶構造解析法から明らかになった [Collins et al., PNAS 2005, 102,16668-16671]。これらの結果から、マイクロ秒からミリ秒オーダーで起こるキャビティー周辺の立体構造の揺らぎはキャビティーへの水分子の出入りを可能とする構造変化と密接に関わっているものと考えられる。

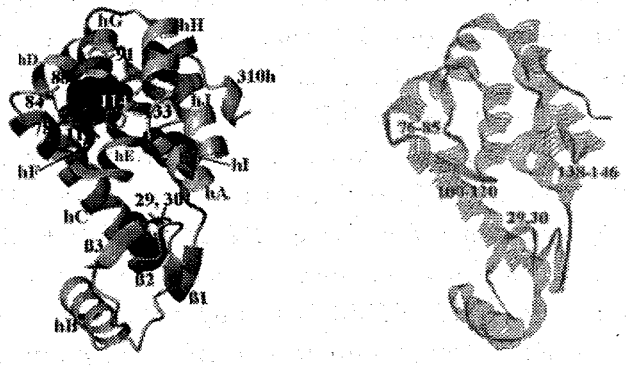

Fig. 1 Conformational fluctuation in L99A cavity mutant of T4 lysozyme. (Left) The cavities are illustrated by blue spheres. The residues showing preferential decreases in cross-peak volumes are colored by red. Side chains of cavity-lining residues showing preferential decreases in the volumes are colored green. (Right) The residues showing chemical exchange in ^{15}N relaxation dispersion NMR [Skrynnikov et al., 2002] are marked by red.

P013

可変圧力NMR法を用いた深海微生物由来ジヒドロ葉酸還元酵素の構造安定特性

○秦 和澄[1,2]、北原 亮[2]、大前英司[3]、Ying Xu[4]、
月向邦彦[3]、横山茂之[2,5,6]、赤坂一之[1,2]
[1]近畿大学生物理工、[2]理研SPring-8センター、[3]広島大学大学院、
[4]南カルフォルニア大学、[5]理研GSC、[6]東京大学大学院

Structural Characteristics of Dihydrofolate Reductase from Deep-sea Bacteria by Variable Pressure NMR

○Kazumi Hata[1,2], Ryo Kitahara[2], Eiji Ohmae[3], Ying Xu[4], Kunihiko Gekko[3], Shigeyuki Yokoyama[2,5,6], Kazuyuki Akasaka[1,2]
[1]Graduate School of Biology-Oriented Science and Technology, Kinki University, [2]RIKEN SPring-8 Center, [3]Graduate School of Science, Hiroshima University, [4]University of Southern California, [5]RIKEN Genomic Science Center, [6]Graduate School of Science, University of Tokyo

The effect of pressure and temperature on the structural and thermodynamic stability of a dihydrofolate reductase (DHFR) from deep-sea bacteria *Moritella profunda* and *Shewanella violacea* has been investigated in their folate-bound form in the pressure range between 3 and 375 MPa and the temperature between -5 and 30 °C, using the on-line cell variable pressure ^{1}H NMR spectroscopy. We determined the free energy difference ΔG^0 extrapolated to 1 bar and the volume difference ΔV between N (Native state) and D (Denature state) at different temperatures. At 15 °C, the stability of MP-DHFR, ΔG^0 = 15.8 /- 4.1 kJ/mol, is smaller than even that of apo *Escherichia coli* DHFR (EC-DHFR), ΔG^0 = 21.2 +/- 5.8. The difference would be increased for folate-bound EC-DHFR, showing marked instability of MP-DHFR against EC-DHFR. On the other hand, ΔV is smaller for folate-bound (-66 +/- 19 mL/mol) than for apo EC-DHFR (-101 +/- 29), suggesting that MP-DHFR is less sensitive to pressure than apo EC-DHFR. Interestingly, the maximum stability of MP-DHFR is around 5 °C (ΔG^0 = 21.4 kJ/mol), close to the temperature of the living environment of *Moritella profunda*.

Key Words: Variable pressure NMR, Deep-sea, DHFR, Thermodynamics

はたかずみ、きたはらりょう、おおまええいじ、Ying Xu、げっこうくにひこ、よこやましげゆき、あかさかかずゆき

高圧・低温下に生息する深海微生物が、このような極限環境に耐えられるメカニズムを知るためには、圧力・温度軸におけるタンパク質の構造や、その安定性を調べなければならない。本研究では、深海微生物*Moritella profunda*と*Shewanella violacea*のジヒドロ葉酸還元酵素 (DHFR)の構造と熱力学量の圧力・温度依存性を、理研・播磨の 800 MHz可変圧力NMR装置を用いて調べ、大腸菌由来DHFR (EC-DHFR) と比較し、深海微生物由来DHFRがどのような特徴を持っているかを調べることを目的としている。測定した深海微生物*Moritella profunda*由来DHFR (MP-DHFR)および*Shewanella violacea*由来DHFR (いずれも葉酸結合型)の^{1}H NMRスペクトルは、EC-DHFR (アポ型)と同じようなスペクトルで、加圧により疎水性アミノ酸由来の信号強度が減少し変性由来の信号強度が増加していった。この疎水性コアの信号強度の減少からN (天然構造) – D (変性構造)間の平衡として熱力学量ΔG^0とΔVを求めたところ、15℃において、MP-DHFRのΔG^0およびΔVは 15.8 ± 4.1 kJ/mol・-66 ± 19 ml/mol、そしてEC-DHFRのΔG^0およびΔVは 21.2 ± 5.8 kJ/mol・-101 ± 29 ml/molであった。EC-DHFRでは、アポ型よりもホロ型の方が構造安定性は高いのにもかかわらず、ホロ型のMP-DHFRはアポ型のEC-DHFRよりも全体的に構造安定性は低く、また圧力に対する感受性も低かった。そして最も特徴的だったことは、MP-DHFRは生息領域付近の温度(5 ℃)において最も安定な構造を獲得していることがわかった。これらのことから、深海微生物由来のタンパク質はその生息領域で最安定構造を有していることが明らかになった。

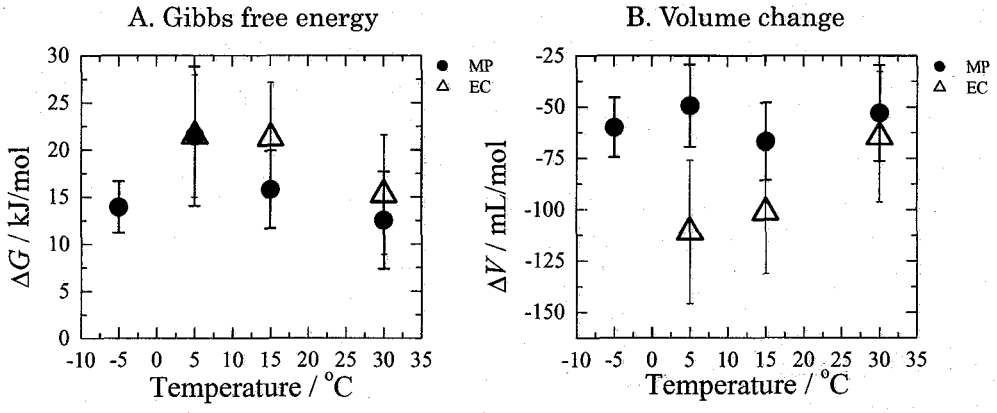

Fig.1. Plots of the standard Gibbs free energy change for unfolding (ΔG_0) (A) and the volume change upon unfolding (ΔV) (B) against temperature, for folate-bound MP-DHFR (●) and apo EC-DHFR (△).

P014

^{19}F NMR によるヘモグロビンのサブユニットの研究

(筑波大院数物[1]、長岡高専物質工[2])
○長尾 聡[1]、長友 重紀[1]、三田 肇[1]、山本泰彦[1]、鈴木秋弘[2]

^{19}F NMR characterization of subunit interaction of tetrameric hemoglobin

Satoshi Nagao,[1] Shigenori Nagatomo,[1] Hajime Mita,[1] Yasuhiko Yamamoto,[1]
and Akihiro Suzuki[2]
[1]*Department of Chemistry, University of Tsukuba, Tsukuba 305-8571*
[2]*Department of Materials Engineering, Nagaoka College of Technology, Nagaoka 940-8532*

The introduction of ring-fluorinated hemes into *b*-type hemoproteins provides spectroscopic probes highly sensitive to heme electronic nature which is relevant to functional properties of the proteins. ^{19}F NMR allowed the determination of the p*K*a value of acid-alkaline transition and oxygenation in individual subunits of tetrameric hemoglobin.

序論

ミオグロビン(Mb)など天然の *b* 型ヘムタンパク質にフッ素を側鎖にもつヘムを導入すると、^{19}F NMR 測定によりヘムタンパク質の活性部位の電子構造の変化を高感度に検出する事ができる。フッ素核の緩和では化学シフト異方性(CSA)が支配的であり、観測対象のタンパク質の分子運動が遅い場合、シグナルがブロードに観測される。そこで、CF_3 基をヘム側鎖にもつ 13,17-bis(2-carboxylatoethyl)-3,8-diethyl-2,12,18-trimethyl-7-trifluoromethylporphyrinatoiron(III)(7-PF, Fig. 1)のヘムタンパク質への導入を検討している。CF_3 基の ^{19}F NMR シグナルは、CF_3 基の C_3 軸まわりの高速回転により CSA が小さくなるため、タンパク質の分子量とは無関係に先鋭化されることが期待されるからである。本研究では、7-PF を利用して、ヒト成人のヘモグロビン四量体(HbA, $\alpha_2\beta_2$)とヒト胎児のヘモグロビン(HbF, $\alpha_2\gamma_2$)の活性部位の電子構造解析を ^{19}F NMR により行った。また、単量体の Mb の解析も行った。

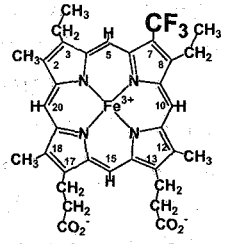

Fig. 1 Structure of 7-PF.

結果と考察

Hb のヘム配向異性体及びサブユニットの帰属

7-PF を組み込んだ Mb 及び HbA、HbF の ^{19}F NMR スペクトルを Fig. 2 に示す。Hb の分子量は約 6 万 5 千であり、Mb の約 4 倍であるにも関わらず、観測されたシグナルの線幅は Mb の約 1.5 倍であり、分子量の増大に伴う線幅の増加が小さい事が確認された。したがって、分子量 10 万を超えるヘムタンパク質の研究にも本手法が有効である事が期待される。Mb の ^{19}F NMR スペクトルでは、シグナルは 2 本観測された。これは、7-PF をヘムタンパク質に導入した際に、ポルフィリン環の 5–15メソ位を通る軸に関して 180 度反転した ***N*** 及び ***R***

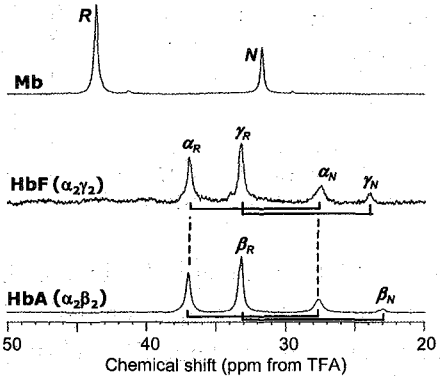

Fig. 2 ^{19}F NMR spectra of Mb(7-PF)N_3^-, HbA(7-PF)N_3^- and HbF(7-PF)N_3^-.

^{19}F NMR, 四次構造変化, ヘモグロビン, フッ素化ヘム, 常磁性 NMR

ながお さとし・ながとも しげのり・みた はじめ・やまもと やすひこ・すずき あきひろ

form のヘム配向異性体が生じるためである。つまり、HbA と HbF のスペクトルのシグナル 4 本は、サブユニット毎にヘム配向異性体が存在することを反映している。ヘム配向異性体のシグナルの帰属は、Mb において CF_3 基から近傍のアミノ酸側鎖への ^{19}F-^{1}H NOE の検出により行い、HbA 及び HbF におけるシグナル帰属の参考にした。α, β, γサブユニットのシグナルは HbA と HbF のスペクトル比較から行った。HbA と HbF で共通するαサブユニットに由来するシグナルのシフト値は、お互いに類似していると予想されるからである。HbA の様々な配位状態において、^{19}F NMR シグナルはヘム鉄の酸化状態及びスピン量子数を反映し、約 100 ppm の範囲に分離良く観測されている(Fig. 3)。これらのシグナルをプローブとして、これまで解析が困難であった Hb 四量体の研究が初めて可能になり、サブユニットやヘムの配向が Hb の機能に及ぼす影響の解明が可能になる。

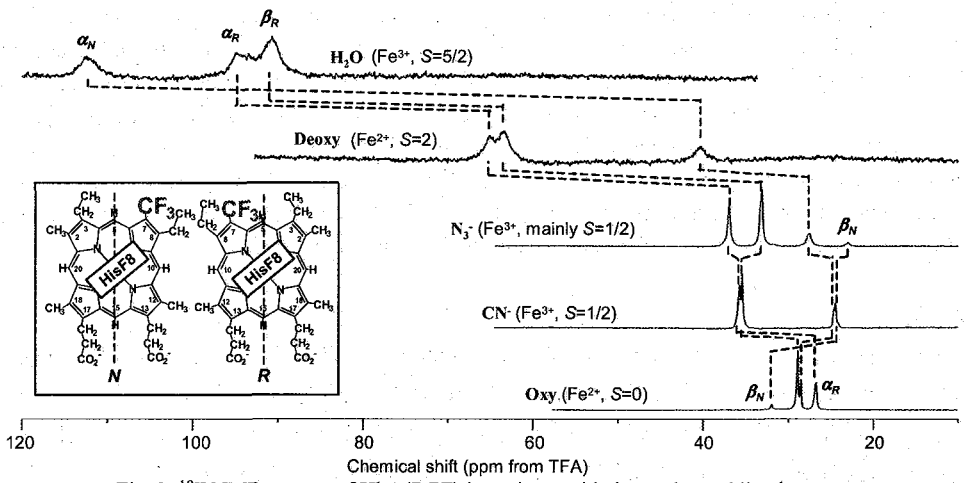

Fig. 3 ^{19}F NMR spectra of HbA(7-PF) in various oxidation, spin, and ligation states.

酸素化過程の解析

^{19}F NMR シグナルの強度の単純な解析により、Hb の各サブユニット及びヘム配向異性体の酸素結合過程を観測する事ができる。酸素分圧が異なる HbA の ^{19}F NMR スペクトルを Fig. 4 に示す。Hb の酸素平衡は NMR のタイムスケールより遅いため、酸素分圧の上昇に従い、Deoxy 体のシグナル強度は減少し、一方、Oxy 体のシグナル強度は増加する。一連の酸素分圧における ^{19}F NMR シグナルの強度を解析すれば、Hb 四量体のサブユニットの酸素親和性を求める事が可能である。

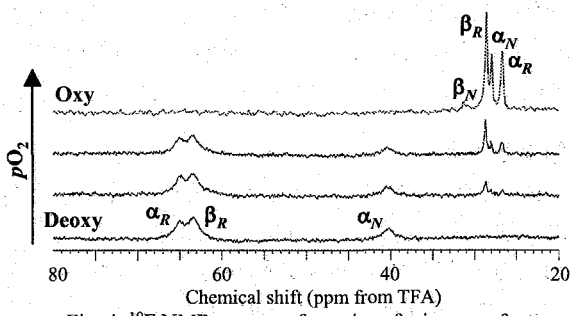

Fig. 4 ^{19}F NMR spectra of a series of mixtures of deoxyHbA(7-PF) and OxyHbA(7-PF) .

References

Yamamoto, Y., Hirai, Y., & Suzuki, A. *J. Biol. Inorg. Chem.* **2000**, 5, 455-462

Hirai, Y., Yamamoto, Y., & Suzuki, A. *Bull. Chem. Soc. Jpn.* **2000**, 73, 2309-2316.

Yamamoto, Y., Nagao, S., Hirai, Y., Inose, T., Terui, N., Mita, H., & Suzuki, A. *J. Biol. Inorg. Chem.* **2004**, 9, 152-160.

Hirai, Y., Nagao, S., Mita, H., Suzuki, A, & Yamamoto, Y. *Bull. Chem. Soc. Jpn.* **2004**, 77, 1485-1486.

Nagao, S., Hirai, Y., Suzuki, A., & Yamamoto, Y. *J. Am. Chem. Soc.* **2005**, 127, 4146-4147.

Yamamoto, Y., Nagao, S., & Suzuki, A., *Modern Magn. Reson.* **2006**, 1-8.

P015

シトクロム c の熱安定性を増大する分子機構の解明

（筑波大院数物）　○高山 J. 真一、佐々木寛明、高橋陽太、入江清史、太 虎林、河野 慎、三田 肇、長友重紀、山本泰彦

Elucidation of molecular mechanism responsible for thermostabillity of cytochrome *c*

○Shin-ichi J. Takayama, Hiroaki Sasaki, Yo-ta Takahashi, Kiyofumi Irie, Hulin Tai, Shin Kawano, Hajime Mita, Shigenori Nagatomo, and Yasuhiko Yamamoto
Department of Chemistry, University of Tsukuba, Tsukuba 305-8571

Thermophile *H. thermophilus* cytochrome c_{552} (HT) and mesophile *P. aeruginosa* cytochrome c_{551} (PA) are small monoheme-containing electron transfer proteins, which exhibit high sequence identity (56 %), and their main-chain folding is almost identical. But HT is much more stable as to heat than PA. From a detailed comparison of the protein interior between HT and PA, stereochemical packing of hydrophobic residues is shown to be crucial to overall thermostability of proteins. In order to further enhance the hydrophobic interactions in HT, we removed hydrophilic OH group of Tyr27, which is located nere hydrophobic core, by substitution of Tyr27 with Phe and sucseeded in constructing HT mutant which exhibit even higher thermostability than wild-type protein.

序　論

好熱性水素細菌 *H. thermophilus* 由来の cytochrome c_{552}（HT、Fig. 1）と緑膿菌 *P. aeruginosa* 由来の cytochrome c_{551}（PA）はアミノ酸配列で 56%の相同性をもち、両者の主鎖のフォールディングは類似しているが，HT の変性温度（T_m）は PA に比べて約 30 ℃も高い。HT と PA の立体構造の比較から、HT 内部ではヘム近傍の疎水性コアが安定化されていることが明らかになっている。このように、タンパク質内部における疎水性コアの安定化は、タンパク質全体の熱安定性の増大に寄与すると考えられる。私共は、HT の疎水性コア近傍に位置する Tyr27 側鎖の OH 基を Phe への置換により除去することにより疎水性コアの安定性を増大し、HT の熱安定性をさらに高くすることに成功した[1]。

結果と考察

HT と PA の Y27F 変異体は、遺伝子工学的手法により調製した。Fig. 2 に HT、PA および調製した変異体の酸化型での ^{1}H NMR スペクトルを示す。酸化型シトクロム c では、ヘム鉄に存在する不対電子の影響によりヘム側鎖メチルプロトンシグナルが低磁場側に常磁性シフトして観測される。

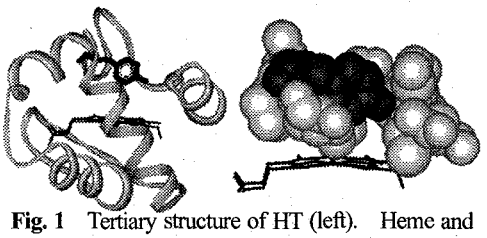

Fig. 1 Tertiary structure of HT (left). Heme and Tyr27 residue are indicated in a stick model. The hydrophobic core near heme (right). The Tyr27 residue is indicated in dark grey.

Keyword: シトクロム c、常磁性 NMR、熱安定性、タンパク質フォールディング、疎水性相互作用

たかやま J.しんいち、ささきひろあき、たかはしようた、いりえきよふみ、たいこりん、かわのしん、みたはじめ、ながともしげのり、やまもとやすひこ

これらのシグナルはヘムの電子状態を鋭敏に反映してシフト変化するが[2]、HT、PA 共に Y27F 変異体の常磁性シグナルのシフトパターンは野生型のものと一致した。このことから、Y27F の変異はヘム活性部位の構造には大きく影響しないことが明らかとなった。また、NOESY スペクトル(Fig. 3)の帰属から得られた主鎖プロトンのシフト値も変異体と野生型の間で本質的には変化がなく、主鎖のフォールディングが保存されていることが示された。

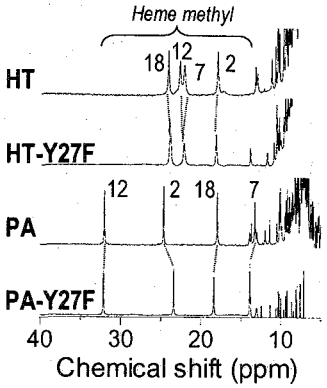

Fig. 2 Downfield portion of ^{1}H NMR spectra of oxidized forms of HT, HT-Y27F, PA, and PA-Y27F. The assignment of heme methyl signals are indicated in the spectra.

タンパク質の T_m は、α-ヘリックス含量に対応する 222 nm の円二色性 (CD) の温度変化より求めた (Fig. 4)。HT は、野生型においても 100 ℃ < T_m なので、試料溶液の沸騰を防ぐため、約 10 気圧の加圧下で測定を行った[3]。その結果求められた酸化型 HT、PA、HT-Y27F および PA-Y27F の T_m はそれぞれ 108.3、82.3、116.1、90.6 ℃となり、HT、PA いずれにおいても変異の導入により、T_m が約 8 ℃上昇した。一方、還元型では、HT、PA 共に野生型と変異体でほとんど T_m に変化はなかった。このことから、Y27F 変異の導入は主に酸化型の熱安定性を増大させることが明らかとなった。また、NMR の解析から Y27F の変異は主鎖のフォールディングにはほとんど影響を与えないことが示されているので、変異導入による熱安定性の上昇は主に側鎖のパッキングの変化と、それに伴う疎水性コアの安定化に起因すると考えられる。

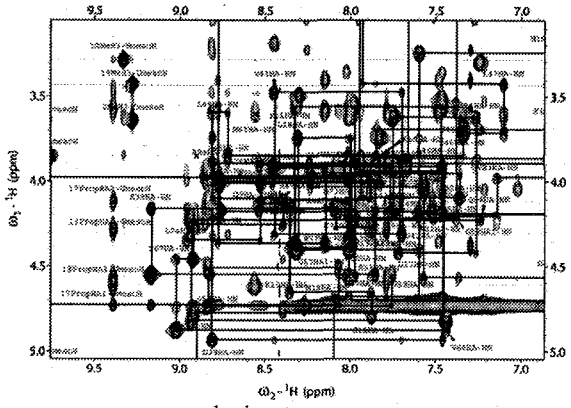

Fig. 3 A portion of ^{1}H-^{1}H NOESY spectrum of HT-Y27F.

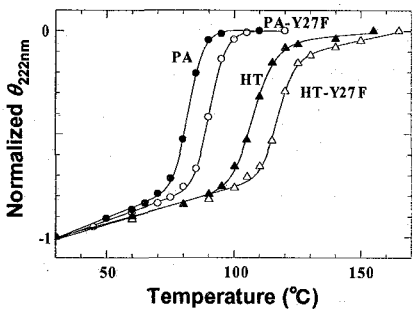

Fig. 4 Temperature dependence of normalized CD at 222 nm of oxidized forms of HT(▲), HT-Y27F(△), PA(●), and PA-Y27F(○).

References

[1] Y. Takahashi, H. Sasaki, S. J. Takayama, S. Mikami, S. Kawano, H. Mita, Y. Sambongi, and Y. Yamamoto (2006) *Biochemistry*, 45, 11005-11011.

[2] N. Tachiiri, H. Hemmi, S. J. Takayama, H. Mita, J. Hasegawa, Y. Sambongi, and Y. Yamamoto (2004) *J. Biol. Inorg. Chem.*, 9, 733-742.

[3] S. Uchiyama, A. Ohshima, S. Nakamura, J. Hasegawa, N. Terui, S. J. Takayama, Y. Yamamoto, Y. Sambongi, and Y. Kobayashi (2004) *J. Am. Chem. Soc.*, 126, 14684-14685.

P016

Structure of the N-terminal domain of SUMO ligase Siz1 from *Succhromyces cerevisiae*

R. Suzuki[1], H. Shindo[1,2,3], S. Tase[1] and T. Yamazaki[1] ([1]Protein Research Unit, National Institute of Agrobiological Sciences, [2]RIKEN Genomic Science Center and [3]School of Pharmacy, Tokyo University of Pharmacy and Life Science)

Post-translational modification by SUMO (small ubiquitin-like modifiers) is an important mechanism that regulates a wide variety of cellular functions such as gene transcription, viral infection, nuclear localization, chromatin organization, cell cycle progression and so on. Sumoylation pathway is very similar to that of ubiquitination which occurs through the thioester cascade of E1 (activating enzyme) to E2 (conjugating enzyme) and E3 function as a ligase for ubiquitin or SUMO to each target protein. However, functional consequence of sumoylation as mentioned above is quite different from that of ubiquitination which involves in protein degradation as its major role.

Siz1 (also called Ull1), a member of the PIAS (protein inhibitor of activated STAT) family, was identified as an E3 SUMO ligase for septin components in budding yeast. The family has several conserved domains such as the N-terminal domain with SAP motif, the PINIT domain and the RING-like zinc finger domain. However, sequence identity between yeast Siz1 and human PIAS1 is not so high. For example, the identity of N-terminal domains is 18.5% between them, and further more the domain of Siz1 is longer by 22 aa than that of PIAS1. Thus, it is interesting to study the structures and function of the extended region of the SAP domains of two proteins.

We have previously determined structure of the N-terminal SAP domain of SUMO ligase PIAS1 from human and have shown that the domain can bind an AT-rich DNA[1)]. Here, we will report the NMR structure of a putative extended SAP domain in the N-terminus of a SUMO ligase Siz1 (1-111). We will discuss structural similarity and distinction between the N-terminal domains of these two SUMO ligases.

Materials and Methods

The N-terminal domain (1-111 aa) with His_6-tag of yeast Siz1 is overexpressed in *E. coli* BL21 in M9 medium containing ^{15}N-enriched ammonium chloride or/and ^{13}C-enriched glucose. The recombinant proteins were purified by Ni^{2+}-column, and His-tag was cleaved by thrombin, followed by gel filtration. The protein was resolved in 10% D_2O containing 300 mM NaCl, 20 mM K-Pi (pH 6.1), 0.2 mM $ZnCl_2$, 5 mM DTT, and multi-dimensional NMR spectra were acquired at 10°C on a Bruker DMX750 spectroscopy. A self-complement

---

Keywords: SUMO, ligase Siz1, ligase PIAS1, NMR structure, DNA binding

DNA 16-mer, d(CAAAAATATATTTTTG)$_2$, was used for DNA binding experiments.

Results and Discussion

Structural Feature of N-terminal Domain: The spectra were analyzed by the program SPARKY3 and the structural calculations were carried out using the program CYANA with its standard protocol. The C_α and C_β secondary chemical shifts indicated that the domain Siz1 (1-111) is composed of five α-helices and that the N-terminal region (1-21) of Siz1, which is absent in PIAS1 (1-85), has no secondary structure (essentially flexible) as shown in Figure 1. Here, the secondary structure of Siz1 (1-111) is compared with the N-terminal extended SAP domain of PIAS1 (1-85) whose structure was previously determined. The primary SAP domains (corresponding to α2 and α3-helices) are very similar between Siz1 and PIAS1, while the α1-helix and the loop between α3 and α4 of Siz1 are much longer than those of PIAS1. It should be mentioned that the C-terminal segment of PIAS1 (65-85) was a flexible, random coil while the corresponding segment of Siz1 was in α-helix (Fig. 1). Preliminary structural calculations indicated that it has a five-bundle like structure in stead of a four-bundle in the case of PIAS1. Further refinements for three-dimensional structure are in progress.

DNA Binding Ability of N-terminal Domain: ^{15}N-labeled Siz1 (1-111) was titrated with DNA 16-mer and the chemical shift perturbations were observed using ^{15}N-^{1}H HSQC spectra upon DNA binding at various P/D ratios. In Fig. 1, the residues strongly perturbed in chemical shift index are labeled with asterisk * at the top and bottom of sequences of PIAS1 and Siz1, respectively. Although the individual perturbed residues are different between two, they are almost all located on the SAP motif (α2 and α3) in both cases, indicating that the pattern of DNA binding is similar.

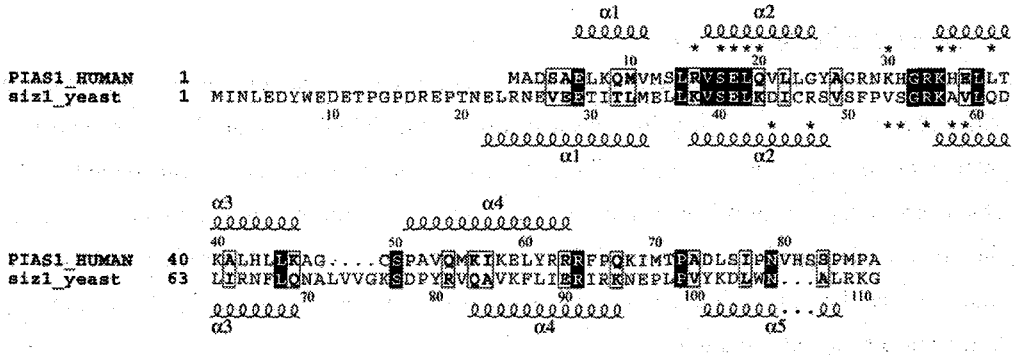

Fig. 1. Amino acid sequence alignments, secondary structures and residues involved in DNA binding (*) of the N-terminal extended SAP domains of PIAS1 and Siz1.

Refs. : 1) S. Okubo et al., J. Biol. Chem., 279, 31455(2004).

P017

920 MHz NMR analyses of causative gene products of neurodegenerative disorders

○Hiroaki Sasakawa[1], Eri Sakata[2], Akira, Sumiyoshi[2], Maho Utusmi[1, 2], Yoshiki Yamaguchi[2] and Koichi Kato[1, 2]

[1] Institute for Molecular Science,

[2] Graduate School of Pharmaceutical Sciences, Nagoya City University

Neurodegenerative disorders such as Alzheimer's disease (AD), Parkinson's disease (PD), and polyglutamine (polyQ) disease are though to be caused by common cellular and molecular mechanisms. The underlying genetic mutations for many familial neurodegenerative disorders have been identified in recent years. Here we report an NMR approach to obtain deeper insights into the pathological mechanisms of molecular interactions of the causative gene products of neurodegenerative disorders, i.e. α-synuclein, amyloid-β (Aβ) and polyQ tracts. These proteins have no apparent ordered secondary structure in the monomeric forms, although recent evidence indices the existence of functionally relevant intra-molecular interactions. NMR analyses of these unfolded proteins are generally precluded by overlap of signals and lack of NOE-derived distance constraints. To cope with these difficulties, we applied ultra-high field (920 MHz) NMR spectroscopy and the spin labeling technique to analyze the intra- and inter-molecular interactions of these proteins in solution.

i) Solution conformation of Aβ

The conversion of monomeric Aβ to its aggregated, toxic form is a crucial step in Alzheimer's disease. Underlying mechanisms of the initial step of the inter-molecular interaction of Aβ leading to its fibrils formation have been poorly understood. We characterized the conformational status of monomeric Aβ by observing line broadening due to the effect of the spin label attached to the N- or C-terminus of Aβ. Inspection of these data indicates that the conformation of Aβ in solution is not completely random but has a tendency to assume a bent conformation.

Keywords: Neurodegenerative disorders, Intrinsically disordered protein, α-synuclein, Amyloid β, Poly-glutamine tract

ii) Intramolecular interaction of Ataxin-3

Ataxin-3 is the product of the causative gene of Machado-Joseph disease, which is one a putative de-ubiquitinating enzyme, and the C-terminal polyubiquitin interacting motifs Pubh1-3 inserting the polyQ tract between Pubh2 and Pubh3. Our NMR data revealed that there exist intra-molecular interactions between the Pubh1-2 motifs and the polyQ-Pubh3 segment.

iii) Identification of epitope exhibited on α-synuclein

α-Synuclein, a causative gene product of PD, is a 140 amino acid phosphorylated protein abundantly expressed in presynaptic terminals of vertebrates. We identified the epitope of α-synuclein recognized by its cognate antibody (LB509) on the basis of the ultra-high resolution NMR spectral data (Fig. 1). We also analyzed the effects of site-specific phosphorylation at Ser129 of α-synuclein. Phosphorylation at Ser129 induced chemical shift changes at Lys34 and Lys45, which are distal from the phosphorylated site. These data suggest that long-rage electrostatic interaction(s) exist in the phosporylated α-synuclein.

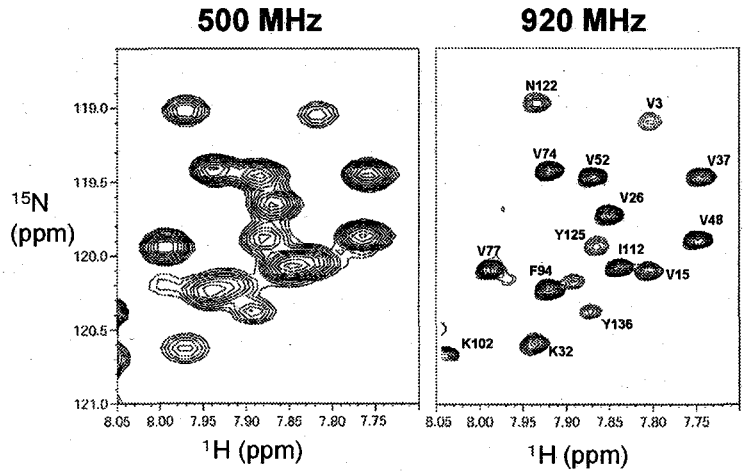

Fig. 1. ^{1}H-^{15}N HSQC spectra of [^{15}N]α-synuclein recorded at ^{1}H observation frequencies of 500 MHz and 920 MHz

Acknowledgements We thank Dr. M. Hasegawa (α-synuclein), Dr. T. Iwatsubo (α-synuclein), Dr. K. Yanagisawa (Aβ), Dr. C.A. Joazeiro (Atx3) and Dr. W. Li (Atx3) for helpful discussions. We also thank M. Nakano for her help in some NMR measurements.

P018

無細胞系によって調製されたイネ NifU1A domain I の NMR 立体構造解析

(北大院・生命科学院[1], 農水省・農生資研[2])
○ 斉尾智英[1], 小椋賢治[1], 久米田博之[1], 横地政志[1],
加藤静恵[2], 加藤悦子[2], 稲垣冬彦[1]

Structual Analysis of *Oryza sativa* NifU1A Domain I Prepared by Cell-Free System

Graduate School of Life Science, Hokkaido University[1]
Biochemistry Department, National Institute of Agrobiological Sciences[2]
○Tomohide Saio[1], Kenji Ogura[1], Hiroyuki Kumeta[1], Masashi Yokochi[1],
Shizue Katoh[2], Etsuko Katoh[2], Fuyuhiko Inagaki[1]

NifU/NifU-like proteins are known to provide a molecular scaffold for the assembly of the iron-sulfur cluster and play important roles not only in electron transfer or metabolic reactions but also in gene expression. The chloroplast-type NifU-like protein has a tandem repeat of NFU domains. N terminal domain has CXXC motif that is suggested to accept iron-sulfur cluster and transfer it to receptor protein, whereas C-terminal domain lacks this motif. This domain arrangement is unique to chloroplast-type NifU-like proteins. The solution structure of C-terminal domain of NifU-like protein from *Oryza sativa* (OsNifU1A) has been solved. Here we discuss the structure of N-terminal domain of OsNifU1A prepared by cell-free system using improved dialyzer.

【序論】

NifU/NifU-like タンパク質は、鉄-硫黄クラスター形成の足場として機能し、電子伝達や代謝反応ばかりでなく、遺伝子の発現調節にも関わっていることがわかっている。葉緑体局在

Key words : cell-free protein synthesis, *Oryza sativa*, photosystem, Fe-S cluster protein

著者ふりがな：さいおともひで、おぐらけんじ、くめたひろゆき、よこちまさし、かとうしずえ、かとうえつこ、いながきふゆひこ

型 NifU-like タンパク質によって形成された鉄-硫黄クラスターは、光合成における電子伝達をになうFerredoxinに受け渡される。葉緑体局在型 NifU-like タンパク質は 2 回の繰り返しドメインを持っていることが明らかにされており、N 末端側の domain I は活性中心であるCXXC モチーフを持つが、C 末端側の domain II では CXXC モチーフが欠けている。このような配列構成はほかの生物の NifU/NifU-like タンパク質では見られず、植物特有のものである。イネ由来の OsNifU1A の CXXC モチーフを持たない domain II はすでに NMR による立体構造解析がなされている。本研究では、大腸菌系無細胞タンパク質合成を用いて調製した OsNifU1A domain I の NMR による立体構造解析を行った。

無細胞タンパク質合成に用いる透析器は、市販されているものの多くが反応内液の出し入れがしにくいことや、透析効率が低くタンパク合成量が少ないといった短所があった。それらの短所を改善するため、改良型透析器を考案・作成し、それを用いて NMR サンプルを調製した。

【実験】

大腸菌 BL21 Star (DE3)菌体を安井器械 Multi Beads Shocker で破砕し、S30 抽出物を調製した。

次に、無細胞タンパク質合成のための透析器の改良を行った。15mL ディスポーザブル遠心管にフィットする形状の透析膜型枠を作成した。この型枠に市販透析膜を密着させ、遠心管をねじ込むことにより透析器を組み立てることができる。この透析器の利点は①あらゆるポアサイズの透析膜を使用できること、②タンパク質合成反応液を遠心によりロスなく回収できることである。実際にこの透析器と SpectraPor 透析器でタンパク質合成の収量を比較したところ、約 2 倍の収量向上を確認した。

次に、この改良型透析器を用いた無細胞タンパク質合成によって$^{13}C^{15}N$ラベルNifU1A domain IをHis-tag融合タンパク質として発現させ、アフィニティークロマトグラフィー、ゲルろ過クロマトグラフィーによって精製した。

NMR測定はVarian社製Unity Inova 600 MHz, 800 MHz分光計を用いて 25°Cにて行った。スペクトル解析にはOliviaを使用し、^{13}C-および^{15}N-NOESYからの距離制限とTALOS由来の二面角制限を用いて、CYANAによって立体構造計算を行った。

【結果・考察】

改良型透析器を用いて OsNifU1A domain I を発現させたところ、1mL 反応内液あたり 2.7mg の収量を得ることができた。

TALOSによる二次構造予測では、OsNifU1A domain Iは 2 本のαヘリックスと 3 本のβシートから構成されるという結果が得られ、これはC末端側のdomain IIの二次構造と一致していた。CXXCモチーフを構成するアミノ酸残基は[$^{1}H^{15}N$]-HSQCでピークが観測されず、その周辺の残基もピーク強度が著しく弱いかもしくは観測されなかったことから、CXXCモチーフは柔軟なループ構造をとっていると考えられる。現在、立体構造解析のためのNMR測定は終了しており、立体構造決定に向けて解析中である。

P019

Acyl-coenzyme A binding proteins from human and their functional analysis

Hiroyuki Onuki[1,2], A. Z. M. Ruhul Momen[1], Yusuke Tsubota[2], Kenichi Yasumuro[1], Kazuhito Satou[1], Takamasa Abe[1], Toshiyuki Hamada[1,2], Fumiaki Hayashi[1], Kohei Saito[1], Seizo Koshiba[1], Takanori Kigawa[1], Shigeyuki Yokoyama[1] and Hiroshi Hirota[1,2]

[1]RIKEN Genomic Sciences Center, [2]Graduate Course of Supramolecular Biology, Yokohama City University

The three dimensional structures of two human ACBPs (acyl-CoA binding proteins) were determined by NMR. Based on the structural information, we examined the interaction of the two human ACBPs (hACBP1 and hACBP2) with acyl-CoAs having various acyl lengths by NMR chemical shift perturbation method. Distribution of the residues corresponding to perturbed signals showed that acyl-CoAs interact with ACBPs site-specifically.

Introduction

ACBPs are proteins with highly conserved amino acids and are present in cells of a wide range of eukaryote organisms from yeast to mammals. They play roles of the storage and intracellular transport of acyl-CoAs.[1] To date, there have been reported numerous eukaryotic ACBPs. Human ACBPs have also been cloned, but no structural information of human originated ACBPs has been reported yet. Here we report the first three-dimensional structures of two human ACBPs (hACBP1 and hACBP2). Based on these structures, we demonstrate interaction of human ACBPs with acyl-CoAs having various acyl lengths.

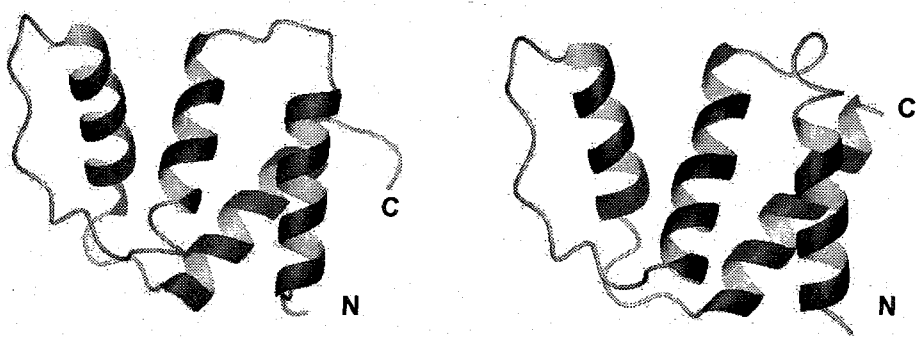

Figure Structure of hACBP1 (left: PDB ID 2CQU) and hACBP2 (right: PDB ID 2 COP)

Key Words: ACBP, acyl-coenzyme A, functional analysis, chemical shift perturbation

Materials and Methods

hACBP1 domain is located at N-terminus of human Δ^3,Δ^2-enoyl-CoA isomerase (364 residues). hACBP2 domain is located nearby N-terminus of a hypothetical protein containing ankyrin repeat (282 residues). The ^{13}C, ^{15}N-labeled proteins were prepared by the *E. coli* cell-free system. NMR spectra were obtained by standard multidimensional measurements. Automated NOE cross peak assignment and structure calculation were performed by CYANA. For perturbation experiment, acyl-CoAs (C12, C14, C16 and C18) were added to the solution of U-[^{15}N]-ACBPs from the molar ratio of 1:0 to 1:5. ^{1}H-^{15}N HSQC spectra were measured under each concentration ratio to obtain perturbed chemical shifts. Dissociation constant (K_d) was calculated by non-linear curve fitting method.

Results and Discussion

The fold of the both proteins shows a down-up-up-down four-alpha-helix bundle. These helices of both proteins were arranged in a bowl shape with a possible acyl-CoA binding site. Most of the residues that might bind to adenosine-3'-phosphate are conserved.

Then we examined interaction of hACBP1 and acyl-CoAs. Clear concentration dependent signal perturbation was observed only in the case of C12-CoA. Intensive analysis of the data for hACBP1 and C12-CoA experiments revealed that distribution of the residues corresponding to perturbed signals showed good agreement with conserved residues reported on other ACBPs. From this observation, acyl-CoA interacts with ACBP site-specifically. According to the chemical shift changes, K_d was estimated as the order of 1×10^{-5} M. This result is consistent with that of surface plasmon resonance experiment: hACBP1 was immobilized on a sensor chip surface and C12-CoA was used as a mobile phase.[2,3] When we used C14, C16 and C18-CoAs, chemical shift changes were also observed, but we observed only two states: free and bound forms, presumably due to slow exchange rate between two states. Though it was difficult to calculate dissociation constant as the similar manner, perturbed signals were observed at the same residues as in the case of using C12-CoA and we could depict residues that interacted with acyl-CoAs. We are also to report the result of NMR chemical shift perturbation experiments of hACBP2 with acyl-CoAs having various acyl lengths as the similar manner. From the analysis of these experiments, we will discuss the acyl-chain specificity for ACBPs with the structural viewpoint.

References

1) van Aalten D. M. F. et al., *J. Mol. Biol.* , **2001,** *309*, 181-192.
2) Tsubota, Y. et al. Abstracts of Papers, 86th Annual Meeting of the Chemical Society of Japan, Chiba; Chemical Society of Japan: 2006; 3 G4-18.
3) Momen, A. Z. M. R. et al. Abstracts of Papers, International Conference on Biodiversity and Natural Products, Kyoto; IUPAC: 2006; P-403.

P020

^{19}F-NMRを用いた4(*R*)-fluoroprolineを含むコラーゲンモデルペプチドに関する研究

(^{1}大阪大学薬学部、^{2}日本電子(株)、^{3}大阪薬科大学薬学部、^{4}和歌山高等専門学校物質工学科、^{5}大阪大学工学部、^{6}奈良女子大学理学部、^{7}(株)ペプチド研究所)
○河原一樹^{1}、根本暢明^{2}、西義則^{3}、土井正光^{4}、内山進^{5}、中沢隆^{6}、西内祐二^{7}、吉田卓也^{1}、大久保忠恭^{1}、小林祐次^{3}

^{19}F-NMR Study of Collagen Model Peptides containing 4(*R*)-fluoroproline

(^{1}Graduate School of Pharmaceutical Sciences, Osaka Univeresity, ^{2} JEOL LTD., ^{3}Devision of Rational Drug Design, Osaka University of Pharmaceutical Sciences, ^{4}Department of Materials Science, Wakayama National College of Technology, ^{5}Graduate School of Engineering, Osaka University, ^{6}Department of Chemistry, Nara Women's University, ^{7}Peptide Institute Inc.)
○ Kazuki Kawahara^{1}, Nobuaki Nemoto^{2}, Yoshinori Nishi^{3}, Masamitsu Doi^{4}, Susumu Uchiyama^{5}, Takashi Nakazawa^{6}, Yuji Nishiuchi^{7}, Takuya Yoshida^{1}, Tadayasu Ohkubo^{1}, and Yuji Kobayashi^{1}

^{19}F-NMR experiments have been carried out on 4(*R*)-fluoroproline (fPro^{R}) containing collagen model peptides. It is known that H-(Pro-fPro^{R}-Gly)$_{7}$-OH takes triple helical structure at lower temperature and shows thermal transition to single coil state. Due to much larger ^{19}F chemical shift dispersion than that of ^{1}H or ^{13}C, we successfully tracked triple helix – monomer transition in a series of temperature dependence experiments. Analyses on ^{19}F–{^{1}H} heteronuclear correlation and relaxation as well as on the temperature dependence helped us to clearly categorize the ^{19}F signals into three; those of monomer, folding intermediate, or triple-helix. The method shown here provides a clue to analyze the conformational transition, dynamics and stability of collagen triple helical structure.

Key Words : ^{19}F-NMR, collagen model peptides, temperature dependence, folding intermediate, relaxation

かわはらかずき、ねもとのぶあき、にしよしのり、どいまさみつ、うちやますすむ、なかざわたかし、にしうちゆうじ、よしだたくや、おおくぼただやす、こばやしゆうじ

[緒言]

コラーゲン分子は$(X\text{-}Y\text{-}Gly)_n$の繰り返しアミノ酸配列を持つペプチド鎖からなり、室温付近では三本のペプチド鎖が螺旋状に絡み合うトリプルヘリックス構造を形成している。配列中のX,Y位にはProや4(*R*)-hydroxyproline(Hyp^R)が頻繁に存在し、I型のコラーゲンにおいてはこれらのイミノ酸の含有量が全体の約 30%を占めることが知られている[1]。モデルペプチドを用いた熱安定性の研究から、Y位のHyp^Rはトリプルヘリックス構造の熱安定性に重要な寄与を示すことが報告され、更に、Hyp^Rを4(*R*)-fluoroproline($fPro^R$)に置換したモデルペプチドがより熱安定性の高いトリプルヘリックス構造を形成することが報告されている[2-4]。この様なコラーゲントリプルヘリックス構造の安定化と一本鎖状態から三本鎖状態へのフォールディングの機構を説明する為これまでにもNMRを使用した様々な研究が行われてきたが、^1Hないし^{13}C-NMRスペクトル上での信号の重なりの問題の為、三本鎖や一本鎖の信号の帰属が非常に困難であった。今回我々は$fPro^R$を含むモデルペプチド(Pro-$fPro^R$-Gly)n (n=1~4, 7)の^{19}F-NMRによる測定を行った。^{19}Fの化学シフトは、^1Hや^{13}Cに比べて、核周辺の小さな環境変化に敏感であり、化学シフトがより広範囲に分散する傾向を持つことが知られている。

[実験]

化学合成した(Pro-$fPro^R$-Gly)n (n=1~4, 7)を 90% H_2O / 10% D_2Oに溶かし測定した。温度変化実験(10°C~80°C)、$\{^1H\}-^{19}F$ HETCOR, $\{^1H\}-^{19}F$ HOESY, ^{19}F-緩和測定などを行った。

[結果と考察]

^{19}F-単一パルス実験より、(Pro-$fPro^R$-Gly)n (n=1~4, 7)の$fPro^R$における$^{19}F\gamma$の化学シフトが比較的広範囲に分散していることが確認された。これは^1H-NMRスペクトル上で1本の信号として観測された$fPro^R$中の$^1H\gamma$の結果と対照的である。更に、温度変化実験(10°C~80°C)と$\{^1H\}-^{19}F$ HOESYおよび^{19}F-緩和測定の測定結果を組み合わせることによって、^{19}F-単一パルス実験により観測された各信号は三本鎖状態、一本鎖状態及び中間状態に大別できることが明らかになった。特に、三本鎖状態と平衡関係にある一本鎖状態及び中間状態の詳細な解析を行うことは、コラーゲントリプルヘリックス構造のフォールディング過程を理解する上で非常に重要である。

[参考文献]

1, P. P. Fietzek and K. Kühn. (1975) *Mol.Cell. Biochem.* **8**, 141-157.
2, Kobayashi, Y. et al. (1970) *Biopolymers*, **9**, 414-425.
3, Holmgren, S. K. et al. (1998) *Nature* **392**, 666-667.
4, Hodges, Jonathan, A., and Raines, R.T. (2003) *J. Am. Chem. Soc.* **125**, 9262-9263.

[謝辞]

名古屋大学物質国際研究センターでの測定に便宜をはかってくださいました前田裕博士ならびに篠原久典教授に感謝致します。

P021

Solution structure of Hex C-terminal domain and the mechanism of the transcriptional activation

Yuki Horie[1], Riyo Yoshikawa[1], Shinichiro Asai[1], Tamio Noguchi[2], Takahisa Ikegami[3], Hideo Akutsu[3], Hiroshi Hirota[4], Shigeyuki Yokoyama[4], Shunsuke Meshitsuka[1,4]

[1]Tottori University Graduate School of Medical Science,Institute of Regenerative Medicine and Biofunction, [2]Osaka Ohtani University Tondabayashi 584-8540, [3]Osaka University Institute for Protein Research, [4]RIKEN Genomic Sciences Center

Transcription factor Hex (haematopoietically expressed homeobox) is a homeobox protein that regulates differentiation and development of liver and monocyte. Hex has three functional domains, N-terminal domain, homeo domain and C-terminal domain, of which functions are repression, DNA binding and activation, respectively. To explain the function of activation by Hex the structural studies have been carried out by NNR. The solution structure of Hex C-terminal domain was determined. Binding of the C3-domain of the transcription factor GATA-2 to Hex C-terminal domain was observed.

Introduction

Homeobox genes encode transcription factors that regulate development and differentiation. Homeobox genes are classified into genomic clusters named HOXA, HOXB, HOXC and HOXD, and there are other types of orphan homeobox genes which are independent of HOX clusters. Hex is one of the orphans identified in human promyelotic leukemia cell line and is found in rat, mouse, chicken, xenopus, zebrafish and C.elegance. Hex is a transcription factor constituted of 271 amino acids and has a proline-rich repressor domain in the N-terminal region (45-136 AA), a homeodomain in the center (137-196 AA) and an activator domain in the C-terminal region which has many negatively charged amino acids such as glutamic acid and aspartic acid (197-271 AA). The knock out mouse of Hex is embryonically lethal around E10.5 due to a lack of substantial liver formation, thyroid gland formation, forebrain formation, and monocyte and B cell differentiation. Recently, several genes such as thyroglobulin, the precursor

Key Words: Hex, transcription factor, transcriptional activation, solution structure, protein-protein interaction

of thyroid hormone, and goosecoid, homeodomain transcription factor involved in development of early embryo were found to be repressed by Hex. In contrast, Hex activates the expression of Smemb, nonmusclė isoform of the myosin heavy chain and sodium dependent bile acid co-transporter. Furthermore, the expressions of GATA-1, flk-1 and fil-1 which are the transcription factors of endothelial and blood cells for differentiation in zebrafish are also activated by Hex. It was also reported that Hex binds directly to transcription factors such as HNF1α and GATA-2, and regulates the transcription of their target genes. However, the detail function of Hex has not been clarified yet.

Experiment

The domains of Hex were expressed separately in homeodomain and C-terminal domain (Hex-C). Also, the domains of GATA-2 were expressed separately in five domains such as N1, N2, C1, C2 and C3 domains. The interactions between Hex and GATA-2 were observed by experiments of the surface plasmon resonance. NMR spectra of N-HSQC, C-HSQC, HNCO, HNCACO, CBCANH, CBCACONH, HCCONH, CCONH, NOESY_N-HSQC, NOESY_C-HSQC, HCCH_TOCSY, TOCSY_N-HSQC, and TOCSY_C-HSQC were measured in 66mM phosphate buffer at pH7.0 with 50mM KCl at 25℃ by Varian Unity Inova (500MHz). Analysis of spectrum was performed by NMRPIPE and Sparky. The solution structure of Hex C-terminal domain was calculated according to the NOE constraints by Cyana.

Results

We obtained a sufficient amount of Hex-C with GST (glutathione S-transferase) tag after sufficient purification with gel chomatography. Hex-C did not provide good NMR spectra for analysis when GST tag was removed by thrombin. Hence, we have measured NMR spectra of Hex-C without cleaving GST. According to the conventional analyses, we obtained the structure of Hex-C, which is abundant of the negatively charged amino acids with the transcriptional activation. Hex-C consists of four α-helices, and the structure is conserved by hydrophobic core. The surface was fully charged negatively as expected. It was observed by binding studies using Biacore instrument that the domain of C3 of the transcription factor GATA-2 binds to Hex-C. NMR spectra of Hex-C have been observed in presence and absence of GATA-2 domains and analyzed.

P022

ジスルフィド結合で拘束したTom20-プレ配列複合体の動的振る舞い

○斉藤貴士[1, 2], 伊倉真由美[2], 小島理恵子[2], 帯田孝之[2], 前仲勝実[2], 神田大輔[2]
[1]九州大学デジタルメディシン・イニシアティブ
[2]九州大学生体防御医学研究所

Dynamic behavior of disulfide-bond tethered Tom20-presequence complex.

○Takashi Saitoh[1, 2], Mayumi Igura[2], Rieko Kojima[2], Takayuki Obita[2], Katsumi Maenaka[2], Daisuke Kohda[2]
[1]Digital Medicine Initiative, Kyushu University, Fukuoka, Japan.
[2]Medical Institute of Bioregulation, Kyushu University, Fukuoka, Japan

Most mitochondrial proteins are synthesized in the cytosol as precursor proteins with a cleavable N-terminal presequences, and are imported into mitochondria. One of the subunits, Tom20, functions as a general protein import receptor by recognizing the presequences of proteins. Two crystal forms of the disulfide bonded Tom20-presequence complex have been obtained in our laboratory with different designs of the linker sequence. In the present study, we performed two NMR ^{15}N relaxation experiments, the model free analysis and transverse cross-correlation rate, to characterize the dynamic properties of the disulfide-bonded Tom20-presequence complex. We found molecular motions in submilli-second time scale at the interface between Tom20 and the presequence peptide. We propose that Tom20 recognizes presequences through dynamic equilibrium of two states revealed by the crystallography.

ミトコンドリアには独自のゲノムDNAが含まれているが、このミトコンドリアゲノムにコードされているタンパク質はごく少数である。ミトコンドリアを構成するタンパク質の大部分は核のゲノムDNAにコードされている。これらのミトコンドリアタンパク質は細胞質にあるリボソームでプレ配列が付加された前駆体蛋白質として合成された後、ミトコンドリアの外膜及び内膜に存在する膜透過装置（タンパク質からなる超分子複合体でそれぞれ Tom及びTim複合体と呼ばれる）によってミトコンドリア・マトリクスへと輸送される（Fig. 1）。このうちプレ配列を最初に認識する受容体がTom20である。プレ配列は15から70残基程度の長さ

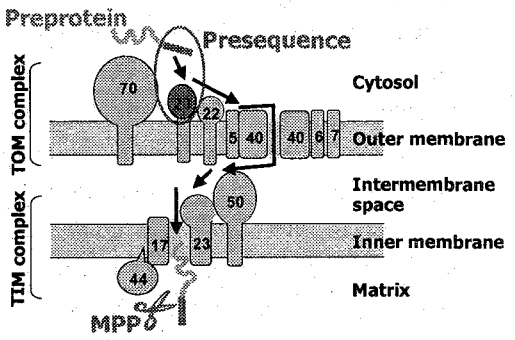

Fig. 1 Diagram of mitochondrial protein transport

Relaxation rate, ModelFree analysis, chemical exchange, Tom20

さいとうたかし、いぐらまゆみ、こじまりえこ、おびたたかゆき、まえなかかつみ、こうだだいすけ

であるがその種類は多種類存在し、Tom20が認識するプレ配列のアミノ酸６残基からなるコンセンサス配列こそ推定されているものの共通のアミノ酸配列は見いだせない。当研究室ではこれまでプレ配列とTom20をSS結合で固定した複合体において二種類の結晶でのX線結晶構造解析に成功している。本研究ではTom20によるプレ配列認識機構のメカニズムを立体構造的な基盤から明らかにすることを目的とし、これまでの立体構造解析に加えて，NMRスペクトル測定による分子運動性の解析をおこなう。＜実験＞Tom20とプレ配列の結合は弱く（Kdでμ Mオーダー）、結合状態と解離状態の交換は速い。そのため複合体の構造情報を得ることは非常に難しい。そこで本研究ではプレ配列にシステイン残基を導入し、Tom20のシステイン残基との間にＳＳ結合を形成することで複合体を安定にトラップする手法を用いた。実験ではアグリゲーションを避けるためにTom20の両末端にあるフレキシブル領域を削除した67残基からなるフラグメント（Asp59-Leu126）を大腸菌で発現し，これに aldehyde dehydrogenase プレ配列の一部（Gly12-Leu19）を分子間ＳＳ結合で固定した複合体を調製した。プレ配列とTom20を繋ぐリンカー部分にはAAG(X=A)を導入した（Fig.2）。Tom20及びプレ配列の運動性を調べるためにTom20、プレ配列ペプチドそれぞれを^{15}Nラベルしたサンプルを調製しNMRスペクトル測定によるModel Free解析並びにtransverse cross correlation rate constant（η_{xy}）の測定を行った。

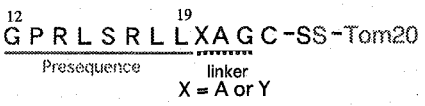

Fig. 2 Design of the presequence peptide

＜結果、考察＞　複合体の T_1、T_2、HetNOE の測定結果を用いて Model Free 解析を行った結果、Tom20 とプレ配列ペプチドの接触領域において R_{ex} が観察された。また同時に行った η_{xy} を用いた解析においても良く一致した結果が得られた（Fig. 3）。この結果は Tom20 とプレ配列ペプチドの接触領域にμs から ms の比較的遅い運動性が存在していることを意味している。これまで当研究室のX線結晶構造解析による研究では、Tom20 とプレ配列の SS 複合体においてリンカー部分のXに Ala 及び Tyr を導入した複合体でそれぞれ Tom20 へのプレ配列の結合様式が異なった結晶が得られている。これらの構造では、A リンカー複合体においては Tom20 がプレ配列の Leu18 と Leu19 を認識しているのに対し、Y リンカー複合体では Leu18 と Leu15 を認識していた。Tom20 が認識するプレ配列の配列パターンは $\phi_1\chi_2\chi_3\phi_4\phi_5$（$\phi$：疎水性残基、$\chi$：任意のアミノ酸残基）であることが知られており、一方の複合体構造のみではこのプレ配列のコンセンサスを説明することはできない。すなわち２つの結合様式を用いてプレ配列を動的に認識しているという新たなモデルが考えられる。本研究で行った緩和解析で得られた Tom20 とプレ配列の接触面で観察された運動性はこのモデルを強く支持するものである。

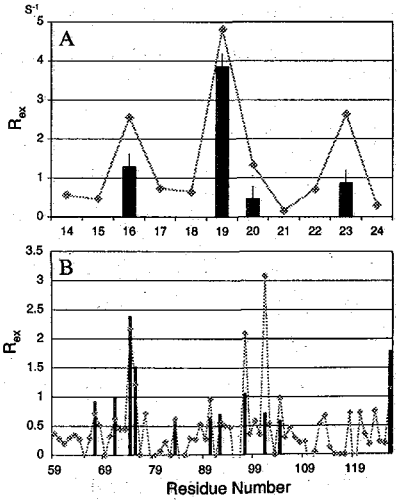

Fig. 3 Comparison of the Rex values determined from Model Free analysis (black bar) and η_{xy} (green line). A: presequence peptide. B: Tom20

P023

Saccharomyces cerevisiae Atg8 の溶液構造

○渡部 正博[1]、鈴木 展生[1]、横地 政志[1]、久米田 博之[1]、
藤岡 優子[1]、中戸川 仁[2]、大隅 良典[2]、稲垣 冬彦[1]
([1]北大院薬、[2]基生研)

Solution Structure of *Saccharomyces cerevisiae* Atg8

○Masahiro Watanabe[1], Nobuo N. Suzuki[1], Masashi Yokochi[1], Hiroyuki Kumeta[1], Yuko Fujioka[1], Hitoshi Nakatogawa[2], Yoshinori Ohsumi[2], Fuyuhiko Inagaki[1]
([1]Graduate School of Pharmaceutical Sciences, Hokkaido University, [2]National Institute for Basic Biology)

Atg8, a member of a novel ubiquitin-like protein family, is an indispensable component of the autophagy machinery in yeast *Saccharomyces cerevisiae*. This protein consists of 117 amino acid residues, and undergoes the reversible conjugation to phosphatidylethanolamine (PE) through a multistep ubiquitin-like process. We determined the solution structure of Atg8 variant K26P by NMR methods. K26P is the mutant that reduces the dynamics of the N-terminal region in Atg8. The structure comprises the N-terminal helical domain and the ubiquitin-like C-terminal domain, which is similar to that of mammalian Atg8 homologues. Previous report suggested that the PE lipidation induces a conformational change in N-terminal region of Atg8. The relationship between the dynamics of the N-terminal domain and autophagic activity will be discussed.

【背景】

オートファジー（自食作用）とは、飢餓状態に陥った細胞が生き延びるために、自己のオルガネラ等を分解してリサイクルするためのシステムである。酵母から哺乳動物に至るまで見出され、基本的な生命維持のシステムと考えられている。1960 年代にその現象が発見され、遺伝学的な研究では、酵母において少なくとも 16 個の *ATG* 遺伝子が関与することが明らかにされているが、分子レベルにおける解析は未知な点が多い。オートファジーでは、初期の過程で隔離膜が湾曲しながら伸張して、細胞質の一部が隔離膜によって取り込まれるオートファゴソームと呼ばれる 2 重膜構造体が形

キーワード：Atg8, autophagy, ubiquitin-like

○わたなべ　まさひろ、すずき　のぶお、よこち　まさし、くめた　ひろゆき、
ふじおか　ゆうこ、なかとがわ　ひとし、おおすみ　よしのり、
いながき　ふゆひこ

成されるが、そのメカニズムは不明な点が多い。オートファゴソームの形成に必須なAtgタンパク質群には、Atg5とAtg12を結合させるAtg12結合系と、脂質のホスファチジルエタノールアミン(PE)とAtg8を結合させるAtg8結合系の2種類のユビキチン様反応系がある。本研究の対象となるAtg8系結合システムにおいて、Atg8は117アミノ酸残基からなる分子量約13.6 kDaの親水性のタンパク質で、N末端ドメインとユビキチン様ドメインの2つからなり、一部がオートファゴソーム膜上に局在化することが報告されている。

本研究の目的は、Atg8のN末端ドメインにおける運動性の解明と、Atg8がPE化して隔離膜に向かってどのようにしてオートファゴソームが形成されるのかを、Atg8系結合システムの反応メカニズムを用いて構造生物学の見地から解明することである。

【結果・考察】

Atg8の溶液中における立体構造をNMR法によって解析した。野生型のAtg8では、^{1}H-^{15}N-HSQCスペクトルでN末端21残基に相当するピークを観測出来なかった。このため、N末端ドメインの運動性を抑制させるAtg8の遺伝子変異体としてK26Pを作成した。アミノ酸残基26番目は、Atg8のホモログにおいて2つのドメインをつなぐリンカー領域に存在し、Atg8のホモログで保存されているプロリン残基に置換した。K26P変異体を調製したところ、野生型よりも収量や安定性が増加した。K26P変異体では、^{1}H-^{15}N-HSQCスペクトルにおいて殆どのピークが観測され、N末端領域の運動性が抑制されたことが示唆される（図1）。

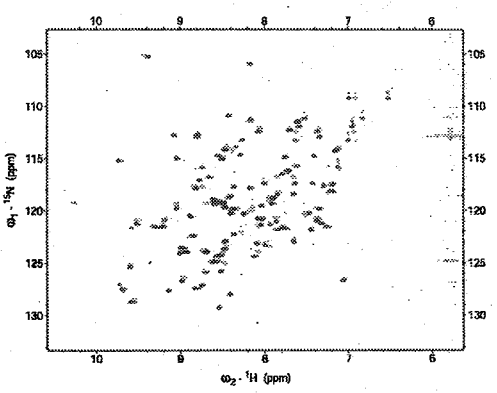

Figure 1 Overlay of 1H-15N-HSQC spectra
thick: K26P, thin: wild-type

K26P変異体の構造解析から、Atg8のホモログと同様にN末端ドメインとユビキチン様ドメインの2つからなる構造をとることが明らかになった。構造が収束しているユビキチン様ドメインとは対照的に、N末端ドメインは1本目のα-ヘリックス周辺を中心に運動性が高いことが示唆された。また、重水素交換実験からの結果もこの領域の運動性の高さを支持している。

本年会では、構造解析に加えてK26P変異体のPE化修飾およびオートファジー活性の結果を踏まえて、立体構造とN末端ドメインの運動性や機能についても議論を行いたい。

P024

Structural study of a transmembrane signal transducer *p*HtrII by NMR and EPR

○Kokoro Hayashi[1], Yuki Sudo[2], Masaki Mishima[1], Hideyuki Hara[3]
Naoki Kamo[2] and Chojiro Kojima[1]

[1]Graduate School of Biological Science, Nara Institute of Science and Technology
[2]Graduate School of Pharmaceutical Sciences, Hokkaido University
[3]ESR Division, Bruker Biospin K.K.

Background

The *pharaonis* halobacterial transducer protein, *p*HtrII and *pharaonis* phoborhodopsin, *p*pR (also called *pharaonis* sensory rhodopsin II, *Np*SRII) are phototaxis proteins from extreme halophile and alkalophilic bacteria, *Natronomonas pharaonis*, and these proteins form complex. Light signals are transmitted to *p*HtrII through *p*pR, and phosphorylation cascades that modulate flagella motors are activated (Fig.1). *p*HtrII is called transducer protein, and composed of transmembrane region, linker region (called HAMP domain), methylation region and signaling region. The HAMP domain has important roles in many taxis signal transductions. However, HAMP domain structure has not been reported, and its function in the signal transduction is poorly understood. In this study, we focused on the structure of *p*HtrII linker region to elucidate the signaling mechanism between *p*HtrII and *p*pR.

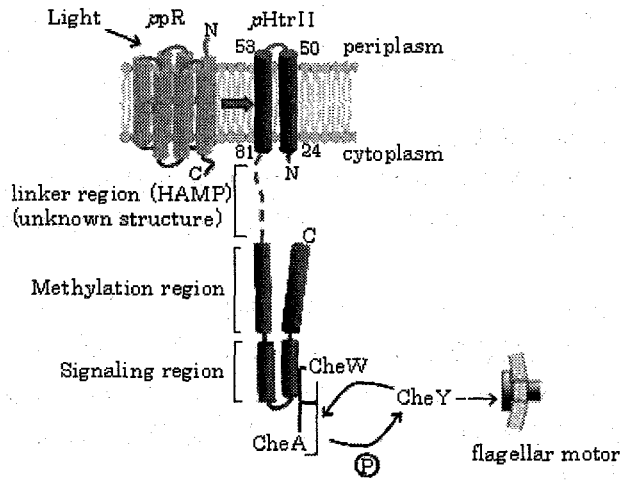

Fig.1 Photo-signal transduction through *p*pR and *p*HtrII

Keywords : membrane protein, HAMP domain, solution NMR, EPR, ELDOR

3D structure determination of HAMP domain by solution NMR

*p*HtrII(1-159) containing linker region and transmembrane region was expressed in *E. coli* and a trypsin resistant fragment (residue 100-159) was found within the linker region. For the structure determination of a trypsin resistant fragment (residue 100-159), ^{15}N- and $^{15}N/^{13}C$-labeled samples were prepared, and the 3D structure of *p*HtrII(100-159) was determined by using the multi-dimensional solution NMR spectroscopy. These results showed that *p*HtrII(100-159) had an α-helix structure (residues D125 to E153).

Structural analysis of HAMP domain in liposome by CW-EPR

In order to exam the structure of this region in liposome, continuous wave (CW) EPR experiments were carried out. In the EPR experiments, *p*HtrII(1-159) which was singly or doubly spin-labeled and reconstituted into phosphatidylcholine was used. Doubly labeled spectra were compared with the sum spectra of singly labeled ones. For two doubly labeled *p*HtrII(1-159) samples (residues 138 and 145, and residues 134 and 145), dipolar broadening were observed. In general, the dipolar broadening is observed for the spin pair with interspin distance of $\leqq 20$ Å. Thus these results suggest that α-helical structure found in solution is kept in liposome.

Distance measurement between *p*pR and *p*HtrII HAMP domain by pulsed EPR

In order to obtain the distance between *p*HtrII linker and *p*pR E-F loop, pulsed electron-electron double resonance (ELDOR/DEER) was applied. The distances between residues 154 of *p*pR and 98 of *p*HtrII, and residues 154 of *p*pR and 134 of *p*HtrII were measured in the dark-state or light-state of *p*pR. These distances of dark-state suggest that *p*HtrII linker region does not form continuous α-helix but same special conformation. The differences between dark-state and light-state were small.

Discussion

R. Moukhametzianov *et al.*(2006) reported the crystal structure of the photoactive form *p*pR and the transmembrane region of *p*HtrII complex. They showed that *p*HtrII responded to the activation of the *p*pR by clockwise rotation of about 15° of helix TM2 and a displacement of this helix by 0.9 Å at the cytoplasmic surface. Our ELDOR data suggest that linker region helix (residue 126-152) does not have direct interaction with *p*pR E-F loop, and linker region structure does not change dramatically in the signal transduction. Here, we revealed that *p*HtrII linker region had a structural domain. The structure can transduce the subtle structural change of transmembrane helix of *p*HtrII to the methylation region and signaling region.

P025

NIPP1 FHA ドメインの立体構造解析

(1北大・院薬・構造生物, 2北大・生命科学院・構造生物,
3北大・遺制研・情報調節)

○久米田博之1, 小椋賢治1,2, 藤岡優子1, 安達聡一郎2,
田沼延公3, 菊池九二三3, 稲垣冬彦1,2

Solution structure of the NIPP1 FHA domain

(1Laboratory of Structural Biology, Graduate School of Pharmaceutical Sciences, Hokkaido University, 2Laboratory of Structural Biology, Graduate School of Life Science, Hokkaido University, 3Division of Biochemical Oncology and Immunology, Institute for Genetic Medicine, Hokkaido University)

○Hiroyuki Kumeta1, Kenji Ogura1,2, Yuko Fujioka1, Soichiro Adachi1,
Nobuhiro Tanuma3, Kunimi Kikuchi3, Fuyuhiko Inagaki1,2

NIPP1 was originally discovered as a potent and specific inhibitor of protein Ser/Thr phosphatase-1 (PP1), hence its name, nuclear inhibitor of PP1. NIPP1 is a ubiquitous nuclear protein that is implicated in transcription and pre-mRNA splicing by mechanisms that do not involve PP1. The N-terminal part of NIPP1 consists of phosphothreonine-interacting Forkhead-associated (FHA) domain. The FHA domain of NIPP1 interacts with phosphorylated mRNA splicing factor proteins. Here, we describe the solution structure of NIPP1 FHA domain by heteronuclear NMR spectroscopy and discuss the recognition of phosphorylated targets.

[はじめに]

NIPP1 は Ser/Thr 残基特異的プロテインフォスファターゼ（PP1）の活性阻害分子として発見された核内タンパク質であり、そのノックアウトマウスは胎生致死となる。近年、NIPP1 の機能として PP1 を介した遺伝子発現の転写後調節への関与ならびに PP1 に関係なく pre-mRNA splicing 抑制に関与することが明らかになった。NIPP1 の N 末側には FHA ドメインが存在し、このドメインは mRNA splicing 関連タンパク質との相互作用が確認されている。

FHA ドメインはリン酸化 Thr（以下 pT）を認識する構造ドメインとして酵母から高等生物に至るまで幅広い生物種に存在し、その立体構造および pT を含むペプチドの認識機構について複数報告されている。酵母由来 Rad53p タンパク質中に存在する二つの FHA ドメイン（FHA1、FHA2）は認識配列の選択性が異なり、それぞれ pTxxD、pTxxI/L を認識する。また、細胞増殖関連タンパク質であるヒト由来 Ki67 の FHA ドメインでは結合相手タンパク質である hNIFK 中の pT を含む 44 残基からなる領域を認識し、Rad53p FHA1 および FHA2 とは大きく異なる認識機構を有している。NIPP1 FHA ドメインは標的分子中の TP に富んだ領域を認識することは明らかになっているが標的とする配列モチーフおよび認識機構はわかっていない。

FHA domain、NIPP1、mRNA splicing

くめたひろゆき、おぐらけんじ、ふじおかゆうこ、あだちそういちろう、たぬまのぶひろ、きくちくにみ、いながきふゆひこ

本発表では、NIPP1 FHA ドメインの立体構造解析を行い他の FHA ドメインとの比較検討を行い、標的であるリン酸化された mRNA splicing 関連タンパク質の認識機構について議論する。

[方法・結果]

NMR 測定サンプルは 0.5 mM $^{13}C/^{15}N$ ラベル体を用いた。多核多次元 NMR 測定は、Varian 社製 UNITY INOVA 800 MHz および 600 MHz 分光計によって行った。スペクトル処理には NMRPipe、スペクトル解析には Sparky をそれぞれ用いた。^{13}C-および ^{15}N-NOESY-HSQC により NOE 信号を取得し、CYANA 2.1 による自動 NOE 信号帰属および立体構造計算を行った。構造計算の結果、安定最終構造 20 個の平均 Target function は 6.11 $Å^2$ になり、Ala20 から Pro130 までの主鎖の RMSD は 0.3 Å、重原子の RMSD は 0.88 Å であった(図)。本構造は、一本の短いαヘリックス(Pro55-Cys58)とストランド六本による逆平行βシート（Leu29-Lys33、Glu39-Ile43、Thr94-Leu96、Ile99-Leu101、Asp112-Ser116、Arg122-Leu126）およびストランド四本による逆平行βシート（Tyr48-Gly52、Ala72-Tyr76、Val83-Asp87、Pro106-Gln108）から構成される。βシートは互いに向き合って位置しており、既知の FHA ドメインと似た構造骨格を持っていた。pT 認識に必須であり FHA ドメイン間で完全に保存された残基（Arg53、Ser68、His71）はループ上に存在していた。His71 側鎖の Hε2-Nε2 ピークが ^{1}H-^{15}N HSQC 上において観測され、他の FHA ドメイン同様にプロトネーションを受けていることが確認された。

[考察]

pT 認識に直接関係する残基は配列上および立体構造上保存されていた。NIPP1 FHA ドメインとの結合が報告されている MELK（Maternal Embryonic Leucine zipper Kinase）中の pT を含む 18 残基ペプチドとの Titration 実験を行った。立体構造から推測された結合領域を構成するアミノ酸の主鎖アミドピークの移動が確認され、NIPP1 FHA ドメインも他の FHA 同様の機構で pT を認識することが確認された。標的の選択性に関して Rad53p FHA1、Rad53p FHA2 との比較を行った。それぞれ pT より＋3位に位置するアミノ酸（Asp または Ile/Leu）の認識部位は配列上および立体構造上保存されておらず、異なる認識機構であることが考えられる。NIPP1 FHA ドメインの標的分子である CDC5L、SAP155、MELK における認識配列中には TP モチーフが存在するが他に配列特異性は見当たらない。今後、標的分子と NIPP1 FHA ドメインの複合体構造解析によって認識機構が明らかになると推察される。

Fig. The solution structure of NIPP1 FHA domain.
(left, ensemble 20 structures. right, rbbon diagram with His71 stick model)

P026

RIG-I C末端CARDの溶液構造

(1北大・生命科学院、2北大・院薬、3京大・ウイルス研)
○ 都築奈津子1、高橋清大2、堀内正隆1,2、藤岡優子2、
久米田博之2、小椋賢治1,2、藤田尚志3、稲垣冬彦1,2

Solution structure of RIG-I C-terminal CARD

(1Graduate School of Life Science, Hokkaido University, 2Department of Structural Biology, Graduate School of Pharmaceutical Sciences, Hokkaido University, 3Laboratory of Molecular Genetics, Department of Genetics and Molecular Biology, Institute for Virus Research, Kyoto University)
○ Natsuko Tsuzuki1, Kiyohiro Takahasi2, Masataka Horiuchi1,2, Yuko Fujioka2, Hiroyuki Kumeta2, Kenji Ogura1,2, Takashi Fujita3, Fuyuhiko Inagaki1,2

RIG-I (Retinoic acid-inducible gene I) is known as a receptor that recognizes viral double-strand RNA (dsRNA) in cytoplasm. RIG-I consists of N-terminal tandem CARD (Caspase recruitment domain) like domains and a C-terminal helicase. Upon viral infection, N-terminal CARDs transduce the signal downstream and induce type-I interferons. Here we report the solution structure of C-terminal domain of tandem CARD and discuss its functional implications.

【序論】

RIG-I (Retinoic acid-inducible gene I)は、自然免疫系において、細胞内のウイルス由来二重鎖RNAを認識し、I型IFN産生へ至るシグナル伝達を仲介する。RIG-IはN末端側にCARD (Caspase recruitment domain)と呼ばれるドメインを2回繰り返して持ち、このCARDを使って下流へシグナルを伝達していると考えられているが、その詳細は未だ明らかでない。そこで今回、RIG-I のシグナル伝達様式を解明するため、CARD領域のNMRによる立体構造解析を行った。

【実験】

RIG-I N末端側の繰り返しCARDのうち、C末端側 (CARD-C, 96残基) をGST融合タンパク質として大腸菌により発現させた。$^{13}C/^{15}N$ラベル体作成にはM9培地を使用し、アフィニティー、ゲルろ過クロマトグラフィーにより精製した。サンプル濃度1.2 mMの$^{13}C/^{15}N$ラベル体を用い、Varian UNITY$_{INOVA}$ 600および800を使用し、25℃にてNMR測定を行った。主鎖帰属用に^{1}H-^{15}N-HSQC、HNCO、HN(CO)CA、

【キーワード】 自然免疫　立体構造　シグナル伝達　CARD

【著者ふりがな】○つづきなつこ、たかはしきよひろ、ほりうちまさたか、ふじおかゆうこ、くめたひろゆき、おぐらけんじ、ふじたたかし、いながきふゆひこ

HNCA、HBHA(CO)NH、HN(CA)HA、CBCA(CO)NH、HNCACB、(HCA) CO(CA)NH、側鎖帰属用に^{1}H-^{13}C-HSQC、C(CO)NH、CCH-TOCSY、HC(C)H-TOCSY、HbCbCgCdHd、HbCbCgCdCeHe、距離制限として^{13}C-edited 3D NOESY、^{15}N-edited 3D NOESYを測定した。データ処理はNMRpipe、スペクトル帰属はSparky、NOE信号並びにTALOSによる二面角制限情報を用いて、CYANA2.0 による立体構造計算を行った。

【結果と考察】

立体構造計算の結果、得られた構造を Fig.1.に示す。RIG-I CARD-C は 6 本のα-ヘリックスから成る球状のコンパクトな構造をとり、主鎖原子の RMSD が 0.30 Å、側鎖重原子を含む RMSD が 0.84 Å (103-189)と、よく収束した構造が得られた。また、分子表面に裏表の対になる形で、それぞれ 3 本のヘリックスから構成される広い酸性面と塩基性面が存在した。

CARD は、一般に分子表面に広い酸性面と塩基性面を持ち、この面を使って静電相互作用により CARD 同士で特異性の高い結合をすることが知られている。今回明らかとなった RIG-I CARD-C の構造を、立体構造既知である Caspase9、Apaf-1 の CARD と比較したところ、ヘリックスの配向が類似していると共に、静電ポテンシャルにおいても、結合に重要とされる広い酸性面・塩基性面の位置は類似していた。しかし今回決定した構造においては、両 CARD に比べると電荷が乏しく、相互作用に重要とされるアミノ酸残基もあまり保存されていなかった。このことから、RIG-I CARD-C は少なくとも既知の CARD ほど強固な結合はせず、別な結合様式をとる可能性も示唆された。

【参考文献】

Yoneyama M, et al. Nature Immunol. 5, 730-737 (2004)
Qin H, et al. Nature 399,549-557 (1999)

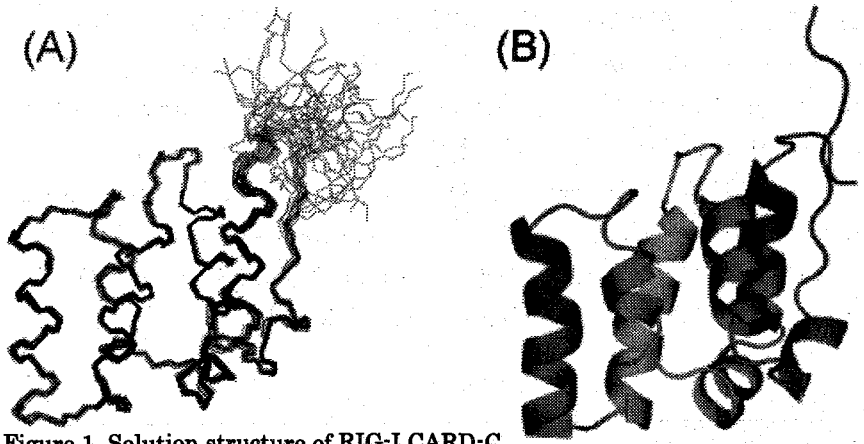

Figure 1. Solution structure of RIG-I CARD-C

(A) Superposition of the backbone atoms of 20 lowest energy structures.

(B) Ribbon model of RIG-I CARD-C.

P027

標的 RNA と Musashi タンパク質との複合体の構造解析

○大山 貴子[1]、宮ノ入 洋平[1]、永田 崇[1]、岡野 栄之[2]、片平 正人[1,3,4]
[1]横浜市立大学・国際総合科学研究科、[2]慶応大学・医学部、[3]理研・ゲノム科学センター、[4]科技振興・さきがけ

Structural analysis of Musashi protein complexed with the target RNA

Takako Ohyama[1], Youhei Miyanoiri[1], Takashi Nagata[1], Hideyuki Okano[2], Masato Katahira[1,3,4]
[1]International Graduate School of Arts and Sciences, Yokohama City University, [2]Keio University School of Medicine, [3]GSC, RIKEN, [4]PRESTO, JST

Musashi1 protein regulates differentiation of central nervous system through translational inhibition of the target gene. Musashi1 has two RNA binding domains (RBD1 and RBD2). We have already determined the structures of each single RBD. Here, we have analyzed the RBD1-RBD2 (connection of two RBDs) in complex with the target RNA. First, we have determined the structure of each RBD in the complex. Secondly, we have determined the relative orientation of two RBDs in the complex on the basis of residual dipolar couplings (RDCs). Thirdly, we are trying to obtain further structural information from paramagnetic relaxation enhancement (PRE). Fourthly, isotope-filtering technique in combination with residue-specific labeling is applied to identify the intermolecular NOE contacts. The features of the complex will be addressed on the basis of these analyses.

序論

Musashi タンパク質は(G/A)U_nGU (n = 1-3)配列を有する標的 mRNA に結合してその翻訳を抑制する事で、神経細胞の分化｜未分化の非対称分裂を制御している。Musashi タンパク質は 2 つの RNA 結合ドメイン(RBD1, RBD2)を有する。我々はこれまでに RBD1 と RBD2 各々の単独の立体構造解析、ダイナミクス、RNA との相互作用を報告し、RBD1 が RBD2 に比して高い結合能を有する理由を明らかにしてきた。Musashi タンパク質においては RBD1 と RBD2 が連結しているが、RBD1-RBD2 連結体は RBD1 よりさらに高い結合能を有する。今回は RBD1-RBD2 連結体と標的 RNA の複合体の構造を残余双極子結合(RDC)、常時性緩和促進(PRE)、残基特異的な標識、他核フィルターを組み合わせて解析した結果を報告する。

キーワード:Musashi, RNA 結合タンパク質, タンパク質－RNA 複合体, NMR, 立体構造

おおやまたかこ、みやのいりようへい、ながたたかし、おかのひでゆき、かたひらまさと

結果と考察

標的 RNA(15mer ないしは 10mer)と複合体を形成した RBD1-RBD2 に関し、NMR の共鳴線の帰属を三重共鳴スペクトルを用いて常法に従って完了した。次に標的 RNA を RBD1-RBD2 連結体に加えた際のケミカルシフトパータベーションを解析した。その結果、RNA の添加に伴い、まず RBD1 に由来する共鳴線の化学シフト値が変化し、その後引き続いて RBD2 に由来する共鳴線の化学シフト値が変化した。このことから、RBD1-RBD2 連結体に RBD1 がまず結合し、引き続いていて RBD2 が結合する事が分かった。これは連結体において、RBD1 と RBD2 が両方ともに RNA と相互作用を行うためには２つの RBD の立体配置のリアレンジメントが必要とされることを示唆している。

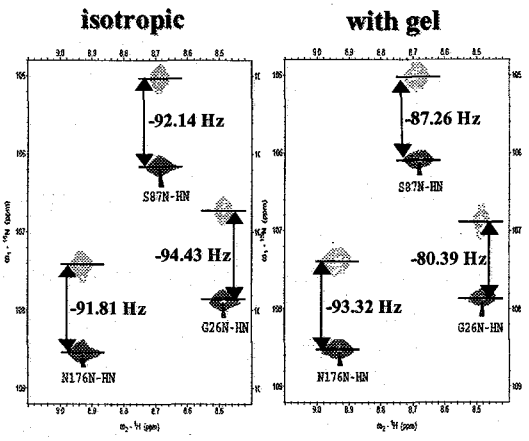

Figure IPAP ^{1}H-^{15}N HSQC spectra of the complex between RBD1-RBD2 and target RNA under isotropic and gel conditions.

そこで、既に報告してきた RBD1 と RBD2 の各々単独の構造と、残余双極子結合(RDC)の値を組み合わせることで、複合体中における RBD1 と RBD2 の相対配向を決定した。その結果、各ドメインのβシートを同じ方向に平面的に配置した構造が示唆された。

さらに、より詳細な RBD1-RBD2 連結体の RNA 認識機構の解明のために、複合体を形成した RBD1-RBD2 連結体について、個々のドメインの立体構造を NOE 情報等に基づき決定した。今回得られた各ドメインの構造に RDC の情報を組み合わせる事で、RBD1 と RBD2 の相対配向をより正確に決定した。しかし、ドメイン間の NOE の観測が困難であったため、相対配向の完全な決定には至らなかった。そこで現在、RDC に加え PRE (paramagnetic relaxation enhancement)を利用することで相対配向の完全な決定を試みている。また、他核フィルターの手法を適用することで、RBD1-RBD2 連結体と RNA 間の分子間 NOE の同定も試みている。これらによって複合体の立体構造の解明を目指している。

P028

昆虫外皮由来新規サイトカインの構造解析

[1]北大院・生命科学、[2]佐賀大・農
○神谷昌克[1]、仲戸川真一[1]、織田康則[2]、上島達郎[1]、相沢智康[1]、熊木康裕[1]、早川洋一[2]、出村誠[1]、河野敬一[1]

Solution structure of a novel cytokine from the larval integument of the armyworm, *Pseudaletia separata*

[1]Grad. Sch. of Life Sci., Hokkaido Univ., [2]Fac. of Agr., Saga Univ.
○Masakatsu Kamiya[1], Shin-ichi Nakatogawa[1], Yasunori Oda[2], Tatsuro Kamijima[1], Tomoyasu Aizawa[1], Yasuhiro Kumaki[1], Yoichi Hayakawa[2], Makoto Demura[1], Keiichi Kawano[1]

Insects are one of the most flourishing species in the worlds and live in almost every habitat on the earth. Insects lack an acquired immune system seen in higher vertebrates, but they can protect themselves from a wide variety of pathogenic microorganisms and parasites by intensely-potent innate immune system. Insect blood cells (hemocytes) play an essential role in cellular immune responses like phagocytosis, nodulation, and encapsulation. In the present study, we focused our attention upon the insect integument where many molecular events must occur following an injury, though any immune reactions in that tissue have not been revealed yet. In integument cell, a certain type of cytokines could physiologically modulate the function of hemocytes. It is reasonably speculated that a class of molecules are secreted from the injured integumental cells and activate hemocytes to agglutinate or form spreading fibriform network around the injured site for defending against the invading microorganisms and sealing the open wound.

The purpose of the present study was to discover the unknown factor that induces plasmatocytes to rapidly aggregate from the larval integument of *Pseudaletia separata*, to isolate and purify, and to characterize the novel factor.

キーワード：　新規サイトカイン、自然免疫、昆虫

著者ふりがな：　かみや まさかつ、なかとがわ しんいち、おだ やすのり、かみじま たつろう、あいざわ ともやす、くまき やすひろ、はやかわ よういち、でむら まこと、かわの けいいち

[序論]

我々生物は、病原性微生物に囲まれて生活しており、常に感染の危険に晒されている。この危険から身を守る手段が免疫である。免疫には、抗体が体内から病原性微生物を排除する獲得免疫と、抗菌ペプチドや血球細胞が体内から病原性微生物を排除する自然免疫がある。ヒトのような高等脊椎動物は獲得免疫と自然免疫を併せもつが、昆虫に代表される無脊椎動物は自然免疫しかもっていない。しかし昆虫は、その強力な生体防御機構と高い適応能力で地球上のいたるところに分布している。

本研究は、昆虫を研究材料に自然免疫に関与する新規のサイトカインを単離・精製し、その性質と機能を解析することを目的としている。

[結果]

アワヨトウ幼虫の外皮組織中には、血球細胞の凝集塊形成を誘起する未知なるサイトカインが存在することが明らかになった(Fig. 1)。この凝集活性を指標に、活性因子を 5 段階のHPLC 操作により単離した。最終精製活性分画をペプチドシーケンサーで解析した。また、外皮由来のcDNAライブラリーからクローニングを行った。最終的に32残基からなるペプチドであることを明らかにし、hemocyte-aggregation factor (AGF)と名づけた(Fig. 2)。

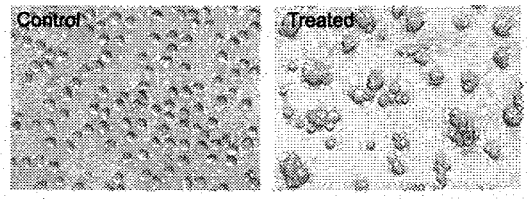

Fig. 1. Aggregation of hemocytes from *P. separata*

S-V-Q-I-L-R-C-P-D-G-M-Q-M-L-R-S-G-
1 10
Q-C-V-A-T-T-E-P-P-F-D-P-D-S-Y
20 30

Fig. 2. Primary structure of AGF

AGFの構造解析を行うために、大腸菌においてTrx融合系による組み換えAGFの大量発現系を構築し、His-tag精製、enterokinase処理により^{15}Nラベル体を調製した。^{15}N-edited TOCSYおよび^{15}N-edited NOESYにより^{1}H/^{15}Nの帰属を行った(Fig. 3)。現在、構造計算のためのNOE情報を収集している。本発表では、AGFの構造の特徴について述べたい。

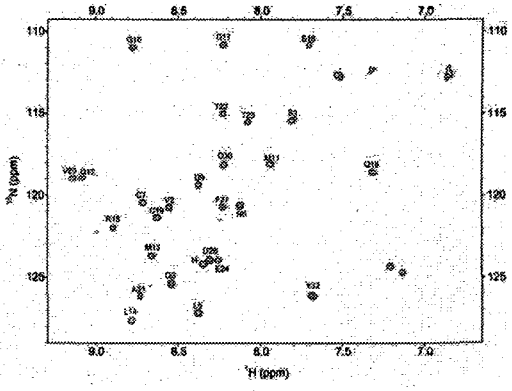

Fig. 3. ^{1}H-^{15}N HSQC spectrum for AGF

[謝辞]

本研究の一部は、新技術・新分野創出のための基礎研究推進事業の補助を受けておこなわれた。

P029

ムスカリン性アセチルコリンレセプター第３細胞内ループ部分ペプチドの溶液構造

（群馬大学工学部[1]、三菱化学生命科学研究所[2]）
○細田和男[1]、小堀可奈子[1]、稲岡斉彦[1]、石井毅[1]、久保田真[1]、向井秀仁[2]、河野俊之[2]、若松馨[1]

Structure of G protein-activating peptide fragment from m4 muscarinic acetylcholine receptor

([1]Department of Biological and Chemical Engineering, Faculty of Engineering, Gunma University, [2]Mitsubishi Kagaku Institute of Life Sciences)
Kazuo Hosoda[1], Kanako Kobori[1], Yoshihiko Inaoka[1], Takeshi Ishii[1], Makoto Kubota[1], Hidehito Mukai[2], Toshiyuki Kohno[2], Kaori Wakamatsu[1]

Abstract

The peptide fragment corresponding to the C-terminal 14 residue of the third intracellular loop of m4 muscarinic acetylcholine receptor, m4I3C(14), selectively activate Gi-type G proteins but not Gs and Gq, as does the parent m4 receptor. Thus the peptide is expected to be useful as a low-molecular-weight mimetic of the receptor. Because the activation of Gi by the peptide is potentiated by the reconstitution of G proteins in lipid vesicles, the conformation of the peptide in the membrane-bound state is preferable for the activation of G protein. We thus analyzed the conformations of the peptide in a G protein-bound state and in a membraneous state.

［緒言］　細胞内情報伝達で重要な役割を果すとともに創薬の最大のターゲットになっているＧ蛋白質共役型レセプター（GPCR）の機能を理解する上で，GPCR とＧ蛋白質との相互作用を解析する事は重要である．しかし，GPCR は大量に調製する事が難しいだけでなく，膜蛋白質であるために構造解析も現状では困難である．m4 ムスカリン性アセチルコリンレセプター（ｍ４レセプター）の細胞内第三ループのＣ末端側 14 残基に相当するペプチド m4I3C(14)は Gi/Go を活性化するが Gs や Gq を活性化せず，元の m4 レセプターの特異性を保持している (1)．そこで，このペプチドは m4 レセプターの良い低分子モデルとなると期待される．

レセプター　Ｇタンパク質　ペプチド　活性化　ミセル

ほそだかずお、こぼりかなこ、いなおかよしひこ、いしいたけし、くぼたまこと、むかいひでひと、こうのとしゆき、わかまつかおり

このペプチドによるG蛋白質の活性化はG蛋白質を脂質ベシクルに再構成すると増強されるので，脂質膜に結合した時の立体構造がG蛋白質の活性化に適している可能性がある．今回，m4I3C(14)についてG蛋白質に結合した時の構造と脂質に結合した時の構造をCDとNMRで解析した．

［実験および結果］　安定同位体ラベルしたm4I3C(14)はユビキチン融合蛋白質として大腸菌で発現させ，YUHで切断することにより調製した．また，ノンラベルのペプチドは化学合成した．

このペプチドは水溶液中で低濃度の場合random coilのCDスペクトルを与えたが，濃度を上げるとβ構造の形成が観察された．ペプチドにαヘリックス構造を誘導する事が知られているTFEを加えてもαヘリックスに特徴的なスペクトルは現れなかった．dodecylphosphocholine (DPC) のミセルやPC/PS/CHAPSOのバイセルの存在下ではβ構造を含むスペクトルが観察された．

m4I3C(14)がG蛋白質に結合した時の構造をTRNOEで決定するために，NMRサンプルチューブに入れたペプチドにGiαを添加したところ，ペプチドとGiαとが沈殿した．この沈殿形成はNMRサンプルチューブをシリコナイズしておく事でかなり回避できた．

［考察］　G蛋白質を直接活性化するペプチドであるマストパラン-XはG蛋白質に結合した時も脂質二重膜に結合した時もαヘリックスを形成するのに対し (2,3)，m4I3C(14)は脂質のミセルやバイセルを共存させても典型的なαヘリックス構造は形成しなかった．m4I3C(14)は二次構造予測でβ構造の形成が強く示唆されたこと．TFEを加えてもαヘリックスを形成しないことから，このペプチドはαヘリックスではない構造（β構造と思われる）でG蛋白質に結合し活性化している可能性が高い．現在，脂質ミセルに結合した時およびGiαに結合した時の構造を解析中であり，立体構造とその生理的意義について当日議論する予定である．

[Reference]

1. F. Kuribayashi, et al., *EMBO J.* 21, 6312–6320 (2002).
2. K. Kusunoki, et al., *Biochemistry* 37, 4782–4790 (1998).
3. T. Fujiwara, et al., *J. Biomol. NMR* 28(4), 311-325 (2004).

P030

Aromatic-amide interactions in tripeptides Ar-Gly-Xaa as revealed by NMR

Yasuhiro Kumaki[1], Manabu Nakano[2], Masakatsu Kamiya[2], Tomoyasu Aizawa[2], Makoto Demura[2], Keiichi Kawano[1,2], and Norio Matsushima[3]

[1]High-Resolution NMR Laboratory and [2]Division of Biological Sciences, Graduate School of Science, Hokkaido University, [3]School of Health Sciences, Sapporo Medical University,

Ice nucleation protein (INP), heterogeneous nuclear ribonucleoprotein (hnRNP), prion, plant glycine-rich RNA-binding protein (GRRBP), Atriplex canescens ozone-inducible proteins and Cicer arietinum glycine-rich proteins (GRPs) contain repetitive glycine-rich sequences intercepted with aromatic residues such as tryptophan or tyrosine. Synthetic peptides corresponding to sections of the sequences of these proteins are analyzed by NMR in order to elucidate the structures[1-6]. The assignment of these peptides indicates that backbone amide proton resonance of the residues located at i+2 in the segment Tyr/Phe/Trp(i)-Gly(i+1)-Xaa(i+2) ("Xaa" means an arbitrary amino acid except Pro) in peptides shows significant negative deviation form the random coil value (upfield shifts). Such upfield shifts can be ascribed to weakly polar interactions between aromatic rings of amino acids at position i and hydrogens of backbone amides at position i+2 (Ar(i)-HN(i+2)). The amide protons which are associated with Ar(i)-HN(i+2) interactions are located above or below aromatic rings, therefore, show upfield ring current shifts. Our results indicates that not only Gly but also other residues at position i+2 show significant upfield shifts of the backbone amide proton resonance, which suggests that non-Gly residues can be the donors in Ar(i)-HN(i+2) interactions in case the residue at position i+1 is Gly. However, according to the statistical survey based on crystal structures presented by Worth and Wade[7], no Ar(i)-HN(i+2) interactions were found in case Gly at position i+1 and any residues other than Gly at position i+2.

To understand the origin of this discrepancy, we investigated the relationship between amino acid sequence and chemical shift deviation of amide protons by use of BMRB chemical shift database. For this investigation, we extracted amide proton chemical shifts for Ar-Gly-Xaa sequences from all ^{1}H chemical shift entries in BMRB database, and obtained their deviation from the random coil values. The result of this investigation shows that the chemical shift deviations of amide protons from the random coil values for Xaa(i+2) are widely distributed, however, Xaa(i+2) residues which is not Gly with significant negative chemical shift deviations certainly exist (Fig.1). This suggests that Ar(i)-HN(i+2) interactions is possible in tripeptide Ar-Gly-Xaa even if Xaa is not Gly. In addition, we investigated the relation between the significant negative chemical shift deviations of the backbone amide protons in BMRB database and their ring current shift values calculated from their corresponding PDB structural data determined by NMR experiments in order to confirm our findings. We will present the result of this survey on poster session.

Keyword: Aromatic-amide interactions, ring current shift, BMRB database

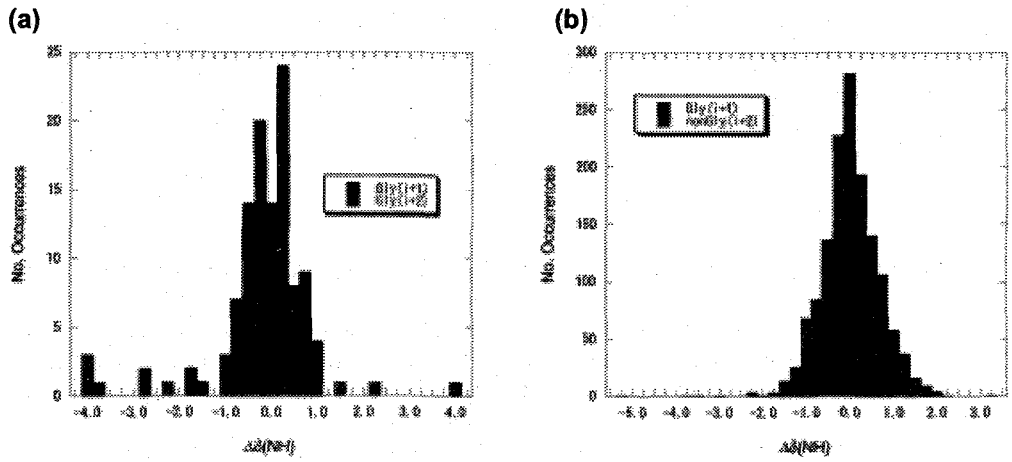

Fig.1 Distribution of the chemical shift deviation from the random coil values for the backbone amide protons[8] ($\Delta\delta$(NH)) of Gly(i+1) and Xaa(i+2) in ArGX tripeptide sequence. **(a)** The case where Xaa(i+2) is Gly. This dataset contains 57 Ar-Gly-Gly tripeptides. The average values of $\Delta\delta$(NH) (and standard deviation) is 0.12 (0.80) for Gly(i+1), and –0.49 (1.25) for Gly(i+2). **(b)** The case where Xaa(i+2) is not Gly (nonGly). This dataset contains 693 Ar-Gly-nonGly tripeptides. The average values of $\Delta\delta$(NH) (and standard deviation) is 0.16 (0.67) for Gly(i+1), and –0.13 (0.64) for nonGly(i+2). $\Delta\delta$(NH) are widely distributed, however, the fact that nonGly(i+2) residues with significant negative $\Delta\delta$(NH) certainly exist suggest that aromatic - (i+2) amide interactions is possible in tripeptide Ar-Gly-Xaa even if Xaa is not Gly.

References

[1] Kumaki Y, Nitta K, Hikichi K, Matsumoto T, Matsushima N. *J. Biochem. (Tokyo).* **136**:29-37, 2004.
[2] Kamiya M, Kumaki Y, Nitta K, Ueno T, Watanabe Y, Yamada K, Matsumoto T, Hikichi K, Matsushima N. *Biochem. Biophys. Res. Commun.* **314**:908-915, 2004.
[3] Kamiya M, Kumaki Y, Nitta K, Matsumoto T,Hikichi K, Matsushima N. *Biochim. Biophys. Acta.* in press.
[4] Kumaki Y, Matsushima N, Yoshida H, Nitta K, Hikichi K. *Biochim Biophys Acta.* **1548**:81-93, 2001.
[5] Yoshida H, Matsushima N, Kumaki Y, Nakata M, Hikichi K. *J. Biochem. (Tokyo).* **128**:271-281, 2000.
[6] Tsuda S, Ito A, Matsushima N, *FEBS Lett.* **409**: 227-231, 1997.
[7] Worth G A, Wade R C. *J. Phys. Chem.* **99**: 17473-17482, 1995.
[8] Andersen N H, Neidigh J W, Harris S M, Lee G M, Liu Z, Tong H, *J. Am. Chem. Soc.* **119**: 8547-856, 1997.

P031

ミミズ由来レクチンのC末端糖結合ドメインの糖との相互作用に関するNMR研究

[1]農研機構・食品総合研究所、[2]産総研・糖鎖工学研究センター、[3]山形大・理学部
○逸見　光[1]、久野　敦[2]、伊藤茂泰[2,3]、鈴木龍一郎[2,3]、長谷川典巳[3]、平林　淳[2]

Interaction of C-terminal domain of a novel galactose-binding protein from earthworm with sugar

[1]National Food Research Institute, National Agriculture and Food Research Organization (NARO), [2]Research Center for Glycoscience, National Institute of Advanced Industrial Science and Technology (AIST), [3]Department of Material and Biological Chemistry, Yamagata University
○ Hikaru Hemmi[1], Atsushi Kuno[2,3], Shigeyasu Ito[2,3], Ryuichiro Suzuki[3], Tsunemi Hasegawa[3], Jun Hirabayashi[2]

A novel 29-kDa lectin (EW29) isolated from the earthworm *Lumbricus terrestris* consists of two homologous domains (14,500 Da) showing 27% identity with each other. Further, the C-terminal domain of EW29 retained its hemagglutinating activity 10-fold lower than the whole protein. The NMR structure of the C-terminal domain of EW29 was characterized by a β-trefoil fold of a typical protein in the R-type lectin family such as galactose specific plant lectins. Further, the chemical shift mapping perturbation of the C-terminal domain of EW29 with sugar by ^{1}H-^{15}N HSQC spectroscopy indicate that the protein has two sugar-binding sites.

1．はじめに

分子量が2万9千のミミズ由来レクチン（EW29）は、27%アミノ酸配列が同一の2つのドメインからなり、さらに、そのアミノ酸配列中に“Gly-X-X-X-Gln-X-Trp”と言うモチーフ構造を持つ[1]。このモチーフ構造は、これまで多くの糖認識タンパク質で発見されており、R-type レクチンファミリーを形成している。従って、EW29 はガレクチン様タンパク質スクリーニング用である asialofetuin-agarose 吸着クロマトで分離精製されたにもかかわらず、そのアミノ酸配列上 R-type レクチンファミリーに属すると思われる。さらに、このレクチンの特徴として、R-type レクチンファミリーに属する他のタンデムリピートタンパク質がドメイン毎に一つの糖結合部位しか持たないことから単独のドメインでは赤血球凝集活性を持たないと考えられているが、EW29 において C

キーワード：レクチン、糖結合タンパク質、糖、相互作用

著者ふりがな：へんみひかる、くのあつし、いとうしげやす、すずきりゅういちろう、はせがわつねみ、ひらばやしじゅん

末端ドメイン単独でもEW29に比べ10倍程度低い活性ではあるが赤血球凝集活性を持つことが知られている。このことから、EW29のC末端ドメインは複数の糖結合部位を持つと考えられるが、未だその糖結合部位は同定されていない。今回、EW29のC末端ドメインのNMR構造とchemical shift mapping perturbation法による糖との相互作用について報告する。

２．方法

NMR測定サンプルは、構造解析用として約1mM $^{15}N/^{13}C$ ラベル体を糖とのNMR滴定実験用として約0.64mM ^{15}N ラベル体を用いた。その立体構造は多核多次元異種核NMR法を用いて決定し、糖とのNMR滴定実験は、^{1}H-^{15}N HSQCによるchemical shift mapping perturbation法により行った。

３．結果と考察

１）NOEから得られた距離拘束条件、HNHA及びTALOS計算から得られた主鎖の二面角制約条件、HNHB及びNOEのパターンから得られたχ_1 anglesの二面角制約条件、NOEのパターン及び初期構造からの水素結合の拘束条件、さらに、RDC拘束条件（H^N-N）からCNSを用いて構造計算を行った。その結果、EW29のC末端ドメインは、R-type レクチンファミリーに特徴的な構造である3つの繰り返し領域からなるβ-trefoil構造をとることが分かった。

２）EW29のC末端ドメインと糖との相互作用を調べるため、ラクトースとのNMRを用いたtitration実験を行った。その結果、EW29のC末端ドメインは交換速度の異なる2箇所の糖結合部位を持つことが示唆された。このことから、EW29のC末端ドメインは、そのドメイン中に2箇所の糖結合部位を持つことより、単独のドメインでも赤血球凝集活性を維持するものと推測された。

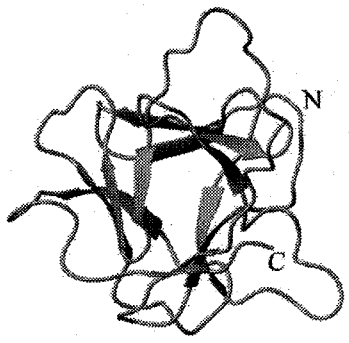

Fig. 1 A ribbon diagram of the C-terminal domain of EW29

References

1. Hirabayashi, J., Dutta, S. K. and Kasai, K. (1998) J. Biol. Chem. 273, 14450-14460.

P032

Solution Structure of a High-affinity Inhibitor with Grb2 SH2 Domain

Kenji Ogura[1], Takanori Shiga[1], Masashi Yokochi[1], Terrence R. Burke Jr.[2], and Fuyuhiko Inagaki[1]

[1] *School of Pharmaceutical Sciences and Pharmacy, Hokkaido University, Sapporo Japan*

[2] *National Cancer Institute at Frederick, NIH, MD, USA*

Summary

The solution structure of growth factor receptor-bound protein 2 (Grb2) SH2 complexed with a high-affinity inhibitor, having a non phosphorus moiety and a macrocyclic peptide mimetic, was determined by nuclear magnetic resonance (NMR) spectroscopy. The solution structure showed that overall conformation of the inhibitor on the molecular surface of Grb2 SH2 was very similar to that of phosphotyrosine-containing ligand peptide derived from BCR-Abl. The binding interaction between the inhibitor and Grb2 SH2 in the solution structure proved that the structure-based drug design was appropriate.

Introduction

Growth factor receptor-bound protein 2 (Grb2) is an adaptor protein with a domain structure of SH3-SH2-SH3. Upon EGF stimulation, Grb2 SH2 binds to the EGF receptor directly or indirectly through proteins such as Shc, FAK, Syp and IRS-1 by recognizing the phosphotyrosine-containing sequences and relocating Sos to the plasma membrane to allow interaction with Ras. Thus, Grb2 mediates signal transduction from a variety of extracellular stimuli to Ras. Among the SH2 domain, the Grb2 SH2 domain directly mediates the activation of mitogenic Ras pathway. Overexpression of Grb2 protein is also related to liver tumorigenesis in mice and human breast cancer cells. Therefore, development of Grb2 SH2 antagonists is an effective approach to block the growth of malignant cells.

Structural basis of SH2 domain is well understood by X-ray crystallography and NMR spectroscopy. These structural studies shows that the phosphotyrosine-containing peptides bind to SH2 at several sites. In the typical SH2 domains, the ligand peptide forms an extended conformation on molecular surface of protein. In contrast to these typical SH2 domains, Grb2 SH2 domain binds the high affinity ligand having a consensus sequence of pTyr-(Leu/Val)-Asn-(Val/Pro) with a β-turn conformation of the peptide backbone. Such a unique binding mode suggested it would be possible to design highly specific inhibitors for the Grb2 SH2 domain.

Keywords: Grb2, structure-based drug design, inhibitor

A pTyr-containing tripeptide Ac-pYIN-NH_2 that was originally reported by Novartis Corp. retaining micro molar affinity to the Grb2 SH2 domain is a starting point to improve the binding affinity. pTyr + 1 Ile was replaced to aminocyclohexanecarboxylic acid (Ac_6c), which stabilize the type-I β-turn. C-terminal 3-naphthalene-1-yl-propyl was appended to make van der Waals contacts with a hydrophobic patch on the surface of the SH2. Because the cytosol has very high levels of constitutive tyrosine phosphatase activity, the stability of the phosphate linkage is a major concern in vivo. Substitution of pTyr with phosphonomethyl phenylalanine (Pmp) led to protection from the phosphatase but a little loss of binding affinity. In order to stabilize the β-turn conformation, Burke and coworkers attempted to constrain the linear peptide mimetic macrocyclization. The cyclic analogue (Fig. 1) exhibited approximately 100-fold enhancement in binding affinity (IC_{50} = 0.02 μM) in vitro relative to its linear counterpart. Therefore, we decided to solve the solution structure of the macrocyclic inhibitor complexed with the Grb2 SH2 domain.

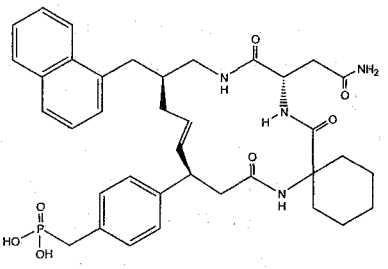

Figure 1. Structure of the macrocyclic inhibitor for Grb2 SH2.

Materials and methods

Protein expression and purification

Grb2 SH2 (residues 58-159) cloned into a pGEX-4T-2 vector was expressed as a GST fusion protein in Escherichia coli BL21(DE3). GST fusion protein was purified using Glutathione Sepharose 4B beads and was cleaved with trypsin. Grb2 SH2 was further purified by a ResourceS column and a Superdex 75 column. The protein was concentrated by Centriprep YM-3 to final conc. of 0.5 mM.

NMR spectroscopy

The macrocyclic inhibitor was dissolved in 20 mM sodium phosphate buffer (pH 6.3) to final concentration of 10 mM solution. The NMR samples contained 0.5 mM Grb2 SH2, with the inhibitor solution added to a concentration of 0.75 mM in order to ensure saturation. The buffer system was 20 mM phosphate buffer pH 6.3; 150 mM NaCl; 0.05% NaN_3.

NMR experiments were run on Varian Unity Inova 800 and 600 MHz spectrometers. Chemical shift assignments and acquisition of NOEs of the Grb2 SH2 were accomplished using a series of 3D heteronuclear experiments recorded on $^{13}C/^{15}N$-labeled Grb2 SH2 complexed with the inhibitor in 90% H_2O / 10% ^2H_2O solution.

To complete the chemical shift assignments of the inhibitor bound on Grb2 SH2, 2D NOESY, 2D DQF-COSY and 2D TOCSY spectra were recorded on the inhibitor complexed with $^2H/^{15}N$-labeled Grb2 SH2 dissolved in ^2H_2O solution and 2D ^{15}N-filtered TOCSY and 2D ^{15}N-filtered NOESY spectra were measured in 90% H_2O solution.

Intermolecular NOEs between Grb2 SH2 and the inhibitor were obtained with a 3D ^{13}C-filtered NOESY experiment recorded on $^{13}C/^{15}N$-labeled Grb2 SH2 complexed with the

inhibitor dissolved in 90% H_2O / 10% ^2H_2O solution and a 3D ^{15}N-edited NOESY experiment recorded on $^2H/^{15}N$-labeled Grb2 SH2 complexed with the inhibitor dissolved in 90% H_2O / 10% ^2H_2O solution.

Structure calculations

Structures were calculated with the program Cyana version 2.0. To calculate molecular complex of proteins and small organic compounds with Cyana, the residue library of the small molecule have to be defined and appended into standard cyana.lib file. First, a PDB-formatted structural model of the inhibitor was created using DunGee PRODRG2 server (http://davapc1.bioch.dundee.ac.uk/programs/prodrg/). Next, the created PDB file was manually converted into a Residue Library-formatted file of Cyana.

Results

NMR assignment of the inhibitor complexed with the Grb2 SH2 domain

We prepared molecular complex samples of the inhibitor and $^{15}N/^2H$-labeled Grb2 SH2 dissolved in ^2H_2O and 90% H_2O / 10% ^2H_2O. Perdeutration of the Grb2 SH2 brought perfect elimination of the signals derived from the SH2, and resulting the simplification of analysis of the spectra. Using 2D TOCSY and NOESY spectra of the molecular complex, we completed the proton assignment of the inhibitor bound on the Grb2 SH2 without ambiguousness. This assignment strategy using perdeutrated protein is generally applicable to NMR structural study of protein-ligand complex.

Structural description of Grb2 SH2 complexed with the inhibitor

A superposition of the backbone of the Grb2 SH2 and the inhibitor complex from the 20 final structures is shown in Fig. 2(a). The atomic rmsd about the mean coordinate positions for the protein residues from Phe61 to Asp150 was 0.51 ± 0.07 Å for the backbone atoms and 0.90 ± 0.08 Å for all heavy atoms.

The topology of the Grb2 SH2 was very similar to those of other SH2 domains. Fig. 2(b) shows a ribbon diagram of the NMR-derived minimized mean structure of Grb2 SH2 complexed

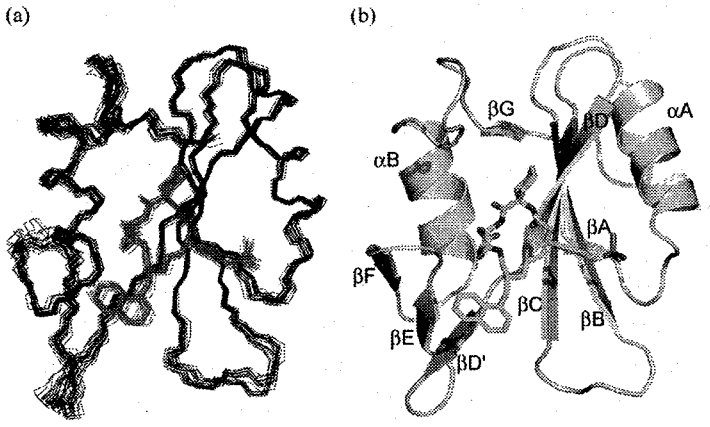

Figure 2. (a) Superposition of 20 lowest energy structures of Grb2 SH2 complexed with the inhibitor. Residues 60-152 of Grb2 SH2 and the inhibitor are shown. Structures were superimposed by least square fit to average N, Cα, and C' coordinates of residues 60-152 of Grb2 SH2. (b) Ribbon diagram of Grb2 SH2 complexed with the inhibitor. The regular secondary structure elements are labeled.

with the inhibitor. The structure consists of a three-stranded antiparallel β-sheet composed of strands βB, βC and βD that is flanked on each side by two a-helices, αA and αB. The central β-sheet is extended by two short parallel strands (βA and βG) located on the opposite side of the inhibitor-binding site. The protein also contains a second, smaller β-sheet-like structure composed of strands βD', βE and βF.

Specific interaction between Grb2 SH2 and the inhibitor

The Ac_6c (pTyr +1) residue of the inhibitor has intermolecular NOEs with Gln106, His107 and Phe108 of the Grb2 SH2 (Fig.3(a)). The cyclohexane group of the Ac_6c residue is stuck into the hydrophobic molecular surface of the Grb2 SH2. The side chain protons of Asn (pTyr +2) had strong intermolecular NOE interactions with Trp121 and Lys109. NMR signals of the Hδ protons of Asn (pTyr +2) were extremely low-field shifted to 8.80 and 8.15 ppm. This low-field shift is due to electric field effects, suggesting that these protons form hydrogen bonds with the carbonyl groups of the Grb2 SH2 as shown in Fig. 3(b). The side chain of naphtylpropylamide (pTyr +3) had many NOE contacts with both of Lys109 and Leu111 (Fig. 3(c)). The residue at pTyr +3 is not conserved or type-conserved in peptidic ligands, but hydrophobic residues are preferred for specific binding with the Grb2 SH2. In the present structure, we confirmed that the naphthalene group hydrophobically contacted with the side chain of Leu111.

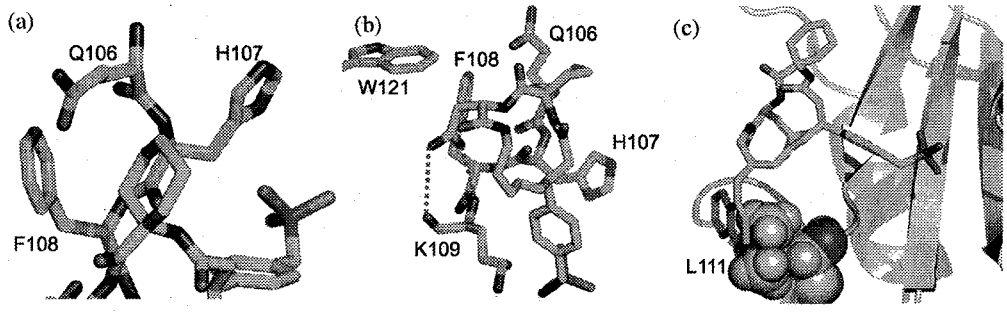

Figure 3. Details of the interaction between the inhibitor and the binding site of Grb2 SH2. (a) pTyr +1 site; (b) pTyr +2 site; (c) pTyr +3 site. The inhibitor are shown in stick model. In (a) and (b), Gln106, His107, Phe108, and Trp121 of Grb2 SH2 are shown in stick model. In (c), Lys109 and Leu111 are shown in CPK model. Dashed red lines in (b) indicate the hydrogen bonds between Hδ of Asn (pTyr +2) and Grb2 SH2.

Conclusion

A high-resolution NMR solution structure has been presented for a complex between Grb2 SH2 and a macrocyclic inhibitor. The inhibitor binds in the same site as does a peptidic ligand. The presented solution structure should be a basis for further development of the inhibitor.

P033

溶液NMRによるVAP-A:OSBP複合体の研究

(1奈良先端科学技術大学院大学　バイオサイエンス研究科、2首都大学東京都市教養学部　理工学系)
○古板恭子[1]、三島正規[1,2]、児嶋長次郎[1]

Solution NMR studies of the VAP-A: OSBP complex

([1]Graduate School of Biological Sciences, Nara Institute of Science and Technology, [2]Graduate School of Sciences and Engineering, Tokyo Metropolitan University)
○Kyoko Furuita[1], Masaki Mishima[1,2] and Chojiro Kojima[1]

Oxysterol binding protein (OSBP) is a cytosolic receptor of oxysterols such as 25-hydroxycholesterol (25-OHC). OSBP localizes to the cytosolic surface of the endoplasmic reticulum (ER), and translocates to Golgi apparatus membranes after addition of 25-OHC. ER localization of OSBP is mediated by complex formation of OSBP with VAMP-associated protein-A (VAP-A). VAP-A is an ER integral membrane protein that contains a cytoplasmic major sperm protein (MSP) domain. There is an FFAT motif in OSBP that is recognized by the MSP domain of VAP-A. In this study, to clarify the structural basis of the ER localization of OSBP, we performed NMR studies of the complex composed of a VAP-A MSP domain and an OSBP peptide containing the FFAT motif.

[序論]

Oxysterol binding protein (OSBP) は、オキシステロール及びコレステロールの細胞内受容体であり、脂質の恒常性に関わっている。OSBP は 25-hydroxycholesterol (25-OHC) と特に強く結合し、25-OHC 低濃度の細胞では、細胞質及び小胞体に局在するが、細胞に 25-OHC を添加すると、ゴルジ体へと移行する。25-OHC 低濃度下での OSBP の小胞体局在は、OSBP と、小胞体膜貫通タンパク質 VAMP-associated protein A (VAP-A)との相互作用による。VAP-A が細胞質側に持つ Major Sperm Protein (MSP)ドメインは、OSBP がその中ほどに持つ FFAT モチーフ (two phenylalanines[FF] in Acidic Tract) と結合する。本研究では、VAP-A との相互作用による OSBP 小胞体局在の構造的基盤を確立する目的で、VAP-A MSP ドメインと、FFAT モチーフを含む OSBP 由来ペプチドからなる複合体の溶液 NMR 研究を行った。

[実験]

大腸菌による大量発現系を用い、非標識、^{15}N標識、及び ^{13}C/ ^{15}N 標識のヒト VAP-A (5-128) 及びヒト OSBP (345-379) のサンプルを作成した。主鎖及び側鎖の帰属には、Bruker AV500 または DRX800 を用いて測定した各種多次元NMRスペクトルを用いた。複合体の主鎖及び側鎖の帰属には、^{13}C/ ^{15}N 標識 VAP-A と非標識 OSBP、非標識 VAP-A と ^{13}C/ ^{15}N 標識 OSBP、及び ^{15}N 標識 VAP-A と ^{15}N 標識 OSBP からなる 3 種の複合体の NMR スペクトルを用いた。

キーワード　OSBP　VAP-A　FFAT モチーフ

著者ふりがな　ふるいた　きょうこ、みしま　まさき、こじま　ちょうじろう

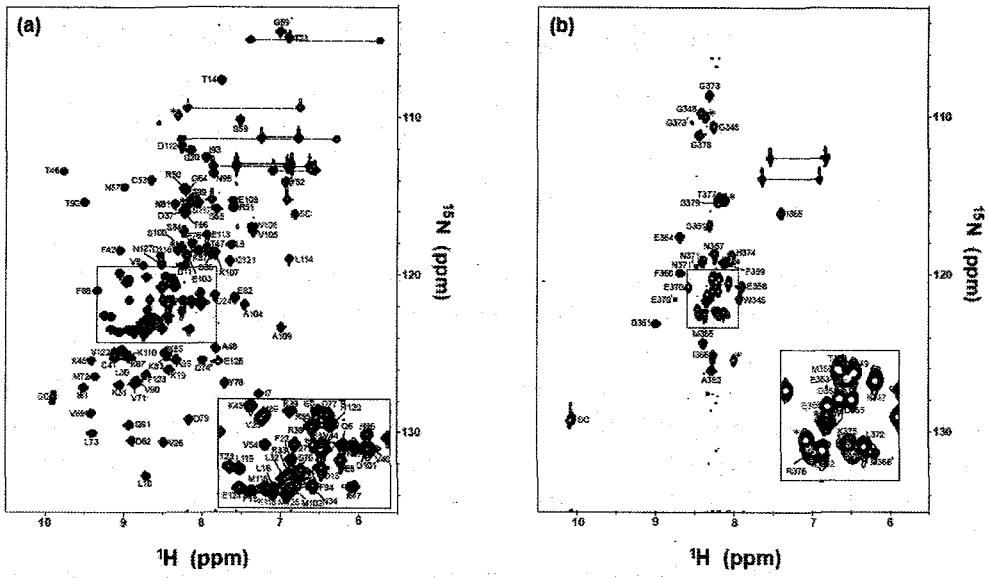

Figure 1. 2D ^{1}H-^{15}N HSQC spectra of ^{13}C/ ^{15}N-labeled VAP-A: non-labeled OSBP peptide complex (a) and ^{13}C/ ^{15}N-labeled OSBP peptide: non-labeled VAP-A complex (b). Assignments are indicated with the one-letter amino acid codes and residue numbers. Asterisks indicate resonances of residues that are not part of the native sequence. Primes indicate the assignments of the minor conformation in Figure 1 (b).

［結果］

VAP-A：OSBP 複合体の主鎖及び側鎖を帰属した（figure 1)。主鎖原子（H_N、N、C´、C_α及びC_β）に関しては 99 %、側鎖原子（主鎖原子を除く脂肪鎖、芳香環、及びアミノ基）に関しては 91 %の帰属を得た。TALOS プログラムによる、複合体のH_N、N、C´C_α、C_β及びH_αの化学シフトを用いた主鎖二面角解析の結果、複合体中の VAP-A は 9 本のβストランドと 2 本のαヘリックスを含むこと、OSBP は FFAT モチーフ及びその周辺が直線状の構造を持つことが示唆された。

OSBP に関しては、単独での主鎖も帰属した。得られた化学シフトを、VAP-A との複合体形成時のものと比較したところ(figure 2)、OSBP の FFAT モチーフ及びその C 末端側が、VAP-A による認識に関与していることが示唆された。

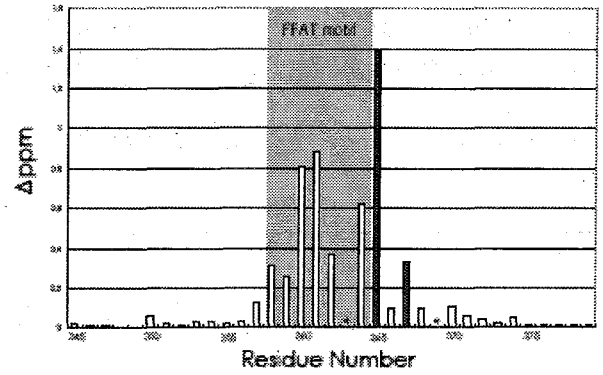

Firure 2. Back bone chemical shift differences of OSBP peptide upon complex formation with VAP-A.

*: proline residue

$\Delta ppm=[(\Delta H_N)^2+(\Delta N/5)^2]^{1/2}$

P034

NMRを用いた高度好熱菌RecXタンパク質の構造・機能解析

首都大学東京大院・理工[1]、理研・遺伝生化学[2]、理研・生体超分子構造機能研究G[3]、横浜市大院・総合理[4]、CREST/JST[5]、理研播磨ストラクチュローム研究G[6]

○ 羽生 香織[1]、井上 仁[2,3,4]、美川 務[2,3,4,5,6]、柴田 武彦[2,3,4]、三島 正規[1,5]、伊藤 隆[1,3,5]

NMR Structural and functional analysis of *Thermus thermophilus* RecX

Kaori Habu[1], Jin Inoue[2,3,4], Tsutomu Mikawa[2,3,4,5,6], Takehiko Shibata[2,3,4], Masaki Mishima[1,5], and Yutaka Ito[1,3,5]

[1]Graduate School of Sciences and Engineering, Tokyo Metropolitan University; [2]Cellular and Molecular Biology Laboratory, RIKEN; [3]Research Group for Bio-supramolecular Structure-Function, RIKEN; [4]Graduate School of Integrated Science, Yokohama City University; [5]CREST/JST; [6]Structurome Research Group, RIKEN/Harima Institute

RecA plays a central role of eubacterial recombinational DNA repair. Even though RecX was identified as an inhibitory regulator of RecA, no structural information has been reported so far for RecX.

In order to delineate the structural basis of the biological functions of RecX, we initiated the NMR studies of *Thermus thermophilus* HB8 RecX (142a.a ,16KDa).

By analyzing six 3D triple-resonance spectra measured with nonlinear sampling scheme on $^{13}C/^{15}N$-labelled RecX, backbone resonances were assigned for 92 out of 138 (67%) non-proline residues in RecX. Chemical Shift Index analysis showed helix-rich structure of this protein. The incompleteness in the assignments was presumably caused by the exchange line broadening of $^{1}H^{N}$-^{15}N correlation cross peaks. For the analysis of the RecA-RecX interaction, NMR titration experiments of ^{15}N-labelled RecX with various fragments of RecA are in progress.

＜序＞

真性細菌において相同組換えを行う中心的なタンパク質としてRecAが知られている。RecXタンパク質はRecAに作用してRecAの組換え活性を阻害することが報告されている。しかし、RecXの立体構造や詳細な阻害機構については明らかにされていない。本研究ではNMR分光法を用いて、RecXの立体構造解析、さらにはRecAとの相互作用のメカニズムの解明を行うことを目標とした。試料としては、高度好熱菌 *Thermus thermophilus* HB8 由来のRecX(ttRecX、142残基、16KDa)を用いた。

今回は、ttRecXの主鎖の帰属と、Chemical Shift Index法を用いた二次構造解析を行ったので、それらの結果について報告する。

キーワード：DNA相同組換え、高度好熱菌

著者ふりがな：はぶ かおり、いのうえ じん、みかわ つとむ、しばた たけひこ、みしま まさき、いとう ゆたか

＜結果・考察＞

^{13}C、^{15}N標識RecX試料(0.2mM)を調製し、2 次元^{1}H-^{15}N HSQCスペクトルを測定したところ、下図のようなスペクトルが得られた。次に異種核多次元NMR法を用いて主鎖$^{1}H^{N}$、$^{13}C^{\alpha}$、$^{13}C^{\beta}$、$^{13}C'$、および^{15}N核の帰属を行った。プロリン 4 残基を除くアミドプロトンが観測可能な 138 残基のうち、約67%について帰属することができた。NMR測定は、CRYOPROBEを装着したBruker DRX600 分光計を用い、測定温度 313Kの条件で行った。データ処理とスペクトルの解析はAZARA v2.7、ANSIG-for-OpenGL v1.0.6 ソフトウェアをそれぞれ用いた。

得られた化学シフトの値から、Chemical Shift Index 法を用いて二次構造解析を行った結果、ほとんどがαヘリックスで構成されていることがわかった。

主鎖シグナルが帰属されない残基は化学交換によるブロードニングが起こっていると考えられる。この化学交換は構造多形によるものと、RecX 間の非特異的な相互作用によるものの 2 つの可能性が考えられた。二次構造予測によると、主鎖NMR シグナルが帰属されない領域は、αヘリックスの構造をとっていることが推定されるため、当該領域が非特異的相互作用のインターフェイスに関与している可能性が高いと考えられる。

今後は RecA とのタイトレーション実験を行い、RecX 上の RecA 相互作用部位の特定を目指している。

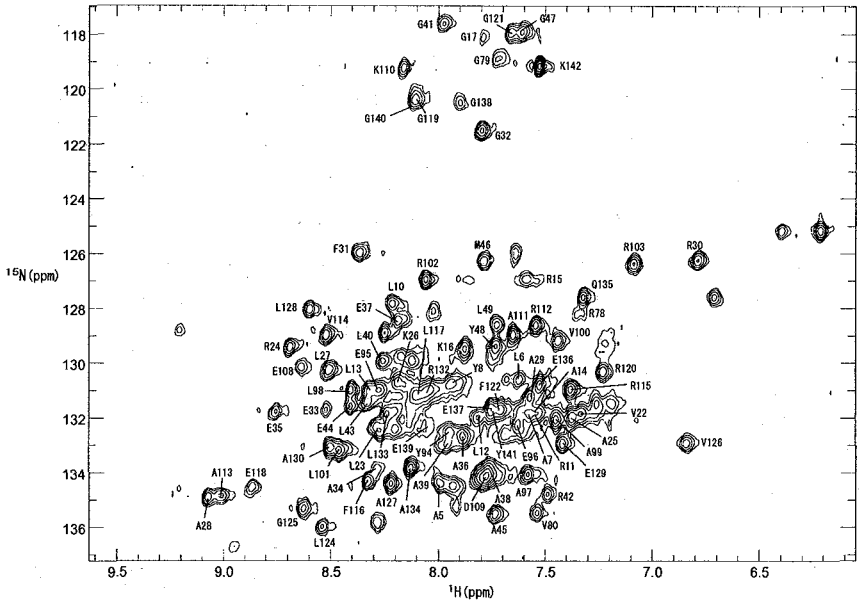

Figure : The ^{1}H-^{15}N HSQC spectrum of $^{13}C/^{15}N$-labelled *Thermus thermophilus* HB8 RecX. Cross peaks are annotated according to the backbone resonance assignments.

P035

NMR法による酵母タンパク質YUH1の立体構造解析

(1横浜市大院・国際総合科学, 2理研・生体超分子構造機能G, 3首都大院・理工学系, 4Univ. of Birmingham, 5理研・和光, 6三菱化学生命科学研, 7CREST/JST)

○ 野尻英里1,2, 池谷鉄兵3, 倉島(伊藤)かおり1,2, Sundaresan Rajesh4, 柴田武彦1,2,5, 河野俊之6, 伊藤隆1,2,3,7

Solution structure of yeast ubiquitin hydrolase, YUH1

Eri Nojiri[1,2], Teppei Ikeya[3], Kaori Kurashima-Ito[1,2], Sundaresan Rajesh[4], Takehiko Shibata[1,2,5], Toshiyuki Kohno[6], and Yutaka Ito[1,2,3,7]

[1]Int. Grad. Sch. of Art. and Sci., Supramol. Biol, Yokohama City Univ; [2]Research Group for Bio-Supramol.Struct.- Func., RIKEN; [3]Dept. of Chem.,Tokyo Metropolitan Univ; [4]Division of cancer studies, Sch. of Medicine, Univ. of Birmingham, UK; [5]Discovery Research Institute, RIKEN; [6]Mitsubishi Kagaku Institute of Life Sciences(MITILS); [7]CREST/JST

Even with the latest technologies of solution NMR, there is considerable difficulty in analyzing three-dimensional structures of larger (> 25kDa) proteins. In order to optimize existing methodologies for larger proteins, we initiated hetrenuclear multidimensional NMR studies of yeast ubiquitin hydrolase ,YUH1 (236a.a, 26.4KDa).

A 50% deuterated and uniformly $^{13}C/^{15}N$-labelled YUH1 sample was prepared. Backbone and side-chain resonance assignments were performed from a set of conventional 3D triple-resonance experiments with deuterium decoupling. 3D TROSY-^{3h}J-HNCO, 3D ^{13}C-separated NOESY-HSQC and ^{15}N-separated NOESY-HSQC spectra were utilised for the analysis of hydrogen bond-derived and NOE-derived distance restraints. Structural calculations with CYANA are in progress.

【序】

近年の飛躍的なNMR技術の進歩に伴い，分子量20KDa程度の蛋白質の立体構造は比較的容易に決定されるようになった．しかし，より大きな蛋白質に関しては，NMRシグナルのオーバーラップや，緩和による線幅の増大や感度の低下といった問題が生じ，依然として解析には困難がつきまとう．

キーワード：YUH1, solution structure, larger protein

著者ふりがな：○のじりえり，いけやてっぺい，くらしま（いとう）かおり，すんだれさんらじぇす，しばたたけひこ，こうのとしゆき，いとうゆたか

ただし，今後さらに様々な生物学的意義を解明していくためにはNMR法を用いた高次構造解析における分子量の壁を押し上げていくことは重要と考えられている．

本研究では，ユビキチンプロテアソーム系において働く，脱ユビキチン化酵素の一つである Yeast Ubiquitin Hydrolase 1(以下 YUH1，約 26.4KDa)をモデル蛋白質として取り上げ，いわゆる一般的な手法を適用する中で，どの程度の構造情報が必要なのか，また，どのような構造制限情報が有用であるのかといった点を検討しながら立体構造決定することを目指し，解析を試みた．

【実験】

大腸菌を用いた大量発現系により 50%-^{2}H/^{13}C/^{15}N標識YUH1 を調製し測定試料とした．主鎖NMRシグナルの帰属および，側鎖NMRシグナルの帰属のために必要な，2 次元^{1}H-^{15}N HSQC，^{1}H-^{13}C HSQCスペクトル，および 3 次元CBCA(CO)NNH，CBCANNH，CC(CO)NNH，HBHA(CBCACO)NNH，H(CCCO)NNH，HCCH-TOCSYスペクトル，TROSY-$^{3h}J_{NC'}$-HNCO関連，^{15}N-separated NOESY，^{13}C-separated NOESYのNMR測定は，Bruker社 DRX600 分光計およびH/C/N 3 重共鳴クライオプローブを用い，測定温度 30℃で測定を行った．

得られた NMR データの処理，解析および構造計算には，Linux/PC 上でそれぞれ，AZARA，ANSIG-for-OpenGL，CYANA ソフトウェアを用いた．

【結果と考察】

高分子量蛋白質の^{1}Hシグナルの線幅の増大や感度低下を引き起こす^{1}H核由来の双極子緩和を軽減し，スペクトルの感度を向上させるために，ランダムに 50%程度重水素化された試料(約 2mM)を用いて一連の測定を行った結果，高分解能のスペクトルを得ることが出来た．

得られたスペクトルを用いて主鎖 NMR シグナルの帰属を行ったところプロリン 11 残基を除く 225 残基中，N 末端 2 残基以外の 223 残基の帰属に成功した．さらに，主鎖の帰属結果に基づき，側鎖 NMR シグナルの帰属を行ったところ 80%程度の帰属が完了している．

続いて，^{15}N-separated NOESY，^{13}C-separated NOESYスペクトルの解析および帰属を行った．現在，NOE由来の水素原子間の距離制限情報，水素結合を介した$^{3h}J_{NC'}$の観測から得た水素結合情報，TALOSを用いた二面角制限情報を基に，CYANAによる立体構造計算を行っている段階である．

今後は，さらなる距離制限情報の取得および解析と構造計算を繰り返し行う中で，立体構造の精密化を図っていき，生物学的解釈をするに十分な精度の立体構造を決定したいと考えている．

P036

成長阻害因子 GBP の C 末端残基伸長部分における生体膜相互作用と機能との相関

(北大院・理[1]、北大院・生命[2]、富山大・薬[3]、佐賀大・農[4])
○梅津喜崇[1]、相沢智康[1,2]、武藤香織[3]、山本宏子[1]、神谷昌克[1,2]、
熊木康裕[1,2]、水口峰之[3]、出村誠[1,2]、早川洋一[4]、河野敬一[1,2]

The elongated C-terminal of Growth-blocking peptide (GBP) undergoes significant changes in conformation upon binding to DPC micelles

[1]Graduate School of Science, Hokkaido University, [2]Graduate School of Life Science, Hokkaido University, [3]Faculty of Pharmaceutical Sciences, Toyama University, [4]Faculty of Agriculture, Saga University
Yoshitaka Umetsu[1], Tomoyasu Aizawa[1,2], Kaori Muto [3],Hiroko Yamamoto[1], Masakatsu Kamiya[1,2], Yasuhiro Kumaki[1,2], Mineyuki Mizuguchi[3], Makoto Demura[1,2], Yoichi Hayakawa[4], and Keiichi Kawano[1,2]

Growth-blocking peptide (GBP) is a 25-amino acid peptide isolated from the lepidopteran insect *Pseudaletia separata* whose development was halted in the last larval instar stage by parasitization with the parasitoid wasp *Cotesia kariyai*. cDNA analysis suggested that 23-amino acid GBP (23GBP) would be expressed in non-parasitized larvae though 28-amino acid GBP (28GBP) would be expressed in parasitized larvae due to translation continue to next stop codon located at nucleotide sequence for 29th amino acid. In this study, we characterized the GBP, which have various C-terminal lengths by comparison of their bioactivity and stability with three-dimensional structure.

【緒言】

Growth-blocking peptide(GBP)は、カリヤコマユバチ *Cotesia kariyai* に寄生されたアワヨトウ *Pseudaletia separata* の幼虫から、幼虫の成長や蛹化変態を阻害する因子として発見された 25 残基からなるペプチドである。その後の研究で、GBP はアワヨトウの遺伝子由来産物であり、未寄生の幼虫では全長 23 残基からなる 23GBP

Growth-blocking peptide, dodecylphosphocholine, cytokine

うめつよしたか, あいざわともやす, むとうかおり, やまもとひろこ, かみやまさかつ, くまきやすひろ, みずぐちみねゆき, でむらまこと, はやかわよういち, かわのけいいち

が発現していること、寄生を受けた場合は感染するポリドナウイルスの影響で、終止コドンがチロシンに翻訳されて 28 残基からなる 28GBP として合成されること、28 残基として発現されたこのペプチドが血清中のプロテアーゼなどによって 25 残基(25GBP)まで分解を受けることが示唆されている。興味深いことに、28GBP は 23,25GBP と比較して強い成長阻害活性を持つことが明らかになっている。しかし一方では、レセプターが完全には同定されておらず、28GBP が強い活性を有するメカニズムについてはわかっていない。本研究では、28GBP がなぜ強い活性を有するのかについての分子レベルでの知見を得るために、主に NMR 法による立体構造の解析から比較を行った。

【実験】

大腸菌を用いてノンラベル、^{15}Nラベル 23,25,28GBPを発現・精製し、実験に使用した。JEOL Alpha 400MHz, ECA 600MHz, Bruker DRX 500MHzのNMR装置を用いて測定を行い、水溶液中における立体構造解析、及びDPCミセル中での化学シフト変化の比較、立体構造解析を行った。

【結果と考察】

23,28GBP の水溶液中での立体構造解析を行った。以前の研究により決定されていた 25GBP の立体構造との比較を行うと、活性に重要とされているコア領域(7-21 残基)の構造には変化がなく、N 末端部分にも明確な違いがないことが明らかになった。従って、これらのペプチドの活性の違いは、フレキシブルな C 末端部分が影響していることが示唆される。また、25,28GBP は生体膜と結合することがモルカット法により示唆されたため、dodecylphosphocholine (DPC)中での立体構造解析を行った。得られた化学シフトは、N 末端、コア領域ではほとんど変化がなくこの領域は膜との相互作用への寄与は低いと考えられる。一方、C 末端部分は DPC ミセルの影響で大きく変化し、立体構造解析の結果、28GBP では両親媒性のαヘリックスをとっていることが明らかになった。 28GBP はこのαヘリックスの疎水性面において生体膜と相互作用をしていると考えられる。

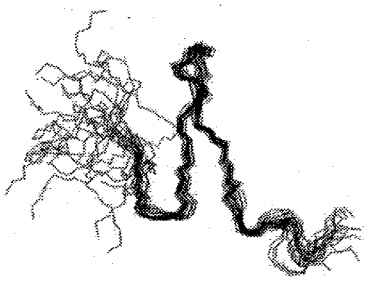

Figure 4. Ensemble of NMR structures of micelle bound 28GBP after superimposing backbone atoms of residues 7-26.

【謝辞】

本研究の一部は、新技術・新分野創出のための基礎研究推進事業の補助を受けておこなわれた。

P037

高度好熱菌由来 RimM のN末ドメインの溶液構造

(1理研 GSC、2東大院理)
○ 鈴木 咲良[1]、龍口 文子[1]、松本 英子[1]、川添 将仁[1]、上西 達也[1]、
白水 美香子[1]、武藤 裕[1]、竹本 千重[1]、横山 茂之[1,2]

Solution structure of the N-terminal domain of *Thermus thermophilus* RimM protein: putative 16S rRNA-processing protein

[1]*RIKEN Genomic Sciences Center,* [2]*Department of Biophysics and Biochemistry, Graduate School of Science, University of Tokyo*
Sakura Suzuki[1], Ayako Tatsuguchi[1], Eiko Matsumoto[1], Masahito Kawazoe[1], Tatsuya Kaminishi[1], Mikako Shirouzu[1], Yutaka Muto[1], Chie Takemoto[1] and Shigeyuki Yokoyama[1,2]

The RimM protein plays an important role in the maturation of the 30S ribosomal subunit. Previous studies suggested that the RimM protein is related to a specific region of the head domain of the 30S subunit. It was also reported that the GST-RimM protein binds to ribosomal protein S19. However, structural information has not been accumulated. With full-length RimM from *Thermus thermophilus*, we first found its N-terminal domain (RimM NTD) folds into a single domain. Using a construct of RimM NTD, we determined its solution structure. RimM NTD adopts a six-stranded β-barrel fold, which resembles the elongation-factor fold observed in domain II of elongation factors Tu and G. However, two characteristic helices cover the top and the bottom of the β-barrel structure, respectively. Successively, this structural information assists our crystal structure analysis.

[序論]

バクテリアで広く保存されているタンパク質 RimM はバクテリア由来リボソームの 30S サブユニット単体には結合するが 70S を形成している 30S サブユニットには結合しない。これにより、RimM はリボソームの成熟に重要な役割を担うタンパク質であると考えられている[1]。変異体実験より RimM は 30S サブユニットの head 領域にある 16S rRNA のヘリックス 31, 33b, リボソームタンパク質 S19, S13 付近をターゲットとすると示唆されている[2]。また、GST-RimM はリボソームタンパク質 S19 に結合する。RimM の立体構造は現在までに得られていないが、RimM の C 末端領域は PRC-barrel ドメインとなることがアミノ酸配列から推測されている[3]。一方 N 末端側の構造については β strand-rich であると推測されているものの、現在までに定義されている他ドメインとの類似性については示唆されていない。本研究ではこの構造未知である RimM N 末端ドメイン(RimM NTD) の構造解析を行ったので、これを報告する。

[方法]

Full-length RimM (残基 1-162) と RimM NTD (残基 1-85) についてはそれぞれ $^{13}C/^{15}N$ 均一標識化タンパクとして大腸菌内で大量発現させ精製した。NMR 測定は Bruker 社製 AVANCE600 および AVANCE 800 MHz を用いてそれぞれ 45 °C、25 °C で多核多次元測定を行った。バッファー条件は 20 mM sodium phosphate buffer (pH 6.5) である。RimM NTD の構造計算については、CYANA 2.0.17 を用いた。

キーワード: RimM、リボソーム、16S rRNA プロセッシング

すずきさくら、たつぐちあやこ、まつもとえいこ、かわぞえまさひと、かみにしたつや、しろうずみかこ、むとうゆたか、たけもとちえ よこやましげゆき

[結果と考察]

初めに高度好熱菌由来 RimM タンパク質 N 末端領域の RimM(1-83) と RimM(1-85) の 2 つのコンストラクトをデザインした。RimM(1-83) についてはサンプルの安定性が低く、最終サンプルの段階で沈殿を生じた。一方、RimM(1-85) については溶解度の高いモノマーとして得られ、RimM (1-85) の ^{1}H-^{15}N HSQC スペクトルにおいては、非常に分散の良いシャープなシグナルが観測された。次に、$^{13}C/^{15}N$-RimM 全長タンパク質 (残基 1-162) を準備し、^{1}H-^{15}N HSQC を測定した。RimM(1-85) と全長 RimM の HSQC スペクトルを比較すると、RimM(1-85) で観測されたシグナルは、全長 RimM の HSQC スペクトル上の同位置に観測された。これは RimM(1-85) が C 末領域の影響を受けずに独立に存在していることを示している。ゆえに、RimM(1-85) は、RimM において単独ドメインとなり得ることが分かった。よって構造解析には RimM (1-85) (以下 RimM NTD)を用いることとした。

RimM NTD の NMR 法によって決定された溶液構造は、6 本の逆平行 β ストランドで形成されるコンパクトな β バレル構造になった。短い 3_{10} ヘリックスが β2 と β3 の間に、また短い α ヘリックスが β5 と β6 間に挿入されており、バレル構造の上下の空間(蓋と底に相当する領域)をふさぐように配置されていた。バクテリア間での RimM NTD のアミノ酸配列アラインメントを行うと多くの疎水性残基が高く保存されていることが分かるが、これらの疎水性残基の側鎖の大半は分子の内部に埋め込まれており、疎水性コアを形成していた。またこれらのうち数残基はバレル構造の側面に存在していた。よって RimM NTD はこれらの高く保存された疎水性残基によって安定化されていることが明らかになった。更に、高く保存されている疎水性残基のうち、その側鎖が溶媒に露出しているものがいくらか存在しており、これらの残基は RimM NTD の N 末端と C 末端領域に集中していることが分かった。ゆえに、N 末端と C 末端領域に位置する残基で形成された疎水性パッチが存在している。

DALI を用いて RimM NTD との構造類似性について調べたところ、RimM NTD は elongation factor Tu (EF-Tu) の domain II に現れる reductase/isomerase/elongation factor fold スーパーファミリーと似ていることが分かった。これらの翻訳タンパク質の多くでは、このフォールドが tRNA もしくは 16S rRNA 結合に関与している。一方、H/ACA RNP のコンポーネントであり Cbf5 タンパク質と直接相互作用する Gar1 タンパク質も RimM NTD と高い構造類似性を示した。このように RimM NTD が保持する 6 本の β バレル構造は、タンパク質–タンパク質相互作用とタンパク質–核酸相互作用の両方に関与している。しかし、EF-Tu domain II と RimM NTD は β バレル構造のトポロジーとして一致するものの、EF-Tu domain II ではバレル構造の蓋に相当する領域に β シートが挿入されているなどの構造的相違が見られる。EF-Tu domain II が RNA を認識するサイトと Gar1 の Cbf5 認識サイトは主にバレル構造の側面であり、これらは空間的に同一であることが報告されている。RimM NTD とこれらの構造を重ねると、EF-Tu と Gar1 の認識サイトに相当する RimM NTD の部位では、芳香環リング、もしくは安定性に寄与している疎水性残基の側鎖で埋められており、ターゲットを認識するだけの十分なスペースがないと思われる。一方、興味深いことに RimM NTD の配列アラインメントから、β1 と β2 の間のループに RimM NTD の中で最も保存が高い配列があるが、EF-Tu や Gar1 で、このループに対応する領域は、ターゲット認識サイトの一部になっている。よって、RimM NTD は、EF-Tu や Gar1 とは異なり、この保存されたループと RimM NTD 特異的な領域でターゲットを認識する可能性がある。

[参考文献]

1. Bylund, G.O., et al., *J Bacteriol*, 1997. **179**(14), 4567-4574.
2. Lovgren, J.M., et al., *RNA*, 2004. **10**(11), 1798-1812.
3. Anantharaman, V. and L. Aravind, *Genome Biol*, 2002. **3**(11): RESEARCH0061.

P038

Preparation, NMR resonance assignments and binding studies with a chromogranin B peptide on a luminal loop region of the Inositol-1,4,5-trisphosphate receptor

Jinho Kang, Sunmi Kang, Seung Hyun Yoo, and Sunghyouk Park

Department of Biochemistry and Center for Advanced Medical Education by BK21 project, College of Medicine, Inha University, Incheon 400-712, Korea

Inositol 1,4,5-trisphosphate receptor (IP3R) is a membrane channel that conduct calcium ions from the intracellular calcium stores. Due to the importance of the calcium control in the cells, a lot of research have been performed on the regulation of the receptor. However, most of the studies were done on the cytoplasmic part of the IP3R and the corresponding regulators. Here, we report the preparation strategies of IP3R intraluminal loop L3-2 region and the studies on its binding to the chromogranin B peptide, as chromogranins are the only known luminal side activator of the IP3R. The L3-2 loop is at the heart of the channel's pore forming region and thus considered critical in regulating the entire channel. We solved the problem of poor expression of L3-2 by attaching the B1 domain of protein G (GB1) in front of the IP3R peptide. We did not cleave the GB1 part and it served both as a reporter for the nativeness of the fusion peptide and as an internal control for monitoring possible non-specific binding. The use of GB1 fusion should be generally applicable to study interactions of other ill-behaved peptides. Using NMR titration approach, we were able to show that a part of the L3-2 is involved in a specific interaction with the chromogranin B peptide. To get a further insights into the interaction, we employed triple resonance NMR experiments with 15N and 13C double-labeled L3-2 samples. We assigned the backbone amide resonances from the data, which revealed that the L3-2 uses residue 14-20 for the binding interaction with the chromogranin B peptide. Our report is the first study on residue-resolution interaction between the luminal loop of the IP3 receptor and its regulator. The sequence specific assignments of the L3-2 reported here should also give valuable information for the mechanistic understanding of the luminal side regulators found in the future.

Key words

Chromogranin, IP3 receptor, binding, assignment

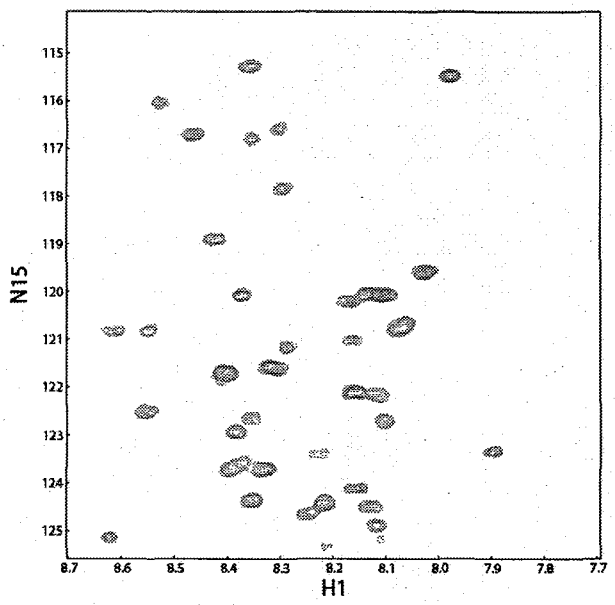

Figure 1. HSQC binding experiments between the IP3RL3-2 GB1 and the chromogranin B peptide. Control spectrum with IP3RL3-2 GB1 only is shown in black while the one with the chromogranin B peptide is in red.

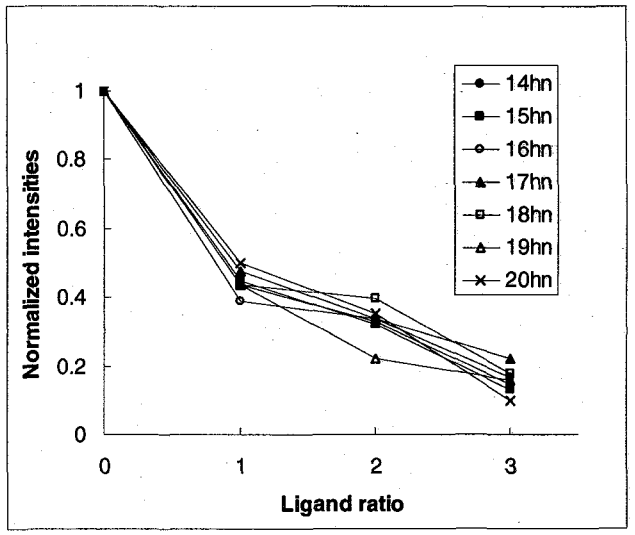

Figure 2. Titration of the IP3RL3-2 GB1 with the chromogranin B peptide. Peak intensity changes following the addition of the indicated molar ratio of the chromogranin B peptide were plotted.

P039

Recombinant expression and interaction studies of calmodulin-binding chromogranin A peptide

Sunmi Kang, Jinho Kang, Seung Hyun Yoo, Sunghyouk Park

Department of Biochemistry and Center for Advanced Medical Education by BK21 project, College of Medicine, Inha University, Incheon 400-712, Korea

Chromogranin-derived peptides have important biological activities and bind to various cellular targets. Despite the importance, the molecular mechanism of the interactions between the peptides and the target proteins have not been studied much. Here, we recombinantly expressed a chromogranin A – derived peptide (CGACaM) and its target protein, calmodulin, and studied the interaction between them with stable isotope labeling and heteronuclear NMR spectroscopy. While calmodulin was prepared with standard recombinant technology, CGACaM required more steps. The CGACaM was not expressed as 6X-His tagged form and needed His-GST as the fusion partner for expression, probably due to the degradation of the small sized peptides. His-GST-fusion peptide was expressed entirely as insoluble inclusion body and was refolded with a step-gradient on-column refolding strategy. The presence of GST also allowed rapid assessment of the folding of the fusion peptide. The subsequent TEV-cleavage and ethanol precipitation of the unwanted proteins gave well-purified peptides. The recombinantly produced peptide had the functional calmodulin binding property as shown by the HSQC binding experiment. By using the reported resonance assignments, we were able to identified the residues in calmodulin most affected by the CGACaM binding and found that the pattern of change is close to that of CaMKIp peptide but is significantly different from that of smMKIP. The results suggest that the CGACaM also binds calmodulin in a wrap-around mechanism and that the conformational change is similar to that induced by CaMKIp peptide. Our approaches should be applicable to interaction studies involving other chromogranin-derived peptides and their cellular target proteins.

Key words

Chromogranin, Calmodulin, Refolding, Fusion peptide

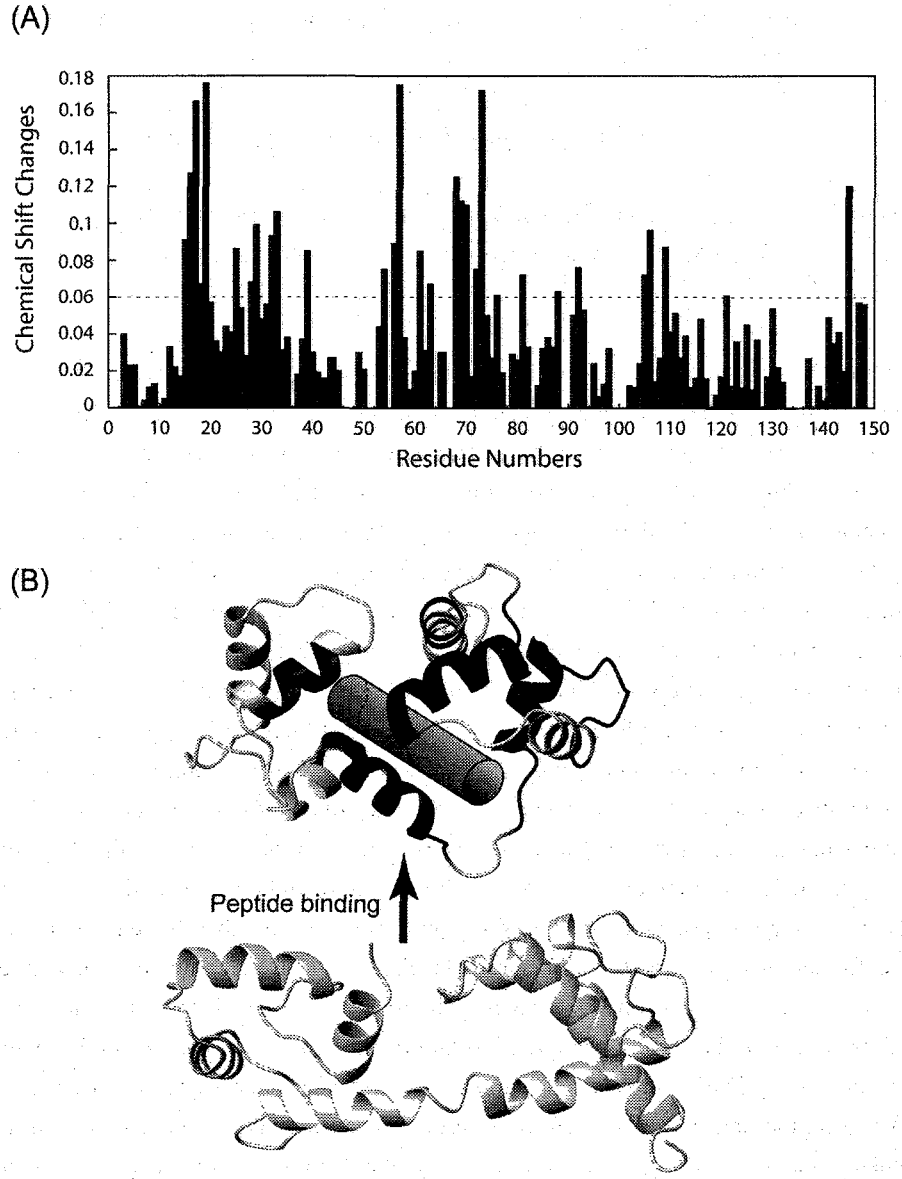

Figure 1. Chemical shift mapping analysis and the suggested binding mechanism between calmodulin and CGACaM. (A) Normalized chemical shift changes after the addition of the CGACaM were plotted against the residue numbers. The chemical shift changes were calculated as described previously [19]. The horizontal dotted line indicates the threshold value of 0.06 ppm. (B) The wrap-around binding mechanism of calmodulin. The solid black color on the upper molecule indicates the residues that shifted significantly in the chemical shift mapping analysis (chemical shift changes > 0.06 ppm). The pdb codes for the calmodulin structures are 2BBM (upper) and 1X02 (lower).

P040

Structural and dynamics studies on the L3V region of the IP3 receptor

Sunmi Kang, Jinho Kang, Seung Hyun Yoo, Sunghyouk Park

Department of Biochemistry and Center for Advanced Medical Education by BK21 project, College of Medicine, Inha University, Incheon 400-712, Korea

Calcium is an important messenger in cellular signaling and its concentration in the cell is very tightly regulated. A major player in mobilizing calcium from the intracellular stores is Inositol 1,4,5-triphosphate receptor (IP3R), a membrane-associated calcium channel. With IP3 and calcium itself being the two major regulators, there are dozens of small- and macromolecules that affect the IP3R channel opening. Although a lot more studies have been done on IP3R regulation in the cytosolic compartment, regulators in the luminal side of the calcium stores also can affect the channel activity. Recently, it was reported that ER luminal environment, especially the redox potential, can significantly affect the IP3R channel activity through a negative regulator ERp44. The redox potential was suggested to alter the oxidation statuses, thus the presence of the free sulfhydryl groups, of the three critical cysteine residues in the L3V region of the IP3R, controlling the binding of the ERp44. Therefore, the cysteine sulfhydryl groups could serve as intraluminal molecular switch for the regulation of the cytoplasmic calcium concentration. Since this is the first demonstration of the negative regulation of the IP3R from the luminal side, it is important to study the detailed mechanism, especially, how the redox potential affect L3V region. Here, we show that the redox potential causes the formation of a very specific intramolecular disulfide bond out of many other possibilities. In addition, the disulfide bond significantly changed the structural and dynamical properties of the L3V which could explain the mechanism of the molecular switch function of the region. During the course of the structural studies, we assigned the resonances of the L3V using the non-linear sampled triple resonance spectra. The approach reduced the experimental time by a factor of 8, requiring only about 13 hours for acquiring all the necessary HNCACB, CBCA(CO)NH, HNCO, HN(CA)CO and C(CO)NH experiments. Our experimental scheme should be generally applicable to obtaining NMR backbone and sidechain data rapidly for relatively small proteins.

Key words

IP3, redox, regulation, non-linear sampling

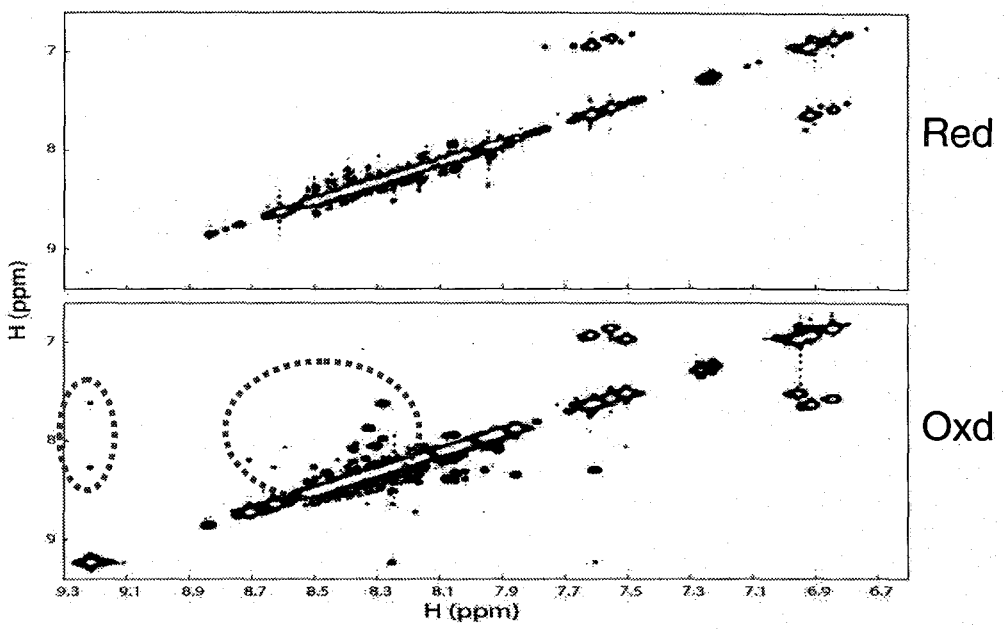

Figure 1. Comparison of the 2 dimensional projection of the 15N-NOESY-HSQC spectra of the reduced and oxidized form of the L3V region of IP3 receptor. The upper spectrum is for the reduced form and the lower of the oxidized form. Cross peaks appearing on the oxidized form only are indicated by the dotted circles.

P041

亜鉛結合タンパク質297Bのtandem repeat zf-C2H2ドメインの溶液中の構造解析

(1理研GSC、2理研・播磨、3理研RCAI、4かずさDNA研究所、5東大院・理)
○井上匡子[1]、斉藤耕平[1]、武藤裕[1]、林文晶[1]、白水美香子[1,2]、
寺田貴帆[1,2]、木川隆則[1]、井上真[1]、矢吹孝[1]、青木雅昭[1]、関英子[1]、
松田貴意[1]、廣田洋[1]、好田真由美[1]、田仲昭子[1]、小原収[3,4]、横山茂之[1,2,5]

Solution structure of tandem repeats of the zf-C2H2 domains of human zinc finger protein 297B.

([1]RIKEN GSC, [2]RIKEN SPring-8 Center, Harima Institute, [3]RIKEN RCAI, [4]KAZUSA DNA Research Institute,[5]Graduate School of Science, The University of Tokyo)
Kyoko Inoue[1], Kohei Saito[1], Yutaka Muto[1], Fumiaki Hayashi[1], Mikako Shirouzu[1,2], Takaho Terada[1,2], Takanori Kigawa[1], Makoto Inoue[1], Takashi Yabuki[1], Masaaki Aoki[1], Eiko Seki[1], Takayoshi Matsuda[1], Hiroshi Hirota[1], Mayumi Yoshida[1], Akiko Tanaka[1], Osamu Ohara[3,4], Shigeyuki Yokoyama[1,2,5]

The zinc binding protein 297B belongs to the kruppel C2H2-type zinc-finger protein family. This protein has the BTB domain in the N-terminus and tandem three repeats of zinc-finger domain which is a DNA-binding motif in the C-terminus.

We have determined the solution structures of the triplet zinc-finger domain in the C-tarminus by using heteronuclear multidimensional spectroscopy and CYANA calculation. As a result of structural analysis, each of three domains independently formed a compact structure with two β-strands and one α-helix. In general, two Cysteins in the β-hairpin and two Histidines on the helix coordinate a zinc ion. The ε 2-nitrogens of both Histidines are used for a ligand of zinc coordination. But we found that for the first Histidine, the δ 1-nitrogen is mainly used for a zinc ion coordination in the first zf-C2H2 domain. We will show these evidences and discuss structural detail.

【序】

Kruppel 型転写因子ファミリーは C 末端側に 3 個の Zinc-finger ドメインを持つ特徴的な構造を持った転写因子群であり、個体の発生、細胞分化あるいは癌を含む病態の形成に重要であることが知られている。

本研究で用いたヒトの亜鉛結合タンパク質 297B は約 470 残基からなり、N 末端に BTB ドメイン、C 末端に 3 個の連続した亜鉛結合ドメイン (C2H2 - C2H2 - C2HC) で構成され、Kruppel C2H2-type zinc-finger protein family に分類される。今回、NMR 分光法により、C 末端の 3 個の亜鉛結合ドメインを含む配列の立体構造を NMR 分光法により解析した。

Keywords: zf-C2H2, DNA-binding

いのうえきょうこ、さいとうこうへい、むとうゆたか、はやしふみあき、しろうずみかこ、きがわたかのり、いのうえまこと、あおきまさあき、せきえいこ、まつだたかよし、ひろたひろし、よしだまゆみ、たなかあきこ、おはらおさむ、よこやましげゆき

【実験】
無細胞タンパク質合成系により13C,15N標識体tandem repeat zf-C2H2 domainsを発現させた。Bruker 社製 AVANCE 600MHz,700MHzと800MHzを用い25℃で多核多次元NMR spectrumを測定した。 試料溶液は、試料 1.18mMを20mM d-Tris-HCl buffer、100mM NaCl、0.02% NaN_3、100uM $ZnCl_2$ (90% H2O/10% D2O)に溶解し、pH=7.0とした。 スペクトルの処理、解析及び構造計算には、NMRPipe、NMRView-Kujira、CYANA /CANDIDを用いた。

【結果と考察】
各亜鉛結合ドメインは一組のβ-sheet と一本のα-helix で構成され、各々約 25 残基のアミノ酸から成る。このモチーフはzf-C2H2 domain として多くのタンパク質に見出され、NMR 分光法による構造も数多く報告されている。しかし、最近まで亜鉛に結合するHistidine の配位はほぼNE2 位(ε配位)で報告されている。今回、1st zinc finger domainにおいて、第三配位残基の Histidine はND1 位で配位 (δ配位) しており、他の亜鉛結合 Histidine はNE2 位で配位していることが実験より得られた。また、このδ配位はε配位と交換していることがNOESY スペクトルより明らかとなった。δ配位構造とε配位構造の交換は空間的に隣接するPhenylalanine 残基のNOESY スペクトルからも裏づけられた。得られた結果からδ&ε配位構造が主構造として存在し、且つε&ε配位構造も同時に系内に存在することがわかった。
今回の発表では、この新しい知見を含む構造の特徴を報告する。

Fig. 1 Ribbon diagram of the three zinc-finger domains.
Fig. 2 Ribbon diagram of the first zinc finger domain.
Fig. 3 Ribbon diagram of the second zinc finger domain.

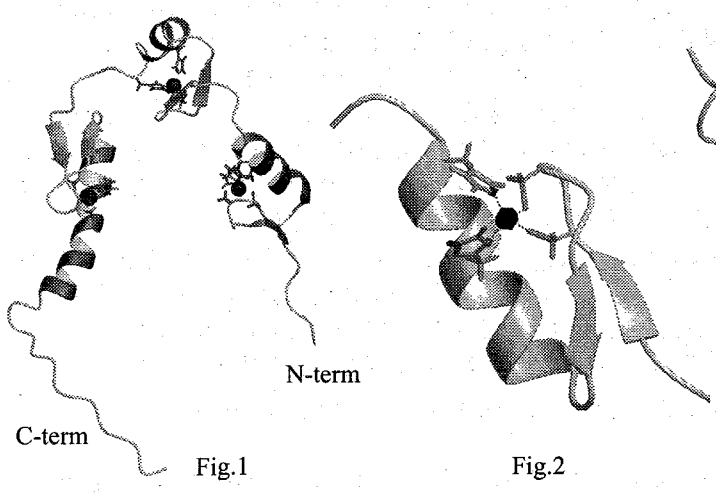

Fig.1 Fig.2 Fig.3

P042

BRCT ドメインの網羅的構造解析

1) 理研 GSC、2) 理研・播磨、3) 理研 RCAI、4) かずさ DNA 研究所、5) 東大医科研、6) 東大院理
○長島 敏雄[1]、林 文晶[1]、白水 美香子[1,2]、寺田 貴帆[1,2]、木川 隆則[1]、井上 真[1]、矢吹 孝[1]、青木 雅昭[1]、関 英子[1]、松田 貴意[1]、廣田 洋[1]、好田 真由美[1]、田仲 昭子[1]、小原 収[3,4]、菅野 純夫[5]、横山 茂之[1,2,6]

Structural and functional analysis of BRCT domain

1) RIKEN GSC, 2) RIKEN Spring-8 Center, 3) RIKEN RCAI, 4) KAZUSA DNA Research Institute, 5) The Institute of Medical Science, The University of Tokyo, 6) Graduate School of Science, The University of Tokyo
Toshio Nagashima[1], Fumiaki Hayashi[1], Mikako Shirouzu[1,2], Takaho Terada[1,2], Takanori Kigawa[1], Makoto Inoue[1], Takashi Yabuki[1], Masaaki Aoki[1], Eiko Seki[1], Takayoshi Matsuda[1], Hiroshi Hirota[1], Mayumi Yoshida[1], Akiko Tanaka[1], Osamu Ohara[3,4], Sumio Sugano[5] and Shigeyuki Yokoyama[1,2,6]

Many copies of BRCA1 C-terminal (BRCT) region are found within various proteins involved in cell cycle checkpoint, DNA repair, and transcription. The function of the domain is mainly protein binding through hetero BRCT-BRCT dimer and BRCT-non-BRCT. Furthermore, it has been reported that tandemly repeated BRCT domain of BRCA1 tumor suppressor could bind phosphopeptide. In this study, we solved solution structures of BRCT domain in various proteins by NMR spectroscopy. Comparing the structures, we found diversity of structure in BRCT-BRCT interaction site and phosphopeptide binding site. The detail of the results will be discussed.

BRCT ドメインは 90-100 残基程度からなり、転写、細胞周期チェックポイントおよび修復に関係するさまざまなタンパク質に見られる。主な機能としてはヘテロ二量化とBRCT-non-BRCTによるタンパク質間相互作用が分かっていた。最近になって、ガン抑制遺伝子である BRCA1 タンパク質のタンデムに並ぶBRCT ドメインの二量体で、リン酸化 Ser を含む pS-X-X-F/Y モチーフと結合した構造が報告された。一般に BRCT ドメインは DNA 損傷応答タンパク質を集約する働きがあると考えられている。今回構造解析した BRCT ドメインは以下の 6 種類のタンパク質に存在するものであり、一部の BRCT ドメインは生化学実験で機能がわかってきているものもある。
Topoisomerase-II binding protein 1 (TopBP1) 8個の BRCT ドメインのみからなるタンパク質で様々な核内タンパク質の足場として機能していると考えられている。3番目のドメインを解析した。
Terminal deoxynucleotidyltransferase (TDT) テンプレートに依存しない DNA ポリメラーゼで、非相同末端結合に関与している。B 細胞での抗体産生に重要な役割を果たしている。

キーワード: BRCT、DNA 修復、細胞周期チェックポイント、リン酸化ペプチド

ながしま としお、はやし ふみあき、しろうず みかこ、てらだ たかほ、きがわ たかのり、いのうえ まこと、やぶき たかし、あおき まさあき、せき えいこ、まつだ たかよし、ひろた ひろし、よしだ まゆみ、たなか あきこ、おはら おさむ、すがの すみお、よこやま しげゆき

Poly(ADP-ribose)polymerase-1 (PARP1) DNA 損傷部位に結合して、自分自身を含め周辺タンパク質を ADP リボシル化することによってシグナル伝達をするタンパク質。
ECT2 protein 有糸分裂の際に RhoGEF として機能しているタンパク質で、ガン細胞で異常発現している。BRCT ドメインが自身の GEF 機能をコントロールしていると考えられている。
XRCC1 塩基除去修復の際に足場タンパク質として機能し、DNA リガーゼ III と DNA ポリメラーゼ β と結合する。
DNA polymerase μ (Pol μ) B 細胞において抗体の体細胞超変異とクラススイッチに関与している。

<方法と考察> すべて BRCT ドメインは無細胞タンパク質発現系を用い、$^{13}C/^{15}N$ 二重同位体標識を用いた。バッファーはすべてのタンパク質で 20mM TrisHCl(pH7.0)、100mM NaCl、1mM DTT、0.02% NaN_3、10% D_2O を用いた。NMR 測定は Varian 社製 INOVA-600、-800、-900 を用い、15～25℃で行った。主鎖帰属用に ^{15}N-HSQC、HNCO、H(CA)CO(CA)NH、HN(CO)CA、CBCA(CO)NH、HNCACB、側鎖帰属用に ^{13}C-HSQC、C(CO)NH、HCCH-TOCSY、CCH-TOCSY、構造解析用に ^{13}C-HSQC NOESY、^{15}N-HSQC NOESY を測定した。データ処理は NMRPipe、スペクトル解析は NMRView およびホームメイドの Kujira、構造計算には CYANA1.0.7 および 2.0.17 を用いた。

構造解析の結果のひとつをリボン図で示した。構造は BRCT ドメインとしてよく保存された alpha/beta/alpha の 3layer で4本ストランドの parallel β シートの構造だった。α2 の部分は ECT2 以外でヘリックスになったが、ヘリックスの角度や長さが異なった。α2 と別の BRCT ドメインのα1 とα3 の部分が head-to-tail の結合をすることでヘテロ二量体を形成することが示唆されているため、立体構造の違いが結合様式の違いになると考えられる。ヒトの BRCT ドメインのアミノ酸配列アライメントの結果、α2 の部分はあまり保存されていなかった。リン酸化 Ser のリン酸部分に結合する Lys もα2 の部分にあるが同様に保存されてなかった。アミノ酸配列からはわからなかったα2 の構造が明らかになり、二量化やリン酸化ペプチドの結合に関して、構造的観点から解明に繋がると考えられる。また、網羅的な BRCT ドメインの構造解析により BRCT ドメイン間の相互作用の全容解明に繋がるものと予想される。

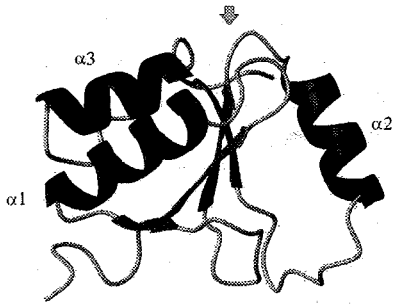

The BRCT domain of terminal deoxynucleotidyltransferase (2COE) A diversity of helix α2 is involved in the specificity of BRCT dimerization. The putative binding site of phosphopeptide is up-side loops indicated by arrow.

P043

Solution structure of CIDE-N domain of human Cell death-inducing DFFA-like effector A (CIDEA)

(RIKEN GSC[1]、RIKEN 播磨[2]、東大院理[3])
○秦旭栄[1]、林文晶[1]、白水美香子[1,2]、寺田貴帆[1]、木川隆則[1]、井上真[1]、矢吹孝[1]、青木雅昭[1]、関英子[1]、松田貴意[1]、廣田洋[1]、好田 真由美[1]、横山茂之[1,2,3]

(RIKEN GSC[1]、RIKEN Harima Institute[2]and University of Tokyo[3])
○Xu-rong Qin[1], Fumiaki Hayashi[1], Mikako Shirouzu[12], Takaho Terada[1], Takanori Kigawa[1], Makoto Inoue[1], Takashi Yabuki[1], Masaaki Aoki[1], Eiko Seki[1], Takayoshi Matsuda[1], Hiroshi Hirota[1], Mayumi Yoshida[1], Shigeyuki Yokoyama[1,2,3]

Introduction

Apoptotic DNA fragmentation and chromatin condensation is mediated by a caspase-activated DFF40/CAD nuclease, which is chaperoned and inhibited by DFF45/ICAD. CAD consists of two domains with differentiated functions. Its C-terminal domain displays DNA nuclease activity, whereas the N-terminal domain shows a regulatory role. N-terminal domain of CAD is similar to N-terminal domain of ICAD and their interaction plays a key role in the proper functioning of this two-component system. There are reports that the N-terminal domain of ICAD alone is unstructured in solution, and its folding is induced upon binding to the N-terminal domain of CAD.

Those homologous N-terminal domain which has been termed as the "cell-death inducing DFF45-like effector"(CIDE) domain are conserved within the family of cell death-inducing proteins.

CIDEA belongs to the family of cell death-inducing proteins and owns an N-terminal domain, the CIDE-N domain, homologous to the N-terminal domain of DFFs. We present here the structure of the CIDE-N domain of human Cell death-inducing DFFA-like effector A (CIDEA) determined by nuclear magnetic resonance spectroscopy. We will discuss the structural characterizition, binding site and relationship between structure and function by comparing with known CIDE-N domains.

Keywords: Structural proteomics, E. coil cell-free protein synthesis system, Apoptotic DNA fragmentation and CIDE-N domain

しんきょくえい、はやしふみあき、しろうずみかこ、てらだたかほ、きがわたかのり、いのうえまこと、やぶきたかし、あおきまさあき、せきえいこ、まつだたかよし、ひろたひろし、よしだまゆみ、よこやましげゆき

Materials and Methods

The ^{13}C- and ^{15}N-labeled protein was produced by the E. coil cell-free synthesis system. All NMR measuremens were performed at 298K under ambient pressure on varian INOVA 600 or, in the case of the NOESY experiments, Varian INOVA 800 spectrometers.

The sequence-specific backbone resonance assignment was achieved through a combination of standard triple resonances techniques using 2D $^{1}H,^{15}N$-HSQC and 3D HNCO, HN(CA)CO, HNCA, HN(CO)CA, HNCACB and CBCA(CO)NH spectra. Side-chain assignment was obtained using 2D $^{1}H,^{13}C$-HSQC and 3D C(CO)NH, (H)CCH-TOCSY and HCCH-TOCSY spectra. 3D ^{15}N-edited ($^{1}H,^{1}H$)-NOESY and ^{13}C-edited ($^{1}H,^{1}H$)-NOESY spectra were used to determine the distance restraints.

The programs NMRPipe, NMRView and Kujira were used for spectral processing and data analysis. Structure calculation were performed with the program CYANA 2.0.17.

Result and Discussion

The domain owns a fold of an α/β-roll and consists of four β-strands arranged into a single β-sheet with helices packed against it (Figure 1a). The domain has a prominent hydrophobic core consisting of conserved hydrophobic residues that support the packing of the helices against the β-sheet. The second hydrophobic cluster is located on the opposite side of the β-sheet and is centered around a conserved Trp residue (Trp 83) in the C-terminal region of the domain. Packing of this tryptophan restrains the orientation of the C-terminal loop relative to the β-sheet.

Residues E62-Q66 form a short helix(α2), which observed in ICAD and CIDEB but absent in CAD. This region in ICAD comprises its binding surface and it is likely that the differences in structure are important for CAD recognition.

There are two clusters of oppositely charged residues located on the opposite side of the protein (Figure 1b), suggesting a possibility of an electrostatic mode for the CIDE-N/CIDE-N interaction.

a b

Fig.1 Ribbon diagram (a) and electrostatic potential map (b) of the CIDE-N (CIDEA)

P044

C_2H_2 タイプ zinc finger タンパクの構造の相違

(理研・GSC[1]、理研・播磨[2]、理研・RCAI[3]、かずさ DNA 研究所[4]、東大院理[5])
○黒崎千智[1]、遠藤弘[1]、林文晶[1]、好田真由美[1]、白水美香子[1,2]、寺田貴帆[1,2]、木川隆則[1]、井上真[1]、矢吹孝[1]、青木雅昭[1]、関英子[1]、松田貴意[1]、廣田洋[1]、田仲昭子[1]、小原収[3,4]、横山茂之[1,2,5]

Structural varieties in C_2H_2-type zinc finger proteins.

Genomic Science Center, RIKEN[1]; Harima institute RIKEN[2]; Research Center for Allergy and Immunology, RIKEN[3]; KAZUSA DNA Research Institute[4]; Graduate School of Science, The University of Tokyo[5]
C. Kurosaki[1], H. Endo[1], F. Hayashi[1], M. Yoshida[1], M. Shirouzu[1,2], T. Terada[1,2], T. Kigawa[1], M. Inoue[1], T. Yabuki[1], M. Aoki[1], E. Seki[1], T. Matsuda[1], H.Hirota[1], A. Tanaka[1], O. Ohara[3,4] and S. Yokoyama[1,2,5]

C_2H_2-type zinc finger domain bind to specific DNA sequences and play an important role in controlling transcription of genes. The domain consists of well-defined sequences and forms a compact structure with two β-strands and one α-helix. Most of the C_2H_2-type zinc finger domains exist as tandem repeats connected by linkers. The halves of this type of zinc fingers have well conserved linkers that play a crucial role in a complex formation with DNA. We present two solution structures of C_2H_2-type of zinc finger domains from KIAA1196 protein and Teashirt homolog 3. Those domains belong to the separated-paired C_2H_2-type zinc finger proteins and structural availability of this type of zinc fingers is limited. We will discuss the detail feature of the structures comparing with the other unusual type of zinc finger proteins.

キーワード：C2H2-type zinc finger proteins, Teashirt homolog 3, zinc finger protein KIAA1196

○くろさきちさと、えんどうひろし、はやしふみあき、よしだまゆみ、しろうずみかこ、てらだたかほ、きがわたかのり、いのうえまこと、やぶきたかし、あおきまさあき、せきえいこ、まつだたかし、ひろたひろし、たなかあきこ、おはらおさむ、よこやましげゆき

【序論】

Zinc finger C_2H_2 ドメイン(zf-C_2H_2) は特定の DNA の配列に選択的に結合し、細胞活性において発達、分化および腫瘍抑制などに分類され、遺伝子の転写制御に重要な役割を果たす。そのドメインの配列はよく保存されており、2 つのβシートと 1 つのαヘリックスおよびループ領域から成る。ほとんどの zf-C_2H_2 はタンデムに並んでおり、その内の約半分はドメイン間に良く保存されたリンカーを持つ。この良く保存されたリンカーは zf-DNA 複合体の形成において非常に重要な役割を果たしている。この良く保存されたリンカー領域を持たない KIAA1196 タンパク質および Teashirt homolog 3 (Tsh3) タンパク質のタンデム zf-C_2H_2 タイプのドメイン構造を NMR を用いて決定し、このドメインの構造上の特徴を述べる事を試みた。

【方法】

Zf-C_2H_2 タイプのドメインを含む KIAA1196 と Tsh3 の $^{13}C/^{15}N$ 標識タンパク質を無細胞タンパク質発現系により調製した。KIAA1196 の zf ドメインは NMR 測定を JEOL 社製 ECA 800、ECA 600 および Varian 社製 INOVA 800 により 25℃で行った。Tsh3 の zf ドメインは Varian 社製 INOVA 800 および INOVA 600 にて NMR 測定を行った。両サンプルともシグナルを帰属するために ^{15}N-HSQC、^{13}C-HSQC、HNCO、HN(CA)CO、HN(CO)CA、CBCA(CO)NH、HNCACB、HBHA(CO)NH、HBHANH、CC(CO)NH、HCCH-TOCSY、CCH-TOCSY を測定した。また側鎖のχアングルを求めるために、HN(CO)HB、HNHB を測定し、さらに原子間距離情報を得るために、^{15}N-edited NOESY-HSQC および ^{13}C-edited NOESY-HQSC を行った。これらのスペクトルの処理と帰属は NMRPipe、NMRView、KUJIRA を用い、構造計算は CYANA/CANDID を用いて行った。また得られた構造の評価には PROCHECK-NMR を用いた。

【結果と考察】

KIAA1196 の領域 493-534 はデータベース上ドメインが見出されていない。この領域を含む領域 493-577 に関して、構造解析を行った。その結果、第三 zf-C_2H_2 の前に、新たに 1 個の zf-C_2H_2 タイプの存在が明らかとなった。解析を行った第一ドメインに関して、N 端側にαヘリックスが追加されていること、第一ドメインの zf-C_2H_2 で保存されたαヘリックスが通常の zf-C_2H_2 より長く、このαヘリックスがドメイン間のリンカー部位になっていることが分かり、このような点で新規な構造であると言える。

Tsh3 のタンデム zf-C_2H_2 タイプドメインは 1 番目と 2 番目のドメインである。一見は通常の zf-C_2H_2 タイプと同様であるが、亜鉛に配位する 2 番目の His 残基がヘリックスから伸びたリンカー（またはヘリックス）に位置すること、そしてこの His の亜鉛の配位がδ窒素原子で行われているところが新規であった。また、2 つのドメインをつなぐリンカーの長さが 35 残基ときわめて長いことも大きな特徴であった。

本発表では今回解析を行った zf-C_2H_2 タイプで保存された構造以外の二次構造を持つ、あるいは特殊なリンカーを持つタンデム zf-C_2H_2 タイプドメインと種々の zf-C_2H_2 とを比較し、議論をする予定である。

P045

網羅的構造解析で見出されたユニークな構造やスペクトルとその特徴

1) 理研 GSC、2) 理研播磨、3) 理研 RCAI、4) かずさ DNA 研究所、5) 東大医科研、6) 東大院理

○林 文晶[1]、長島 敏雄[1]、秦 旭栄[1]、末武 徹也[1]、泉 顕也[1]、遠藤 弘[1]、井上 匡子[1]、佐野(八田)玲子[1]、清宮 恭子[1]、黒崎 千智[1]、長嶋 嘉代子[1]、好田 真由美[1]、白水 美香子[1,2]、寺田 貴帆[1,2]、木川 隆則[1]、井上 真[1]、矢吹 孝[1]、青木、雅昭[1]、関 英子[1]、松田 貴意[1]、廣田 洋[1]、田仲 昭子[1]、林崎 良英[1]、小原 収[3,4]、菅野 純夫[5]、横山 茂之[1,2,6]

Unique structural environments and spectral patterns found in structural genomics

1) RIKEN GSC, 2) RIKEN Spring-8 Center, 3) RIKEN RCAI, 4) KAZUSA DNA Research Institute, 5) The Institute of Medical Science, The University of Tokyo, 6) The Graduate School of Science, The University of Tokyo

Fumiaki Hayashi[1], Toshio Nagashima[1], Xu-rong Qin[1], Tetsuya Suetake[1], Kenya Izumi[1], Hiroshi Endo[1], Kyoko Inoue[1], Reiko Sano[1], Kyoko Seimiya[1], Chisato Kurosaki[1], Kayoko Nagashima[1], M.ayumi Yoshida[1], Mikako Shirouzu[1,2], Takaho Terada[1,2], Takanori Kigawa[1], Makoto Inoue[1], T.akashiYabuki[1], Masaaki Aoki[1], Eiko Seki[1], Takashi Matsuda[1], Hiroshi Hirota[1], Akiko Tanaka[1], Yoshihide Hayashizaki[1], Osamu Ohara[3,4], Sumio Sugano[5] and Shigeyuki Yokoyama[1,2,6]

We have determined nearly a thousand solution structures in the comprehensive analysis program of "Protein 3000 project" conducted at RIKEN GSC. We will present several examples of unique local structures and unique spectral patterns as follows, 1) buried lysins, 2) a unique spectral pattern of restrained histidine with special environments, 3) a few topics of proteins with cis-peptide bonds.

はじめに

理研GSCで担当している「タンパク3000プロジェクト」の網羅的解析プログラムにおいて、これまで多数の構造解析が行われてきた。この内、構造やスペクトルにおいて特に特徴的と思われる例についていくつか紹介したい。

結果と考察

埋もれたLys　Lys、Arg、Glu、Asp等の残基は中性条件においては電荷をもち、通常典型的な親水性残基と考えられている。我々は、CSおよびnuclear moveタンパクファミリーに属するドメインの構造解析の結果、Lys残基が、蛋白質の疎水性コア内に埋もれていることを見出した。CS、nuclear moveドメインはHsp20スーパーファミリーに属し、この埋もれたLysは酵母からヒトまで完全に保存された残基であることがわかった。このLysは疎水コア中ではNH2 の形で電荷を持たず、主鎖のカルボニル基と水素結合を形成して安定化していた。

Keywords: buried lysine, restrained histidine, cis-peptide bonds, structural genomics

はやしふみあき、ながしまとしお、しんきょくえい、すえたけてつや、いずみけんや、えんどうひろし、いのうえきょうこ、さのれいこ、せいみやきょうこ、くろさきちさと、ながしまかよこ、よしだまゆみ、しろうずみかこ、てらだたかほ、きがわたかのり、いのうえまこと、やぶきたかし、あおきまさあき、せきえいこ、まつだたかし、ひろたひろし、たなかあきこ、はやしざきよしひで、おはらおさむ、すがのすみお、よこやましげゆき

δ炭素が炭素方向に強く広幅化したHis　数多くの蛋白質の芳香族領域のHSQCを測定中、まれに表記のようなHisを観測することがある。ところが、LIMドメインの構造解析の際には、ずっと高い頻度でこの特徴的なHisシグナルの広幅化が観測された。このことは、LIMドメインにおいては特徴的なHisの広幅化が起こる構造が保存されていることを示している。この構造がどんな特徴を持ち、なぜ広幅化が起こるのか検討を行った。

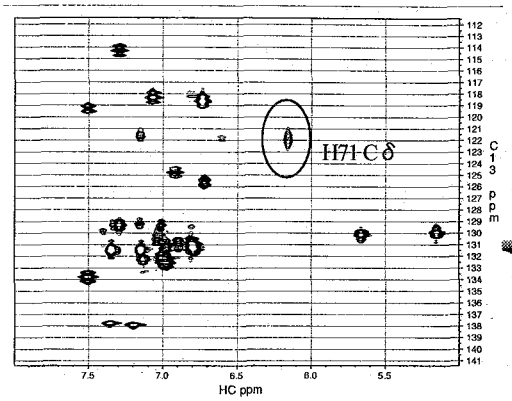

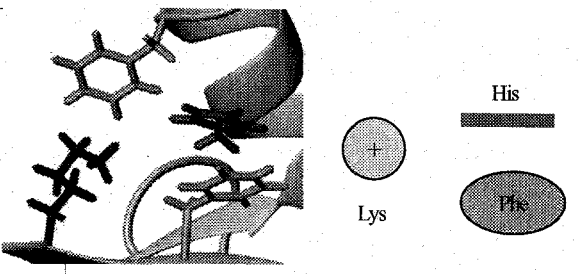

A unique broadening of the delta carbon of His71 is shown on the left. Side chain arrangements around the His are shown on the right.

上図の例のように、広幅化が起こっているHisは例外なくχ_2軸に関する回転が束縛されていた。また、イミダゾール環の横に電荷または水素結合できる官能基を持った側鎖が位置していた。このことから、Hisの広幅化の原因は次のように考えることができる。回転が束縛されているためイミダゾール環の横には常に特定の官能基が存在し、この存在のために窒素原子のローンペアはイミダゾール環のフリップフロップ時にも、常に片側(この場合Lys側)にあるほうが有利となる。その結果、HNはイミダゾール環のフリップフロップと同期して、δN1位とεN2位を交換することになる。δN1位またはεN2位がプロトン化された時のδCの化学シフトは10ppmほど異なるため、このような広幅化が観測されると考えられる。

シスペプチド結合　蛋白質中のポリペプチド鎖のペプチド結合は通常トランス型を取るが、まれにシス型の配座となる。また、シス型のペプチド結合は、Proの直前のペプチド結合で見られることが多い。現在のところ相同な蛋白質で保存されたcis-Proを持つことがわかっているもの以外でシス型ペプチド結合の存在を予測することは困難である。ここでは 2 つの観点からシスペプチド結合に関して考察を加えたい。1)相同蛋白質において保存されたcis-Proの位置が別の残基に置き換わったときどうなるか、2)cis-Proが頻繁に現れる領域を持つドメインに関して立体構造とシス型ペプチド結合との関係はどうか。1)に関してユビキチン共役酵素ファミリー(UQ_con)の例を示したい。UQ_conはβ3 とβ4 をつなぐループ部分によく保存されたcis-Proを持つ。ところが我々が構造解析したUQ_conでは、このProはAsnに置換されていた。構造解析の結果、興味深いことに、このAsnの3-4残基後ろにPro-Proという配列を持つにもかかわらず、このAsnのところでcis配座をとっていた。このことは、この蛋白質の場合、残基の種類よりもむしろ保存された残基の周りの構造がcis配座をとる決め手となっていることを意味する。2)に関して、免疫グロブリン様ドメインはβ2とβ3をつなぐループでしばしばcis-Proの存在が確認されている。1)の場合とは異なり、cis-Proの位置は配列上保存されておらず、このループ上にProがあるからといって必ずしもシス型になるとは限らない。この場合のシス配座と構造の関係について現在解析を進めている。

P046

Human Structure Proteomics: Solution Structure of the SMR Domain of Human Blc-3 Binding Protein (B3BP)

([1]理研 GSC、[2]理研播磨、[3]理研 RCAI、[4]かずさ DNA、[5]東大院理)
○張 恵平[1]、林 文晶[1]、黒崎 千智[1]、好田 真由美[1]、白水 美香子[1,2]、
寺田 貴帆[1,2]、木川 隆則[1]、井上 真[1]、矢吹 孝[1]、青木 雅昭[1]、関 英子[1]、
松田 貴意[1]、廣 田洋[1]、田仲 昭子[1]、小原 收[3,4]、横山 茂之[1,2,5]

Human Structure Proteomics: Solution Structure of the SMR Domain of Human Blc-3 Binding Protein (B3BP)

([1]RIKEN GSC, [2]RIKEN HARIMA, [3]RIKEN RCAI, [4]KAZUSA DNA Research Institute, [5]Graduate School of Science, The University of Tokyo)
○Huiping Zhang[1], Fumiaki Hayashi[1], Chisato Kurosaki[1], Mayumi Yoshida[1], Mikako Shirouzu[1,2], Takaho Terada[1,2], Takanori Kigawa[1], Makoto Inoue[1], Takashi Yabuki[1], Masaaki Aoki[1], Eiko Seki[1], Takayoshi Matsuda[1], Hiroshi Hirota[1], Akiko Tanaka[1], Osamu Ohara3,4 and Shigeyuki Yokoyama[1,2,5]

Abstract: The solution structures of the SMR domain, which is involved in the human Blc-3 binding protein (B3BP), has been revealed by using multidimensional NMR spectroscopy. In this presentation, we describe the structural detail and discuss relationship between structure and function by comparing with other domains from Dali Sever search.

Introduction: SMR domain is an around 90-residue domain found in the small mutS related (SMR) proteins from bacteria and eukaryotes. Usually, SMR proteins could be involved in mismatch repair (MMR) or/and chromosome crossing-over and segregation. The precise biological function of this protein has not been yet clear, although it has been supposed that the SMR domain may act as a nicking endonuclease. In order to understand the detail biological function, it is important to elucidate the structure of SMR domain. As a part of the project PROTEIN 3000, we have determined the NMR structure of the SMR domain in Blc-3 binding protein (B3BP), which is only human protein containing the SMR domain.

Keywords: SMR domain; Blc-3 binding protein; NMR; Solution structure; Cell-free protein expression system

ちょうけいへい、はやしふみあき、くろさきちさと、よしだまゆみ、しろうずみかこ、てらだたかほ、きがわたかのり、いのうえまこと、やぶきたかし、あおきまさあき、せきえいこ、まつだたかよし、ひろたひろし、たなかあきこ、おはらおさむ、よこやましげゆき

Materials and Methods

The $^{13}C/^{15}N$-labeled protein was produced by the cell-free synthesis system. All NMR measurements were performed at 20 °C under ambient pressure on JEOL ECA 600, JEOL ECA 800 and Varian INOVA 800 spectrometers. The sequence-specific backbone resonance assignment was achieved through a combination of standard triple resonances techniques using 2D ^{15}N-HSQC and 3D HNCO, HN(CA)CO, HN(CO) CA, HNCACB and CBCA (CO)NH spectra. Side-chain assignment was obtained using 2D ^{13}C-HSQC and 3D HBHA(CO)NH, HBHANH, C(CO)NH, HCCH-TOCSY and CCH-TOCSY spectra. Distance restraints were established using 3D ^{15}N-edited-NOESY and ^{13}C-edited-NOESY spectra. The programs NMRPipe, NMRView and Kujira were used for spectral processing and data analysis. Structure calculations were performed with the program CYANA2.0.17.

Results and Discussion

100 conformers were calculated; of those 20 CYANA conformers with the lowest target function were selected to represent the structure (Figure 1a). The structure of SMR domain folds into a two-layered alpha/beta-sandwich structure with a beta-alpha-beta-alpha-beta-beta topology, comprising a mixed four-stranded beta-sheet stacked against two alpha-helices, both of which are nearly parallel to the strands of the beta-sheet, as shown as the ribbon diagram (Figure 1b). We have elucidated the structure of the SMR domain for the first time. In this presentation, we describe the structural detail and discuss relationship between structure and function by comparing with other domains from Dali Server search.

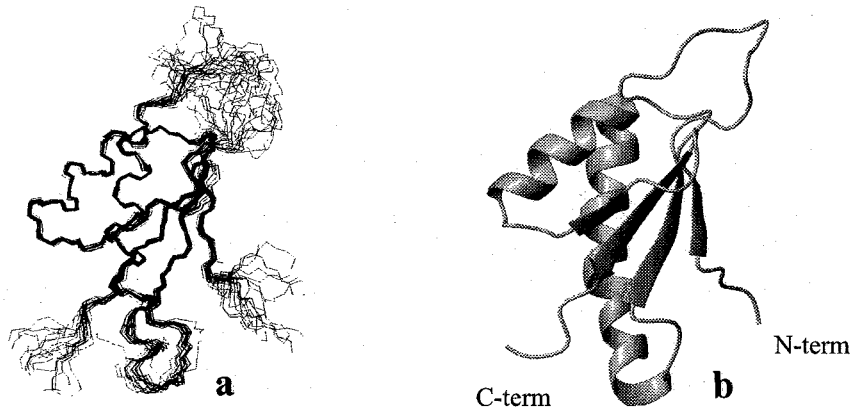

Fig.1 Ensemble of 20 structures of the lowest energy in 100 (a) and ribbon diagram (b).

P047

2D selective-TOCSY-DQFCOSY を用いたラクトースの水酸基シグナルの完全帰属とグリコシド結合の同定

[1]ブルカーバイオスピン, [2]横浜市立大学大学院国際総合科学研究科

○佐藤一[1], 梶原康宏[2]

A Complete Assignment of Hydroxyl ^{1}H Signals and Identification of Glycosidic Linkage by 2D Selective-TOCSY-DQFCOSY

[1]Bruker Biospin,

[2]International Graduate School of Arts and Sciences, Yokohama City University

○Hajime Sato[1], Yasuhiro Kajihara[2]

[Abstract] We have achieved a complete assignment of non-exchangeable ^{1}H and ^{13}C NMR signals of a biantennary undecasaccharide by the 2D selective-TOCSY-DQFCOSY and selective-TOCSY-HSQC experiments. In this poster, we expand the experiments into assignment of hydroxyl proton signals (OH's). The experiments were examined on lactose. Finally, all hydroxyl proton signals were unambiguously assigned. By using the assignment, OH-4's in α- and β-glucose and OH-1 in β-galactose were not observed. This evidence potentially suggests that the linkage is to be the β-1,4 mode.

[要旨] 我々はすでに 11 糖から二分岐のN型糖鎖の ^{1}H と ^{13}Cシグナルを非経験的に完全帰属するための方法を開発している. この測定法は, 選択励起パルスを伴ったTOCSYとDQF-COSY法およびHSQC法を組み合わせた二次元NMR法であり, 得られるスペクトルでは単糖ごとのシグナルのみが観測されるので, 解析が容易となる. 本研究では, この方法を用いて糖水酸基のシグナルの帰属を試みた.

近年, 遊離水酸基を有する糖受容体にグリコシル化反応を行って, 糖鎖を短工程で合成する技術が進歩している. したがって, 糖の連結位置を容易に同定する手法が必要となる. 糖水酸基は, 保護基の導入や脱保護, またはグリコシル化反応において, 対象となる官能基であるにもかかわらず, 通常, NMRを用いて反応前後の解析は行われていない. 本研究では, 上記測定法をまずラクトースに応用した. その結果, α-およびβ-グルコースならびにβ-ガラクトース残基の水酸基プロトンシグナルを容易に帰属できた. また, この実験において, α-およびβ-グルコースの 4 位ならびにβ-ガラクトース残基の 1 位の水酸基は観測されず, グリコシド結合様式が, 1-4 結合であることを確認できるとともに, 未知の糖鎖のグリコシド結合様式を推定する手法にも利用できることが判明した.

キーワード: グリコシド結合, 水酸基プロトンシグナル, 2D selective-TOCSY-DQFCOSY

著者ふりがな: さとう はじめ, かじはら やすひろ

[実験] 本研究ではラクトースを用いた．この試料(2.55 mg)を重DMSO(0.5 mL)に溶かしてNMR測定試料とした．全ての測定はBRUKER社製5mmTXI-Zプローブを装着したAV-400機を用いて行った．温度は293Kに設定した．2D selective-TOCSY-DQFCOSYにおいて，各糖残基の分離したシグナルを選択励起するためにRE-BURP(80 ms-100 ms)を用いた．この測定においてTOCSY混合時間を200 msに設定し，積算回数を16回，展開側を640ポイント取り込んだ．この測定を合計三残基に対して行った．

[結果と考察] まず，単糖分のDQFCOSYスペクトルを得るために，6.34 ppmのシグナルを選択励起した測定を行った．Fig. 1(A)に示すように，6.34 ppmの対角ピークから連鎖帰属を開始して，クロスピークへつなぎ，クロスピークから対角ピークへつないだ．このシグナルパターンは明らかにα-グルコース残基由来であることがわかった．つぎに，Fig. 1(B)に示すように，6.68 ppmのシグナルを選択励起したDQFCOSYスペクトルにおいて，Fig. 1(A)と同様な解析を行った．その結果，このシグナルパターンは，β-グルコース残基由来であることがわかった．最後に，Fig. 1(C)に示すように，4.18 ppmのシグナルを選択励起したDQF-COSYスペクトルにおいて，Fig. 1(A)と同様な解析を行った．その結果，このシグナルパターンは，β-ガラクトース残基由来であることがわかった．ガラクトース残基において，カップリング定数J_{H4-H5}が1 Hz以下であることから，H-4からH-5へTOCSYによる磁化移動が効果的に起こらない．したがって，H-5,H-6およびOH-6は，検出されなかった．2D selective-TOCSY-DQFCOSY法を用いて，ガラクトース残基のH-5,H-6およびOH-6を除く全ての非交換性および水酸基^{1}Hシグナルを非経験的に帰属することができた．この方法で検出されないシグナルの帰属は2D HSQC-TOCSY法により行った．帰属の結果，α-およびβ-グルコース残基のOH-4ならびにβ-ガラクトース残基のOH-1シグナルが観測されず，グリコシド結合様式が，1-4結合であることを確認できた．この方法は，三残基程度の糖鎖に対して有効であり，また，OHシグナルを全て帰属できた場合には，グリコシル位を推定する簡便な手法であることが判明した．現在，この方法を用いて，より大きい糖鎖への応用を試みている．

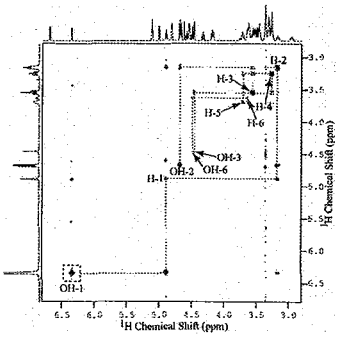

Fig. 1(A)

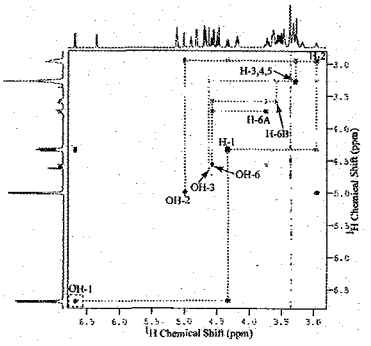

Fig. 1(B)

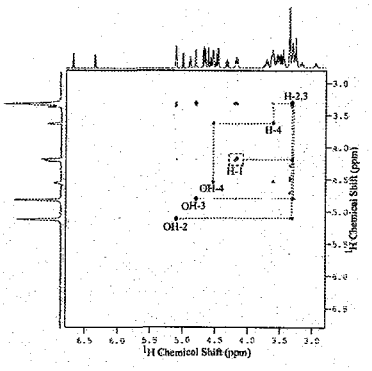

Fig. 1(C)

Fig. 1. 400MHz 2D selective-TOCSY-DQFCOSY spectra for α- (A) and β-glucose (B) and β-galactose (C) in lactose. Normal 1D ^{1}H and 1D selective-TOCSY spectra are shown on top and the left of the 2D spectra, respectively.

P048

HMBC 法の新しい応用測定---Sel-HR-HMBC 法について,

東大院農・応生化、＊東大・分生研
○降旗一夫、＊瀬戸治男

Selective HR-HMBC, A New Method for Measuring Heteronuclear Long Range Coupling Constants of Methine Proton Signals Attached to a Methyl Group

We present an improved version of the HR-HMBC (High Resolution HMBC) technique named Selective HR-HMBC. This method enhances the sensitivity of cross peaks of methine proton signals attached to a methyl group in the HR-HMBC spectra and enables to determine the long range J_{CH} couplings of methine signals. HR-HMBC was developed to observe long range J_{CH} couplings by incorporating the J-scaling pulse sequence into HMBC.

A methine proton adjacent to a methyl group splits into a multiplet with weak signal intensity due to several spin couplings with surrounding vicinal protons. This phenomenon causes determination of long range J_{CH} couplings of methine protons in HR-HMBC spectra difficult.

The important point of Selective HR-HMBC is to transfer selectively the magnetization of a methyl group to its adjacent methine proton. As a result, the cross peaks of the corresponding methine proton are enhanced to enable easy determination of long range J_{CH} coupling constants in HR-HMBC spectra.

Application of this new technique to model compounds, portmicin and monazomycin, proved that this method is useful for determination of J_{CH} of complicated molecules.

天然有機化合物の構造解析において、long range J_{CH}を如何にして効率よく観測するかが重要な課題の一つである。すでに、HMBC 法を利用した long range J_{CH}を観測する方法として J-resolved HMBC 法[1]、HR-HMBC 法[2]を報告し、相対立体の決定に有効であることを示した。しかし、multiplet に分裂したプロトンからは、long range J_{CH}の観測は依然として困難な問題として残っている。例えば、ポリケタイド抗生物質には -CH-CH(CH3)-CH-といったメチル基を多く含んだ化合物が存在する。メチル基の付け根のメチンプロトンは隣接プロトンが多く、multiplet に分裂しブロードとなる。この分裂の度合いがシグナルの高さを決定づける。そのため、通常の HMBC スペクトルでも、S/N の低い cross peak となって観測され、検出が困難になることがしばしばある。また、メチル基の付け根のメチン炭素はアシメ炭素であることが多く、この炭素に結合した置換基の相対立体の解析には、この炭素に結合したプロトンからのスピン結合の解析は重要なポイントになる。そこで、メチル基の付け根のプロトンの感度を高め、なおかつ long range J_{CH}を観測する方法として、Selective(Sel) HR-HMBC-1,-2 の検討を試みた。

<u>パルス系列</u>

この Sel-HR-HMBC 法は、1D-COSY 法と HR-HMBC のコンビネーションからなっている。この方法は、感度の高いメチル基の磁化をメチンプロトンに移動し、その磁化を HR-HMBC 展開することにある。図 1 に Sel-HR-HMBC の模式図を示す。

メチル基を有する-Ha(CH3)-Hb-Hc-のスピン系を考える。通常の HMBC スペクトル (図 a) では、Ha から炭素 Cb と Cc にクロスピークを観測するとする。これに対して、Sel-HR-HMBC-1 スペクトル (図 b) は、メチル基の磁化を選択的に励起しプロトン Ha に移動させる。そして、Ha の磁化とメチル基の磁化を足し合わせて HMBC スペクトルを測定する。この場合、

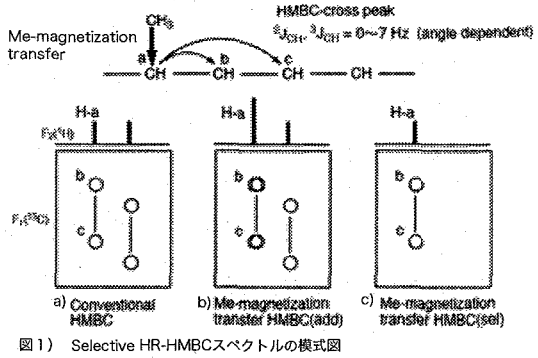

図 1) Selective HR-HMBCスペクトルの模式図
a) Conventional HMBC, b) SEL-HR-HMBC-1, c) SEL-HR-HMBC-2

Ha のクロスピークは自分自身の磁化に対してメチル基からの磁化が加わり、感度の増加したスペクトルとなる。このスペクトルではメチル基のシグナルは観測されないか感度は低下するが、その他のプロトンでは、通常の HMBC スペクトルとして使用することは可能である。Sel-HR-HMBC-2 スペクトル（図 c）は、メチル基の磁化を Ha に移動させ、この磁化のみを観測する。このスペクトルでは目的とするクロスピークのみが観測される。そのため、複雑なスペクトルでは解析は容易となる。

図 2 に Sel-HR-HMBC-1,-2 のパルス系列を示す。

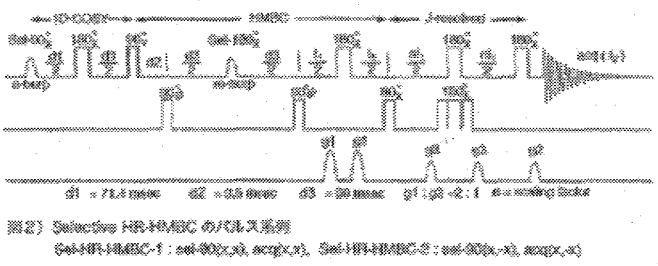

Sel-HR-HMBC-1 は、メチル基の付け根のメチンプロトンの感度の向上とともに、このメチンプロトン以外のプロトンは通常の HR-HMBC スペクトルを測定することを目的とする。このパルス系列は 1D-COSY(90x(sel)-d1/2-180x -d1/2-90y)法と HR-HMBC 法の結合である。HR-HMBC 法は通常の HMBC 法に J-scaling 法を結合した long range J_{CH} を観測する方法である [2]。1D-COSY 法では、90x(sel)パルスはメチル基のみを励起し、90y パルスはメチル基の磁化をメチンプロトンへ移動させる。それと同時に、メチル基以外のプロトンに対しては HR-HMBC 磁化を励起する。そのため、メチル基に結合したプロトンはメチル基の磁化とそれ自身の磁化が合わさって励起するために、シグナル感度を高めることになる。また、それ以外のプロトンは selective pulse の影響を受けないために、通常の HR-HMBC スペクトルの観測を可能にする。Selective pulse としては、pulse 巾が短く、複数のメチル基を同時に励起しても、スピン結合にも化学シフトにも影響されず位相が揃い、なおかつシグナルの選択性が高いことが重要である。ここでは、e-burp を使用した [3]。この e-burp を使用するにあたっては、pulse 巾を短くするために、他のシグナルに影響しない程度に出来るだけ広い範囲を励起するように設定することが重要である。

SEL-HR-HMBC-2 のパルス系列は、メチル基の付け根、メチンプロトンのみを観測し、スペクトルを単純化することを目的にする。この pulse 系列は SEL-HR-HMBC-1 の pulse 系列をそのままに、selective pulse と reciver の位相を可変しメチル基に結合したメチンプロトンのみを観測する。SEL-HR-HMBC-2 の selective pulse としては、DPFGSE 法に置き換えることは可能であるが、この pulse は、二つの soft pulse と四つの fg-pulse を使用しているため、e-burp のような pulse ではパルス巾が長くなり S/N の低下の原因となる。そのため、ここでは使用しない。使用する場合は square pulse か gaus pulse が良いと思われる。

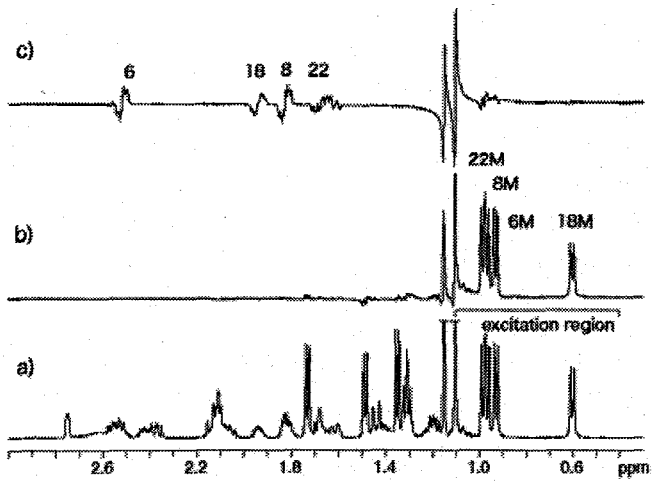

図3) Portmicine Selective 1D-COSY スペクトル
a) 1D-NMR b) Selective 1D-NMR c) Selective 1D-COSY
E-BURP 90 pulse = 12.8 msec delay time(d1) = 69 msec

SEL-HR-HMBC-1,-2 のどちらにおいても HMBC の delay time の中間に、selective180 パルス（re-burp）を導入している。このパルスは、メチル基との J-moduration を消去するためにある。その結果、メチンプロトンにおいて、さらなる感度の向上があった。

図 3 では e-burp の selective 1D スペクトルと、selective-1D-COSY のスペクトルを示す。E-burp の設定は 0.4ppm～1.1ppm(350Hz)を励起範囲とし、pulse 巾は 12.8mse であった。Selective 1D スペクトルでは、Portmicin の 6-Me、8-Me、22-Me、そして、18-Me のみが選択的に、なおかつスペクトルの位相が揃って観測されている。複数のメチル基を同時に測定したときの 1D スペクトルにおいて、観測シグナルの位相が揃うことが phase mode での 1D-COSY スペクトルでは重要になる。Selective-1D-COSY のスペクトルでは、6-Me、8-Me、22-Me、18-Me の付け根のメチンプロトン、6-H、8-H、18-H、22-H のシグナルを観測した。SEL-HR-HMBC-2 スペクトルでは、この磁化を HR-HMBC 測定することになる。

ポートミシンの Sel-HR-HMBC スペクトル

図 4 に portmicin の SEL-HR-HMBC-2 のスペクトルを示す。

通常の HMBC スペクトルでは、ポートミシンの H8 のプロトンはクロスピークが重なり S/N が低いために解析が困難となっている。この H8 からの long range J_{CH} を観測するために SEL-HR-HMBC-2 スペクトルを測定した。その結果、H8 からのクロスピーク、C6, C7, C9 と 8-Me が斜め二本線となって観測した。スピロケタール環の 6 員環において、H8 のプロトンと H7 はスピン結合が 3.9Hz と小さく、また、H7 がエカトリアルであることから、H8 がアクシャルなのかエカトリアルなのかは、プロトンのスピン結合からは判断できない。この H8 と C6 は J_{CH} が 2.8Hz であり、gauche の配置を取る。

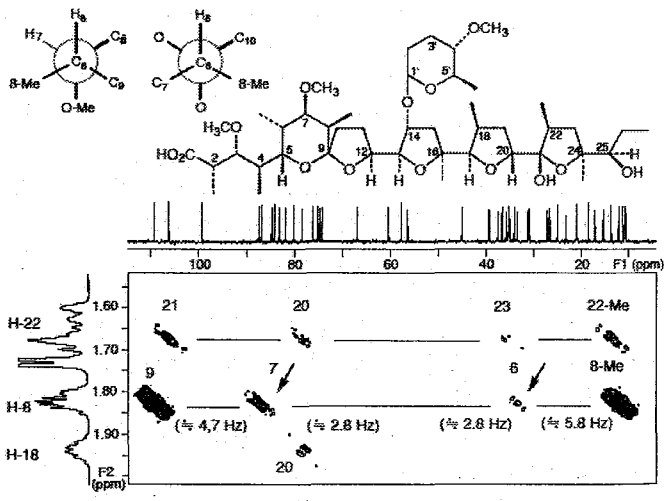

図4) Portmicin SEL-HR-HMBC-2 スペクトル

F1 x F2 = 14000 x 2250(Hz), t1 x t2 = 256 x 4000(point)

d1 = 69 msec, d3 = 69 msec, scans = 64, scaling factor=25,

E-Burp 90 pulse = 12.8 ms (0.4ppm - 1.1ppm)

また、H8 と C7 は $^2J_{CH}$ が 2.8Hz と小さいことからで H 8 と O-Me は anti の関係である。この関係から H8 はアクシャルであることが判明する。また、H8 と C9 は $^2J_{CH}$ は 4.7Hz と大きく分裂する。これは、H8 と C9 に結合した二つの酸素原子が一つは gauche に一つは anti に結合することを指示する。また、H 8 と C10 にクロスピークが観測されないことは、H8 と C10 はスピン結合が小さく、H8 と C10 は gauche の関係であることを示す。

モナゾマアイシンへの応用

図 5 には monazomycin の SEL-HR-HMBC-1 のスペクトルを示す。

Monazomycin のメチル基の付けのメチンプロトンはブロードなマルチプレットに分裂し、通常の HMBC スペクトルでも、クロスピークの観測は困難である。そのため、少しでも感度を得るために SEL-HR-HMBC-1 を測定した。しかも、クロスピー

クの S/N を高めるために、nt_1max（253ms）が短くなるように f1 軸データ点(204point)を少なく設定した。H46 からのクロスピーク、C44, C45, C47 と 46-Me が斜め二本線として観測することが可能であった。H46 と H45 は 3.0Hz に分裂し gauche の関係にあるが、45-OH と C44 は H46 に対してどちらが anti で、どちらが gauche であるか判明することが出来ない。しかし、スペクトルから、H46 と C44 の間で $^2J_{CH}$ が 5.5Hz と観測されたことから、H46 と C44 は anti の関係にあることが容易に判明した。また、H46 と C45 の間で $^2J_{CH}$ が 5.5Hz を観測し、H45 と 46-OH が gauche であることが判明した。

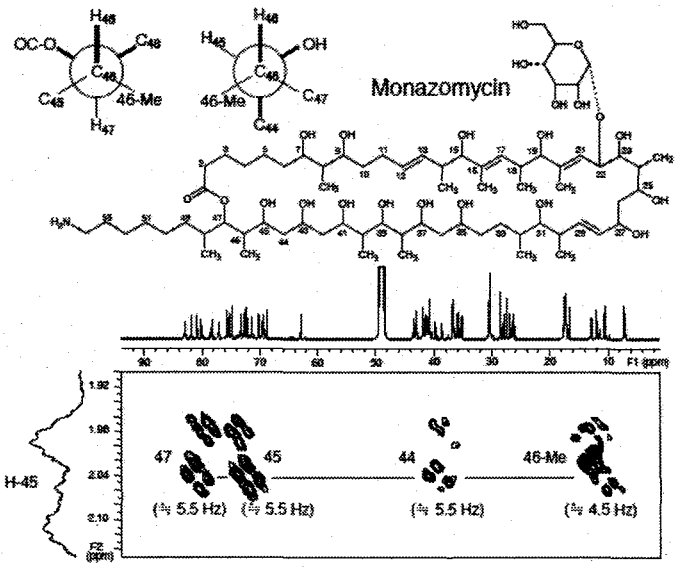

図5） Monazomycin SEL-HR-HMBC-1スペクトル
F1 x F2 = 20000 x 3000(Hz), t1 x t2 = 204 x 5146(point),
d1 = 69ms, d3 = 69ms, scans = 400,
scaling factor =25, nt1max=253 ms,
E-Burp 90 pulse = 12.9 ms (0.4ppm - 1.1ppm)

一方、H46 と H47 は 9.7Hz であることから、47-O と C48 はともに gauche の関係にあることが予想され、C47 に $^2J_{CH}$ が 5.5Hz が観測され、また、C48 とはスピン結合が小さく観測されなかった。

まとめ

SEL-HR-HMBC-1,2 の二つの方法は観測が困難になるメチル基の付け根のメチンプロトンを強調して観測する方法である。SEL-HR-HMBC-1 法は Me 基のシグナル強度は低下するものの通常の HMBC 法と同様のスペクトルを得ることができる。これに対して、SEL-HR-HMBC-2 は Me 基の付け根のメチンプロトンを選択的に観測することが可能である。

どちらの方法においても、HR-HMBC 法を使用し、long range J_{CH} を観測することを目的にしている。そのため、nt_1max を 250msec(4Hz)から 500msec(2Hz)位と長い値をとるように設定するために、通常の HMBC 法に比べて、かなりスペクトルの S/N が低下する。実際の測定に当たっては、この S/N の低下を考慮して積算時間を設定することが重要である。SEL-HR-HMBC-1,2 の二つの方法は Me 基の付け根のメチンプロトンという限られたスピン系の解析手段であるが、このブロードなシグナルからのクロスピークを如何に観測するかという問題の一つの解決法である。これらの方法により、従来法では解析が困難な化合物の構造解析が容易になることが期待される。

1) 第 37 回 NMR 討論会講演要旨集、横浜、100pp, (1998)
2) 第 40 回 NMR 討論会講演要旨集、京都、218pp, (2001)
3) H. Geen, R. Freeman, J. Magn. Reson. 87, 4125, 1990

P049

NMR を用いた *Escherichia coli* ATCC23505 由来 lipopolysaccharide O-antigen の構造解析

東京薬科大学大学院薬学研究科，○多田塁[1]，三浦典子[1]，安達禎之[1]，大野尚仁[1]

An unambiguous assignment and structural analysis using solution NMR experiments of O-antigen from *Escherichia coli* ATCC23505 (serotype O9), [1]Laboratory for Immunopharmacology of Microbial Products, School of Pharmacy, Tokyo University of Pharmacy and Life Science, ○Rui Tada[1], Noriko Nagi-Miura[1], Yoshiyuki Adachi[1], Naohito Ohno[1]

Bacterial lipopolysaccharide from *Escherichia coli* O9 (O9 LPS) has various characteristic biological activities other than endotoxic activities. The biological activities exhibited depend on the structure of the O-antigen. The O-antigen region of O9 LPS is composed of the mannose homopolysaccharide (MHP). This structure was reported previously, but not all its proton and carbon signals were assigned. In the present study, we completely assign all proton and carbon signals of the O-antigen of O9 LPS using ^{1}H- and ^{13}C-NMR spectroscopy, including the DQF-COSY, TOCSY, 2D-selective TOCSY-DQFCOSY, NOESY, HSQC, H2BC and HMBC methods.

【背景】

Lipopolysaccharide (LPS)はグラム陰性菌の外膜に存在し，グラム陰性菌感染の病原性に関わる糖脂質である．LPS は lipid A, core region および，菌の抗原性を担う O-antigen より構成されている．エンドトキシンショックやサイトカイン誘導など LPS の持つ多くの生物活性は lipid A 部分により toll-like receptor 4 (TLR4)を介して発現する．しかしながら，一部の O-antigen に mannose homopolymer (MHP)を有する LPS は通常のエンドトキシンショックではない特徴的なアナフィラキシー様ショックを惹起することが知られている．これらの活性は mannose-binding lectin (MBL)を介した O-antigen の認識により誘導される．これらの O-antigen が関与する生物活性のメカニズム理解には構造情報が有益である．*E.coli* O9 の O-antigen 構造は 1D-^{1}H NMR，メチル化分析およびスミス分解等を用いた構造決定が既報であるものの，各々の ^{1}H および ^{13}C の詳細な帰属はなされていない．

そこで本研究では，溶液 NMR を用い，DQF-COSY, TOCSY, 2D-selective TOCSY-DQFCOSY, NOESY, HSQC, H2BC ならびに HMBC 等，様々なパルス系列を用

Escherichia coli O9; O-antigen; lipopolysaccharide; high mannose type

ただるい，みうらのりこ，あだちよしゆき，おおのなおひと

い *E.coli* O9 lipopolysaccharide 由来 O-antigen 構造中に存在する全ての ^{1}H および ^{13}C の明瞭かつ完全帰属を試みた.

【方法】

LPS は既報に従い, フェノール-水抽出により得た. O-antigen は 1% HOAc, 100℃, 1h で加水分解し, ゲル濾過法により分画した. 糖組成は常法に従い GLC で分析した. NMR は O-antigen を D_2O に溶解し, TXI-*xyz* gradient probe (^{13}C 検出のみ BBO-*z* gradient probe)が備わった Bruker Avance 500 spectrometer を用い, 測定温度 35℃で測定した.

【結果および考察】

糖組成を GLC を用い分析したところ, mannose より構成されていた. 1D-^{1}H NMR spectrum (Fig.1)より, anomeric 領域には糖残基 5 つ分のシグナルが観測された. これらのシグナルを低磁場側から A, B, B', C, D とした. 全ての糖残基は, 取り込み中に decoupling しない ^{1}H, ^{13}C-HSQC を用い測定した $^{1}J_{H1,\,C1}$ よりα-configuration であった. すべての ^{1}H と ^{13}C シグナルを DQF-COSY, TOCSY, 2D-selective TOCSY-DQFCOSY, ^{13}C-edited HSQC ならびに H2BC を用いて帰属した(Fig.2 & Table 1). さらに, NOE と HMBC から, 結合様式と配列を決定した(Fig.3). この構造は既報でメチル化分析, 化学分解や化学合成などの手法で決定した構造と一致していた.

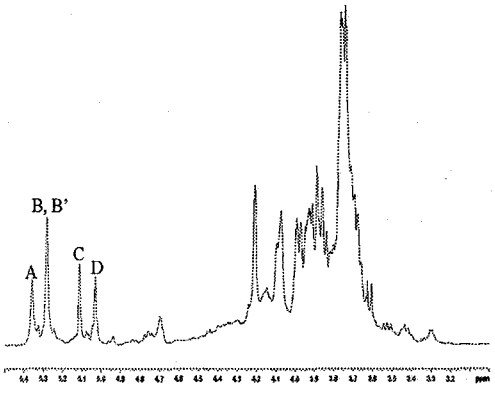

Fig.1. 1D-^{1}H NMR spectrum of O-antigen from O9 LPS

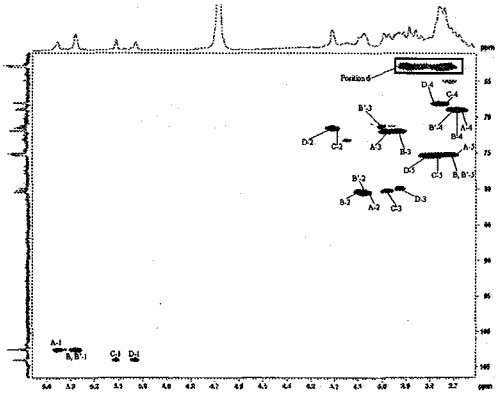

Fig.2. ^{13}C-edited HSQC spectrum of O-antigen from O9 LPS

Table 1. Chemical shifts (ppm) of ^{1}H and ^{13}C NMR signals

	$^{1}H/^{13}C$						
Sugar Residue	1	2	3	4	5	6a	6b
A	5.36	4.07	3.99	3.68	3.77	3.90	3.78
	102.5	80.60	72.02	69.03	75.28	62.90	
B	5.28	4.10	3.94	3.70	3.75	3.90	3.78
	102.5	80.37	71.97	68.87	75.41	62.90	
B'	5.28	4.08	3.96	3.73	3.75	3.90	3.78
	102.5	80.56	71.29	68.87	75.41	62.90	
C	5.12	4.21	3.99	3.76	3.82	3.93	3.78
	103.9	71.61	80.32	68.11	75.20	63.01	
D	5.03	4.21	3.93	3.77	3.84	3.93	3.75
	103.9	71.55	79.97	68.11	75.34	63.01	

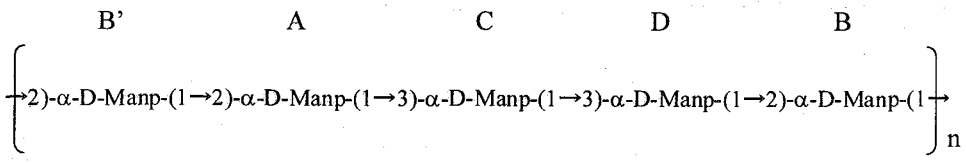

Fig.4. Chemical structure of O-antigen polysaccharide from O9 LPS

P050

J値を用いたブチルアルコールの水和メカニズムについての研究

福井大・院工　○山村卓矢，水野和子

A study of Hydration mechanism of the Butyl alcohol in terms of J value

Department of Applied Chemistry and Biotechnology, University of Fukui,
○Takuya Yamamura, Kazuko Mizuno

Four structural isomers of butyl alcohol are miscible with water in different concentration area. We estimated that the differences in the miscibility should come from those in the Hydrogen bond and the C-H$\cdots$O$_w$ interactions. To demonstrate this, we carried out IR･NMR studies and simulation(MO). NMR measured with NON･NOE(25℃) using External double reference method, and analyzed J value and Chemical shifts. The simulation was executed by the DFT method by using Gaussian03. The result obtained show that weak C-H$\cdots$O$_w$ interaction to strong O-H$_{BuOH}\cdots$Ow and contribute to the difference.

【緒言】

我々の研究室では，これまでに様々な極性基を持つ有機化合物と水との溶液中での相互作用についてIR・NMRを用いた実験と，コンピュータを用いた分子シミュレーションによって詳細な解析を行ってきた．

本研究では，溶質に低分子アルコールであるButyl alcohol (BuOH)を用いてこれまでの研究を発展させることを目的とした．BuOHには4種の構造異性体が存在し，それぞれ水との混合領域が異なっている．(Fig.2)

t-BuOH以外の3種は，水と相分離する領域が存在しており，これらの混合性の違いに注目し実験・計算を行うことを目的として，[BuOH-水]系のサンプルを作成しIRとNMRを用いた実験を行った．また，実験に加えてMO（分子軌道）法による分子シミュレーションによる[アルコール-水]系について構造解析を行い実験結果の補足データとした．

【実験と計算】

4種のBuOHと純水を用いて各濃度の溶液を調整しBuOHの多い混合領域と，水の多い混合領域それぞれについてIR (BuOH/D_2O)とNMR (BuOH/H_2O) の測定を行った．非混合領域については，今回測定は行っていない．

NMRの測定では，Fig.1のような外部複基準法 (External double reference method) による測定法を用いた．内管には，基準物質としてHMDO (Hexamethyldisioxane) を，外管には目的となるサンプル溶液 (BuOH/H_2O) を割り当てている．各濃度のサンプルについてNON・NOE（25℃）で測定を行い，ケミカルシフトとJ値に

Keyword ： 外部複基準法，J値，水素結合，　CH...O interaction

やまむらたくや，みずのかずこ

よる解析と同サンプルの IR スペクトルとの比較・考察を行った.
また実験に加えて，Gaussian03 アプリケーションを用いた分子シミュレーションによる解析を行った．計算方法には密度半関数法（B3LYP）を用いて，構造最適化，振動数，ケミカルシフト・J 値の計算を各 BuOH 分子単体と BuOH-水混合系についてそれぞれ計算を行った．得られた計算結果を実験で得られた IR・NMR のデータと比較を行い，データの補足と更なる詳細な構造解析を行った.

【結果と考察】

得られた IR スペクトルの C-H 伸縮振動バンドの濃度変化（Fig.3）から，水が増えるにしたがって C-H バンドの高波数側へのシフト（ブルーシフト）が生じていることが分かる．溶媒分子である水が多い場合と，溶質分子が多い場合とでは C-H 基への寄与が異なることが予想され，これらの結果を詳細に解析する為に現在 NMR で得られたデータから，J 値とケミカルシフトの解析を行っている.
また，計算結果と比較することによって水素結合をメインとした溶液中での相互作用について詳細な解析を行っており，アルキル基水和のメカニズムの解明が期待できる.

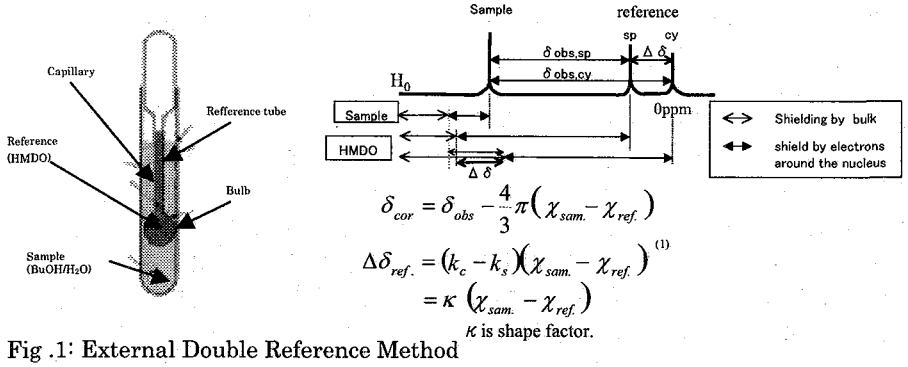

$$\delta_{cor} = \delta_{obs} - \frac{4}{3}\pi(\chi_{sam.} - \chi_{ref.})$$

$$\Delta\delta_{ref.} = (k_c - k_s)(\chi_{sam.} - \chi_{ref.}) = \kappa(\chi_{sam.} - \chi_{ref.}) \quad (1)$$

κ is shape factor.

Fig .1: External Double Reference Method

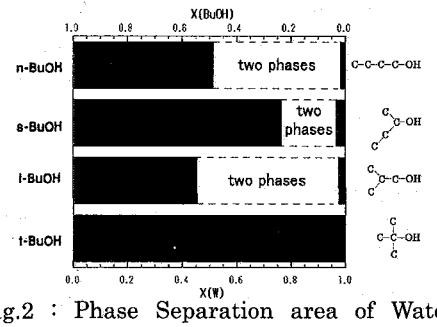

Fig.2 ： Phase Separation area of Water – BuOH mixture

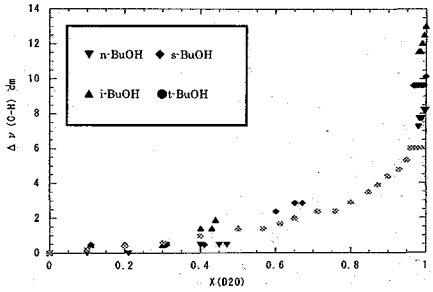

Fig.3 ： Concentration dependency of the wavenumber at the peak of $\Delta\nu$ -CH3 in D_2O as functions of XD_2O

【Reference】

Mizuno.K, Yuka Tamiya, Mamoru Mekata Pure Aool. Chem. Vol.76, No.1,pp.105-114,2004.

P051

エチレングリコール誘導体－水系のケミカルシフトの温度依存性

(福井大・院工) ○林真弘，兵藤公彦，市丸哲也，水野和子

Temperature dependency of chemical shifts of [ethylene glycol derivative/water] system

Department of Applied Chemistry and Biotechnology, University of Fukui,
Masahiro Hayashi , Kimihiko Hyoudou , Tetsuya Ichimaru , Kazuko Mizuno

In order to study concentration and temperature dependence of chemical shifts exactly, the ^{1}H chemical shifts of [1,2-Dimethoxyethane(1,2DME)/water] system were measured by External double reference method with bulk magnetic susceptibilities corrected. It was observed that more polarized water molecules than that of pure water were formed at X[1,2DME]<0.1. On the other hand, it was also found that less polarized water molecules than that of pure water were formed at X[1,2DME]>0.1. The changes in the polarization increases with decreasing temperature. We are going to investigate origins of the changes in the polarization of the water molecules in the mixture.

緒言

非イオン性界面活性剤の親水性基であるポリオキシエチレン(POE)鎖の水和メカニズムを明らかにすることは，基礎化学と応用化学の両方の観点から興味深い研究課題である．本研究ではこの POE を構成する最小単位の化合物として 1,2-ジメトキシエタン(1,2DME)を用いている．我々はこれまでに 1,2DME を[D_2O/H_2O=95/5]に溶かした時の IR スペクトルの O—H 伸縮バンドの測定から，X[1,2DME]=0.05 以下で純水な水よりも分極の大きい水分子が出来ていることをピークの波数から結論してきた．しかし，バンドの吸収強度が波数によって変化するので，ピークの波数は,水素結合の強さと定量的に関係づけることはできない.水分子の水素結合の強さを表す量として水プロトンのケミカルシフト δ_{H2O} がある．δ_{H2O} はすべての化学種の幾何平均値として定量的に得られる．そこで本研究では δ_{H2O} の濃度を測定した．ここでは濃度依存性と温度依存性を厳密に議論できるケミカルシフトの測定法として用いた外部複基準法とその温度補正についても述べる．

外部複基準法について

異なる試料で測定したケミカルシフトを正確に比較するためには，外部基準法を使うことと，試料と基準物質のバルクの磁気遮蔽の差を補正することが必須である．この両方を満たすための方法として我々は外部複基準法で測定してきた．

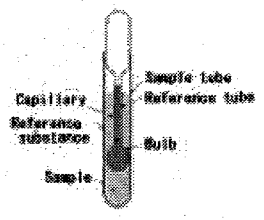

Fig.1：External double reference method

キーワード：外部複基準法(External Double Reference Method)，ケミカルシフトの温度依存性

はやしまさひろ，ひょうどうきみひこ，いちまるてつや，みずのかずこ

外部複基準法によるケミカルシフトは次の式で求めることができる.

$$\delta_{cor} = \delta_{obs} - \frac{4\pi}{3}\left(\chi_{sample} - \chi_{reference}\right) = \delta_{obs} - \frac{4\pi}{3\kappa}\Delta\delta_{reference}$$

ここで, δ_{cor} は補正後のケミカルシフト, δ_{obs} はシリンダー内の reference のピークを 0ppm として観測されたサンプルのケミカルシフト, $\Delta\delta_{reference}$ はシリンダー部分と球部分とにある reference ピークの差, そして, κ は球部分の形状因子である.

ケミカルシフトの温度依存性

ケミカルシフトの温度依存性を厳密に測定するためには, 基準物質の体積磁化率の温度変化の効果を補正する必要がある. Fig. 2 のように, 1℃と 20℃でヘキサメチルジシロキサンを基準物質とした場合, 0ppm の位置のずれは超伝導磁石の外部磁場の測定時間内のゆらぎをはるかに超える.

そこで今回我々は, 20℃での液体のヘキサメチルジシロキサン (HMDO) の共鳴線を 0ppm として, 測定した全ての温度でのケミカルシフトを統一したスケールで表わした. これによってケミカルシフトの温度依存性を厳密に議論できるようになる.

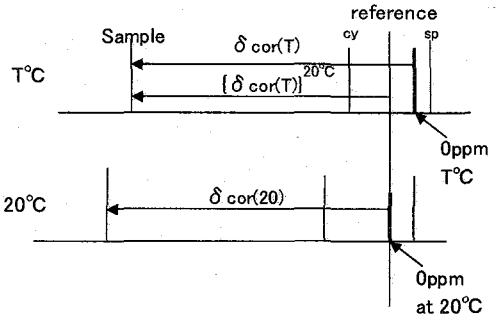

Fig.2 : The chemical shifts δ cor(T) measured at T℃ and {δ cor(T)}20℃ referred to the reference peak at a reference temperature, 20℃.

結果

Fig.3 は 1,2DME を HOD で希釈し IR で測定した O-H 伸縮のピークの変化をまとめたものである. これと対応して, Fig.4 より NMR の結果からも X[1,2DME]<0.1 では純粋な水よりも分極の大きな水分子が存在し, X[1,2DME]>0.1 では分極の小さな水分子が存在していることが確認できた. また, 温度が下がると分極が大きくなっていることからこれは水素結合によるものだと考えられる.

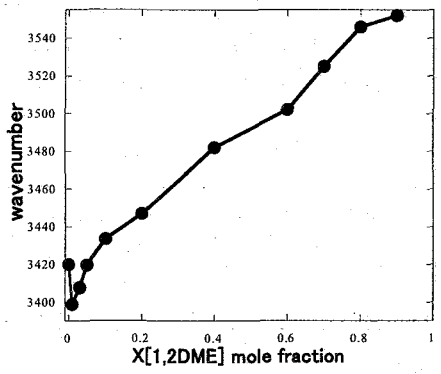

Fig.3 : Concentration dependency of the wavenumber at the peak of ν(O—H) band for HOD in [D_2O+H_2O] solutions of 1,2DME

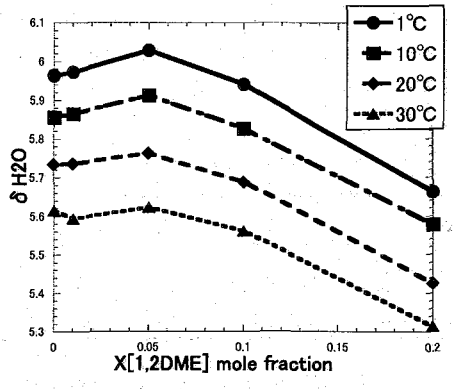

Fig.4 : Temperature and concentration dependence of the chemical shifts of the water protons in aqueous binary mixtures of 1,2DME

NMR ANALYSIS OF CARRAGEENAN EXTRACTED FROM RED SEAWEED *KAPPAPHYCUS ALVAREZII* IN VIETNAM SEA.

Thanh Thi Thu Thuy, Dang Vu Luong, Nguyen Tien Tai
Institute of Chemistry, Vietnamese Academy for Science and Technology

Introduction: Carrageenans are sulfated polysaccharide extracted from the cell wall of red seaweed. Since their nontoxicity and characteristic properties, carrageenans are applied to many fields of daily life, including food, pharmaceutical and cosmetic industries [1].

In previous paper [2], we reported the experimental procedure of isolation and purification of carrageenan extracted from red seaweed, *Kappaphycus alvarezii*, in Ninh Thuan province of Vietnam, and we proposed that this carrageenan is κ-carrageenan, which has an idealized chemical structure consisting of β-(1-3)-D-galactose-4-sulfate (Galp4S : G residue) and α-(1-4)-3,6-anhydro-D-galactose (AnGalp: A residue) repeating units as illustrated in Figure 1.

In this work, we decided to undertake a detailed examination into the structure of this carrageenan by using 1D, 2D NMR spectroscopy.

Experimental: The carrageenan extracted from red seaweed, Kappaphycus alvarezii was then passed through an Amberlite ion exchanged resin 120 H+ column immediately followed by neutralization with a 0.1M NaOH solution and subsequent lyophilization. The Na dissociated form of carrageenan was used for structural analysis.

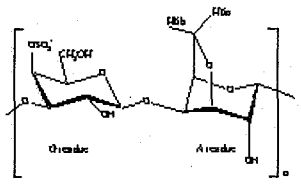

Fig.1: Idealized chemical structure of a disaccharide unit of κ-carrageenan

1D and 2D NMR spectra of 2% (w/w) D_2O solutions of carrageenan sample were measured on a Bruker AVANCE 500MHz. All measurements were performed at 80°C to avoid gel formation.

Results and Discussions: Twelve signals were observed on well resolved ^{13}C spectrum, assigned to the major disaccharide repeat unit of 1,3 linked β -D –galactopyranosyl units alternating with 1,4 linked α -D- galactopyranosyl units. The ^{13}C chemical shift assignments are summarized in Table 1.

Table 1: Chemical shift (ppm) assignments in the ^{13}C NMR measured at 80°C

Residues	α-(1-3)-D-galactose-4-sulfate (G residue)						β-(1-4)-3,6-anhydro-D-galactose (A residue)					
Position	C1	C2	C3	C4	C5	C6	C1	C2	C3	C4	C5	C6
Chem. shifts	102.5	69.6	78.9	74.1	74.7	61.3	95.3	69.9	79.1	78.3	76.8	69.4

Keywords: NMR, assignment, carrageenan, red seaweed.

H-H COSY, H-H TOCSY and HMQC spectra were measuresed for full struture illucidation. Assignment of chemical shift data of COSY and 1H spectra to the structure were shown in tables 2 and 3, respectly.

Table 2: Connectivities arising from COSY spectrum

Cross-peak	Coordinates (ppm)
AH1/AH2	5.14/4.18
AH2/AH3	4.18/4.55
GH1/GH2	4.67/3.65
GH2/GH3	3.65/4.00
GH3/GH4	4.00/4.86

Table 3: Chemical shift (ppm) assignments in the 1H NMR

Residues	α-(1-3)-D-galactose-4-sulfate (G residue)							β-(1-4)-3,6-anhydro-D-galactose (A residue)						
Position	H1	H2	H3	H4	H5	H6a	H6b	H1	H2	H3	H4	H5	H6a	H6b
Chem. shifts	4.67	3.65	4.00	4.86	3.84	3.84	3.84	5.14	4.18	4.55	4.66	4.66	4.18	4.18

Conclusion: We confirm structure of the κ-carrageenan consisting of alternating β-(1-3)-D-galactose-4-sulfate (Galp4S) and α-(1-4)-3,6-anhydro-D-galactose (AnGalp) repeating units of studied carrageenan, extracted from Kappaphycus alvalezii at Ninh Thuan province by more detailed assignments of 1D and 2D NMR spectroscopy. The availability of these chemical shift assignments support to interprete more complex spectra. In addition, the assignments provide novel reference data of galactan compounds.

References

1. Proceeding of National workshop on carrageenan and carrageenophytes, 23rd to 25th Nov., 2002. India.
2. Thanh TT Thuy, Tran TT Van, Qui-Tran Cong Myata, H. Urakawa, κ-carrageenan from *Kappaphycus alvarezii*: Isolation and characterization. *Journal of Chemistry*. Vol.3 , 379-383, 2004.
3. Thanh Thi Thu Thuy, Doctoral Thesis, Kyoto Institute of Technology, 2002
4. I.J.Miller and J.W.Blunt, Botanical Marina, 43, 239, 2000.
5. R. Falshaw, R.H. Furneaux et all, Carbohydrate research, 285, 81-98, 1996.

P053

Homogeneity study of reference material using ^{1}H NMR

Takeshi SAITO
National Metrology Institute of Japan, AIST

Introduction

Producing a reference material requires three important requirements. These are its property value to be certified, homogeneity and stability of the material. In this study, homogeneity study was performed using quantitative ^{1}H NMR. In this study, ERETIC method (Electronic REference To access In vivo Concentrations)[1], which used a pseudo signal that was generated by own NMR synthesizer, was introduced in order to obtain reference signal though out the homogeneity test.

Experimental

All NMR experiments were preformed on a Varian ^{UNITY}INOVA 600A spectrometer; a ^{1}H{^{15}N-^{31}P} 5 mm XYZ PFG Indirect Detection Probe was used.

ERETIC method

ERETIC method uses pseudo FID signal that is generated by synthesizer. The pseudo FID signal was observed through NMR probe. Figure 2 shows the basic ERETIC configuration used in this work. We used a ^{1}H channel synthesizer; the signal was split into two channels. The first channel generates observing pulse. The second channel was used for passing thorough ERETIC signal to probe. Figure 1 shows the ^{1}H NMR spectrum of allyl glycidyl ether (AGE) in $CDCl_3$. ERETIC signal was found around -0.7 ppm in this spectrum. Note that there TMS, water and $CHCl_3$ signals are also there.

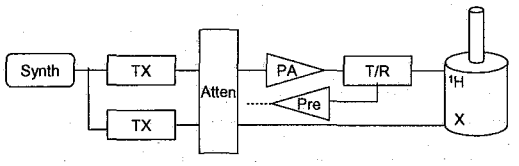

Figure 2 A block diagram of ERETIC method used in this study.

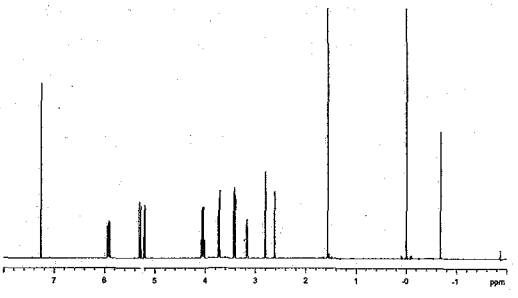

Figure 1 ^{1}H NMR spectrum of AGE in $CDCl_3$. This spectrum was acquired with sw=15,000Hz, at=4s, pw=6.5us (pw90), d1=45s.

Quantitative NMR, ERETIC, homogeneity study, reference materials, reproducibility

さいとう たけし

In this method, we can control frequency or position of the reference signal in a spectrum, amplitude, phase, shape and length of this pseudo FID. When the FID is generated by NMR console, then stability of this signal is expected to be similar or better than NMR signal observed with the same instrument. Furthermore, once the pseudo signal is calibrated in its magnitude, there is no need to re-calibrate the magnitude of the signal as long as the system uses same condition. Thus this signal is an ideal for a reference signal for the quantitative analysis.

Results and discussion

In order to perform a stability test with ERETIC method, the reference signal must have certain level of stability. Table 1 shows the stability of ERETIC signal and other NMR signals for AGE shown in Figure 1. The stronger the signal intensity is, the better the stability was, whoever, this result suggested that some unknown source of noise interfere ERETIC signal. As explained above, stability of ERETIC signal is expected to be similar or better than the NMR signals. One possible solution to stabilize ERETIC signal is just make the signal intensity stronger. Unfortunately this approach is not practical because the pseudo FID was generated and fed into the probe during the acquisition period. If strong ERETIC signal was fed during such a period, the signal interferer to the real signals; make the quality of spectrum worse. Therefore, for applying the ERETIC method to the stability test of the reference materials, further modification is required.

Table 1 Stability of ERETIC signal and NMR signals of AGE.

Run	$CHCl_3$	AGE 1H	AGE 2H	AGE 2H	AGE 1H	AGE 1H	AGE 1H	AGE 1H	AGE 1H	water	TMS	ERETIC
1	4.0526	6.6670	13.3251	13.3091	6.7301	6.6162	6.5552	6.6046	6.6219	12.9400	14.9411	1.6371
2	4.0574	6.6591	13.3064	13.3111	6.7393	6.6222	6.5634	6.6084	6.6293	12.9287	14.9344	1.6402
3	4.0479	6.6689	13.3147	13.3048	6.7365	6.6283	6.5642	6.6109	6.6300	12.9261	14.9268	1.6411
4	4.0503	6.6686	13.3161	13.3094	6.7280	6.6180	6.5634	6.6251	6.6133	12.9343	14.9272	1.6464
5	4.0516	6.6684	13.3118	13.3110	6.7347	6.6238	6.5667	6.6060	6.6325	12.9365	14.9187	1.6384
Average	4.0520	6.6664	13.3148	13.3091	6.7337	6.6217	6.5626	6.6110	6.6254	12.9331	14.9296	1.6406
STD	0.0035	0.0041	0.0068	0.0026	0.0046	0.0048	0.0043	0.0082	0.0078	0.0057	0.0085	0.0036
CV(%)	0.0871%	0.0618%	0.0514%	0.0192%	0.0688%	0.0724%	0.0660%	0.1246%	0.1183%	0.0439%	0.0568%	0.2191%

I would like to discuss some approach to make the ERETIC signal stable and application to the homogeneity study of reference materials at the poster.

Reference

[1] Akoka, Serge; Barantin, Laurent; Trierweiler, Michel *Anal. Chem.* **1999**, *71*, 2554-2557.

P054

Cross Polarization with Simultaneous Adiabatic Frequency Sweep on I and S spins

OWeng Kung Peng and Kazuyuki Takeda
Graduate School of Engineering Science,
Osaka University, Japan

ABSTRACT

We propose an improved heteronuclear cross polarization [1, 2] scheme, which provides higher transfer efficiency than our previously proposed NICP technique (Fig. 1(i)) [3]. NICP, which utilizes adiabatic frequency from far off-resonance to on-resonance on I spins, allows all the spin packets to be locked efficiently with moderate rf power. This technique is particularly important for spin species with large spectral distribution or experiments under high static field, when high rf power is not readily available. Since the effective field of I spin is swept through a wide range of values, similarly to existing phase or amplitude modulated CP schemes [4–10], flat Hartmann-Hahn matching profile can be restored for experiment under high speed MAS. With NICP, 'complete transfer' is possible provided that the sweeping over the Hartmann-Hahn condition be made sufficiently slow. This however, came at the expense of relaxation. Thus, NICP may not be of advantage for S spin species with extremely short $T_{1\rho}$.

In order to overcome this drawback, in the present work, adiabatic frequency sweep is applied on S spin as well (Fig. 1(ii)). As the technique implies, we would like to call this scheme as Simultaneous ADIabatic Spin-locking Cross Polarization (SADIS CP) [11]. Adiabatic spin locking provides robust spin-locking with moderate rf power, while simultaneous irradiations allow us to minimize the rate effective field mismatching in zero-quantum subspace and thereby increasing the transfer efficiency. In other words, high efficiency in polarization transfer increase the number of contacts between I and S spins without having to increase the entire 'mixing time', which will limit the effect of $T_{1\rho}$ relaxation. Four controllable parameters (W_{1I}, W_{1S}, $\Delta\omega_I$, $\Delta\omega_S$) introduced here, offer the flexibility to control the adiabaticity, which have direct implication on the efficiency of polarization transfer (Fig. 2(i)). It is experimentally demonstrated that ^{13}C magnetization in uniformly enriched L-Alanine under fast sample spinning were greatly enhanced over wider range of rf powers (Fig. 2(i)) and contact times (Fig.2 (ii)).

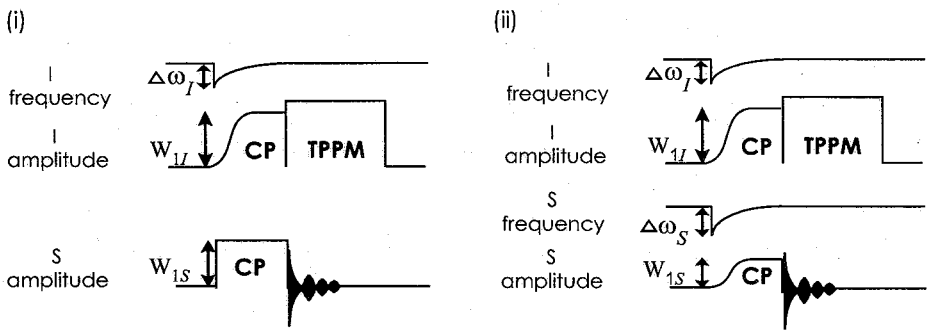

Figure 1. Pulse sequence for (i) NICP and (ii) SADIS CP used in this work.

Keywords: Cross polarization, Simultaneous Adiabatic Sweep, Spin-locking, short $T_{1\rho}$

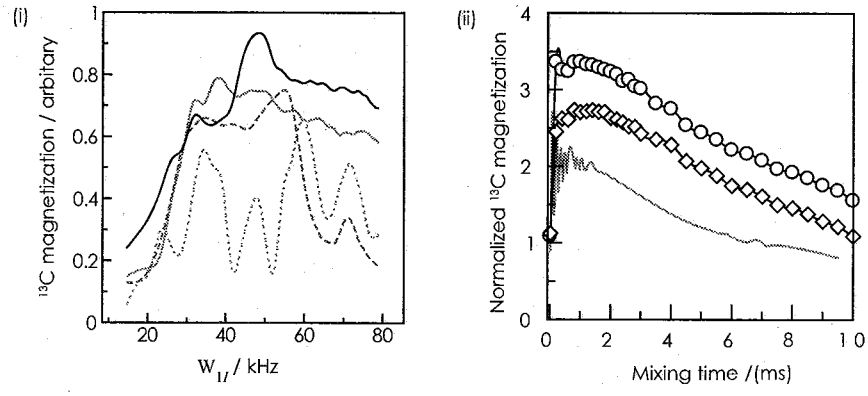

Figure 2. (i) Magnetization of ^{13}C as a function rf power, W_{1I} for various adiabaticity in zero-quantum subscape, Q_{ZQ}. Efficiency of polarization transfer (quantified as Q_{ZQ}) in SADIS CP can be controlled by manipulating experimental parameters as mentioned in the text. SADIS CP of high Q_{ZQ} (solid line) has higher transfer efficiency than that of lower Q_{ZQ} (light solid line). NICP (dash line), which has the lowest Q_{ZQ}, resulting in low transfer efficiency and narrower matching profile. For comparison, conventional CP (light dot) at W_{1S}=45 kHz for a mixing time = 0.20 ms is shown. Data taken from methine (^{13}CH) at spinning frequency, 13.86 kHz under magnetic field of 11.7 T.

(ii) Magnetization of ^{13}C (normalized to single pulse excitation) as a function of mixing time, measured with three different techniques conventional CP (solid line), NICP (diamond) and SADIS CP (circle). For conventional CP, rf amplitudes were set to match at sideband (+1) condition. Data taken from methine (^{13}CH) at sample spinning frequency, 13.86 kHz under magnetic field of 11.7 T.

[1] S.R. Hartmann, E.L. Hahn, Phys. Rev. 128 (1962) 2042.
[2] A. Pines, M.G. Gibby, J.S. Waugh, J. Chem. Phys. 59 (1973) 569.
[3] W.K.Peng, K.Takeda, M.Kitagawa, Chem. Phys. Lett. 417 (2006) 58.
[4] S. Hediger, B.H. Meier, R.R. Ernst, Chem. Phys. Lett. 213 (1993) 627.
[5] S. Hediger, B.H. Meier, Narayanan D.Kurur, G.Bodenhausen, R.R. Ernst, Chem. Phys. Lett. 223 (1994) 283.
[6] G. Metz, X. Xiaoling, S. Smith, J. Magn. Reson. A110 (1994) 219.
[7] S. Hediger, B.H. Meier, R.R. Ernst, Chem. Phys. Lett. 240 (1995) 449.
[8] A.C. Kolbert, A. Bielecki, J. Magn. Reson. A116 (1995) 29.
[9] R. Fu, P. Pelupessy, G. Bodenhausen, Chem. Phys. Lett. 264 (1997) 63.
[10] S. Hediger, P. Signer, M. Tomaselli, R.R. Ernst, B.H. Meier, J. Magn. Reson. 125 (1997) 291.
[11] W.K.Peng, K.Takeda, J. Magn. Reson. (to be submitted).

P055

Ultra Fast MAS プローブにおける二重共鳴測定

Siegfried Hafner[1], Allen Palmer[2], Mircea Cormos[2], ○芦田淳[3]
(Varian Deutschland GmbH[1]、Varian Inc.[2]、
バリアンテクノロジーズジャパン[3])

Double Resonance Solid State NMR Spectroscopy with Ultra Fast MAS Probe.

Siegfried Hafner[1], Allen Palmer[2], Mircea Cormos[2], and Jun Ashida[3]
(Varian Deutschland GmbH[3], Varian Inc.[2], Varian Technologies Japan Ltd.[3])

Small rotor size means small sample volume, however does not always means low sensitivity, because the sensitivity also depends on sample coil volume. Indeed, the sample volume of Ultra Fast MAS™ probe is only ca. 1% of that of standard 5mmϕ MAS probe, however sensitivity of Ultra Fast MAS™ probe is ca. 6%. Therefore, for small molecule work, Ultra Fast MAS™ probe will be practical for not only ^{1}H but ^{13}C experiments. Furthermore, under fast MAS condition, conventional high power ^{1}H decoupling is not necessary, and can be replaced by low power decoupling, which is essential when heat sensitive samples are investigated.

In this work, we present some double resonance experiments with a new ^{1}H decoupling scheme.

【緒言】

サンプル管が小さくなるということは、必然的にサンプル量も少なくなる。しかしこれは必ずしも感度が低くなるということと同義ではない。ソレノイドコイルの場合、サンプルコイルの長さと直径が小さいほどNMRの感度は高くなる[1]。つまり単位重量あたりの感度は、サンプル管が小さくなるほど大きくできる。

Ultra Fast MAS™プローブでは、通常よく用いられている5mmϕと比較するとサンプル容量が約1/100と非常に少ない。しかしサンプルコイルの径もローターに合わせて小さくなるため、結果として感度の低下は約1/16程度に抑えられている。従って^{1}Hだけでなく、^{13}Cなどの多核種の測定も可能である。

また^{13}C測定において高分解能スペクトルを得るためには、$^{13}C/^{1}H$異種核間双極子相互作用を消去することが必要である。20kHz程度以下の試料回転速度では、100kHz程度の高出力^{1}Hデカップリングが必要であるが、50kHz以上の超高速回転下ではそれほど強い^{1}Hデカップリングは必要なく、回転速度よりもはるかに弱いラジオ波磁場を照射するだけで十分であることが知られている[2]。従ってデカップリングパルス照射によるサンプルの温度上昇を抑えられるので、温度に敏感な試料にとっては非常に有用である。

本発表では、新しく開発した65kHzで試料回転できるUltra Fast MAS™プローブを用いた^{13}Cの二重共鳴測定について報告する。また、別掲のポスターでは^{1}Hの1次元、および同種核間2次元測定についても報告しているので、そちらも参照されたい。

低出力CP、高速MAS、プローブ、^{1}Hデカップリング

Siegfried Hafner、Allen Palmer、Mircea Cormos、あしだ　じゅん

【^{1}Hデカップリング　PIPS】

これまでに、高速試料回転下で有効な低出力CWやXiXデカップリング[2,3]が発表されているが、ここでは試料回転に同期したHahnエコーパルスデカップリング[4]を基にしたPI-Pulse Synchronized (PIPS) デカップリングを提案する。図1にPIPSデカップリングのスキームを示す。2つの異なった位相を持つπパルスを試料回転周期のn倍に同期して照射する。ここでnが大きいほどduty cycleが小さくなるので、デカップリングによる発熱を抑えることができる。

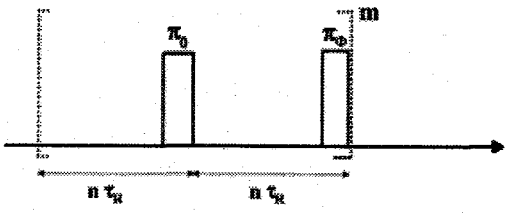

Fig.1 Basic cycle of PIPS decoupling. It consists of two phase shifted p pulses which are synchronized to n times the rotor period.

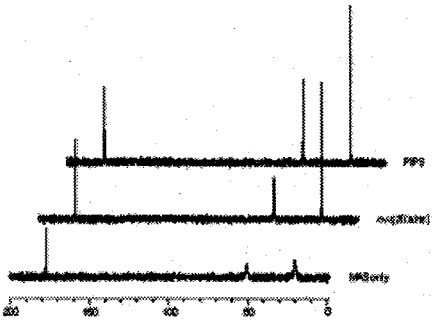

Fig.2 60kHz MAS ^{13}C-CPMAS spectra of L-alanine. (Bottom) MAS only, (middle) high power CW decoupling, and (top) PIPS decoupling.

図2にグリシンの60kHz試料回転下での様々な^{1}Hデカップリング条件における^{13}C-CPMASスペクトルを示す。PIPSデカップリング(n=6)ではduty cycleはCWと比較して約1/50だが、より高分解能のスペクトルが得られる。

緒言で述べたように、感度はサンプル量の割には悪くないので、HETCORなどの2次元測定も可能である。しかも通常のHETCORとは異なり、T_1次元に多重パルスを照射する必要がないので、ここでもパルス照射によって生じるサンプルの温度上昇の問題から解放される。図3にバニリン1mgの^{1}H/^{13}C HETCORスペクトルを示す。非常に少量のサンプル量だが、一晩の積算で十分な感度の信号が得られている。

発表当日は、Ultra Fast MAS^{TM}プローブの他の応用面についても言及する予定である。

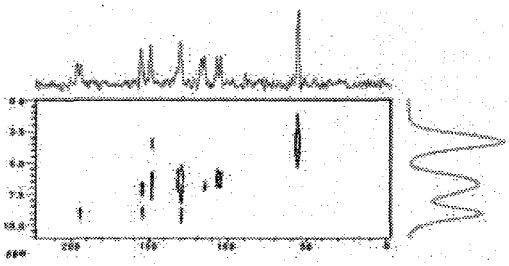

Fig.3 HETCOR spectrum of 1mg vanillin with 60kHz MAS and PIPS decoupling. The experiment time was 10 hours.

【参考文献】

1) 山内一夫, 今田悌三, 朝倉哲郎, 第43回NMR討論会, 3L9, 東京 (2004)
2) M. Ernst, A. Samoson, and B. H. Meier, *J. Magn. Reson.*, **163**, 332 (2003)
3) J. Ashida, and T. Asakura, *J. Magn. Reson.*, **165**, 180 (2003)
4) X. Filip, C. Tripon, and C. Filip, *J. Magn. Reson.*, **176**, 239 (2005)

P056

Peptide secondary structure analysis using selective ^{13}C NMR spectrum line broadening due to overtone NMR irradiation to neighboring ^{14}N

o[1]J. U. N. Fukazawa, [1]K. Takegoshi, [2]Akira Shoji

[1]Department of Chemistry, Graduate School of Science, Kyoto University

[2]Department of Biological Sciences, University of Gunma

Nitrogen constitutes the main chain of polypeptides is an important atom about this function and structures, such as a hydrogen bonding. Although the isotope, ^{14}N has a natural existence ratio as high as 99.63%, it is very difficult to obtain its high resolution solid state NMR spectrum since it is spin-1 nucleus and it has quadrupolar coupling. In order to conquer this problem, overtone NMR was designed. Although traditional ^{14}N solid state NMR spectra have a few MHz line width come from first order quadrupolar shift, overtone spectra line width is only several hundreds kHz because of second order shift. But several hundreds kHz is too large to obtain high resolution ^{14}N NMR spectra. On the other hand, it is advocated from before that you can get the knowledge of dihedral angles of main chain by the second order shift. But it is difficult to observe it using these overtone spectra because of the lowness of overtone excitation probability. In recent years, our group developed ^{14}N indirect spectroscopy obtained from the line width of ^{13}C under ^{14}N overtone irradiating and ^{13}C-^{14}N recoupling under MAS to the powder sample.

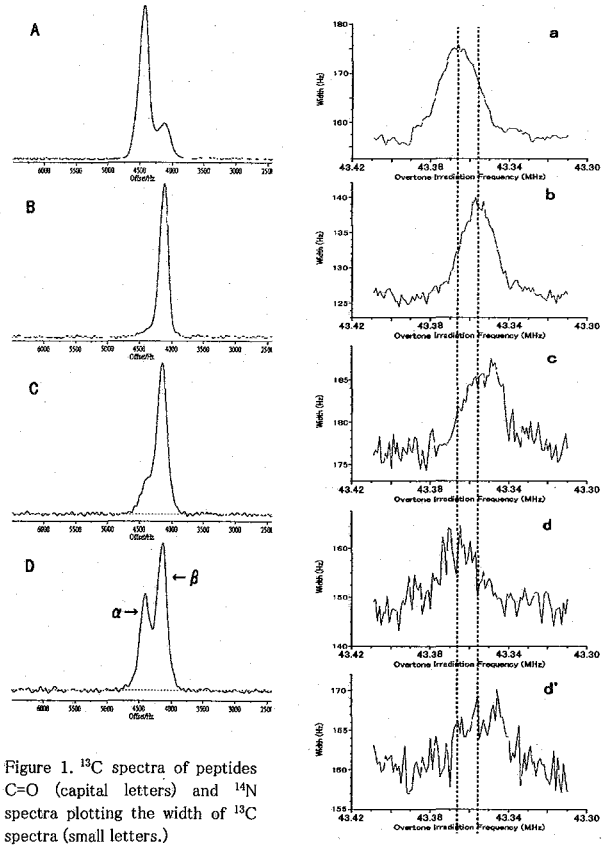

Figure 1. ^{13}C spectra of peptides C=O (capital letters) and ^{14}N spectra plotting the width of ^{13}C spectra (small letters.)
A, a: (Ala*, Ala)=50:50(α)
B, b: $(Ala)_3$-Ala*-$(Ala)_3$ (β)
C, c: (Ala*,Val)=20:80(β)
D, d, d': (Ala*,Val)=30:70
d: left peak(α), d': right peak (β)

^{14}N, overtone NMR, quadrupole, structure, selective recoupling

In this research, fundamental examination for performing the structural analysis of polypeptides was performed using ^{14}N overtone spectrum obtained by this indirect spectroscopy. ^{14}N overtone spectra were actually measured using ^{13}C indirect assay to several powder samples from which the secondary structure (α-helix/β-sheet) differ, each were compared, and it was shown that those secondary structure distinction is possible from ^{14}N overtone spectra (Figure 1).
Furthermore, by ab initio calculation by Gaussian, to each secondary structure, quadrupolar interaction of ^{14}N was calculated, the simulation of the form of a spectra were carried out using them, and there is a correlation between the peak position of the ^{14}N overtone spectrum and the structure of the structure of polypeptide (Figure 2). The line shape is not so matching but the peak position is matching.

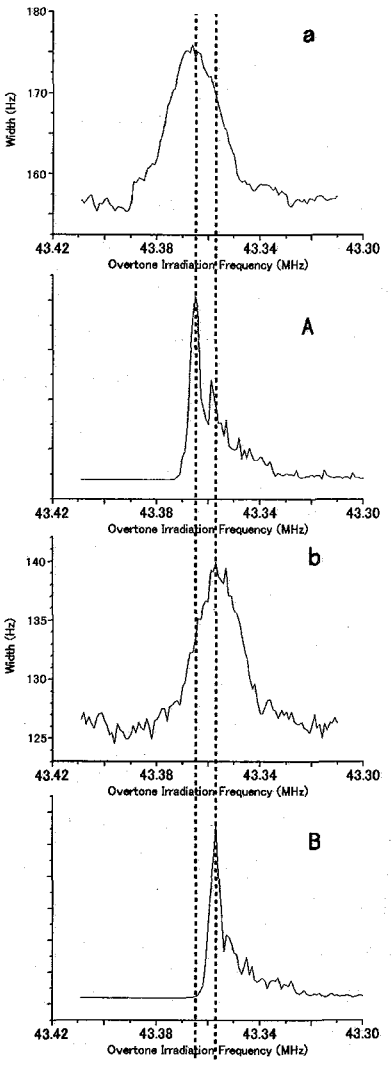

Figure 2. 14N indirect overtone spectra plotting the width of 13C spectra (small letters) and simulation of them (capital letters.)
a, A: (Ala*, Ala)=50:50(α)
and the simulation (eQq=−4.305MHz, η =0.2931)
b, B: $(Ala)_3$-Ala*-$(Ala)_3$(β)
and the simulation (eQq=−4.023MHz, η =0.4399)

References

[1]K. Takegoshi, T. Yano, K. Takeda, and T. Terao, *J. Am. Chem. Soc.* **123**, 10786(2001).

[2] Gaussian 03, Revision C.02,
M. J. Frisch, G. W. Trucks, H. B. Schlegel, G. E. Scuseria, M. A. Robb, J. R. Cheeseman, J. A. Montgomery, Jr., T. Vreven, K. N. Kudin, J. C. Burant, J. M. Millam, S. S. Iyengar, J. Tomasi, V. Barone, B. Mennucci, M. Cossi, G. Scalmani, N. Rega, G. A. Petersson, H. Nakatsuji, M. Hada, M. Ehara, K. Toyota, R. Fukuda, J. Hasegawa, M. Ishida, T. Nakajima, Y. Honda, O. Kitao, H. Nakai, M. Klene, X. Li, J. E. Knox, H. P. Hratchian, J. B. Cross, C. Adamo, J. Jaramillo, R. Gomperts, R. E. Stratmann, O. Yazyev, A. J. Austin, R. Cammi, C. Pomelli, J. W. Ochterski, P. Y. Ayala, K. Morokuma, G. A. Voth, P. Salvador, J. J. Dannenberg, V. G. Zakrzewski, S. Dapprich, A. D. Daniels, M. C. Strain, O. Farkas, D. K. Malick, A. D. Rabuck, K. Raghavachari, J. B. Foresman, J. V. Ortiz, Q. Cui, A. G. Baboul, S. Clifford, J. Cioslowski, B. B. Stefanov, G. Liu, A. Liashenko, P. Piskorz, I. Komaromi, R. L. Martin, D. J. Fox, T. Keith, M. A. Al-Laham, C. Y. Peng, A. Nanayakkara, M. Challacombe, P. M. W. Gill, B. Johnson, W. Chen, M. W. Wong, C. Gonzalez, and J. A. Pople, Gaussian, Inc., Wallingford CT, 2004.

[3]R. Tycko and S. J. Opella, *J. Chem. Phys.* **86**, 1761(1987).

[4]P. L. Stewart, R. Tycko, and S. J. Opella, *J. Chem. Soc., Faraday Trans. I*, **84**(11), 3803(1988).

[5]S. Wi, L. Frydman, *J. Am. Chem. Soc.* **123**, 10354(2001).

P057

Theoretical and Experimental Verification of Time Averaged Nutation in Solid State NMR.

Institute for Molecular Science ○ Katsuyuki Nishimura

The scaling factors of heteronuclear dipolar interaction under a series of time-averaged nutation schemes obtained from zero-order average Hamiltonian theory, numerical calculation, and experimental results were compared. Under normal experimental settings, the scaling factor for heteronuclear dipolar interaction from 0-order average Hamiltonian exhibited identical values to those obtained from numerical calculation.

Author has been successfully developed a series of new cross-polarization techniques[1,4] and spin exchange type of separated local field experiments[2,3] using time-averaged nutaion technique. In this study, scaling factors for heteronuclear dipolar interaction of time-averaged nutation schemes from 0-order Average Hamiltonian (AH) theory and numerical calculation were compared.

The numerical analyses of scaling factors have been carried out using SIMPSON software based on the scripts written by author. The results were compared with those obtained from 0-order average Hamiltonian (AH) which author corrected from previously reported. All time-averaged nutation schemes are shown in Figure 1. Figure 2 shows the plot of the scaling factors of heteronuclear dipolar interaction for duration time-averaged nutation (DTAN) scheme at complete cycle for the case of duration time averaging factor (DTAF) of 1/3. Thus the rf field of observed nuclei is 1/3 of ^{1}H effective field. The longitudinal and horizontal axes are scaling factor and τ_C/τ_{LG}, respectively. Where τ_{LG} and τ_C are 2π rotation period of LG and a unit cycle time of time-averaging, respectively. Normally experiments will be carried out at the condition of $\tau_{LG}/\tau_C<1.5$, thus under such conditions, the 0-order AH gives sufficiently accurate scaling factors for heteronuclear dipolar interaction under time-averaging schemes. Although numerical analysis can be carried out easily using available software such as SIMPSON and GAMMA, numerical calculation dose not provide any insight of the factors affecting to spin dynamics. Thus analytical form of scaling factor from 0-order AH calculated by author gives simple perspective of spin dynamics for time-averaging scheme.

Author will show about the comparison of scaling factors between numerical and analytical solutions for other time-averaging schemes such as amplitude time-averaged

---

solid-state NMR, time averaged nutation, weak rf power

nutation (ATAN), and duration & amplitude time-averaged nutaion (DATAN) schemes. Then the comparison between experimental and theoretical results will be discussed for liquid crystalline solvent.

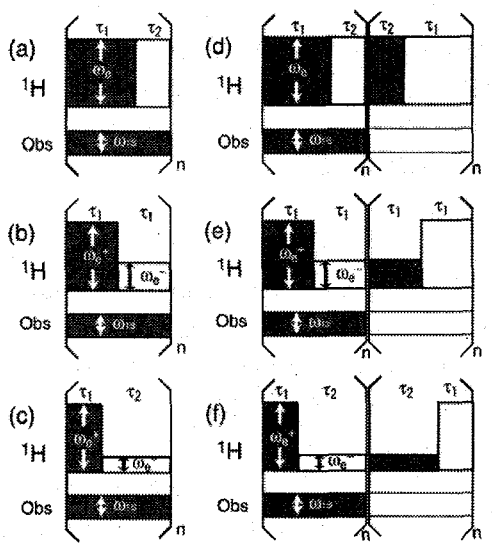

Figure 1. Various time-averaged nutation schemes evaluated in this study. (a) duration time-averaged nutation (DTAN), (b) amplitude time-averaged nutation (ATAN), (c) duration & amplitude time averaged nutation (DATAN), respectively. And (d)-(f) are the complete cycle of (a)-(c), respectively. Grayed and white colored box indicate + and –LG condition for ^{1}H, and +X and –X phase spin locking for observed nuclei, respectively. Where $\tau_c = \tau_1 + \tau_2$. The number of "n" must be integer satisfying the relationship of $n = (\tau_{LG}/DTAN \times t_c)$.

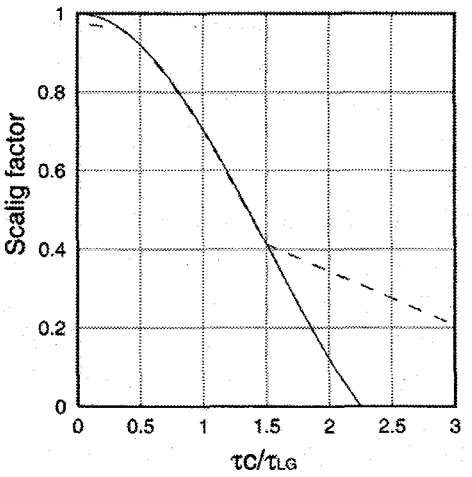

Figure 2. The plot of scaling factors for duration time-averaging nutation scheme at complete cycle for DTAF =1/3 obtained from corrected 0-order AH (solid line), numerical simulation (dashed line), respectively.

References

1) K. Nishimura, A. Naito, Chem. Phys. Lett. **380**, 569 (2003).

2) K. Nishimura, A. Naito, Chem. Phys. Lett. **402**, 245 (2005).

3) K. Nishimura, A. Naito, Chem. Phys. Lett. **402**, 245 (2006)

4) K. Nishimura, A. Naito, NMR conference, Tokyo, (2004), manuscript has been submitted.

P058

RheoNMR のタンパク質溶液への応用

1.農工大工、2.ドレスデン高分子研究所
○大郷耕輔[1]、Frank Bagusat[2]、Ulrich Scheler[2]、朝倉哲郎[1]

Application of RheoNMR for Investigation of Protein Solutions

Kosuke Ohgo[1], Frank Bagusat[2], Ulrich Scheler[2], Tetsuo Asakura[1]
[1]Department of Biotechnology, Tokyo University of Agriculture and Technology
[2]Institute for Polymer Research Dresden

Abstract : We applied RheoNMR method to investigate the structural change of *Bombyx mori* silk fibroin aqueous solution under shear. Decreasing and sudden jump of peak intensities were observed during shearing. After experiments the aggregates of silk were found in the rheometric cell, thus we successfully observed the process of structural change of silk fibroin by using RheoNMR.

【緒言】RheoNMR は、Rheology すなわち“ずり”と核磁気共鳴法を組み合わせた測定法であり、NMR 分光計内で測定試料に“ずり”をかけながら高分子挙動の観察を行う手法である。これまで Callaghan グループ[1)]が精力的に研究を進める一方、共同著者である Scheler グループも RheoNMR を用いた研究を推進している。[2)]
一方、朝倉グループは、これまで NMR による構造解析をベースとして、絹フィブロインの機能解明及び応用研究を推し進めてきた。[3)] その中の一つとして興味深いテーマが、絹フィブロイン繊維化過程の解明である。絹フィブロインは、カイコ体内では絹水溶液として蓄えられ、これが吐糸管を通過する際、常温常圧下で繊維化が起こる事から、機構解明は工業的な応用も含め、大変興味深い。これまでの繊維化過程の研究から、吐糸管内で発生すると考えられる“ずり”が絹の繊維化に関与していると考えられている。実際に絹水溶液に一定のずりを与えると、絹の凝固が起こることはよく知られている。
そこで我々は、RhoNMR 装置により、NMR 分光計内で絹の繊維化過程を人為的に起こし、その際の絹の構造情報を NMR により検出することを試みたので報告する。
【実験】絹繊維を 9M LiBr 水溶液に溶解後、透析する事で絹水溶液を得た。また絹水溶液を凍結乾燥することにより得られるスポンジ状試料は水に可溶であることから、このスポンジを D_2O に溶解させることで、絹フィブロイン重水溶液を作成した。溶液の pH は NaOH を加え pH=9-11 に調製した。RheoNMR 測定は Bruker 社

Key words: RheoNMR, Shearing, Rheology, *B. mori* Silk Fibroin solution, Structural Change

著者ふりがな：おおごう　こうすけ、ふらんく　ばぐさっと、うるりっひ　しぇらー、あさくら　てつお

Avance300 NMR 分光計を用いて行った。プローブに内径 20mm のバードゲージ型プローブヘッドを装着して用いた。モーター、ドライブシャフトを分光計に装着、自作の Couette Cell(内筒外径 6.8mm、外筒内径 8.8mm、ギャップ 1.0mm) を用いて (Fig.1)、内筒の回転速度を 2Hz で絹溶液にずりを印加した。これらの装置を用い、1D ^{1}H NMR スペクトル (水溶液では water suppression も併用) 及び z 軸 profile 像を経時的に測定 (時間分解能 : 2 − 3 分に設定)、ピーク、信号強度の挙動を観測した。

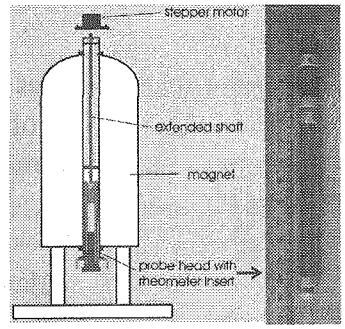

Figure 1. RheoNMR system (left) and Couette cell (right).

【結果・考察】絹水溶液について NMR 測定を行った結果、絹の ^{1}H ピークは約 3 時間ほどで半減し、約 5 時間でピークはほぼ観測されなくなった (Fig. 2a)。また同時にコイル中心から±10mm の profile 像 (主に H_2O の信号が寄与) を観測したところ、信号強度が、絹の ^{1}H NMR ピーク強度とほぼ同期して減少している (Fig.2b)。測定後、絹凝固物が Cell 内に見られた事から、双方の結果は絹分子の繊維化過程を検出した結果であると結論づけられる。更に詳細なピークの変化を観察するために、H_2O ピークの影響が少ない絹重水溶液で測定を行った。その結果、^{1}H ピークの経時変化中に、急激な強度変化が数回見られた (Fig.3)。各ピークで同時的に見られることから、これは Cell 内に出来た絹凝集塊近辺でずり速度が上昇し、その結果、更なる絹の構造転移が引き起こされたものと考えられる。今後は、ずり印加後の絹凝集塊の固体 NMR 測定及び溶液−固体の中間状態を検出する事で、絹繊維化過程の解明を行っていく。

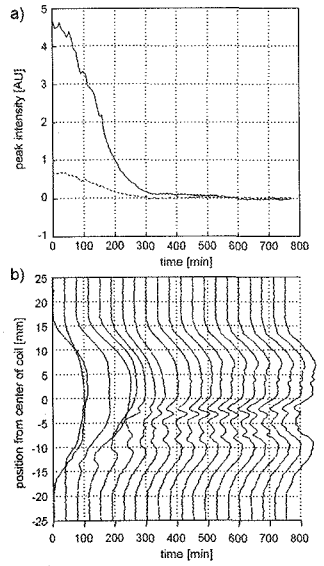

Figure 2. Peak intensities of Ala $C^{\beta}H_3$ (solid line) and Val $C^{\gamma}H_3$ (broken line) in H_2O solution (a) and water signal projections along the B_0 direction (b).

なお本研究は一部、平成 18 年度科学研究費補助金基盤 S (18105007) で行われた。

【参考文献】

1) P. T. Callaghan *Encyclopedia NMR* **9**, 737-750 (2002).

2) A. Gottwald, P. Kuran, U. Scheler *J. Magn. Reson.* **162**, 364-370 (2003).

3) C. Zhao, T. Asakura, *Prog. NMR Spec.* **39**, 301-352 (2001).

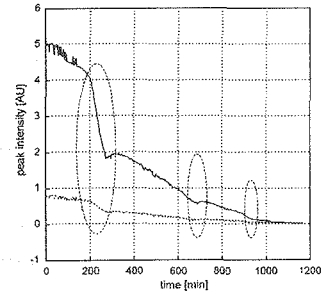

Figure 3. Peak intensities of Ala $C^{\beta}H_3$ (solid line) and Val $C^{\gamma}H_3$ (broken line) in D_2O solution. Sudden jump of peak intensities were observed (shown by circles).

P059

Effect of membrane curvature on the structure of the phospholipase C-δ1 PH domain detected by solid-state NMR spectroscopy

○Naoko Uekama, Takahiro Aoki, Akiko Hatakeyama, Masashi Okada, Hitoshi Yagisawa, Satoru Tuzi
Graduate School of Life Science, University of Hyogo

The PH domain of PLC-δ1 is known to dominate the membrane localization of PLC-δ1. Previously, we reported that local conformation of the PH domain alters at the membrane surface due to an interaction between the amphipathic α2 helix and the interface of the lipid bilayer. In this work, we investigated influence of the membrane curvature on the structure of the PH domain of PLC-δ1. The conformational alternation was induced as the PH domain was bound to the vesicle with a diameter greater than 300 Å, whereas no such conformational alternation was observed for the PH domain forming complex with the micelle.

Introduction Phospholipase C-δ1 (PLC-δ1) hydrolyzes phosphatidylinositol 4,5-bisphosphate (PIP_2) in the plasma membrane to produce the second messengers, inositol 1,4,5-trisphosphate (IP_3) and diacylglycerol. PH domain located at the N-terminus of PLC-δ1 selectively forms high affinity complex with PIP_2 in the plasma membrane and IP_3 in the cytoplasm, and consequently regulates membrane localization of PLC-δ1. Previously, we have reported that structure of the PH domain of PLC-δ1 bound to PIP_2 embedded in a phosphatidylcholine (PC) multilamellar vesicle (MLV) containing 5% PIP_2 differs from that of the PH domain forming complex with IP_3 in solution[1]. This conformational change at the membrane surface would be induced by an interaction between the amphipathic α2 helix of the PH domain and the interface of the lipid bilayer.

Since a diameter of MLV is greater than 1000 Å, a curvature of the outer surface of MLV is very small and virtually negligible. The curvatures of the membranes of the living cell are, however, expected to be altered dynamically, and a local membrane structure with a great curvature could be formed.

Keywords membrane curvature, solid-state NMR, PLC-δ1 PH domain, signal transduction

Such alternations of the curvature may affect the structure of the PH domain at the membrane surface.

In this study, we investigated the structure of the PH domain of PLC-δ1 which is bound to vesicles and a micelle with different diameters by using solid-state ^{13}C NMR spectroscopy.

Experimental Procedure [3-^{13}C]Ala labeled PH domain of PLC-δ1 was expressed as GST fusion protein in *E. coli.* After isolation from GST-tag by thrombin cleavage, the obtained protein was mixed with lipid bilayer or micelle shown below and used for solid-state ^{13}C NMR measurements. The mole ratios of the PH domain and PIP_2 was adjusted to 1 : 2.

	diameter (Å)	curvature ($Å^{-1}$)	mole ratio
Micelle	40.2	0.04975	PIP_2 : n-Dodecyl-β-D-maltoside = 1 : 40
SUV	314	0.00159	PIP_2 : POPC = 1 : 20
MLV	>1280	>0.00039	PIP_2 : PC = 1 : 20

Solid state ^{13}C NMR spectra were recorded on a Chemagnetics CMX Infinity-400 spectrometer (^{13}C: 100.6 MHz), using single pulse excitation dipolar decoupled-magic angle spinning (DD-MAS) method, at 20℃.

Results and Discussion Fig. 2 shows the DD-MAS ^{13}C NMR spectra of [3-^{13}C]Ala labeled PH domain of PLC-δ1 forming complex with PIP_2 in MLV, SUV, and micelle (Fig. 2A-C), and with IP_3 (Fig. 2D). In the previous work, the signals of Ala residues in the PH domain bound to MLV have been assigned as follows; Ala118: 15.3 ppm, Ala116: 15.8 ppm, Ala112: 18.6-19.2 ppm. The chemical shifts of these residues coincide with those in the spectrum of PH domain bound to SUV (Fig. 2B) except for the signal of Ala112 at 18-19 ppm. This indicates that the conformation of Ala88 located at the C-terminus of α2 helix and Ala116 and Ala118 involved in the α3 helix (Fig. 1) are not affected by the size of the vesicles. Ala112 is resonated at 18.8 ppm in Fig.2B as a peak with narrow line width in contrast to the broad peak of Ala112 at 18.6- 19.2 ppm in Fig. 2A. This reveals that the conformational inhomogeneity of Ala 112 at the surface of MLV would be averaged out by a conformational exchange with a frequency greater than 60 Hz at the surface of SUV.

In the spectrum of the PH domain bound to the micelle (Fig. 2C), the Ala88 peak at 16.8 ppm is reduced compared with that in the spectra of the PH

domain forming complex with MLV and SUV, and a new peak at 17.6 ppm which is not observed for the PH domain bound to MUV or SUV (Fig. 2A, 2B) appears. The chemical shift of the latter peak coincides with that of the Ala88 signal in the PH domain forming complex with IP_3 (17.5 ppm). The chemical shift of the signal of Ala112 (18.5 ppm) in the spectrum of the PH domain forming complex with the micelle (Fig. 2C) also agrees with that in the spectrum of the PH domain-IP_3 complex (Fig. 2D). These chemical shift displacements of Ala88 and Ala112 observed for the PH domain bound to the micelle compare with the PH domain bound to MLV and SUV indicate that the conformation of Ala88 and Ala112 of the PH domain forming complex with the micelle is different from those at the surface of the lipid bilayer. On the contrary, the signals of Ala116 and Ala118 which is identical among the spectra in Fig. 2 indicate that conformations of these residues are insensitive to the membrane environment around PIP_2.

In conclusion, the difference of membrane curvature between MLV and SUV has no drastic effect on the conformation of the PH domain, expect for the probable increase in mobility of Ala112 at the surface of SUV. On the contrary, the local conformational change of the PH domain induced at the membrane surface is not induced at the interface of the micelle. This suggests that the interaction between the α2 helix and the aqueous phase/ hydrophobic phase interface is eliminated at the surface of the micelle with the diameter smaller than 40 Å.

Reference

1) Tuzi, S., Uekama, N., Okada, M., Yamaguchi, S., Saitô, S., and Yagisawa, H. (2003) *J. Biol. Chem.* **278,** 28019-28025

2) Ferguson, K. M., Lemmon M. A., Schlessinger, J., and Sigler, P.B. (1995) *Cell* **83,** 1037-1046

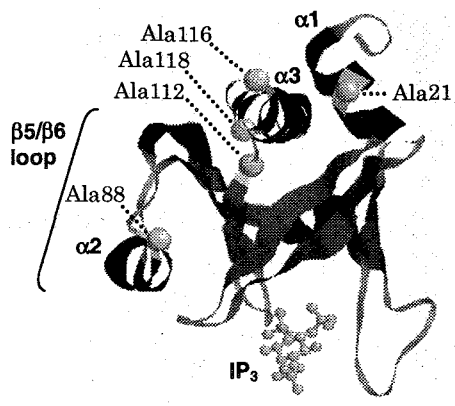

Fig. 1 Three-dimensional model structure of PLC-δ1 PH domain -IP_3 complex[1]. Positions of Ala residues are indicated as white spheres with residue numbers. Position of α helices (α1, α2 and α3) and β5/β6 loop are indicated.

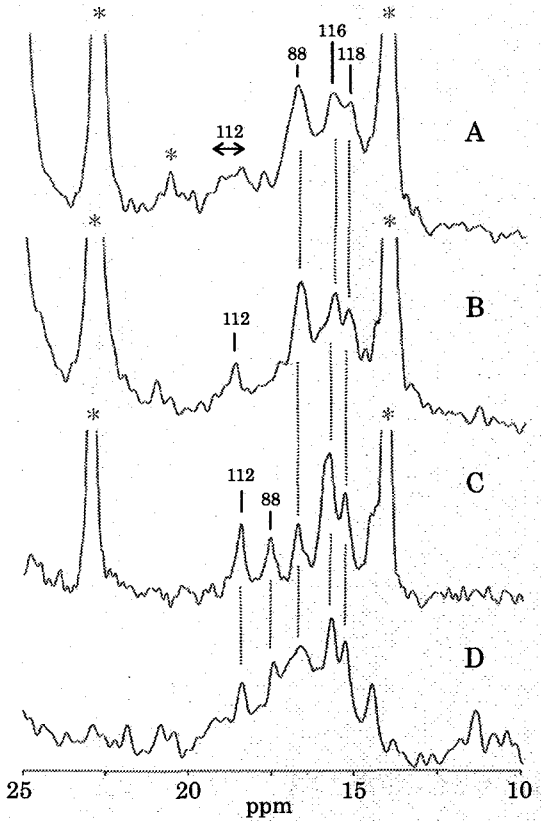

Fig. 2 The DD-MAS ^{13}C NMR spectra of [3-^{13}C]Ala labeled PH domain of PLC-δ1 forming complex with MLV (A), SUV (B), micelle (C) and IP_3 (D). Residue numbers of Ala residues are shown at the top of the peaks. Asterisks indicate signals from lipid molecules.

P060

固体高分解能 NMR による
L−フェニルアラニン含有ジペプチド誘導体の構造研究

（群馬大 工）○新村素晴、荘司顯、尾崎拓男

Structural Studies of Dipeptide Derivatives Containing L-Phenylalanine Residue by High-resolution Solid-state NMR

Subaru Niimura, Akira Shoji, Takuo Ozaki
Dept. Biological Sciences, Faculty of Engineering, Gunma University

We studied the structural feature of model dipeptide derivatives containing L-phenylalanine residue, Ac–Xaa–Phe–NHMe [Xaa = Gly, L-Val, L-Ile, L-Glu, L-Pro], by ^{13}C and ^{15}N CP–MAS NMR measurements, in order to demonstrate the neighboring amino-acid sequence effect for L-phenylalanine residue in proteins. As a result, we found that the ^{13}C and ^{15}N chemical shifts of the L-phenylalanine residue were changed depending on the nature of the Xaa residue.

序論：タンパク質は約 20 種類の標準アミノ酸がペプチド結合によって連結した鎖状高分子として解釈される。本研究では、この解釈からさらに「連続した 2 残基から構成されるジペプチド連鎖がタンパク質の構造（及び機能）発現の基本単位となる」ことを提唱し実証を試みた。そのため、生理活性部分に多く見られるL-フェニルアラニン残基(Phe)に着目し、アセチルジペプチドメチルアミド、Ac–Xaa–Phe–NHMe (Scheme 1)を合成し、固体^{13}Cおよび^{15}N CP–MAS NMRスペクトルを測定し、その固体状態における構造特性を調べた。Xaa残基には、グリシン(Gly)、L-バリン(Val)、L-イソロイシン(Ile)、L-グルタミン酸(Glu)およびL-プロリン(Pro)を導入した。

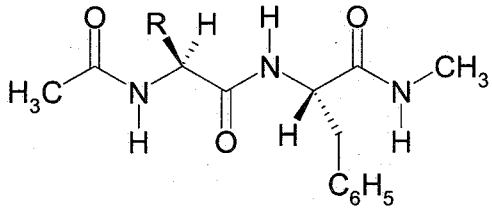

Scheme 1. Chemical structure of Ac–Xaa–Phe–NHMe [Xaa = Gly, Val, Ile, Glu, Pro].

キーワード：dipeptide; L-phenylalanine; CP–MAS NMR; chemical shift

著者：にいむらすばる　しょうじあきら　おざきたくお

測定法： 固体高分解能NMR測定はBruker DSX300 分光計 (^{13}C共鳴周波数 75 MHz、^{15}N共鳴周波数 30 MHz) により、4 mm(または 2.5 mm) CP-MASプローブを用いて行った。^{13}C NMRの測定条件は、CP接触時間：2-3 ms、繰り返し時間：6 s、MAS速度：6000～11000 Hz、積算回数：800～2048 とした。^{13}C化学シフトはアダマンタン(29.50 ppm ; TMS:0 ppm) を二次基準として使用した。^{13}C化学シフト値の実験誤差は±0.3 ppmである。ピーク分離にはDmfitプログラム[1] を使用した。

結果及び考察： Ac-Val-Phe-NHMeの^{13}C CP-MAS NMRスペクトルをFigure 1 に示す。L-フェニルアラニン残基のピークはC_α(53.6 ppm)、C_β(40.7)、C_γ(136.9)、フェニルC_δ-C_ζ(128.9-127.0) に帰属した。その他のピークはアセチルCH_3(24.4)、メチルアミドCH_3(26.4)、L-バリン残基のC_α(58.6)、C_β(33.3)、C_γ(20.1, 19.7) に帰属した。カルボニル領域の一部重複したピークは 171.4、170.8、170.6 ppmの三本に分離されたがそれぞれの帰属は現在検討中である。本研究で用いたすべてのジペプチド試料について得られたL-フェニルアラニン残基の^{13}C化学シフト値を比較した結果、C_α、C_β、C_γの化学シフト値がXaa残基の種類によって変化することが明らかになった。特にC_βの化学シフト値の変化量は大きく 3 ppmにも及ぶことを見出した。これらの^{13}C化学シフトの変化は、試料の主鎖および側鎖のコンホメーションの違いを反映していると考えられる。発表では^{13}Cの結果と併せてアミノ酸配列効果を評価できる^{15}N化学シフト値の結果についても考察する。

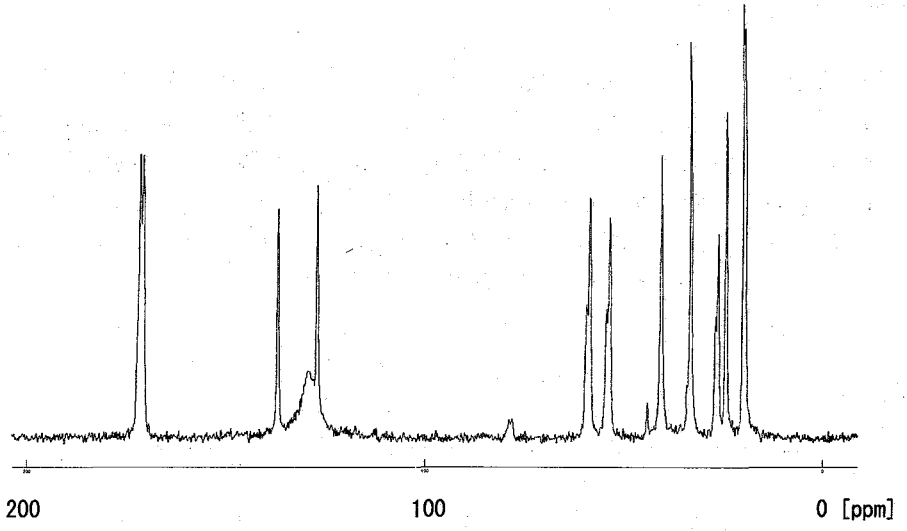

Figure 1. 75 MHz ^{13}C CP-MAS NMR spectrum of Ac-Val-Phe-NHMe.

参考文献

[1] D.Massiot et. al., "Modelling one- and two-dimensional Solid State NMR spectra", *Magnetic Resonance in Chemistry, 40*, 70-76, **2002**.

P061

固体高分解能 NMR による
L-プロリン含有ジペプチド誘導体の構造研究

（群馬大工） ○相馬洋之，荘司顯，尾崎拓男

Structural Studies of Dipeptide Derivatives Containing L-Proline Residue by High-resolution Solid-state NMR

Hiroyuki Souma, Akira Shoji, Takuo Ozaki
Dept. Biological Sciences, Faculty of Engineering, Gunma University

We studied the structural feature of model dipeptide derivatives containing L-proline residue, Ac-Xaa-Pro-NHMe [Xaa = Gly, L-Ala, L-Leu, L-Ile, L-Phe, and L-Met], by ^{13}C CP-MAS NMR method, in order to demonstrate the neighboring amino-acid sequence effect for L-proline residue in proteins. As a result, we found that the ^{13}C chemical shifts of the L-proline residue were changed among these dipeptide derivertives.

序論：本研究ではタンパク質内におけるL-プロリン残基の構造特性を明らかにするため，L-プロリン残基を含むアセチルジペプチドメチルアミドAc–Xaa–Pro–NHMe (Scheme.1) を合成し、^{13}C CP-MAS NMR法によりその隣接残基間相互作用（隣接アミノ酸残基効果）を固体高分解能NMRにより研究を行なった．Xaa残基には，グリシン(Gly)，L-アラニン(Ala)，L-ロイシン(Leu)，L-イソロイシン(Ile)，L-フェニルアラニン(Phe)およびL-メチオン(Met)を導入した．

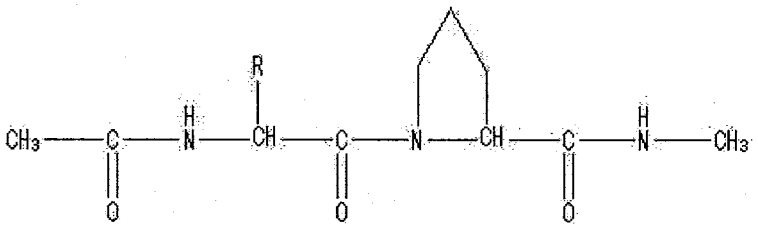

Scheme 1. Chemical structure of Ac–Xaa–Pro–NHMe.

Key Words: dipeptide; L-proline; CP-MAS NMR; chemical shift

著者： そうまひろゆき，しょうじあきら，おざきたくお

NMR測定：固体高分解能^{13}C CP-MAS NMR測定は，Bruker DSX 300分光計（^{13}C: 共鳴周波数75.48 MHz)で，4mm CP-MASプローブを用いて行った．測定条件は，CP接触時間：3 ms，繰り返し時間：6 s，$\pi/2$パルス幅：2.8 μs，MAS速度：6000 Hz，積算回数：800とした．^{13}C化学シフトはアダマンタン(δ=29.5)を二次基準（TMS：δ=0)とした．^{13}C化学シフトの実験誤差は±0.3 ppm以内である．ピーク分離にはDmfitプログラム[1]を使用した．

結果および考察：Ac–Gly–Pro–NHMeの^{13}C CP-MAS NMRスペクトルをFigure 1に例示する．L-プロリン残基の各ピークは低磁場側からC=O(169.5 ppm)，C_α(60.5)，C_δ(48.1)，C_β(30.5)，C_γ(25.9)と帰属した．その他のピークは，低磁場からGly C=O(173.4)，アセチルC=O (171.4)，Gly C_α (42.6)，メチルアミドCH_3(25.9)，アセチルCH_3(22.8)と帰属できた．本研究で用いたすべてのジペプチド誘導体について得られたL-プロリン残基の^{13}C化学シフト値を比較すると，各試料間で次のような^{13}Cシフト値の変化が観測された．すなわち、主鎖C=O：3.2 ppm，C_α：0.6 ppm，ピロリジン環のC_δ：1.2 ppm，C_β：1.8 ppm，C_γ：2.6 ppmであり，この中で，C=OおよびC_γのシフト変化が非常に大きいことが注目される．以上の結果は，ジペプチド誘導体におけるL-プロリン残基の主鎖及び側鎖のコンホメーションが隣接アミノ酸残基の影響を受けて変化していることを示している．すなわち，Xaa残基の種類によってL-プロリン残基の二面角(ϕ，ψ，ω)および環構造に変化が生じている可能性が示唆される．本研究では，これらのことを実証するため，量子化学計算による局所的安定構造と化学シフトの計算、および^{15}N CP-MAS NMRスペクトル測定による構造解析を進めており，これらの結果についてもあわせて発表する．

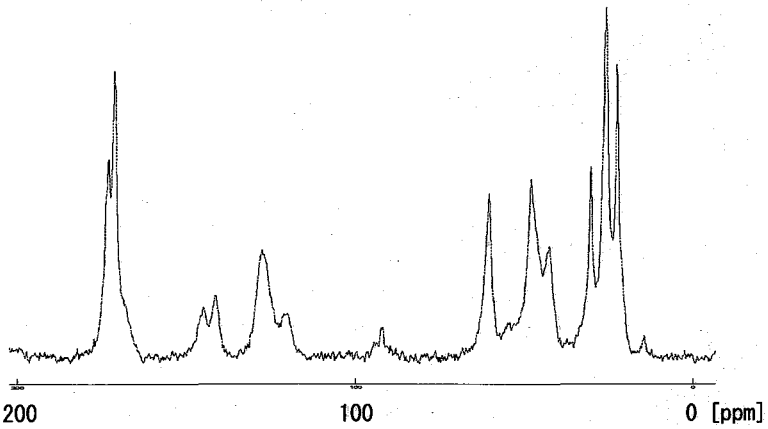

Figure 1. ^{13}C CP-MAS NMR spectrum of Ac–Gly–Pro–NHMe.

引用文献

[1] D. Massiot et. al., "Modelling one- and two-dimensional solid state NMR spectra", *Magnetic Resonance in Chemistry, 40*, 70–76 (2002).

P062

Comparison of solution-state and MAS-NMR spectra of stable isotope labeled *Populus*

OTetsuya Mori[1], Takashi Hirayama[1,2] and Jun Kikuchi[1,3,4]

([1] Int. Grad. Sch. Arts Sci., Yokohama City Univ, [2] Environ Mol. Biol. Lab., RIKEN, [3] RIKEN Plant Science Center and [4] Grad. Sch. Bioagri. Sci., Nagoya Univ.)

1. Introduction

Measurements of extracted soluble fraction of biological samples by certain solvents are major methods in current metabolome analysis. However, in case of plants, insoluble fractions are mixed with insoluble metabolites and useful macromolecular materials including biomass. Thus, analysis of these metabolites might contribute in not only basic science, but also in industrial applications. We are willing to follow carbon fixation and assimilation by $^{13}C_6$-glucose, $^{13}CO_2$ labeling in plants and their multi-dimensional NMR using the potential ability of molecular identification and non-invasive measurement (Fig. 1).

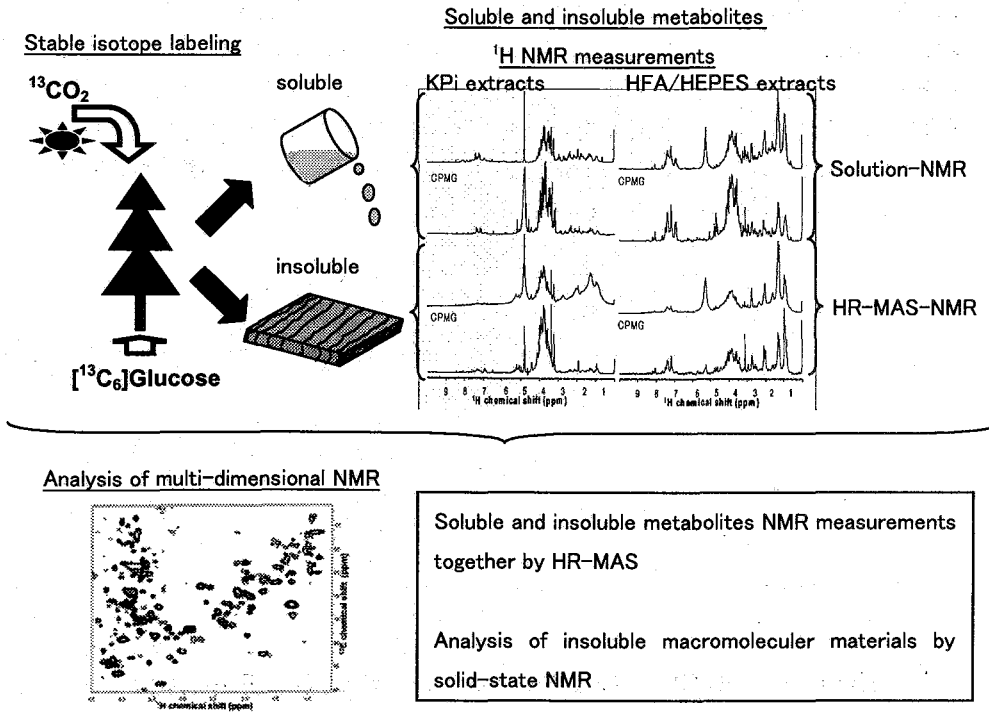

Figure 1. Scheme of multi-dimensional NMR metabolome analysis in this study

MAS, Stable isotope labeling, insoluble metabolites, plant biomass, molecular association

2. ^{13}C stable isotope labeling of *Populus* for multi-dimensional NMR analysis

Firstly, we monitored incorporations of $^{13}C_6$-glucose and $^{13}CO_2$ into *Populus* by ^{13}C HSQC signal intensities of their extracted solutions.

3. Comparison of HR-MAS non-invasive, extracted sample, and insoluble sample measurements

Next, we measured the non-extracted *Populus*, by non-invasive magic angle spinning (MAS) method. Although ordinal solution NMR suffers problem of solubility in metabolite mixture solution, whereas MAS-NMR exhibits both soluble and insoluble metabolites. In spite of this, several metabolites measured in only solution NMR but not in MAS-NMR. These metabolites could not be detected by MAS-NMR, suggesting that non-invasive measurement might reflect information on intracellular localization. Furthermore, detecting same signals with insoluble cell wall fraction by MAS-NMR exhibits its ability to observe macromolecular materials (Fig. 2).

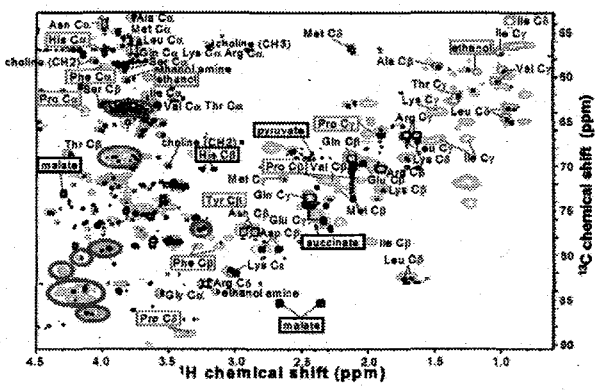

Figure 2. Superposition of non-invasive(MAS), KPi extract, and cell-wall insoluble fraction in ^{13}C HSQC spectra of ^{13}C uniformly labeled *Populus*.

: non-invasive : KPi extract : cell wall fraction

4. Physicochemical characterization of plant biomass by solid-state NMR

Further, we have analyzed cell-wall components and their physical characterization by solid-state NMR. Future perspective of physicochemical characterization of plant biomass as useful materials in human life will be discussed in the conference.

References

1) Reddy, N. and Yang, Y. "Biofibers from agricultural byproducts for industrial applications" *Trends Biotech.* **23**, 22-27 (2005).

2) Kikuchi, J., Shinozaki, K. & Hirayama, T. "Stable isotope labeling of *Arabidopsis thaliana* for an NMR-based metabolomics approach" *Plant Cell Physiol.* **45**, 1099-1104 (2004).

3) Kikuchi, J. & Hirayama, T. "Hetero-nuclear NMR-based metabolomics" *Biotech. Agri. Forest.* **57**, 94-101 (2006).

4) Kikuchi, J. & Hirayama, T. "Practical aspects of uniform stable isotope labeling of higher plants for a hetero-nuclear NMR-based metabolomics" *Methods Mol Biol*, (in press).

P063

N-H distances and the secondary structures of polypeptides

Masashi Fukuchi[1], Hiroki Ishii[1], Kiyonori Takegoshi[1],
and Akira Shoji[2]

[1]**Department of Chemistry, Graduate School of Science, Kyoto University,**
[2]**Department of Biological Science, Faculty of Engineer, Gunma University**

Abstract

To examine correlation of the N-H distances and the secondary structures of polypeptides, we measured the N-H distances of various polypeptides of known secondary structures with the PMLG (phase modulated Lee-Goldburg) [1]-$m\bar{2}mm$ sequence [2], which is a variation of the FSLG (frequency-switched Lee-Goldburg)-$m\bar{2}mm$ sequence [3].

Hydrogen bonds are important for stabilizing the secondary structures of polypeptides and proteins. So far, N-H ··· O=C distances or N-H ··· O distances over the hydrogen bonds have been extensively examined. In this work, we evaluated N-H distances by measuring a ^{15}N-^{1}H heteronuclear dipolar interaction.

For this purpose, the FSLG-$m\bar{2}mm$ sequence proposed by Takegoshi et al. [3] for recoupling heteronuclear dipolar interaction under fast magic-angle spinning (MAS) is used. Because of some limitation of our machine, FSLG-$m\bar{2}mm$ was modified to use phase-modulated RF irradiation (PMLG-$m\bar{2}mm$ [2]). The FSLG-$m\bar{2}mm$ (PMLG-$m\bar{2}mm$) sequence is applicable under fast MAS to recouple heteronuclear dipolar interaction and to decouple homonuclear dipolar interaction.

Fig.1 shows N-H dipolar powder patterns of fully ^{15}N-labeled poly(L-alanine) (PLA) adopting right-handed α-helix (the solid line) and antiparallel β-sheet (the dotted line) conformations obtained by applying PMLG-$m\bar{2}mm$ under MAS (ν_r = 10 kHz). The strength of the ^{1}H rf field was 62.5kHz, and that of the PMLG effective field was 80kHz. The experiments were performed on a 300 MHz CMX Infinity NMR spectrometer using a Doty double resonance 5 mm MAS probe.

Keywords: Solid-state NMR, PMLG, secondary structure

Table.1 shows N-H distances in peptides which were obtained by fitting the experimental lineshapes (Fig.1) to theoretical ones with the N-H distances as an adjusting parameter. We also examined PBLA (poly(β-benzyl L-aspartate)). Table.1 shows that the N-H distance of β-sheet is longer than that of α-helix.

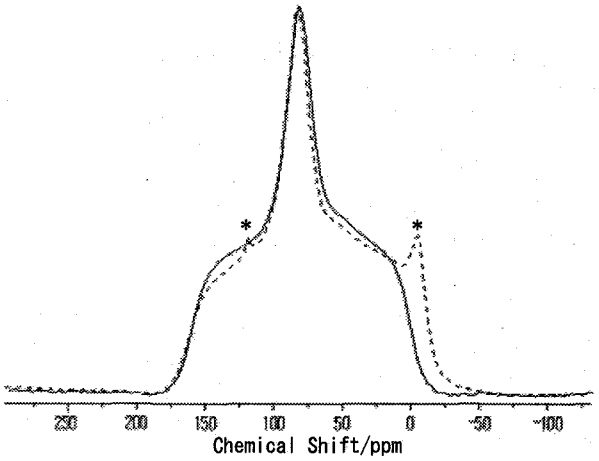

Fig.1 N-H powder patterns of fully ^{15}N-labeled PLA adopting α-helix (the solid line) and β-sheet (the dotted line) conformations.
***; impurities?**

Peptide	Secondary structure	N-H distance (our studies)	N-H distance[4]
PBLA	ω-helix (left turn)	**1.005 Å ± 0.005 Å**	
	α-helix (left turn)	**1.005 Å ± 0.005 Å**	
	α-helix (right turn)	**1.005 Å ± 0.005 Å**	
	β-sheet (anti-parallel)	**1.025 Å ± 0.005 Å**	
PLA	α-helix	**1.025 Å ± 0.005 Å**	**1.09 Å**
	β-sheet	**1.035 Å ± 0.005 Å**	**1.12 Å**

Table.1 N-H distances in peptides which were analyzed from this method. PBLA: poly(β-benzyl L-aspartate), PLA: poly(L-alanine).

References

[1] E. Vinogradov, P. K. Madhu, and S. Vega, Chem. Phys. Lett. 314, 443 (1999)

[2] H. Ishii, M. Fukuchi, K. Takegoshi, and A. Shoji, the 44th annual NMR meeting NP119 (Yokohama, Japan 2005)

[3] K. Takegoshi, and T. Terao, Solid State Nucl. Magn. Reson. 13, 203 (1999)

[4] H. Kimura, A. Shoji, H. Sugisawa, K. Deguchi, A. Naito, and H. Saito, Macromolecules 33, 6627 (2000)

P064

固体 ^{13}C NMR を用いた Poly(β-benzyl L-aspartate)の構造転移の研究

○中西　梓、笠原 慎一、水野　敬、竹腰　清乃理、荘司 顯*
京都大学大学院理学研究科
*群馬大学工学部生物化学工学科

Solid-State ^{13}C NMR studies on conformational transformation of Poly(β-benzyl L-aspartate)

A.Nakanishi, S.Kasahara, T.Mizuno, K.Takegoshi, and A.Shoji*
Department of Chemistry, Graduate School of Science, Kyoto University, Kyoto, 606-8502
**Department of Biological and Chemical Engineering, Faculty of Engineering, Gunma University, Gunma,376-8515*

We studied dynamics in conformational transformation of Poly(β-benzyl L-aspartate) (PBLA) by high resolutional solid-state ^{13}C NMR. The α_R-helical PBLA is transformed into the ω_L-helix with a change of the helix sense by heating at about 70-140 ℃ , and further heat treatment causes the change of conformation from the ω_L-helix form to the β-sheet form [1].

Figure 1 shows the C=O signal of PBLA after heat-treatment at 140℃. The lineshape change observed for C=O peaks indicates that the longer the heating time the more PBLA transforms into the ω_L-helix and the β-sheet forms. Interestingly the ω_L-helix didn't transform into the β-sheet form completely contrary to the observation at 150℃ [2]; the ω_L-helix changed almost completely into the β-sheet form.

The relative peak intensities of these conformers are determined by fitting the signal to a sum of Gaussian lineshapes(Figure 2) and using this result, the reaction rate constant of the transformation from the α_R-helical to the another conformer is obtained to be $3.78*10^{-3}$ s^{-1} at 140℃ ,which is comparable to the value ($4.0*10^{-3}$ s^{-1}) determined at 150℃[2].

Similar experiments at different heat-treatment are undergoing to determine the transformation energy.

[1] T.Akieda, H.Miura, S.Kurosu, and I.Ando *Macromolecules*, 1992, *25*, 5794
[2] S.Kasahara, K.Takegoshi, and A,Shoji
The 44th Annual NMR Meeting of the NMR Society of Japan , Abstracts, *page204*

key words: solid-state 13C NMR　Poly(β-benzyl L-aspartate)

なかにし　あずさ

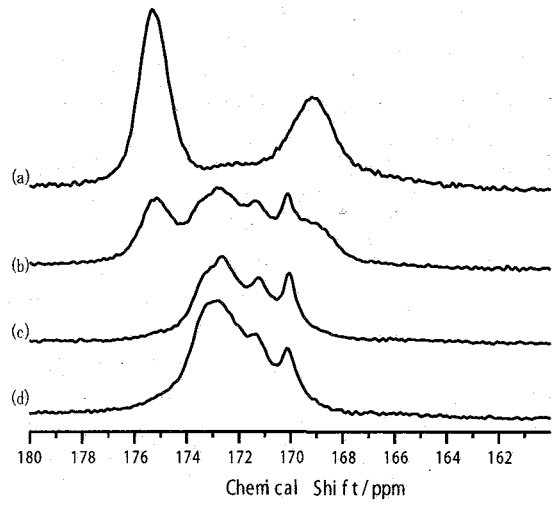

Figure 1.
13C CP/MAS spectra of PBLA
(a) with no thermal treatment
(b) heated at 140℃ for 1min
(c) heated at 140℃ for 2min
(d) heated at 140℃ for 3min

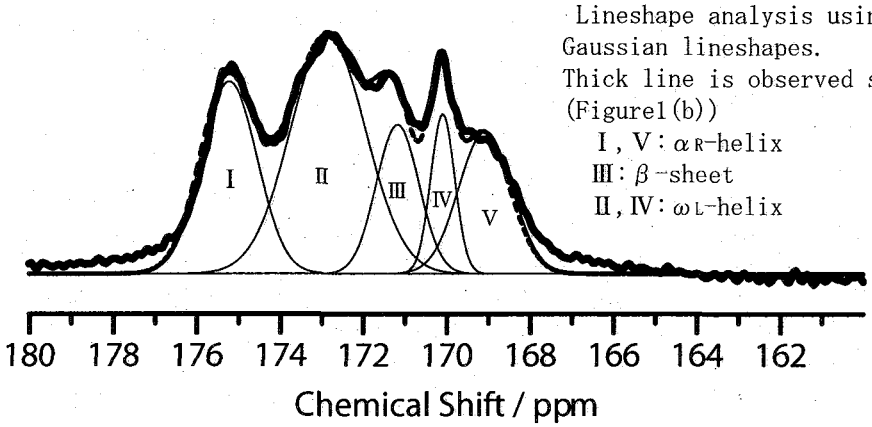

Figure 2.
Lineshape analysis using Gaussian lineshapes.
Thick line is observed spectrum (Figure1(b))
I, V: α_R-helix
III: β-sheet
II, IV: ω_L-helix

sec	Cα	ω_L	β-sheet
0	86.8	8.8	4.2
30	52.9	36.2	13.5
60	38.5	47.2	13.7
120	17.3	68.9	15.4
180	13.4	73.9	12.9

Table1.

Relative peak intensity(%) of C=O carbon at 140℃

P065

固体 NMR 法を用いた各種水溶性絹モデルペプチドの精密構造解析

農工大・工　○中澤靖元・山口恵理香・菊池有加・佐藤博彦・朝倉哲郎

Structural Analysis of water-soluble silk model peptides using Solid-state NMR

Yasumoto Nakazawa, Erika Yamaguchi, Yuka Kikuchi, Hirohiko Sato, Tetsuo Asakura
Department of Biotechnology and Life Science, Tokyo University of Agriculture and Technology, Koganei, Tokyo, 184-8588, Japan

Abstract　Selective isotope labeling can be introduced in synthetic peptides more easily than in the native materials and one can focus on the specific local areas of interest in the proteins in the solid-state NMR analysis. In recent works we have shown that torsion-angle distributions in several silk model peptides can be analyzed using a combination of 2D spin-diffusion NMR and REDOR techniques. Here we present an alternative approach, which allows a more detailed determination of the torsion-angle distribution, by using the double-quantum single-quantum correlation experiment (DOQSY). We have applied this approach to several model peptides, with sequences based on silk and the related analysis.

【緒言】　本研究ではこれまで、家蚕、エリ蚕、クモなどが生産する絹の繊維化前後における構造を精度良く決定するため、特定アミノ酸残基に安定同位体ラベルを施したモデルペプチドを合成、固体 NMR 法を用いた内部回転角決定法を用いて、繊維タンパク質の詳細な構造解析を行ってきた[1-3]。

絹フィブロインやクモ牽引糸はカイコ体内において可溶化して存在しているが、吐糸されることにより、劇的な構造変化を遂げ、繊維状態になる[1]。当研究室では既に、エリ蚕絹フィブロインについて各種固体 NMR 法を用いて、α-ヘリックス構造を中心とする繊維化前の構造のモデルペプチドを合成し、その精密な構造を決定するとともに[2]、繊維化後の構造についても、固体 NMR 法を中心とした解析を進めている[3,4]。

本研究では、これら一連の構造分布を踏まえた、二次元スピン拡散法、DOQSY 法などの各種構造解析手法を用い、モデルペプチドの特定アミノ酸の内部回転角を定量的に評価した結果について述べる。また、これまで作成してきた絹モデルペプチドに加え、新たに水溶性を付与したモデルペプチドを作成、繊維化に伴う構造変化に関する検討を行う。

【実験】　ペプチドはすべて、Fmoc 固相合成法により合成した(Table 1)。

Table 1 Primary structures of model peptides of the silks from *S. c. ricini*, *B. mori* and *N. clavipes*

Sample #	Peptide Sequences	Origin
#1	GGAGGGYGGDGGAAAAA[1-^{13}C]A^{18}[1-^{13}C]A^{19}AAAAAGGAGDGYGAG	*S. c. ricini*
#2	GGAGGGYGGDG[1-^{13}C]G^{12}[1-^{13}C]A^{13}AAAAAAAAAAAGGAGDGYGAG	*S. c. ricini*
#3	AGG AGG AGG AGG AG[1-^{13}C]G^{15} [1-^{13}C]A^{16}GG AGG AGG AGG AGG	*N. clavipes*
#4	AGG AGG AGG AGG AGG A[1-^{13}C]G^{14}[1-^{13}C]G^{15} AGG AGG AGG AGG	*N. clavipes*
#5	(E)$_8$GGLGGQGAGAAAAAAGGAGQGGYGG	*N. clavipes*
#6	(E)$_8$AGSGAGAGSGAGAGSGAGAGSGAGAGSGAG	*B. mori*

Sample #1~4 に関しては、エリ蚕絹フィブロインおよび *N. clavipes* 牽引糸のモデルペプチドであり、また Sample #5, #6 では、水溶性を付与するため、N 末端側に poly-Glu を導入している。

Solid-state NMR, DOQSY, 2D spin-diffusion NMR, isotope-labeled model peptide, Silk fibroin

なかざわやすもと，やまぐちえりか，きくちゆか，さとうひろひこ，あさくらてつお

DOQSY 法は Varian Infinity Plus(300MHz)を用いて行った。Single exitation cycle 1.5msec、Contact time 1.4msec、^{13}C Frequency 75MHz, Recycle delay 4sec、試料は 30~70mg、スペクトルのプロセッシングは matNMR[4] を用いた。

【結果・考察】　本研究では、これまで当研究で行ってきた各種絹フィブロインの構造解析に加え、DOQSY 法を用い、内部回転角の分布を考慮した構造解析について検討した。Figure 1 にはエリ蚕絹モデルペプチドの DOQSY スペクトルを示した。Sample #1 の実測スペクトル(Figure 1(a))に関して、取り得る内部回転角の分布を検討するため、確率分布関数のプロットを Figure 1(e)に示した。この結果、Sample #1 のスペクトルは、おおむね単一の構造から構成されており、(ϕ, ψ)=(-60°, -45°)の内部回転角、すなわち、α-helix 構造に対応することが明らかとなった。一方、Ala 連鎖領域の N 末端側に存在する Ala[13] の内部回転角を決定するための Sample #3 に関しても同様の検討を行った。実測スペクトル(Figure 1(b))の確率分布関数による内部回転角の分布では((Figure 1(f))、Sample #1 と同様の内部回転角である(ϕ, ψ)=(-60°, -45°)に加え、(ϕ, ψ)=(-75°, -30°)が存在することがわかった。この内部回転角は以前、当研究室で決定した(ϕ, ψ)=(-70°, -30°)とおおむね一致する。この内部回転角を持つ helix 構造は、helix 末端の水素結合が i+3 となることで、安定化していることがわかっている。Ala 連鎖領域 N 末端側にこれら二種類の構造成分が存在する理由として、水溶液状態ではエリ蚕絹フィブロインの Ala 連鎖領域の N 末端側は典型的なα-helix 構造と末端がすぼまった安定化構造の間の平衡状態にあり、固体状態においては、それら二状態が独立して観測されたものと推測した。

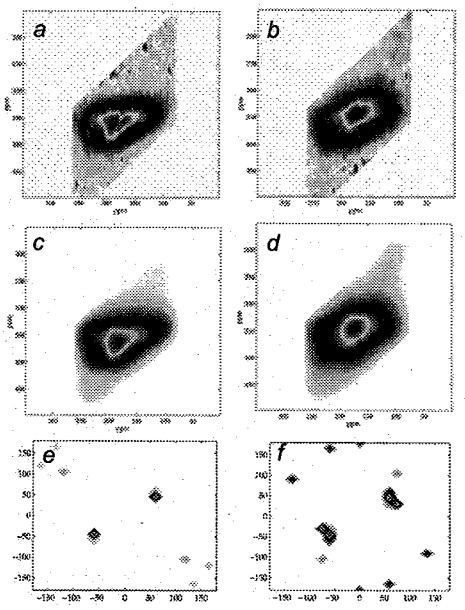

Figure 1　(a) Experimental 2D DOQSY spectra of the model peptide #1 and (b) model peptide #3 taken at room temperature. Spectra processed using the MatNMR[4] processing package. (c) and (d) show the corresponding best fits. (e) and (f) show the respective probability distribution functions P(ϕ, ψ).

尚、本発表では、エリ蚕絹フィブロインの他にも、各種絹モデルペプチドの内部回転角決定を中心とした解析を報告する。特に、Sample #5 および Sample #6 のモデルペプチドに関しては、Glu 残基の導入により、これまで困難であった水溶性が付与された絹モデルペプチドの作製に成功、さらに、pH の変化によって、比較的均一なβ-sheet 構造を形成することが確認された。発表では、これら水溶性ペプチドの解析についても報告する予定である。

【参考文献】

(1) Nakazawa, Y.; Asakura, T. *FEBS Lett.* **2002**, *529*, 188-192.
(2) Nakazawa, Y.; Asakura, T. *J. Am. Chem. Soc.* **2003**, *125*, 7230-7237.
(3) Asakura, T.; Yao, J.; Yamane, T.; Umemura, K.; Ulrich, A. S. *J. Am. Chem. Soc.* **2002**, *124*, 8794-8795.
(4) MatNMR is a toolbox for processing NMR / EPR data under MATLAB and can be downroaded freely at http://matnmr.sourceforge.net/.

P066

脂質2重膜結合ペプチドの固体NMRによる測定

阪大蛋白研[1]、京大院工[2]、武田薬品工業[3]

○ 小見伸泰[1]、大河佳代[1]、立石寛之[2]、井ノ岡博[3]、 白川昌宏[2]、藤原敏道[1]、
阿久津秀雄[1]

Solid-State NMR measurement of PACAP Bound to Lipid Membrane

[1]Institute for Protein Resarch, Osaka University, [2]Graduate School of Engineering, Kyoto Univiersity, [3]Takeda Chemical Industries Ltd.

○ Nobuyasu Komi[1], Kayo Okawa[1], Hiroyuki Tateishi[2], Hiroshi Inooka[3], Masahiro Shirakawa[2], Toshimichi Fujiwara[1],and Hideo Akustu[1]

Pituitary adenylate-cyclase activating peptide (PACAP) is one of hormone peptides. PACAP regulates the cardiovascular, endocrine, and immune systems by raising cAMP levels. We studied stable isotope-labeled PACAP27 and 21 by high-resolution multidimensional solid-state NMR. We have assigned ^{13}C signals of PACAP27 by ^{13}C correlation experiments using RFDR and DQ dipolar recoupling sequences, and predicted the secondary structure from chemical shifts by TALOS. TALOS predicted membrane bound PACAP27 takes an all-extend form. Our solid-state NMR results differ from the previously determined structure (Inooka 2001).

序

PACAPは視床下部より分泌されるペプチドで神経伝達物質として神経系の活性化に働く。このペプチドの受容体は脳だけでなく全身に存在しており筋収縮や、血管拡張を促すホルモンとしても作用する。PACAPの1次構造は哺乳類では完全に保存されており原索動物のものとも高い相同性を示す。しかしながら、その受容体活性化の分子メカニズムは明らかになっていない。近年、trNOEにより溶液中のミセルに結合したPACAPの構造が解析されている[1]。しかし、この測定法は膜に結合した状態のPACAPを直接測定するものではない。我々は膜受容体に結合した状態でのPACAP構造解析を行うことを目標とし、その第一歩として脂質二重膜結合PACAPの固体

キーワード： 固体NMR、ホルモンペプチド

こみのぶやす、おおかわかよ、たていしひろゆき、いのおかひろし、しらかわまさひろ、ふじわらとしみち、あくつひでお

NMR 測定を開始した。

実験

PACAP は ^{13}C 安定同位体標識 M9 培地で培養した大腸菌 BL21(DE3)株にチオレドキシン融合蛋白として発現させ、精製したのち酵素処理により、チオレドキシンの切断と C 末端のアミド化を行って得た。脂質二重膜は脂肪鎖が重水素化された脂質を凍結融解し調製した。測定に用いた試料は PACAP を脂質二重膜に結合させ、相対湿度を 32%に調整したものである。用いた装置は Varian 社 Infinity Plus 500 (3.2mm φ spinner)、(4mm φ spinner)と Infinity Plus 700 (3.2mm φ spinner)であり、^{13}C 共鳴周波数はそれぞれ 125.6、175.9 MHz である。測定に際してマジック角試料回転を 12.5 或いは 16 kHz で行った。我々が用いた測定法は 0 量子 ^{13}C 双極子相関法(RFDR)、2 量子 ^{13}C 双極子相関 (SPC5)、残基内、残基間 ^{13}C-^{15}N 相関測定法、そして ^{13}C スピン拡散法である。

結果・考察

残基毎の信号帰属には RFDR(混合時間 1.5、2.5、2.96 ms)、SPC5(混合時間 1.25、1.75 ms)、残基内 ^{15}N-$^{13}C^{\alpha}$$^{13}C^{\beta}$ 相関測定(混合時間 7 ms)を用いた。SPC5 のスペクトルから各側鎖の同定を行い RFDR のスペクトルでカルボニル残基内 ^{15}N-$^{13}C^{\alpha}$ $^{13}C^{\beta}$ 相関でアミドの信号を各残基に帰属した。これらの情報を基に残基間 $^{15}N_{i+1}$-$^{13}C'_i$ $^{13}C^{\alpha}{}_i$ 相関測定(N-C 混合時間 5 ms C'-C^{α} 混合時間 2.24ms)で各信号をアミノ酸配列に対応させた。

このようにして帰属した脂質膜(d_{54}-DMPC)結合 PACAP27(モル比　ペプチド:脂質 = 1:20)の C'、C^{α}、C^{β}、N の化学シフト値から 2 次構造予測プログラム (TALOS) で予測した結果、全長にわたりβストランド構造を示した。又、脂質膜(d_{62}-DPPC:d_{62}DPPG = 4:1)に結合した PACAP21(モル比　ペプチド:脂質=1:32)の ^{13}C スピン拡散スペクトル(混合時間 17 ms)と比較すると、ピーク位置がよく一致していること、主鎖カルボニルのピークがベータ構造に特有の位置に偏っていることから PACAP21 も大部分がβストランドで占められた構造をとっていると予測される。ピーク位置のシフトは 5 から 7 番目の残基のイソロイシン、フェニルアラニン、スレオニンで見られた。これらのピークすべてがαヘリックス構造と予想される側に 1ppm 程度移動していた。trNOE で決定された溶液中の構造は N 末端 7 残基がβターンで他の残基αヘリックスをとっている。この違いを引き起こした原因として脂質の電荷、ペプチドの濃度が挙げられる(trNOE の測定では　モル比　ペプチド:脂質 = 1:100)。

Reference

1)　H. Inooka, et al. *Nature Struc. Biol.*8, 161-165 (2001).

P067

The characterization of hydrogen bonding in native cellulose by high-field solid-state NMR

Qing Luo[1], Shinji Suzuki[1], Yasumasa Kanie[1], Hironori Kaji[1], Fumitaka Horii[1], Tadashi Shimizu[2], Masataka Tansho[2], Takahiro Nemoto[3], Takashi Mizuno[4] and Kiyonori Takegoshi[4]

1 Institute for Chemical Research, Kyoto University, Uji, Kyoto 611-0011, Japan

2 High Magnetic Field Center, NIMS, Tsukuba, Japan

3 JEOL, Akishima, Japan

4 Faculty of Science, Kyoto University, Japan

[Introduction] It is well known that the native cellulose crystals consist of two allormorphs, cellulose I_α and I_β. Recently, Nishiyama et al.[1)] reported the precise crystal structures including the positions of hydrogen atoms for cellulose I_α and I_β by using highly crystalline and highly uniaxially oriented samples. However, different kinds of inter- and intra-molecular hydrogen bondings, particularly associated with the CH_2OH side groups, are distributed almost statistically in each allomorph and their dynamic structure is not unclear. In this paper, we characterize the hydrogen bonding in native cellulose by using ^1H CRAMPS, $^1H/^{13}C$ HETCOR and ^2H MAS and $^1H/^2H$ HETCOR detection. The chemical shifts of different OH groups are first assigned.

[Experimental] ^1H CRAMPS, $^1H/^{13}C$ PMLG HETCOR and ^2H MAS spectra were measured on a CMX-400 ECA-500 and ECA-930 solid-state NMR spectrometers, respectively. OH deuterated samples were prepared by treating with $NaOD/D_2O$ at 190 -210 .In the HETCOR experiments, the LG-CP was applied in the cross polarization process to prevent the homonuclear spin diffusion.

[Results and Discussion] The deuteration phenomenon can be used to measure the accessibility of cellulose. ^1H CRAMPS spectra were measured for the tunicate samples of deuterated at 190 for 30, 60 and 90 min respectively. The ^1H CRAMPS spectra show that the process time of 60 min is enough to fully induce the H-D exchange process. The H-D exchange rate of the different OH group is almost the same, indicating no selectivity of the exchange reaction. Figure 1 shows the ^1H CRAMPS spectra of the native tunicate cellulose and the fully OH-deuterated one. The difference spectrum of these two spectra shows the ^1H resonance lines of OH groups. 3 broad peaks can be distinguished in the difference spectrum. Although the resolution is not high, Although the resolution is not high, it is clear that the ratio of the 3 peaks is not

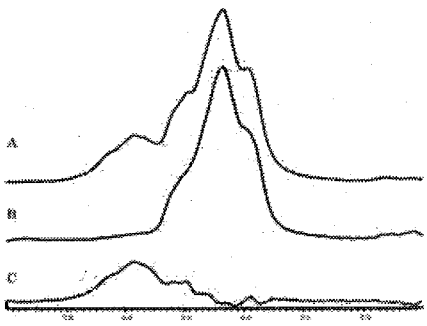

Figure 1. The ^1H CRAMPS spectra. (a): the fully OH-deuterated tunicate cellulose. (b) the native tunicate cellulose. (c) the difference spectrum of a and b.

Key words: Hydrogen bonding, Native cellulose, ^1H CRAMPS, High-field solid-state NMR, ^2H CP/MAS

1:1:1. Thus, these 3 peaks can not be assigned to OH(2), OH(3) and OH(6), respectively directly.

As it is well known, the ^{2}H NMR shows a similar chemical shift as that of ^{1}H NMR. By using ultrahigh-field 930 MHz NMR spectrometer, ECA-930, high resolution ^{2}H MAS NMR spectra of the OH-deuterated tunicate cellulose samples were measured. Figure2 shows the central band of the ^{2}H CP/MAS spectra of the deuterated tunicate cellulose which shows a much higher resolution compared with the CRAMPS spectra. This hints that the low resolution of OH signals in ^{1}H CRAMPS spectra is not due to the chemical shift distribution but the residue dipolar interaction. At least 4 peaks can be distinguished by curve fitting.

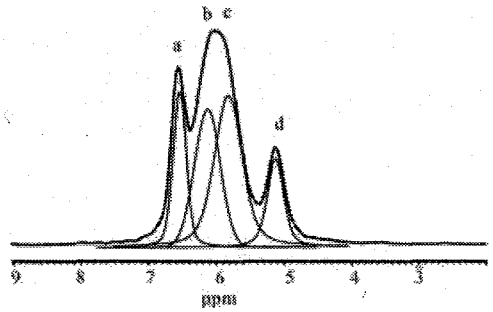

Figure 2. The CP/MAS ^{2}H spectrum of OH-deuterated tunicate cellulose.

Figure 3 shows the $^{1}H/^{13}C$ PMLG HETCOR spectra of the native tunicate cellulose. A relative long contact time (0.7ms) was used. The range of the chemical shift of the OH proton has already been determined by the ^{1}H CRAMPS measurements. By establishing the correlation of the carbon and OH proton in the PMLG HETCOR spectrum, the assignments of the OH peaks is available, and so of the assignment of the ^{2}H spectrum. Peak a and b in the ^{2}H spectrum is from as OH-2, OH-6, and c, d are from OH-3 with different local environment.

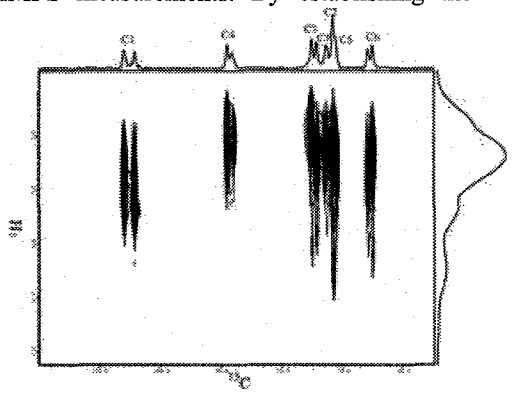

Figure 3. The PMLG HETCOR spectrum of native tunicate cellulose. The contact time is 0.7 ms.

Since the chemical shifts of the OH protons are assigned, further $^{1}H/^{13}C$ HETCOR experiments with different contact time can be performed to establish the correlation between those OH groups with C-1 and C-4. Because there is no OH group connecting with C-1 and C-4 directly, the correlation may through the hydrogen bonding. $^{1}H/^{2}H$ HETCOR experiment of partially deuterated sample was also performed to provide more detailed information about the hydrogen bonding.

1) Nishiyama *et al., J. Am. Chem. Soc.* 124, 9074 (2002); *J. Am. Chem. Soc.* 125, 14300 (2003)

P068

固体 NMR によるポリエチレン単斜晶に関する研究

群馬大工　橋爪憲司、上原宏樹、○山延　健、甲本忠史

Solid-State NMR Study of Monoclinic Form of Polyethylene (Gunma University)Kenji Hashizume, Hiroki Uehara, Takeshi Yamanobe, Tadashi Komoto

[Abstract] Polyethylene has two stable crystal structures. One is orthorhombic form in which all-trans zigzag planes are perpendicular to each other, the other is monoclinic form in which those planes are parallel to each other. Monoclinic form is produced by drawing and compression. The amount of monoclinic form depends on the compression pressure, the draw ratio and the compression temperature. At high temperature, monoclinic form is transformed to orthorhombic one. By 2D exchange NMR, the cross peaks between the monoclinic and orthorhombic forms and intermediate phase are observed. Therefore, at high temperature, there is a component which exchanges between the monoclinic and orthorhombic forms and intermediate phase. By the spin diffusion experiments, the domain sizes will be discussed.

【緒言】ポリエチレン(PE)は斜方晶と単斜晶の２つの結晶構造を持つことが知られている。常圧下で溶融結晶化を行うと斜方晶の結晶をとる。これに対して、延伸、圧縮などを行うと単斜晶が生じる。また、低温で重合された超高分子量ポリエチレンにおいて単斜晶が多く生成する。これら２つの結晶形では分子鎖はall-trans zig-zagのコンフォメーションをとっており、分子鎖間の相対的な方向が異なっている。一方で、生成した単斜晶は融点以下での熱処理により斜方晶へと転移する。本研究では ^{13}C 固体高分解能 NMR 法を用いることにより単斜晶の生成、消失についての検討を行った。

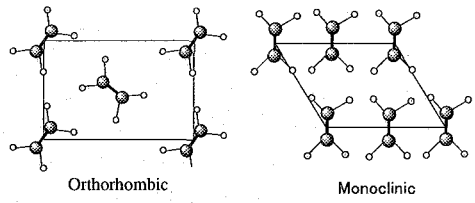

Fig.1 Crystalline Structure of orthorhombic and monoclinic form of polyethylene

【実験】試料として超高分子量ポリエチレン(UHMWPE:Mw=2.0×10^6)を使用した。パウダーから180℃にて溶融結晶化フィルムを作製し、様々な条件にて延伸・圧縮して試料とした。固体 NMR 測定は Bruker 製 AVANCE　DSX300WB により行った。

【結果・考察】

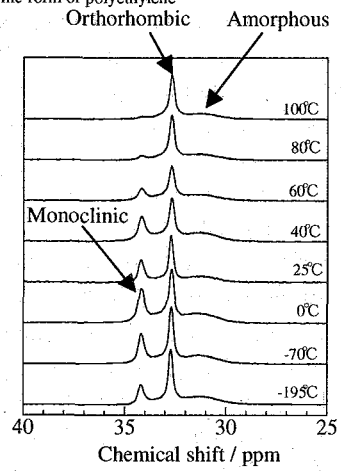

Fig.2 Press temperature dependence of ^{13}C CPMAS NMR spectra.

単斜晶の生成条件　Fig.2 に延伸試料を圧縮することにより得られた試料の ^{13}C CPMAS NMR スペクトルの圧縮温度依存性を示した。スペクトルにおいて約 31ppm の幅広なピークは非晶、約 33ppm のピークは斜方晶、34ppm のピークは単斜晶のピークである。単斜晶のピークは 0℃での圧縮により最も強いことがわかる。室温以上ではポリエチレン鎖の分子運動の開始により、分子鎖の滑りが生じ単斜晶から斜方晶への構造緩和が生じるために単斜晶の生成が少なくなる。これに対して、低温では非晶部分の運動性が著しく悪いために、結晶面の移動が生じにくく斜方晶から単斜晶への転移が生じにくいために 0℃付近で単斜晶の生成が最大になると考えられる。単斜晶の生成は圧縮温度のみならず、圧力、延伸倍率、圧縮方向によっても影響される。高延伸倍率の試料に対して、分子鎖に垂直に

なるように高圧力で圧縮することにより、より多くの単斜晶を生成することが明らかになった。

単斜晶の消滅機構　Fig.3に各温度で熱処理した延伸-圧縮試料（9倍延伸後520MPaで圧縮、熱処理）の固体高分解能NMRスペクトルを示した。熱処理温度の上昇とともに単斜晶が減少している。特に熱処理温度が60℃から単斜晶は急激に減少している。しかし、90℃熱処理試料でも単斜晶の存在がわずかながら確認された。更に、90℃で熱処理した試料を室温で測定すると90℃で存在した単斜晶のピーク強度より強くなっていることがわかった。ピーク分離を行うと非晶、斜方晶、単斜晶に加えて、斜方晶と単斜晶の間の中間相が存在しており、60℃以上では中間相の分率が増加することが明らかになった。単結晶ポリエチレンではこの温度でラメラの厚化が生じ、結晶化度の増加が観測されている。このことからポリエチレンの主鎖のすべりの開始とともに単斜晶から斜方晶への転移が生じると考えられる。ほとんどの単斜晶はこれにより斜方晶へと転移する。これに対して、冷却すると再び単斜晶が現れることは高温で斜方晶へ転移していたものが室温に戻る際に逆に単斜晶に戻る成分が存在する場合と、高温で単斜晶と斜方晶の間で交換していたものが低温で単斜晶に安定化する場合が考えられる。最初の状況はFig.4に示すエネルギーの状態で考えると、通常は斜方晶が安定であるため、一度単斜晶から転移した斜方晶は戻ることは考えられない。しかし、局所的に圧縮により加えられた応力が緩和できない状態があるとすると斜方晶のエネルギーは上昇し、単斜晶よりも不安定になる可能性もある。２番目の理由である交換が生じているとすると２次元交換スペクトルを測定することにより観測できるはずである。実際に２次元交換測定をしてみると、高温で３つの相の間の交換ピークを観測することができた。このことは高温で中間相の割合が非常に多くなることを考えても理解できる。これらのことより、高温では分子鎖の滑りの開始とともにほとんどの単斜晶が斜方晶へ転移するが、一部の成分は単斜晶と斜方晶の間を交換しており、それが室温に戻る段階で、単斜晶、中間相、斜方晶へと安定化するものと考えられる。

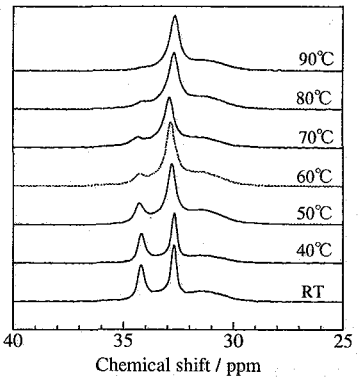

Fig.3 NMR spectra of heat-treated sample as a function of thermal treatment temperature.

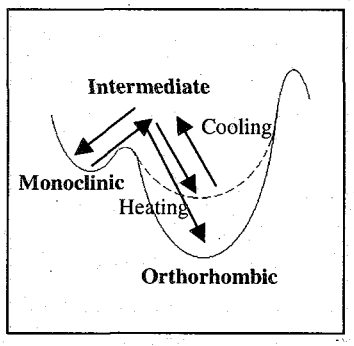

Fig.4 Mechanism for transformation from Monoclinic to Orthorhombic forms.

単斜晶、斜方晶、非晶のドメイン　単斜晶、斜方晶、非晶のそれぞれのドメインがどれくらいの大きさで、どの様な配列になっているかというのは興味深い問題である。このような情報は電子顕微鏡を用いて行われる。しかし、延伸試料等では延伸による分子配向により、結晶、非晶のコントラストが付きにくくなり観察することができない。そこで、スピン拡散を用いてこれらの相の付いての情報を得ることを試みた。非晶成分からのスピン拡散の挙動を見てみると最初に単斜晶成分のピークが回復し、それに続いて、斜方晶成分のピークが回復した。このことから、単斜晶成分が非晶成分に近い部分にあることがわかった。

P069

Characterization of Microbial Poly(ε-L-lysine)/ Poly(L-lactic acid) Blend Films

Shiro Maeda[1], Osamu Kinoshita[1], Yasuhiro Fujiwara[1], Kensuke Sakurai[2], and Ko-Ki Kunimoto[3]

[1]Division of Applied Chemistry and Biotechnology, and [2]Division of Materials Science, Graduate School of Engineering, University of Fukui, Fukui 910-8507, Japan, and [3]Division of Material Engineering, Graduate School of Natural Science and Technology, Kanazawa University, Kanazawa 920-1192, Japan.

Structural analysis of biodegradable poly(L-lactic acid)/poly(ε-L-lysine) (PLLA/ε-PL) blend film cast from chloroform/methanol solution and that from hexafluoroisopropanol solution were done by using solid-state NMR, IR and DSC. Chemical shifts of ε-PL peaks of the former are almost the same as those of ε-PL powder. However, those of the latter shift toward upfield and are almost the same as those of hydrochloric acid salt of ε-PL (ε-PL/HCl). Conformation of methylene carbon chain of ε-PL in the former film and the latter film may have almost the same conformation of ε-PL powder and ε-PL/HCl, respectively.

Introduction

In recent years, there has been considerable interest in biopolymers because of concern over the environmental impacts arising from the disposal of petroleum based plastics. It is important to develop novel biodegradable materials which substitute for non-biodegradable synthetic polymers made from petroleum. Poly(L-lactic acid) (PLLA) is most expected material as a biodegradable polymer made from natural resources such as corn starch. Microbial poly(ε-L-Lysine) (ε-PL) is a product of a variant of *Streptomyces albulus*, having amide linkage between ε-amino and α-carboxyl group. Due to antibacterial activities against a broad spectrum of microorganisms, ε-PL has found application as a preservative for various food products[1]. It may be an effective way of obtaining more useful characteristics and improving defects of both PLLA and ε-PL to make a polymer blend of PLLA and ε-PL.

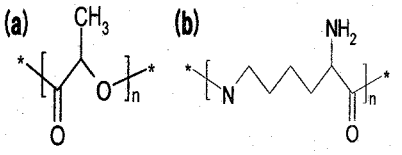

Figure 1. Structure of (a) Poly(L-lactic acid) and (b) poly(ε-L-Lysine), respectively.

Experimental

PLLA (Mitsui chemicals, LACEA) and ε-PL (Chisso Corp.) were dissolved in $CHCl_3/CH_3OH$ mixed solvent and hexafluoroisopropanol (HFIP). The solutions were cast on a Teflon dishes and dried at room temperature to make a film, then dried in vacuo. The PLLA/ε-PL blend films were characterized by using solid-state NMR, IR and DSC. ^{13}C Solid-state NMR spectra were measured with Chemagnetics CMX Infinity 300 operating at 75 MHz. MAS speed was 5.0 kHz. ^{13}C chemical shifts were referenced to the methyl resonance of hexamethylbenzene (17.35 ppm from Me_4Si).

Key words: Poly(L-lactic acid), Poly(ε-L-lysine), Solid-State NMR, DSC, polymer blend

Results and Discussion

PLLA/ε-L-PL blend film cast from $CHCl_3/CH_3OH$ mixed solvent was not transparent but cloudy. Figure 2 shows honeycomb structure observed on the surface of PLLA/ε-PL blend film (4/1) by using optical microscope. A diameter of a hollow is about 4.2 μm. Honeycomb structure may be formed because two solvents have different properties; methanol is hydrophilic and chloroform is hydrophobic. On the other hand, the blend film cast from HFIP is transparent.

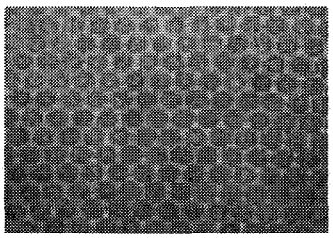

Figure 2. The microscopic photograph of blend film PLLA/ε-PL (4/1) cast from $CHCl_3/CH_3OH$.

Figure 3 shows solid-state ^{13}C CP/MAS spectra of ε-PL, PLLA, and PLLA/ε-PL (1/1) blend film cast from $CHCl_3/CH_3OH$ and HFIP. Chemical shifts of ε-PL are summarized in Table 1. Chemical shifts of ε-PL in the blend film cast from $CHCl_3/CH_3OH$ are almost the same as in ε-PL. It implies that conformation of ε-PL in the crystal component of the blend film is maintained as in ε-PL which has β-sheet like conformation[2]. On the other hand, those cast from HFIP show upfield shift probably due to γ-gauche effect. It suggests that the conformation is changed in the blend film cast from HFIP. Peak profile of PLLA in the blend film cast from $CHCl_3/CH_3OH$ looks like that of α-crystal form of PLLA. It implies that the ratio of crystal component has increased with addition of ε-PL; it may accelerate crystallization of PLLA.

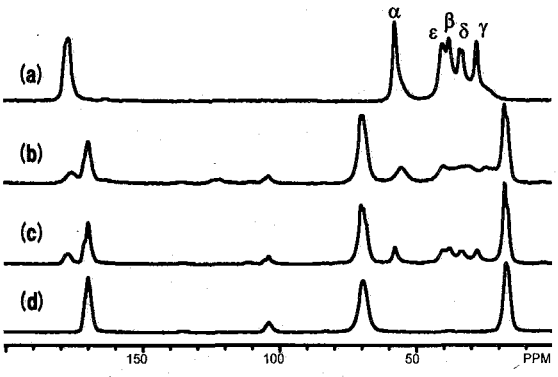

Figure 3. ^{13}C CP/MAS NMR spectra of (a) ε-PL, (b)PLLA/ε-PL (1/1) cast from HFIP solution, (c)PLLA/ε-PL (1/1) cast from $CHCl_3/CH_3OH$ solution, and (d) PLLA.

As described above, crystal structure of the blend film changes with solvent although constituent parts of the blend film and its ratio is the same. It may result from the difference in miscibility of the blend film. The correlation of miscibility and change of crystal structure is under investigation by measurements of ^1H relaxation time of PLLA/ε-PL blend films.

Table 1. Chemical shifts of ε-PL in ε-PL powder and PLLA/ε-PL (1/1) blend films cast from chloroform/methanol and HFIP in ppm.

Carbon	ε-PL powder	PLLA/ε-PL (1/1) blend film cast from chloroform/methanol	PLLA/ε-PL (1/1) blend film cast from HFIP
α	57.9	57.9	55.3
ε	40.4	40.3	39.8
β	38.1	38.0	30.9
δ	34.0	34.0	24.6
γ	27.9	27.9	
C=O	177.6	177.5	176.5

References

1) S. Maeda, T. Mori, C. Sasaki, and K. Kunimoto, *Kobunshikako*, **52**, 516-522 (2003).
2) S. Maeda, K. Kunimoto, C. Sasaki, A. Kuwae, and K. Hanai, *J. Mol. Struct.*, **655**, 149-155(2003)..

P070

Characterization of microbial poly(ε-L-lysine) by solid state NMR and solid state CD

Shiro MAEDA[1], Junnosuke MURANAKA[1] and Ko-Ki KUNIMOTO[2]
[1]Division of Applied Chemistry and Biotechnology, Graduate School of Engineering, University of Fukui, 910-8507 Fukui, and [2]Division of Material Engineering, Graduate School of Natural Science and Technology, Kanazawa University, 920-1192 Kanazawa, Japan

Structural analysis of microbial poly (ε-L-lysine) (MPL) was done by using solid state NMR and solid state circular dichroism (CD). We had elucidated that MPL takes β-sheet like conformation in the solid state and degree of crystallinity was estimated to 63% by using solid-state NMR. In addition, solid state circular dichroism (CD) measurements with the artifact free method which was derived by using Mueller matrix approach to eliminate an artifact from apparent CD signal show that conformation of MPL films cast from aqueous solutions at various pH depends on its pH. The solid state NMR spectrum of MPL film cast from aqueous solution shows broad linewidth compared with that of MPL powder due to heterogeneity of the molecular conformation. The molecular structure and conformation of MPL films cast from aqueous solution with various pH studied by using solid state NMR and solid state CD are also discussed.

Introduction

In recent years, there has been considerable interest in biopolymers because of concern over the environmental impacts arising from the disposal of petroleum based plastics. Poly(amino acid)s provide a class of biopolymers based on natural amino acids linked by amide bonds. Microbial poly(ε-L-lysine) (MPL) is made of L-lysine, having linkage between ε-amino and α-carboxyl group. MPL is biodegradable, antibiotic and water soluble. Applications of MPL as biodegradable fibers, food preservatives and drug carriers have been investigated. MPL has a highly reactive side chain, α-NH_2, therefore its derivatives are expected to have a wide variety of applications. CD spectra of solid sample with macroscopic anisotropy show apparent CD with artifact resulted from linear birefringence and linear dichroism[1)].

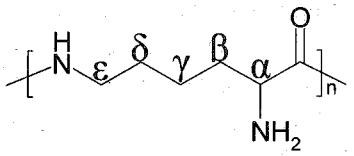

Figure 1. Structure of poly(ε-L-lysine)

Experimental

MPL was produced from the culture broth of a variant of *Streptomyces albulus* by Chisso Corp. Mn = 4090, Tm = 172.8°C and Tg = 88°C. ^{13}C solid state NMR spectra were measured with Chemagnetics CMX Infinity 300 operating at 75.0 MHz at room temperature. MAS speed was 7 kHz. Solid state CD spectra were measured with modified JASCO J-500 by using artifact free method[2)].

Keywords: Microbial polymer, Solid State NMR, Solid State CD, poly (ε-L-lysine), poly (amino acid)

Results and discussion

Solid state CD spectra

The CD spectra of the MPL films cast from a basic and an acidic pH aqueous solution are shown in Figure 2a and Figure 2b, respectively. The former have a negative band at about 220nm and a positive band at about 200nm. It suggests MPL film cast from a basic pH aqueous solution takes β-sheet like conformation. On the other hand, the latter have an only positive band at about 200nm. It suggests the conformation of MPL film cast from an acidic pH aqueous solution takes an electrostatically expanded chain. The similar CD spectra had been observed by Kushwaha *et al.*[3] and by us[4] in the solution CD measurements of synthesized and microbial ε-PL, respectively.

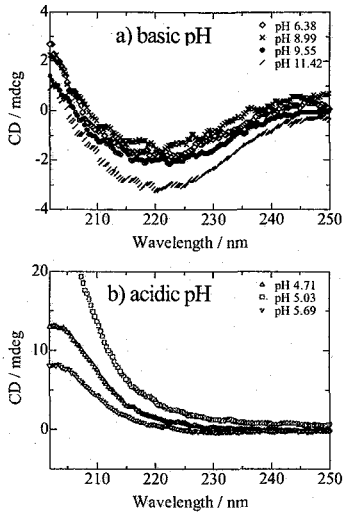

Figure 2. Solid state CD spectra of MPL film cast from a) basic pH, and b) acidic pH aqueous solution, respectively.

Solid state ^{13}C NMR spectra

^{13}C CP/MAS spectra of MPL film cast from aqueous solution of pH9, pH5 and pH3 are shown in Figure 3a, 3b, and 3c, respectively. Peaks are assigned based on the assignment of MPL[5]. The chemical shifts of aliphatic carbons in high field region of pH9 are almost the same as those of MPL. It suggests MPL film cast from a basic pH aqueous solution takes β-sheet like conformation in crystalline component. On the other hand, the chemical shifts of aliphatic carbons of pH5 and pH3 show a little upfield shift as compared with those of pH9 and they are almost the same as those of MPL/HCl. The peaks of carbonyl carbon were observed at 176.9ppm, 171.9ppm and 170.4ppm for pH9, pH5 and pH3, respectively. The chemical shifts of carbonyl carbon of pH5 and pH3 show about 5 ppm upfield shift as compared with that of pH9. It suggests the distance of intermolecular hydrogen bonding between α-carbonyl group and ε-amino group become longer as compared with that of pH9 or the hydrogen bonding brakes.

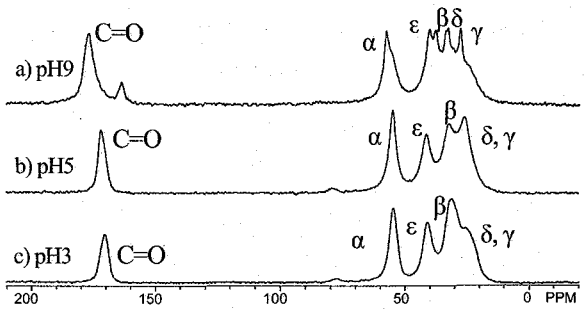

Figure 3. ^{13}C CP/MAS NMR spectra of MPL film cast from aqueous solution of a) pH9, b) pH5 and c) pH3, respectively.

References 1). Y. Shindo, M. Nishio and S. Maeda, *Biopolymers*, **30**, 405-413 (1990). 2) Y. Shindo, *et al.*, *J. Plast. Film Sheet.*, **17**, 164-183 (2001). 3) D. R. S. Kushwaha, *et. al.*, *Biopolymers*, **19**, 219-229 (1980). 4) H. Lee, *et. al.*, *Chem. Express.*, **6**, 683-686 (1991). 5) S. Maeda, *et. al.*, *J. Mol. Struct.*, **655**, 149-155 (2003).

P071

Characterization of Chitosan/Carboxymethyl Cellulose Complex by Solid NMR

Shiro Maeda[1], Yuko Fujimoto[1], Kensuke Sakurai[2]

[1]Division of Applied Chemistry and Biotechnology and [2]Division of Materials Science and Engineering, Graduate School of Engineering, University of Fukui, 3-9-1, Bunkyo, Fukui 910-8507, Japan

Molecular structure and formation mechanism of chitosan (CS) / carboxymethyl cellulose (CMC) polymer complex (CS/CMC) were elucidated by using high resolution solid state ^{13}C NMR and IR spectroscopies. Dilute hydrochloric acid aqueous solution was used for the solvent. A carbonyl carbon peak in 1:1 CS/CMC appeared at about 175ppm, which is slightly upfield compared with 178ppm in CMC-Na. This upfield shift was attributed to poly-ionic polymer complex formation between CS and CMC.

【Introduction】

There are many studies on chitosan/polysaccharide polymer complex and they are characterized by means of infrared spectroscopy (IR), differential scanning calorimetry (DSC), X-ray diffraction analysis, scanning electron microscopy, etc. In this work, solid-state NMR analysis was undertaken to elucidate intermolecular interaction between CS and CMC. A uniform cast film is obtained when a formic acid aqueous solution is used as a solvent because intermolecular interaction is weak. However, formylation of CS takes place and it causes complicated problem to elucidate intermolecular interaction. Therefore dilute hydrochloric acid aqueous solution was used as a solvent in this study, whereas intermolecular interaction between CS and CMC is strong, and mixture of two polymer solutions is cloudy.

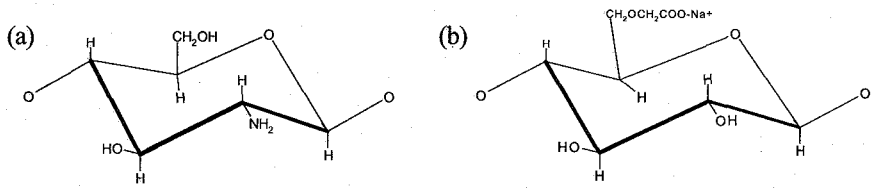

Figure1. Chemical structures of (a) chitosan and (b) carboxymethylcellulose.

【Experimental】

CS (Katakura Chikkarin Co. Ltd., the degree of deacetylation DAC=96%) was stirred for 8 hrs in 5% sodium perborate aqueous solution, filtered, washed with distilled water, and dried in vacuo for 24 hrs. Degree of polymerization of depolymerized CS was 479. CS and CMC-Na were dissolved in

Keywords: chitosan, carboxymethyl cellulose, solid NMR, polymer complex.

1% hydrochloric acid aqueous solution and in water, respectively, to make 2 wt% solution. CS/CMC polymer complex was prepared as follows. Each solution was mixed to be the ratio of 3:1, 1:1, and 1:3 stoichiometrically. Cloudy whitish mixtures were centrifuged and the precipitate was filtered and dried under vacuum. Solid state ^{13}C CP/MAS NMR spectra were measured with Chemagnetics CMX Infinity 300 operating at 300MHz for ^{1}H and 75MHz for ^{13}C at room temperature. Chemical shifts were referenced to hexamethylbenzene (17.35 ppm from Me_4Si).

【Results and Discussion】

Figure 2 shows the ^{13}C CP/MAS NMR spectra of (a) CS, (b) 1:1 CS/CMC polymer complex, and (c) CMC-Na, respectively. Peaks appeared in the region from 50 to 100 ppm are carbon peaks of glucosamine ring of CS. Carbonyl carbon peak in 1:1 CS/CMC appeared at about 175 ppm, which is slightly upfield compared with 178 ppm in CMC-Na. Carbonyl carbon peaks in CS/CMC complex with a ratio of 1:1, 1:3, and 3:1 are deconvoluted into two peaks; a peak which has the same chemical shift with CMC-Na is assigned to carbonyl carbon peak of CMC-Na without complex formation, and another peak which has the same chemical shift with 3:1 CS/CMC complex is assigned to that with complex formation. The ratio of the latter peak is 25 % and 90 % in 1:3 and 1:1 CS/CMC complex, respectively. Upfield shift of carbonyl carbon peak via complex formation are considered as follows. Complex formation breaks intermolecular hydrogen bonding between carboxyl groups in CMC-Na which causes downfield shift of carbonyl carbon and makes poly-ionic complex between NH_3^+ of CS and COO^- of CMC resulting into upfield shift of carbonyl carbon. The formation mechanism of CS/CMC polymer complex derived from solid state NMR measurements agrees with that reported based on IR measurements[1,2].

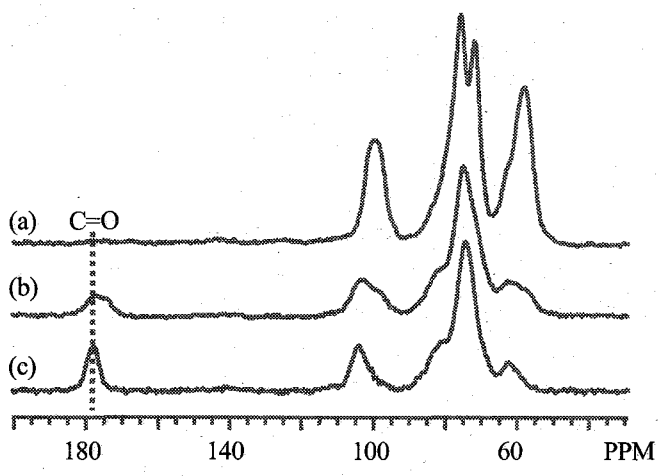

Figure 2. ^{13}C CP/MAS NMR spectra of (a)CS castfilm from 1% hydrochloric acid aqueous solution, (b) 1:1 CS/CMC complex, and (c) CMC-Na castfilm from aqueous solution.

【References】

1) C. Rosca, M. Popa, G. Lisa, G. Chitanu, *Carbohydrate Polym.*, 62, 35-41 (2005).

2) K.V. Harish Prashanth, F. S.Kittur, R.N.Tharanathan, *Carbohydrate Polym.*, 50, 27-33 (2002)

P072

固体 NMR による poly(ethylene-*co*-1,5-hexadiene)の構造と運動性

(奈良女院・生環)○山本優理、藤川亜紀、(東工大・精密工学)曽根正人、
(芝浦工大・工)永直文、(奈良女子大院・共生自然科学)黒子弘道

Structure and Dynamics of Poly(ethylene-*co*-1,5-hexadiene) as Studied by Solid State ^{13}C NMR

○Yuuri Yamamoto[1], Aki Fujikawa[1], Masato Sone[2],
Naofumi Naga[3] and Hiromichi Kurosu[1]
1) Nara Women's University, 2) Tokyo Institute of Technology, 3) Shibaura Institute of Technology

《Abstruct》
Poly(ethylene-co-1,5-hexadien) were prepared by copolymerization of ethylene and 1,5-hexadien(HD) and higher-order structure was studied by solid state ^{13}C NMR. The methylene peaks of the observed ^{13}C CP/MAS NMR spectra for the three samples are decomposed into three peaks. Three decomposed peaks of the methylene carbon are designated peaks α, β, γ from downfield. The highest field peak γ (31.4ppm) shifts lower field as compared with the amorphous polyethylene peak and the T_1 measurement shows that the mobility of the polymer become higher as the HD content is increased. This shows that even in the sample with the smallest content of HD, the conformation of peak γ is restricted to the structure of the trans rich conformation.

＜緒言＞

ポリエチレン主鎖に五員環構造を有する共重合体は、架橋ジルコノセン触媒によるエチレンと 1,5－ヘキサジエン（HD）の環化反応を伴う共重合により得られる。この共重合体の結晶構造を明らかにし、有用性を示すことは様々な高分子材料の構造決定や、分子設計につながると期待される。そこで、本研究ではポリエチレンの主鎖に五員環構造を形成することにより結晶構造にどのような変化が生じているのかを分子運動性や分子構造に着目して考察した。

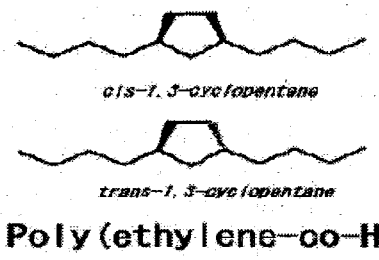

キーワード：Structure, Dynamics, Isomorphism

著者ふりがな：やまもと　ゆうり、ふじかわ　あき、そね　まさと、
なが　なおふみ、くろす　ひろみち

＜試料＞

試料は、架橋ジルコノセン触媒を用い、エチレンと1,5－ヘキサジエン（HD）の環化反応により HD 含量が 1.8%,9.7%,20.3%の 3 種の（エチレン－HD）共重合体を得た。それぞれ sample a, b, c とした。

＜測定＞

上記 3 種の試料についてJEOL EX-270 を用いて^{13}C CP/MAS測定、PST/MAS測定、T_1^c測定を行った。さらにメルトクエンチ処理を施した後にCP/MAS測定、PST/MAS測定を行った。

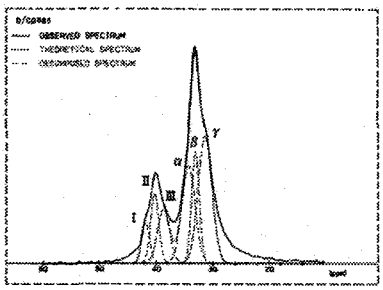

Figure.1 CP/MAS spectrum of sample b.

＜結果と考察＞

試料bのメルトクエンチ処理前の^{13}C CP/MASスペクトルをFig.1にスペクトルフィッティングの結果と共に示す。

また、各試料のメルトクエンチ前後の化学シフトをTable 1に示す。Fig.1およびTable 1にあるようにメチレン鎖は低磁場からピークα、β、γに分けられ、その化学シフト値から単斜晶、斜方晶、非晶に対応すると考えられる。

Table 1 ^{13}C chemical shifts of samples a, b and c(CP/MAS)

		Chemical shift/ppm		
		α	β	γ
Before Melt-quench	Sample a	34.30	32.90	31.35
	Sample b	34.30	33.05	31.35
	Sample c	34.30	33.20	31.35
After Melt-quench	Sample a	34.30	32.95	31.10
	Sample b	34.00	33.05	31.25
	Sample c	34.50	33.05	31.30

ヘキサジエン（HD）含有量の異なる 3 種の一番高磁場側のピーク(ピークγ)に着目すると、わずか 1.8 mol%の HD の取り込みがポリエチレン非晶とは異なるコンホメーションを形成させることが分かった。また、メルトクエンチ処理後において化学シフト値は処理前よりも高磁場シフトし、トランスコンホメーションをとる割合が増加していることから、メルトしてもその直後にトランスの構造をとろうとする傾向が強く、HD 含有量が多いサンプルほどよりトランスリッチな構造をとりやすいのではないかと考えられる。緩和時間測定において、1.8 と 9.7mol%のサンプルは 2 成分あらわれた。低磁場側の結晶系のピークに短い成分があらわれたのであるが、これは五員環がパッキング中に入ったことにより共結晶が起こり、パッキングの緩みにより運動性が高くなったためではないかと考えられる。以上のことより、HD を取り込むことでポリエチレン分子全体の運動性が大きく向上し、HD 含有量が多くなることで分子運動性が高くなることが分かった。

P073

固体NMRによるポリグルタミン酸金属錯体の構造研究

北大院工　○藤江正樹・鈴木晃生・平沖敏文

Metal ion Complexes of Poly(D-glutamic acid) by solid state NMR

Graduate School of Engineering, Hokkaido University, Sapporo, 060-8628.
Masaki FUJIE, Kouo SUZUKI, and Toshifumi HIRAOKI

The conformation of poly(D-glutamic acid)-metal ion complexes with Mg, Ca, Cd, and Pb was characterized by ^{13}C CP/MAS NMR spectroscopy. All complexes prepared in ambient temperature have an α-helical conformation as judged from the chemical shift values of the main chain carbon resonances. The chemical shift values of C_δ and $C_\gamma$resonances depend on the ionic radius of the metal ion used. The annealing effect of the complexes was investigated in order to elucidate their conformational stabilities. Ca-PGA keeps its comformation as an α-helix till 240 ℃, while conformations of other complexes show disordered states over 180 ℃.

1. 緒言

ポリペプチドは様々な規則構造をとることが知られている。Keith らはポリグルタミン酸 (PGA) の側鎖に Mg、Ca、Ba、Sr が結合した錯体の固体構造を X 線回折、電子線回折により調べ、Mg-PGA は α-helix、その他の PGA 金属錯体は β-sheet であることを示した。(1) この構造の差は用いた金属のイオン半径に起因すると考えられている。本研究では試料の調製温度に着目し、イオン半径の異なる幾つかの金属イオンが結合した PGA 金属錯体の二次構造を ^{13}C CP/MAS NMR により検討した。また構造安定性を調べるため、熱処理温度依存性を調べた。

2. 実験

Na-PGA と金属イオンからなる混合水溶液を、(1) 室温でエタノールを加えて沈殿させて得た試料 (室温調製) と、(2)90 ℃まで加熱し、その後冷却して得られた試料 (90 ℃調製) を用いた。また熱処理実験では、室温調製試料を真空下で約 20 時間加熱し、その後ゆっくりと室温まで戻した。固体 ^{13}C CP/MAS NMR は共鳴周波数 75MHz で、全て室温で測定した。$\frac{\pi}{2}$ パルスは 3.5μs、MAS 速度は 4kHz である。

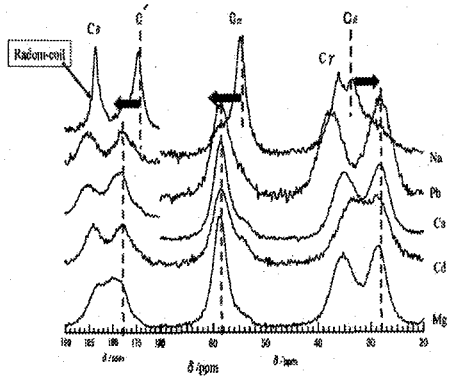

Fig.1 ^{13}C CP/MAS NMR spectra of PGA-metal ion complexes prepared in ambient temperature.

keyword: Poly(glutamic acid), secondary structure, metal ion
○ふじえ　まさき、すずき　こうお、ひらおき　としふみ

3. 結果と考察

調製温度依存性

室温調製試料の ^{13}C CP/MAS NMR スペクトルを Fig.1 に示す。ランダムコイル構造をとる Na-PGA に比べ、[2]PGA 金属錯体主鎖の C_α、C' のシグナルは低磁場側へ、側鎖の C_β のシグナルは高磁場側へ変化した。これは室温調製の試料は全て α-helix 構造をとることを示している。また側鎖 C_δ と C_γ の化学シフト量は金属イオン半径に依存して変化することがわかった。一方、90 ℃調製の試料のうち Mg-PGA は α-helix 構造をとり、Ca-と Pb-PGA はランダムコイルであることがわかった。これらの結果は PGA 金属錯体の二次構造は試料調製温度に依存することを示している。

熱処理温度依存性

Fig.2(a)～(d) にそれぞれ Mg-、Cd-、Ca-、Pb-PGA の熱処理温度を変えた試料の ^{13}C CP/MAS NMR スペクトルを示す。Ca-PGA では熱処理温度を 240 ℃に上げても化学シフト値は変化しておらず、α-helix 構造を保っているが、各シグナルの線幅は広がった。一方 Ca-PGA 以外の 3 つの試料では、180 ℃から 200 ℃以上の温度で化学シフトの変化や新たなピークの出現がみられた。これは高温で不規則構造に変化したことを示している。

以上の結果は、Ca-PGA の α-helix 構造は他の金属錯体に比べ安定であることを示している。

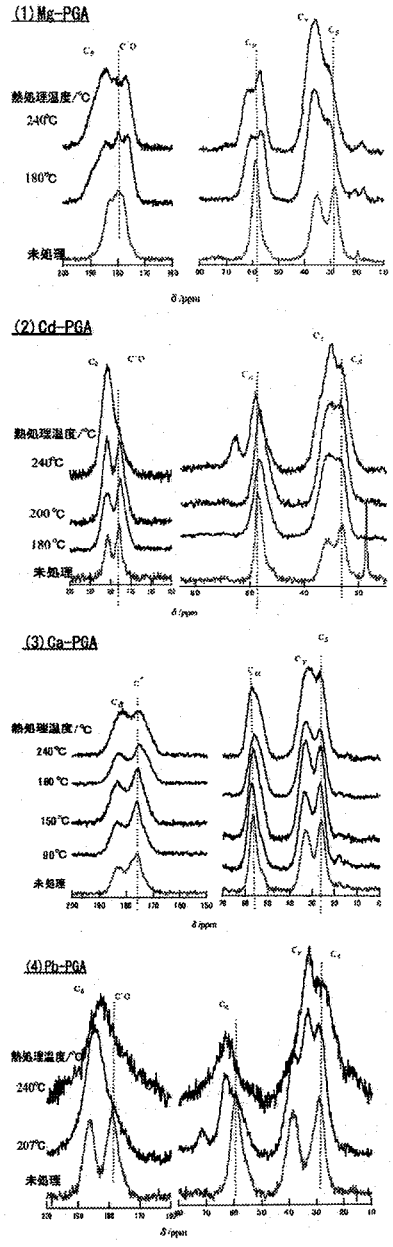

Fig.2 ^{13}C CP/MAS NMR spectra of PGA-metal ion complexes annealed at various temperatures. (a)Mg-PGA,(b)Cd-PGA, (c)Ca-PGA,(d)Pb-PGA.

References

(1)H. D. Keith, G. Giannoni, and F .J. Padde, *Biopolymers*, 7, 775(1969).

(2)H. Pivcova, V. Saudek, P. Schmidt, D. Hlavata, and J. Plestil, *Polymer*, 28, 991(1987).

P074

固体NMRによるポリ（アルキルプロピオレート）の研究

北大院工 ○鈴木晃生・馬渡康輝・田畑昌祥・平沖敏文

Poly(alkyl propiolate)s as Studied by Solid State NMR

Graduate School of Engineering, Hokkaido University, Sapporo 060-8628
Kouo SUZUKI, Yasuteru MAWATARI, Masayoshi TABATA and Toshifumi HIRAOKI

Poly(n-alkyl propiolate)s with methyl to pentyl groups were characterized by ^{13}C CP/MAS NMR spectroscopy. Their conformations were estimated form heteronuclear dipolar-coupled correlation measurements. With increasing the side chain length, the C_α resonances in the main chain for all polymers became sharper, with keeping their chemical shift values. On the other hand, the C_β resonances in the main chain showed broad singlet for methyl and ethyl groups, and doublet for propyl, butyl and pentyl groups. Any change was not observed in other resonances. These results suggest slow internal rotation in the side chain, due to the conjugation of π electrons from the main chain to the carbonyl group.

＜諸言＞Rh系触媒により合成された置換ポリアセチレンはcis-transoid構造をもち、その主鎖はらせん構造をとると推定されている立体規則性高分子である。[1] 置換ポリアセチレンのうち側鎖がエステル型のポリプロピオレートは固体状態で擬六方晶の構造をとることが見出された。本研究では側鎖エステル基のアルキル鎖長がメチル基からペンチル基までのポリ（n-アルキルプロピオレート）**(Scheme.1)**についてそれぞれ固体^{13}C CP/MAS NMR測定を行い、その構造を比較検討した。

＜実験＞モノマーは既知の方法で合成し、Rh錯体触媒の存在下、MeOH溶媒中で40℃、4時間重合して、目的の高分子を得た。^{13}C NMR測定はBruker DSX300（75MHz）とJEOL ECA920（230MHz）を用いて、室温で行った。

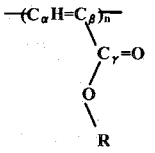

Scheme.1 Poly(n-alkyl propiolate)

＜結果・考察＞**Fig.1** にアルキル鎖長がメチル基からペンチル基までのポリ（n-アルキルプロピオレート）の^{13}C CP/MAS NMRスペクトル（コンタクトタイム 1ms）を示す。主鎖の帰属はdipolar dephasing法を用いて行い、135.1ppmのシグナルがC_α、128ppm付近のシグナルがC_βであることがわかった。またプロピル基では 128.0ppmのシグナルはシャープになり、さらに 126.1ppmに新たなシグナルが表れ、ダブレットになった。ダブレットの線幅はアルキル鎖長が長くなるにつれてシャープになった。一方、主鎖C_βに直接結合している側鎖C_γシグナルは一本のシャープな線形を示し、化学シフト値はエステル基の違いに依存せず変化しない。

Key Word: polyacetylene derivative / poly(propiolate) / structure
○すずき　こうお、まわたり　やすてる、たばた　まさよし、ひらおき　としふみ

これらの結果は、主鎖と側鎖カルボニル基が超共役しているために、側鎖は限られたコンフォメーションをとり、しかも大きな磁気的異方性を持つカルボニル基が主鎖に対して限られた配向をとることを示唆している。

Fig.2 に 230MHzにおける^{13}C-^{1}H dipolar-hetcor法で測定したポリ（n-ブチルプロピオレート）の二次元スペクトルを示す。混合時間が 0.3msでは空間的距離が近い直接結合したC_α-H_α間、C_β-H_α間とブチル基間内のC-H対に相関ピークが現れた。0.5msでは、新たにC_γ-H_αとC_γ-H_ε間にも相関ピークが現れた。1msでは、カルボニル基を含むエステル基内ではすべてのC-H間で相関ピークが現れ、スピン拡散が生じていることを示している。3msでは、C_βとエステル基のすべての水素原子間で強度が小さい相関ピークが現れた。しかも二本のC_βの相関ピークのパターンとピーク強度はほぼ同じである。一方主鎖のC_αとエステル基水素間には相関ピークが観測できなかった。

これらの結果はポリ(n-ブチル プロピオレート)の主鎖はランダムではなく規則構造を形成し、C_αとC_βの相関ピークの出方の違いから、側鎖は延びきったtransジグザグ構造をとることを示唆している。他のn-プロピル基、n-ペンチル基を持つポリ(プロピオレート)でも上記と同様なhetcorスペクトルが得られ、ポリ(n-ブチルプロピオレート)と同様な固体構造をとるものと考えられる。

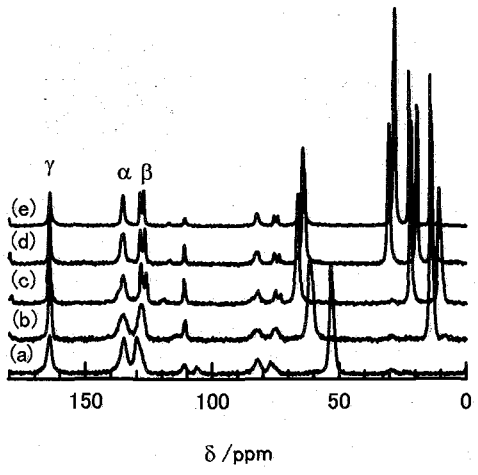

Fig.1 ^{13}C CP/MAS NMR spectra of Poly(alkyl propiolate) ; (a)methyl, (b)ethyl, (c) propyl, (d) butyl, (e)pentyl.

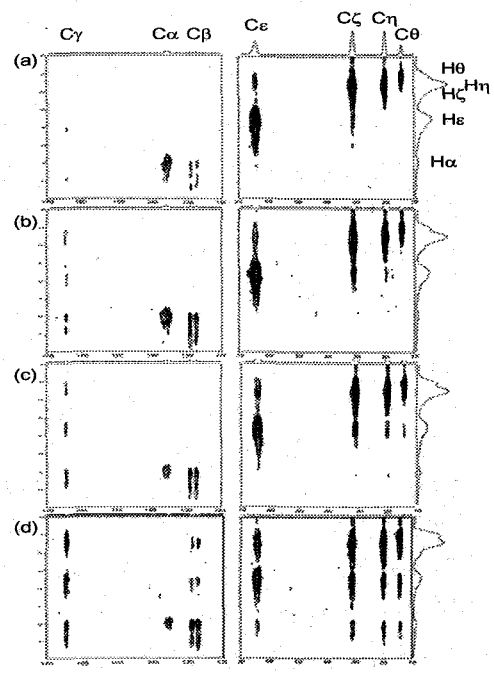

Fig.2 Dipolar-hetcor spectra of Poly(n-butyl propiolate) at 230MHz. Mixing time is (a)0.3ms, (b)0.5ms, (c)1ms, and (d)3ms from the top to the bottom.

本研究は、分子科学研究所「分子物質ナノサイエンス」の支援を得た。

1) M. Tabata, Y. Inaba, K. Yokota, Y. Nozaki, J. Polym., Sci., Pure Appl. Chem., A31(1998), 465.

P075

エリ蚕絹繊維の構造解析と関連した βシート構造を有するアラニンオリゴマーの固体 NMR 研究

(東京農工大工[1]、奈良女子大[2])
○小此木 美智[1]、堀口 久美子[1]、山内 一夫[1]、黒子 弘道[2]、朝倉 哲郎[1]

Solid-State NMR Analysis of Alanine Oligomers with β-Sheet Structures in Relation to the Structure of *Samia cynthia ricini* Silk Fiber

(Tokyo University of Agriculture and Technology[1], Nara Women's University[2])
○Michi OKONOGI[1], Kumiko HORIGUCHI[1], Kazuo YAMAUCHI[1],
Hiromichi KUROSU[2], Tetsuo ASAKURA[1]

To gain further insights for the precise structure of polyalanine regions in *Samia cynthia ricini* silk fibroin after spinning, we performed solid-state NMR analysis on a series of alanine oligomers. ^{13}C CP/MAS NMR spectra and ^{13}C spin-lattice relaxation times (T_1) were observed in accordance to β-sheet structure types and chain lengths. Especially for the well-known alanine tripeptide (Ala_3) with antiparallel[1)] and parallel[2)] β-sheet structures (AP-Ala_3 and P-Ala_3), we additionally observed ^{15}N and ^{17}O solid-state NMR chemical shifts for the central residue and made comparisons with theoretical chemical shift calculations.

【緒言】各種絹の構造・物性に関する知見の蓄積は、絹をベースとした新しい機能性材料の創製に必要不可欠である。その中で、野蚕種であるエリ蚕(*S.c.ricini*)の絹フィブロインは、Ala 連鎖領域と Gly リッチ領域が繰り返されたユニークな構造を有する(Fig.1)。本研究では、Ala 連鎖領域の詳細な構造解明を目標とし、一連のアラニンオリゴマーを用いた多角的な固体 NMR 研究を行なった。逆平行(AP)と平行(P) β-sheet 構造の違い、および、連鎖長に応じて形成されうる二次構造の違いを、^{13}C CP/MAS NMR や ^{13}C スピン-格子緩和時間(T_1)測定を行なうことで順次評価した。また、二種類の β-sheet 構造をとるアラニン三量体(Ala_3)[1),2)]については、中央残基に着目した ^{15}N および ^{17}O 固体 NMR 観測も行ない、化学シフトの理論計算と合わせて帰属と構造の検討を行なった。

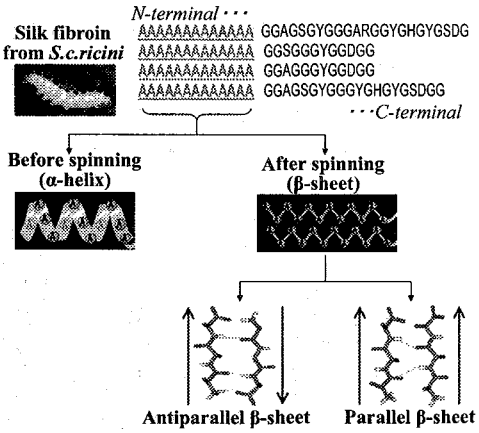

Fig.1 The primary sequence of *S .c. ricini* silk fibroin, together with a schematic diagram of the structural transition occurring in the polyalanine region before and after spinning.

【実験】P-Ala_3 と P-Ala_4 は各々、40%~DMF 水溶液と 75%~メタノール水溶液に溶解後、再沈殿させることにより調製し、IR にて構造を確認した(調製前は全て AP-構造)。^{13}C と ^{15}N CP/MAS NMR、および T_1 測定(Torchia 法)は CMX Infinity400 にて、^{17}O MAS NMR 測定は JEOL ECA930 にて行なった。化学シフト計算には Gaussian03 プログラムを利用し、GIAO-CHF 法にて行なった[基底関数:6-311G(d,p)]。

Keywords: アラニンオリゴマー、エリ蚕絹繊維、逆平行および平行 β-sheet 構造、スピン-格子緩和時間、化学シフト計算
おこのぎみち、ほりぐちくみこ、やまうちかずお、くろすひろみち、あさくらてつお

【結果・考察】 ① Ala_3、Ala_4 の ^{13}C CP/MAS NMR および T_1 緩和時間測定

Ala_4 は沈殿処理を工夫することにより、AP-と P-構造を形成することができた。各 ^{13}C CP/MAS スペクトルパターンは Ala_3 の場合と類似していた (Fig.2)。Ala_4 の詳細なピーク帰属は現在進行中であるが、Ala_3 の場合と同様、P-構造は AP-構造よりもペプチド鎖全体の運動性が著しく高いことが T_1 より示唆された。この差異は、不均一な β-sheet 構造を有するエリ蚕絹繊維での AP-、P-構造を検出するための有用なレファレンスデータとなった。

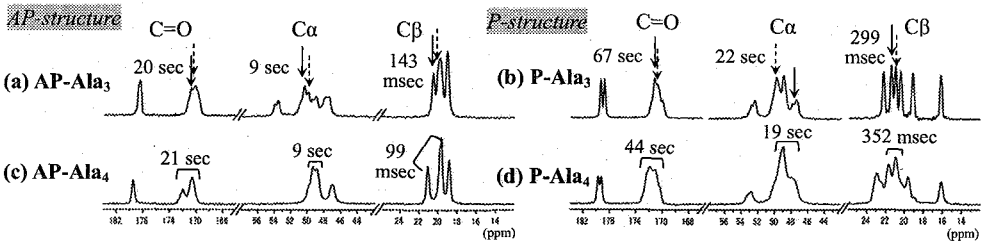

Fig.2 ^{13}C CP/MAS spectra of (a,b)Ala_3 and (c,d)Ala_4 with either AP- or P-structure. ⟶ and ⇢ indicate the peaks which were previously assigned[3] to the central residue (each representing the 2 crystallographically independent molecules A and B). The average T_1 values of Ala_3 and Ala_4 are also shown.)

② Ala_3 中央残基の ^{15}N、^{17}O 化学シフト計算値と実測値との比較

AP-と P-Ala_3 はともに、非対称単位中に 2 分子 A、B を有する。中央残基に着目した際、^{15}N CP/MAS スペクトル(Fig.3a,b)では P-構造の場合に 2.9ppm の化学シフト差が、^{17}O MAS スペクトル(Fig.3c,d)では AP 構造の場合に 33ppm の化学シフト差が観測された。AP-と P-構造の原子座標に基づいた化学シフト計算は、この実測パターンをよく再現し、A と B 分子の帰属を可能にさせた。本研究ではさらに、Ala_{12} を含んだ 32mer のエリ蚕絹モデルペプチドについても ^{17}O MAS スペクトルを測定し、異なる二次構造の観測に成功した。

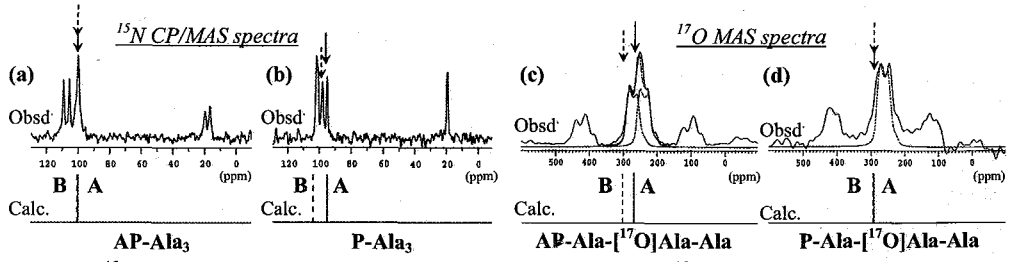

Fig.3 (a,b)^{15}N CP/MAS spectra of (a)AP- and (b)P-Ala_3, together with calculated ^{15}N chemical shifts for the central residue. (c,d)^{17}O MAS NMR spectra of (c)AP- and (d)P-Ala-[^{17}O]Ala-Ala, together with calculated ^{17}O chemical shifts for the central residue. Assignments to molecules A and B were achieved on the basis of well-reproduced chemical shift calculations.

【まとめ】Ala_3、Ala_4 を用いて得た ^{13}C 化学シフトおよび ^{13}C T_1 は、AP-と P-構造を区別するための有用なレファレンスデータとなった。Ala_3 の ^{15}N、^{17}O 固体 NMR 観測においても両構造の差異は明確であった。発表においては、連鎖長がさらに長いアラニンオリゴマー、および、エリ蚕絹繊維モデルペプチドについての測定結果も合わせて報告する予定である。

【参考文献】

1) J. Fawcett, N. Camerman, and A. Camerman, *Acta Crystallogr.* B31, 658(1975).
2) A. Hempel, N. Camerman, and A. Camerman, *Biopolymers* 31, 187 (1991).
3) T. Asakura, M. Okonogi, Y. Nakazawa, and K. Yamauchi, *J. Am. Chem. Soc.* 128, 6231 (2006).

P076

DEVELOPMENT OF A DYNAMICAL IMAGING SPECTROMETER USING A SMALL FERROMAGNET AND APPLICATION TO POLYMERIC GRADED MATERIALS *

Naoki Asakawa† and Yoshio Inoue

Department of Biomolecular Engineering, Tokyo Institute of Technology,
4259 B-55 Nagatsuta-cho, Midori-ku, Yokohama, Kanagawa 226-8501,
JAPAN email: nasakawa@bio.titech.ac.jp, Phone: 045-924-5796, FAX: 045-924-5827

Abstract: We have developed an instrument for dynamical imaging by NMR relaxation spectroscopy. We call "dynamical imaging" a imaging method for dynamical properties such as spectrum density function of local magnetic field fluctuation or the spatio-temporal correlation function. We built a versatile low field NMR spectrometer and a probe equiped with a small ferromagnet, which is a source of large magnetic field gradient up to 86T/m. The method will be applicable to polymeric graded materials.

Introduction

HUGE MAGNETIC FIELD GRADIENT by a small ferromagnet reaches from 10^2 up to 10^5 T/m, and it would be approximately 10^4 times larger than those by pulsed field gradient(PFG, ~20T/m), superconducting fringe field(SFF,~60T/m), and anti-Helmholtz superconducting magnet(~200T/m). Our final research object is to visualize not only the static but also dynamical structure using the huge magnetic field gradient. We are interested in dynamical properties such as spatial distribution of molecular dynamics or spatial variation of dimensionality of local field fluctuation. For our understanding of highly functionalized advanced matarials and devices, it is important for us to make visualization of molecular structure and molecular dynamics from the viewpoint of the wide range of continuous length and time scales. In this research, we seek for establishment of an NMR imaging method for visualization of spatio-temporal local correlation function. This can be done by frequency dependent relaxation time imaging. So far several MRI techniques for solids have been developed including PFG, SFF or stray field imaging(STRAFI). However, the PFG method suffers from a lack of gradient magnitude to achieve the sufficient spatial resolution for imaging of solid materials such as polymer films. Although SFF and STRAFI methods have been proved to be applicable to micro imaging, these methods are unfortunately not straightforward to perform variable frequency(variable field) measurements. In SFF based STRAFI measurements, one can vary the resonance frequency by changing the probe position in the superconducting magnet, but at the same time the magnetic field gradient can be inevitably changed. Therefore, one cannot perform variable frequency measurements under the constant gradient. As for STRAFI measurements with GarField type permanent magnet,[2] the fixed resonace frequency is mainly used. In order to overcome the issue, we have examined the possibility of an imaging method using huge magnetic field gradient from a small ferromagnet.

Experimental

We have developed a PulseBlaster-DDS(SpinCore, Inc.) and Linux based home-built versatile low field NMR/NQR spectrometer(5-30MHz) and NMR probes with a small ferromagnet(Fig.1)。 We employed a neodymium ($Nd_2Fe_{14}B$) magnet as a source of magnetic field gradient. A gauss-meter(Lake Shore 410) was

Key Words: NMR relaxation spectroscopy, instrumentation, magnetic field gradient, small ferromagnet, polymeric graded materials

†あさかわなおき、いのうえよしお

used for measurements of magnetic field from the magnet. We used ^{35}Cl nuclear quadrupole resonance of $KClO_3$ powders and ^1H NMR of water and two layer film of poly(vinylchloride)/poly(L-lactic acid)[PVC/PLLA] for the calibration of our instrument. The thickness of PVC and PLLA films are 200μm and 150μm, respectively.

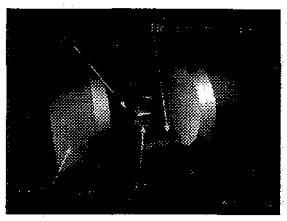

FIG. 1: Schematics of a versatile low field NMR instruments under static magnetic field by a small ferromagnet.

Results and Discussion

Fig.2 shows the magnetic field profile from the neodymium magnet. The value of x denotes the distance(mm) from the surface of the ferromagnet. At the surface, the magnetic field gradient was estimated as G = 86T/m, which is comparable to typical magnitudes of superconducting magnetic field gradient(~60T/m)[1] and of GarField magnet for STRAFI measurements(~20T/m)[2].

We succeeded in observation of ^1H NMR Hahn spin echo measurements under the static magnetic field gradient using the neodymium magnet. Fig.3 shows the two pulse Hahn echo spectra of the PVC film under the condition of x = 2mm(14.7T/m) and the PVC/PLLA two layer film at x = 5mm (3.5T/m). The effective magnetic field gradient was calculated by the following equation: $G = \frac{dB_{\mathrm{eff}}}{dy} = \frac{B(y)}{\sqrt{B_0^2+B(y)^2}} \cdot \frac{dB(y)}{dy}$, where B_0, $B(y)$, and B_{eff} respectively denote the external static field from electromagnet, the field from the neodymium magnet, and effective external field.

We will perform variable frequency longitudinal relaxation measurements in order to obtain information about dimensionality of fluctuation of the local field, namely functional shape of spectrum density function.

Acknowledgments

This work is supported by Ministry of Education, Culture, Sports, Science and Technology(Japan) through a Grant-in-Aid for young scientist category A(No.16685012).

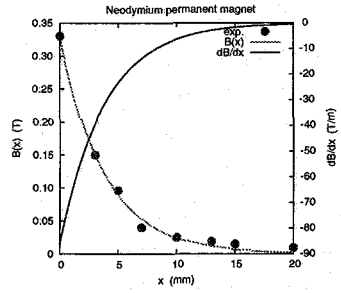

FIG. 2: The profiles for magnetic field and magnetic field gradient by a small neodymium magnet($Nd_2Fe_{14}B$).

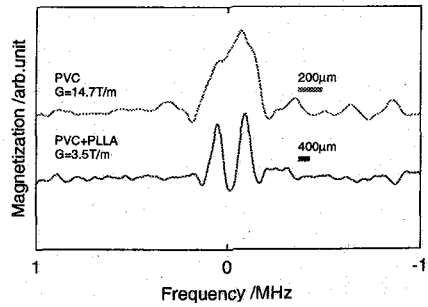

FIG. 3: One-dimensional ^1H imaging of polymer films by two pulse Hahn echo measurements at the resonance frequency of 28.1MHz(echo time:100μs).

[1] R.Kimmich et al., *J. Magn. Reson.*, **91**, 136(1991).

[2] P.M.Glover et al., *J.Magn.Reson.*, **139**, 90(1999).

P077

Solid-State NMR Observation of Strain-Induced β-Form in Poly[(*R*)-3-hydroxybutyrate]

Yusuke Nishiyama[1], Toshihisa Tanaka[2], Toshio Yamazaki[1], and Tadahisa Iwata[2]

[1]Genomic Sciences Center, RIKEN Institute, Tsurumi-ku, Yokohama, Kanagawa 230-0045, Japan, and [2]Polymer Chemistry Laboratory, RIKEN Institute, 2-1 Hirosawa, Wako-shi, Saitama 351-0198, Japan

Poly[(*R*)-3-hydroxybutyrate] (P(3HB)) has been extensively studied as a biodegradable and biocompatible thermotropic polymer. Iwata et al. succeeded in processing uniaxial P(3HB) films and fibers with high tensile strength by two-step drawing and annealing procedures [1]. Two types of molecular conformations of P(3HB) are observed in wide-angle X-ray diffraction (WAXD) measurement: the 2/1 helix conformation (α-form) [2] and the planar zigzag conformation (β-form) [3] (Fig. 1). β-form is responsible for a good mechanical properties of the two-step-drawn P(3HB) sample. However, no other methods besides WAXD have detected β-form in the P(3HB) films and fibers. Furthermore, no experimental observation of the molecular conformation of β-form has been reported: a β-form model was proposed on the basis of an empirical energy calculation [3].

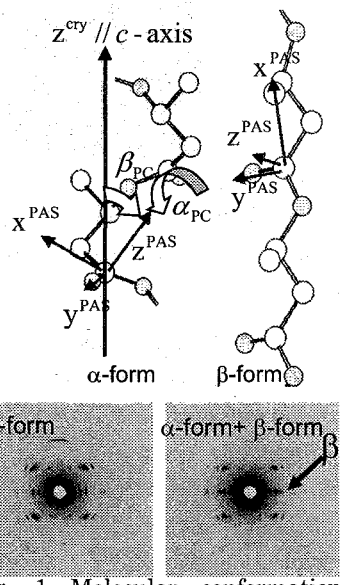

Fig. 1 Molecular conformation (PAS of the carbonyl carbon CSA tensor) and WAXD diagrams of α-form and β-form of P(3HB)

In this paper, we observe β-form separately from α-form and determine each molecular conformation by 2D NMR method. We observed $\sigma_2/\bar{\sigma}$ 2D NMR spectra under off-magic-angle spinning [4, 5, 6]. The σ_2 and $\bar{\sigma}$ terms represent chemical shift anisotropy (CSA) which depends on molecular conformation other than the angle around the spinning axis (γ-encoded). Thus the 2D spectra provide a sharp peak for a uniaxially oriented sample in which the molecules are rotationally distributed around the spinning axis. The peak position reflects the molecular conformation and is directly transformed into the principal axis system (PAS) orientation of the CSA tensor in the rotor-fixed frame [4]. The PAS orientation is closely related to the molecular conformation. For the carbonyl carbon, it is known that σ_{22} (y^{PAS}) tends to lie along the C=O bond axis, that σ_{33} (z^{PAS}) along the axis perpendicular to the O=C-C plane, and that σ_{11} (x^{PAS}) tends to lie in the O=C-C plane [7]. Thus, we can determine the orientation of the O=C-C moiety of α-form and β-form from each peak position of the carbonyl carbon in the $\sigma_2/\bar{\sigma}$ spectra.

The 2D NMR spectrum of the uniaxially cold-drawn P(3HB) film was recorded to observe α-form (Fig.2). A peak from α-form appeared in the 2D spectrum. The 2D peak is broadened due to the distribution of the crystal *c*-axis in the rotor-fixed frame. Taking account of this effect, we calculate the spectra for various (α_{PC}, β_{PC}) angles which describe orientation of PAS in the crystal frame with z^{cry} axis parallel to the *c*-axis (Fig. 1). We obtain the plot of the root-mean-squared deviation (RMSD) between the experimental spectra and the calculated spectra. Minimun RMSD structures were obtained for (α_{PC}, β_{PC})=(14°, 32°), which agrees well the previously proposed angle of (α_{PC}, β_{PC})=(26°, 31°) based on WAXD analysis.

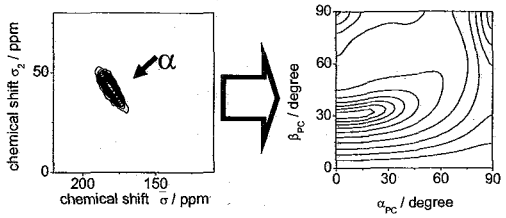

Fig. 2 $\sigma_2/\bar{\sigma}$ 2D NMR spectrum and RMSD plot of the cold-drawn P(3HB)

We observed the 2D NMR spectrum of the uniaxially two-step-drawn P(3HB) films (Fig. 3). A new peak from β-form appears at $\bar{\sigma}$=130 ppm. The RMSD plot gives a minimum value at (α_{PC}, β_{PC})=(10°, 76°(104°)), which is completely different from that of α-form. The agreement between the present result and the previously proposed model ((α_{PC}, β_{PC})=(4°, 10°) is satisfactory. While the WAXD experiment provides only the fiber repeat length, the present results reveal the orientation of the carbonyl carbon. This result strongly supports the molecular model of β-form.

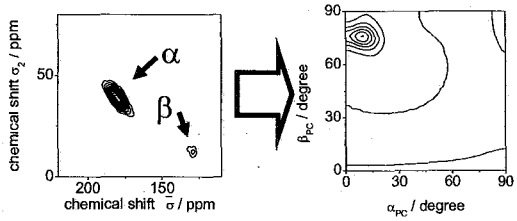

Fig. 3 $\sigma_2/\bar{\sigma}$ 2D NMR spectrum and RMSD plot of the two-step-drawn P(3HB)

References

[1] T. Iwata, Y. Aoyagi, M. Fujita, H. Yamane, Y. Doi, Y. Suzuki, A. Takeuchi, K. Uesugi, Macromol. Rapid Commun. 25 (2004) 1100.

[2] M. Yokouchi, Y. Chatani, H. Tadokoro, K. Teranishi, H. Tani, Polymer 14 (1973) 267.

[3] W.J. Orts, R.H. Marchessault, T.L. Bluhm, G.K. Hamer, Macromolecules 23 (1990) 5368.

[4] Y. Nishiyama, A. Kubo, T. Terao, J. Chem. Phys. 119 (2003) 3297.

[5] Y. Nishiyama, T. Yamazaki, T. Terao, J. Chem. Phys. 124 (2006) 064304.

[6] Y. Nishiyama, T. Tanaka, T. Yamazaki, T. Iwata, Macromolecules 39 (2006) 4086.

[7] N. Asakawa, T. Kameda, S. Kuroki, H. Kurosu, S. Ando, I. Ando, A. Shoji, Annual Reports on NMR spec. 35 (1998) 55.

Keywords: uniaxially drawn samples, biodegradable polymer, CSA

P078

固体重水素 NMR 法による有機 EL 非晶薄膜の検出

京大化研　○美濃 明良, 瀬々井 巌士, 梶 弘典, 堀井 文敬

Detection of amorphous thin films in organic LEDs by solid-state ^{2}H NMR

Institute for Chemical Research, Kyoto University, Gokasho, Uji, Kyoto 611-0011, Japan
○Akira Mino, Takashi Sesei, Hironori Kaji, and Fumitaka Horii

Abstract

In organic light-emitting devices(LEDs), it is considered that the hole transport property is closely related to the molecular structure. However, the analysis has been difficult because materials in organic LEDs are in amorphous thin film state. *N,N'*-diphenyl-*N,N'*-di(*m*-tolyl) benzidine(TPD) is widely used as a hole transport material in organic LEDs. In this study, we attempted solid-state ^{2}H NMR detection of vacuum-deposited TPD thin films with 100 nm thicknesses. For the deuterated TPD thin films, we could successfully observe clear Pake patterns both for methyl-^{2}H and aromatic-^{2}H in TPD. The detailed orientational distributions will be discussed in the presentation.

1. 緒言

近年、有機エレクトロルミネッセンス(EL)素子は注目を集めており、そこに用いられる有機非晶質材料の電荷輸送特性の解明が期待されている。電荷輸送特性の解明には素子中における分子の構造解析が必要であるが、非晶状態であることに加え、超薄膜であることからその解析は容易ではない。本研究では、有機 EL 素子の正孔輸送材料として知られる *N,N'*-diphenyl-*N,N'*-di(*m*-tolyl)benzidine (TPD)(図 1)の重水素化試料を合成し、100 nm 程度有機非晶薄膜に対して ^{2}H NMR シグナルの検出が可能であるか、さらには分子の構造解析への検討を行った。

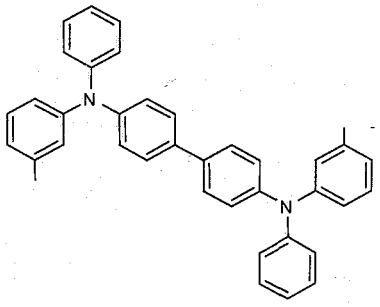

Fig. 1. The structure of TPD

2. 実験

測定に際して、Aldrich 社製の TPD の重水素化を行った。得られた重水素化試料(D-TPD)に対して溶液 ^{1}H および溶液 ^{2}H NMR 測定を行った結果、TPD の重水素化率はそれぞれメチル基で 95 %および 91%、芳香環で 85 %および 81 %であった。この D-TPD を真空蒸着法を用いて NMR 測定用ガラス基板に膜厚 100 nm となるように蒸着した。これを 150 枚作製し、すべてを NMR 試料管に供した。静磁場($\boldsymbol{B}_0$)に対し平行および垂直となるように設置した試料基板に対しての固体 ^{2}H NMR 測定を行った(図 2)。リファレンスとして D-TPD を 200 ℃の溶融状態から 0 ℃まで急冷することによって得た非晶粉末状試料に対しても同様の測定を行った。測定は全て Chemagnitics CMX-400 infinity 分光計を用いて、9.4 T の静磁場下、室温にて行った。

Keywords : 有機 EL, 非晶, 薄膜, 固体 NMR, ^{2}H NMR

○みのあきら, せせいたかし, かじひろのり, ほりいふみたか

3. 結果と考察

飽和回復法により D-TPD 非晶粉末試料のスピン－格子緩和時間(T_{1D})を測定した結果、メチル基では 5.6±0.3 s、芳香環では 12.3±0.2 s という値が得られ、メチル基の緩和時間は予想よりも長い値となった。

図3には各試料に対する固体 ^{2}H NMR 測定の結果得られたスペクトルを示している。(a) は D-TPD 非晶粉末試料に対する測定によるスペクトルである。メチル基の共鳴線が±17 をピークに持つ Pake パターンとして、また芳香環由来の共鳴線が±64 をピークに持つ Pake パターンとしてそれぞれ現れている。図 3(b), (c)にはそれぞれ薄膜試料を $\boldsymbol{B}_0$ に対して垂直および平行に配置した場合の ^{2}H NMR スペクトルを示す。これらのスペクトルから、100 nm 程度の薄い蒸着膜に対しても固体 NMR 測定が可能であることが分かる。図 3(b), (c)を比較すると、$\boldsymbol{B}_0$ に対する基板の向きによるスペクトルの形状変化があまり見られないことから、巨視的には基板に対する分子の配向がないことが示唆される。しかし、(b)と(c)とのスペクトルではメチル基と芳香環のシグナル強度比に若干の違いが見受けられる。この違いに対しては、今後、さらに充分な S / N を有するスペクトルを得ることにより検討を行う予定である。また、有機 EL 素子において正孔注入層に用いられるフタロシアニン系材料に対しても重水素化により同様の検討を行う予定である。

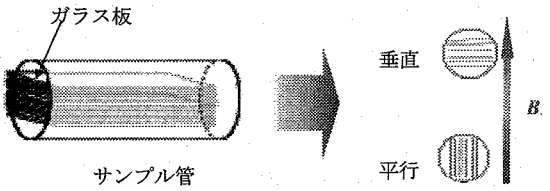

Fig. 2. The arrangement of substrate

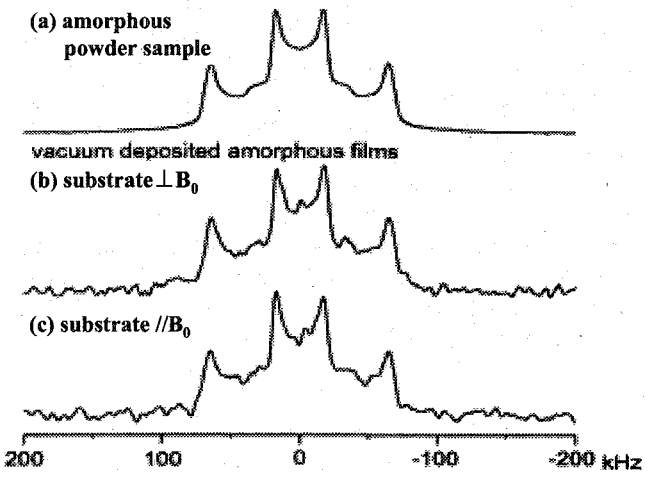

Fig. 3. Solid-state ^{2}H NMR spectra of vacuum deposited amorphous D-TPD; (b) substrate⊥$\boldsymbol{B}_0$, (c) substrate//$\boldsymbol{B}_0$. The spectrum of amorphous powder D-TPD is also shown in (a) for reference.

P079

Molecular dynamics in paramagnetic materials as studied by magic-angle spinning deuterium NMR

Motohiro Mizuno, You Suzuki, Kazunaka Endo
Graduate School of Natural Science and Technology, Kanazawa University, Kanazawa Kakuma-machi 920-1192, Japan

The technique of ^{2}H MAS NMR spectroscopy is presented for the investigation of molecular dynamics in paramagnetic materials. For paramagnetic samples with several structurally nonequivalent sites, the isotropic paramagnetic shift due to Fermi-contact interaction is useful for separation of the spinning sideband patterns from the deuterons in the different sites. The use of two-dimensional NMR spectroscopy for separation of the spinning sidebands is discussed. The simulation of two-dimensional ^{2}H NMR spectrum including paramagnetic effects and molecular motions is performed.

Introduction

^{2}H NMR spectroscopy is a powerful method for studying molecular dynamics and local structure in solids. However, the line broadening of a few hundred kHz for the static-powder ^{2}H NMR spectrum and the molecular motion with intermediate rate obviously lead to poor spectral resolution and low sensitivity. To remove these difficulties, the enhancements of the signal-to-noise ratio and of the sensitivity to dynamic processes due to the MAS ^{2}H NMR method have been demonstrated for the diamagnetic materials. The ^{2}H MAS NMR spectra with spinning sideband is sensitive to the motion with the rates, $k<10^3$ s^{-1}, $k>10^7$ s^{-1}, which are almost undetectable in the static-powder ^{2}H NMR spectrum. Therefore, the ^{2}H MAS NMR spectral analysis is effective for studying molecular dynamics in paramagnetic samples. We have developed the simulation method of the static-powder ^{2}H NMR spectrum for the paramagnetic materials. The reliable information about the molecular motion, the local structure and the paramagnetic ion can be obtained from the ^{2}H NMR spectral simulation including both the quadrupole interaction and the paramagnetic interaction. In the present study, we investigated experimentally and numerically the application of the MAS ^{2}H NMR method to the paramagnetic materials. The use of two-dimensional NMR spectroscopy for separation of the spinning sidebands is discussed. The simulation of two-dimensional ^{2}H NMR spectrum including paramagnetic effects and molecular motions is performed.

Experimental

The ^{2}H NMR spectra were measured by a Chemagnetics CMX-300 spectrometer at 45.826 MHz. The ^{2}H NMR MAS spectra of deuterated $NiCl_2 \cdot 6H_2O$ crystal were obtained using 7.5 mm rotor at 5 kHz.

Results and Discussion

The time evolution of the magnetization vector $\boldsymbol{M}^+(t)$ under MAS can be written as $\boldsymbol{M}^+(t) = \boldsymbol{L}(t)\boldsymbol{M}^+(0)$, where $\boldsymbol{L}(t) = \exp\{(i\boldsymbol{\Omega}(t) + \boldsymbol{W} + \boldsymbol{R}(t))t\}$. $\boldsymbol{\Omega}(t)$ is the diagonal matrix composed by the frequencies at each deuterium site determined by the quadrupole interaction and the paramagnetic interactions. $\boldsymbol{W}$ is a kinetic matrix composed by the rate k of the deuterium jumping between each site. $\boldsymbol{R}(t)$ is a matrix of the spin-spin relaxation due to the paramagnetic interaction. For the short time period Δt , by assuming time–independent $\boldsymbol{\Omega}(n\Delta t)$,

Keywords: deuterium NMR, magic-angle spinning, paramagnetic material

$\boldsymbol{L}(n\Delta t) \approx \exp\{(i\boldsymbol{\Omega}(n\Delta t) + \boldsymbol{W})\Delta t\}\boldsymbol{L}((n-1)\Delta t)$ is obtained. $\boldsymbol{M}^{+}(n\Delta t)$ is calculated by diagonalizing $(i\boldsymbol{\Omega}(n\Delta t) + \boldsymbol{W})$. The ^{2}H NMR MAS spectrum can be obtained by Fourier transform of $\boldsymbol{M}^{+}(n\Delta t)$. Fig. 1 shows the experimental ^{2}H NMR MAS spectra at 293 K obtained by chemical shift echo (π-τ-π/2) sequence. For six water molecules in $NiCl_2 \cdot 6H_2O$, four coordinated waters are directly coordinated to the metals, whereas two crystallization waters do not. So, the deuterons of coordinated waters show larger isotropic paramagnetic shift than those of crystallization waters. The asymmetric line shape of the spectrum is caused by the dipolar interaction between ^{2}H nucleus and Ni^{2+}. The spinning side-band patterns reveal that the electric field gradient (EFG) at ^{2}H nuclei in coordinated and crystallization waters are already averaged by the fast 180° flip of the water molecule at 293 K. Fig.2 shows two-dimensional one-pulse (TOP) spectrum. The ^{2}H NMR broad-line spectra of deuterons of coordinated and crystallization waters in the paramagnetic $NiCl_2 \cdot 6H_2O$ crystal could be separated by the TOP spectrum. The TOP method is convenient for the separation of the ^{2}H NMR spectra of the deuterons with different contact shifts, since a two-dimensional data matrix is obtained from a one-dimensional MAS spectrum [1]. However, the TOP spectra are represented by a superposition of absorption and dispersion lineshapes which reduces the resolution of the spectra. The methods for separation of ^{2}H NMR spectra using isotropic paramagnetic shift are discussed by comparing TOP and other two-dimensional methods.

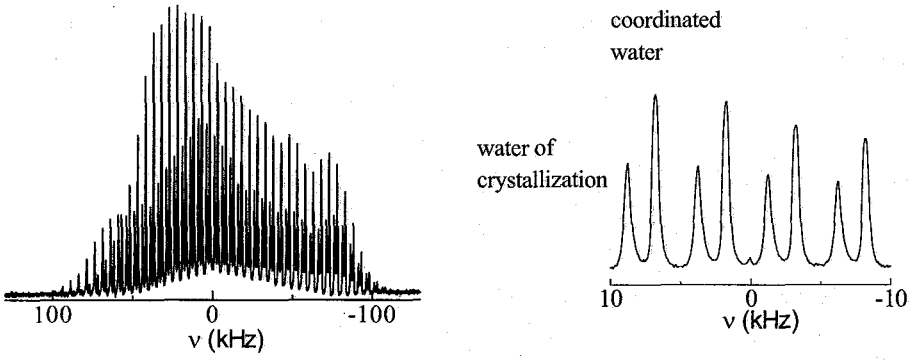

Fig. 1 ^{2}H MAS NMR spectrum of $NiCl_2 \cdot 6H_2O$ at 293 K

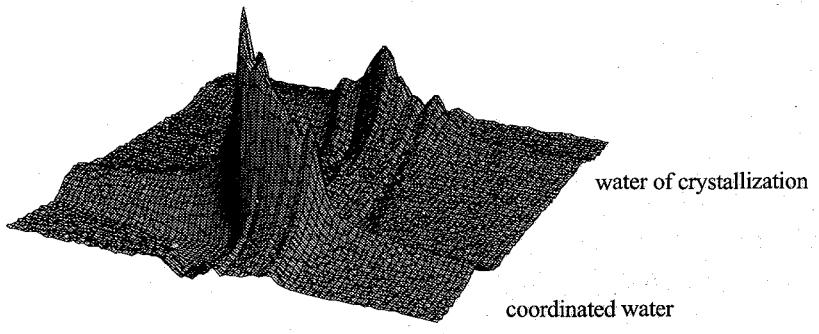

Fig.2 ^{2}H NMR TOP spectrum of $NiCl_2 \cdot 6H_2O$ at 293 K

[1] B. Blümich, P. Blümler and J. Jansen, Solid State Nucl. Magn. Reson. **1**, 111 (1992).

P080

N,N'-diphenyl-*N,N'*-di(*m*-tolyl)benzidine の中性、カチオン、ジカチオン状態における反磁性、常磁性、フェルミコンタクトシフト

京大化研　○山田知典、塚本直樹、日下康成、梶弘典、堀井文敬

Diamagnetic, paramagnetic, and Fermi contact shifts of *N,N'*-diphenyl-*N,N'*-di(*m*-tolyl)benzidine in neutral, cationic, and dicationic states

Institute for Chemical Research, Kyoto University, Gokasho, Uji, Kyoto 611-0011, Japan
○Tomonori Yamada, Naoki Tsukamoto, Yasunari Kusaka, Hironori Kaji, and Fumitaka Horii

N,N'-diphenyl-*N,N'*-di(*m*-tolyl)benzidine (TPD) is a widely used hole transport material in organic LEDs. In this study, we have analyzed the ^{15}N chemical shift changes accompanying dicationization of TPD, measured by solid-state ^{15}N NMR. Quantum chemical calculations clarify that the change of the chemical shifts originate from the changes of xx and yy components of paramagnetic term, both of which are perpendicular to the nitrogen lone pair, $2p_z$. Compared to the two terms, the changes of the paramagnetic zz components and all the diamagnetic components are found to be negligible. Since the paramagnetic term depends on the orbital angular momentum of p-orbital, the changes of the paramagnetic xx and yy components should be related to the occupancy of $2p_z$ orbital. This is supported by natural population analysis, which indicates the decrease of $2p_z$ occupancy with dicationization. The analysis for cationic TPD will be also discussed.

[緒言] 有機 EL 正孔輸送材料の電子状態を明確にすることは、その正孔輸送特性を考察する上で重要である。本研究では、有機 EL 正孔輸送材料として広く知られている *N, N'*-diphenyl-*N, N'*-di(*m*-tolyl)benzidine (TPD、図 1) の、非晶およびジカチオン状態における電子状態に関する知見を得ることを目的として、固体 ^{15}N NMR 測定から得られた化学シフトに関し、その理論的解釈を量子化学計算によって行った。

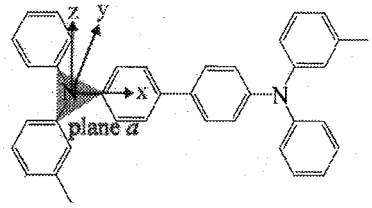

Fig. 1. Constitutional formula of TPD. x and y axes are in the plane *a*, and z axis is perpendicular to the plane *a*.

[実験] ^{15}N 同位体ラベルした TPD (^{15}N-TPD) を合成し、これを用いて中性 (非晶) 試料および五塩化アンチモンドープ試料を作製した。中性試料は、^{15}N-TPD を 200 °C の溶融状態から 0 °C に急冷することによって作製した。五塩化アンチモンドープ試料は、^{15}N-TPD のクロロホルム溶液に、三当量の五塩化アンチモンのクロロホルム溶液を混合した後、減圧乾燥することによって作製した。これらの試料に対して、等方化学シフトを与える CP/MAS ^{15}N NMR 測定および ^{15}N 化学シフト異方性 (CSA) 測定を行った。測定はすべて Chemagnetics CMX-400 分光計を用い、9.4 T の静磁場下、室温にて行った。

キーワード：有機 EL、反磁性、常磁性、フェルミコンタクト、量子化学計算

○やまだとものり、つかもとなおき、くさかやすなり、かじひろのり、ほりいふみたか

TPDの中性、ジカチオン状態について、量子化学計算によって構造最適化を行った。得られた構造に対して、遮蔽テンソルの反磁性項と常磁性項を計算した。計算は、密度汎関数法 (DFT) にてB3LYP汎関数および6-31G(d) 基底関数を用い、Gaussian03によって行った。

[結果・考察] 図2に固体 ^{15}N NMR測定を行った結果を示す。縦線で示したのは、量子化学計算によって得られた中性およびジカチオン状態におけるTPDの^{15}N核の等方化学シフトσ_{iso}および化学シフトテンソルの主値σ_{11}、σ_{22}、σ_{33}である。実測のスペクトルとの比較から、五塩化アンチモンドープ試料がジカチオンであることが示唆された。

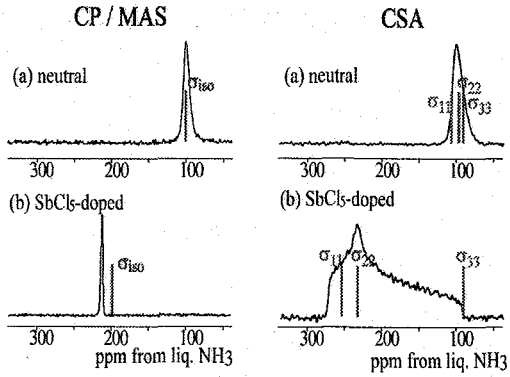

Fig. 2. CP/MAS ^{15}N NMR spectra and ^{15}N CSA spectra of neutral (a) and $SbCl_5$-doped (b) samples. Vertical lines indicate σ_{iso}, σ_{11}, σ_{22}, and σ_{33} of neutral (a) and dicationic (b) TPD obtained by quantum chemical calculations.

量子化学計算による構造最適化の結果、TPDは、中性、ジカチオンのいずれの状態においても、N原子とこれに結合した三つのC原子が同一平面 (図1の平面 *a*) 上に存在することがわかった。

表1に、中性およびジカチオン状態における、^{15}N核のσ_{iso}および化学シフトテンソルの対角成分σ_{xx}、σ_{yy}、σ_{zz}の、反磁性項ならびに常磁性項の計算結果を示す。ここで、xおよびy軸は平面 *a* 内にあり、z軸は平面 *a* に垂直であるとした (図1)。この結果から、σ_{xx}およびσ_{yy}の常磁性項が大きく変化することが明らかになった。遮蔽テンソルの $\alpha\beta$ 成分 ($\alpha\beta$= xx, xy, ⋯, zz) の常磁性項が

$$\sigma'_{\alpha\beta} = \frac{\partial}{\partial B_\alpha} \langle \psi(B_\alpha) | \frac{-i\hbar e}{2mc} \sum_j \frac{L_{j\beta}}{r_j^3} | \psi(B_\alpha) \rangle |_{B=0}$$

で表されることから、この変化はN核周りの電子の軌道角運動量 *L* のxおよびy成分の変化に起因すると考えられる。ここで、$\psi(B_\alpha)$は磁場 B_α 存在下での波動関数、r_j は核と電子 *j* の距離を表す。この軌道角運動量の変化は、natural population 解析によって示された、軌道角運動量のz成分が0である、N原子の$2p_z$軌道の占有数の減少と密接に関係していると考えられる。発表当日には、カチオン状態におけるフェルミコンタクトシフトについて検討を行った結果も報告する予定である。

Table 1. The diamagnetic and the paramagnetic terms of the chemical shift tensor for ^{15}N of neutral and dicationic TPD obtained by quantum chemical calculations. The values are relative to the diamagnetic isotopic shielding of neutral TPD.

	diamgnetic term / ppm		paramagnetic term / ppm	
	neutral	dication	neutral	dication
σ_{iso}	0.0	-1.2	100.5	199.1
σ_{xx} *	-2.8	-5.3	99.8	243.5
σ_{yy} *	-10.6	-4.6	105.4	263.1
σ_{zz} *	13.2	6.3	96.3	90.6

* (σ_{xx}, σ_{yy}, σ_{zz}) corresponds to (σ_{22}, σ_{33}, σ_{11}) and (σ_{11}, σ_{22}, σ_{33}) for neutral and dicationic TPD, respectively.

P081

Structure of hydrous aluminosilicate melts (glasses): ending a long-standing controversy by ^{1}H-^{27}Al HETCOR and 3QMAS/HETCOR NMR

Xianyu Xue* and Masami Kanzaki
Institute for Study of the Earth's Interior, Okayama University, Misasa, Tottori 682-0193 Japan. *E-mail: xianyu@misasa.okayama-u.ac.jp

Introduction

The dissolution mechanisms of water in silicate melts and glasses is an issue of major interest in both earth sciences and materials sciences, because a small amount of water may have dramatic effects on their phase relations and physical properties, and these effects are strongly compositional dependent. Although it is now generally accepted that water is dissolved in (alumino)silicate melts/glasses as both molecular H_2O and hydroxyls (OH), controversy remains as to the form of OH groups. For Al-free silica and alkali silicate compositions, SiOH has been confirmed to be a major OH species by ^{29}Si MAS and $^{1}H \rightarrow ^{29}Si$ cross-polarization (CP) MAS NMR studies; its formation is thought to be largely responsible for the reduction of melt viscosity, via breakage of the strong Si-O-Si linkages. However, for aluminosilicate compositions, debate continues as to whether similar depolymerization occurs (e.g. Zeng et al., 2000), or whether the dissolution of water merely involves M-H cation exchange and formation of bridging OH (Si(OH)Al) and MOH complexes (e.g. Kohn et al., 1989). The controversy arose mainly due to ambiguities in the interpretations of ^{29}Si and ^{27}Al NMR and vibrational spectra, as their resolutions tend to be lowered in the presence of Al.

In this study, we have applied 1D ^{1}H MAS NMR and $^{27}Al \rightarrow ^{1}H$ CP MAS NMR, as well as 2D ^{27}Al triple-quantum (3Q) MAS NMR, $^{27}Al \rightarrow ^{1}H$ heteronuclear correlation (HETCOR) (2D CP MAS) and high-resolution 3QMAS/HETCOR NMR techniques to anhydrous and hydrous $KAlSi_3O_8$ (Or), $NaAlSi_3O_8$ (Ab) and $NaAlSiO_4$ (Ne) glasses containing 1~2 wt% H_2O to shed new light on the dissolution mechanisms of water in aluminosilicate melts (glasses). The $^{27}Al \rightarrow ^{1}H$ CP MAS NMR technique provides direct information about H-Al proximity and, combined with knowledge from ab initio calculations, leads to unambiguous identification of AlOH. The 2D $^{27}Al \rightarrow ^{1}H$ HETCOR and 3QMAS/HETCOR NMR results allowed the ^{27}Al NMR parameters of Al(Q^3)-OH to be revealed for the first time.

Experimental

Anhydrous glasses were synthesized from analytical-grade Na_2CO_3/K_2CO_3, Al_2O_3 and SiO_2 via melting at 1500~1650°C. Hydrous glasses were synthesized by melting anhydrous glass plus deionized water in a sealed Pt capsule at 2 kbar and 1400~1500°C, followed by isobaric quenching, using an internally heated gas pressure vessel, similar to that described in Xue and Kanzaki (2004). The NMR spectra were obtained using a Varian Unity-Inova 400 spectrometer and a Doty 4 mm CP MAS probe at a resonance frequency of 104.3 MHz for ^{27}Al and 400.4 MHz for ^{1}H. Chemical shifts are referenced to tetramethyl silane (TMS) for ^{1}H and 1 M aqueous $Al(NO_3)_3$ for ^{27}Al.

Keywords: hydrous, aluminosilicate, glass, ^{1}H-^{27}Al, HETCOR, 3QMAS/HETCOR

Results and Discussions

The ^{1}H MAS NMR spectra of hydrous glasses show peaks near 1.4-1.7, 4, and 6.5 ppm (Fig. 1). The ^{27}Al→^{1}H CP MAS NMR spectra acquired with a range of contact times (0.25-20 ms) (Fig. 2) suggest that the components near 1.4-1.9 ppm, 6.5 ppm and 4 ppm represent protons increasingly farther away from Al (less enhanced by CP). In combination with knowledge from ab initio calculations (Xue and Kanzaki 2001, 2004), the peak near 1.4-1.9 ppm can be unambiguously attributed to AlOH. Peaks near 6.5 ppm can be best attributed to SiOH in the vicinity of Al, and that near 4 ppm may be due to SiOH farther away from Al (plus minor molecular H_2O).

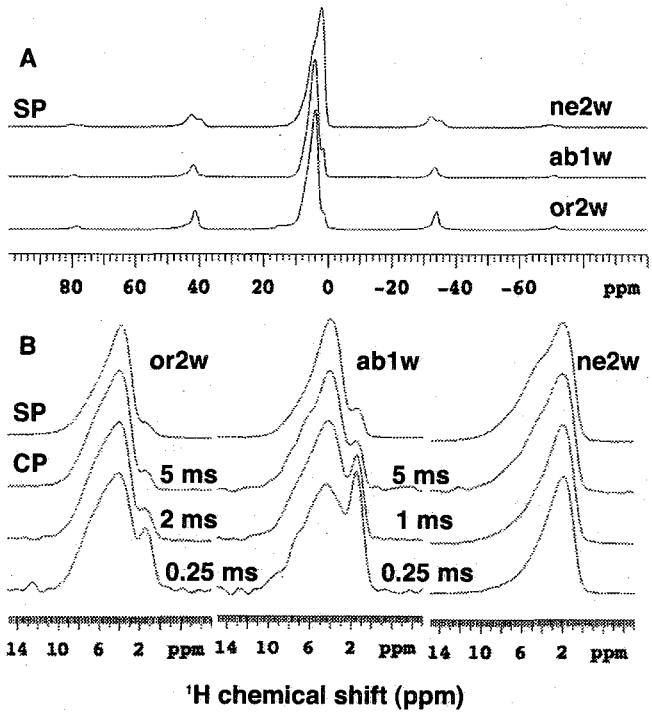

Fig. 1. ^{1}H MAS NMR (SP) and ^{27}Al→^{1}H CP MAS NMR (CP) spectra (**a**), and an enlarged view near the central band (**b**) for hydrous Or glass with 2.3 wt% H_2O (or2w), Ab glass with 1.2 wt% H_2O (ab1w) and Ne glass with 2.0 wt% H_2O (ne2w). Contact times for the CP spectra (0.25, 1, 2 and 5 ms) are as marked.

All the ^{27}Al MAS NMR and 3QMAS NMR spectra contain a single, unresolved peak attributable to four-coordinate Al (Fig. 2). On the other hand, the 2D ^{27}Al →^{1}H HETCOR and 3QMAS/HETCOR NMR spectra acquired with a contact time of 1 ms for hydrous Or and Ab glasses (Fig. 3) clearly show two peaks: a main peak with a maximum near 4 ppm and a smaller one near 1.2 ppm in the ^{1}H dimension. From the ^{1}H chemical shift information, the former may be attributed to the dominant Al Q^4 and the latter to Al Q^3-OH. The estimated mean ^{27}Al isotropic chemical shift (δ_i^{Al}) for Al Q^3-OH are 64~68 ppm, about 3~6 ppm larger than those of Al Q^4. Their quadrupolar coupling constants are within the range of the latter.

Despite the difference in δ_i^{Al}, it is only through $^{27}Al \rightarrow {}^{1}H$ HETCOR and 3QMAS/HETCOR, but not ^{27}Al MAS or 3QMAS NMR that the peaks are resolved.

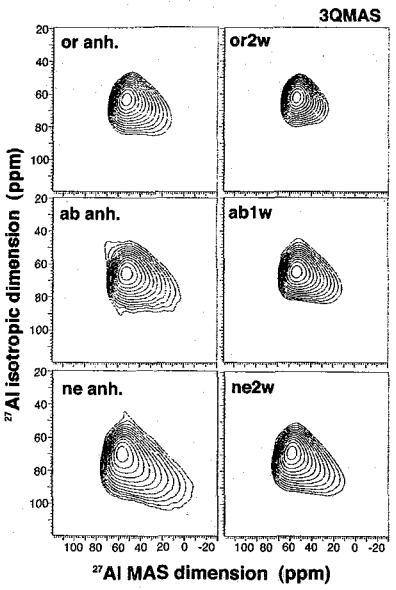

Fig. 2. ^{27}Al 3QMAS MAS NMR spectra of anhydrous (anh.) and hydrous Or, Ab and Ne glasses. All contours are drawn in logarithmic scale with 12 levels and a spacing factor of 1.4.

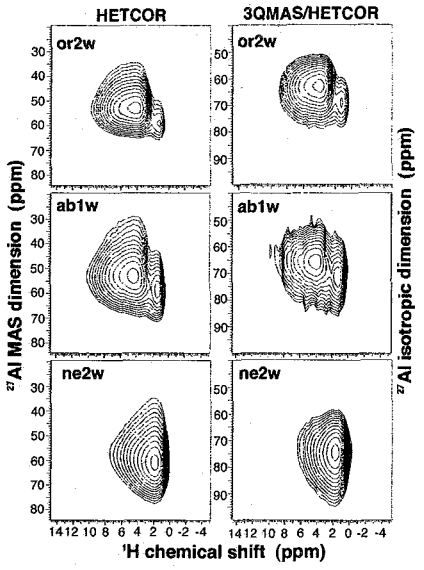

Fig. 3. $^{27}Al \rightarrow {}^{1}H$ HETCOR (left) and 3QMAS/HETCOR spectra (right), acquired with a contact time of 1 ms, for hydrous Or, Ab and Ne glasses (as labeled in Fig. 1). All contours are drawn in logarithmic scale with 12 levels and a spacing factor of 1.2.

Conclusions

Our ^{1}H MAS and $^{27}Al \rightarrow {}^{1}H$ CP-MAS NMR data, combined with ab initio calculation results, indicate that the OH species in hydrous Or, Ab and Ne glasses are in the form of SiOH and AlOH, with the abundance of the latter increasing with bulk Al/Si ratio. Our 2D $^{27}Al \rightarrow {}^{1}H$ HETCOR and 3QMAS/HETCOR results provided the first direct information for the ^{27}Al NMR parameters for Al Q^3-OH in hydrous aluminosilicate glasses.

This study has demonstrated that depolymerization and formation of AlOH/SiOH is a general water dissolution mechanism for polymerized aluminosilicate melts (glasses), and HETCOR and 3QMAS/HETCOR NMR experiments involving ^{1}H are the key to its revelation.

References

Kohn, S.C., Dupree, R., and Smith, M.E. (1989) A multinuclear magnetic resonance study of the structure of hydrous albite glasses. Geochimica et Cosmochimica Acta, 53, 2925-2935.

Xue, X. and Kanzaki, M. (2001) An ab initio calculation of the ^{17}O and ^{1}H NMR parameters for various OH groups: Implications to the speciation and dynamics of dissolved water in silicate glasses. Journal of Physical Chemistry B, 105, 3422-3434.

Xue, X. and Kanzaki, M. (2004) Dissolution mechanisms of water in depolymerized silicate melts: Constraints from ^{1}H and ^{29}Si NMR spectroscopy and ab initio calculations. Geochimica et Cosmochimica Acta, 68(24), 5027-5057.

Zeng, Q., Nekvasil, H., and Grey, C.P. (2000) In support of a depolymerization model for water in sodium aluminosilicate glasses: Information from NMR spectroscopy. Geochimica et Cosmochimica Acta, 64, 883-896.

P082

金属錯体Alq_3の構造－発光特性相関の解明

京大化研　○久我香子・日下康成・梶 弘典・小野山吾郎・堀井文敬

Two-Dimensional Double-Quantum ^{15}N Solid-State NMR Characterization of the Isomeric States in Tris(8-hydroxyquinoline) Aluminum(III) (Alq_3)

Takako Kuga, Yasunari Kusaka, Hironori Kaji, Goro Onoyama, Fumitaka Horii
Chemical Research, Kyoto University, Uji, Kyoto 611-0011, JAPAN

Abstract: The isomeric states of tris(8-hydroxyquinoline) aluminum(III) (Alq_3) have been analyzed by an advanced solid-state NMR technique, ^{15}N two-dimensional double-quantum (2D DOQSY) NMR. This experiment correlates the principal axis directions of the two relevant ^{15}N chemical shift tensors. Therefore, the meridional (*mer*) and facial (*fac*) isomers are expected to be clearly distinguished by this technique. The experimental 2D DOQSY spectra of the ^{15}N-labeled Alq_3 (^{15}N-Alq_3) in the α- and amorphous forms are well reproduced by the calculated spectrum for *mer*-Alq_3. In contrast, δ-Alq_3 provides a clearly different spectral pattern, which agrees well with the calculated pattern for *fac*-Alq_3. These results provide clear experimental evidence that the α- and amorphous Alq_3 are composed of *mer*-Alq_3 whereas δ-Alq_3 is composed of *fac*-Alq_3.

＜緒言＞　金属錯体tris(8-hydroxyquinoline) aluminum(III) (Alq_3、図 1)は、電子輸送特性と発光特性を併せ持つ優れた材料である。1987 年に有機electroluminescence (EL)デバイスに用いられて以来[1]、そのデバイス応用に関する研究が広く行われてきた一方で、その基礎的研究はほとんど行われてこなかった。2000 年にはじめて結晶構造が広角X線回折法(WAXD)によって調べられ[2]、その後、Alq_3にはα, β, γ, δ型の四つの結晶形が存在することがわかった[2,3] (最近では、ε型[4]も報告されている)。また、その構造がその発光特性、特に発光波長に大きく影響することは興味深い。

Alq_3分子には、図 1 に示した 2 つの構造異性体、meridional (*mer*)体とfacial (*fac*)体が存在する。Brinkmannら[2]はα-Alq_3をmeridional体からなると報告しており、多くの論文でそのように認知されている。しかし、昨年、Kodakのグループ[4]は単結晶構造解析の結果からα-Alq_3はfacial体からなるとの報告を行っている。また、™-Alq_3に対し、Cölliらはfacial体からなると報告している[10]。しかし、その粉末WAXDパターンはmeridional体からなると仮定してもわずかにR因子が大きくなるのみであり、facial対であると明確に断定するには至っていない。これらの背景に基づき、我々はこれまで^{27}Alおよび^{13}C固体NMR測定によるAlq_3の局所構造解析[5,6]を行ってきた。本発表では、^{15}N核を用いた二次元二量子固体(2D DOQSY) NMR法[7-9]を用いて、Alq_3分子の構造異性に関する明確な実験的確証を得るとともに、発光特性との相関について検討を行った。

＜実験＞　^{15}N核を同位体ラベルしたAlq_3 (^{15}N-Alq_3)は、$H^{15}NO_3$より合成した。昇華精

Key Word: Alq_3 / solid-state NMR / organic LED / double-quantum NMR
(くが たかこ, くさか やすなり, かじ ひろのり, おのやま ごろう, ほりい ふみたか)

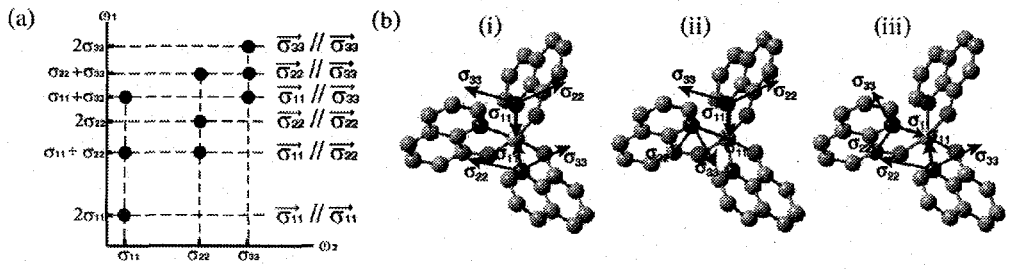

Fig. 1. (a)Schematic form of 2D DOQSY spectrum. (b)Schematic representation of chemical-shift tensor orientations in *mer*-Alq_3. There are three patterns of the coupled sites.

製によりα-Alq_3を、その熱処理によりδ-Alq_3を得た。非晶Alq_3は425 °Cからの急冷により得た。測定はChemagnetics CMX-400 Infinity分光計により、室温で行った。

＜原理＞ 2D DOQSY NMR測定では、二量子励起により2つのdipole間の配向相関を明らかにすることができる[7-9]。その2次元スペクトルの模式図を図1(a)に示す。縦軸ω_1は二量子遷移（2つの核の化学シフト異方性(CSA)の和、$\omega_A+\omega_B$）であり、横軸ω_2は一量子遷移（各サイトのCSA、ω_A及びω_B）である。二量子遷移（$\omega_A+\omega_B$）は核の配向関係を反映する。本実験では、^{15}N-Alq_3を用いることにより、2つの^{15}N核間の相関から、Alq_3の構造についての情報を得た。図1(b)に示したように、例えば*mer*-Alq_3でのdipole-dipoleカップリングの場合、考え得るカップリングは分子内だけで3通りある。シミュレーションでは、各カップリングによるスペクトルの合計として結晶のスペクトルを得た。

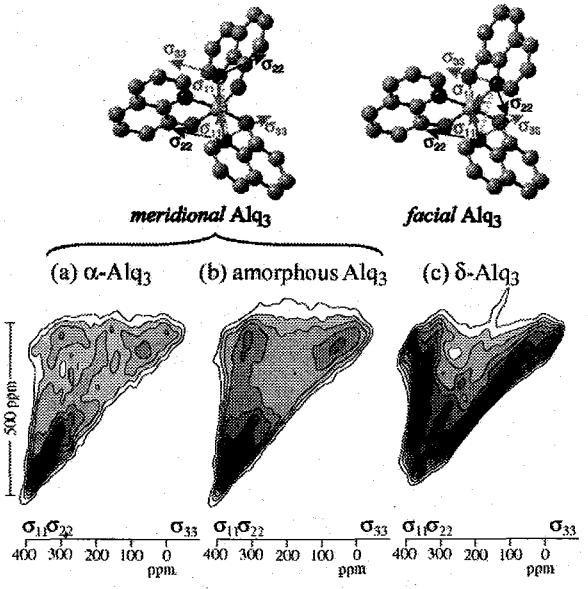

Fig. 2. Experimental ^{15}N 2D DOQSY spectra of (a) α-, (b) amorphous, and (c) δ-Alq_3. The corresponding photographs under UV light are shown below. Alq_3 in the meridional and facial isomeric states are shown above.

＜結果・考察＞ 図2にα-、非晶、およびδ-Alq_3に対する2D DOQSYスペクトルを等高線表示で示す。色が濃い方がスペクトル強度が高いことを示す。α-Alq_3、非晶Alq_3では、(σ_{11}, $2\sigma_{11}$)近傍でシグナル強度が最大となっているのに対し、δ-Alq_3ではこの部分にピークが見られない(図2(c))。

この違いは分子内$^{15}N-^{15}N$配向相関の違い、すなわち構造異性に起因すると考えられる。*mer*-Alq_3では図 1(b)のように 3 パターンの分子内のdipole-dipole カップリングが存在し、パターン(i)では向かい合った^{15}N核のσ_{11}方向がほぼ反平行に並んだ配向をとるため、(σ_{11}, $2\sigma_{11}$)に強いピークが観測される（図 1(a)参照）。一方*fac*-Alq_3での分子内カップリングでは全て図 1(b-ii)のような配向をとり、σ_{11}は互いにほぼ直交しており、この場合(σ_{11}, $2\sigma_{11}$)近傍にピークが出ないと予想される。

δ-Alq_3の結晶構造についてはCölleらが、その構成分子をそれぞれmeridional体、facial体と仮定した場合のX線構造解析結果を公表している[10]。これらを用いて、2D DOQSYシミュレーションを行った（図 3(a)(b)）。この結果からも分子の構造異性が 2D DOQSYのスペクトルパターンによって区別できることが明確であろう。実測スペクトル（図 2(c)）と比較すると、図 3(b) において (σ_{11},$\sigma_{11}+\sigma_{33}$) (σ_{33}, $\sigma_{22}+\sigma_{33}$)付近に実測スペクトルに見られないピークが生じている。3つリガンドが互いに直交性が高い場合には、このようなピークが生じるが、リガンドの直交性・等価性を低くした構造を仮定すると、より実測に近いスペクトルが得られた（図 3(c)）。

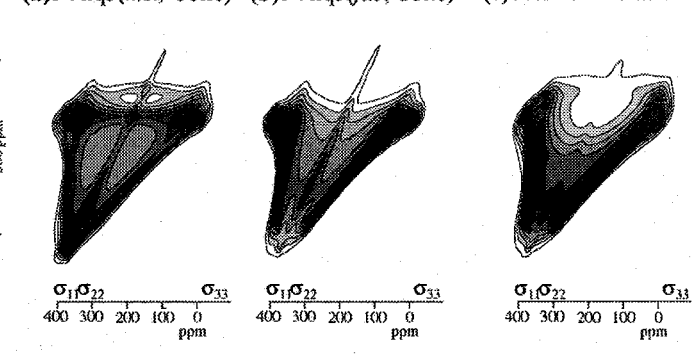

Fig. 3. Calculated ^{15}N 2D DOQSY spectra of δ-Alq_3 in the case when the crystal are considered contains (a)the meridional isomer reported by Cölle, (b)the facial isomer reported by Cölle, (c) Best-fit simulation for δ-Alq_3.

さらにα-Alq_3について、Brinkmannらの示したmeridional分子からなるα-Alq_3の結晶構造に基づく 2D DOQSYシミュレーションを行った（図 4）。(a)が隣接分子間の相互作用を無視した場合、(b)が考慮した場合である。これらの比較から分子間の相互作用の影響が(σ_{11}, $2\sigma_{11}$) (σ_{22}, $2\sigma_{22}$) (σ_{33}, $2\sigma_{33}$)を通る傾き 2 の稜線として現れるのがわかった。(c)(d)では、さらに構造の乱れを考慮して化学シフトテンソルの主軸方向に分布をもたせた。(c)は隣接分子間の相互作用を無視した場合、(d)が考慮した場合である。(a)との比較から構造の乱れにより、スペクトル上部で等高線の幅が広がることがわかった。

これらを図 2 の実測スペクトルと比較すると、α-および非晶Alq_3においても構造のdisorderが観測されていることがわかる。スペクトル上部の等高線の幅は非晶Alq_3の方が広く、α-Alq_3より大きなdisorderがあると示唆される。

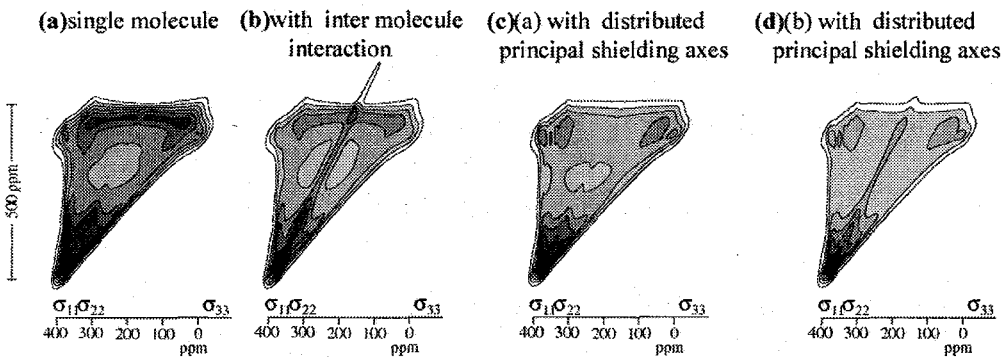

Fig. 4. Calculated ^{15}N 2D DOQSY spectra of *mer*-Alq_3 in the α crystal form (a) without inter-molecular interaction, (b) with inter-molecular interaction, (c) without inter-molecular interaction and with distributed principal shielding axes and (d) with inter-molecular interaction and with distributed principal shielding axes.

一方、分子間の相互作用による稜線はα-Alq_3で明瞭に観測される。非晶Alq_3で、稜線が見えないのは、隣接分子との配向が一定でないため、相互作用が平均化されるからと考えられる。

以上の解析から、α-Alq_3はmeridional体、δ-Alq_3はfacial体であることがこの解析より明確となった。また、非晶Alq_3の実験結果は、図 4(c)に示した分子間相互作用を考慮しない一分子のdisorderのあるmeridional体に対する計算スペクトルとして、うまく再現されることから、非晶Alq_3もmeridional体からなっていること、および非晶試料においては分子間相互作用が平均化されて観測されないことが示された。

さらにAlq_3分子の発光特性という観点では、α-Alq_3や非晶Alq_3が黄緑色の発光をしているのに対してδ-Alq_3が青色発光をしている。よって、構成する分子が*mer*-Alq_3ならば黄緑色*fac*-Alq_3ならば青色の発光になり、発光色とAlq_3分子の構造異性との相関が示されたといえる。

＜References＞

(1) Tang, C. W.; VanSlyke, S. A. *Appl. Phys. Lett.* **1987,** 51, 913.
(2) Brinkmann, M.; Gadret, G.; Muccini, M.; Taliani, C.; Masciocchi, N.; Sironi, A. *J. Am. Chem. Soc.* **2000,** 122, 5147.
(3) Braun, M., et al. *J. Chem. Phys.* **2001,** 114, 9625.
(4) Rajeswaran, M.; Blanton, T. N. *J. Chem. Crystallogr.* **2005,** 35, 71.
(5) Kaji, H.; Kusaka, Y.; Onoyama, G.; Horii, F. *Jpn. J. Appl. Phys.* **2005,** 44, 3706.
(6) Kaji, H.; Kusaka, Y.; Onoyama, G.; Horii, F. *J. Am. Chem. Soc.* **2006,** 128, 4292.
(7) Schmidt-Rohr, K. *Macromolecules* **1996,** 29, 3975.
(8) Schmidt-Rohr, K.; Hu, W.; Zumbulyadis, N. *Science* **1998,** 280, 714.
(9) Kaji, H.; Schmidt-Rohr, K. *Macromolecules* **2000**, 33, 5169; **2001,** 34, 7368; **2001**, 34, 7382.
(10) Cölle, M.; Dinnebier, R. E.; Brütting, W. *Chem. Commun.* **2002,** 23, 2908.

P083

1次元固体状態スピン交換 NMR による 9-ヒドロキシフェナレノンの互変異性の研究

（電気通信大学量子･物質工学科[1]・東邦大学理学部[2]）
○中村英章[1]・桑原大介[1]・古家野宏行[1]・間中泰輔[1]・持田智行[2]

Research of the tautomerisum for 9-hydroxyphenalenone by one-dimensional solid-state spin exchange NMR

Hideaki Nakamura[1], Daisuke Kuwahara[1], Hiroyuki Koyano[1], Taisuke Manaka[1], and Tomoyuki Mochida[2]
(Department of applied Physics and Chemistry , The University of Electro-Communications[1] , Department of Chemistry , Faculty of Science , Toho University[2])

We present a new NMR method to clarify the dynamics of proton tautomerism in solid 9-hydroxyphenalenone. Two ^{13}C resonance lines influenced by the proton tautomerism have a chemical-shift difference between them. In order to depict the precise potential curve of the proton tautomerism, the chemical-shift difference when the proton tautomerism is completely frozen is necessary. If the freezing temperature is under -100 ℃, it is very difficult to obtain the shift difference. The NMR experiments based on this new method are performed at a temperature significantly higher than -100 ℃. The new method yields the ^{13}C spin relaxation rates, the rates for the proton tautomerism, and the populations of the two tautomers. Using the populations and the ^{13}C chemical-shift difference at that temperature, we determine the chemical-shift difference at the freezing temperature.

プロトン互変異性、緩和速度、交換速度、ポテンシャルプロファイル

なかむらひであき、くわはらだいすけ、こやのひろゆき、まなかたいすけ、
もちだともゆき

1.緒言

9-ヒドロキシフェナレノン誘導体は互変異性に基づいた誘電応答を示す。その互変異性はプロトン移動と同期して引き起こされる。最近、9-ヒドロキシフェナレノンの相転移の振る舞いが持田らによって報告された[1]。彼らは、これらの誘導体の誘電応答が、プロトン互変異性と関連した分極反転によって引き起こされることを示した。

分子内または分子間水素結合は固体状態中でプロトン互変異性を生み出す重要な要因の1つである。9-ヒドロキシフェナレノン誘導体に関して、プロトン移動は分子内の水素結合に沿って起こる。加えて、分子は水素結合を持った孤立系と見なすことができる。それ故、それらは、水素結合によるプロトン互変異性と、誘電応答の関連性を研究するための理想的な系である。

Fig.1は9-ヒドロキシフェナレノンの2つの互変体を示す。プロトン互変異性に対するポテンシャル曲線の略図はFig.2示されている。プロトン移動のダイナミクスは反応座標に沿ったポテンシャルの形に大いに依存する。一般には、以下のパラメーター（交換速度k_1, k_{-1}、エネルギー差ΔG、反応エネルギー$\Delta G^{\dagger}$）がポテンシャル曲線を記述するために使われる。2つの互変体は図の上で左右対称であるが、結晶学的環境の差によるポテンシャルエネルギー差を持っている。

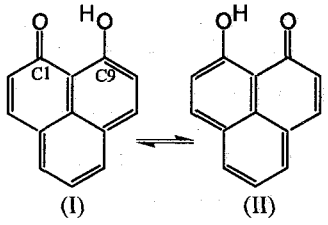

Figure 1. Two tautomers (Ⅰ) and (Ⅱ) of 9-hydoxyphenalenone.

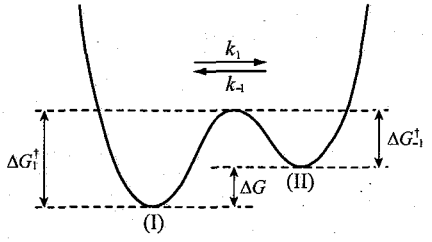

Figure 2. Potential curve for the proton transfer between two the tautomers (Ⅰ) and (Ⅱ) of 9-hydroxyphenalenone.

Limbachらは、ポリフィリン誘導体のプロトン移動のダイナミクスの研究において、^{15}Nマジックアングルスピニング（MAS）NMRスペクトルの分裂幅$\delta\nu$が、

$$\delta\nu = \frac{1-K}{1+K}\Delta\nu \tag{1}$$

で与えられることを見出した[2]。ここで$\Delta\nu$はプロトン互変異性が完全に止まっ

ている時の化学シフト差（静的な分裂幅と呼ぶことにする）、Kは平衡定数である。しかし、9-ヒドロキシフェナレノンの場合、互変異性が完全に止まる時の温度は-100℃以下である。安定した高速試料回転が実現可能な温度範囲の下限は、普通-100℃である。それ故、Doty Super-TV MAS プローブのような特殊なMASプローブでない限り、$\Delta\nu$の値を得ることはできない。たとえ特殊なプローブを使用したとしても、-140℃以下において 5kHz以上の試料回転速度を実現することは非常に難しい。

本研究において、我々はMAS NMR 実験からの静的な分裂幅$\Delta\nu$を求めるための新しい方法を提案する。我々は以下の 2 つの方法、交差分極マジックアングルスピニング（CP/MAS）と 1 次元（1D）固体状態スピン交換 NMR の組み合わせを用いた。

2.実験

NMRスペクトルは、Bruker MAS 4mm プローブを備えたBruker Avance 300 分光計を用いて記録した。NMR実験は^{13}Cに対して 75.43MHzで行った。試料回転速度は 9kHz、CP時間は 1mmであった。

我々が新しく考案した 1 次元スピン交換 NMR パルス系列は、

^{1}H : (π/2) (CP) Decoupling
^{13}C : (CP) (π/2) (π/2)$_{s.e.}$- τ -(π/2) acquision

である。ここでτは交換時間である。(π/2)$_{s.e.}$はC1 に対する共鳴線（共鳴Aとする）またはC9 対する共鳴線（共鳴B）の選択的励起を行う 90° パルスである。サンプルの温度はサマリウムアセテートのカルボキシル炭素の化学シフトを使って修正した。すべてのNMR実験は-100℃よりも高い温度で行った。高速試料回転下でCPを効率的に行うためにRAMP CP法を用いた。^{1}Hデカップリングには TPPMデカップリング系列を使用した。

3.結果と考察

Fig.3 は 1 次元スピン交換NMRパルス系列を用いて-70.6℃において記録された ^{13}C NMRスペクトルである。共鳴Aはスピン緩和やプロトン交換によって次第に大きくなる。従って、これらの強度の変化は、一般に、T_{1A}, T_{1B}, $1/k_1$, $1/k_{-1}$という時定数を使って表現することができる。

9-ヒドロキシフェナレノンは Tc=−18.2 ℃ で構造相転移を持つ。分裂幅$\delta\nu$は温

度の減少と共に 11.6ppm に漸近して近づくことが分かった。-70.6℃において$\delta\nu$は 7.26ppm なので、9-ヒドロキシフェナレノンの静的な分裂幅が 12ppm 付近と仮定すると、その時の平衡定数 K は方程式(1)から、-70.6℃において約 0.23 である。交換速度は 0.1s のオーダーである。よって交換速度は 0.01s のオーダーになる。これらの結果を元に最終的に磁化 A, B に対して、

$$\frac{M_{A,z}^{(A,+z)}(\tau)-M_{B,Z}^{(A,+z)}(\tau)}{\alpha M_A^{eq}}=1-P\cdot\tau+Q\cdot\tau^2 \qquad (2)$$

が導かれた。但し、$P=2x_2k_{-1}$, $Q=\frac{1}{4}Pk_{-1}$,

x_2は互変体(Ⅱ)の占有数である。最小二乗法を用いてP, Qの値はそれぞれ、$P=0.048\pm0.007$, $Q=0.0015\pm0.0006$ と求まった。これより、$k_{-1}=0.12\pm0.05s^{-1}$, $x_2=0.20\pm0.08$, $x_1=0.80\pm0.08$ が得られた。占有数からKは-70.6℃において 0.25 ± 0.10 である。-70.6℃におけるKと$\delta\nu$の値を用いて、我々は、静止な分裂幅が $\Delta\nu=12.1\pm2.6$ ppmであることを見出した。この値は9-ヒドロキシフェナレノンに対する上記の見積もりに非常に近い。この結果は本研究のNMR実験が静的な分裂幅$\Delta\nu$を正確に決定できることを示している。本研究で考案した新しいパルス系列の詳細及びポテンシャル曲線を特徴付けるその他のすべてのパラメーターについては会場にて報告する。

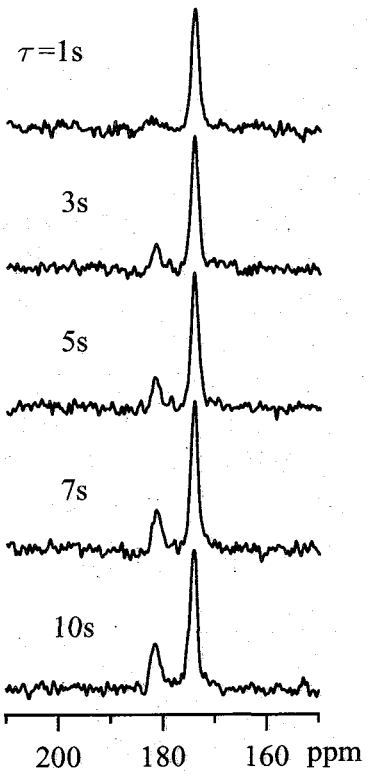

Figure 3. Variation in resonances A and B with the indicated exchange periods.

4.文献

(1) Mochida, T.; Kuwahara, D.; Miyajima, S.; Sugawara, T. *J. Phys. Chem. B* **2003**, *107*, 12315.
(2) Limbach, H.H.; Wehrle, B.; Schlabach, M.; Kendrick, R.; Yannoni, C.S. *J. Magn. Reson.* **1988**, *77*, 84.

P084

^{13}C-NMR 緩和時間および誘電緩和時間に基づく非晶質ジヒドロピリジン系薬物の分子運動性の測定

(国立衛研) ○阿曽幸男、吉岡澄江、宮崎玉樹、川西徹

Molecular mobility of some 1,4-dihydropyridines in the amorphous state determined by ^{13}C-NMR relaxation and dielectric relaxation measurements.

(National Institute of Health Sciences) Yukio Aso, Sumie Yoshioka, Tamaki Miyazaki, Toru Kawanishi

The crystallization rate of 1,4-dihydropyridines studied was in the order: nifedipine> nitrendipine> nilvadipine. The local mobility of amorphous nilvadipine, as indicated by β-relaxation time, was lower than that of nifedipine or nitrendipine. ^{13}C-NMR relaxation time measurements showed that crystalline nilvadipine exhibited higher molecular mobility than the other two drugs did. These results suggest that the crystallization rate of these drugs correlates with local mobility, and that local mobility affects stability of amorphous drugs as well as global mobility indicated by glass transition temperature.

はじめに

水に溶けにくい医薬品の溶解性を改善するために、非晶質化することが多くの医薬品において行われている。非晶質化した医薬品は結晶に比べ運動性が高く、保存中に結晶化しやすいが、ガラス転移温度(T_g)の高い高分子添加剤は非晶質薬物を安定化することが知られている。高分子はT_gを高めマトリックスのグローバルな運動を低下させる作用に加え、薬物と相互作用し、薬物のローカルな運動性を低下させることによって安定化することが示唆されている。本研究においてはFig. 1に示すジヒドロピリジン系薬物について、^{13}C-NMRスピン格子緩和時間(T_1)および誘電緩和時間の測定を行い、非晶質薬物の結晶化速度に及ぼすローカルな運動性の影響を考察した。

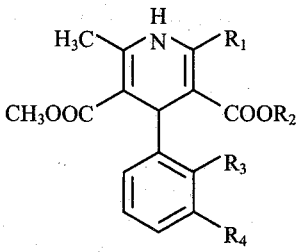

	R_1	R_2	R_3	R_4
nifedipine	CH_3	CH_3	NO_2	H
nitrendipine	CH_3	C_2H_5	H	NO_2
nilvadipine	CN	$(CH_3)_2CH$	H	NO_2

Fig. 1 Chemical structure of 1,4-dihydropyridines.

緩和時間、結晶化、非晶質

あそゆきお、よしおかすみえ、みやざきたまき、かわにしとおる

実験

非晶質薬物は結晶を融点以上に加熱し、急冷することによって調製した。薬物炭素の T_1 は固体高分解能 NMR（Varian、400MHz）を用いて 27℃で測定した。誘電緩和時間は DEA 2970 Dielectric Analyzer (TA Instrument)を用い、-50~90℃で測定した。

結果および考察

昇温速度 1℃/min において測定したニフェジピン、ニルバジピン、ニトレンジピンの T_g はそれぞれの 41、43、27℃であった。ニルバジピンの T_g はニフェジピンより 2℃高いが、その結晶化はニフェジピンに比べ 2 オーダー以上遅かった。また、ニトレンジピンの T_g はニフェジピンに比べ 4℃低いにもかかわらずニフェジピンと同様の速度で結晶化した。これらの薬物の結晶化速度は T_g を指標とするマトリックスのグローバルな運動性とは密接な関連が見られず、同様のグローバルな運動性を有する温度において比較すると、ニフェジピン＞ニトレンジピン＞ニルバジピンの順であった。

非晶質ニフェジピン、ニルバジピン、ニトレンジピンの誘電緩和時間測定の結果、ガラス転移の動きと関連するα-緩和とそれよりも速い動きと関連するβ-緩和が観測された。ニフェジピンにくらべニルバジピンのβ-緩和時間は 2 オーダー長く、ニフェジピンにくらべローカルな運動性が低いことが示された。

フェニル基の結合した CH 炭素のスピン-格子緩和の減衰曲線を Fig. 2 に示す。非晶質状態においては T_g の低いニトレンジピンが最も減衰が速やかであった。誘電緩和測定において観測されたβ-緩和の動きよりも、T_g を指標とするマトリックスのグローバルな運動性が、非晶質状態の CH 炭素のスピン-格子緩和に大きく影響するものと考えられる。それに対し、結晶状態においては、結晶化の最も遅いニルバジピンの CH 炭素が速やかに緩和した。これは、ニルバジピンでは他の薬物に比べ、結晶相にある薬物分子が非晶質相へ移動しやすいことを示唆し、それがニルバジピンの結晶化が他の薬物より遅い理由のひとつと考えることができる。

誘電緩和時間や NMR 緩和時間の測定によって得られるローカルな運動性もグローバルな運動性と共に非晶質薬物の安定性に大きく影響することが示された。

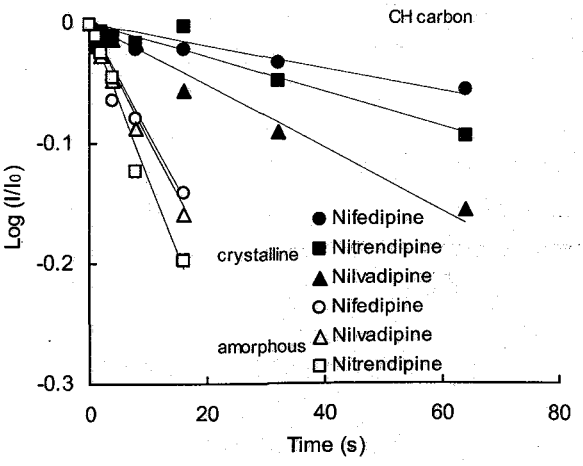

Fig. 2 T_1 decay of CH carbon of 1,4-dihydropyridines.

P085

^{1}H MAS NMR による水素結合ネットワーク系における プロトン拡散

(産総研 計測フロンティア) ○尾身 洋典、鈴木 浩一、林 繁信

Proton diffusion in hydrogen bond network systems probed by ^{1}H MAS NMR

(Research Institute of Instrumentation Frontier, National Institute of Advanced Industrial Science and Technology (AIST))
Hironori Omi, Koh-ichi Suzuki and Shigenobu Hayashi

Inorganic solid acid salts have much attracted attention as candidates for solid electrolytes in fuel cells. In the present study, ^{1}H MAS NMR spectra of $Cs_3(HSO_4)_2(H_2PO_4)$ were measured in the temperature range of 185 K−340 K in order to study the proton diffusion in hydrogen bond network systems. In the low temperature region, the broad and complicated peak attributed to the acidic proton was observed around 13 ppm. This complicated peak was composed of several peaks arising from the inequivalent sites for the acidic protons. This peak became sharp and could be represented by single component as the result of chemical exchange of acidic proton with increasing in temperature.

【序】$CsHSO_4$などに代表される無機固体酸塩では、AO_4型の四面体イオン(A = S, P)が水素結合のネットワークを形成している。これらの物質は、無加湿の状態で、かつ100℃以上の温度において高いプロトン伝導性を示すために中温作動型燃料電池の固体電解質の有力な候補として注目されている。我々のグループでは、これまでに幾つかの硫酸塩や硫酸-リン酸混合塩について研究を行い、SO_4 (PO_4)四面体の回転運動がプロトン並進拡散の律速過程であることを報告した[1,2]。本研究では、$Cs_3(HSO_4)_2(H_2PO_4)$を取り上げ、^{1}H MAS NMR スペクトルの温度変化の測定から、水素結合ネットワーク上のプロトン拡散を支配する水素結合について調べた。

【実験】NMR 測定には、$Cs_3(HSO_4)_2(H_2PO_4)$の粉末試料を 350 K, 真空排気下で加熱乾燥させたものを用いた。^{1}H MAS NMR の測定は、Bruker MSL400 分光計（共鳴周波数 400.13 MHz）を用い、185 K − 340 K の温度範囲で行った。

【結果・考察】$Cs_3(HSO_4)_2(H_2PO_4)$に対する ^{1}H MAS NMR スペクトルの温度変化を Figure 1 に示す。13 ppm 付近に酸性プロトンに対応するブロードな信号が観測された。また、6 ppm 付近に付着水に由来するシャープな信号が観測された。低温では、酸性

プロトンダイナミクス、水素結合ネットワーク、プロトン拡散、無機固体酸塩、固体 NMR

おみ ひろのり、すずき こういち、はやし しげのぶ

プロトンに対応する信号が、複雑な線形を示しており、複数の信号が重なり合っていると考えられる。温度が上昇するにつれて徐々にそれぞれの信号が区別できなくなる。室温付近においては、約 11 ppm および 16 ppm に shoulder が観測される。高温にすると、高磁場側の shoulder が徐々に消失し、さらに温度を上げると低磁場側の shoulder もみえなくなり、330 K より高温では酸性プロトンに対応する信号をひとつの成分として表すことができるようになる。

^{1}H NMR 化学シフト値と水素結合距離(O－H…O)には式(1)のような相関があることが知られている。

$$\delta_{iso}(\mathrm{ppm}) = 79.05 - 255d(\mathrm{O-H\cdots O})(\mathrm{nm}) \quad (1)$$

ここで δ_{iso} は化学シフトの等方値、d(O－H…O)は O－H…O 距離である。$Cs_3(HSO_4)_2(H_2PO_4)$の室温相において、酸性プロトンに対して 5 つの非等価なサイトが報告されており、式(1)から予想される化学シフト値は、それぞれ 12.42, 14.31, 14.59, 16.22, 16.47 ppm である。このスペクトルの線形の温度変化は、温度の上昇により、これらの水素結合が切断され、プロトン同士の交換が起こるためだと考えられる。これより、$Cs_3(HSO_4)_2(H_2PO_4)$において P－O－H－O－P 水素結合の方が、P－O－H－O－S や S－O－H－O－S 水素結合よりも切断されにくいことが示された。このように ^{1}H MAS NMR を用いて、プロトン拡散を支配する水素結合の解裂過程に関する知見が得られた。

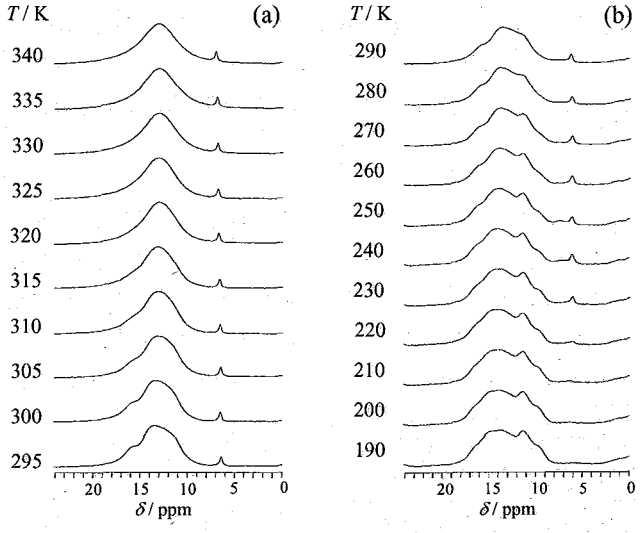

Figure 1. Temperature dependence of ^{1}H MAS NMR spectra in $Cs_3(HSO_4)_2(H_2PO_4)$. The spinning rate of the sample was set at (a) 8 kHz and (b) 6 kHz.

【参考文献】

[1] S. Hayashi and M. Mizuno, *Solid State Ionics*, **171**, 289 (2004).

[2] S. Hayashi and M. Mizuno, *Solid State Ionics*, **176**, 745 (2005).

P086

様々な水酸化物における CP 条件の検討と考察

（日鐵テクノリサーチ）○畠山盛明
（新日本製鐵（株）先端研）齋藤公児、藤部康弘

Study of CP conditions for various inorganic compounds

(Nippon Steel Techno Research) Moriaki Hatakeyama
(Nippon Steel Corporation Advanced Research Lab.) Koji Saito,Yasuhiro Toubu

CP/MAS technique is very popular for various materials to get chemical information using solid state NMR. In the case of ^{13}C and ^{15}N nuclei, there are many papers about CP conditions, but on the other hand, very few reports are reported in the case of quadrapolar nuclei. In this paper, we have demonstrated the optimized CP conditions for various quadrapolar nuclei (^{25}Mg,^{43}Ca,^{23}Na etc.) samples which have hydroxyl groups. Individual CP build-up curve profile shows each optimized conditions, respectively. In the case of quadrapolar nuclei, CP technique is not sensitive to the enhanced S/N but the effect of the selectivity, which is via the bond connectivity through the space from proton to quadrapolar nuclei.

1．はじめに

固体NMRの測定手法の一つであるCP/MAS法は構造解析を行うには不可欠な手法であるが CP 条件の検討には材料や測定核によって多くの時間が必要になる場合がある。特に contact time については重要なパラメーターのひとつであるが、典型的な核種である炭素や窒素については既に多くの知見[1)]がある。しかし、その他の核種、特に四極子核については報告例[2)]が非常に少ない。実際に、四極子核はそのものの感度や共鳴周波数が低い場合が多く、実用材料での含有量が低い場合があり、CP 条件の検討は困難な場合が珍しくない。そこで、今回は四極子核を含む様々な水酸化物を実用材料でのモデルとして選び、それらについて contact time の検討を行った。また、MAS および CP/MAS 測定の測定条件も検討し、その感度向上効果に関しても検討したので報告する。

2．実験

NMR 測定は、VARIAN UNITY INOVA 500(NB)を使用し、測定した試料とそれぞれの共鳴周波数については Table 1 に示す。プローブは T3 プローブの 3.2mm を使用した。低周波数（^{25}Mg、^{43}Ca）では Low Gamma Box を使用し測定した。回転数は 20 kHz とした。化学シフトは外部基準とし、それぞれのケミカルシフト値及び実験に使用した標準試料については、

Table 1　Resonance Frequency for model samples

Sample	Spin	Frequencies
Na(OH)	3/2	132.218 MHz
$Al(OH)_2$	5/2	130.247 MHz
Saponaite(Si)	-1/2	99.305 MHz
$Ca(OH)_2$	-7/2	33.639 MHz
$Mg(OH)_2$	-5/2	30.599 MHz

Table 2　Standard Chemical shift values

	Chemical shift	
^{23}Na	NaCl	(0.0 ppm)
^{27}Al	AlCl	(-0.1 ppm)
^{29}Si	PDMS	(-34.0 ppm)
^{43}Ca	CaCl	(0.0 ppm)
^{25}Mg	$MgSO_4$	(0.0 ppm)

solid state NMR,CP/MAS, inorganic materials

はたけやまもりあき、さいとうこうじ、とうぶやすひろ

Table 2 に示す。尚、NaOH と KCl については水分に敏感なため、簡易的な無菌パックを使用して窒素ガス雰囲気中で試料管に詰めて、ただちに測定を実施した。

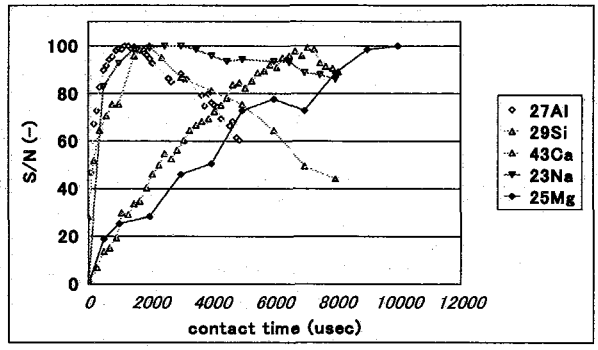

Fig.1 CP conditions profile for various quadrapolar nuclei

3．結果・考察

それぞれのサンプルについて

①^{1}H 90° Pulse

②^{1}H 緩和時間

③測定核の 90° Pulse と緩和時間

を求めた。CP/MAS 測定の条件については contact time について検討した。各試料で得られた CP 条件の検討結果（CP でのビルドアップカーブ）を Fig.1 に示す。S/N に関しては規格化している。明らかに核種毎にその CP 条件での信号強度の挙動は異なることがわかる。また ^{25}Mg や ^{43}Ca ではその CP 条件の最適値は、コンタクト時間が長いのに対して、^{23}Na や ^{27}Al ではコンタクト時間は短い。それは OH 基と対象となる四極子核との距離や化学構造等に依存していると考えられるが、得られる結果は非常に興味深く、今後様々な四極子核を含む材料系を測定する際に適用できると考えている。

Fig.2 に $Ca(OH)_2$ の MAS 及び CP/MAS のスペクトルを示す。FFT のデータ処理条件等は同じである。S/N は同等に見えるが積算回数は MAS が 20 回、CP/MAS は 1024 回と 50 倍強となっている。よって、明らかに CP/MAS の結果の方が S/N が低いことがわかる。この結果は OH 基からの CP 条件であるが、期待される S/N 向上効果は観察されていない。化学構造にも依存しているが、^{25}Mg や ^{43}Ca のような四極子核での CP はどちらかというと、感度向上効果ではなく結合に依存した効果が反映されると思われ、この結果は P と O での実験結果[3]と矛盾しない。

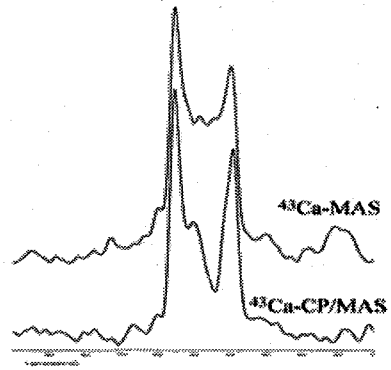

Fig.2 ^{43}Ca-CP/MAS spectra of $Ca(OH)_2$

4．まとめ

本研究では、様々な四極子核と水酸基との CP 条件を検討し、その最適化を行った。CP でのビルドアップカーブでは核種に応じて大きくその挙動が異なっており、それは化学構造等に依存していると考えられる。また四極子核と水素核との CP では、最適化を実施しても感度向上効果は少なく、どちらかというと水酸基との結合による選択効果の方が強いことがわかった。

参考文献

1)例えば高分子学会編「高分子の構造(1) 磁気共鳴法」共立出版

2)Koji Saito, Koji Kanehashi and Ikuo Komaki,;Annual Reports on NMR spectroscopy,vol.44, 23-74, (2001)

3)Koji Kanehashi and Koji Saito ; Chemistry Letters., No.7,668-669, (2002)

P087

全核高分解固体 NMR を用いた珪酸塩スラグの構造解析

○下田景士[1]、藤部康弘[1]、金橋康二[1]、根本貴宏[2]、齋藤公児[1]
[1]新日本製鐵先端技術研究所、[2]日本電子

Total understanding of amorphous slag structure: perspective from multi-nuclear (^{29}Si, ^{27}Al, ^{17}O, ^{25}Mg, and ^{43}Ca) solid state NMR

Keiji Shimoda [1], YasuhiroTobu [1], Koji Kanehashi [1], Takahiro Nemoto [2], Koji Saito [1]
[1]*Advanced Technology Research Laboratories, Nippon Steel Corporation,* kshimoda@re.nsc.co.jp, [2]*JEOL Ltd.*

We applied multiple-quantum magic-angle spinning nuclear magnetic resonance (MQMAS NMR) spectroscopy to understand the local environments of the constituting elements in a silicate slag structure. Si and Al atoms were tetrahedrally coordinated by oxygens as have already been reported. ^{17}O MQMAS spectrum showed that the oxygens occupy several sites, depending on their bridging nature. ^{43}Ca and ^{25}Mg MQMAS spectra demonstrated that these cations also showed multi-site occupancy, and that the average coordination numbers were estimated to about 7 and 6, respectively. Our results underscore the impact of the high magnetic field MQMAS technique when applied to non-crystalline solids.

導入

高炉スラグは製鉄・製鋼の過程で大量に生じる副産物であり、主にCaO, Al_2O_3, SiO_2等の酸化物から構成される。冷却プロセスの違いにより徐冷スラグと水砕スラグに大別され、徐冷スラグは結晶質である一方、水砕スラグは非晶質であることが知られている。しかしながら、"副産物"として扱われてきたが故に、高炉スラグ、とりわけ水砕スラグの構造について詳細な解析例は極めて少ない。

水砕スラグは非晶質であるためアルミノ珪酸塩ガラスとして取り扱うことができる。ガラスの構造解析法として主にX線回折やラマン・赤外分光といった手法が挙げられるが、原則的に特定元素に関する情報は抜き出すことができないという欠点がある。

核磁気共鳴(NMR)法はそのような場合に効力を発揮する。NMRは特定の原子種のみに焦点を当てる解析法の1つであり、ほぼ全ての核種が対象となるため、ガラス組成の全ての元素について多角的な情報を得ることができるという大きな利点がある。NMRによるスラグの構造解析は^{29}Si, ^{27}Al及び、より少ない例として^{19}F(製鋼スラグの場合)のMAS測定に限定されている。

本研究では水砕スラグの非晶質構造に焦点を当て、スラグを構成する全ての核種について高磁場下での NMR 測定を行うことで包括的な構造情報を得ることに成功した。とりわけ、半整数スピン核種に関しては MQMAS 法によって詳細なサイト分布を明らかにした。

実験

用いた合成試料は典型的な高炉スラグの主成分組成に準じている(43.0 wt%CaO, 7.0 wt%MgO, 15.0 wt%Al_2O_3, 35.0 wt %SiO_2)。水砕スラグをモデル化するため、試薬粉末を

Keywords: ^{43}Ca, ^{25}Mg, solid state NMR, MQMAS, slag

しもだけいじ、とうぶやすひろ、かねはしこうじ、ねもとたかひろ、さいとうこうじ

1500℃で30分熔融し急冷することで、無色透明なガラスが作成された[1]。

NMR測定のためにスラグ中のCa, Mg, O核種は同位体エンリッチされている。^{43}Caの天然存在比は 0.135%であり、66%エンリッチ$^{43}CaCO_3$試薬をスターティングマテリアルとして用いた。^{25}Mg核(天然存在比 10.13%)は 99%エンリッチ^{25}MgOを、^{17}O核(天然存在比 0.037%)は25%エンリッチ$H_2{}^{17}O$(ISOTEC)を用いた。

NMR測定はJNM-ECA700 (16.4 T)で行った。^{29}Si, ^{27}Al, ^{17}O, ^{25}Mg及び^{43}Ca核の操作周波数は各々139.1 MHz, 182.4 MHz, 94.9 MHz, 42.9 MHz及び47.1 MHzである。全ての測定は18 kHzでMAS回転させて行った。^{27}Al, ^{17}O, ^{25}Mg及び^{43}Ca同位体核種は半整数核スピン(それぞれI = 5/2, -5/2, -5/2, -7/2)を持つため、高分解能なMQMAS測定を行った。

結果と考察

Spin echo法による^{25}Mg MASスペクトルをFig.1 に示す。スラグ中のMg含有量は少ないためにS/Nは悪いが、~ -80 ppmにピークトップを持つブロードなシングルピークが得られた。3QMASスペクトルはS/Nが極めて悪いものの、幾つかのサイトの存在を示唆した。真の化学シフトδ_{CS}値は~14 ppmと見積もられ、スラグ中のMgは六配位であることが結論付けられる。また、QIS軸に沿ったピーク分布は六配位Mgの配位環境が歪んでいるということを意味している。これらの結果は、実際の製鋼スラグに対して天然存在比での^{25}Mg 3QMAS測定を行ったHatakeyama et al.[2]とも調和的である。

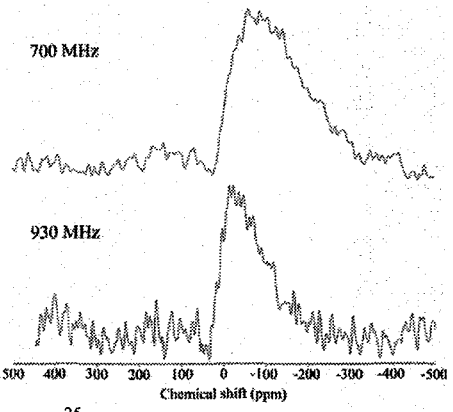

Fig.1 ^{25}Mg MAS spectra of the slag at 700 and 930 MHz.

^{17}O MASスペクトルは130 ppm及び55 ppm付近にトップを持つダブルピークが観察される。高分解能な 5QMASスペクトルではさらに多数のサイトが確認できる(Fig.2)。これらのサイトのアサインメントは容易ではないが、120 ppm付近のピークはCa-NBO-Siに関係したサイトであり、Mg-NBO-Siサイトはおそらく90 ppm付近のピークであると考えられる[3]。一方、90 ppm以下の高磁場領域はSi-O-Si, Si-O-Al, Al-O-Alといった架橋酸素サイトで占められていると考えられる。

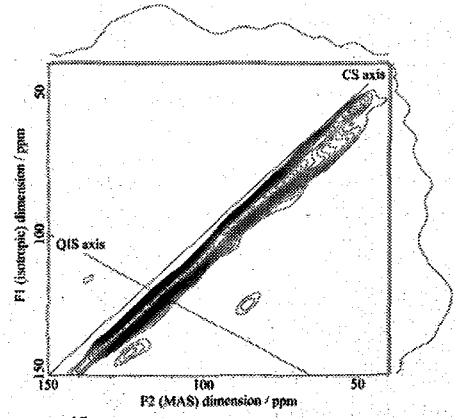

Fig.2 ^{17}O 5QMAS spectrum of the slag at 700 MHz.

我々は、さらに^{28}Si, ^{27}Al, ^{43}Ca NMRスペクトルも含め、ポスター紙上にて高炉スラグの全体像について考察する。本研究の一部は科学振興調整費で行われている。930 MHzマグネット使用許可に関して、物質材料研究機構の清水禎先生に感謝します。

参照

[1] Shimoda et al. (2006), *Solid State Nucl Magn Reson* **30**, 114; [2] Hatakeyama et al. (2005), *Chem Lett* **34**, 864; [3] Allwardt & Stebbins (2004), *Am Mineral* **89**, 777.

P088

NMR Study of Ammonium Sulfate

Kwan Soo Hong[1)] and Insuk Yu[2)]

1) Advanced Magnetic-Resonance Research Building, Korea Basic Science Institute, Oh Chang, Chung Won, Choongbuk, 363-883, Korea.
2) Department of Physics and Astronomy and the Nano Systems Institute(NSI-NCRC), Seoul National University, Seoul, 151-742, Korea

Ammonium sulfate ($(NH_4)_2SO_4$) is a pseudo-proper ferroelectrics which shows a transition to ferroelectric phase at T_c = 223 K. Its Curie-Weiss constant is very small and the temperature dependence of spontaneous polarization is anomalous. The two sub-lattice structures with NH_4^+(I) and NH_4^+(II) ions are playing an important role in the characteristics of ammonium sulfate. We study the dynamic properties of NH_4^+ ions by using the pulse NMR techniques.

^{1}H NMR spectra and relaxation times are investigated for ammonium sulfate powder sample at temperatures ranging from 102 K to 440 K using the Bruker MSL 200 and Avance II 500 MHz Solid NMR spectrometers. Above 100 K, the intra-molecular dipolar interaction of NH_4^+ ions are averaged out due to the fast rotational motion of the ions and the NMR line width is determined by the inter-molecular interaction of the ammonium ions. The line width is further reduced by magic angle spinning over 5 kHz. ^{1}H spin-lattice relaxation time T_1 is mainly reflecting the hindered rotation of the ammonium ions. At temperatures below 318 K the initial ^{1}H spin-lattice relaxation has non-exponential behavior with the exponent $1 < n < 2$, *i.e.*, $S(t) = S(0)\exp\{-(t/T_1)^n\}$. Above 318 K the relaxation is single-exponential. We believe this is a manifestation of the bottleneck effect in the spin-lattice relaxation of the nuclear spin system through the hindered rotation of ammonium ions. This is compared with the measurement of spin-lattice relaxation with different initial condition of the spin system. In the ferroelectric phase the correlation time for the hindered rotation of NH_4^+(I) ions is longer than that of NH_4^+(II) ions, but the difference between the two correlation times becomes smaller as temperature approaches the T_c. From the temperature dependent spin-lattice relaxation time in the ferroelectric phase, the activation energies for the hindered rotation are found for the two types of NH_4 ions as, E_a^I = 0.27±0.02 eV and E_a^{II} = 0.12±0.01 eV. In the paraelectric phase the relaxation is determined by the NH_4^+(II) ions.

Keywords: Ammonium sulfate, ferroelectric transition, hindered rotation, spin-lattice relaxation, bottleneck effect.

^{2}D NMR spectra and relaxation times are studied for the deuterated ammonium sulfate, $(ND_4)_2SO_4$ at temperatures 180 K ~ 430 K. The ^{2}D NMR spectra are typical of the quadrupole broaden lines. The quadrupole coupling constants estimated from the line shapes are different for the two ammonium ions, ND_4^+(I) and ND_4^+(II). The spin-lattice relaxation is of the double exponential form in the ferroelectric phase, but it becomes single exponential at the ferroelectric phase transition temperature T_c = 223 K. The discontinuous changes of relaxation times, correlation times, and quadrupole coupling constants of ^{2}D nuclei are observed at T_c.

^{15}N NMR is also studied for the ^{15}N enriched ammonium sulfate $(^{15}NH_4)_2SO_4$. In contrast to the ^{1}H and ^{2}D NMR, the ^{15}N nuclei show only the single exponential relaxation behavior at all temperatures. However, the relaxation time T_1 shows an abrupt change at the ferroelectric phase transition temperature T_c = 223 K. The activation energy obtained from the temperature dependent spin-lattice relaxation times in the paraelectric phase is the same as the one obtained for the NH_4^+(II) ions.

It is noticed that the ferroelectric phase transition temperature T_c is the same for all the three ammonium sulfates $(NH_4)_2SO_4$, $(ND_4)_2SO_4$ and $(^{15}NH_4)_2SO_4$. This is suggestive that the motion of NH_4^+ ions is not the driving force for the phase transition. On the other hand, the NMR spectra and relaxation times show abrupt changes at the transition temperature which fact is an indication that the transition changes the dynamics of NH_4^+ ions largely. We will try to explain the observed results, as well as some new findings, in a united way.

This work was supported by part by the Korea Science and Engineering Foundation through the National Core Research Center program (Nano Systems Institute, Seoul National University). The experiments in this work were performed using the NMR facilities of the Korea Basic Science Institute and the National Center for Inter-University Research Facility, Seoul National University.

P089

Improved sensitivity and resolution in the indirect dimension of HSQC experiment for probe molecules aligned in strongly orienting media

Bikash Baishya[a,b], Raghav G Mavinkurve[c], Suresh Kumar Vasa[c] and N. Suryaprakash[b,d]

[a]Solid State and Structural Chemistry Unit, [b]NMR Research Centre, [c]Department of Physics, Indian Institute of Science, Bangalore 560 012, India

The spectra of molecules oriented in liquid crystalline media are dominated by partially averaged dipolar couplings. In the ^{13}C-^{1}H HSQC, due to inefficient hetero-nuclear dipolar decoupling in the indirect dimension, normally carried out by using a π pulse, there is a considerable loss of resolution. Furthermore, in such strongly orienting media the ^{1}H-^{1}H and ^{1}H-^{13}C dipolar couplings leads to fast dephasing of transverse magnetization causing inefficient polarization transfer and hence the loss of sensitivity in the indirect dimension.

We have carried out HSQC experiment with efficient polarization transfer from ^{1}H to ^{13}C for molecules aligned in liquid crystalline media. The homonuclear dipolar decoupling using FSLG during the INEPT transfer delays and also during evolution period combined with the π pulse heteronuclear decoupling in the t1 period has been applied. The studies resulted in a significant reduction in RDC and thereby resolution and sensitivity enhancement in the indirect dimension. This has been demonstrated on pyridazine and

pyrimidine oriented in the liquid crystal. The two closely resonating carbons in pyrimidine which were broad and unresolved in earlier experiments have been resolved.

P090

Fractional anisotropy と Trace index に基づくマウス脳 MR 画像の取得

○若松永憲、横井美佳、今泉好偉、杉原文徳、荻野孝史、瀬尾芳輝

獨協医科大学／医学部／生理学(生体制御)

Mouse brain MR imaging based on fractional anisotropy and trace index

○H. Wakamatsu[1], M. Yokoi[1], Y. Imaizumi[1], F. Sugihara[2], T. Ogino[3], Y. Seo[1]
[1]Dept of Regulatory Physiology, Dokkyo University School of Medicine,
[2]Graduate School of Integrated Science, Yokohama City University,
[3]Dept of Biochemistry and Cellular Biology, National Institute of Neuroscience,
National Center of Neurology and Psychiatry

We are working on the calculation of tensor value from DWI, the conversion of the tensor value into fractional anisotropy (FA) and trace index (TI), and the production of the parameter image of the brain to achieve the diagnosis at the early stage of the nerve disease. In order to establish a basic system in vertical high-field MR micro-imaging system, we had made a probe with the stereotaxic coordinates for mice inside a gradient system. FA indices provide clear images of brain structures. It is high in numerical value in corpus callosum. But there was little difference between cerebral cortexes. However, TI is high in ventricles, and show low contrast images. Though other areas hardly showed the difference of TI, the part of the dentate gyrus showed a numerical value that was lower than other areas.

はじめに

我々は現在、「揺さぶられっこ症候群」のような症例における神経性疾患を早期に診断する手法を確立するプロジェクトに参画している。幼少期における脳内微小出血は成長とともに解剖学的な痕跡は消失し、障害部位の検出は困難となる。しかし、その後遺症は思春期の素行不良や社会生活不順応という形で現れてくると考えられている。また、虚血や外傷による神経変性は白質神経線維の脱髄による所が大きく、髄鞘形成過程にある小児、幼少期の脳内の傷害を検出する手法の開発は必須の課題である。以上の要求に対する答えとして、拡散強調画像を中心とした MR イメージング手法が最適な手法であると考えられる。我々の達成目標は脳内微小出血を発症するモデル動物を用いて基礎データを収集するための小型動物を対象とした MR イメージング手法の開発である。

Key words: diffusion, tensor imaging, fractional anisotropy, trace index

著者ふりがな:わかまつひさのり、よこいみか、いまいずみよしえ、すぎはらふみのり、おぎのたかし、せおよしてる

手法と材料

実験動物

本計画の基本戦略として、揺さぶりの障害を受けたモデルラットの解析を計画の中心に据えている。そのため、幼齢ラットと同サイズで簡便に扱える実験動物として C57BL 系のマウス（5-7 週齢）を用いて計画初期の装置開発と測定条件の調整を行った。

MRI 測定装置

本研究において、幼齢ラットの成長段階にともなった脳画像を取得するための装置の開発が達成目標の一つである。よって、成獣マウスの測定に適したサイズと感度を備える Micro 2.5 gradient system (Bruker Biospin) を採用した。また、この装置に適合する脳定位固定装置は市販されていないため、併せてそれも開発した。(Fig1).

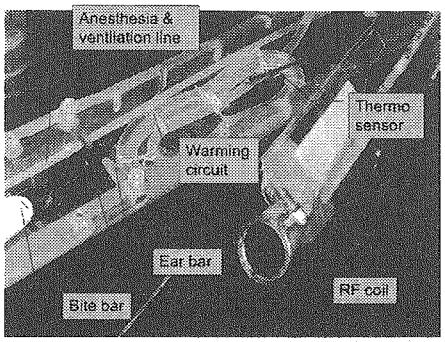

Fig1 Layout of stereotaxiccordinate probe

拡散強調画像の撮像

全てのボクセルについての拡散テンソルは ^{1}H 拡散強調画像から計算によって得られた。画像取得の際のパラーメターとして FOV,1.5 x 1.5 cm^2;matrix size ,128 x 128。b 値は 50 から 2800s/mm^2 に渡る5つの画像から取得。ボクセルサイズは 117x117x500 μ m^3、スライス厚は 0.5mm とした。次に、固有値の算出を行った。一つのボクセルに対し X,Y,X の3つの軸とそれらの中間である XY、XZ、YZ の3軸、合計6つの軸の画像情報が得られることになり、これらは拡散テンソルとしてまとめられる。この拡散テンソルに対角化を用いることで固有値 λ_1, λ_2, λ_3 を得る。これらを元に下式に従って FA と TI を算出した。FA は拡散による分子の拡散の異方性を知る指標であり、TI はその分子の拡散ベクトルの絶対値を反映している。拡散現象に影響を与える脳の微細な組織構造に外傷あるいは脱髄のような変化が起れば、これら FA,TI に変化が現れると推測される。それぞれ FA 画像と拡散係数絶対値画像(TI 画像)を取得した。

$$D=\begin{bmatrix} D_{XX} & D_{XY} & D_{XZ} \\ D_{YX} & D_{YY} & D_{YZ} \\ D_{ZX} & D_{ZY} & D_{ZZ} \end{bmatrix}$$

$$(\lambda 1= D_{XX},\ \lambda 2=D_{YY},\ \lambda 3 =D_{ZZ})$$

Fractional Anisotropy(FA)

$$=\frac{3 \times S.D.(\lambda 1, \lambda 2, \lambda 3)}{\sqrt{2} \times \sqrt{\lambda 1^2+\lambda 2^2+\lambda 3^2}}$$

Trace Index(TI)

$$=\sqrt{(\lambda 1^2+\lambda 2^2+\lambda 3^2)} \quad (mm^2/sec)$$

実験結果

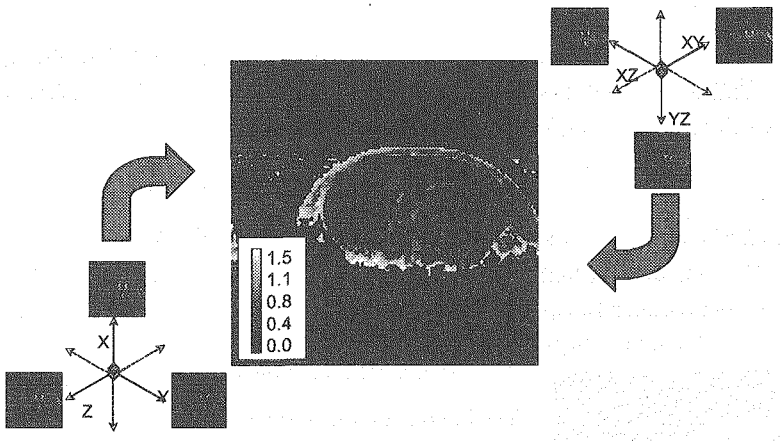

Fig2　FA coronal slice images integrated from water diffusion coefficient of six axes

FA 画像では組織の解剖学的な構造が明確に表現されていた。特に数値が高かったのは側脳室や第Ⅲ脳室の辺縁の部分、脳梁の部分であった。その他の脳実質領域は低い数値を示していた (Fig.2)。多くの神経軸索は髄鞘によって被膜されているために、細胞内の水の拡散に対して強固な障壁となる。髄鞘化された白質線維が集中する脳梁のような場所において高い FA が示されるのはこの有髄神経内での水分子の制限拡散を反映した結果と考えられる。脳室内での水は何ら制約を受けていないため、あらゆる方向に拡散でき、FA は低くなると予想される。にもかかわらず、これらの領域の辺縁で FA が高く見えるのは部分体積効果によるアーティファクトと考えられる。一方、TI 画像では脳室領域の数値が著明に高く、その他の脳実質間での数値の差を見て取るのは困難であった。(Fig.3)。

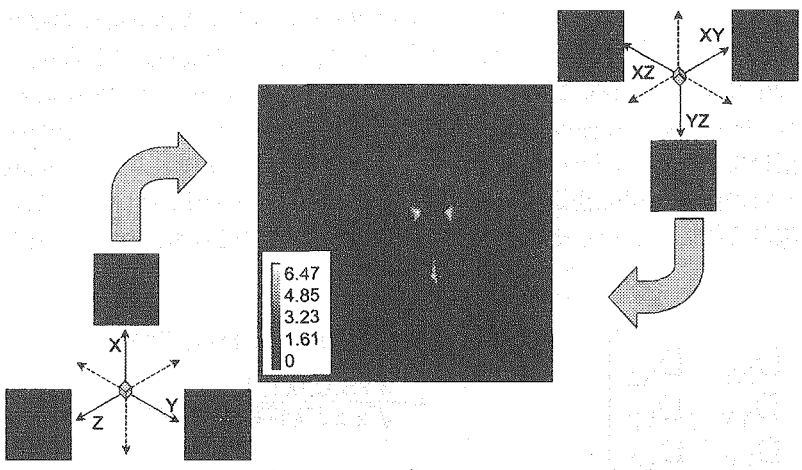

Fig3 TI coronal slice images integrated from water diffusion coefficient of six axes

我々はより詳細な数値のデータを得るために、いくつかの脳領域についてFA, TI両方の画像の数値を集計した(Fig4)。FA画像においてはやはり脳梁部分がもっとも高く(0.65±0.02 n=4)、大脳皮質の間でほとんど差は見られなかった。

TI画像では検索対象外とした脳室以外の領域はほとんど差が見られなかったが、海馬において歯状回の部分(0.87±0.01)が他よりも低いと言う結果を示した。これは海馬内の他の2領域(mol: 1.07±0.01;Py: 1.02±0.01)のみならず、他の大脳皮質領域に対しても同様である。

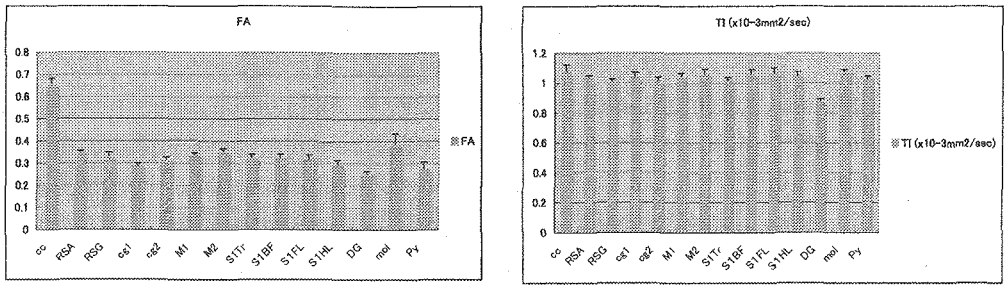

Fig.4 Comparison of numerical values between brain areas in FA and TI

まとめ

本研究では小動物用に調整したMR画像装置によってFAとTIからなるテンソル画像を取得することができた。

海馬の領域について歯状回だけがTI値が低いという結果になったが、その理由については現時点では示唆する証拠は得られていない。歯状回と比較して計算した他の領域に錐体細胞が集中している領域があるため、当初は単純に細胞の種類や形状の差によるものかと推測もした。しかし、歯状回の中においても顆粒細胞層、分子層、多形細胞層と細分化されており、今回そこまでの測定精度が発揮できたとは言いがたい。まして、大脳皮質領域との差を鑑みれば、投射する神経の走行や複数の細胞層の配置についても考察せねばならない。受傷モデル動物の解析に取り組むためのスタンダードの第一段階はクリアしたものの、まだ、改良すべき点は多分にある。

次のステップとしては、現在正常の幼齢ラットの成長段階に沿った画像の取得に取り組んでいる。正常ラットの画像を蓄積しつつ、受傷ラットの画像取得にも順次平行して取りかかる。さらに、ガドリニウム等の造影剤の利用による画像の鮮明化も今後の計画の一環として粛々と準備中である。

P092

T_1強調３D画像からの脳梁断面の抽出：脳梁断面の性差について

国立環境研究所　○高屋　展宏，渡邉　英宏，三森　文行

Segmentation of the corpus callosum from T_1-weighted 3D image: Sex differences in the corpus callosum

National Institute for Environmental Studies
Nobuhiro Takaya, Hidehiro Watanabe, Fumiyuki Mitsumori

It was reported that there are sex differences in the human brain morphology. Despite decades of research, there is still no agreement over the presence of sex-differences in the human corpus callosum (CC). In this study, the mid-sagittal slice of CC was extracted from T1W 3D image with 1mm^3 spatial resolution obtained by 3D MDEFT sequence at 4.7T. Average area of CC in healthy subjects were 5.44±0.98cm^2 in male (n=33) and 5.35±0.64cm^2 in female (n=36) . Student t-test gives no significant difference. The mid-sagiital CC area normalized with the intracranial volume in female was significantly higher than that of male. In addition, the area of the CC showed a positive correlation with the brain volume in male, while no correlation was found in female.

【序】

脳梁は左右の大脳半球を連結する重要な神経組織である。今までに大きさ、形状について脳梁の性差に関する研究は多くあるが、今もなお MR による測定で脳梁の解剖学的な性差に関する議論が盛んである。今回我々は、1mm の空間分解能を持つ T1 強調の３次元画像から脳梁正中断面を抽出、断面積を計測して、その性差について論じる。

【方法】

装置はVarian社製 4.7T/92.5cmシステムに^{1}H TEMコイルを使用した。4.7T用に最適化した測定条件で空間分解能１ｍｍのヒト脳の３D MDEFT画像を取得した。被験者は健常な成人６９人。脳梁断面は白質画像から抽出するため、MDEFT画像を灰白質、白質、CSFに組織分画した。得られたMDEFT画像は強いB1 不均一のために画像の中心が明るいため、組織分画の前に信号強度の補正を行った。組織分画後、正中断面を得るために、SPM99 のcoregister toolで白質画像をテンプレートに合わせて座標変換して、画像の中心断面を脳梁の正中断面とした。最後は白質の確率画像の正中断面よりMEDxソフトウエアをつかって手作業で脳梁正中断面を抽出した。脳梁断面積は各ピクセルの確率値にピクセルの面積(0.01cm^2)を乗算した値を合計して求めた。

キーワード：high field MRI, human brain, corpus callosum, MDEFT, tissue segmentation

著者ふりがな：たかや　のぶひろ，わたなべ　ひでひろ，みつもり　ふみゆき

【結果と考察】

脳梁断面積の平均値は男性：5.44±0.98cm^2，女性：5.35±0.64cm^{2}であった。年齢による傾向は見られなかった。t検定の結果、男女間に有意な差は見られなかった。この結果は、これまでに報告されている文献値と比較して若干小さい。しかし、日本人を対象にしたMRI測定の報告は我々の値に近い。

個体差を補正するため、脳梁断面積を頭蓋内体積で標準化（脳梁断面積／頭蓋内体積）した場合は、男性：3.45×10^{-3}(cm^{-1})，女性：3.87×10^{-3}(cm^{-1})でｔ検定の結果、男女間に有意な差が見られた(P<0.001)。他の文献でも標準化した値に性差があり、女性において脳梁断面積の割合が男性より高いと報告されている。

頭蓋内体積が大きい男性群と小さい女性群で比較を行っているが、頭蓋内体積が同じ男女を比較した場合も女性の脳梁の割合が高いか否かを調べるために、脳梁断面積と頭蓋内体積の関係を調べた。

その結果、脳梁断面積と頭蓋内体積との間に、女性では相関があまりみられなかった(r=0.25)のに対して、男性では中程度の相関がみられた(r=0.48, P<0.01)。
脳梁は白質中のもっとも大きな組織であるため、白質体積と脳梁断面積の関係も調べた。その結果、男性には中程度の相関が見られた(r=0.43, P<0.05)のに対して、女性では相関がほとんど見られなかった(r=−0.03)。

以上の結果を総合して、女性では脳梁断面積が、頭蓋内体積、白質体積等、頭の大きさを示す指標に対して独立しているのに対して、男性では頭の大きさに依存する新たな性差が浮かび上がってきた。すなわち、脳梁の性差の有無の判断は単に脳梁断面積や頭蓋内体積による標準化した値の比較のみでなく、頭の大きさに対する依存性の有無も考慮する必要がある。依存性になぜ男女差が認められるかは、これまでの結果からは明らかでない。

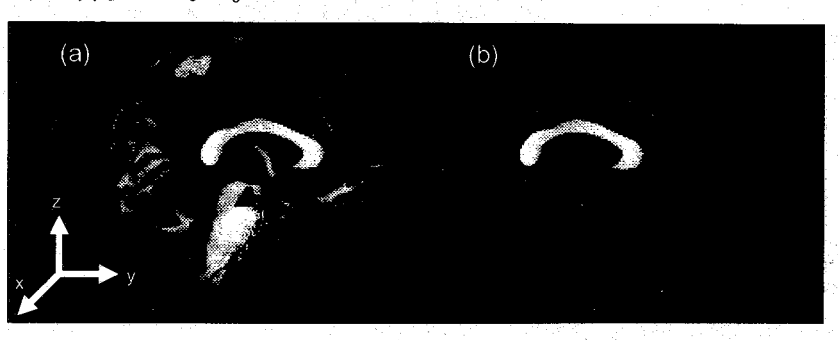

Fig. Mid-sagittal slice images of white matter (a) and corpus callosum (b).
Mid-sagittal plane of CC was manually extracted from a WM probability image using MEDx software. Before extraction of CC, the probability image of WM was rotated to align the mid-sagittal plane in the sagittal slice.

P093

Simultaneous quantitation of glutamate and GABA in the human brain using a localized 2D constant time COSY

H. Watanabe, N. Takaya, F. Mitsumori
National Institute for Environmental Studies

Introduction

Glutamate and GABA are major neurotransmitters in the human brain. Glutamine is a precursor of glutamate, localized in astrocytes. Then, *in vivo* peak detection of these metabolites is one of the important themes in ^{1}H magnetic resonance spectroscopy. However, since these have complex spin systems, it is difficult. So, we have developed a localized 2D constant time COSY method and have demonstrated *in vivo* peak detection in the human brain on a 2D spectrum at 4.7 T. In this work, I will present an absolute quantitation method and demonstrate an absolute quantitation of glutamate and GABA in the human brain.

Methods

On the localized 2D CT-COSY spectra of the human brain, three peaks related to glutamate and GABA were able to be resolved; the diagonal peaks of Glu C4H at 2.35 ppm and GABA C2H at 2.28 ppm, and the cross peak between Glu C4H and Glu C3H (1). We used two diagonal peaks of Glu C4H and GABA C2H for quantitation here.

In the localized CT-COSY sequence, T_2 decay occurs during T_{ct}. In addition to this decay, the signal intensities are varied due to ^{1}H-^{1}H coupling, J_{HH}. We calculated this dependence function, $f(T_{ct})$, using GAMMA (2) with the reported values of the chemical shifts and J_{HH} (3). Then, the net signal intensities were proportional to a function, $e^{-Tct/T2} * f(T_{ct})$. Thus, T_2 was calculated by curve-fitting the measured data to this function.

In case of glutamate, the peak of Glu C4H on the human brain spectrum was curve-fitted using the peak on the spectrum of the 50 mM glutamate phantom. Then, the peak volume ratio, PV_{ratio}, which is the quotient of the peak volume on the human brain spectrum to that on the phantom was calculated. We used the phantom immersed in a bath of 0.9 % saline solution for realizing a similar coil-loading condition to the human brain. The difference of coil-loading factor was corrected using water reference method. Then, the concentration of glutamate in the human brain, $Conc_{brain}$, was written as follows using the concentration of the glutamate phantom, $Conc_{phantom}$; where Vol_{brain} and $Vol_{phantom}$ denote the voxel volumes in the human brain and in the phantom, respectively. The concentration of GABA was also obtained using this

Keywords: human brain, glutamate, GABA, CT COSY, *in vivo*

procedure.

$$Conc_{brain} = Conc_{phantom} \times PV_{ratio}(T_{ct}) \times \frac{Vol_{phantom}}{Vol_{brain}} \times \frac{1/e^{-T_{ct}/T_{2brain}}}{1/e^{-T_{ct}/T_{2phantom}}} \times \frac{Conc_{water\_brain} \times Vol_{water\_brain} / A_{water\_brain}}{Conc_{water\_phantom} \times Vol_{water\_phantom} / A_{water\_phantom}}$$

All experiments were performed using a 4.7 T whole-body NMR spectrometer (*INOVA*, Varian). First, for validation of this proposed metod, we did phantom experiments using a 10 mM glutamate phantom. Next, human volunteer studies were performed. The volume of interest was 36 ml and was set inside the parieto-occipital lobe. Four spectra with *T*ct of 110ms, 130 ms, 150 ms, and 270 ms were obtained for T_2 measurement. Concentrations of glutamate and GABA were obtained after peak volume calculation, T_2 corrections and water reference calculation.

Results & Discussion

In the 50 mM phantom experiments, the measured peak volumes of Glu C4H were well fitted to the proposed function, A*exp(-*T*ct/T_2)*f(*T*ct) (Fig. 1 (a)). The calculated T_2 value was 580 ms, which was used as $T_{2phantom}$ in the proposed quantitation equation. In validation experiments using the 10 mM glutamate phantom, the calculated concentration was 9.62 mM.

In the human volunteer studies, T_2 value of Glu C4H was calculated as 117 ms (Fig. 1 (b)). After T_2 corrections, the calculated concentrations of glutamate and GABA in the human brain were 11.7 mM and 0.95 mM, respectively. Those two values were in good agreement with the previously reported values.

Conclusions

Glutamate and GABA in the human brain were quantitated by the proposed method with T_2 correction and peak volume calculation. The calculated concentrations were within the previously reported values.

References

1. Watanebe, H., Takaya, N., Mitsumori, F., Proc. Intl. Soc. *Mag. Reson. Med.*, 13, 2496, 2005.
2. Smith, SA., Levante, TO., Meier, BH., Ernst, RR., *J Magn. Reson.* Ser A, 106:75-105, 1994.
3. Govindaraju, V., Young, K., Maudsley, AA., *NMR Biomed.*;13(3):129-153, 2000.

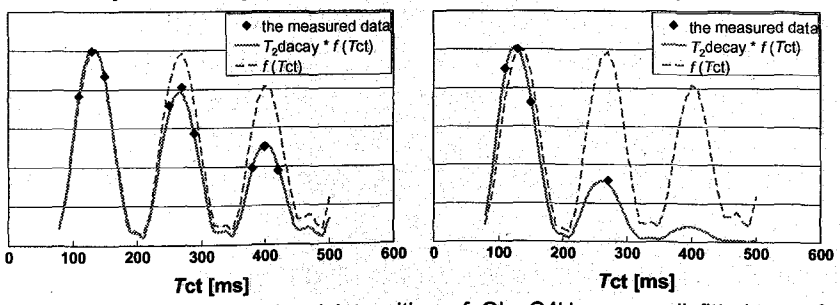

Fig. 1. The measured signal intensities of Glu C4H were well fitted to a function, A*exp(-*T*ct/T_2)*f(*T*ct). The function, f(*T*ct) is a *T*ct dependence function due to J_{HH}. (a): the 50 mM glutamate phantom data, (b): the human brain data.

P094

異種核多次元 NMR を用いた細胞内大量発現蛋白質の解析

(1 首都大学東京・院理工, 2CREST/JST, 3 理研, 4 藤田保衛大)
○佐々木敦子 1,2, 榊原大介 1,2, 飯島亜季 1, 末永智子 1, 吉益雅俊 3,
林 宣宏 4, 三島正規 1,2, 伊藤 隆 1,2

Heteronuclear multidimensional NMR of proteins overexpressed in cells

Atsuko Sasaki[1,2], Daisuke Sakakibara[1,2], Aki Iijima[1], Satoko Suenaga[1],
Masatoshi Yoshimasu[3], Nobuhiro Hayashi[4], Masaki Mishima[1,2] and Yutaka Ito[1,2]
[1]Department of Chemistry, Tokyo Metropolitan University; [2]CREST, JST; [3]RIKEN; [4]Fujita Health University

Recent developments of NMR spectroscopy allowed us to observe high resolution heteronuclear multi-dimensional NMR spectra of overexpressed proteins inside living cells.

In this presentation, we report our recent studies on this "In-Cell NMR" method applied to several proteins expressed in *E. coli* cells. For the measurement of 3D "in-cell" triple-resonance NMR spectra, a nonlinear sampling scheme for indirectly acquired dimensions was shown to be very effective, in order to overcome the low sensitivity and instability of samples. Further, we succeeded to obtain long-range NOEs from In-Cell NMR samples, which were prepared with selective protonation at methyl-groups with deuterated background. Based on these results we will discuss future perspectives on the methodological developments of In-Cell NMR.

【序】 In-Cell NMR 法は, 蛋白質を発現させた細胞そのものを測定試料として異種核多次元 NMR スペクトルを測定するものである. In-Cell NMR が提唱された当時は, 大腸菌などのバクテリアで発現させた蛋白質の ^{1}H-^{15}N もしくは ^{1}H-^{13}C 異種核相関 NMR の測定例が報告されたのみであったが, 最近になって, 大腸菌内発現系を用いた蛋白質の主鎖 NMR シグナルの帰属や, 蛋白質間相互作用解析の例が報告され, さらにアフリカツメカエル卵へのマイクロインジェクションの系を利用した異種核相関 NMR 測定や蛋白質間相互作用解析の例も報告されるようになってきている. しかし, 細胞と標的蛋白質の適切な組み合わせでは驚くほど明瞭なスペクトルを与えてくれるこの手法も, 様々な細胞と蛋白質の組み合わせで普遍的に測定が可能になるまでには, まだ多くの方法論的改良がなされなければならない. NMR 測定については, 特に短時間で高感度のスペクトルを観測する手法が

キーワード In-Cell NMR, 異種核多次元 NMR, 非線形サンプリング, 立体構造

ささき あつこ, さかきばら だいすけ, いいじま あき, すえなが さとこ,
よします まさとし, はやし のぶひろ, みしま まさき, いとう ゆたか

希求されている. また, 細胞内蛋白質の高次構造情報(NOE など)を如何にして取得するか, という点についても方法論的検討を要する.

今回の報告では, われわれの研究室が現在試みている In-Cell NMR 測定法の研究の中から, 主として「非線形サンプリング法を用いた高感度高分解能 In-Cell NMR スペクトルの迅速な測定」, および「選択的プロトン標識を用いた細胞内蛋白質の高次構造情報の取得」の試みについて紹介し, In-Cell NMR 法についての展望についても議論を行う.

【実験, 結果, および今後の展望】 本研究ではカルモジュリン(CaM)を標的蛋白質とし, 大腸菌内発現系を用いて, In-Cell NMR 法による細胞内 CaM の ^{1}H-^{15}N HSQC 測定, および 3D HNCA, HN(CO)CA, HNCO, HN(CA)CO, CBCANH, CBCA(CO)NH 測定を行った. 3D 三重共鳴 NMR の間接観測軸には非線形サンプリング法を用い, 測定感度を損なわずに測定時間を著しく短縮することに成功した. Figure に, CBCA(CO)NH, HN(CA)CO および HNCO スペクトルの一部を示した. 現在までに主鎖シグナルの部分帰属に成功しているが, 完全帰属のためには, より効率的な 3 重共鳴 NMR 測定法が必要である. 非線形サンプリング法の最適化およびデータ処理法の改良を行なっている.

また, 細胞内 CaM の高次構造情報の取得も試みた. CaM の In-Cell NMR スペクトルは, 主としてシグナルの線幅の増大によってスペクトル中のクロスピークの分離が著しく低下する. これを克服するために, メチル基を選択的にプロトン標識し, 残りを重水素化した In-Cell NMR 試料を調製し, 選択的 NOE 情報の観測を試みた. 現在までに ^{1}H-^{13}C HMQC, および 3D ^{13}C/^{13}C-separated NOESY を測定することで, 細胞内 CaM が選択的プロトン標識されていることを確認するとともに, いくつかのメチル基間の NOE の観測に成功した. 現在は芳香環選択的標識法などを併用して, さらなる高次構造情報の収集を試みており, 細胞内 CaM のグローバルフォールドの決定を目指す.

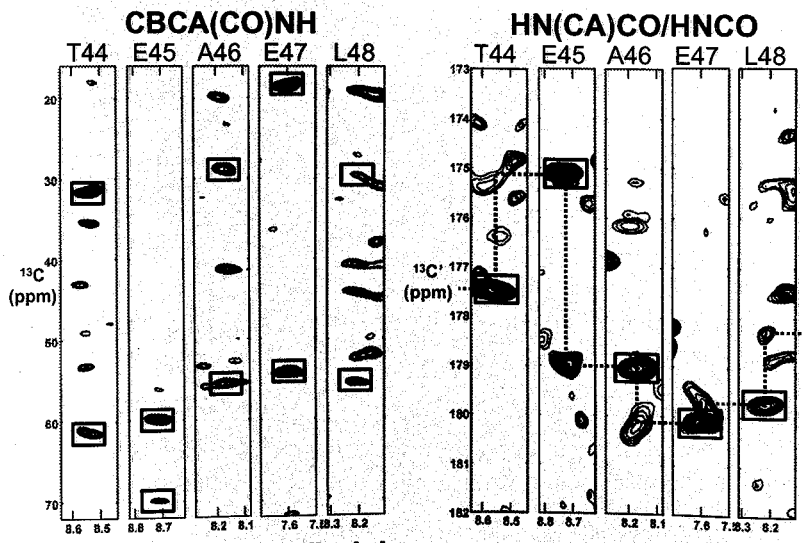

Figure. 3D "In-Cell" triple-resonance spectra of CaM

P095

Atomic redistribution of metabolism in a plant cell system

OMami Okamoto[1], Takashi Hirayama[1,2] and Jun Kikuchi[1,3,4]
[1]Int. Grad. Sch. Arts. Sci., Yokohama City Univ, [2]Environ Mol. Biol. Lab., RIKEN
[3]RIKEN Plant Science Center and [4]Grad. Sch. Bioagri. Sci., Nagoya Univ.

Key words; stable isotope labeling, plant cell, metabolic pathway analysis, ^{13}C-^{13}C coupling, atomic redistribution

Plant metabolomics has been recently growing rapidly. However most of their reports tend to rely on statistical analysis without molecular identification. Whereas, we are developing methodologies for metabolites identification by a combination of multi-dimensional NMR measurements of uniformly stable isotope labeled plants and signal assignment with our standard ^{1}H, ^{13}C chemical shifts data base [1-3]. Here, we discuss atomic redistribution [4] of protons and carbons in isotope labeled plant cells.

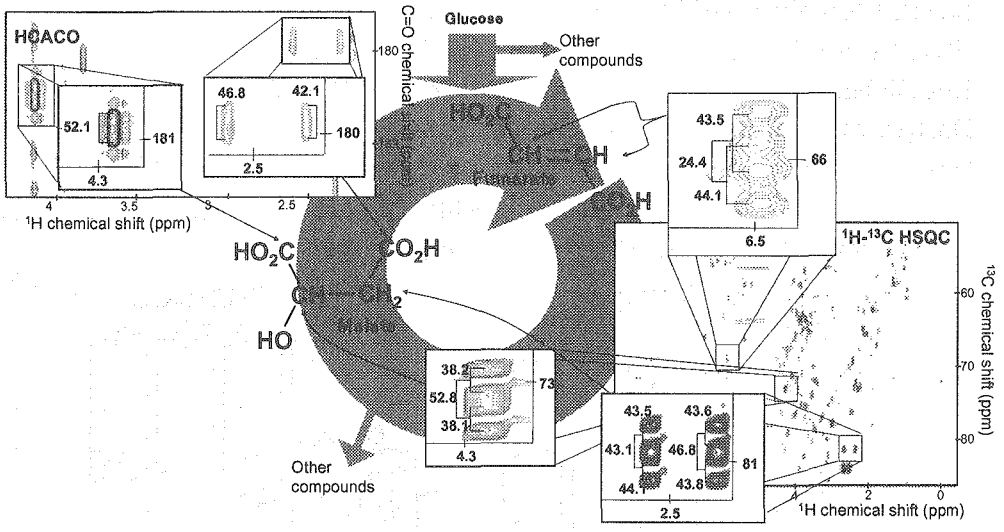

Figure 1; Schematic representation of our strategy for following ^{13}C-^{13}C couplings in the metabolism of [$^{13}C_6$]-glucose incorporated plant cells. Both ^{1}H-^{13}C HSQC and $^{13}C_{aliphatic}$-coupled HCACO spectra exhibit atomic reconstruction from $^{1}J_{C\text{-}C}$ coupling constants (Hz) and signal intensities. Gray arrows indicate the course of the metabolic pathway, and their line width show metabolic flux at the analysis point.

We optimized the culture condition of *Arabidopsis* T87 cells to pursuer the metabolic changes by labeling from [$^{13}C_6$] glucose. The 0.1 M-KPi extracted metabolites were analyzed on ^{1}H-^{13}C-HSQC and ^{13}C-^{13}C coupling constants exhibited time-dependent changes of signal intensities of major metabolites. In same cases, signal intensity rates changed among the atoms in a compound. Therefore, we found that relative ^{1}H-^{13}C signal intensity changes within the assigned metabolites can be applied to metabolic flux analysis at the atomic level. Additionally in ^{1}H-^{13}C-HSQC spectra, the information of carbonyl carbon is indirect, we also examined HCACO spectra that enable us to analyze the carbonyl carbons directly. For example, $^{1}J_{C\alpha\text{-}C'}$ values in malate carbon exhibited almost same values observed in ^{1}H-^{13}C-HSQC and $^{13}C_{aliphatic}$-coupled HCACO spectra, that indicates ^{13}C-^{13}C atomic redistribution in carbonyl carbon can be monitored in this method (Fig.1). From these result, we suppose the new methodologies for the direct analysis of carbonyl carbon, whereas conventional approach has not described (5).

In addition to ^{13}C labeling, we investigated deuterium (D_2O or [$^{2}H_7$] glucose) incorporation into the T87 cells. Firstly, the T87 cells were cultured with [$^{2}H_7$] glucose and D_2O. [$^{2}H_7$] glucose didn't inhibit the growth and cells were deuterium labeled. We also discuss the efficient labeling methodologies of D_2O without any growth inhibition.

We show here the development of novel methodologies for the analysis of "dynamic change" of metabolism at atomic level. Future perspective of their capability will be discussed at this conference.

References

1) Kikuchi, J. Hirayama, T. "Hetero-nuclear NMR-based metabolomics" *Biotech. Agri. Forest.* 57, 94-101 (2006)
2) Kikuchi, J. Shinozaki, K. & Hirayama T. "Stable isotope labeling of *Arabidopsis thaliana* for an NMR-based metabolomics approach" *Plant cell Physiol.* 45, 1099-1104 (2004)
3) Kikuchi, J. & Hirayama T. "Practical aspects of uniform stable isotope labeling of higher plants for a hetero-nuclear NMR-based metabolomics" *Methods Mol Biol,* (in press).
4) Arita, M. "Atomic reconstruction of metabolism" *Proc. Natl. Acad. Sci. USA* 101, 1543-1547 (2004).
5) Ratcliffe, R. G. and Shachar-Hill, Y. "Measuring multiple fluxes through plant metabolic networks" *Plant J.* 45, 490-511 (2006).

P096

Strategies of metabolic profiling of bacterial and animal systems

Yumiko Nakanishi[1], Shinji Fukuda[1,2], Hiroshi Ohno[1,3] and Jun Kikuchi[1,4]
[1]Int. Grad. Sch. Arts. Sci.,Yokohama City Univ, [2]RIKEN GSC,
[3]RIKEN RCAI and [4]RIKEN PSC

Key words: metabolic profiling, bacteria, murine tissue, *in vivo*, co-culture

Introduction

Although methodologies for meta-genomic analysis have been published in recent years [1,2], molecular mechanism in symbiotic systems is still unclear due to lack of strategy to investigate it. For example, huge time and costs are required for transcriptome and proteome analysis, resulting that time-dependent those analysis could be waste for laboratory' s resources. However, analysis of chemical responses influenced on interaction among organisms by time-dependent manner might gain insight in this problem. Therefore, we have been developing *in vivo* real-time NMR measurement of the metabolites [3]. In this study, we used *Escherichia coli* O157:H7 and *Bifidobacterium longum* as the symbiosis model, since their complete genome sequences are available.

Bacterial symbiotic systems

Firstly, we found these two bacteria could grow by living together and reached full-growth in NMR tube after optimization of a rich medium under anaerobic condition. These bacteria were cultured for 8 hr in NMR magnet at 37℃, and measured 1D-^{1}H and ^{1}H-^{13}C HSQC by every 30 minutes. ^{1}H-NMR analysis was used to examine global changes of the metabolites. Z-scores in aliphatic region exhibited dramatic changes in three kinds of bacterial media (Fig.1).

From this result, we focused on organic acids, and their signal assignments were performed by ^{1}H-^{13}C HSQC spectra. There, we found increase of acetate and decrease of pyruvate intensities in co-culture state. Furthermore, microarray analysis showed related metabolic gene expressions.

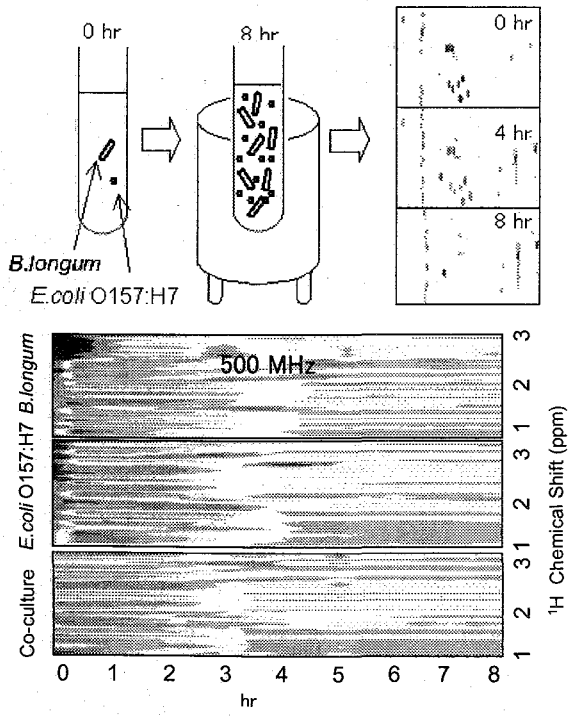

Figure 1. Methods of *in vivo* NMR of three kinds of bacterial systems. : (bottom) Z-matrix is introduced as calculated ^{1}H-NMR intensities, defined as $Z=(I_i - I_{ave}) / \sigma$.

These measurements showed bacterial intakes of nutrients and metabolism during growth and their differences of the metabolic movements in between mono-culture and co-culture states. In addition to this, we rationalized from gene to the metabolite better than the

transcriptome analysis alone.

Animal symbiotic systems

Secondly, we have investigated how these metabolite changes in three kinds of bacterial systems can affect on metabolism in symbiotic animal system. Then, these bacteria were orally administered into germ-free mice. When *E.coli* O157:H7 administrated, these mice died during almost one week, whereas *B.longum* administered mice could alive. Therefore, we collected cecal contents samples from *E.coli* O157:H7 administered mice at day 1, 3 and 5, *B.longum* administered mice at day 1, 8 and 14, and *E.coli* O157:H7/*B.longum* administered mice at day 8, 10, 12 and 14. These samples were extracted by 0.1 M-KPi and ^{1}H-NMR metabolic profiling (principal component analysis, PCA) were performed to quantify these metabolic differences. As expected from previous bacterial metabolomic studies, the PCA of mice samples were also classified as these associated bacterial systems.

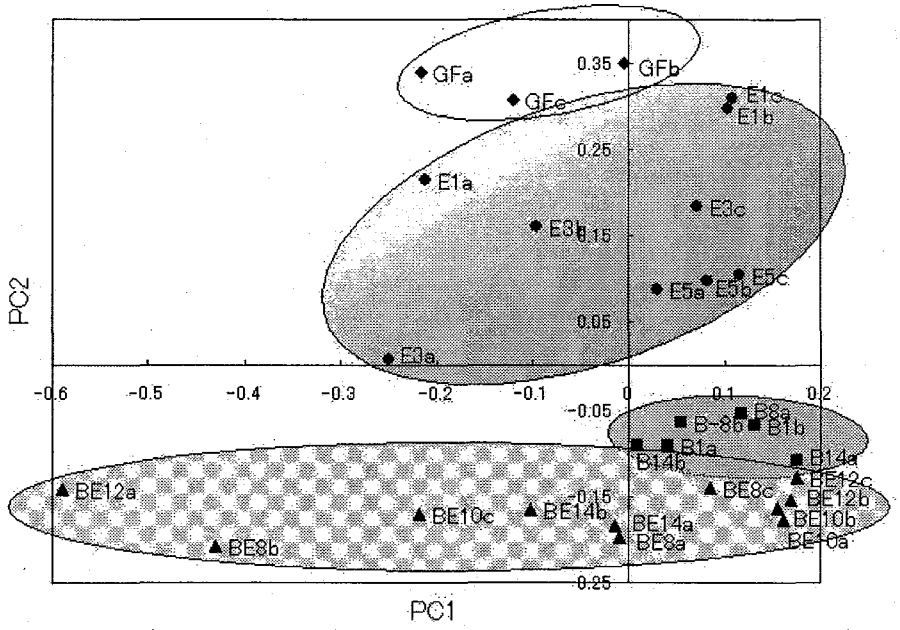

Figure 2. PCA score plots of cecal contents extracts. Each administered bacteria is denoted by different symbols. GF: germ-free, E: *E.coli* O157:H7, B: *B.longum*, BE: *E.coli*O157:H7+*B.longum* . Note that numbers 1, 3, 5, 8, 10, 12, 14 are days after each bacterial administrations, respectively.

References

1) Friedrich, M. W. (2006) *Curr. Opin. Biotech.* 17, 59-66.

2) Cowan, D. et al. (2005) *Trends Biotech.* 23, 321-329.

3) Kikuchi, J. and Akamine, K. (2006) *J. Spec. Soc.* (in press).

P097

NMR メタボローム解析技術を用いたラット組織の死後変化に関する代謝学的研究

日本医科大学　法医学講座およびNMR研究施設[1)]
京都大学　初期診療・救急医学講座[2)]
富士通(株)　バイオIT事業開発本部[3)]

○平川慶子[1)]、植草協子[1)]、小池薫[2)]、湯田浩太郎[3)]、大野曜吉[1)]

An NMR metabolomic investigation of metabolic disturbances after death in the rat tissues.

Department of Legal medicine and NMR laboratory, Nippon Medical School [1)]
Department of Primary Care & Emergency Medicine, Kyoto University [2)]
Bio-IT Group, Fujitsu Co.Ltd. 3)

Keiko Hirkawa[1)], Kyoko Uekusa[1)], Kaoru Koike[2)], Kohtaro Yuta[3)] and Youkichi Ohno[1)]

In this study pattern recognition of spectra derived from ^{1}H NMR spectroscopy was used to investigate metabolic disturbances after death in the rat skeletal muscles and brain. In early stage after death, principal component analysis (PCA) readily differentiated the NMR spectra of skeletal muscle extracts of the rat killed by different modes. PCA scores of the spectra of the tissue extract from the rat died of hypoxia varied by the hour.
NMR based metabolomic data may provide useful informations to estimate postmortem interval and to investigate the cause of death of the cadaver.

【背景】我々は、NMRデータを用いた死後経過時間の推定法の確立を目指している。これまでにラットを用いた基礎的実験で、死体大腿部骨格筋の*in vivo* ^{31}P NMRおよび摘出脳・骨格筋試料の^{1}H NMRデータによる検討を行った結果、スペクトル上で観測可能な数種の代謝物質のうち、アラニンや酢酸などの分析値が死後経過時間と高い相関関係示すことを明らかにすることができた。これらの分析値を用いて死後経過時間の推定法の確立を目指したが、残念ながら正確な予測モデルを作成するにはいたらなかった。そこで、組織中の代謝物について網羅的な分析を行う必要があると考え、あらたに^{1}H NMR based metabolomicsを用いた死体組織の代謝物プロファイリングを行い、死因による死体組織の代謝像の違いや死後経過時間との関連を検討した。死後経過時間の推定根拠に応用されている死体現象である死後硬直の発現時期や強度との関連についても検討を加えた。

Key Words: NMR-based metabolomics, postmortem changes, skeletal muscle, brain, rat

【方法】

(1)動物実験および試料の前処理:Wistar系雄ラットを用いてTable 1 に示す条件でと殺実験を行った。と殺は、酸素欠乏のほか死後硬直の発現開始時期や強度との関連を調べる目的でコカインおよび臭化パンクロニウムの大量投与にて行った。心停止確認後死体を 20℃の恒温槽内に保存した。15分以内、1、4、8、16、24、および48時間後に大腿部骨格筋および脳を迅速に採取、液体窒素中で凍結し、クライオプレス™(マイクロテックニチオン)にて液体窒素中で凍結粉砕した。さらに冷0.6N過塩素酸溶液を加えて攪拌し、その遠心上清にロック用D_2O、内部標準物質TSPを一定量添加したものを^{1}H NMR測定試料とした。**(2)^{1}H NMR-based metabolomics**:300MHzFT-NMR装置(LA-300、JEOL)で得た^{1}H NMR スペクトルデータを**Alice2 for metabolome™ ver.1.0**(日本電子データム(株))にて数値化し、主成分分析法(principal component analysis, PCA)によるデータの可視化とSIMCA法による分類を試みた。同様に**ADOMEWORKS / ModelBuilder™ ver3.1**(富士通)を用いて主成分分析その他の手法での解析を行い解析結果を比較した。

【結果および考察】

動物実験の概要はTable 1に示すとおりで、心停止前の運動量や痙攣の有無や程度と死後硬直の発現時期および強度に強い関連性があることが確認できた。

採取した骨格筋および脳組織抽出物の^{1}H NMRスペクトルデータについてAlice2 for metabolome™を用いて行ったメタボローム解析の結果は以下のとおりである。**(1)骨格筋抽出物**:主成分分析(PCA)の結果、心停止 15 分以内でのデータ群では、score plot上でと殺条件の違いによる明らかなクラスター化が視覚的に観察された。時間の経過に伴って死因によるscoreの差は小さくなり、4 時間後では死因を特徴づける代謝像を抽出することは困難となった(Fig. 1)。同一死因(hypoxia)では、死後 1 時間以内、4～8 時間後、16～24 時間後および 48 時間のデータ群でそれぞれクラスター化が認められ、死後硬直発現開始前、死後硬直発現期および緩解期から腐敗開始に至るまでの骨格筋の死後変化を特徴づける代謝像を抽出することが可能であった(Fig. 2)。クラスター化したデータ群を用いて、SIMCA法を用いた分類を試みたところ同一の死後経過時間での死因や、同一の死因での死後経過時間について良好な結果を得ることができた。**(2)脳抽出物**:主成分分析(PCA)の結果、脳抽出物では、今回のと殺条件では、脳組織に関しては、同一の死後経過時間で死因を特徴づけるようなscoreの違いは観察されなかった。同一死因(hypoxia)では、心停止後 15 分以内、1 時間後、4～16 時間後、24 時間および 48 時間後のデータ群でクラスター化が認められ、死後経過時間にともなう組織の死後変化を特徴づける代謝像を抽出することが可能であった(Fig. 3)。SIMCA法を用いて骨格筋と同様の検討を行ったところ、死因の異なるデータ群を用いても死後経過時間についてデータ群の分類が可能である結果が得られた。

以上の結果から、死体組織中の代謝物をNMR メタボローム解析法によって網羅的に分析することにより、死後経過時間をより客観的に推定しうる可能性が示された。

Table 1 Summary of observations of the experiment in this study

modes of killing	surviving time (min)	muscular activity	convulsion	rigor mortis	
				onset	intensity
hypoxia (100% N_2 gas chamber)	3	+++	−	hastened	+++
cocaine hydrochloride (200 mg/kg i.p.)	4–11	+++	+++	hastened	+++++
pancuronium bromide (1 mg/kg i.p.)	1.5–4	−	−	delayed	±

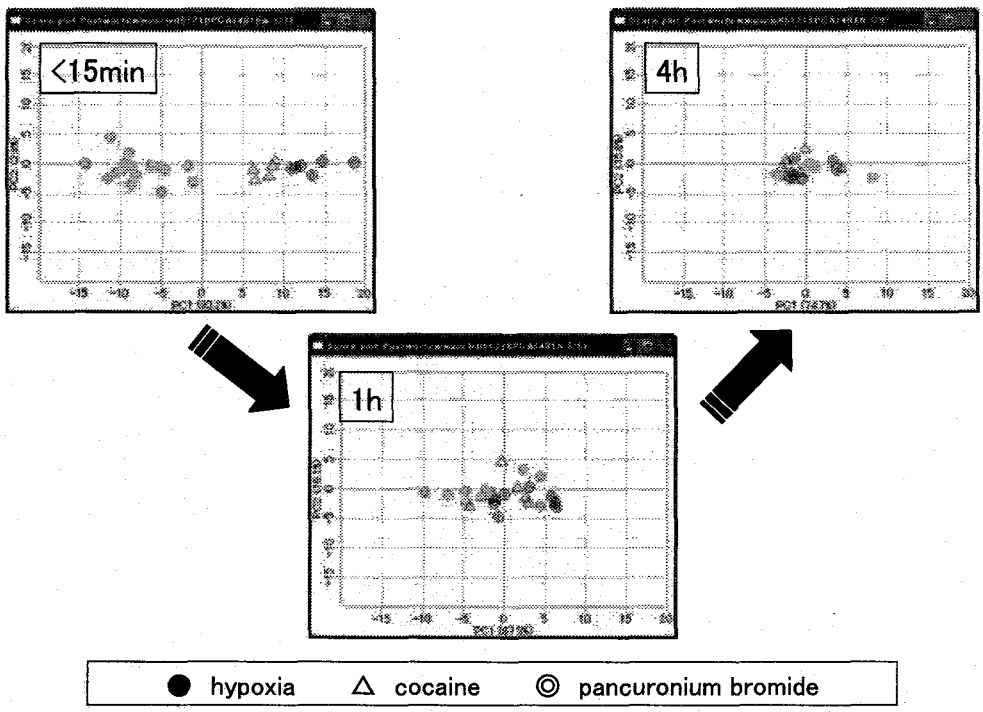

Fig. 1 Principal component analysis (PCA) of ^{1}H NMR spectra from the acid soluble metabolites extracted from skeletal muscular tissues in the rat cadaver.

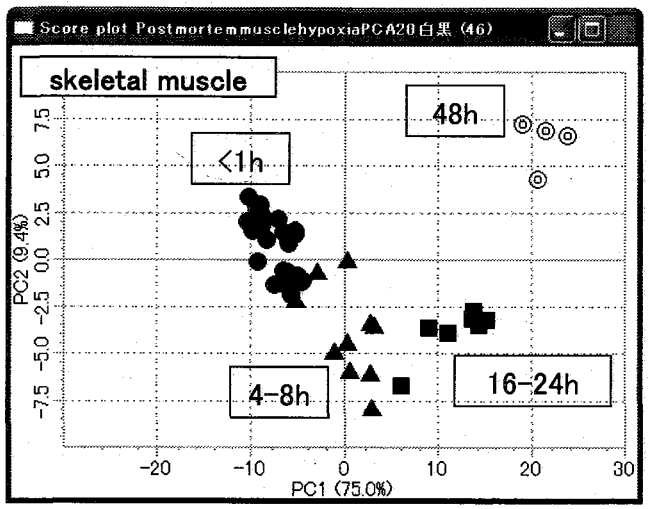

Fig. 2 Principal component analysis (PCA) of ^{1}H NMR spectra from the acid soluble metabolites extracted from skeletal muscular tissues in the rat cadaver died of hypoxia.

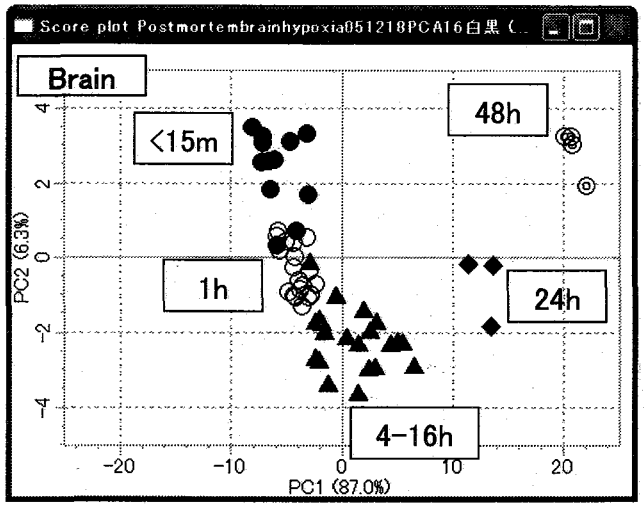

Fig. 3 Principal component analysis (PCA) of ^{1}H NMR spectra from the acid soluble metabolites extracted from cerebral tissues in the rat cadaver died of hypoxia.

P098

Non-targeted NMR Metabolomics: Evaluation of metabolic variation in female spontaneous hypertensive model rats using 1H spectra of urine

* Itiro Ando[1,2], Taeko Kataoka[2], Masako Fujiwara[3], Kazunori Arifuku[3], Kenji Kanazawa[2], Katsuo Asakura[4] and Tadashi Nemoto[2]

[1]Environmental Research Center Ltd., [2]Biological Information Research Center, National Institute of Advanced Industrial Science and Technology(AIST), [3]JEOL DATUM LTD., [4]JEOL LTD.

We have been developing a new method of non-targeted NMR analysis of mixture samples.[1)] We had analyzed male spontaneously hypertensive model rats (SHR) and normal (control) rats of 10-week-old by this method to reveal diurnal variation of their urine, and their difference between the two strains.[2)] The numbers of measured spectra from each strain were 10 which were fairly insufficient to high statistical reliability.

Therefore, we collected about 900 urine samples from 6-week- to 15-week-old female rats and acquired water-suppressed ^{1}H-NMR spectra by JEOL ECA800 spectrometer. All the data were processed by 'ALICE 2 for Metabolome' software package (ver.1.0). In the score plot by principal component analysis (PCA), clustering patterns of urine of morning, day and night are differentiated from each other as in the case of male rats that we have published[2)]. Fig. 1 shows an example of the PCA score plot of day (131 points) and night (116) urine data from female SHR rats. In this figure, ☆ and ○ indicate the datasets of night and day, respectively. The left lower cluster was datasets from night; the right upper one was that of from daytime.

In figure 2, it is shown the discrimination of the datasets of SHR strain against controls. In this figure, ☆ and * indicate the datasets of 116 SHR rats and 129 controls, respectively.

We also tried to observe the estrus cycle of each female rat combined with vaginal smear check data. A sub-space method of multivariate analysis methods (SIMCA) was submitting to differentiate the estrus cycle of pubertal female rat s' urine.

Data analysis for extremely complicated elements of the datasets (growth, circadian rhythm, estrus cycle, hypertensive and so on) will be discussed.

Keywords: metabolomics, multivariate analysis, hypertensive, urine, rat

References

1) Multivariate Analysis for ^{1}H-NMR Spectra of Two Hundred Kinds of Tea in the World, M. Fujiwara, I. Ando, and K. Arifuku, Anal. Sci. 2006, vol. 22, No.10 in press

2) Pattern Recognition Analysis for Classification of Hypertensive Model Rats and Diurnal Variation Using 1H-NMR Spectroscopy of Urine, M. Fujiwara, K. Arifuku, I. Ando, and T. Nemoto, Anal. Sci. 2005, vol. 21, 1259-1262.

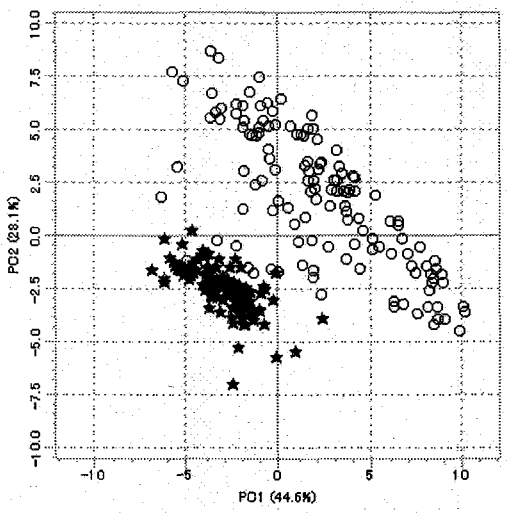

Fig. 1

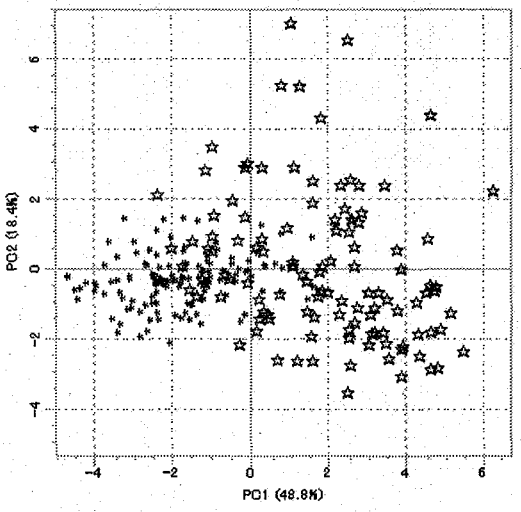

Fig. 2

P099

Non-targeted NMR Metabolomics: Detection and evaluation for disease status of inborn errors of metabolism using ^{1}H spectra of human urine

*Masako Fujiwara,[1] Itiro Ando,[2,3] Kazunori Arifuku,[1] Taeko Kataoka,[3] Kenji Kanazawa,[3] Tadashi Nemoto,[3] and Tomiko Kuhara[4]

[1]JEOL DATUM LTD, [2]Environmental Research Center Ltd., [3]Biological Information Research Center, National Institute of Advanced Industrial Science and Technology (AIST), [4]Division of Human Genetics, Kanazawa Medical University

We propose NMR-based Metabolomics using Non-targeted profiling, which provides not only excellent discriminant analysis for mixture samples[1,2] but also promising scope for clinical use. The pioneer work of metabolic research for clinical applications had performed by Prof. Kuhara's group using the gas chromatographic – mass spectroscopy (GC-MS) technique.[3] Their urease method captures wide class of metabolites and they have established diagnostic method for over 130 kinds of inborn errors of metabolism.

Our pilot study has done using urine samples from babies including inborn errors of metabolism. Eighteen urine samples were given, 10 were normal, and other 8 were abnormal samples with several inherited disorders resulted from GC-MS diagnosis. Samples were prepared by adding phosphate buffer and measured ^{1}H-NMR spectra using JEOL ECA-500 spectrometer. All the FID data were processed and analyzed by `ALICE2 for Metabolome' version1.0 (JEOL) software package to get plots of Principal Component Analysis (PCA) and a sub-space method (SIMCA). The spectra showed very different patterns from each other (in the right figure). PCA score plot submitted by18 spectra resulted in clear classification of two groups consisting of 10 and 3 samples respectively, from others. As far we concluded that 10 might be normal and 3 might be one of disorders. Then, the two groups were made as independent mathematical models for conducting SIMCA, and the remainder 5 were fitted onto the Cooman's plot which visualizes the similarity of each sample to pre-defined models. As shown in the left figure, 5 samples lined up, which revealed to discriminate each disease and also disease status from mild to severe. Three methylmalonic aciduria samples ($A_{1,2,3}$) contain methylmalonic acid as its biomarker (indicated ▲ in the spectra). They can not be differentiated by conventional single marker-detective analysis. This non-targeted profiling, however, enables us to recognize a spectral pattern as possessing multi-biomarkers and to evaluate definite disease status, e.g., attack with or without treatment, onset, or remission (well-controlled and masked condition of disease) even in the same disease. This method will be directly applicable to clinical use for the first and fast screening.

Keywords: non-targeted metabolomics, multivariate analysis, inborn error, urine, GC-MS

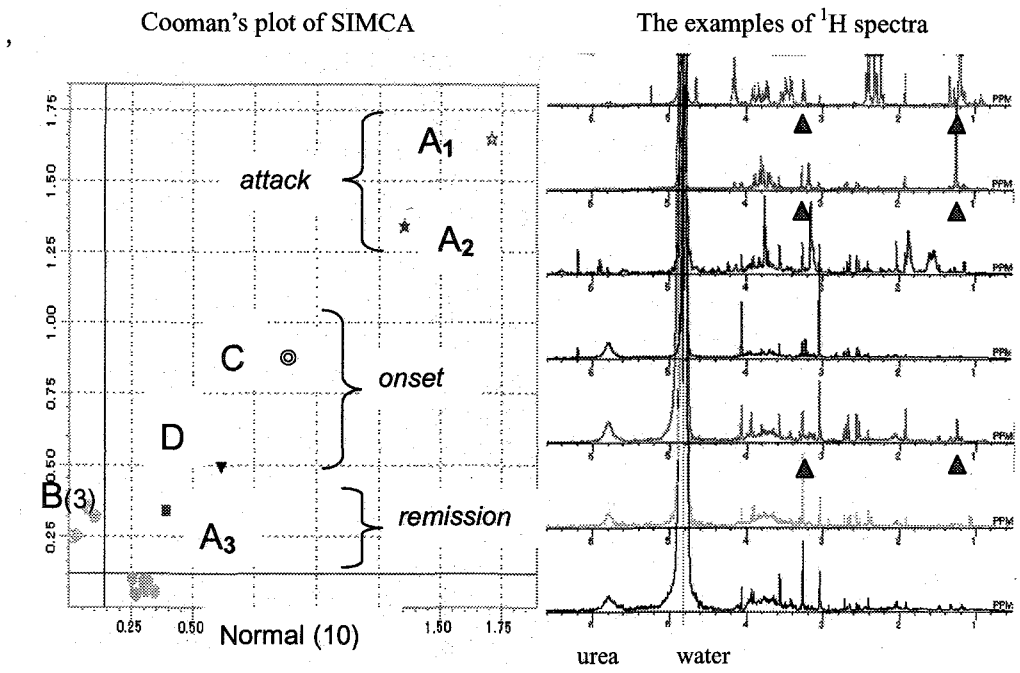

In the left figure, X axis represents normal model (n=10), Y axis represents B model (n=3) of β–Ureidopropyonase deficiency. A_1 is during severe attack treated with glucose, A_2 is during attack without treatment and A_3 is in remission, of Methylmalonic acduria. C is Citrullunemia, D is OTC (ornithine carbamoyl trasferase) deficiency, C and D are both during onset. A_3 and B are both during remission.

References

1) Pattern Recognition Analysis for Classification of Hypertensive Model Rats and Diurral Variation Using ^{1}H-NMR Spectroscopy of Urine, M. Fujiwara, K. Arifuku, I. Ando, and T. Nemoto, Anal. Sci. 2005, vol. 21, 1259-1262
2) Multivariate Analysis for ^{1}H-NMR Spectra of Two Hundred Kinds of Tea in the World, M. Fujiwara, I. Ando, and K. Arifuku, Anal. Sci. 2006, vol. 22, No.10 in press
3) Diagnosis of inborn errors of metabolism using paper urine, urease treatment, isotope dilution and gas chromatography-mass spectrometry, T. Kuhara, J. Chromatography B, 2001, 758, 3-25

P100

An efficient strategy for the screening and characterization of Arabidopsis mutants with visible phenotypes by one- and multi-dimensional NMR spectra analysis

Chunjie Tian[1], Yuri Tsuboi[1], Eisuke Chikayama[2], Yasuyo Sekiyama[2], Takashi Kuromori[3], Kazuo Shinozaki[2] and Jun Kikuchi[2], Takashi Hirayama[1,3,4],
[1]Env. Mol. Bio., RIKEN; [2]PSC, RIKEN, [3]GSC, RIKEN, [4]Yokohama City Univ.

Metabolomics is well known to be producing vast useful data which might be needed to describe the biological problem adequately, so it is an ideal strategy to use high-dimensional data from metabolic profiling to elucidate the function of gene which is still a main focus in the post-genomic era. Gene disruption mutant plants with visible phenotype are often used for the gene function analysis. As a result of a multiplicity of regulatory interactions at all levels in plant cells, different gene mutations may result in similar phenotypes, such as *albino* mutants which may owe to different gene mutation. Accordingly, it is necessary to find an efficient way to clarify the difference of mutants with similar phenotype for explaining the complex responses of single point mutation.

Unbiased metabolite analysis will offer a direct link between a gene sequence and function with the metabolic network in plants, which is an important complement for existing functional genomics methodologies. The method for metabolite profiling should be fast, reliable, sensitive, and suitable for automation, as well as covering a significant number of metabolites. In accordance with these requests, Nuclear magnetic resonance (NMR) techniques, based upon the observation and characterization of the magnetizations of nuclear spins in different chemical environments, now play an important role in investigating the physiology and metabolism of living systems. The metabolic profiling based on NMR measurement offers easier sample preparation and higher cost-effective technology than other omics methods such as transcriptome and proteome. In addition, since the metabolites, as the end products of cellular regulatory process, may represent the ultimate and direct responses of plants to genetic or environmental change, the comprehensive measurement of them can reveal the effect of most mutations.

As a test case, here several Ds transposon insertion mutants of *Arabidopsis* with albino phenotype were selected for NMR measurement based on the detection and quantification of compounds from plant leaf extract. Our goals were 1. to obtain and compare the metabolic profiling of different albino mutants for the elucidation of gene function of different mutations; 2. to establish a practical system for metabolic analysis, and confirm the efficiency of 1D-^{1}H fast screening together with 2D spectra assignment for characterization of mutants. To

Key word: Metabolic profiling, Nuclear magnetic resonance, *Arabidopsis thaliana*, albino, mutant

compare the overall chemical composition of samples, the unassigned 1D-^{1}H NMR spectra were used for fast screening of several albino mutants in terms of metabolite accumulations. Then, we labeled the mutants with ^{13}C uniformly by $^{13}C_6$-glucose uptake, and the 2D-^{13}C-HSQC spectra were acquired. These well-separated 2D-spectra allow the accurate identification of major metabolites by our original Java program, SpinAssign.

By Z-matrix and PC analysis for 1D spectroscopy, the albino mutants and control were well-differentiated, and the unique chemical regions for different lines were identified and the key metabolites were deduced. Different statistical methods based on 1D-NMR spectroscopy analysis not only made it easy to screen and characterization lines with different metabolite profiles, but also to clarify which chemical region is unique for different lines, since the relative intensity of chemical region provided the direct spectra pattern for comparison within lines. So, it suggested that this approach could be used for the selection of mutants with interesting metabolic phenotype for further analysis, especially for screening a large amount of mutants.

However, although with the advantage for the fast screening and characterizing amounts of mutants, ^{1}H-1D spectra analysis showed the deficiency: most of the chemical compounds represented in the chemical shift were unknown and difficult to be assigned according to the database available until now. An attractive alternative is to introduce of ^{13}C chemical shifts in second dimension by stable isotope labeling techniques in NMR samples, which will not only enhance the ^{13}C-signals, but also trace the metabolic movement of carbon element. In addition, the enhanced and separated signals in 2D-^{13}C-HSQC spectroscopy are more feasible for assignment comparing with 1D spectroscopy, which will offer more detail information for characterizing different mutants by metabolic approach. After labeled with^{13}C uniformly by $^{13}C_6$-glucose uptake of the seedlings, 2D-^{13}C-HSQC spectra was investigated, and the well-separated 2D-spectra provided accurate identification of major metabolites by our original Java program, *SpinAssign*. By statistics, it was found that Asn and Pro were key metabolites for distinguishing albino mutants from control lines besides the higher content of sucrose in albino mutants, and Glu, Gln and Ser were key metabolites for the difference within albino mutants. The gene expression pattern for albino mutant was studied by use of microarray analysis, and the correlation between metabolome and transcriptome in some way was confirmed.

In conclusion, for the first time, a metabolic profiling by using NMR spectroscopy analysis for albino mutants was provided by our research. Furthermore, because of the significant difference in ^{1}H-^{13}C cross-peak intensities of some metabolites not only in comparing between mutants and WT but also within albino mutants, an efficient approach for screening and characterization of mutants by using unassigned 1D-^{1}H NMR spectra combined with detailed 2D-NMR analysis was proposed, which could be used to unravel the effects of different gene mutations. Using this approach, metabolic characterization of sugar-related silent mutants is investigated now. The results will be presented and discussed.

P101

量子化学計算による α ヘリックス形ポリ(L-アラニン)の精密な構造解析

(群馬大工) ○荘司顯、相馬洋之、(奈良女) 黒子弘道、(東京工大) 安藤勲

Precise Structure Analysis of α-Helical Poly(L-alanine) by Quantum Chemical Calculation

Akira Shoji[1], Hiroyuki Souma[1],Hiromichi Kurosu[2], Isao Ando[3]

[1]Dept.Biological Sciences, Faculty of Engineering, Gunma University, [2]Graduate School of Humanities and Sciences, Nara Women's University, [3]Joint Graduate School Program of Tokyo Institute of Technology-Tsinghua University (Beijing).

We calculated the chemical shifts of α-helical poly(L-alanine) based on the quantum chemistry with Gaussian 03 software. As a result, the calculated ^{13}C chemical shifts of the main-chain C=O and C_α signals were identical with those of measurement, whereas the calculated ^{13}C chemical shift of the side-chain C_β signal was different by 2.8 ppm from that of measurement. Furthermore, we developed the hydrogen-bonding feature of α-helical poly(L-alanine).

緒言：ポリペプチドのαヘリックス構造は分子内水素結合により安定化されるため、分子間相互作用は小さいと考えられる。したがって、一本鎖ポリペプチドの量子化学計算に基づく構造最適化と化学シフトの計算結果を固体高分解能NMR測定による化学シフト実測値と比較することは意義深い。

本研究では、Gaussian 03 ソフトウエアを用いて、αヘリックスコンホメーションをとる一本鎖ポリ(L-アラニン)をモデル分子とし、その化学シフト値を計算した。その結果、主鎖カルボニル(C=O)とα炭素(C_α)の^{13}C化学シフトの計算値と実測値との間に極めてよい一致が見られた。またこの計算によって得られた最適化構造の二面角(ϕ, ψ, ω)、水素結合距離などの構造特性パラメータを基にαヘリックス形ポリ(L-アラニン)に関する精密な構造解析を行った。蛋白質の立体構造解析に量子化学計算がどの程度有用であるかについて検討する。

キーワード：ポリ(L-アラニン)、αヘリックス、構造計算、量子化学

著者：しょうじあきら、そうまひろゆき、くろすひろみち、あんどういさお

計算方法： 量子化学計算はGaussian 03ソフトウエアにより行った。構造計算にはDFT(b3lyp)法を用い、6-31G(d)の基底関数を用いて構造最適化を行い、化学シフトはDFT/6-311G(d,p)を用いGIAO-CHF法により評価した。分子構造パラメータの初期条件として、二面角(ϕ, ψ, ω)を(−57, −47, 180)と設定した。

実験： ^{15}N標識した(ヘリックス形ポリ(L-アラニン)試料[1]の固体高分解能^{13}Cおよび^{15}N NMR測定には、Bruker DRX-600 分光計を用いた（測定にご協力いただいたLeipzig大学（ドイツ）分析化学研究所のStefan Berger教授に感謝する)。

結果および考察： αヘリックス形ポリ(L-アラニン)の^{13}Cおよび^{15}N等方性化学シフトの計算値及び実測値をTable 1に示す。化学シフト値の基準にはそれぞれテトラメチルシラン($Si(CH_3)_4$)および硝酸アンモニウム($^{15}NH_4NO_3$)を採用した。

Table 1. ^{13}C and ^{15}N chemical shifts of α-helical poly(L-alanine) calculated and measured.

	^{13}C chemical shifts, δ_{iso} (ppm)			^{15}N chemical shifts, δ_{iso} (ppm)
	C=O	C_α	C_β	
Calculation	176.9	53.8	12.8	98.9
Measurement	177.0	53.2	15.6	98.8

Table 1からわかるように、ポリ(L-アラニン)の主鎖C=OおよびC_αの計算された^{13}C化学シフト値は実測値と非常によい一致を示した。一方、側鎖C_βの^{13}C化学シフトの計算値は実測値より約3 ppm小さかった。この差は分子間における側鎖間相互作用に起因すると考えられる。従って、一本鎖のαヘリックス形ポリペプチドの量子化学計算による構造最適化と化学シフトの計算結果は、その主鎖コンホメーション（二次構造）を議論する上で信頼に値する重要な知見を呈することが明らかとなった。更に分子間相互作用を考慮した量子化学計算を行なうことによって、より精密な立体構造解析が行えるものと期待できる。

本研究では、α ヘリックス形ポリ(L-アラニン)の二面角(ϕ, ψ, ω)、水素結合距離、化学シフトテンソルなどの構造パラメータの解析結果についても発表する予定であり、蛋白質の精密な立体構造解析に量子化学計算が有用であることを示す。

文献：[1] H. Kimura, T. Ozaki, H. Sugisawa, K. Deguchi, A. Shoji, *Macromolecules* *31*, 7398–7403, **1998**.

P102

モデル構造を用いた自動帰属法

[1]大阪大学大学院薬学研究科, [2]大阪薬科大学
○吉田卓也[1], 小林祐次[2], 大久保忠恭[1]

Automatic resonance assignment method based on homology model

[1]Graduate School of Pharmaceutical Sciences, Osaka University, [2]Osaka University of Pharmaceutical Sciences
Takuya Yoshida[1], Yuji Kobayashi[2], Tadayasu Ohkubo[1]

Here, we report an approach to solve the assignment problem automatically from structural information of a homologus protein. In this approach, sets of chemical shifts are predicted from a determined structure or a model structure of the target protein constructed by homology modeling. They are combined to the observed resonances of the target by using a bipartite graph matching algorithm. At first, we tested this procedure with proteins which had been analyzed by both of NMR and X-ray crystallography. When the known structure of a target protein was used as an ideal model structure (reverse assignment), about 60% of backbone assignments were correctly obtained. Then, this method was applied to parkin and ribosome recycling factor. The homology structure based method with an additional optimization using NOE information yielded almost all correct assignments.

[緒言] タンパク質の NMR における帰属は、しばしば X 線結晶構造解析における位相問題に例えられる。X 線結晶構造解析においては、対象分子と相同性が高い分子の立体構造が既に決定されている場合、分子置換法がもっとも効率の良い位相決定法として確立されている。一方、NMR 法において確立している帰属法では多数のスペクトルや、異なった標識試料が必要であり、その効率は高いとはいえない。NMR 法は、分子内運動やフォールディング、分子間相互作用といった様々な情報をアミノ酸残基レベル、あるいは原子レベルで得ることができる大変優れた手法である。従って近年構造ゲノム科学の成果により多くのタンパク質の立体構造が決定されていることを考慮すれば、今後立体構造が既知であるか、あるいはホモロジーモデルが構築可能な

帰属、自動化、ホモロジーモデル

よしだたくや、こばやしゆうじ、おおくぼただやす

タンパク質についてその帰属を簡便に行う手法が重要になると考えられる。本研究では、そのような手法の開発をおこなった。

[方法] まず、主鎖化学シフト情報のみに基づく逆帰属法の検討を行った。この方法では、既知立体構造から、期待される化学シフトを計算し、観測された化学シフトとの差を最小化することによって帰属をおこなう。この場合計算値と観測値は 1:1 に対応し、その組み合わせは N!通りあるが、それぞれを独立に評価できるので、2 部グラフのマッチングアルゴリズムを応用し多項式時間で最適化できる。次に、アミドプロトン間の距離情報(NOE)を用いた手法を検討した。NOE は２つのプロトンの帰属に依存するため、上述の手法では最適化できない。そこで、遺伝的アルゴリズムを用いた探索法及び予測 NOE パターンと実測 NOE パターンの類似性を評価し最適化する手法を検討した。

[結果と考察] 立体構造及び主鎖の化学シフト帰属が既知のタンパク質数種類について、化学シフト情報に基づく逆帰属法を評価した。主鎖 H^N,N,C'を用いた場合平均 20%の化学シフトを正しく帰属できた。これは 3D HNCO 実験のみを使用した場合に相当する。また主鎖 H^N,N,Cα, Cα(-1)を用いた場合(3D HNCA 実験のみを使用した場合に相当)、Cαの連結性を用いることなく平均 60%の化学シフトを正しく帰属でき、Cαの連結性を用いればほぼ完全な帰属が可能であった。

アミドプロトン間の NOE 情報を用いた場合の結果は探索の初期解に依存した。シミュレーションの結果初期解が 20%以上正しければ、NOE 情報によってその間違いが訂正でき、最終的にほぼ 100%正しい帰属が可能であることが示された。従って構造既知のタンパク質においては、HNCO 及び ^{15}N-edited NOESY のみで、主鎖 H^N,N,C'核の帰属が可能であることが示唆された。これらの実験は比較的高分子量のタンパク質でも感度良く測定可能であり、X 線結晶構造解析で得られた高分子量タンパク質の構造情報を NMR 解析に活用する上で有用であると考えられる。

最後にこれらの手法を、ホモロジーモデリングによって構築したモデル構造に対して用いることを検討した。対象として NMR 帰属情報が既知である parkin(78 残基)及び緑膿菌 ribosome recycling factor (RRF, 185 残基)を用いた。モデル構造はそれぞれユビキチン及び超好熱菌 RRF を用い構築した。アミノ酸の同一性はそれぞれ 34%,41%である。parkin の場合、主鎖 H^N,N,C'を用い 17%の化学シフトを正しく帰属できた。さらにその結果をアミドプロトン間の距離情報を用いて改良したところ、90%以上の帰属を正しく得ることに成功した。一方 RRF の場合、主鎖 H^N,N,C'及び距離情報だけでは探索過程が十分に収束しなかったため、現在パラメータの最適化を行っている。

P103

フラグメント（FMO）分子軌道法による生体分子のNMRシフトの推算

[1]東京工業大学，生命理工学研究科，[2]三菱化学科学技術研究センター.
&JST-CREST，[3]三菱化学生命科学研究所センター
コウチ○[1]，横島智[2]，小林高雄[2]，河野俊之[3]，中村振一郎[2]

Ab initio calculations of NMR chemical shift of bimolecular system by FMO method

[1]Department of Biomolecular Engineering, Tokyo Institute of Technology, [2] Science and Technology Research Center, Mitsubishi Chemical Group, & JST-CREST, [3]Mitsubishi Kagaku Institute of Life Sciences
Qi. Gao○[1], Satoshi. Yokojima[2], Takao. Kobayashi[2], Kohno.Toshiyuki[3], Shinichiro. Nakamura[2]

Abstract

Fragment molecular orbital (FMO) approach together with the gauge invariant atomic orbital (GIAO) method has been used to calculate the chemical shift values of several bio-molecular systems (i.e. small peptide and ubiquitin protein). The chemical shifts calculated by the FMO-GIAO method accurately reproduce those obtained by the full GIAO calculation. The calculated values of ubiquitin protein are in good agreement with the experimental data, which is observed in a natural environment. This ab initio quantum approach also allows us to calculate chemical shifts for large bio-molecular system with an acceptable computational cost.

本文

今日、NMR（nuclear magnetic resonance）スペクトル法はひとつの強力な実験手法として生体分子（例：たんぱく質、DNAなど）の構造やダイナミックなどの情報を調べるのにひろく使用されている。しかし、一方では、生体分子の揺らぎや実験装置自身の限界などの問題で、完全に生体分子の構造、とくに局小的な情報が現時点でのNMR実験で測定できないことも事実である。これらの問題を解決するひとつの方法としてはコンピュータを駆使し、計算科学の理論を基づいて、生体分子のケミカルシフトを推算することである。

キーワード: FMO Protein Abinitio Chemical shift

著者ふりがな：こう ち、よこじま さとし、こばやし たかお、こうの としゆき、なかむら しんいちろう

NMR のケミカルシフトの理論的な推算がこの半世紀に渡って多くの研究者たちによって取り組まれてきた。現在では比較的小さい有機分子の炭素なら、とても高い精度のケミカルシフトが推算できる。しかし、環境に敏感な水素や窒素などの原子種に対する正確な理論推算はまだ難しい。またコンピュータのコストを考えると、生体分子全体のケミカルシフトの推算は困難である。本研究では FMO（Fragment Molecular Orbital）という計算手法を用いて、ab initio 法によるたんぱく質のケミカルシフトの理論推算が実行した。テスト計算としてユビキチンが用いられた。計算の結果と実験値を比較し、炭素、水素と窒素がすべてにわたって実験値とよい一致をみた（Fig. 1）。従って、この手法によって、大きな系でも比較的小さな計算コストでケミカルシフトの推算ができるようになった。さらに精度や計算時間などを改善していけば、将来的にきっと多くの研究（ex：構造解析や分子相互作用など）に不可欠な存在になるだろう。

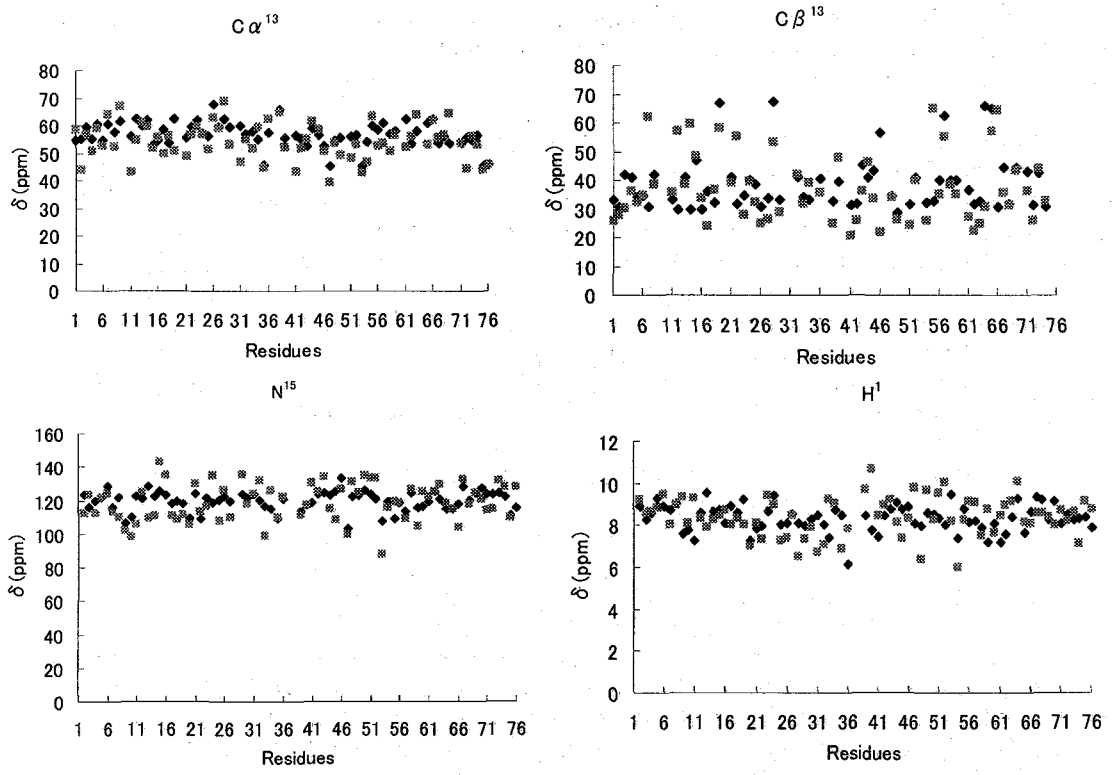

Fig. 1 The comparisons between FMO-NMR calculations (pink dots) and experimental (blue dots) results for C_{α}^{13}, C_{β}^{13}, N^{15} and H^{1} atoms.

P104

Expected peak overlap in multidimensional NMR spectra

Roland Schmucki[1,2], Peter Güntert[1]

[1]RIKEN Genomic Sciences Center
[2]Graduate School of Science, The University of Tokyo

The major problems when analyzing multidimensional NMR spectra for the determination of three-dimensional protein structures are peak overlap, low signal-to-noise ratios, and spectral artifacts. Peaks can readily be identified and analyzed only if they are above the noise level and not overlapped with other peaks or spectral artifacts.

The extent of peak overlap depends on the size and amino acid composition of the protein, the sample conditions and relaxation properties which are manifested mainly in the resonance line widths, the type of experiment, and the type of cross peak under investigation.

Here, we present a measure for estimating expected peak overlap in protein NMR spectra. Given the amino sequence of the protein, all theoretically expected peaks in a given NMR spectrum are determined on the basis of the knowledge of the protein sequence and the magnetization transfer pathways of the pulse sequence that was used to acquire the spectrum (1). Then, the probability that an expected peak overlaps with other expected peaks in the spectrum is calculated. For this calculation, we assume that the chemical shift values of each ^{1}H, ^{13}C and ^{15}N atom in a protein are distributed according to a Gaussian probability distribution. Its mean value and standard deviation are derived from a statistics over a large number of proteins for which chemical shift assignments are stored in the BioMagResBank (BMRB) (2).

The main goal of the expected peak overlap probability calculation is to provide a measure that can be computed readily before measuring or analyzing the spectrum for predicting which peaks in a spectrum will be likely to show overlap.

Our measure for the expected peak overlap in multidimensional NMR spectra formalizes and quantifies with only a small number of assumptions the common experience of NMR spectroscopists that certain kinds of spectra, signals and spectral regions are "easy" or "difficult" to analyze because they show few or extensive peak overlap. For instance, the crowding of NOEs between aliphatic side-chain protons or in the vicinity of the diagonal result naturally from the expected peak overlap calculation without additional, heuristic assumptions.

This information can be used in the design of new sample preparation methods, including optimal isotope labeling, and to guide the development of novel pulse

Keywords: Peak picking; Overlap probability; Resonance assignment; Automated spectra analysis; Automated structure determination

sequences in NMR experiments. The feasibility of resonance assignment strategies that rely on the interpretation of certain classes of cross peaks can be estimated before performing the NMR measurements. Such a prediction is particularly advantageous when the sample preparation is demanding, as for example in the case of larger proteins which result in more and broader peaks than small proteins, or when studying membrane proteins under conditions that result in increased linewidths, e.g., in mixed protein-detergent micelles (3).

Furthermore, the knowledge of expected peak overlap is useful in the process of automatically assigning the resonance frequencies by automated computer algorithms (1, 4). The information about the expected peak overlap can help the automated algorithm to score possible peak identifications and assignments. For instance, it is possible to objectively impose a higher penalty if an expected cross peak is not found in a virtually non-overlapping spectral region, e.g., in a triple resonance spectrum for the assignment of the polypeptide backbone, than if another cross peak in a crowded region of an HCCH-TOCSY spectrum is missed.

References:

(1) Bartels, C., Güntert, P., Billeter, M. & Wüthrich, K. GARANT - A general algorithm for resonance assignment of multidimensional nuclear magnetic resonance spectra. *J. Comp. Chem.* 18, 139-149 (1997).

(2) Seavey, B. R., Farr, E. A., Westler, W. M. & Markley, J. L. A relational database for sequence-specific protein NMR data. *J. Biomol. NMR* 1, 217-236 (1991).

(3) Fernández, C., Hilty, C., Wider, G., Güntert, P. & Wüthrich, K. NMR structure of the integral membrane protein OmpX. *J. Mol. Biol.* 336, 1211-1221 (2004).

(4) Gronwald, W. & Kalbitzer, H. R. Automated structure determination of proteins by NMR spectroscopy. *Prog. NMR Spectrosc.* 44, 33-96 (2004).

P105

SpinAssign: 多次元NMRメタボミクスのためのコンピューター支援スペクトル解析システム

[1]理化学研究所　植物科学研究センター、[2]横市院国際総合、[3]CREST JST、[4]名大院生命農
○近山英輔[1]、平山隆志[1,2,3]、篠崎一雄[1]、菊地淳[1,3,4]

SpinAssign: a Computer-Aided Spectral Analysis System for Multi-dimensional NMR-based Metabomics

[1]RIKEN Plant Science Center, [2]Int. Grad. Sch. Arts Sci., Yokohama City Univ., [3]CREST, JST, [4]Grad. Sch. Bioagr. Sci., Nagoya Univ.
Eisuke Chikayama[1], Takashi Hirayama[1,2,3], Kazuo Shinozaki[1] and Jun Kikuchi[1,3,4]

Abstract: Conventional NMR-based metabomics approaches based on multivariate analysis show global aspects of NMR spectra of metabolite mixtures without assignments of individual signals. We are aiming at precisely identifying metabolites from biological samples by *in vitro* or *in vivo* NMR, assigning the individual peaks as many as possible. Therefore, we developed a computer-aided spectral analysis system for hetero-nuclear multi-dimensional NMR-based metabomics named as **SpinAssign**. Using our system, which contains standard chemical shifts data for 140 metabolites, we obtained more than 100 unique assignments (about 50 metabolites) for each peaks in ^{13}C-HSQC spectra. Furthermore, we confirmed exact assignment of them by through-bond connectivity in the 3D HCCH-COSY spectra of uniformly ^{13}C-labeled *Arabidopsis* T87 cells using our developed system.

我々はNMRを用いたメタボローム研究の方法論構築を目指している。従来は、多変量解析的方法論を用いて全体スペクトルの変動で生命システムの輪郭を描き出すことが重要視されてきた。代謝活動は、分子群のネットワークとバランスで成立しており、これらの全体像を輪郭として捉える従来法のアプローチは重要である。

Keywords:
Metabomics, HSQC, Signal assignment, Database, Java,

ふりがな:
ちかやまえいすけ、ひらやまたかし、しのざきかずお、きくちじゅん

しかしながら、ゲノム機能に関連づけてトランスクリプトームやプロテオームとの統合的解析を将来目指すのであれば、個々の代謝産物の網羅的な同定を行うことが必要になると考える。従って我々は、生物試料の *in vitro* / *in vivo* NMR による代謝産物一斉帰属方法論の開発を遂行している。これを従来の方法論と統合することで、複雑な生命システムを理解するメタボローム研究の基礎方法論が完成すると期待する。ここでは、NMR メタボミクス研究の基盤ソフトウエアとしてスペクトル解析システム **SpinAssign**（**Fig.1**）の開発現状を報告する。現在までに代謝経路中に存在する 140 の代謝産物について、標準化合物を用い^{13}C-HSQCを個々に測定、^{1}Hと^{13}Cケミカルシフトを標準データベースとして収集し、スペクトル解析システムに実装した。関心のある生物試料からの^{13}C-HSQCスペクトルは、このシステムにより標準ケミカルシフトデータベースと照合され、代謝産物の有無が一斉に帰属される。このシステムでは、さらに信頼性を追及するために 3Dスペクトルにも対応しており、3Dスペクトル内のピークを 2D ^{13}C-HSQC スペクトルの帰属結果と連動して探索できる設計により、効率的な帰属の検証を行うことができる。また関連するスペクトルファイルと更新時間や帰属時の注釈などを含む帰属テーブルファイルを 1 つのプロジェクトとして保存しておくことができ、長期間の帰属作業も容易に行うことができる。今回我々は^{13}C標識化カイコ体液およびシロイヌナズナT87 培養細胞からNMRサンプルを調整し、^{13}C-HSQCと 3D HCCH-COSYを測定した。その結果、代謝産物由来の約 550 のHSQCピークを 1 つのNMRサンプル管から得た。そしてこのシステムを用いて代謝産物の一斉帰属を行った結果、約 50 種の代謝産物に相当する約 100 のピークが標準データベースとユニークにマッチし帰属された（**Table 1**）。さらに 3D HCCH-COSYのスペクトルを帰属結果と連動させてシステマティックに解析し、T87 に関しては 24 種の代謝産物について 2D の帰属結果と整合する相関ピークを見出すことができ、極めて高い確率でその代謝産物が存在していることを証明することができた（**Table 2**）。結果として代謝産物24 種 89 原子の帰属テーブルを得た。

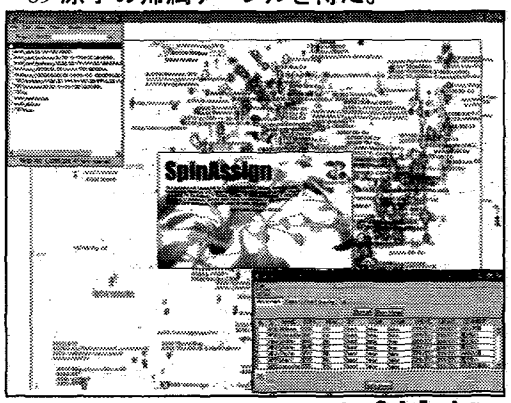

Figure 1. A snapshot of **SpinAssign**, computer-aided spectrum analysis system for hetero-nuclear multi-dimensional NMR-based metabomics

Table 1. Summary of batch-assigned peaks and compounds (in parentheses)

	Total	Assigned	Unique
Silkworm	552	188	125
		(97)	(64)
T87	544	192	122
		(108)	(60)

Table 2. Confirmation by 3D HCCH-COSY

	Confirmed assignments
Silkworm	34 (11)
T87	89 (24)

低温 MAS-NMR プローブの開発にむけて

○水野　敬 (日本電子㈱)、竹腰清乃理 (京都大・理)

The Depvelopment of Cryogenic MAS-NMR probe

Takashi Mizuno[1] and K. Takegoshi[2]
([1]JEOL ltd., [2]Faculty of Science, Kyoto University)

固体NMRは、様々な相互作用からもたらされる磁気的環境を反映したスペクトルを得られ情報量が多く、化合物の同定だけでなく、複合材料の構造・ダイナミクス情報の解析を行ううえで、非常に強力な測定手段である。その一方、NMRは静磁場下の核スピンの磁気モーメントからなる統計集団を観測対象としており、分光学的にエネルギーの最も低いラジオ波領域の遷移を扱うため、雑音の影響を受けやすく、感度が低いことが分析装置としての最大の弱点であった。

我々は、NMRの感度を向上させる方法の一つとして、磁化信号の検出機構であるNMRプローブの熱雑音に注目した。NMR分光法における雑音源の大部分は、試料磁化による誘導起電力を生じる検出コイルにおける熱雑音であり、信号の初段アンプにおける付加的雑音がそれに次ぐ。よく知られているように、ある帯域幅 B[Hz] における抵抗 R [Ω] の抵抗体の熱雑音の雑音スペクトル強度 e_n[V] は、周囲と熱平衡にある温度 T[K] のとき、

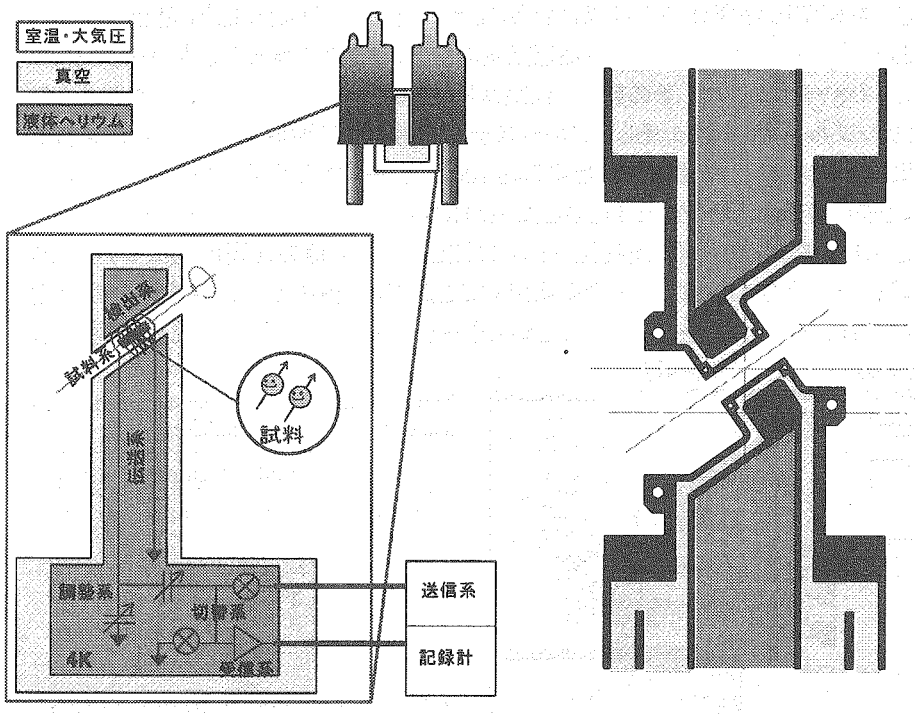

Figure 1: 低温 MAS-NMR プローブの構成概念図。試料を室温空間に保持しながら、検出系や信号受信系をヘリウム温度に冷却する構造とする。

[1]○みずの　たかし、たけごし　きよのり
Key Words: MAS, probe, cryo, solid-state NMR

$$e_n = \sqrt{4kTRB} \tag{1}$$

として表され、温度の1/2乗に比例する (ただし、kはボルツマン定数)。そこで、NMRプローブ電気回路を冷却することによって、これらの雑音が減少すれば、NMR信号の感度が増加する。このアイディアは、「クライオプローブ」として研究が進められ、溶液NMRにおいてはすでに実用化に至っている。このアイディアを固体高分解能NMR法に適用するには、まず検出器冷却システムを備えた低温プローブに試料管回転システムを据え付ける必要がある。我々は、300 MHz用のワイドボアマグネットに適用可能な、低温プローブ用の試料管回転システムを設計した。Figure.1 (下) は、5 ϕの試料管を常温下に、サンプルコイルを4 K下に置くように熱設計を最適化した場合のプローブ上部の、検出コイル付近の断面概念図である。中心に、試料管がマジック角になるように配置し、試料回転システムは両脇の凹んだところに入る。濃い網掛で示した空間に液体ヘリウムが充填される。薄い網掛は真空層である。今後、回路性能や熱特性などを検討し、プローブの製作を行う予定である。

信号の初段アンプは能動素子であるため、その雑音は上式の熱雑音のみに由来しないけれども、低温で動作させることによって、あるていど感度が改善されることは見出される。MITEQ社より液体ヘリウム温度での動作を謳っているもの (AFS3) を購入して自作NMR装置 (7T) において雑音の温度依存性について検討した。室温測定用のプローブを用いて、信号アンプだけを室温から10度おきに-150Kまで冷却して信号雑音比 (SN比) を測定した (下図左) ところ、300Kから240Kまでアンプ冷却による約1.5倍のSN比の向上が観測されたが、それ以下の温度でのSN比の向上は観測されなかった (下図右)。これは雑音がコイルの熱雑音に支配される領域になったためであると考えられ、現在、コイルを液体ヘリウムに漬す構造のプローブを作成して、コイル温度とSN比の関係を測定する準備を行っている。

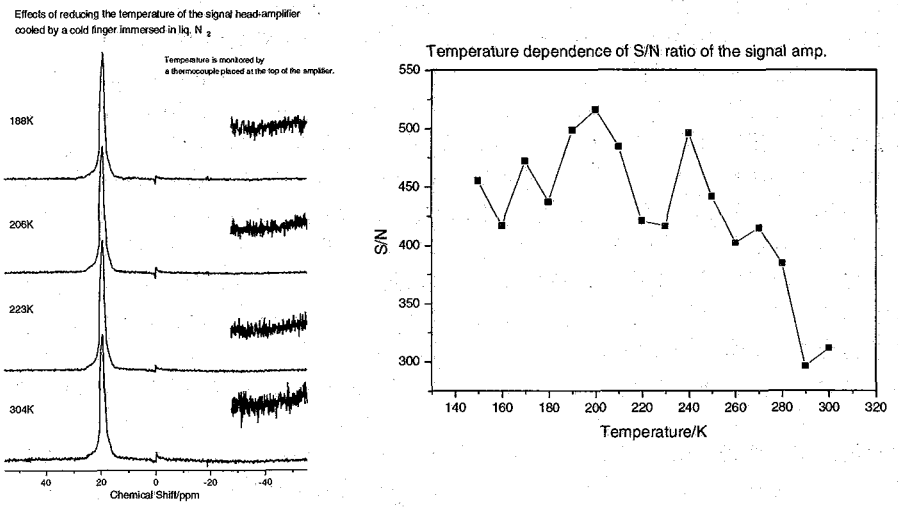

Figure 2: NMRスペクトルのプリアンプの温度に対する依存性。(左図) 各プリアンプ温度におけるベンゼンの^{1}H-NMRスペクトル。右はノイズ部分を50倍に拡大したもの。(右図) S/N強度比をプリアンプ温度に対してプロットしたもの。ノイズ強度は、検出されたノイズのRMSとしている。

P107

揺動磁場下での高分解能NMR

(京大院理[1]、物材機構[2])
○飯島隆広[1]、竹腰清乃理[1]、端健二郎[2]、藤戸輝昭[2]、清水　禎[2]

High-resolution NMR under an unstable magnetic field

T. Iijima[1], K. Takegoshi[1], K. Hashi[2], T. Fujito[2], and T. Shimizu[2]
[1]*Department of Chemistry, Kyoto University*
[2]*National Institute for Materials Science (NIMS)*

A method for compensating effect of field fluctuation is examined to attain high-resolution NMR spectra under an unstable magnetic field. In this method, time dependence of electromotive force induced for a pickup coil attached near a sample is measured synchronously with an acquisition of NMR. Observed voltage across the pickup coil is then converted to field fluctuation data, which is used to deconvolute NMR signals. The feasibility of the method is studied by ^{79}Br MAS NMR of KBr under a 30 T magnetic field of a hybrid magnet. Twenty single-scan NMR signals were accumulated after the manipulation, resulting in a spectrum of a single main peak with its spinning sidebands.

【始めに】平衡磁化や化学シフトの大きさは印加磁場の大きさに比例するため、感度や分解能の向上のために磁場の強磁場化は極めて有用である。高分解能NMRを行うには、磁場の強度に加え安定性が重要となる。

NMR用の強磁場磁石としては超伝導磁石、水冷銅磁石、ハイブリッド磁石、パルス磁石がある。このうち、かなり安定した磁場を提供する超伝導磁石がこれまでほとんどの高分解能NMRに用いられてきたが、その磁場強度はせいぜい22-23 Tである。一方、パルス磁石は非常に大きな磁場を提供可能で、58 Tまでの磁場でのNMR測定が行われている[1]。しかし、磁場の持続時間はミリ秒のオーダーであり、種々のNMR測定には短すぎる。更に、磁場の再現性は不十分であり、また均一度も極めて悪いため、現状ではパルス磁石は高分解能NMRには適さない。そのため、磁場が1時間以上持続し、かつ、良好な均一度も望める水冷銅磁石やハイブリッド磁石が、高分解能NMR用の強磁場磁石として期待される。実際に、Ganらはフロリダの NHMFL に設置されているハイブリッド磁石を用いて、40 Tの磁場での^{27}Al MAS NMRスペクトルを報告している[2]。しかし、通常は水冷銅磁石やハイブリッド磁石の磁場の安定度は悪く、これらの磁石を使った高分解能NMRは一般的でない。例えば、筑波のNIMSのハイブリッド磁石では、数10 Hz付近の周波数成分をもつ振幅3 mT程度の磁場揺動が起こっている[3]。従って、このような磁石で高分解能NMRスペクトルを測定するには、磁場揺動の影響を取り除くことが必須である。

磁場の変化は超伝導磁石にも存在している。ドリフトと呼ばれるこの変化は通常NMRロックにより補正されている。しかし、NMRロックは周波数1 Hz以下、かつ振幅1 mT

high-field NMR, field fluctuation, pickup coil, hybrid magnet

いいじまたかひろ、たけごしきよのり、はしけんじろう、ふじとてるあき、しみずただし

以下の小さな変化しか補正できず、上記のハイブリッド磁石で生じるような速い、大きな揺らぎをNMRロックで補正することはできない。

水冷銅磁石やハイブリッド磁石で高分解能NMRスペクトルを測定するための方法は、これまでに幾つか報告されている。しかしながら、それらの多くは試料などに制約がある。そこで本研究では、NMR測定は通常通り行い、これとの同期測定によって得られる磁場揺動データを用いて、NMR信号中の磁場揺動成分を補正する方法を開発する。NIMSのハイブリッド磁石を用い、KBr試料の^{79}Br MAS NMRで本法の実証実験を行った。

【原理】 水冷銅またはハイブリッド磁石によって提供される磁場$B(t)$は以下で表すことができる。

$$B(t) = B_0 + B_{\rm f}(t), \tag{1}$$

ここでB_0は数10テスラのstaticな強磁場、$B_{\rm f}(t)$はミリテスラのオーダーの振幅を持つ時間に依存した揺動磁場である。(1)式の磁場下でシングル・スキャンのNMR測定を行った場合、n個のLorentzianカーブのFID信号$g(t)$は次式で表される。

$$g(t) = \sum_{j=1}^{n} a_j \exp[-{\rm i}(\Delta\omega_j t + \phi_{\rm f}(t) + \phi_{0j}) - t/T_{2j}], \tag{2}$$

ここで、a_j, $\Delta\omega_j$, ϕ_{0j}及びT_{2j}はそれぞれj番目のスペクトル成分の強度、磁場B_0でのNMR周波数、初期位相、及びスピン－スピン緩和時間を表す。$\phi_{\rm f}(t)$が揺動磁場$B_{\rm f}(t)$のために生じる、時間に依存した位相角であり、次式で与えられる。

$$\phi_{\rm f}(t) = \gamma \int_{-\tau_{\rm d}}^{t} B_{\rm f}(t')\,{\rm d}t', \tag{3}$$

ここでγは観測核の磁気回転比である。$\tau_{\rm d}$は照射rfのパルス幅とacquisition delayの和である。時間の原点はFID信号の取り込み開始時間に一致している。

本研究では$B_{\rm f}(t)$を、サンプル近くに取り付けたピックアップ・コイルに発生する誘導起電力(induced electromotive force, IEF)の信号$V(t)$の測定により求める。$V(t)$の測定はFID信号$g(t)$の測定と同期して行う。この場合、$B_{\rm f}(t)$は以下の式を用いて$V(t)$から見積もることが出来る。

$$B_{\rm f}(t) = B_{\rm f0} - \frac{c}{mS}\int_{-t_{\rm ini}}^{t} V(t')\,{\rm d}t'. \tag{4}$$

ここで、mとSはそれぞれピックアップ・コイルの巻き数と断面積である。cはコイルの内部にある物質の透磁率を表すパラメータである。$V(t)$の取り込みは、条件$t_{\rm ini} \geq \tau_{\rm d}$を満たす$-t_{\rm ini}$から始まる。$B_{\rm f0}$は揺動磁場のオフセットであるが、これは以下の2つの理由により生ずる。一つは、$t = -t_{\rm ini}$での揺動磁場はゼロとは限らないことである。もう一つのより重要な理由は、周期が数10 msを超える遅い揺動が起こり得るが、そのような遅い揺動をピックアップ・コイルで正しく検出するのは困難だからである。尚、cと$B_{\rm f0}$はフィッティング・パラメータとして扱い、数値的に求める。NMR信号の磁場揺動成分の補正は、IEF信号$V(t)$と式(3), (4)から$\phi_{\rm f}(t)$を求めた後に補正信号$\exp[{\rm i}\phi_{\rm f}(t)]$を作成し、FID信号$g(t)$を以下のようにdeconvolutionすることにより行う。

$$\begin{aligned} g'(t) &= g(t) \times \exp[{\rm i}\phi_{\rm f}(t)] \\ &= \sum_{j=1}^{n} a_j \exp[-{\rm i}(\Delta\omega_j t + \phi_{0j}) - t/T_{2j}]. \end{aligned} \tag{5}$$

生成される信号 $g'(t)$ は $\phi_f(t)$ を含まず、static な磁場 B_0 の下での FID 信号になる。

【実験】 NMR と IEF の信号測定は NIMS のハイブリッド磁石を用いて行った。印加磁場 30 T の内訳は超伝導磁石による磁場 14 T と水冷銅磁石による磁場 16 T であった。

プローブには、JEOL 社製 4 mmϕ MAS ユニットを装着したナローボア用単核 NMR プローブを用いた。プローブ・ヘッドを厚さ 0.5 mm のシールド管で覆い、0.435 mmϕ の銅線を長さ 100 mm に渡ってこれに巻きつけ磁場揺動読取用のピックアップ・コイルとした。IEF 信号は 0.4 μs の dwell time でデジタル・オシロスコープにより測定した。

粉末 KBr 試料の ^{79}Br MAS NMR は Tecmag APOLLO 分光器を用い、共鳴周波数 324.0 MHz で測定した。MAS 周波数は $\nu_r = 15.23$ kHz であった。rf パルスの幅は 5 μs、acquisition delay は 6 μs であり、0.8 μs の dwell time で FID を測定した。分光器からオシロスコープへ同期信号を送り、FID と IEF 信号の同期測定を行った。IEF 測定の開始は $t_{ini} = 50$ ms であった。

【結果と考察】 KBr の ^{79}Br MAS NMR のシングル・ショットの測定と、これと同期して行う誘導起電力 (IEF) の測定を、30 T に励磁したハイブリッド磁石で 20 回実行した。20 個のうちの 1 個の FID 信号とそのスペクトルを Figs. 1(a-i), 1(a-ii) にそれぞれ示す。KBr の ^{79}Br MAS NMR スペクトルは、一本のメインピーク (ν') と ν' から MAS 周波数の整数倍だけ離れた位置 ($\nu' \pm n\nu_r$) に現れる複数のスピニング・サイドバンドから成る。Fig. 1(a-ii) のスペクトルはおおよそそのような線形であり、$\nu' = -82$ ppm のメインピークと n が 2 程度までのサイドバンドによるスペクトルであった。しかし、ハイブリッド磁石の磁場揺動のため、測定の度にピーク位置及びスペクトルの位相は大きく変化し、また、ピークの片方の脇にはリップルが生じた。20 個の NMR 信号を補正なしで足し合わせた結果が Fig. 1(e) である。スペクトルは約 206 ppm (−183-23 ppm) にも及んでおり、補正なしでは高分解能 NMR が測定できないことが分かる。尚、メインピークの半値幅を位相補正の後に見積もったところ、Fig. 1(a-ii) のスペクトルでは 4.7 ppm であり、20 個のスペクトルの平均は 4.4 ± 1.6 ppm であった。

Fig. 2(a) に、NMR プローブの周りに巻いたピックアップ・コイルで、Fig. 1(a) の FID 信号と同期測定した IEF 信号 $V(t)$ の時間依存性を示す。Fig. 2(b) は、この $V(t)$ を式 (4) により変換した揺動磁場 $B_f(t)$ である。2 つのパラメータ c, B_{f0} のうち、c の値は 20 個のデータ全てに共通で、5.0×10^4 Tm^{2}V^{-1}s^{-1} であった。一方、B_{f0} は各データにより異なり、−3.0-2.7 mT の間の値であった。Fig. 2 のデータでは B_{f0} は 0.4 mT であった。Fig. 2(c) に、Fig. 2(b) の $B_f(t)$ と式 (3) を用いて見積もった位相角 $\phi_f(t)$ の時間依存性を示す。

Fig. 1(b-i) に、Fig. 2(c) で求められた $\phi_f(t)$ から計算した補正信号 $\exp[i\phi_f(t)]$ を示す。式 (5) に従い、$g(t)$ (Fig. 1(a-i)) と $\exp[i\phi_f(t)]$ (Fig. 1(b-i)) を掛け合わせ deconvolution した信号 $g'(t)$ が Fig. 1(c-i) である。補正によりスペクトル (Fig. 1(c-ii)) のメインピークは位置が約 −82 ppm から −60 ppm へシフトし、位相は out-of-phase から in-phase へ変化し、また半値幅は 4.7 ppm から 3.2 ppm へと減少した。更に、ピークの高周波側にあったリップルは取り除かれた。サイドバンドも補正後のメインピーク位置に対して ν_r の整数倍の位置へシフトした。

Fig. 1(d) に補正後の 20 個のデータを足し合わせた結果を示す。積算により、Fig. 1(d-ii) のスペクトルは Fig. 1(c-ii) のスペクトルと比べて SN 比が向上していることが分かる。補正と積算を行ったスペクトルでは、4 次 ($\nu' \pm 4\nu_r$) またはそれ以上のスピニング・サイドバンドが明瞭になった。Fig. 1(d-ii) のスペクトルの半値幅は 3.3 ppm であり、補正前の

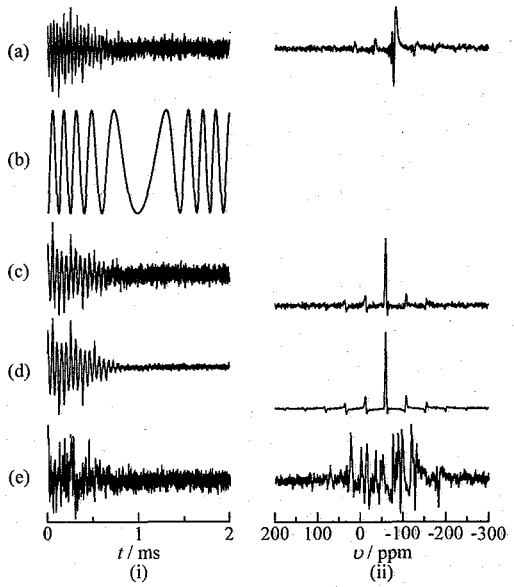

Fig. 1: (a) and (c)-(e): FID signals of MAS NMR of ^{79}Br in KBr measured with the hybrid magnet at 30 T (i) and the corresponding FT spectra (ii). (a) shows the single-scan raw signal. (b-i) represents the compensation signal for (a), $\cos\phi_{\rm f}(t)$, fabricated from the IEF data shown in Fig. 2. (c-i) shows the deconvoluted signal obtained by multiplying the raw signal (a-i) and the compensation signal (b-i) (see Eq. (5)). (d) and (e) show the accumulated data of twenty deconvoluted and raw signals, respectively. All the data are normalized.

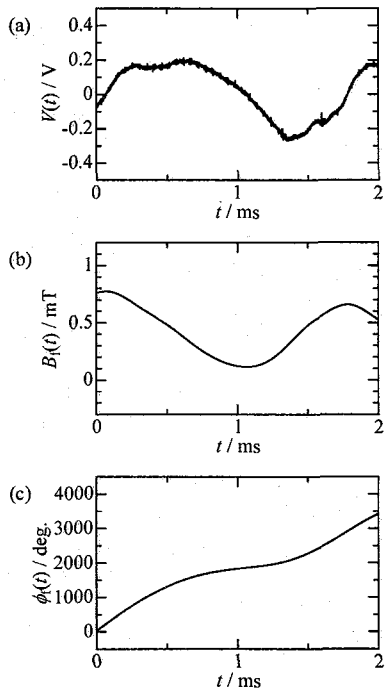

Fig. 2: Time dependence of (a) the IEF signal $V(t)$ measured synchronously with the FID siganl of Fig. 1(a-i), (b) the corresponding field fluctuation $B_{\rm f}(t)$ calculated by Eq. (4), and (c) the phase angle $\phi_{\rm f}(t)$ by Eq. (3).

平均半値幅 4.4 ppm よりもかなり小さくなった。補正後にも残った線幅は磁場の不均一性による。

【終わりに】 本研究では、ピックアップ・コイルに生ずる IEF 信号を FID 信号と同期測定し、得られたデータを用いて FID 信号を deconvolution することで、揺動磁場下で高分解能 NMR スペクトルを得る方法を開発した。NIMS の 30 T のハイブリッド磁石を用い KBr の ^{79}Br MAS NMR で本法の有効性を実証した。強磁場 NMR は、半整数スピン四極子核の高分解能スペクトルの取得に特に有用である。今後、四極子核を用いた無機物質の精密構造解析等に進展が期待できる。

【謝辞】 本研究は文部科学省科学技術振興調整費及び科学研究費補助金によって行われた。

【参考文献】

[1] J. Haase, *Appl. Magn. Reson.* **27**, 297 (2004).
[2] Z. Gan, *et. al*, *J. Am. Chem. Soc.* **124**, 5634 (2002).
[3] K. Hashi, *et. al*, *Jpn. J. Appl. Phys.* **44**, 4194 (2005).

P108

Ultra Fast MASプローブにおける^{1}H測定

○芦田淳[1]、Allen Palmer[2], Mircea Cormos[2],
Charles E. Bronnimann[2], and Siegfried Hafner[3]
(バリアンテクノロジーズジャパン[1]、Varian Inc.[2]、
Varian Deutschland GmbH[3])

^{1}H Solid State NMR Spectroscopy with Ultra Fast MAS Probe.

Jun Ashida[1], Allen Palmer[2], Mircea Cormos[2], Charles E. Bronnimann[2], and Siegfried Hafner[3]
(Varian Technologies Japan Ltd.[1], Varian Inc.[2], Varian Deutschland GmbH[3])

It has been shown that very fast MAS is an effective means for partially averaging the homonuclear ^{1}H dipole interaction in solid samples, allowing in many cases for the simple acquisition of chemical shift resolved ^{1}H spectra. In both theory[2] and experiment[3], the linewidth contribution from dipolar coupling is approximately linear with 1/ωr, and the resulting linewidths in typical organic molecules over 60kHz spinning have been reduced to a few hundred Hz.

For this contribution we present new ^{1}H NMR data using new Ultra Fast MAS™ spinner mounted on a narrow bore T3 probe and report on the spectroscopic performance up to the maximum spinning speed.

【緒言】

固体NMRの実験手法が溶液NMRのそれと最も異なっている点は、あまり^{1}H-NMRを測定しないことであろう。ゼオライト中に吸着された水などのように^{1}Hの含有量が少ない場合は測定することはあるが、有機物では^{1}H-^{1}Hの同種核間双極子相互作用が～100kHzと非常に大きく、単純な１パルスの測定では非常に線幅の広いスペクトルになってしまい、ほとんど情報を得ることができない。水素中のプロトン(^{1}H)の存在比は～99%と多くてしかも磁気回転比が大きいので^{13}Cと比較して圧倒的に感度は良いが、固体NMRでは逆にたくさんありすぎることが高分解能スペクトルを得られない原因となる。

固体^{1}H -NMR測定法としては、Magic Angle Spinningと多重パルスを組み合わせたCRAMPS法[1]がよく知られているが、パルス幅が有限値であるため双極子相互作用を完全に消去することができないこと、パルス設定時に波形の不完全性の補正が必要なこと、多重パルスを用いているため正確な化学シフト値を求めるためには補正が必要なことなど様々な問題があるため、それほど広く使われているとは言い難い状況である。

本発表では、新しく開発した65kHzで試料回転できるUltra Fast MAS™プローブおよびそれを用いた^{1}H-NMR測定について報告する。また、別掲のポスターでは^{1}H以外の核種での測定についても報告しているので、そちらも参照されたい。

固体^{1}H NMR、高速MAS、プローブ

あしだ　じゅん、Allen Palmer、Mircea Cormos、Charles E. Bronnimann、Siegfried Hafner

【プローブ】

スピナーモジュールおよびローターは、これまで我々が開発してきたPENCIL™タイプを踏襲している。このプローブでは^{1}H測定を前提としているため、バックグラウンドを除くためにスピナーモジュールのサンプルコイル周辺部は^{1}Hを含まないフッ素樹脂で作られている。また、ローター本体はジルコニア製、ドライブチップとエンドキャップはポリアミドイミド樹脂製で、^{1}Hのバックグラウンドを除くためにスペーサーにはやはりフッ素樹脂を用いている。

【スペクトル例】

図１に試料回転速度を 20～70kHzまで変化させたアラニンの^{1}H-MASスペクトルを示す。^{1}H MASスペクトルの線幅は試料回転速度が～100kHz程度までは、試料回転速度に反比例することが理論的にも[2]実験的にも[3]報告されているが、図１でもそれが示されている。これまでの市販プローブの最高速度であった～30kHzのスペクトルでは、メチル、メチン、カルボキシル水素の信号の分離が十分ではなかったが、70kHzの試料回転下では、それぞれのプロトンのピークがほぼ完全に分離測定できる。

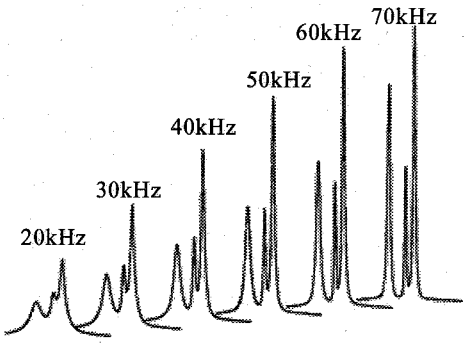

Fig.1 600MHz ^{1}H spectra of L-alanine at spinning speed between 20 and 70kHz.

このように低分子試料に対してはUltra Fast MAS™プローブの優位性を示すことができたが、プロトンのネットワークが強い高分子などの試料では、70kHzの高速回転でもまだ不十分でCRAMPS法の方が高分解能スペクトルが得られる場合がある。しかし溶液NMRと同様に、固体NMRでも多次元化によって重なっている信号を分離することが可能になる場合がある。

図２にモノエチルフマル酸の^{1}H２次元NOESYスペクトルを示す。CRAMPS法では、T_1次元、T_2次元ともに多重パルスを照射しなければならないのでパルスの最適化が煩雑であるが、高速回転下では３つの 90 度パルスを照射するだけで高分解能の^{1}H２次元スペクトルを観測できる。

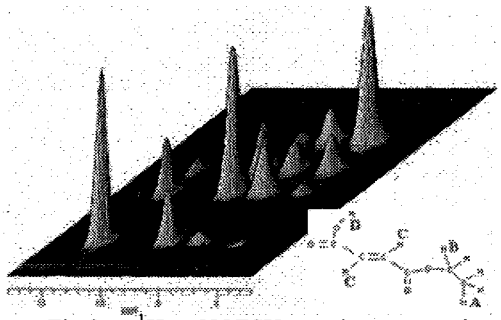

Fig.2 ^{1}H NOESY spectrum of ethylfumarate at 65kHz MAS and 500ms. mixing time.

発表当日はCRAMPS法との比較についてももう少し詳細に議論する予定である。

【参考文献】

1) L. M. Ryan, R. E. Taylor, A. J. Paff, and B. C. Berstein, *J. Chem. Phys.*, **72**, 508 (1980)
2) P. Filip, S. Hafner, I. Schnell, D. E. Decmo, and H. W. Spiess, *J. Chem. Phys.*, **110**, 423 (1999)
3) A. Samoson, T. Tuherm, and Z. Gan, *Solid State Nucl. Magn. Reson.*, **20**, 130 (2001)

P109

Packing digital circuits for an NMR spectrometer into a single chip[1]

Kazuyuki Takeda [2]
Graduate School of Engineering Science, Osaka University, Japan

ABSTRACT: In order to develop a compact-sized, home-made NMR spectrometer, digital circuits required for the spectrometer are incorporated into a single FPGA (Field-Programmable Gate-Array) chip.

A Field-Programmable Gate-Array (FPGA) is an LSI composed of a large number of *programmable* logic gates, in which digital circuits, called IP-cores ("IP" stands for "Intellectual Property"), can be built with hardware description codes. An FPGA is attractive in the sense that

(1) circuit components are, once developed, re-usable,

(2) the individual circuits built in an FPGA run *concurrently*,

(3) the circuits in the FPGA chip are re-configurable as many times as necessary, and

(4) development requires only a personal computer and a download cable.

In principle, an FPGA can realize any digital circuits within limitations set by the available number of logic elements and the operation speed. In this work the author aimed at letting *a single FPGA chip* do all the digital jobs required for an NMR spectrometer. These include

(a) triple pulse programmers[1],

(b) Direct Digital Synthesizers (DDS),

(c) phase-cycle memory arrays,

(d) digital receiver composed of digital quadrature demodulator and digital low-pass filter, and

(e) PC interfaces for command/data transfer.

The FPGA chip used in this work is EP2C70F672C8, which is one of "Cyclone II" devices by Altera Inc. Its 27x27 mm package has 68,416 logic elements, 1,152,000 RAM bits, 150 multipliers, 4 PLLs, and 622 I/O pins. The Cyclone II breadboard was purchased from HuMANDATA Ltd., and development was carried out on a software, Quartus II Web edition, which is provided for free by Altera. VHDL codes for (a)-(e) have been written, debugged, and finally programmed into the Cyclone II chip. As a result, the FPGA chip serves as a very compact digital module, and can be used to control non-digiral NMR peripherals, which are described in another presentation in this conference[2].

[1] *Key Words:* Field-Programmable Gate Array (FPGA), IP-core, Pulse programmer, Direct Digital Synthesizer (DDS), Digital receiver

(a)

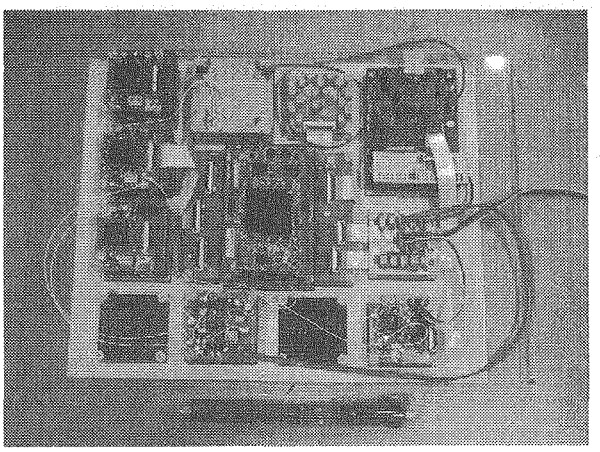

(b)

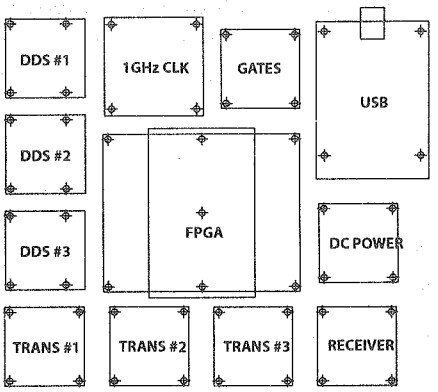

Fig. 1. (a) A snapshot of the laptop-sized NMR spectrometer, which is also presented in the oral session[2]. For a feel of its size, a ballpoint pen is also shown in the picture. The assembly of modules are shown in (b). The schematic of these modules are described in Ref. [2]

References

[1] K. Takeda, *Single-chip pulse programmer on field-programmable gate-array*, 47th ENC (2006).

[2] K. Takeda, *A laptop NMR spectrometer*, oral session.

P110

偏極キセノンポンピングセル加熱方法の検討

(秋田県立脳血管研究センター) ○中村和浩、近藤靖、David Wright、三浦修一
(放射線医学総合研究所) 若井篤志、Jeff Kershaw、菅野巖、
(東横化学株式会社) 大竹紀夫、外間省吾

An effective method for heating hyperpolarized Xenon pumping cell

○K.Nakamura, Y. Kondoh, D. Wright, S. Miura (Akita Research Institute for Brain and Blood Vessels) A.Wakai, J. Kershaw, I. Kanno (National Institute for Radiological Sciences), N. Ohtake, S. Sotoma (Toyoko Kagaku Co. Ltd.)

We have evaluated nine pumping cells to date. Of these, only three cells provided sufficient levels of polarization. Three other cells also showed some minor polarization that was too small to be considered for biological applications. We were unable to moderate temperature in the remaining three cells due to uncontrollable heating by pumping laser irradiation resulting in a high density of Rb vapor and an excessive coating of Rb on the walls of the cell. A jacket-type electrical heater with thermal insulation was ineffective in solving the problem and we have since developed a new method for heating the pumping cell using a glass hood and heated airflow that provides proper temperature control of the pumping cell.

1. はじめに

アルカリ金属原子を用いた光ポンピング法により ^{129}Xe 原子核の偏極率を熱平衡状態の１万倍以上にできることが知られており、感度が非常に低い分光法である核磁気共鳴法においては画期的な手法である。臨床応用においては、肺といった空隙部分の撮像に大きな意味があるが、脳血流量測定といったトレーサーを用いる測定法にも、その応用が期待されている。我々もここ数年偏極キセノンの臨床応用研究を進めているが、研究において問題となっているのは、生成偏極ガスの偏極率についてその再現性が悪いことである。東横化学社製の偏極装置（HPXE2-04H）を用いることで経時的な変化は少なくなったが、ルビジウム(Rb)金属を封入したガラスセル（偏極セル）によるばらつきが大きい。満足のいく高偏極率が得られた偏極セルにおいてもその初期状態は様々であった。こうした偏極セルの初期状態について報告すると共に、偏極セルが温度制御不能となる状態を改善するため、加熱方法を検討したので報告する。

キーワード：高偏極, Xe, ポンピングセル

著者：なかむら かずひろ、こんどう やすし、でいびっど らいと、みうら しゅういち、わかい あつし、じぇふ かーしょう、かんの いわお、おおたけ のりお、そとま しょうご

2．偏極セルの初期状態評価方法

東横化学社製偏極装置（HPXE2-04H）を用い、9 個の異なる偏極セル（RBCP2101）について計測をおこなった。偏極セルは周囲に配置された電熱線と断熱素材からなるジャケットヒーターにより加熱され、セル外壁部の温度を熱電対により測定することにより、偏極セル温度を制御した（Fig. 1）。偏極ガスは自然配合比のキセノン 70%、窒素 30%の混合ガスを用い、ガス圧は 1.4 気圧、ポンピング用の波長 795nm のレーザーパワーは 80W とした。偏極セルは電気ヒーターにより、110℃に保持された。レーザーを 24 時間連続的に照射し、光ポンピングによる偏極操作を連続的におこなった状態で、一時間毎に 30cc のガスを取り出した。このガスを 4.7テスラ MR スペクトロメータ内のガラス容器（内容積約 50cc）に封入した。その後、ガラス容器の周囲に配置したサドル型高周波コイルから核磁気共鳴信号を計測した。取得した核磁気共鳴信号に指数関数による重み付け乗算（バンド幅 80Hz 増相当）をおこなった後、フーリエ変換をおこない、スペクトラム強度の最大値を測定値とした。得られた測定値は ^{129}Xe の偏極率を反映した値となり、測定値が大きいほど高い偏極率が得られたといえる。

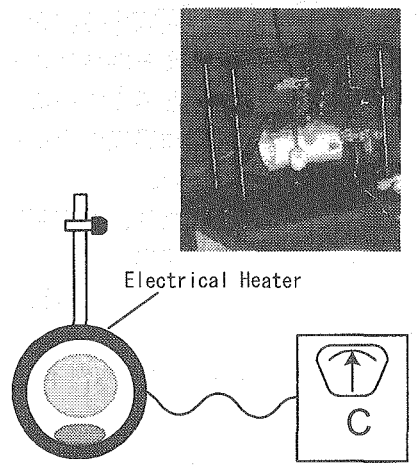

Fig. 1：Schematic of the experiment setup. Pumping cell temperature was monitored by thermo-coupler and heated by jacket-type electrical heater.

3．偏極セルの初期状態評価結果

これまでの実験から測定値が 1×10^6 程度あれば、およそ 10%の偏極率であり、動物実験に利用して十分な信号強度が得られることがわかっている。偏極セル設置後、評価した 9 個の偏極セルにおいて、満足のいく高偏極信号が得られる偏極セルは 3 個であり、3 個は低い測定値を示し、3 個はレーザー照射時に温度制御不能となった。高偏極信号が得られる偏極セルについても測定値の時間変遷は様々であった。開始から 5 時間後に最高値に達した後、その後減少し、１２時間後には最高値の 1/2 から 1/4 程度に落ち着く現象が見られた偏極セル＃４（Fig. 2a）もあれば、30 分ほどで、最高値に達し、２４時間測定値が変化しない偏極セル＃６(Fig.2 b)もあった。高偏極信号が得られた偏極セル＃１は偏極セル＃６と同様の傾向を示した。また、偏極セル＃６は設置直後には、低い測定値を示したが、48 時間といった長い時間を経て次第に測定値が上昇する傾向が認められた。Fig2b において、11 日後の測定結果に代表される測定値の時間変遷は従来報告されているものとよく一致しているが、設置直後に見られる現象や、Fig2a で観察されるような時間変遷を説明することは難しい。偏極率を決めるパラメータとして、アルカリ金属原子の光ポンピング率とスピン崩壊率、ア

ルカリ原子と ^{129}Xe 原子核とのスピン交換反応の確率、^{129}Xe スピンの緩和率（壁緩和、磁場不均一性に起因する緩和、キセノン間の双極子―双極子相互作用等を含む）が考えられるが、これらのパラメータが時間に依存しない定数であれば、従来のモデルでは説明できないと考えている。ひとつの原因として、Rb 金属の容器内壁への付着によるキセノン緩和過程の変化を考えているが、内壁面の状態を実測することは難しく仮説の域をでない。

低い測定値を示したり、温度制御不能となった偏極セルでは、Rb 金属が偏極セル内に飛散した状態が観察された。特に、温度制御不能となった偏極セルではレーザー光入射面に金属の付着が認められた。飛び散ってガラス内壁面に付着した Rb 金属はキセノンの壁緩和時間を短くし、測定値を低くする原因になっている可能性がある。また、偏極セル表面に付着した Rb 金属がレーザー照射により過剰に蒸発することで、レーザー光から供給される熱量が放熱量を上回り、過剰な加熱により温度制御不能になったと考えている。特に断熱素材からなるジャケットヒーターは放熱を抑えるため、温度制御が困難になりやすいと考えた。

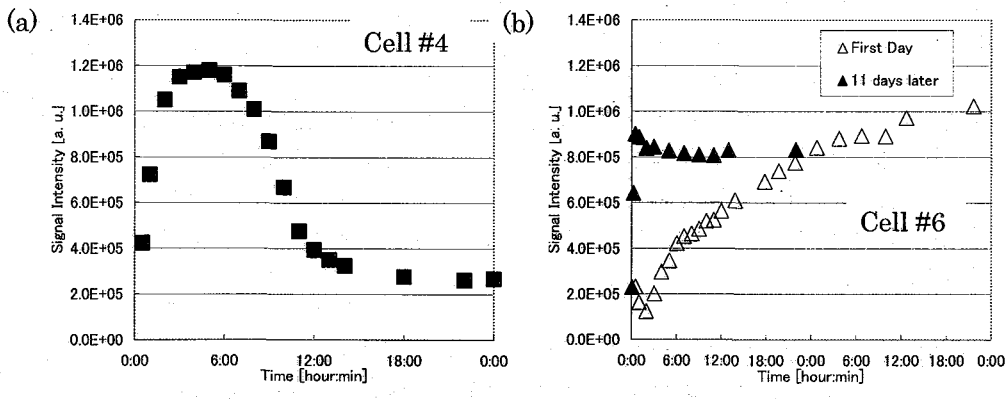

Fig. 2：Typical signal changes of polarized xenon in pumping cells. Two different cells were shown in (a) and (b). The data acquired immediately after cell setting were shown by open triangle and the data after eleven days were shown in solid triangle.

4．偏極セル加熱方法の検討

偏極セル 9 個の初期状態を検討した結果、Rb 金属を封入する際飛散しないようにすることが望ましく、加熱だけではなく、放熱も可能な温度制御方法が必要であると考えた。まず、Rb 金属を飛散せずに封入するため、偏極セルの中央部に溝上の凹部を形成し、Rb 金属が自然に流れ落ちるようにした。加熱方法については、Fig. 3 に示すように、偏極セルの外部を覆うガラス製のフードを作製し、高温の空気を送風することにした。偏極セル表面の温度を熱電対で検出し、ヒーター（ライスター3300 型）に印加する電流をサイリスタレギュレータ（チノー JB-2040）で制御した。送風機（ライスターロングライフ型）から 900ℓ/分の流量で送風されているため、レーザー光により偏極セルが加熱された場合でも放熱可能となる。本手法において偏極セ

ルが 180℃程度まで加熱できることを確認し、レーザー光の照射により温度制御不能になることもなくなった。

新たに作成した偏極セルを本手法により加熱し、レーザーを照射しキセノンガスを偏極して得られた測定値を Fig. 4 に示す。動物実験に十分使用可能な高い偏極信号が得られている。また、偏極セル＃6ほど顕著ではないが、時間と共に次第に信号値が増大していく傾向が認められた。照射するレーザー光を 160W とすると、ほぼ2倍の信号強度が得られた。

5．まとめ

高温の空気を送風することにより偏極セルを加熱する手法は有効であり、高偏極率を有する偏極 ^{129}Xe ガスを再現性良く供給することに役立つと考えられる。

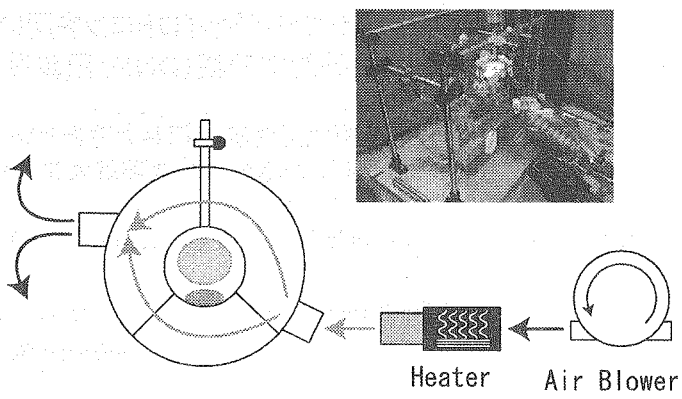

Fig. 3 : Schematic of pumping cell heating. Blown air through the heater was induced to the glass hood. The temperature of airflow was controlled by electric current to the heater depending on the temperature measured by thermo-coupler on the cell.

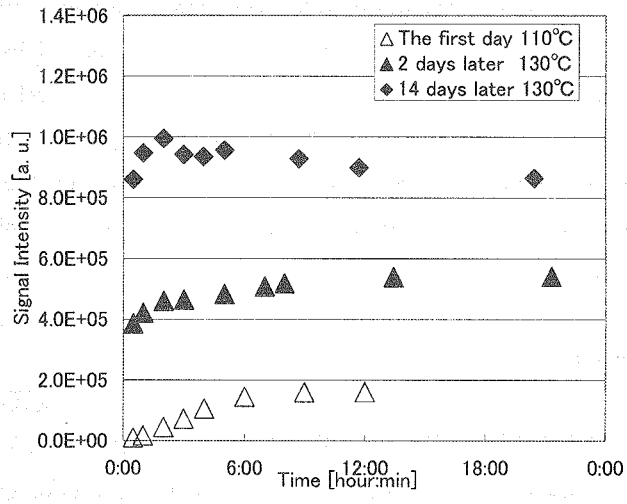

Fig. 4 : Signal changes of xenon in the newly developed pumping cell. The data acquired immediately after cell setting at 110 degrees were shown by open triangle and the data after 2 days and 14 days at 130 degrees were shown in solid triangle and square, respectively.

P111

394-GHzジャイロトロンを用いた 高磁場動的核分極(DNP)用装置の開発

(阪大蛋白研[1]、福井大遠赤センター[2])
○高橋大樹[1]、出原敏孝[2]、斉藤輝雄[2]、光藤誠太郎[2]、阿久津秀雄[1]、藤原敏道[1]

Instrumentation for Dynamic Nuclear Polarization at 14 T with a 394-GHz Gyrotron

1 Institute for Protein Research, Osaka University
2 Research Center for Development of Far-Infrared Region, University of Fukui

Hiroki Takahashi[1], Toshitaka Idehara[2], Teruo Saito[2], Seitaro Mitsudo[2], Hideo Akutsu[1], and Toshimichi Fujiwara[1]

High-field dynamic nuclear polarization (DNP) using electron spins is a promising technique for biological systems which can significantly enhance the sensitivity of high-resolution solid-state NMR. This report presents the instrumentation for dynamic nuclear polarization at 14 T with a 394-GHz second harmonic gyrotron. The gyrotron oscillator generates continuous waves at a power level of 0.7 kW in the TE_{26} mode. A sub-millimeter wave is transmitted to a liquid-N_2 temperature magic-angle-spinning probe through a circular waveguide. The temperature of the sample is controlled by low temperature N_2 gas purified from the air. The mechanism of high-field DNP is also discussed.

【緒言】

固体NMR法は超分子システムの構造解析法として重要な役割を果たしている。そのようなシステム(膜蛋白質など)は単結晶が得られなかったり、可溶化すると機能を失ったりするので、X線結晶構造解析法や溶液NMRに不向きである。近年、固体 NMR による構造決定法の様々なテクニックが開発されてきているが、いずれも分解能や感度の低さのため巨大分子への応用は難しい。感度を上げる方法として電子スピンの分極を核スピンに移す動的核分極法(DNP)がある。電子スピンの磁気回転比は ^1H に比べて約660倍大きいので、DNP法を用いれば感度が劇的に増大する。1953年にOverhauser効果が示されて以来、低磁場

キーワード:DNP, Gyrotron, Solid-State NMR, Electron Spin, Sensitivity Enhancement
たかはしひろき、 いではらとしたか、 さいとうてるお、 みつどうせいたろう、 あくつひでお、 ふじわらとしみち

においてDNPの研究が数多くされてきたが、生体系の高分解能NMRには高磁場が必要である。しかし、高磁場DNPは電子スピンを飽和させる高出力(100W 以上)テラヘルツ波光源の欠如のためほとんど手付かずであった。そこで、我々は高磁場DNP用の光源(ジャイロトロン)を作成した。また、電子スピンの緩和を抑えるため、試料を液体窒素温度にして長時間測定するシステムも開発した。さらに、これまで行われてきた低磁場でのDNPとは異なり、高磁場DNPではメカニズムが明らかにされておらず、効率的な分極移動を行うためにラジカル密度などを考慮に入れた理論的研究も重要となっている。

【394GHz ジャイロトロン】

ジャイロトロンはサイクロトロンメーザー作用を発振原理とする高周波光源である。電子銃により放射された電子は軸方向磁場に沿って螺旋運動をしながら空洞共振器部分に入る。そこで電場と相互作用をしてサブミリ波が発生し、上部のウィンドウから伝送系を通りプローブへと伝わる。また、空洞部を通り抜けた電子は冷却水によって冷やされコレクターで回収される。

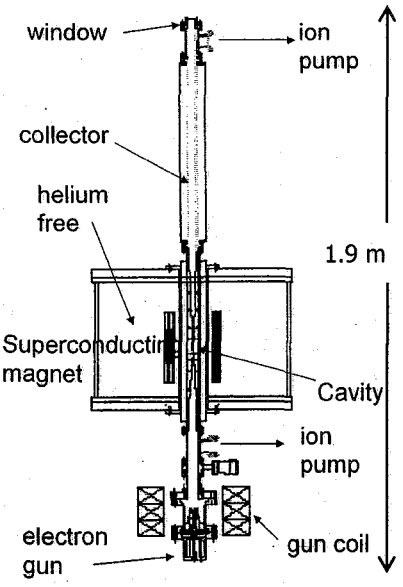

Fig.1 : 394 GHz Gyrotron

我々が作成した 394GHz ジャイロトロンは 7T の無冷媒超伝導マグネットを用い、2次の高調波で作動する。空洞共振器の径を小さく(半径:1.95 mm)してモード分離を行い、TE_{26}モードで最高出力 0.7kW のCWを発振する。伝送系での損失を考えてもDNP実験には十分な出力である。伝送系には銅製の円形導波管を使用した。電子銃部でのカソード、アノード電圧はそれぞれ 18kV、14.4kV であり、電流は 0.4A である。

【液体窒素温度DNP用マジック角試料回転プローブシステム】

また、DNP実験用にNMRマグネット及びプローブを改良した。NMR測定には 14T Varian CMX600 Infinity+、4mmϕ二重共鳴 T3 プローブを用いた。今回作成したジャイロトロンは周波数固定のため、高分解能NMRマグネット(14.1T wide-bore)の磁場を掃引しサブミリ波照射の効果を最適化する。プローブ内は 6mmϕの円形導波管で伝送し、テーパーで 2.1mm まで絞って試料にローターと平行にマジック角方向から照射する。第 44 回NMR討論会(ポスター番号:AP153)では窒素ガスセパレータを用いて大気中から窒素を分離し、少ない窒素消費量で長時間低温測定ができるシステムを発表した。現在、MAS 周波数 8kHz において試料温度が 120K まで到達できた。

500 MHz 溶液 NMR 用 4K 極低温プローブの高性能化

[1] 理研 GSC, [2] 横市大院, [3] 東工大院総理工, [4] 東大院理, [5] 理研播磨
○ 高橋雅人 [1,2], 由本富巳 [1,3], 保母史郎 [1,2], 岡村哲至 [3], 横山茂之 [1,4,5], 前田秀明 [1,2]

Performance of a 4 Kelvin Cryogenic Probe for 500 MHz Solution NMR

[1]GSC, RIKEN Yokohama Inst.; [2]Grad. Sch. Integ. Sci., Yokohama City Univ.; [3]Grad. Sch. Integ. Sci. Eng., Tokyo Tech.; [4]Grad. Sch. Sci., Univ. Tokyo; [5]Cell. Sign. Lab., RIKEN Harima Inst.
○Masato Takahashi[1,2], Fumi Yoshimoto[1,3], Fumio Hobo[1, 2], Tetsuji Okamura[3], Shigeyuki Yokoyama[1,4,5] and Hideaki Maeda[1,2]

A 4K cryogenic probe system has been developed for higher sensitivity gain than commercial system. When a RF coil of NMR is cooled down to 4K, higher sensitivity, temperature stability at the RF coil against large heat input can be achieved. A cryogenic preamplifier and a RF switch have been developed and installed into the cryogenic probe to reduce thermal noise. The effect on the sensitivity is demonstrated.

緒言

NMR 法の弱点である感度を向上させるために **Fig. 1** に示すような 4 ケルビン極低温プローブの開発を行っている(1)。RF コイルを 4 ケルビンに冷却することで、従来の GM 冷凍機のみ利用の極低温プローブ（25 ケルビン）に比べて更なる高感度化が期待できるとともに、RF パルスによる発熱に対する温度変化が小さくなるためより高性能な極低温プローブが実現可能である。

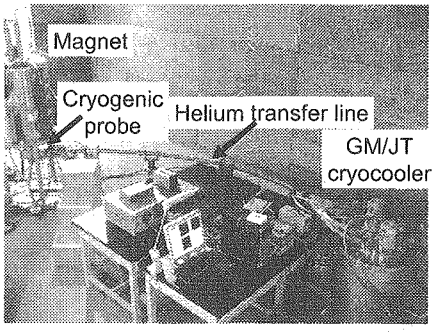

Fig. 1. 500 MHz Cryogenic probe

冷却技術の開発

溶液用 NMR プローブではサンプルを室温に保つ必要があるため、極低温に冷却される RF コイルとの間に大きな温度差が存在する。また、計測の都合上電磁波を遮ることはできないため熱輻射が大きな熱侵入源として残る。本研究のプローブでは熱輻射も含めた 4K 冷却ステージへの熱侵入は実験により 1.7W 程度と見積もることがで

キーワード：極低温プローブ、 4 ケルビン冷却、 高感度化

たかはしまさと、よしもとふみ、ほぼふみお、おかむらてつじ、よこやましげゆき、まえだひであき

きた。この値は極低温部分への熱侵入としては非常に大きく、冷却ステージと RF コイル近傍で大きな温度差が発生した。そこで熱接触抵抗を減らす改良とともに熱伝導部品を超高純度アルミニウムに変更した。これにより RF コイル近傍の温度は 7.5K 程度になった。

熱雑音の低減

極低温用の RF スイッチとプリアンプを新たに開発した。この RF スイッチは高周波用 PIN ダイオードを使用し、送信系と受信系のアイソレーションが-65dB、送信系と送受信コイル間（受信系も同様）の通過特性が約 1dB である。今回開発した 500MHz 用初段プリアンプは HEMT を用い、極低温時の安定性を重視した設計を行った。その結果、室温で、ゲイン 18dB、ノイズ温度 72K(NF0.97dB)、77K でゲイン 20dB、ノイズ温度 24K(NF0.35dB)の特性が得られた。

NMR 測定結果

本極低温プローブにおける線形測定試料（1%$CDCl_3$）におけるピークの 0.55%の線幅が 9Hz、0.11%で 22Hz、50%で 0.54Hz であった。0.1%Ethylbenzene で測定した感度は室温で 300、極低温で 1746 であった。また、極低温プローブで測定した重水溶媒リゾチームの 2D NOESY スペクトルを **Fig. 2** に示す。

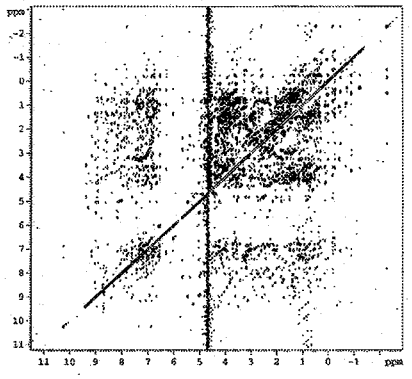

Fig. 2. NOESY for Lysozyme

Fig. 3 は計算で求めた感度上昇率と実験結果を比較したものである（横軸は RF コイル近傍の温度）。プリアンプを 68K に冷却（実線）すると、プリアンプが室温の時（1 点鎖線）より感度が 50%向上するが、プリアンプのノイズが無い理想的な場合（点線)より特性が低い。従って、4K 極低温プローブの更なる高感度化にはプリアンプの改良による熱雑音の低減が重要である。ただし、現状の構成でも、RF コイルを 10K まで冷やすことで、RF コイルの 25K 冷却より感度が 30%向上している。今後、プリアンプの改良とともに基本性能を向上させることで4K極低温プローブの感度向上を行っていく予定である。

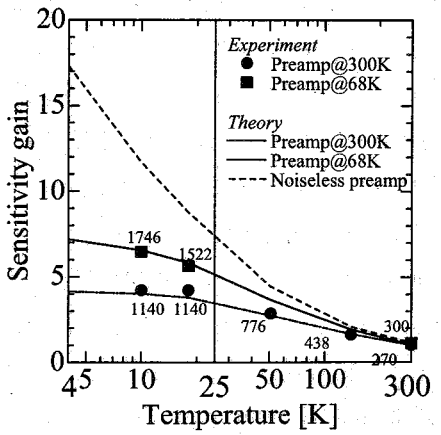

Fig. 3. Sensitivity gain by the cryogenic probe

参考文献

(1) F. Yoshimoto, M. Takahashi, T. Horiuchi, F. Hobo, K. Inoue, T. Miki, M. Hamada, T. Okamura, S. Yokoyama and H. Maeda Advances in Cryogenic Engineering, (2006) **51** p. 704-711

P113

ガラス容器中のアルカリ金属相転移と不純物

兵庫県立大[A], Princeton University

○石川潔[A], B. Patton, Y. -Y. Jau, and W. Happer

Phase transition and intrinsic impurities in glass alkali-vapor cells

University of Hyogo[A], Princeton University

K. Ishikawa[A], B. Patton, Y. -Y. Jau, and W. Happer

We report NMR spectra of metallic ^{133}Cs in glass cells. The cells were cycled in temperature and the solid-liquid phase transition was studied. NMR lines in these phases are resolvable at 9.4 T because of difference in Knight shift of metal nuclei. Moreover, two other NMR peaks were observed at temperatures below the melting point. We attribute these extraneous signals to two distinct chemical impurities. One of the peaks was confirmed by intentional oxidization.

アルカリ金属原子は、原子分光で使うために、ガラス容器に封入されることが多い。GPS原子時計や原子磁束計、核スピン偏極希ガスメーザーでは、電子や核のスピン偏極などを利用する。精密計測のためには、それら量子状態の壁における緩和を抑えることが重要である。特に、携帯機器に搭載する目的で開発中の原子時計は、小型のガラス容器に封入されるので、アルカリ金属やガラス表面の性質が計測精度に及ぼす影響をできる限り小さくしたい。また、アルカリ金属を少しだけ酸化させると、偏極Heガスのスピン緩和時間が長くなることが報告されている。しかし、壁におけるスピン緩和機構と、その経年変化は、いまだに明らかになっていない。本研究は、化学反応性の高いアルカリ金属のガラス容器

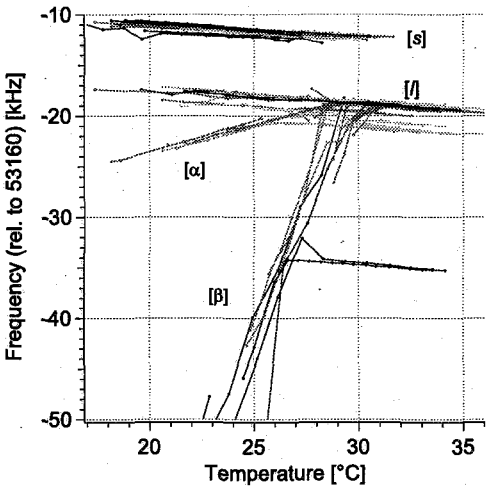

Figure 1: Resonance frequencies of ^{133}Cs nuclei measured by temperature cycles for many glass cells. In addition to [s] solid and [l] liquid peaks, extraneous α and β peaks were observed. Knight shifts of these additional peaks depend strongly on temperature. Supercooled liquid was also observed below melting point of pure Cs metal (28.52 °C).

alkali-metal, glass cell, phase transition, Knight shift

いしかわ きよし、 ぱっとん ぶらいあん、じゃう やんゆう、はーぱー うぃりあむ

内における状態を明らかにし、スピン緩和機構を調べることを目的とする。

実験では、磁場 9.4 T におけるガラス面上の ^{133}Cs 金属の NMR 信号 (53 MHz) を計測し、金属の相転移を観測した。表皮効果のため高周波磁場が金属に浸透する厚さは、室温で 30 μm であり、ガラス表面の金属を観測するのに都合がよい。金属内の NMR 共鳴周波数は、伝導電子の影響でシフトする (Knight shift)。高磁場では固体と液体の共鳴線は分解でき、実際に光学実験で使用する容器内のアルカリ金属の状態を調べるのに、NMR 計測が適している。

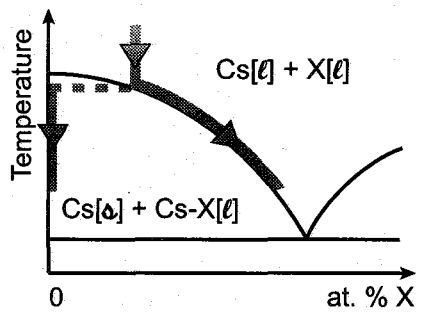

Figure 2: Phase diagram and Knight shift. As contaminated liquid is cooled down, a part of liquid is solidified and the ratio of impurities in liquid increases along the equilibrium curve. Since impurities take electrons out of liquid metal, Knight shift decreases and approaches to the frequency of compounds.

図 1 は、多くのガラス容器で観測した Cs NMR 共鳴周波数の温度依存性である。固体 [s] と液体 [l] の共鳴以外に、2 種類の共鳴線 [α, β] を観測できる。これら共鳴周波数の温度依存性は大きく、純粋な金属の理論では説明できない。凝固点効果が見られるので不純物が混入していると仮定し、図 2 のような相図を使うと実験結果を説明できる。不純物が金属から電子を奪うので、Knight shift が小さくなる。温度が下がり純粋な固体が析出し、不純物濃度が高くなるほど、共鳴が低周波側に移動する。これを証明するため、容器に酸素を導入し、アルカリ金属を酸化した。酸素ガス圧を 10^{-5} Torr 程度にし、均一な亜酸化物 (suboxide) が得られるようにすると、β 共鳴線と一致する信号が得られた。β 共鳴線は、蒸留により除去可能なことも確認した。一方、α 共鳴線は、容器を清浄にするほど現れるようである。特定できていないが、アルカリ金属がガラスと反応し、ガラスの成分あるいは Si 自身が溶け出している可能性が高い。これが本当であれば、ガラス容器が容器の体をなしている間、アルカリ金属と反応を続け、精密分光実験の結果に影響を与え続けることになり、非常に深刻な問題である。

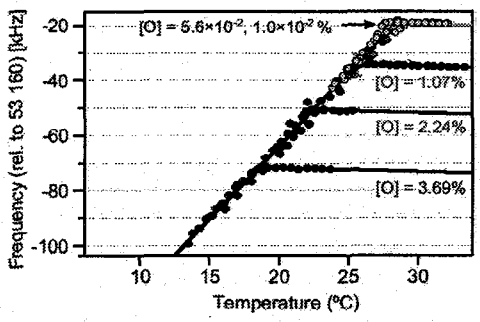

Figure 3: Resonance Frequencies of Cs suboxide. The numbers are the contamination ratios of oxygen.

P114

Universal control of a qubit system under Lee-Goldburg irradiation for solid-state NMR quantum computing

○ **Makoto Negoro**, Shogo Yamanaka, Akinori Kagawa,
Kazuyuki Takeda and Masahiro Kitagawa
Graduate School of Engineering Science, Osaka University

Abstract: We show theoretically and experimentally that universal control of solid-state NMR quantum computer is possible under continuous decoupling of homonuclear dipolar interactions.

Recently, the focus of interest in quantum computing by means of NMR has been shifted from experiments in liquids to those in solids, mainly because high nuclear spin polarization can be attained[1]. In solid-state NMR quantum computing, controlled two-qubit gate operation is driven by the dipolar interaction between the nuclear spins under interest. However, as an inevitable consequence of using the through-space dipolar interaction, time evolution of the system is affected by dipolar interactions across the molecules that constitute an ensemble quantum computer. Since the individual elements of the ensemble system should be independent from one another, the intermolecular dipolar interactions are not welcome from the viewpoint of solid-state NMR quantum computing. In particular, the dipolar interactions among like spins should be eliminated, because the on-speaking flip-flop term causes considerable decoherence. In this work, we propose a new approach to universal gate operation under continuous application of homonuclear decoupling.

In this approach, the homonuclear dipolar interactions are eliminated by the Lee-Goldburg (LG) technique[2], which employs RF irradiation with carefully chosen amplitude ω_1 and offset frequency $\Delta\omega$ such that $\omega_1/\Delta\omega = \sqrt{2}$. Taking advantage of the fact that the phase ϕ of the RF irradiation can arbitrarily be chosen without violating the LG condition, we show that appropriate modulation of ϕ enables universal one-qubit gate operation under continuous LG irradiation. Two-qubit operation is also shown to be possible under LG with the LGCP technique[3], where the flip-flop Hamiltonian between the qubits can be utilized to implement the ISWAP gate.

Experimental demonstrations were carried out in a single crystal sample of 2-^{13}C-labeled l-alanine. As demonstrated in Fig.1, the decay of oscillation caused by the ^{1}H-^{1}H homonuclear interactions has successfully been suppressed in both the one-qubit rotation under LG irradiation and the LGCP experiments as compared to the conventional quantum gate operation using on-resonance irradiation.

The combination of the ISWAP gate and an arbitrary one-qubit gate can implement any quantum circuits. Thus, this work opens a new way toward universal control of a solid-state NMR quantum computer under continuous decoupling of homonuclear dipolar interactions across the individual molecules in the bulk ensemble quantum computer. An attempt to combine the

Key Word: quantum computer, Lee-Goldburg irradiation, LGCP

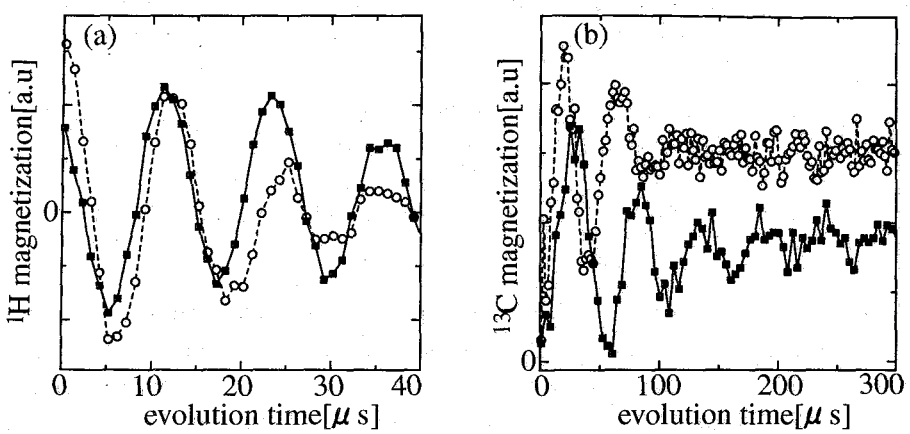

Fig. 1: (a)Evolution of the ^{1}H magnetization under one qubit rotation in the conventional (open circles) and the present (filled squares) approaches. It was indirectly monitored through the ^{13}C magnetization by transferring polarization from the ^{1}H spins to ^{13}C spins by the LGCP scheme. (b)^{1}H-to-^{13}C magnetization transfer under cross polarization (open circles) and LGCP (filled squares) sequences.

present work with dynamic nuclear polarization is also under progress, which is presented in another poster[4].

References

[1] D.G. Cory *et al.* Fortschr. Phys. 48, 875 (2000).

[2] M. Lee and W.I. Goldburg, Phys. Rev. 140, A1261 (1965).

[3] R.K. Hester, J.L. Ackerman, V.R. Cross and J.S. Waugh, Phys. Rev. Lett. 34, 993 (1975).

[4] A. Kagawa, M. Negoro, S. Yamanaka, Y. Murokawa, K. Takeda and M. Kitagawa, "Initialization of a solid-state NMR quantum computer by DNP using photo-excited triplet electron spins", poster session

P115

Initialization of a solid-state NMR quantum computer by DNP using photo-excited triplet electron spins

○Akinori Kagawa, Makoto Negoro, Shogo Yamanaka, Yu Murokawa, Kazuyuki Takeda and Masahiro Kitagawa

Graduate School of Engineering Science, Osaka University, Japan

Abstract: In order to realize NMR quantum computing with high nuclear polarization beyond the entanglement threshold, dynamic nuclear polarization using electron spins in the photo-excited triplet state was utilized. In order both to attain high polarization and to implement quantum computing, an experimental setup is developed. Requirements on the material is also discussed.

Previous experiments on NMR quantum computing (NMRQC) are not "true" implementations of quantum computing, owing to the low nuclear polarization, with which one must rely on pseudo-initialization schemes. The pseudo-initialization schemes require exponentially increasing experimental steps with the number of qubits. Furthermore, the quantum state of the system started from the pseudo-initialized state cannot be entangled, unless the initial nuclear polarization exceeds a certain threshold given by the separability criterion [2]. The only example of NMRQC experiment above the entanglement threshold reported so far has utilized para-hydrogen induced high polarization in a liquid sample. In this work we propose an alternative approach toward NMRQC with high polarization, in which dynamic nuclear polarization (DNP) using electron spins in the photo-excited triplet state, which we henceforth refer to as "triplet-DNP", is utilized. Toward the ultimate goal of realizing NMRQC with high polarization above the entanglement threshold, we set the following three mid-term tasks.

1. Design of the material suitable for both triplet-DNP and NMRQC with up to several qubits
2. Hardware development for triplet-DNP togther with NMR experiments
3. Development of pulse sequences for quantum gate operations specific to the material found out in 1

Although the material quest is still underway, we are fairly sure about some features that the appropriate materials should have as follows.

a. The sample has to be host/guest single crystal, in which the guest molecules are photo-excitable to the triplet state having the large electron polarization, and serves as the sources of polarization.

Key Words : quantum computer, DNP, photo-excited triplet electron spins

b. The guest also has to act as a quantum computer, or the second guest material for the quantum computer may be co-doped.

c. The ^{1}H spin diffusion rate of the host material should appropriately be controlled by adjusting the deuteration factor, because the host protons are irrelevant to NMRQC and used only to transport the polarization from the triplet electrons to the co-doped molecules for quantum computing.

Here, we performed triplet-DNP experiments in a system that is known one can attain high nuclear polarization: pentacene-doped in naphthalene or p-terphenyl. We aimed at letting one of the ^{13}C spins in a naphthalene molecule and its adjacent ^{1}H spin serve as a 2-qubit system. Since ^{1}H spins in the host naphthalene has successfully been built up to the ultimate value (0.69) that coincides with the electron polarization of the photo-excited triplet state of pentacene [3], NMRQC with polarization beyond the entanglement threshold (0.41) is expected with this approach. The issue of pulse sequences for quantum gate operation is dealt with in another poster [5].

For the host naphthalene, we used two differently labeled materials : (a) ~ 99 % deuterated naphthalene, and (b) 1-^{13}C naphthalene (undeuterated). (a) and (b) were mixed with a ratio of 9:1 together with a small amount (~ 0.01 mol%) of pentacene, and single crystal was grown from the melt. In this sample, the residual protons in (a) and those in (b) transport polarization by spin diffusion, and the e ^{13}C spin, which is intended to be used as the first qubit, can also be polarized with CP. In order to let the nearest ^{1}H spin to the ^{13}C spin act as the second qubit, Lee-Goldburg (LG) irradiation [4] is applied after the DNP process, so that the dipolar couplings among the protons are eliminated. We showed that appropriate phase modulation that keeps the LG condition enables 1-qubit gate as well as controlled gate operations [5].

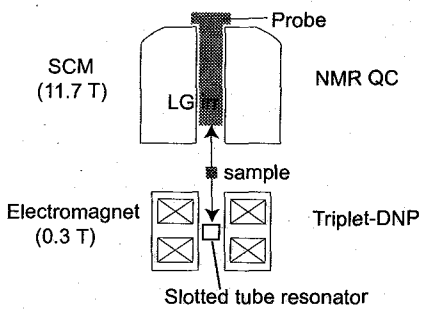

Fig. 1: A schematic diagram of an experimental system

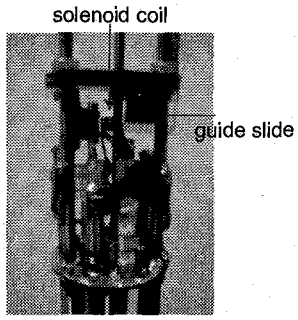

Fig. 2: triple-resonance probe head

For practical reasons, relatively low magnetic fields around 0.3 T are suitable for the triplet-DNP experiments, while NMRQC is desirable to be carried out in the conventional high fields. In order to meet both of these demands, we have developed

an X-band ESR system with an electromagnet, a ^{1}H-^{13}C-^{2}H triple-resonance probe for NMR experiments in a 11.7 T wide bore superconducting magnet, and a sample shuttle system between the low and high magnetic fields (Fig.1). The X-band ESR system consists of a resonator and a field sweep coil. For the microwave irradiation, we used a slotted-tube resonator, which has a sample access along the resonator's cylindrical axis and is easily accommodated to the sample-shuttle system. For the NMR coil in the high field, on the other hand, the priority was given to rf-irradiation efficiency, and accordingly, a solenoid coil was employed. In order to put samples into the solenoid coil smoothly, a guide slide is placed in the NMR probe head (Fig.2).

The demonstration of triplet-DNP with a shuttle system have been performed at room temperature in single crystal of pentacened-doped p-terphenyl (3mg). For the triplet-DNP experiment, the Integrated Cross Polarization (ICP) technique [3] was used with a repetition rate of 20Hz, as depicted in Fig.3.

After 10min repetition of the ICP sequence, the ^{1}H polarization was enhanced to ca. 0.01 (Fig.4), which is 250 times larger than that in thermal equilibrium. The enhanced ^{1}H polarization can further be transferred to the ^{13}C spins by CP, as demonstrated in Fig.5. The attained ^{13}C polarization was ca. 0.0027.

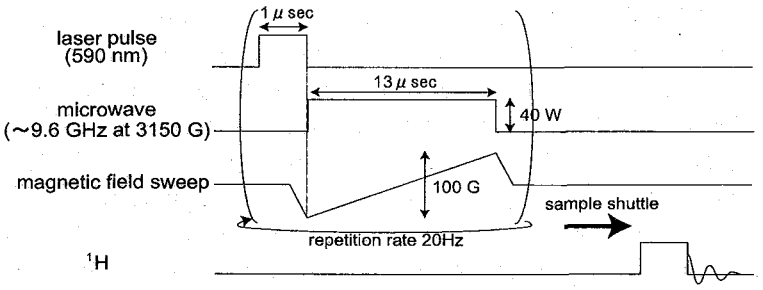

Fig. 3: a pulse sequence for the ICP technique

To summarize, we have successfully implemented triplet-DNP with the sample shuttle system. The nuclear polarizations attained here are rather small, due to relatively short T1 at room temperature. In order to suppress ^{1}H spin-lattice relaxation, we are now developing a cryogenic system, with which significant enhancement of nuclear polarization beyond the entanglement threshold is expected. Thus, the present work on triplet-DNP combined with our new approach toward universal quantum gate operation [5] would realize "ture" NMR quantum computing.

References

[1] M. S. Anwar, D. Blazina, H. Carteret, S. B. Duckett, J. A. Jones, Phys. Rev. A **70**, 032324 (2004).

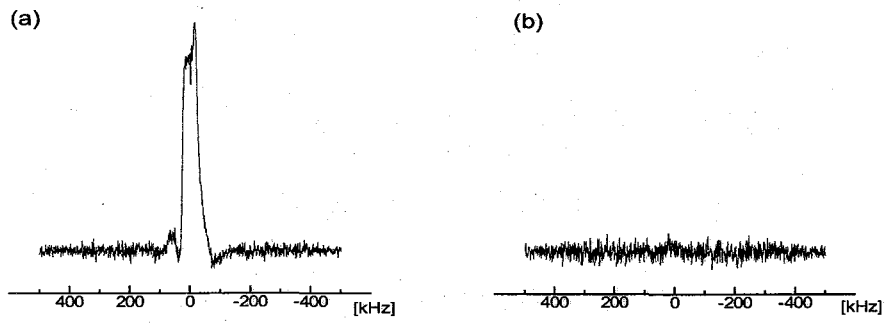

Fig. 4: Single scan ^{1}H spectra in single crystal of 0.05 mol% pentacene-doped p-terphenyl obtained (a) by applying the ICP sequence for 10 min at a repetition rate of 20Hz. (b) under thermal equilibrium. In order to avoid receiver saturation, the preamplifier was not used.

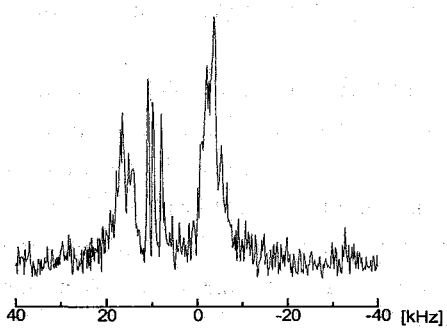

Fig. 5: Single scan ^{13}C CP spectrum in p-terphenyl (3 mg) after polarizing the protons by the ICP technique.

[2] A. Peres, Phys. Rev. Lett. 77, 1413-1415 (1996).

[3] K. Takeda, K. Takegoshi, T. Terao, J. Phys. Soc. Japan 73 2313 (2004).

[4] M. Lee, W.I. Goldburg, Phys. Rev. **140**, A1261 (1965).

[5] M. Negoro, S. Yamanaka, A. Kagawa, K. Takeda and M. Kitagawa, "Universal control of a qubit system under Lee-Goldburg irradiation for solid-state NMR quantum computing", poster session.

P116

高速フーリエ変換法によるNMR量子コンピュータ用ラジオ波パルス列の生成法

松山大学経営学部　福見　俊夫
790-8578 松山市文京 4-2

FFT method of rf-pulse generation in NMR quantum computer

Toshio Fukumi
Faculty of Business Administration, Matsuyama University
4-2 Bunkyo, Matsuyama, Ehime 790 8578, Japan

NMR quantum computation is to employ evolving of spins according to unitary operators.[1] For this purpose we must encode unitary operator into rf-pulses. Up to date no clear technique for rf-pulse sequence has not been described explicitly, although researchers have been using it implicitly. The purpose of the present paper is to explore the method of rf-pulse sequence form unitary operator. The schematic of rf-pulse generation can be summarized as follows.

Step 1. Factorization of unitary matrix into direct products.
Step 2. Rewrite factorized matrix by spin operator.
Step3 . Construction of infinitesimal operator.
Step 4. Exponential homomorphism of infinitesimal operator provides rf-sequence.

Unfortunately, however, factorization of matrix is a NP-Problem, that is, exponentially complex problem. Generic algorithm is a recent attempt.[3]

In the present study, the author would like to propose to employ operator valued FFT technique to generate a large rf-pulse sequence. The amplitude spectrum provides the measure of the importance of individual elementary gates. In case, in which underlying group has a large automorphism, FFTs for many finite groups exists. As a simple example, in the case in which the underlying group is abelian, the classical Cooley-Turkey FFT provides a fast algorithm. More generally, FFTs work for symmetric groups, super-solvable groups, and the Lie groups of finite type. At a first glance, quantum Fourier transform(QFT) seems promising as the method of implementation into

NMR quantum computer is known. Unfortunately, however, QFT is a quantum version of Cooley-Turkey FFT which was originally aimed to factorize large integers and so it can not factorize unitary matrixes. For this reason we must rely on conventional computers to factorize large unitary matrixes employing a group theoretic FFT for the present purpose. Finally, it should be noted that FFT method is sometimes not effective as we may encounter TSP(Traveling Salesman Problem) which is a typical NP-Complete problem which is exponentially complex.

References

1. U.Sakaguchi, H.Ozawa, and T.Fukumi, "NMR Quantum Computing" in "Coherence and Statistics of Phtons and Atoms" ed. J.Perina (Wiley 2000).
2. M.J.Rethinan, A.K.Javal, E.C.Behrman, J.F.Steck, and S.R.Skinner, "A generic algorithm for finding pulse sequences for NMR quantum computing" e-print arXiv:quant-ph/04041710 29 Apr. 2004.

NMR データベース; BMRB の新登録インターフェイス (ADIT-NMR)

○中谷 英一[1,2], 原野 陽子[1], 藤原 敏道[1], 中村 春木[1], 阿久津 秀雄[1]
[1]大阪大学蛋白質研究所, [2]科学技術振興機構-BIRD

New deposition web interface (ADIT-NMR) of BMRB as a NMR database.

[1]Institute for Protein Research, Osaka University, [2]Japan Science and Technology Agency - BIRD

Eiichi Nakatani[1,2], Yoko Harano[1], Toshimichi Fujiwara[1], Haruki Nakamura[1], Hideo Akutsu[1]

The β version of data deposition web interface (ADIT-NMR) of BMRB database (BioMagResBank, University of Wisconsin Madison, USA, PI. John L. Markley) had been released in September, 2006 at Madison. In near future, the ADIT-NMR will be renewed as a production version instead of current ADIT-NMR. The new ADIT-NMR allows to deposit both NMR experimental and structural data of a protein to either BMRB and PDB (Protein Data Bank) via a web interface. Furthermore, the description for solid-state NMR data are developed in cooperation with PDBj (Protein Data Bank japan, Head; Haruki Nakamura).

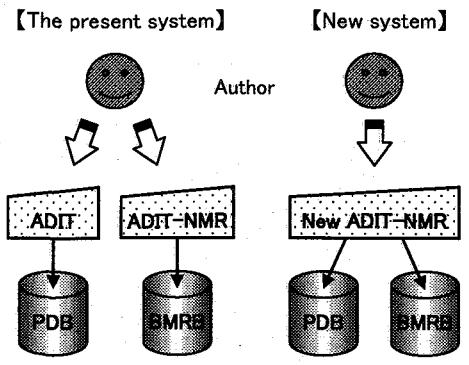

Fig.1 The flow of data deposition to PDB and BMRB.

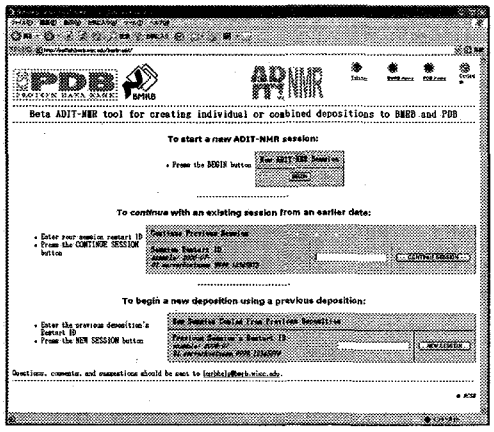

Fig.2 The top page of new ADIT-NMR (β version).

従来の PDB と BMRB の登録ではそれぞれ独自の登録ウェブサイト（ADIT および ADIT-NMR）を公開して研究者が実験で求めた蛋白質の立体構造データと NMR データの登録を受け付けていた。今回、ADIT-NMR の改良でそれらは一つのインターフェイスに統合された。その結果、一度の登録作業で両データベースにデータ登録を行うことが可能となり、同じようなデータを重複してそれぞれのインターフェイスに入力する必要がなくなった。

キーワード：BMRB、NMR データベース、PDBj
なかたにえいいち、はらのようこ、ふじわらとしみち、なかむらはるき、あくつひでお

新 ADIT-NMR では PDB と BMRB 登録のためのデータ入力の表示モード（Fig.3）が設けられた。両登録に必要な入力項目の組はそれぞれのモードで異なるが、共通項目において一方のモード上で入力されたデータは両モードで共有される。入力の完了後、PDB モードで登録すると PDB の登録が、BMRB モードでは BMRB の登録がそれぞれ行われる。

Fig.3 A switch for exchanging screen between PDB and BMRB input layout.

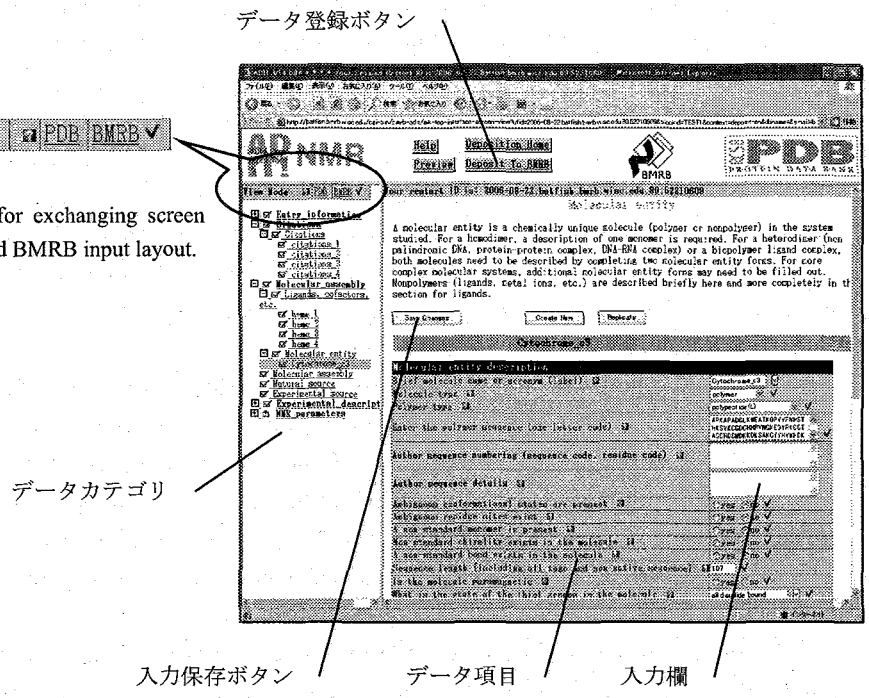

Fig.4 The input screen of new ADIT-NMR.

PDB や BMRB の既存の登録ファイルを新 ADIT-NMR にアップロードすると、そのファイルから抽出されたデータが入力欄に既定表示される。登録者はそれらのデータを修正、あるいは不足するデータを補うことで新規の登録を行うことが可能となった。この結果、登録を行う際の入力作業の負担を減らす事ができた。

PDBj（Protein Data Bank japan, 統括; 中村春木）では、固体 NMR 特有のデータを BMRB フォーマットに記述することを可能とするためのデータ項目の追加と、ADIT-NMR 利用勝手向上のための開発を BioMagResBank と共同で行っている。本討論会では、新 ADIT-NMR が旧バージョンから変更された点や新 ADIT-NMR を使用した PDB と BMRB データ登録の方法、固体 NMR に関連するデータ項目、および BMRB データベースの利用統計について説明する。

P118

Restricted diffusion of water in clay gel saturated porous media

Takahiro Ohkubo[1] and Makoto Yamaguchi[2]
[1]Geological Isolation Research and Development Directorate, Japan Atomic Energy Agency
[2]Institute of Research and Innovation

The time-dependent diffusion coefficients of fluid molecules in confining geometries have been studied by NMR experiments with magnetic gradient. The characteristics of porous media such as the ratio of the surface area to pore volume, S/V_p, and tortuosity, Υ, are extracted by analyzing the diffusion coefficient of fluid molecules as a function of diffusion time, Δ_{eff}. Since S/V_p and Υ are related to permeability, it have been a very powerful technique for investigating the transport phenomena of fluids in porous media. Therefore, we attempted to apply these methods to clay saturated porous media which would be considered as barrier environment in geological disposal system of high-level radioactive waste. NMR measurements of time-dependent diffusion coefficient were performed to estimate S/V_p and Υ for water and clay gel saturated porous media modeled by glass beads beds.

The purified natural Na-montmorillonite (purity is over 98 %), from Tsukinuno Mine, Yamagata, Japan (~1 μm particle size) were used as clay minerals. This clay contains paramagnetic ions like Fe^{2+} and Fe^{3+} in a crystal structure. Hence, a low field permanent magnet at 0.55 T was used to avoid the short relaxation time in higher magnetic field due to paramagnetic ions. The clay gel saturated porous media were prepared by mixing glass beads beds (50 μm and 150 μm with 10 % error catalog values) and clay gel, which was prepared by mixing clay and deionized water at a weight rate of 1 to 20. The sample was put into the glass container (ϕ = 14 mm), sonicated and centrifuged to remove air bubbles. 17 interval bipolar gradient stimulated echo[1] (Δ_{eff} = 6 ms ~ 200 ms) and oscillating gradient spin echo sequences[2] (Δ_{eff} = 0.625 ms ~ 5.626 ms) were used to measure time-dependent diffusion coefficients. All measurements were carrying out on a Resonance Instrument Maran Ultra NMR spectrometer equipped with a 250 G/cm at 30 ℃. Mitra equation[3] and Pade approximation[4] give by Eqs. (1) and (2) were applied to analyze time-dependent diffusion coefficient for the purpose of extracting Υ and S/V_p.

$$D(\Delta_{\mathrm{eff}}) = D_0(1-c) \tag{1}$$

$$D(\Delta_{\mathrm{eff}}) = D_0 - D_0\left(1-\frac{1}{\Upsilon}\right)\times\frac{c+(1-1/\Upsilon)\Delta_{\mathrm{eff}}/\theta}{(1-1/\Upsilon)+c+(1-1/\Upsilon)\Delta_{\mathrm{eff}}/\theta} \tag{2}$$

$$c = \frac{4}{9\sqrt{\pi}}\frac{S}{V_p}\sqrt{D_0\Delta_{\mathrm{eff}}}.$$

where θ is related to the sphere diameter of pore.

The diffusion coefficients of water and bulk clay gel were 2.54×10^{-9} m^2/s and 1.64×10^{-9} m^2/s with independent of Δ_{eff}, respectively. The result of bulk clay gel means that the minimum Δ_{eff}

keywords: Clay gel, porous media, 17 interval bipolar gradient stimulated echo, Oscillating gradient spin echo, Restricted diffusion

of 0.625 ms was already over the range of restricted diffusion regime of water molecules in clay gel.

Figures 1 and 2 show that Mitra equation for Δ_{eff}<6 ms and Pade approximation for Δ_{eff}<200 ms were applied to fit time-dependent diffusion coefficients for each samples. The fitting procedures with variable D_0 in Fig. 2 were not able to obtain a valid fitting result. Therefore, we performed fitting procedure with fixed D_0 to 2.54 $\times 10^{-9}$ m^2/s and 1.64 $\times 10^{-9}$ m^2/s for water and clay gel saturated media, respectively. S/V_p values estimated from Mitra equation in water saturated 50 and 150 μm glass beads beds were 1890 cm^{-1} and 629 cm^{-1}, respectively. Assuming close packed structure, beads diameters were calculated to be 52 and 156 μm, indicating very good agreement with the ideal values of the glass beads. On the other hand, estimation of S/V_p for clay gel saturated samples were 1462 cm^{-1} and 517 cm^{-1}, respectively. Similarly, Υ were evaluated from Pade approximation for time-dependent diffusion coefficients of all samples, and were 1.79 and 1.57 for clay gel saturated 50 μm and 150 μm glass beads samples, and 1.86 and 1.49 for water saturated 50 μm and 150 μm glass beads samples, respectively. It would appear from these results that the evaluation of S/V_p and Υ in clay saturated porous media by measuring time-dependent diffusion coefficients is feasibility.

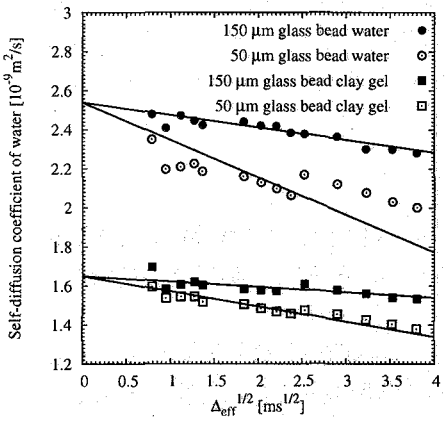

Figure 1: Diffusion coefficient as a function of the square root of diffusion time. The lines indicate fitting results of Mitra equation.

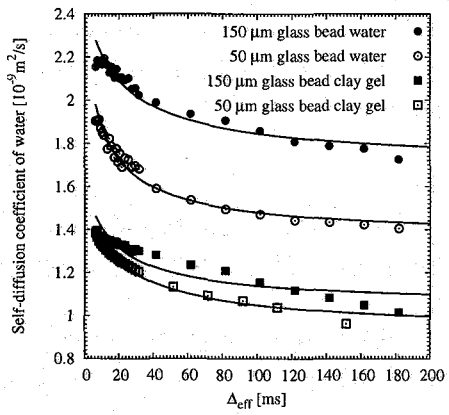

Figure 2: Diffusion coefficient as a function of diffusion time. The lines indicate fitting results of Pade approximation.

References

[1] R. M. Cotts, M. J. R. Hoch, T. Sun and J. T. Markert, *J. Magn. Reson.*, **83**, 252 (1989)

[2] B. Gross and R. Kosfeld, *Messtechnik*, **77**, 171 (1969)

[3] P. P. Mitra, P. N. Sen, L. M. Schwartz and P. Le Doussal, *Phys. Rev. Lett.*, **68**, 3555 (1992)

[4] L. L. Latour, P. P. Mitra, R. L. Kleinberg and C. H. Sotak, *J. Magn. Reson. A*, **101**, 3442 (1993)

P119

地雷探知のためのNQRパルスシーケンス

大阪大学基礎工学研究科(1)、物質・材料研究機構(2)
小林和彦 1、太田剛 1、Jammie Barras1、田村潤 1、糸崎秀夫 1、立木実 2

NQR Pulse Sequence for Explosive Detection

1Graduate School of Science Engineering,Osaka University,
2National Institute for Materials Science
Kazuhiko Kobayashi1, Go Ota1, Jammie Barras1, Jun Tamura1, Hideo Itozaki1,
Minoru Tachiki2

Abstract

Nuclear quadrupole resonance (NQR) has been paid attention to as an explosive detection technique, which detects the ^{14}N nuclei in an explosive material. The explosive materials widely contained in a landmine, RDX and TNT have resonant frequency in the range from 700 kHz to 5 MHz. It is so necessary to detect the NQR signal from a landmine quickly and robustly for a practical application that we considered rapid pulse sequences of SLSE and SORC instead of a usual sequence of FID detection. The signal from RDX and TNT were identified efficiently by these sequences.

本文

核四極共鳴(Nuclear Quadrupole Resonance;NQR)は化学物質を直接探知できる手法であるため、金属探知機等に代わる地雷探知の新しい方法として実用化が期待されている。

NQR とは各種物質中の原子核スピンに、ある特定の共鳴周波数の電波を照射することで核スピンを励起し、そのスピンが緩和する際に同じ共鳴周波数の電波を放出する、という現象である。共鳴周波数はスピンの周りの電場勾配によって決定される。電場勾配はそれぞれの化学物質により異なるため、共鳴周波数は物質ごとに異なる数値を取る。このため、NQR を利用することにより物質の特定ができるだけでなく、想定している物質の有無を調べることも可能となる。また、NMR が静磁場をかけてスピンを整列させるのに対し、NQR は分子の電場勾配を利用するため、超伝導磁石のような大規模な装置を必要としない。

現在、NQRでは一般的にパルス法が用いられている。単一のパルスによる励起で得られるFID 信号は一般に S/N 比が低く、何回も積算することで S/N 比を高める必要がある。積

Key Words: NQR, pulse sequence, explosive, land mine, sensitivity
著者ふりがな:こばやし かずひこ

算する際には励起されたスピンが緩和して元の状態に戻るのを待ってから、次のパルスを照射したほうが強い信号が得られる。

この、励起されたスピンが緩和するまでの時間がT_1である。実際にはパルスを照射する間隔をT_1の 3～4 倍以上取ったときに最大強度の信号が得られる。T_1に依存する緩和は縦緩和であり、エネルギーのやり取りによるものである。スピンの緩和には縦緩和の他に、横緩和がある。横緩和の時定数はT_2*である。

地雷に含まれる代表的な爆薬としてはRDXとTNTが挙げられるが、RDXのT_1は 32 ミリ秒であるのに対してTNTのT_1は約 3 秒と非常に長い。このため、RDXは 1 分間にFID信号を 100 回以上積算できるが、TNTは 1 分間に 3～4 回程度しか積算できない。実際の地雷探知では数分程度で地雷を見つける必要があるため、FID信号の観測のみでは地雷探知に応用することは極めて難しい。ゆえに現在、シングルパルスによるFID信号観測だけでなく、パルスの位相や照射するタイミングなど、パルスの当て方を工夫してスピンを効率的に励起する様々なパルスシーケンスが研究されている。

NQR 信号を効率的に得るシーケンスの 1 つの例として、SLSE(Spin Locking Spin Echo)シーケンスが挙げられる。SLSE は主に NMR で用いられているシーケンスで、スピンが横緩和していくのをマルチパルスにより抑制する、という考えに基づいている。この、横緩和を抑制する SLSE により、TNT のような縦緩和に非常に長い時間がかかる物質においても短時間で積算回数を多く取る事ができると考えた。今回、我々は TNT に SLSE を適用することで効率よく NQR 信号を取得することに成功した。

また、RDX は通常の FID 信号の観測である程度の S/N 比を持つ信号を得ることができるが、更に短時間に積算回数を増やすことでノイズの多い環境でも信号を観測することができると考え、RDX にも FID 以外のパルスシーケンスの適用を検討した。そこで、我々は SORC(Strong Off Resonance Comb)シーケンスに着目した。SORC シーケンスは FID 信号とエコー信号を重ね合わせて擬似的な定常信号を得るものである。そこで、SORC シーケンスを用いることで更に積算回数を増やすことができると考え、実際に SORC シーケンスを用いて RDX の NQR 信号を取得することに成功した。

P120

磁場勾配NMRによるベシクル内包分子の選択的検出

（花王㈱）○中村文彦、川口高広、香春武史

Selective Detection of Molecules in Vesicle by Pulse Field Gradient NMR (Kao Corporation) ○Fumihiko Nakamura, Takahiro Kawaguchi, and Takeshi Kaharu

Vesicle and multi-emulsion include water molecules in dispersed phase and continuous phase respectively. We developed a novel method for detecting a signal only from dispersed phase selectively, by making good use of PFG-NMR. We found that by increasing diffusion time extremely, a signal from continuous phase is eliminated, besides a signal from dispersed phase remains because of restricted diffusion. By this method, we can estimate the molecules distribution, relaxation time of molecules in dispersed phase and so on.

We applied this method to typical sample that includes multi-lamellar vesicles, and estimate proportion of molecules in vesicle. The order of these estimated proportion agreed with an observation by polarizing microscope.

【序論】ベシクルや多重ミセルのような、分散相と連続相に同種の化合物が存在する溶液構造を有する組成物がある。こうした組成物において、分散相と連続相の違いというのは巨視的なものであり、２つの領域に分かれて存在している分子を、NMRスペクトルやその緩和時間といった、微視的な環境しか反映しない情報によって見分けることは不可能である。しかし、事実、これらは異なる状態にある分子であって、これらの比率が巨視的な物性に影響を与えることもある。したがって、分光的にこれらを識別することができれば、意義深いと考えられる。今回、我々は磁場勾配NMRを応用することで、分散相に存在する分子だけを選択的に検出できる方法を開発したので報告する。

【原理】磁場勾配スピンエコー法によれば、注目した化合物の拡散の程度を式（１）に示したシグナルの強度変化として捉えることができる。

$$M = M_0 \exp\left\{-\gamma^2\delta^2 g^2\left(\Delta-\frac{\delta}{3}\right)D-\frac{\tau}{T_2}\right\} \qquad (1)$$

M_0 ： 減衰を受けない場合のシグナル強度　γ ：磁気回転比
δ ：磁場勾配パルス幅　g ： 磁場勾配強度　Δ ：拡散観測時間
D ： 自己拡散係数　τ ：遅延時間（$=2\Delta$）　T_2 ：横緩和時間

キーワード：磁場勾配NMR、溶液構造、ベシクル
著者ふりがな：なかむらふみひこ、かわぐちたかひろ、かはるたけし

拡散時間Δの間の２乗平均移動距離$<x^2>$は自己拡散係数がDのとき式（２）のように表されることから、$\Delta \gg \delta/3$のとき、式（１）は、式（３）のように、$<x^2>$に対する式に書きなおせる。

$$\left\langle x^2 \right\rangle = 2D\Delta \qquad (2)$$

$$M = M_0 \exp\left\{-\frac{1}{2}\gamma^2\delta^2 g^2 \left\langle x^2 \right\rangle - \frac{\tau}{T_2}\right\} \qquad (3)$$

さらに、本研究で注目しているような組成物においては、分散相と連続相のそれぞれに存在する分子からのシグナル強度の足し合わせとして、式（４）のように導ける。なお、式（４）中、添え字のＡは分散相を、Ｂは連続相を意味する。

$$M = M_A \exp\left\{-\frac{1}{2}\gamma^2\delta^2 g^2 \left\langle x^2 \right\rangle_A - \frac{\tau}{T_{2A}}\right\} + M_B \exp\left\{-\frac{1}{2}\gamma^2\delta^2 g^2 \left\langle x^2 \right\rangle_B - \frac{\tau}{T_{2B}}\right\} \qquad (4)$$

このとき、Δを充分長くとれば、連続相では分子の拡散が著しく進行するため$<x^2>_B \rightarrow \infty$となり、式（４）の第２項全体が消失する。それに対し、分散構造自体の拡散が無視できるとすると、閉じた分散相内での分子の拡散には限界が有り、$<x^2>_A$はある一定の値$<x^2>_{A\infty}$に収束する。その結果、Δを充分大きくとれば式（４）は式（５）のように単純化できる。

$$M = M_A \exp\left\{-\frac{1}{2}\gamma^2\delta^2 g^2 \left\langle x^2 \right\rangle_{A\infty} - \frac{\tau}{T_{2A}}\right\} \qquad (5)$$

したがって、以上の条件が満たされるとき、連続相からのシグナルが消失し、分散相からのシグナルのみを検出できることになる。このとき、連続相のシグナルが消失したことは、シグナル強度のτ（＝２Δ）に対する対数プロットがｇによらず同じ傾き（$-1/T_{2A}$）の直線に収束することで確認される。

こうして得られた直線から、分散相の分子のT_2を求められるが、さらにτ、g^2に対して外挿を行うことにより、M_Aが得られ、分散相と連続相の存在比を見積もることができる。また、ここでは詳細は略すが、$<x^2>_{A\infty}$を求め、分散相の大きさも見積もることも可能である。

【実験】主な成分としてカチオン界面活性剤と高級アルコールを含む水系の化粧料用組成物を種々の乳化条件の下で調製し、マルチラメラベシクル量の異なる３つの試料

を得た。これらの試料中の水（～84%）のシグナルを磁場勾配スピンエコー法により測定し、原理の項で説明した方法により、分散相からのシグナルを分離した。磁場勾配の大きさgは0～300Gauss/cm、磁場勾配パルス幅は1000μsecとし、Δは最大で0.5sec（τで1.0sec）まで伸ばした。

【結果と考察】Fig.1に、得られたシグナル強度変化の一例を示す。gが100Gauss/cm以上になると、τの大きい領域ではgによらず、同じ傾きの直線に収束していることが読み取れる。この領域が分散相に由来するシグナルのみになっていると考えられ、これから分散相の比率を算出した。他の2つの試料に対しても同様にプロットを行い、それぞれ分散相比率を算出した。各試料について算出した分散相比率を、試料の偏光顕微鏡写真とともにFig.2に示す。本法で求められた分散相比率の序列は、偏光顕微鏡で観測されるマルチラメラベシクルの多さの序列に一致し、分散相であるベシクル内部からのシグナルの選択的な検出に成功しているものと考えられた。

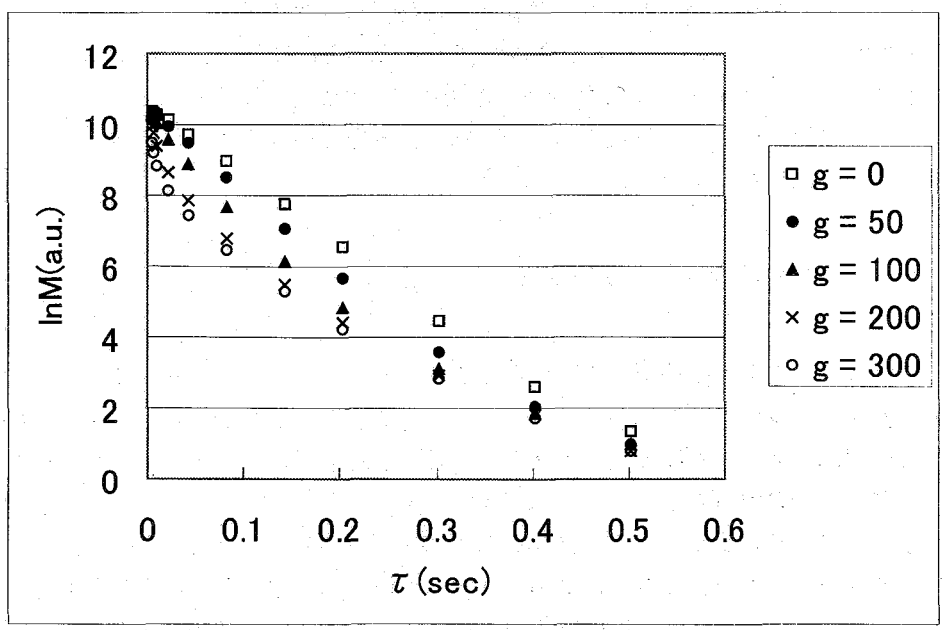

Fig.1 An example of signal intensity plot.
(Dispersed phase proportion of this sample was estimated at 1.3%.)

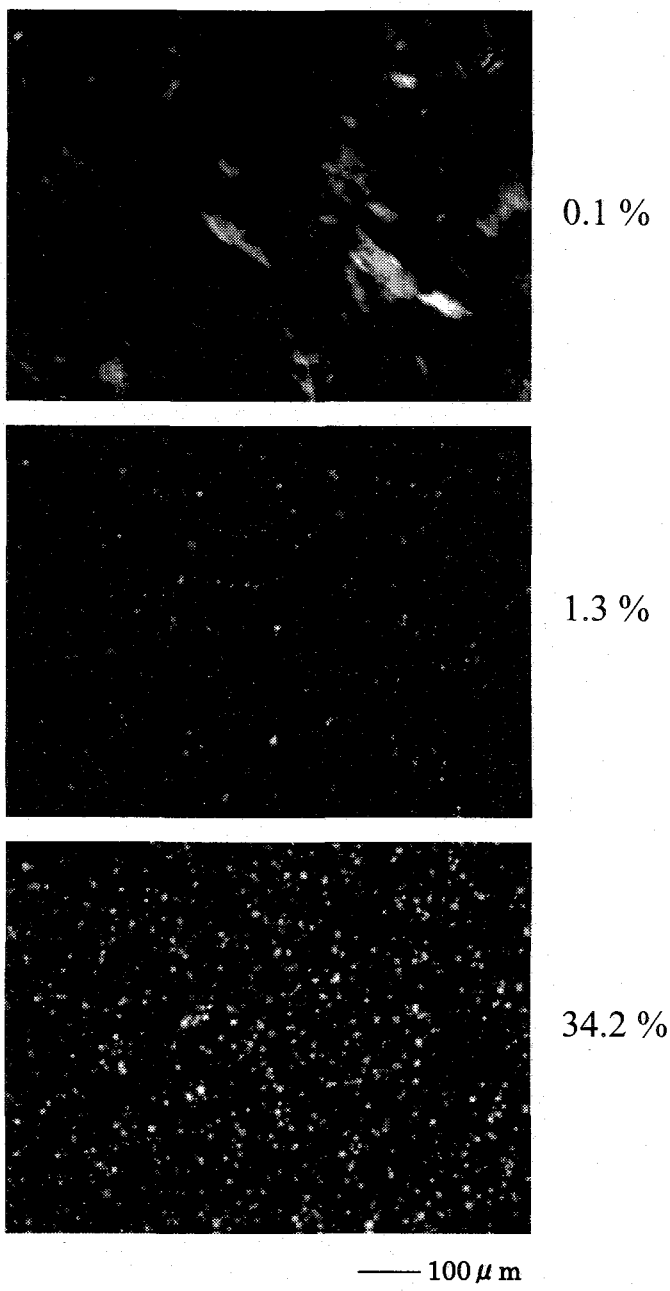

Fig.2 Optical texture of sample by a polarizing microscope and their dispersed phase proportion estimated by this method.

キーワード索引

著者索引

参加者名簿（予約者）

キーワード索引

参加者名簿 名前	所属
相沢　智康 Tomoyasu Aizawa	北海道大学大学院先端生命科学研究院 Hokkaido University
赤木　謙一 Ken-ichi Akagi	医薬基盤研究所 National Institute of Biomedical Innovation
秋山　かずえ Kazue Akiyama	大阪大学大学院医学系研究科保健学専攻
阿久津　秀雄 Hideo Akutsu	大阪大学蛋白質研究所 Institute for Protein Research, Osaka University
朝倉　哲郎 Tetsuo Asakura	東京農工大学 Tokyo University of Agriculture and Technology
浅野　敦志 Atsushi Asano	防衛大学校 National Defense Academy
浅野　朋子 Tomoko Asano	名古屋工業大学大学院工学研究科物質工学専攻
淺野間　文夫 Fumio Asanoma	奈良先端科学技術大学院大学
芦田　淳 Jun Ashida	バリアンテクノロジーズジャパンリミテッド Varian Technologies Japan Limited
阿曽　幸男 Yukio Aso	国立医薬品食品衛生研究所 National Institute of Health Sciences
阿部　孝政 Takamasa Abe	理化学研究所　ゲノム科学総合研究センター RIKEN, GSC
飯島　隆広 Takahiro Iijima	京都大学大学院理学研究科 Department of Chemistry, Kyoto University
池上　貴久 Takahisa Ikegami	大阪大学蛋白質研究所構造プロテオミクス Institute for Protein Research, Osaka University
石川　潔 kiyoshi ishikawa	兵庫県立大学
石川　洋土 Hiroto Ishikawa	京都大学大学院理学研究科化学専攻
泉川　美穂 Miho Izumikawa	独立行政法人　理化学研究所 RIKEN Yokohama Institute
射手園　佳子 Yoshiko Itezono	中外製薬
出田　圭子 Keiko Ideta	九州大学先導物質化学研究所 Institute for Materials Chemisitry and Engineering, Kyushu Univ.
犬飼　宗弘 Munehiro Inukai	大阪大学大学院基礎工学研究科 Graduate School of Engineering Science, Osaka University, Japan
井上　匡子 Kyoko Inoue	理化学研究所　横浜研究所　ゲノム科学総合研究センター RIKEN Yokohama Institute Genomic Sciences Center

参加者名簿 名前	所属
井上　暁 Satoru Inoue	京都大学理学部理学科化学専攻
井ノ岡　博 Hiroshi Inooka	武田薬品工業株式会社 Takeda Pharmaceutical Company Ltd.
今泉　好偉 Yoshie Imaizumi	獨協医科大学　医学部　生理学（生体制御） Dokkyo University School of Medicine, Department of Regulatory Physiology
井町　美佐子 Imachi Misako	ブルカーバイオスピン（株）
岩澤　秀樹 Hideki Iwasawa	横浜市立大学大学院　国際総合科学研究科　生体超分子科学専攻
岩下　孝 Takashi Iwashita	（財）サントリー生物有機科学研究所 Suntory Institute for Bioorganic Research
岩瀬　由紀子 Yukiko Iwase	福岡大学　薬学部 Fukuoka University Faculty of Pharmaceutical Science
上釜　奈緒子 Naoko Uekama	兵庫県立大学大学院　生命理学研究科 Grad. Schl. Life Sci., Univ. Hyogo
植木　定雄 Ueki Sadao	ブルカーバイオスピン（株）
上松　照幸 Teruyuki Uematsu	株式会社巴商会 Tomoe Shokai Co., Ltd.
内田　健一 Kenichi Uchida	帝京大学理工学部バイオサイエンス学科
内海　博明 Hiroaki Utsumi	日本電子株式会社　分析機器本部 JEOL　Ltd
梅川　雄一 Yuichi Umegawa	大阪大学大学院理学研究科 Osaka Univ.
梅津　喜崇 Yoshitaka Umetsu	北海道大学大学院理学研究科 Graduate School of Science, Hokkaido University
梅山　万左子 Masako Umeyama	横浜国立大学大学院工学府 Yokohama National University
大郷　耕輔 Kosuke　Ohgo	東京農工大学 Tokyo Univ. Agri. Tech.
大島（坂本）　曜子 Yohko　Ohshima	東邦大学　薬学部　ＮＭＲ Faculty of Pharmaceutical Sciences, Toho University
太田　将信 Masanobu Ota	田辺製薬株式会社医薬化学研究所
大竹　紀夫 Norio Ohtake	東横化学株式会社　研究開発室
大貫　裕之 Hiroyuki Onuki	理化学研究所ゲノム科学総合研究センター RIKEN Genomic Sciences Center

参加者名簿 名前	所属
大野　靖 Yasushi Ohno	日本たばこ産業株式会社　医薬総合研究所
大橋　竜太郎 Ryutaro Ohashi	京都大学大学院理学研究科
大橋　若奈 Wakana Ohashi	理化学研究所ゲノム科学総合研究センター RIKEN GSC
尾身　洋典 Hironori Omi	産業技術総合研究所 計測フロンティア研究部門 ナノ移動解析研究グループ National Institute of Advanced Industrial Science and Technology (AIST)
大山　貴子 Takako Ohyama	横浜市立大学 Yokohama City University
岡田　敦司 Atsushi Okada	大正製薬株式会社 Taisho pharmaceutical co ltd
岡本　真美 Mami Okamoto	横浜市立大学大学院国際総合科学研究科 Int. Grad. Sch. Arts Sci.,Yokohama City Univ.
小川　潔 Kiyoshi Ogawa	旭化成ファーマ（株）　創薬研究所 Asahi-Kasei Pharma Corpolation
小川　雄大 Yuta Ogawa	東京大学大学院薬学系研究科 Graduate School of Pharmaceutical Sciences, the University of Tokyo
荻野　孝史 Takashi Ogino	国立精神・神経センター神経研究所 National Institute of Neuroscience
小此木　美智 Michi Okonogi	東京農工大学　工学府
香川　晃徳 Akinori Kagawa	大阪大学大学院基礎工学研究科 graduate school of engineering science, osaka university
垣田　信吾 Shingo Kakita	協和発酵工業株式会社 Kyowa Hakko Kogyo Co., Ltd.
加鳩　洋祐 Yousuke Kashima	塩野義製薬株式会社
片平　正人 Masato Katahira	横浜市立大学国際総合科学研究科 Yokohama City University
門　良一 Ryoichi Kado	京都産業大学理学部 Kyoto Sangyo University
加藤　久美子 Kumiko Katou	福井大学　生物応用化学科　生物物理化学グループ university of FUKUI
門原　寛 Kadohara Hiroshi	ブルカーバイオスピン（株）大阪営業
神原　孝之 Takayuki Kamihara	京都大学大学院理学研究科
神谷　昌克 Masakatsu Kamiya	北海道大学大学院先端生命科学研究院 Graduate School of Life Science, Hokkaido University

参加者名簿 名前	所属
亀田　篤司 Atsushi Kameda	大阪大学蛋白質研究所　蛋白質構造形成研究室 Laboratory of Protein Folding, Institute for Protein Research
川島　裕之 Hiroyuki Kawashima	産業技術総合研究所
河野　敬一 Keiichi Kawano	北海道大学大学院理学研究院 Hokkaido University, Faculty of Science
川村　出 Izuru Kawamura	横浜国立大学大学院　工学府　機能発現工学専攻 Graduate School of Engineering, Yokohama National University
木川　隆則 Takanori Kigawa	理化学研究所 RIKEN
菊地　淳 Jun Kikuchi	理化学研究所植物科学研究センター RIKEN Plant Science Center
北原　亮 Ryo Kitahara	理化学研究所スプリング８センター RIKEN SPring-8
木下　理 Osamu Kinoshita	福井大学 University of FUKUI
木村　一雄 Kazuo Kimura	（株）東レリサーチセンター
薛　献宇 Xianyu Xue	岡山大学地球物質科学研究センター Institute for Study of the Earth's Interior, Okayama University
久我　香子 Takako Kuga	京都大学化学研究所 Kyouto Univ. Institute of Chemical Research
串田　克彦 Katsuhiko Kushida	バリアンテクノロジーズジャパンリミテッド Varian Technologies Japan Ltd.
熊木　康裕 Yasuhiro Kumaki	北海道大学大学院理学研究院高分解能核磁気共鳴装置研究室 High-Resolution NMR Laboratory, Graduate School of Science, Hokkaido University
熊沢　茂則 Shigenori Kumazawa	静岡県立大学 University of Shizuoka
久米田　博之 Hiroyuki Kumeta	北海道大学薬学部構造生物学研究室 Laboratory of Structural Biology, Graduate School of Pharmaceutical Sciences, Hokkaido University
栗田　順一 Junichi Kurita	バリアンテクノロジーズジャパンリミテッド Varian Technologies Japan Ltd.
栗林　秀人 Hideto Kuribayashi	バリアンテクノロジーズジャパンリミテッド Varian Technologies Japan Limited
黒木　重樹 Shigeki Kuroki	東京工業大学大学院理工学研究科物質科学専攻 Tokyo Institute of Technology, Department of Chemistry and Materials Science
黒崎　千智 Chisato Kurosaki	理研GSC RIKEN, GSC
黒子　弘道 Hiromichi Kurosu	奈良女子大学 Nara Women's University

参加者名簿 名前	所属
黒田　幸夫 Kuroda Yukio	ブルカーバイオスピン（株）
河野　俊之 Toshiyuki Kohno	三菱化学生命科学研究所 Mitsubishi Kagaku Institute of Life Sciences
甲野　裕之 Kouno Hiroyuki	ブルカーバイオスピン（株）
越野　広雪 Hiroyuki Koshino	独立行政法人理化学研究所 RIKEN
小柴　生造 Seizo Koshiba	理化学研究所ゲノム科学総合研究センター Genomic Sciences Center RIKEN Yokohama Institute
児嶋　長次郎 Chojiro Kojima	奈良先端科学技術大学院大学 Nara Institute of Science and Technology
小橋川　敬博 Yoshihiro Kobashigawa	北海道大學大学院薬学研究院 Graduate School of Pharmaceutical Sciences, Hokkaido University
小林　広和 Hirokazu Kobayashi	大阪大学大学院基礎工学研究科 Graduate School of Engineering Science, Osaka University,
小林　将俊 Masatoshi Kobayashi	大阪大学　蛋白質研究所 Osaka University, Institute for Protein Research
齋藤　公児 Koji Saito	新日本製鐵（株）先端技術研究所
斉藤　貴士 Takashi Saitoh	九州大学　デジタルメディシン・イニシアティブ Kyushu univ.
齋藤　剛 Takeshi Saito	独立行政法人産業技術総合研究所
斉藤　肇 Hazime Saito	広島大学量子生命科学プロジェクトセンター QuLis, Hiroshima University
坂本　泰一 Taiichi Sakamoto	千葉工業大学工学部生命環境科学科 Department of Life and Environmental Sciences, Faculty of Engineering, Chiba Institute of Technology
佐久間　千勢子 Chiseko Sakuma	東京薬科大学
櫻井　愛子 Aiko Sakurai	（株）三菱化学科学技術研究センター Mitsubishi Chemical Group Science And Technology Research Center, Inc.
櫻井　智司 Satoshi Sakurai	日本電子株式会社分析機器本部応用研究グループ JEOL Ltd. Analytical Instrument Division Application & Research Group
笹川　拡明 Hiroaki Sasakawa	自然科学研究機構　分子科学研究所 National Institutes of Natural Science, Institute for Molecular Science
佐藤　一 Satou Hajime	ブルカーバイオスピン（株）
佐野　玲子 Reiko Sano	理化学研究所　ゲノム科学総合研究センター RIKEN GSC

参加者名簿 名前	所属
沢辺　紀子 Noriko Sawabe	東京理科大学　薬学部
品川　麻衣 Mai Shinagawa	味の素株式会社 AJINOMOTO
篠田　安弘 Yasuhiro Shinoda	京都大学理学部化学専攻 Department of Chemistry Graduate School of Science Kyoto University
下田　景士 Keiji Shimoda	新日本製鐵株式会社 Nippon Steel Corporation
荘司　顯 Akira Shoji	群馬大学 Gunma University
秦　旭栄 Xu-rong Qin	理化学研究所 RIKEN
神藤　平三郎 Heisaburo Shindo	（独）農業生物資源研究所 National Institute of Agricultural Sciences
榛葉　信久 nobuhisa Shimba	味の素株式会社 AJINOMOTO
菅瀬　謙治 Kenji Sugase	財団法人サントリー生物有機科学研究所 Suntory Institute for Bioorganic Research
杉浦　眞喜子 Makiko Sugiura	神戸薬科大学 Kobe Pharmaceutical University
鈴木　榮一郎 eiichiro Suzuki	味の素株式会社 AJINOMOTO
鈴木　浩一 Koh-ichi Suzuki	ソニー株式会社　コアコンポーネント事業グループ　エナジー事業本部　開発部門　材料解析室 Materials Analysis Section, R&D Division, Energy Business Group, Core Component Business Unit, Sony Corporation
鈴木　晃生 Kouo Suzuki	北海道大学大学院工学研究科応用物理学専攻
鈴木　咲良 Sakura Suzuki	理化学研究所ＧＳＣタンパク質構造機能解析グループ
鈴木　英男 Hideo Suzuki	スペクトラガス　インク
鈴木　陽 You Suzuki	金沢大学大学院　自然科学研究科
鈴木　倫太郎 Rintaro Suzuki	農業生物資源研究所 National Institute of Agrobiological Sciences
清宮　恭子 Kyoko Seimiya	独立行政法人理化学研究所　ゲノム科学総合研究センター RIKEN Genomic Sciences Center
瀬尾　芳輝 Yoshiteru Seo	獨協医科大学　医学部　生理学（生体制御） Dokkyo University School of Medicine, Department of Regulatory Physiology
関口　真二 Shinji Sekiguchi	北海道大学大学院 薬学研究院 構造生物学研究室 Graduate School of Pharmaceutical Sciences, Hokkaido University, Sapporo, Japan.

参加者名簿 名前	所属
相馬　洋之 Hiroyuki Souma	群馬大学工学部 Faculty of Engineering, Gunma University
高橋　征三 Seizo Takahashi	日本女子大学理学部物質生物科学科 Dept. Chem. &Biol. Sci., Fac. Science, Japan Women's University
高橋　栄夫 Hideo Takahashi	産総研・生物情報解析研究センター BIRC/AIST
高橋　宏和 Hirokazu Takahashi	金沢大学大学院　自然科学研究科
高橋　大樹 Hiroki Takahashi	大阪大学蛋白質研究所 Institute for Protein Research, Osaka University
高橋　雅人 Masato Takahashi	理化学研究所 RIKEN
高橋　豊 Yutaka Takahashi	日本電子（株）分析機器本部MSG技術T R&D-T, MSG, Analytical Instrument Division, JEOL Ltd.
高屋　展宏 Nobuhiro Takaya	国立環境研究所 National Institute for Environmental Studies
髙山　真一 Shin-ichi Takayama	筑波大学大学院数理物質科学研究科 Univ. of Tsukuba Dept. of chem
滝沢　剛 Takeshi Takizawa	三共株式会社　創薬基盤研究所1G
竹腰　清乃理 Kiyonori Takegoshi	京都大学大学院理学研究科化学
武田　和行 Kazuyuki Takeda	大阪大学大学院基礎工学研究科 Osaka University
多田　塁 Rui Tada	東京薬科大学　免疫学教室 Tokyo university of Pharmacy and Life Science, Laboratory for Immunopharmacology of Microbial Products
田中　千香子 Chikako Tanaka	防衛大学校　応用化学科 National Defense Academy
田中　彬嗣 Yoshitsugu Tanaka	九州大学　大学院薬学研究院 Graduate School of Pharmaceutical Sciences, Kyushu University
田中　利好 Rikou Tanaka	三菱化学生命科学研究所　蛋白質立体構造研究グループ
谷生　道一 Michikazu Tanio	三菱化学生命科学研究所 Mitsubishi Kagaku Institute of Life Sciences
玉井　潤野 Junya Tamai	京都大学理学部理学科化学専攻
田村　友美 Tamura Tomomi	ブルカーバイオスピン（株）大阪営業
近山　英輔 Eisuke Chikayama	理化学研究所 RIKEN

参加者名簿 名前	所属
趙　晨華 Chenhua Zhao	萬有製薬株式会社 BANYU PHARMACEUTICAL CO.,LTD.
張　恵平 Keihei Cho	理化学研究所 RIKEN
津野　慎治 Shinji Tuno	富士フイルム株式会社
出村　誠 Makoto Demura	北海道大学 Hokkaido Univ.
寺本　由衣 Yui Teramoto	奈良女子大学生活環境学部生活環境学科アパレル科学専攻
堂本　竹雄 Takeo Domoto	ブルカー・バイオスピン株式会社 Bruker BioSpin K.K.
土江　松美 Matsumi Doe	大阪市立大学理学研究科 Osaka City University
都出　千里 Chisato Tode	神戸薬科大学 Kobe Pharmaceutical University
内藤　晶 Akira Naito	横浜国立大学 Yokohama National University
長尾　聡 Satoshi Nagao	筑波大学大学院数理物質科学研究科山本研究室
中澤　靖元 Yasumoto Nakazawa	東京農工大学　工学部 Tokyo Univerisity of Agriculture and Technology
長嶋　恵美 Megumi Nagashima	株式会社渡商会 Watari Co.,Ltd.
長島　敏雄 Toshio Nagashima	理化学研究所ゲノム科学総合研究センター タンパク質構造・機能研究グループ RIKEN GSC Protein Research Group
永田　崇 Takashi Nagata	横浜市立大学 Yokohama City University
中西　梓 Azusa Nakanishi	京都大学理学研究科分子構造化学研究室
中西　裕美子 Yumiko Nakanishi	横浜市立大学 Yokohama City University.
中村　和浩 Kazuhiro Nakamura	秋田県立脳血管研究センター Akita Research Institute for Brain and Blood Vessels
中村　英章 Hideaki Nakamura	電気通信大学量子・物質工学科 Department of applied Physics and Chemistry , The University of Electro-Communications
中村　文彦 Fumihiko Nakamura	花王株式会社 Kao Corporation
新村　素晴 Subaru Niimura	群馬大学大学院工学研究科 Faculty of Engineering, Gunma University

参加者名簿 名前	所属
西村　勝之 Katsuyuki Nishimura	分子科学研究所 Institute for Molecular Science
西村　文月 Fuzuki Nishimura	京都大学理学部分子構造研究室
西山　裕介 Yusuke Nishiyama	理化学研究所 GSC RIKEN Institute GSC
根来　誠 Makoto Negoro	大阪大学大学院基礎工学研究科 Graduate School of Engineering Science, Osaka University
根本　直 Tadashi Nemoto	産業技術総合研究所 National Institute of Advanced Industrial Science and Technology
野尻　英里 Eri Nojiri	横浜市立大学大学院　国際総合科学研究科
野田　康夫 Yasuo Noda	関西学院大学 Kwansei Gakuin Univ.
野村　薫 Kaoru Nomura	（財）サントリー生物有機科学研究所 suntory institute fo bioorganic research
秦　和澄 Kazumi Hata	近畿大学大学院生物理工学研究科 Graduate School of Biology-Oriented Science and Technology, Kinki University
服部　峰之 Mineyuki Hattori	（独）産業技術総合研究所 AIST
林　繁信 Shigenobu Hayashi	産業技術総合研究所 National Institute of Advanced Industrial Science and Technology (AIST)
林　文晶 Fumiaki Hayashi	理化学研究所 RIKEN
半沢　宏之 Hiroyuki Hanzawa	三共株式会社創薬基盤研究所
平沖　敏文 Toshifumi Hiraoki	北海道大学大学院工学研究科 Hokkaido University
平川　慶子 Keiko Hirakawa	日本医科大学 Nippon Medical School
平田　清美 Kiyomi Hirata	株式会社巴商会 Tomoe Shokai Co., Ltd.
廣田　洋 Hiroshi Hirota	独立行政法人理化学研究所 RIKEN
深澤　隼 Jun Fukazawa	京都大学大学院理学研究科化学専攻 Kyoto University
福地　将志 Masashi Fukuchi	京都大学大学院理学研究科化学専攻 Department of Chemistry, Graduate School of Science, Kyoto University
藤江　正樹 Masaki Fujie	北海道大学工学研究科応用物理学専攻 Graduate School of Engineering, Hokkaido University

参加者名簿 名前	所属
藤本　侑子 Yuko Fujimoto	福井大学大学院工学研究科生物応用化学専攻
藤原　敏道 Toshimichi Fujiwara	大阪大学　蛋白質研究所 Institute for Protein Research, Osaka university
藤原　英明 Hideaki Fujiwara	大阪大学大学院医学系研究科 Osaka University, Graduate School of Medicine
藤原　康博 Yasuhiro Fujiwara	福井大学 University of Fukui
古板　恭子 Kyoko Furuita	奈良先端科学技術大学院大学 NARA INSTITUTE of SCIENCE and TECHNOLOGY
古田　浩祐 Hirosuke Furuta	キョーリン製薬（株）創薬研究所 kyorin pharmaceutical co.,ltd
降旗　一夫 Kazuo Furihata	東京大学農学生命科学研究科応用生命化学専攻 University of Tokyo
ベルヒリ　マーカス	ブルカーバイオスピン（株）
逸見　光 Hikaru Hemmi	独立行政法人農業・食品産業技術総合研究機構　食品総合研究所 National Food Research Institute, National Agriculture and Food Research Organization (NARO)
星加　博光 Hiromitsu Hoshika	奈良先端科学技術大学院大学 Nara Institute of Science and Technology
細田　和男 Kazuo Hosoda	群馬大学工学部生物化学工学科 Department of Biological and Chemical Engineering, Faculty of Engineering, Gunma University
蓬台　俊宏 Toshihiro Hodai	住友化学株式会社
前川　英己 Hideki Maekawa	東北大学 Tohoku University
前田　史郎 Shiro Maeda	福井大学大学院工学研究科生物応用化学専攻 Division of Applied Chemistry and Biotechnology, Graduate School of Engineering, University of Fukui
増田　裕洪 Hiromitsu Masuda	日本電子株式会社
Hidefumi Masumoto	University of Tsukuba
松原　康史 Koshi Matsubara	三菱化学科学技術研究センター　横浜分析センター　有機分析グループ
松森　信明 Nobuaki Matsumori	大阪大学大学院理学研究科 Graduate School of Science, Osaka University
丸吉　京介 Keisuke Maruyoshi	三共株式会社 SANKYO CO., LTD.
まろにゅ　みはる Michal Malon	独立行政法人理化学研究所 RIKEN

参加者名簿 名前	所属
マンレイオ　スラージ Suraj Manrao	スペクトラガス　インク Spectragases Inc.
水野　和子 Kazuko Mizuno	福井大学大学院 University of Fukui
水野　敬 Takashi Mizuno	日本電子株式会社 JEOL Ltd.
水野　元博 Motohiro Mizuno	金沢大学大学院自然科学研究科 Graduate School of Natural Science and Technology, Kanazawa University
三森　文行 Fumiyuki Mitsumori	国立環境研究所 National Institute for Environmental Studies
宮本　和英 Kazuhide Miyamoto	理化学研究所　GSC　タンパク質構造・機能研究グループ RIKEN GSC Protein Research Group
三好　利一 Toshikazu Miyoshi	産業技術総合研究所 AIST
村上　美和 Miwa Murakami	物質・材料研究機構 National Institute for Materials Science
村中　淳之介 Junnosuke Muranaka	福井大学大学院工学研究科 Graduate School of Engineering, Universoty of Fukui
村山　守男 Morio Murayama	東横化学株式会社 Toyoko Kagaku CO.,LTD.
飯塚　舜介 Shunsuke Meshitsuka	鳥取大学大学院医学系研究科 Ｔｏｔｔｏｒｉ University Grad Sch Medical Science
最上　祐貴 Yuuki Mogami	京都大学理学部化学科
森　哲哉 Tetsuya Mori	横浜市立大学大学院　国際総合科学研究科　生体超分子科学専攻　環境分子生物学研究室 Division of Enviromental Molecular Biology, Supramolecular Biology, International Graduate School of Arts and Sciences, Yokohama City University
森田　勇人 Hayato　Morita	愛媛大学総合科学研究支援センター Ehime University, Intergrated Center for Sciences
八木　宏昌 Hiromasa Yagi	大阪大学蛋白質研究所 Institute for protein research
八島　秀仁 Hidehito Yashima	ブルカーバイオスピン（株）
山内　一夫 Kazuo Yamauchi	東京農工大学 Tokyo University of Agriculture and Technology
山口　徹 Tohru Yamaguchi	塩野義製薬株式会社 Shionogi & Co., Ltd.
山口　秀幸 Hideyuki Yamaguchi	味の素株式会社 AJINOMOTO
山崎　俊正	農業生物資源研究所

参加者名簿 名前	所属
Toshimasa Yamazaki	National Institute of Agrobiological Sciences
山路　俊樹 Toshiki Yamaji	京都大学理学研究科化学専攻 Department of Chemistry, Graduate School of Science, Kyoto University
山田　知典 Tomonori Yamada	京大化研 Institute for Chemical Research, Kyoto University
山延　健 Takeshi Yamanobe	群馬大学工学部 Gunma University
山本　昭彦 Akihiko Yamamoto	ブルカーバイオスピン（株）
山本　泰彦 Yasuhiko Yamamoto	筑波大学大学院数理物質科学研究科 Graduate School of Pure and Applied Sciences, University of Tsukuba
山本　優理 Yuuri Yamamoto	奈良女子大学大学院 Nara Women's University
横井　実佳 Mika Yokoi	獨協医科大学　医学部　生理学（生体制御） Dokkyo University School of Medicine, Department of Regulatory Physiology
好田　真由美 Mayumi Yoshida	独立行政法人理化学研究所 RIKEN
吉水　広明 Hiroaki Yoshimizu	名古屋工業大学大学院工学研究科 Nagoya Institute of Technology
李　華 Hua Li	理化学研究所ゲノム科学総合研究センター
若松　馨 Kaori Wakamatsu	群馬大学 Gunma University
若松　永憲 Hisanori Wakamatsu	獨協医科大学 Dokkyo University School of Medicine
和田　武 Takeshi Wada	ブルカーバイオスピン（株）
渡邉　永治 Eiji Watanabe	順天堂大学 Juntendo Univ.
渡邉　英宏 Hidehiro Watanabe	独立行政法人国立環境研究所化学環境研究領域 National Institutes for Environmental Studies
渡辺　裕之 Hiroyuki Watanabe	バリアン　テクノロジーズ　ジャパン　リミテッド
Astrid Eijkelenboom	none
Hyuk Nam Kwon	INHA University
Insuk Yu	Seoul National University, Seoul, Korea
Jin Ho Kang	INHA University
Johan Sagemark	Karolinska institute

参加者名簿 名前	所属
N. Suryaprakash	NMR Research Centre, Indian Institute of Science
Sun mi Kang	INHA University
Sunghyouk Park	INHA University
Tobias Elgan	Biosciences and Nutrition at Novum
Weng Peng Weng	大阪大学、基礎工研究科 Osaka University, Faculty of Engineering Science
Yohei Miyanciri	HongKong University of Science & Technology
Yu-Keung Mok	Natioanl University of Singapore and Institute of Molecular and Cell Biology